STUDY OF MECHANISMS OF GRAIN DUST EXPLOSION AS AFFECTED BY PARTICLE SIZE AND COMPOSITION

by

DAVID WAYNE GARRETT

B.S., Kansas State University, 1977

A MASTER'S THESIS

submitted in partial fulfillment of the

requirements for the degree

MASTER OF SCIENCE

Department of Chemical Engineering

KANSAS STATE UNIVERSITY
Manhattan, Kansas

1981

Approved by:

J. S. Lai
Co-Major Professor

L. T. Fan
Co-Major Professor

TABLE OF CONTENTS

CHAPTER PAGE

CHAPTER PAGE

CHAPTER PAGE

CHAPTER PAGE

LIST OF FIGURES

Figure | Page

Figure | Page

Figure | Page

LIST OF TABLES

THIS BOOK
CONTAINS
NUMEROUS PAGES
WITH THE ORIGINAL
PRINTING BEING
SKEWED
DIFFERENTLY FROM
THE TOP OF THE
PAGE TO THE
BOTTOM.

THIS IS AS RECEIVED
FROM THE
CUSTOMER.

CHAPTER 1

INTRODUCTION

Research on dust explosions has been conducted since 1917 but the progress has been painfully slow (see, e.g., Aldis and Lai, 1979). Relatively limited work has been carried out to systematically explore and quantify the effects of basic parameters governing the dust explosion. A dust explosion consists of a very rapid combustion reaction that liberates heat and results in the expansion of the gases surrounding the dust. When this expansion occurs in a vessel or enclosure, the pressure in it rises rapidly; this may lead to structural damage to the vessel or the enclosure. Two of the basic parameters are the diameter and composition of the grain dust particles.

The overall objective of this work was to study the effects of the particle diameter and composition on the explosibility of the grain dust. Specifically, the explosibility was characterized in this work by four parameters from Hartmann bomb tests (Dorsett et al., 1960). These four parameters were the maximum explosion pressure, P_{max}, the maximum rate of pressure rise, $(dP/dt)_{max}$, the average rate of pressure rise, $(dP/dt)_{ave}$, and the minimum explosible concentration, C_{min}.

Four types of powder were tested. They were corn dust, wheat dust, and sorghum dust, which had been collected from cyclone dust systems in commercial elevators, and a commercial grade cornstarch. Each of these was separated into different particle size fractions, and the particle size distribution of each fraction was determined. The composition of the grain dust was characterized by the moisture content, ash content, protein content, and starch and fiber content.

This thesis contains six chapters. The first is the present introductory chapter delineating the objectives and scope of the work. The works by previous researchers are reviewed in the second chapter. The third chapter describes characterization of dust particles with the emphasis on particle size and composition. Determination of the minimum explosible concentration is described in chapter four; the effects of the particle size and composition on it are discussed. Measurements of the maximum explosion pressure, the maximum rate of pressure rise, and the average rate of pressure rise are given in chapter five. The conclusions and recommendations are given in chapter six.

REFERENCES

Aldis, D.F., and Lai, F.S. 1979. Review of literature related to engineering aspects of grain dust explosions. USDA Miscellaneous Publication Number 1375.

Dorsett, H.G., Jr., Jacobson, M., Nagy, John, and Williams, R.P. 1960. Laboratory equipment and test procedures for evaluating explosibility of dusts. U.S. Bureau of Mines, Report of Investigations 5624, 21 pp.

CHAPTER 2

REVIEW OF LITERATURE

I. INTRODUCTION

This review deals with publications related to the effects of particle size and composition of grain dust on its explosion characteristics. The characteristics considered are the minimum explosible concentration, the maximum explosion pressure, the maximum rate of pressure rise, and the average rate of pressure rise. This survey is concerned with mainly dust from grains, including wheat, corn, and grain sorghum.

II. EXPERIMENTAL STUDIES

A relatively limited number of publications are available, which are concerned with the effects of particle size and composition on the four explosion characteristics. Some of the publications reporting the results of experimental study present the data graphically and/or tabularly with minimal analysis. The majority of such publications are from the U.S. Bureau of Mines (Hartmann and Nagy, 1944; Jacobson et al., 1964; and Hertzberg et al., 1979). Other publications include empirical correlations of data (Jacobson and Nagy, 1961; Eckhoff, 1976).

A. Particle Size

Hartmann and Nagy (1944) used a series of sieves to separate their dust into four size ranges; 20-65, 65-100, 100-200, and greater than 200 mesh. They calculated an average particle diameter for each of the size ranges, i.e., the arithmetic mean of the particle diameter corresponding to the sieves used to determine the upper and lower bounds of each range. The geometric mean should have been used instead of the arithmetic mean because particle

size distributions are characteristically lognormal. Herdan (1960) stated that for the lognormal distribution, the geometric mean better represents the particle size than the arithmetic mean. For each range, Hartmann and Nagy (1944) plotted the minimum explosible concentration, the maximum pressure rise, and several other quantities against the average particle diameter. They observed that the minimum explosible concentration decreased with decreasing particle size; however, for several kinds of dust, it changed very little when the particle sizes were less than approximately 102 μm (0.004 in.) for cellulose acetate molding powder with a dust cloud concentration of 0.005 kg/m^3 (0.005 oz/cu.ft.), the maximum pressure increased with decreasing particle size but remained essentially constant for diameters smaller than 102 μm (0.004 in.). The maximum and average rates increased with a decrease in the particle size.

Jacobson et al. (1961) separated, by sieving, each of eleven types of dust into two or more size fractions. They obtained twelve fractions for aluminum, nine for magnesium, five for cornstarch, and two to four for the rest. They further separated, with a series of sieves, each of the fractions and calculated the average particle diameters with a method described by Dallavalle (1948). The arithmetic mean of the respective size openings of a pair in the series of sieves was multiplied by the fraction of dust retained on the finer of the two sieves. The average particle diameter was the summation of the latter quantities for the entire series of sieves. Again, the geometric mean should have been used in place of the arithmetic mean because of the lognormality of the particle size distributions (Herdan, 1960). The average particle diameters of these fractions ranged from 18 to 171 μm. Jacobson et al. (1961) plotted the results of the experiments performed on all eleven types of dust on a single graph. They plotted the ratio of explosion

characteristics against the ratio of average particle diameters. The ratio of explosion characteristics (e.g., maximum explosion pressure) is defined as the explosion characteristics of a given dust divided by that of a through no. -200 sieve sample of the same type of dust. The *maximum* pressure, as one of the explosion characteristics, showed a slight increase as the ratio of average particle diameters decreased. The ratio of minimum explosible concentrations decreased with the decrease in the ratio of average particle diameters for coarse dust (> 74 μm); however, for fine dusts there was only a slight change with the ratio of average particle diameters.

Jacobson and Nagy (1961) empirically correlated the ratio of explosibility indexes, I_R, with the ratio of average particle diameter, D_R. The explosibility index is the product of the maximum explosion pressure and the maximum rate of pressure rise divided by the product of the minimum ignition temperature, the minimum ignition energy and the minimum explosible concentration for the sample dust divided by that for standard Pittsburg coal dust. The relationship obtained by them is:

$$I_R = D_R^{-3} \tag{1}$$

Jacobson et al. (1964) used dust samples of various metals including zinc, iron, cobalt, etc. that were obtained from different processes, e.g., milling, stamping, and atomizing. They determined the particle size distribution by sieving and calculated the average particle diameter for each sample. The effect of average particle diameter on minimum explosible concentration, maximum pressure rise, maximum rate of pressure rise, and average rate of pressure rise for atomized aluminum dust was similar to those reported by Jacobson et al. (1961).

Hertzberg et al. (1979) performed a study on explosion of coal dust-air mixtures. They separated their dust into nine size ranges with average particle diameters spanning from 2.7 to 65 μm. Six of the nine size ranges were classified by a Donaldson centrifugal classifier, two by sieve-classification, and one was unclassified pulverized coal. The surface mean diameter was determined for each size range by a Coulter size analyzer. The experiments were performed to determine the minimum explosible concentration, the maximum pressure, and the maximum rate of pressure rise in a modified Hartmann bomb. The volume of the explosion chamber was 7.8 liters instead of the standard 1.2 liters and the inside configuration of the chamber was altered to achieve a more uniformed dust dispersion than in the original Hartmann bomb. The standard criterion for determining the minimum explosible concentration is the lowest concentration of dust that when ignited will cause a paper diaphram to rupture (Dorsett et al., 1960). The criterion used by Hertzberg et al. (1979) was the lowest concentration of dust that when ignited would create a maximum pressure that reached a value twice that of the initial pressure just prior to ignition. They altered the standard procedure by partially evacuating the explosion chamber to a pressure of 0.2 to 0.3 atm, so that the pressure reached approximately 1 atm after the air for dispersing the dust was injected into the chamber. Instead of the standard procedure imploring a continuous electric spark initiated prior to the injection of the dust, they used electric matches ignited after a spatially uniformed dust cloud was achieved. Hertzberg et al. (1979) observed the minimum explosible concentration to be virtually independent of particle size in the range of size 2.7 to 65 μm. At dust concentrations close to the minimum explosible concentration, the maximum pressure rise and maximum rate of pressure rise did not depend markedly on the particle size. However, at high dust concentrations

(0.4 to 0.5 kg/m^3) these quantities did increase somewhat with decreasing particle diameter.

Eckhoff (1976) determined the maximum explosion pressures, and the maximum rates of pressure rise, of several types of dust from agricultural grains and feedstuffs (e.g., corn, wheat, rye, fish powder, soya meal, and potato starch). The dust samples were obtained from elevators in different countries (e.g., the United States, and Norway), and from various locations in the elevators (e.g., the bottom of the bucket elevator, and the dust filter). To determine the particle size distribution Eckhoff (1976) used a series of sieves for the coarse (> 74 μm) and of the distribution and a Coulter Counter analysis for the fine end. A specific surface area (the "envelope" surface area) was approximated for each sample. The shape of the dust particle approximated by a sphere, and the corresponding mass average particle diameter was used as the radius in the measurement of particle size distribution. BET measurements were conducted to obtain another approximate average surface area. He used the Hartmann apparatus to determine the maximum explosion pressure and maximum rate of pressure rise for each sample. He also obtained the relation between the maximum rate of pressure rise and the specific "envelope" surface area by means of a least squares regression line for starch and protein, i.e.,

$$\left(\frac{dP}{dt}\right)_{max} = KS \tag{2}$$

where

$\left(\frac{dP}{dt}\right)_{max}$ = maximum rate of pressure rise

K = constant

S = specific surface area

Each regression line was forced through the origin and two data points were used to determine the slope. Two different sizes of fish powder were used for the protein, and two different types of starch, potato and maize, were used for the starch. He obtained a good correlation with slope values of 450 bar·g/(s·m^2) for protein and 1250 bar·g/(s·m^2) for starch.

Bartknecht (1978) performed explosion tests in a one cubis meter spherical explosion chamber. He studied four types of dusts: flour, methylcellulose, polyethylene, and polyvinylchloride. The average particle diameters of each dust ranged from approximately 10 to 400 μm. The maximum explosion pressure and rate of pressure rise were plotted against the average particle diameter. From the methylcellulose and the polyvinylchloride dusts, Bartknecht separated, for each dust, a non-explosive coarse fraction and an explosive fine fraction. From these fractions he prepared five samples, each having unique ratio, the weight percent of coarse fraction to that of the fine fraction. For example, a ratio of 75/25 indicates that the sample contained 75 percent coarse fraction and 25 percent fine fraction. He plotted the maximum explosion pressure and the maximum rate of pressure rise against those ratios. The result for each type of dust was graphed separately. Methylcellulose showed that the maximum explosion pressure and the maximum rate of pressure rise increased with the ratio decreased. The highest value of maximum explosive pressure and maximum rate of pressure rise occurred at the ratio of 0/100 (that is the sample contained no coarse fraction and 100 percent fine fraction). For polyethylene dust, the highest value of the maximum explosion pressure and the maximum rate of pressure rise occurred when there was some coarse fraction mixed with the fine fraction. These maximum approximately occurred at the ratio of 75/25 for the maximum explosion pressure and 25/75 for the maximum rate of pressure rise.

Price (1922) separated oat and corn dust, wheat flour, wheat flour dust, and potato starch into four different size fractions by elutriation. The particles in a sample from each fraction were microscopically sized. The average particle diameter for each fraction was the arithmetic average of the maximum particle diameter in the fraction and that in the next smaller fraction. The average particle diameters ranged from 10 to 100 μm. He used the standard Bureau of Mines apparatus for inflammability to perform experiments. The standard procedure was altered by using 0.000075 kg (75 mg) of the dust sample instead of 0.0001 kg (100 mg), and by dispersing the dust sample with pressurized air instead of oxygen. The maximum explosion pressure measurements from the tests were plotted against the average particle diameter. The maximum explosion pressures increased with decreasing average particle diameters; however, for wheat flour and "wheat flour dust" with particle sizes less than approximately 35 μm, the maximum explosion pressure decreased with decreasing particle size. Price (1922) concluded that particle size was a very important factor in governing the explosibility of the dust.

B. Composition

Eckhoff (1976), in his work on agricultural dust, characterized the composition of the dust by the percent moisture, ash, protein, starch and fiber. He discovered a reasonable correlation between the maximum rate of pressure rise and the percent of starch and fiber. To separate the particle size effect from the correlation, he assumed that Eq. (2) could be used to correlate the maximum rate of pressure rise with a specific "envelope" surface area. He assumed the proportionality constant, K, in Eq. (2) to be a function of composition. This functionality was

$$K = \sum_{i}^{n} K_i X_i \qquad (3)$$

where

n = total number of all components

K_i = the value of K for pure component i

X_i = the weight fraction of component i

He experimentally determined the value of K_i for starch using wheat starch and corn starch and for protein using fine and coarse fish powder. The value of K_i for starch was considered applicable to the starch and the fiber fractions because of the similarity between the molecular structures of the two. The value of K_i for the fish powder was considered applicable to the rest of the components: protein, fat, and N-free soluble organic compounds other than starch. The resultant correlation is

$$K = \left(800 \cdot \frac{(\%\ \text{Starch \& Fiber})}{100} + 450\right) ; \frac{kp \cdot gm}{cm^2 \cdot s \cdot m^2} . \qquad (4)$$

Eckhoff (1977/78) also correlated the maximum rate of pressure rise with the weight percent moisture. He selected four dusts: maize starch, cellulose powder, potato starch, and Norwegian oat dust, and prepared several samples from each with varying weight percents of moisture. He obtained an approximate correlation given by

$$\left(\frac{dP}{dt}\right)\Big|_y = \left(\frac{dP}{dt}\right)\Big|_{y=0} \left(1 - \frac{y}{y_{min}}\right) \qquad (5)$$

where

y = weight percent of moisture

y_{min} = the weight percent of moisture above which no explosion can occur.

y_{min} was assumed by Eckhoff (1977/78) to be approximately 15% for all types of dusts.

Enomoto (1977) performed his study using two different apparatuses. Each apparatus generated a sufficiently uniform dust cloud over a specific concentration range. The range of concentration was 0 to 0.300 kg/m^3 for the apparatus developed by Ishihama (1961) and 0.300 to 4.000 kg/m^3 for the apparatus developed by Ishihama and Enomoto (1973). Neither of the apparatuses used compressed air to disperse the dust as the standard Hartmann apparatus did. The first used a mechanical vibrator to shake the dust through a sieve into the explosion chamber below. The second apparatus generated a dust cloud by rotating the explosion chamber. The faster the chamber rotated and the more dust placed in the chamber, the denser the cloud became. Gun cotton was also used as the ignition source in the second apparatus instead of the standard electric spark. Enomoto (1977) performed his experiments on four types of coal dust: Yamagata lignite, Horonai, Ponbetis, and Liddel. Each of the Horonai and Ponbetia had five separate particle size fractions and each of the Yamagata lignite and Liddel had two. He added small amounts of magnesium oxide to increase the dispersibility of the dust. Graphs of explosion strength plotted against average particle diameter were presented. The explosion strength is the maximum explosion pressure multiplied by the highest maximum rate of pressure rise. The explosion strength increased as the particle size decreased.

Eckhoff (1978) studied the effect of moisture on the rate of pressure rise in the Hartmann bomb tests. He attempted to eliminate the effects of moisture on the quality of the dust dispersion, the effective particle size distribution and the turbulence. Corn flour was the only sample used. In a test apparatus similar to the Hartmann, the effective particle size distribution was measured. This apparatus uses the same dispersion system as the Hartmann apparatus and also had the same shape; however, there is no ignition

system and the tube is fitted with a piston. Double adhesive tape was attached on the bottom of the piston. When the dust was dispersed, the tape captured a sample of the dust dispersed and an effective particle size distribution was determined by microscopic examination. He concluded that moisture does not affect the effective particle size distribution greatly.

The ignition delay (the time interval between the dispersion and the ignition of the dust) was taken as an indicator of the degree of turbulence, e.g., if the ignition delays of two explosions were equal, the degree of turbulence was considered to be the same. Therefore, to eliminate the effect of turbulence on the correlation of the maximum rate of pressure rise with weight percent moisture, only those data from the explosion tests with similar ignition delays were compared. This correlation was significantly different from the correlation of the maximum rate of pressure rise with weight percent moisture where the differences in ignition delay were not considered. At short ignition delay times (approximately 0.005 sec.) there were significant maximum rates of pressure rise for moisture contents considerably higher than 30%. When the delay time was not considered, there were few significant maximum rates of pressure rise for moisture contents higher than 22%.

Price (1922) studied the effect of volatile matter, ash, and moisture content on the maximum pressure rise. His samples included different types of coal dust and other carbonaceous types of dust. The apparatus and procedure that he used are described earlier in this chapter. He obtained no apparent correlation between the maximum explosion pressure developed and the weight percent of volatile matter for the carbonaceous dusts. From a table presented by Bautling (1918) on volatile matter produced by complete distillation (to 500° C) of cellulose and starch, Price (1922) showed that most of the volatile matter given off is not inflammable. He also found that the ash

content did not have a marked effect on the pressure rise by the carbonaceous dusts when the weight percent of ash was below normal limits; however, at weight percents of ash above normal limits, the higher the ash content, the lower the explosion pressure rise. His results indicate an increase in moisture content decreases the explosion pressure rise by both acting as a heat sink and by causing the effective particle size to increase due to agglomeration. The effect was not pronounced enough to make moisture a practical inertant.

III. THEORETICAL STUDIES

There is also a very limited number of publications that attempt a theoretical prediction of the explosion characteristics: minimum explosible concentration, maximum explosion pressure, maximum rate of pressure rise, and average rate of pressure rise. Jaeckel (1924) and Tanaka (1977) developed expressions to predict the minimum explosible concentration. Normura and Tanaka (1979) and Nagy et al. (1969) developed expressions for the prediction of the maximum explosion pressure and rate of pressure rise.

Jaeckel (1924) performed a heat balance on the dust-air system to predict the minimum explosible concentration. He considered the minimum explosible concentration, C_{min}, to be the smallest concentration of dust capable of producing enough heat, when completely combusted, to elevate the temperature of the dust cloud and the air to the ignition temperature. He has obtained the following expression:

$$C_{min} = \frac{(T_1 - T_o)\rho_a C_p}{q - (T_1 - T_o)C_{ps}} \qquad (6)$$

where

q = heat generated per unit mass of dust

T_1 = ignition temperature

T_o = initial temperature

ρ_a = density of the air

C_p = specific heat capacity of the air

C_{ps} = specific heat capacity of the dust

This model depicts the system as being a spatially uniformed dust cloud throughout the entire explosion and does not take into account the dependence of C_{min} on the dust particle size. Jaeckel (1924) reported that Eq. (6) predicted a minimum explosible concentration of 0.022 kg/m^3 for sugar powder; in contrast, Jacobson et al. (1961) reported an experimental value of 0.045 kg/m^3.

Tanaka (1977) also developed a model to predict the minimum explosible concentration. He considered a particle at the center of the dust cloud that was ignited by an outside source. The ignited particle now is heating its nearest neighbor, a second particle at a distance L. The minimum concentration, C_{min}, is the smallest concentration that allows the flame to propagate from the ignited particle to its nearest neighbor. In his model, an equation for the calculation of the flame height, b, is that taken from a publication on the burning of liquid droplets by Meise (1957). Tanaka (1977) has assumed that the gas phase between the two particles is stagnant. He then estimated the gas temperature at the gas-solid interface of the second particle, T_{gL}, by solving the conduction equation

$$\frac{\partial T_{gr}}{\partial t} = \alpha \left(\frac{\partial^2 T_{gr}}{\partial r^2} + \frac{2}{r^2} \frac{\partial T_{gr}}{\partial r} \right) \tag{7}$$

where

α = thermal diffusivity of the air

r = radial distance from the center of the ignited particle

T_{gr} = temperature of the gas at any radial position r

The resultant equation was

$$T_{gL}(\eta) = (T_f - T_i)\left(\frac{6}{L}\right) \operatorname{erfc}\left[\frac{(L-b)}{2\sqrt{\alpha K_p D_p^2 \eta}}\right] + T_i \tag{8}$$

where

D_p = particle diameter

η = t/T

T = time required to completely combust the particle

K_p = proportionality constant between T and D_p^2

T_f = temperature of the flame

T_i = initial temperature of the system

He performed an energy balance around the second dust particle to determine the temperature of the particle, T_{dL}, as follows:

$$\rho_s \frac{\pi}{6} D_p^3 C_{ps} \frac{d(T_{dL})}{dt} = \pi D_p^2 L (T_{gL} - T_{dL}) + \frac{\pi}{2} D_p^2 E_p E_f F \cdot \sigma T_f^4 - \pi D_p^2 E_p \sigma T_{dL}^4 \tag{9}$$

where

ρ_s = density of the dust particle

C_{ps} = specific heat capacity of the dust particle

E_p = emissivity of the particle

E_f = emissivity of the flame

σ = Stephan-Boltzmann constant

F = shape factor

h = heat transfer coefficient, $2K/D_p^2$

k - thermal conductivity of the air

The resultant equation is

$$T_{dL}(\eta) = \frac{1}{e^{C\eta}} \left[\int_0^{\eta} e^{C\eta} \left[C\, T_{gL}(\eta) + D \cdot T_f^4 \right] d\eta + T_{do} \right] \tag{10}$$

where

$C = 12K_D k/\rho_s \cdot C_{ps}$

$D = 3K_D E_p E_f F D_p/\rho_s C_{ps}$

T_{do} = initial temperature of the particle

The value of η, t/T, at which T_{dL} reaches the ignition temperature, T_i, can be calculated from Eqs. (8) and (10) by selecting a distance L. The minimum distance, L_o, is the distance L which allows the second particle to reach the ignition temperature, $T_{dL} = T_i$, at the moment that the initial particle is completely consumed, $\eta = 1$. The minimum explosible concentration is calculated from L_o by the following equation:

$$C_{min} = \frac{\frac{\pi}{6} D_p^3 \rho_s}{L_o^3} \tag{11}$$

Tanaka (1977) has defined his ignition temperature, T_i, differently from that experimentally determined by the Gobert-Greenwald furnace. The ignition temperature defined in the model is the temperature of the dust particle that causes it to ignite; however, the experimentally determined ignition temperature is the minimum gas temperature that causes a particle immersed in it to ignite (Dorsett et al., 1960).

Nagy et al. (1969) has derived an expression to predict the rate of pressure rise as a function of time. He has assumed that the pressure developed is affected by changes in temperature and increases in the total number of moles of gas in the explosion chamber.

Nagy et al. (1960) based their derivation on an equation empirically derived from gaseous explosions, which is

$$\frac{1}{A}\left(\frac{\Delta V_u}{\Delta t}\right) = K_r \left(\frac{T_u}{T_r}\right)^2 \left(\frac{P_r}{P}\right)^{\beta} \qquad (12)$$

where

A = surface area of the flame front

V_u = volume of unburned fuel and gas

K_r = burning velocity reference at 1.0013 bar (1 atm) and 298 K (537°R)

T_r = reference temperature, 298 K (537°R)

P_r = reference pressure, 1.013 bar (1 atm)

β = constant

They have assumed that the air and combustion gases behave ideally and that any solid present has negligible heat capacity and volume. At any time during

the explosion, the combustion chamber is assumed to be divided into two zones, the burned and unburned zones, by a very thin combustion zone.

Nagy et al. (1960) have considered two cases. In one case, the system is assumed to be isothermal, and in the other it is assumed to be adiabatic. For the isothermal system, the rate of pressure rise is

$$\frac{dP}{dt} = \frac{3 K_r T_o^2 P_r P_m^{\frac{2}{3}}}{a T_r^2 P_o} \left(P_{max} - P_o \right)^{\frac{1}{3}} \left(1 - \frac{P_o}{P} \right)^{\frac{2}{3}} P^{1-\beta} \qquad (13)$$

where

P_{max} = maximum explosion pressure

P_o = initial pressure

T_o = initial temperature

a = radius of the vessel

For the adiabatic system, the rate of pressure rise is

$$\frac{dP}{dt} = \frac{3\nu K_r T_o^2 P_r^{\beta} P_{max}^{\frac{2}{3}\nu}}{a T_r^2 P_o^{2-\frac{1}{2}}} \left(P_{max}^{\frac{1}{2}} - P_o^{\frac{1}{2}} \right)^{\frac{1}{3}} \left[1 - \left(\frac{P_o}{P} \right) \right]^{\frac{2}{3}} P^{3-\frac{2}{\nu\beta}} \qquad (14)$$

In either case, the expression for pressure as a function of time is obtained by the integration of its equation for the rate of pressure rise, Eqs. (13) or (14). Note that neither Eq. (13) nor Eq. (14) is a function of particle size.

The expressions for the rate of pressure rise, Eq. (13) and (14), are explicit functions of neither concentration nor their models to experimental results involving several gases and cornstarch. They obtained a good

agreement with an exception when the explosion was nearly complete and the heat loss to the walls of the vessel became significant.

Normura and Tanaka (1979) have theoretically derived the experimentally determined "cubic law" used by Bartnecht (1971). The "cubical law" is

$$K_G = \left(\frac{dP}{dt}\right)_{max} \cdot V_o^{\frac{1}{3}} \tag{15}$$

where

$(dP/dt)_{max}$ = maximum rate of pressure rise

V_o = enclosure volume (constant with time)

They have assumed the dust cloud to be stagnant with the particles uniformly spaced in a fixed geometry. The geometry is shown in Fig. 2.1. The flame in the n-th spherical shell of dust particles is assumed to propagate by transfering heat to the (n+1)-th spherical shell of particles until the temperature of the particles in the (n+1)-th shell reached the ignition temperature and the particles ignited. The flame continues to propagate from one shell to the next until the dust is completely consumed. Normura and Tanaka (1979) have also assumed the heat is transported by only conduction and radiation because of the stagnant cloud assumption. By performing an energy balance, the time interval, t_n, between the ignition of the particles in the n-th shell and the ignition of the particles in the (n+1)-th shell is calculated for each pair of shells. For n between 1 and approximately 10, the time interval t_n decreases; however, for n greater than 10 it remains constant. Because t_n becomes constant rapidly, a fixed t is used as the time interval for the entire flame propagation (n+1). At any time t, after the ignition of the first particle, the number of shells that have been ignited is calculated from t. From the

geometry, the total number of particles in each shell is known, and thus, the total number of particles ignited at any time t can be calculated. To determine the total mass of dust burned at any time t, M(t), Normura and Tanaka (1979) have assumed that the burning rate of each particle is controlled by the diffusion of oxygen through a layer of burned dust into the unburned center. From this, they have found a relationship between the length of time a particle had been burning, θ, and the mass of the particle that was consumed, $m(\theta)$. Therefore, M(t) is the summation over all of the ignited shells of the product of the total number of particles in a shell and the mass of each particle that has been burned. The relationship used for $m(\theta)$ is

$$\frac{m(\theta)}{m_o} = 1 - \left(1 - \frac{\theta}{\tau}\right)^3 \tag{16}$$

where

τ = time necessary to completely combust the particle

m_o = total amount of mass initially contained in the particle

However, this relationship is for a heterogeneous reaction in which the rate of the particle consumption is controlled by the rate of a first order reaction. The expression for which the controlling mechanism is the diffusion of oxygen through an ash layer is

$$\frac{m(\theta)}{m_o} = 1 - \frac{3}{2}\left(1 - \frac{m(\theta)}{m_o}\right)^{\frac{3}{2}} + \frac{1}{2}\left(1 - \frac{\theta}{\tau}\right) \tag{17}$$

Equation (17) is more complicated than Eq. (16) and would also complicate the solution of the model. Therefore, if from Eq. (16) the fraction of the initial mass that has been consumed, $m(\theta)/m_o$ is within 0.1 of that from Eq. (17) for all θ/T then Eq. (16) is the better choice. Figure 2.2 presents both Eq. (16) and Eq. (17) and the difference between $m(\theta)/m_o$ from Eq. (16) and $m(\theta)/m_o$ from Eq. (17). The difference is greater than 0.10 for $m(\theta)/m_o$ between 0.11 and 0.68 with a maximum of 0.21.

Normura and Tanaka (1979) have derived an expression for the pressure at any t from the expression for the amount of mass burned at any t, M(t) by making three more assumptions. They have assumed that the pressure developed was the result of a net increase in the total number of moles of gas produced by the reaction and the increase in temperature produced by the heat released from the reaction. They also have assumed that the system of the dust and air is adiabatic. The expression obtained by them for the pressure, P(t), is

$$P(t) = \left[\left(P_{max}^{1/\nu_u} - P_o^{1/\nu_u} \right) \frac{M(t)}{M_o} + P_o^{1/\nu_u} \right]^{\nu_u} \qquad (18)$$

where

M_o = total mass of dust initially present

ν_u = ratio of the heat capacity of the unburned gas at constant pressure to that at constant volume

$$\frac{M(t)}{M_o} = \frac{8m_o}{\Delta t_\infty^3} \left(1 - \frac{3\Delta t_\infty}{2\tau}\right) t^3$$

P_{max} = maximum explosion pressure attainable

P_o = initial pressure

They assumed that the maximum explosion pressure occurred when all of the dust initially present had been combusted. Hertzberg et al. (1979) showed that dust explosions were oxygen limited for concentration greater than 0.4 to 0.5 kg/m^3. Therefore, from Hertzberg et al. (1979), all of the initially present dust would not be burned, and maximum explosion pressure would be a function of the total amount of oxygen present. Therefore, P_{max} that Normura and Tanaka (1979) calculated would be too large for high concentration. When they assumed their system to be adiabatic, this caused the maximum explosion pressure and the maximum rate of pressure rise to occur at the same time. Therefore maximum rate of pressure rise will also be too high. To obtain their derived expression for the "cubical law," they differentiated Eq. (18) with respect to time, and evaluated the derivative at the time when it was maximum. As previously stated, the rate of pressure rise became a maximum when all of the dust was consumed. After some rearrangement they obtained

$$V_o^{\frac{1}{3}}\left(\frac{dP}{dt}\right)_{max} = \frac{\nu_n D_p}{\Delta t_\infty}\left[\frac{36\pi\rho_s}{a}\left(1-\frac{3\Delta t_\infty}{2\tau}\right)\right]^{\frac{1}{3}} P_{max}\left[1-\left(\frac{P_o}{P_{max}}\right)^{1/\nu_n}\right] \tag{19}$$

where

ρ_s = the density of the dust

D_p = the dust particles diameter

$a = 0.2 \cdot M_o/V_o$

Therefore,

$$K_G = \frac{\nu_a D_p}{\Delta t_\infty}\left[\frac{36\pi\rho_s}{a}\left(1-\frac{3\Delta t_\infty}{2\tau}\right)\right]^{1/3} P_{max}\left[1-\left(\frac{P_o}{P_{max}}\right)^{1/4}\right] \qquad (20)$$

The values of K_G calculated from Eq. (20) when compared with experimental data for starch, were significantly larger than those of the experimental values but are in the same order of magnitude.

REFERENCES

Bartknecht, W. 1978. Explosionen-ablauf und Schutzmassnahmen. (The course of explosions and preventive measures.) Springer Verlag, Berlin.

Dallavalle, J.M. 1948. Micromeritics, Ch. 5 in The Technology of Fine Particles. Pitman, New York, N.Y. 2nd ed., p. 113.

Dorsett, H.G., Jr., Jacobson, M., Nagy, J., and Williams, R.P. 1960. Laboratory equipment and test procedures for evaluating explosibility of dusts. U.S. Department of the Interior, Bureau of Mines, Report of Investigations, RI-5624.

Eckhoff, R.K. 1977/78. Pressure development during explosions in clouds of dusts from grain, feedstuffs and other orgain materials. Fire Research 1:71-85.

Eckhoff, R.K., and Mathisen, K.P. 1977/78. A critical examination of the effect of dust moisture on the rate of pressure rise in Hartmann bomb tests. Fire Research 1:273-280.

Enomoto, H. 1977. Explosion characteristics of agricultural dust clouds. Proceedings of the International Symposium on Grain Dust Explosions. Grain Elevator and Processing Society, Minneapolis, Minn. pp. 143-170.

Hartmann, I., and Nagy, J. 1944. Inflammability and explosibility of powders used in the plastics industry. U.S. Department of the Interior, Bureau of Mines, Report of Investigations, RI-3751.

Herdan, G., Smith, M.L., and Hardwick, W.H. 1960. Small Particle Statistics. Bulterworth and Co.

Hertzberg, M., Cashdollar, K.L., and Operman, J. 1979. The flammability of coal dust-air mixtures and particle size effects. U.S. Department of the Interior, Bureau of Mines, Report of Investigations, RI-8360.

Ishihama, W., and Enomoto, H. 1973. New experimental method for studies of dust explosions. Combustion and Flame 21:177-186.

Jacobson, M., Cooper, A.R., and Ball, F.J. 1961. Explosibility of Agricultural Dust. U.S. Department of the Interior, Bureau of Mines, Report of Investigations, RI-5753.

Jacobson, M., Cooper, A.R., and Nagy, J. 1964. Explosibility of metal powders. U.S. Department of the Interior, Bureau of Mines, Report of Investigations, RI-6516.

Jaeckel, G. 1922. Die Staubexplosionen. (Dust explosions.) Zeitschtift fur Technische Physik 3:67-78.

Miesse, C.C. 1957. Symp. Combust., 6th. 732.

Nagy, J., Conn, J.W., Verakis, H.C. 1969. Explosion development in a spherical vessel. U.S. Department of the Interior, Bureau of Mines, Report of Investigations, RI-7279.

Nagy, J., Seiter, E.C., Conn, J.W., and Verakis, H.C. 1971. Explosion development in closed vessels. U.S. Department of the Interior, Bureau of Mines, Report of Investigations, RI-7507.

Normura, S. and Tanaka, T. 1979. Theoretical study of the rate of pressure rise due to a dust explosion in a spherical vessel. Kagaku-Kogaku. pp. 601-608.

Price, D.J., and Brown, H.H. 1922. Dust explosions. National Fire and Protection Association, Boston, Mass.

Tanaka, T. 1977. Predicting ignition temperature, minimum explosive limit and flame propagation velocity. Proceedings of the International Symposium on Grain Dust Explosions. Grain Elevator and Processing Society, Minneapolis, Minn. pp. 79-99.

Yagi, S., and Kunii, D. 1955. 5th Symposium (International) on Combustion. Reinhold, New York. p. 231.

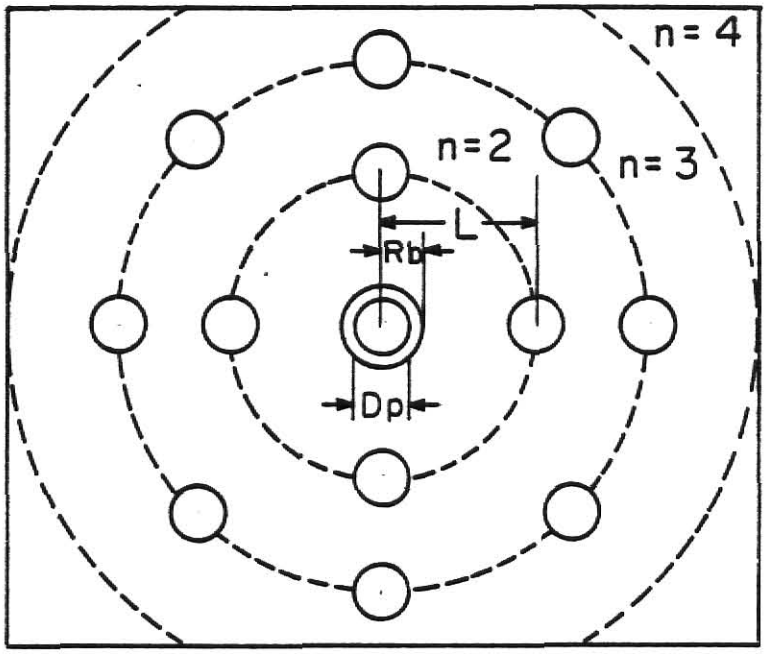

Fig. 2.1 Model of Dust Particles (Normura and Tanaka, 1977)

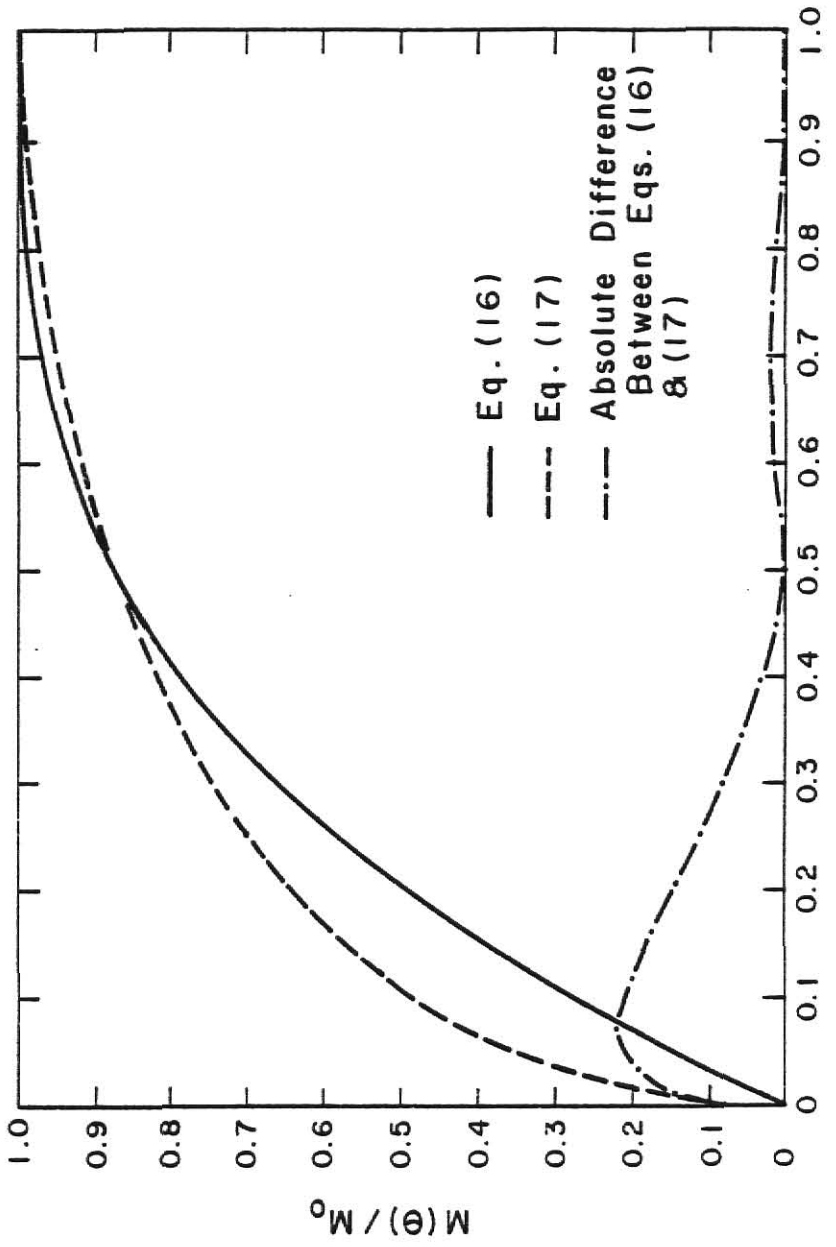

Fig. 2.2 Comparison of the Actual Expression for $M(\Theta)/M_o$ in Yagi and Kungi (1955) to that Used by Normura and Tanaka (1977)

CHAPTER 3

CHARACTERIZATION OF THE PARTICLE SIZE AND COMPOSITION OF GRAIN DUST

I. INTRODUCTION

In this investigation, studies were carried out on the effects of dust particle size and composition on the minimum explosible concentration, the maximum explosion pressure, the maximum rate of pressure rise, and the average rate of pressure rise. To study the effect of particle size requires a sample with the narrowest possible particle size distribution. To study the effect of composition requires the determination of the contents of moisture, ash, protein, and starch & fiber in each sample. This chapter is concerned with the collection of the dust samples from grain sorghum, wheat, and corn, the separation of those samples into size fractions, the determination of the particle size distribution of each fraction, the calculation of the average particle diameter of each distribution, and the determination of the composition of each fraction.

II. THEORETICAL

A. Determination of the Particle Size

1. Particle size distribution. The particle size distribution in each of the eleven size fractions was determined by the AACC method 50-10 (1975), namely, the Whitby sedimentation method. This is a centrifugal sedimentation method in which dust is allowed to settle in a capillary tube filled with liquid termed the sedimentation liquid. The Whitby sedimentation method classified particles hydrodynamically. The diameter obtained by this method corresponds to the diameter of a sphere that falls with the same velocity as

the real particles. Though the physical dimension of the particles obtained by this method might be different from those of the real particles in many cases, the distribution obtained is one for spheres that behave hydrodynamically; however, the distribution is obtained by measuring the cumulative volume of dust.

2. Mass mean diameter. Two properties of the mass mean diameter, D_w, render it to be a convenient choice as an average particle diameter. The first is that one-half of the total mass of the sample is contained in particles with diameters less than the mass mean diameter. The second is that the mass mean diameter approaches the geometric mean diameter based on weight, $D_{g,3}$, as the particle size distribution approaches a log normal distribution (Irani and Clayton, 1963). A log normal distribution is characterized completely by the geometric mean, $D_{g,3}$, and the geometric standard deviation, σ_g.

The mass mean diameter is determined from the cumulative weight distribution. Particle size distributions obtained from air and sieve classification are typically log normal with varying degrees of distortion with the upper and lower ends of the distribution. This distortion depends on the preciseness of the classification. Typically there exists an interval about the cumulative weight percent of 50 that is log normal. Therefore, all of the data in this interval can be utilized in determining the mass mean diameter. However, the interval must contain at least two data points of which one is above a cumulative weight percent of 50 and the other below.

To determine the interval about the cumulative weight percent of 50 that is log normal, the following transformation is introduced:

$$w = \frac{1}{\sqrt{2\pi}} \int_{-\infty}^{Z} \exp\left(-\frac{1}{2}x^2\right) dx \qquad (1)$$

where

w = cumulative weight percent

Z = standard normal deviate

When the data in the interval under consideration are from a log normal distribution,

$$Z = \frac{1}{\ln \sigma_{g,3}} \ln D - \frac{\ln D_{g,3}}{\ln \sigma_{g,3}} \qquad (2)$$

where

D = particle diameter

$D_{g,3}$ = geometric mean diameter for a log normal distribution based on weight (the mass mean diameter, D_w)

$\sigma_{g,3}$ = standard deviation for a log normal distribution based on weight

To determine if the data in the interval under consideration are from a log normal distribution, a criterion on the 95% confidence interval for the population correlation coefficient is established. The confidence interval has to contain 0.99; however, the lower boundary cannot be less than 0.95.

3. Mean diameter based on the external surface area. The mean based on the external surface area, $D_{a,2}$, is defined by Herdan, et al. (1960) as

$$D_{a,2} = \left[\frac{1}{\pi N_{tot}} \int_0^\infty \pi D^2 n(D) \, dD \right]^{\frac{1}{2}} \tag{3}$$

where

N_{tot} = total number of particles in the sample

n(D) = particle size number distribution with diameter D as the distributed variable

$D_{a,2}$ is equivalent to the diameter of the particle in a monodispersed particulate system that has the same total external surface area, A_{tot}, as that of a particulate system with a particle size distribution, n(D). In other words,

$$A_{tot} = N_{tot} (\pi D_{a,2}^2) = \int_0^\infty \pi D^2 n(D) \, dD \tag{4}$$

Herdan et al. (1960) have integrated Eq. (3), by assuming n(D) to be a log normal distribution, and obtained

$$D_{a,2} = D_{g,s} \exp(-2 \ln^2 \sigma_{g,s}) \tag{5}$$

To calculate $D_{a,2}$, for a non-log normal distribution, it can be assumed to be log normal between two adjacent, data points (see Fig. 3.1). The distribution function of the fraction of the total mass contained in particles of diameter D, w(D), is then given by

$$w(D) = \left\{ w_i(D), \; i = 1, 2, \cdots, m-1 \right\} \tag{6}$$

where

$$w_i(D) = \frac{1}{\ln \sigma_{g,3,i} (\sqrt{2\pi})} \exp\left[- \frac{\ln^2 \left(\frac{D}{D_{g,3,i}} \right)}{2 \ln^2 \sigma_{g,3,i}} \right] \frac{1}{D} \qquad D_i \le D \le D_{i+1}$$

m = total number of data points

To calculate $D_{a,2}$ from Eq. (3), the total number of particles with diameters in the range of D to D+dD, n(D)dD, is related to w(D)dD by

$$n(D)dD = \frac{W_{tot} \, w(D) dD}{\frac{\pi}{6} \rho_d D^3} \tag{7}$$

where

W_{tot} = total mass of the sample

ρ_d = density of the dust particle

Substitution of Eqs. (6) and (7) into Eq. (3) yields

$$D_{a,2} = \left[\frac{W_{tot}}{N_{tot}} \left(\frac{6}{\rho_d \pi} \right) \sum_{i=1}^{m-1} \int_{D_i}^{D_{i+1}} w_i(x) \frac{dx}{x} \right]^{\frac{1}{2}} \tag{8}$$

or

$$D_{a,2} = \left[\frac{W_{tot}}{N_{tot}} \left(\frac{6}{\rho_d \pi} \right) \sum_{i=1}^{m-1} \int_{D_i}^{D_{i+1}} \frac{1}{\ln \sigma_{g,3,i} (\sqrt{2\pi})} \exp \left[- \frac{\ln^2 \left(\frac{x}{D_{g,3,i}} \right)}{2 \ln^2 \sigma_{g,3,i}} \right] \frac{dx}{x^2} \right]^{\frac{1}{2}} \tag{9}$$

It can be shown (see Appendix 1) that the integration of Eq. (9) yields

$$D_{a,2} = \left\{ \frac{W_{tot}}{N_{tot}} \left(\frac{6}{\rho_d \pi} \right) \left[\frac{1}{2} \sum_{i=1}^{m-1} \frac{\exp \left(\frac{1}{2} \ln^2 \sigma_{g,3,i} \right)}{D_{g,3,i}} \left(\operatorname{erf}(y_{i+1}) - \operatorname{erf}(y_i) \right) \right] \right\}^{\frac{1}{2}} \tag{10}$$

where

$$y_n = \frac{\ln \left(\frac{D_n}{D_{g,3,i}} \right)}{\sqrt{2} \ln \sigma_{g,3,i}} + \frac{\ln \sigma_{g,3,i}}{\sqrt{2}} \qquad n = i, i+1$$

It can also be shown (see Appendix 2) that

$$\frac{W_{tot}}{N_{tot}} = \left\{ \frac{6}{\rho_a \pi} \sum_{i=1}^{m-1} \frac{1}{2} \frac{\exp\left[\frac{9}{2} \ln^2 \sigma_{g,3,i}\right]}{D_{g,3,i}^3} \left[\operatorname{erf}(X_{i+1}) - \operatorname{erf}(X_i) \right] \right\}^{-1} \tag{11}$$

where

$$X_n = \frac{\ln\left(\frac{D_n}{D_{g,3,i}}\right)}{\sqrt{2} \ln \sigma_{g,3,i}} + 3 \frac{\ln \sigma_{g,3,i}}{\sqrt{2}} \qquad n = i, i+1$$

Substitution of Eq. (11) into Eq. (10) yields

$$D_{a,2} = \left\{ \frac{\sum_{i=1}^{m-1} \left\{ \frac{\exp(1/2 \ln^2 \sigma_{g,3,i})}{D_{g,3,i}} \left[\operatorname{erf}(y_{i+1}) - \operatorname{erf}(y_i) \right] \right\}}{\sum_{i=1}^{m-1} \left\{ \frac{\exp(9/2 \ln^2 \sigma_{g,3,i})}{D_{g,3,i}} \left[\operatorname{erf}(X_{i+1}) - \operatorname{erf}(X_i) \right] \right\}} \right\}^{\frac{1}{2}} \tag{12}$$

As the entire distribution approaches a log normal distribution, the geometric mean, $D_{g,3,i}$, and the geometric standard deviation, $\sigma_{g,3,i}$, of each log normal section in Eq. (12) reduces, respectively, to $D_{g,3}$ and $\sigma_{g,3}$, which are common for the entire distribution. The resultant expression is

$$D_{a,2} = D_{g,3} \exp\left(-2 \ln^2 \sigma_{g,3}\right) \left[\frac{\operatorname{erf}(y_m) - \operatorname{erf}(y_1)}{\operatorname{erf}(X_m) - \operatorname{erf}(X_1)} \right]^{1/2} \tag{13}$$

In addition, the maximum diameter, D_m, and the minimum diameter, D_1, of the distribution will approach infinity and zero, respectively. This causes y_m and x_m to approach positive infinity and y_1 and x_1 to approach negative infinity. This gives, from Eq. (13)

$$D_{a,2} = D_{g,3} \exp\left(-2 \ln^2 \sigma_{g,3}\right) \left[\frac{1-(-1)}{1-(-1)}\right]^{1/2} \tag{14}$$

or

$$D_{a,2} = D_{g,3} \exp\left(-2 \ln^2 \sigma_{g,3}\right) \tag{15}$$

Note that Eq. (15) is identical to Eq. (5).

4. Mean diameter based on the mass. The mean diameter based on mass, $D_{a,3}$, is

$$D_{a,3} = \left[\frac{6}{\rho_a \pi N_{tot}} \int_0^\infty \pi/6 \, \rho_a \, D^3 \, n(D) \, dD\right]^{1/3} \tag{16}$$

$D_{a,3}$ can be interpreted as the effective diameter of the particles in the mono-disperse system that has the same total mass, M_{tot}, as the actual particulate system with a particle size distribution of n(D). Note that

$$M_{tot} = \int_0^\infty \pi/6 \, \rho_d \, D^3 \, n(D) \, dD = \frac{\pi}{6} \rho_d \left(D_{g,3} \right)^3 N_{tot} \tag{17}$$

Herdan et al. (1960) have integrated Eq. (16) for a log normal distribution and obtained

$$D_{a,3} = D_{g,3} \exp \left[-1.5 \ln^2 \sigma_{g,3} \right] \tag{18}$$

Again the assumption that the non-log normal type of distribution can be approximated by a distribution that is log normal between two adjacent data points is made (see Fig. 3.1). Substitution of the relationship for n(D)dD in Eq. (3) into Eq. (16) yields

$$D_{a,3} = \left[\frac{6}{\rho_d \pi N_{tot}} \int_0^\infty W_{tot} \, w(D) \, dD \right]^{1/3} \tag{19}$$

or, if $w(D) = 0$ for $D_1 > D > D_m$,

$$D_{a,3} = \left\{ \frac{6}{\pi \rho_d} \left(\frac{W_{tot}}{N_{tot}} \right) \sum_{i=1}^{m-1} \int_{D_i}^{D_{i+1}} \frac{1}{\ln \sigma_{g,3,i} (\sqrt{2\pi})} \exp\left[- \frac{\ln^2 \left(\frac{x}{D_{g,3,i}} \right)}{2 \ln^2 \sigma_{g,3,i}} \right] \frac{dx}{x} \right\}^{\frac{1}{3}} \tag{20}$$

This, in turn, gives rise to (see Appendix 1)

$$D_{a,3} = \left\{ \frac{6}{\pi \rho_d} \left(\frac{W_{tot}}{N_{tot}} \right) \sum_{i=1}^{m-1} \frac{1}{2} \left[erf(Z_{i+1}) - erf(Z_i) \right] \right\}^{\frac{1}{3}} \tag{21}$$

where

$$Z_n = \frac{\ln \left(\frac{D_n}{D_{g,3,i}} \right)}{\sqrt{2} \ln \sigma_{g,3,i}} \qquad n = i, i+1$$

Substitution of Eq. (11) into Eq. (21) gives

$$D_{a,3} = \left\{ \frac{\sum_{i=1}^{m-1} \left[erf(Z_{i+1}) - erf(Z_i) \right]}{\sum_{i=1}^{m-1} \frac{\exp\left(\frac{9}{2} \ln^2 \sigma_{g,3,i} \right)}{D_{g,3,i}^3} \left[erf(X_{i+1}) - erf(X_i) \right]} \right\}^{\frac{1}{3}} \tag{22}$$

As the entire distribution approaches a log normal distribution, or as

$$D_{g,3,i} \rightarrow D_{g,3}$$

$$\sigma_{g,3,i} \rightarrow \sigma_{g,3}$$

Eq. (22) is transformed into

$$D_{a,3} = D_{g,3} \exp(-1.5 \ln^2 \sigma_{g,3}) \left[\frac{\mathrm{erf}(Z_m) - \mathrm{erf}(Z_1)}{\mathrm{erf}(X_m) - \mathrm{erf}(X_1)} \right]^{\frac{1}{3}} \tag{23}$$

Furthermore, as log normality is approached, we obtain

$$D_m \rightarrow \infty$$

$$D_1 \rightarrow 0$$

which causes

$$Z_m, x_m \rightarrow \infty$$

$$Z_1, x_1 \rightarrow -\infty$$

Thus, Eq. (23) becomes

$$D_{a,3} = D_{g,3} \exp(-1.5 \ln^2 \sigma_{g,3}) \tag{24}$$

Note that Eq. (24) is identical to Eq. (18).

B. Determination of the Composition

The composition of each size fraction is usually characterized by determining the contents of moisture, ash, protein, and starch & fiber. The weight fraction of moisture, ash, and protein can be determined by the AACC methods 44-46, 08-01, and 46-10, respectively (AACC, 1975). The weight fraction of starch & fiber can be obtained from the difference.

III. EXPERIMENTAL

A. Collection of the Dust Samples

The dust samples from grain sorghum, wheat, and corn were collected from the storage bins of the dust removal systems, cyclones or baghouses, in three commercial grain elevators. Dust was removed from several locations in the elevator. The wheat dust and corn dust were collected with cyclones and the grain sorghum dust was collected with a baghouse. Each sample was 2 to 3 kg in weight, and a sieve with a 1.0 mm mesh opening was used to remove very large "trash." One hundred pounds of cornstarch were obtained in bulk from a mill (General Mills; Minneapolis, MN).

B. Separation of the Dust Samples into Size Fractions

A 250 Tyler mesh sieve was used to initially divide each dust sample into a coarse fraction (having particle diameters approximately greater than 61 μm) and a fine fraction. This separation was performed because the series 6000 Microparticle Classifier used to further separate the fine fraction of each sample could not effectively classify grain dust particles with diameters larger than 61 μm.

The series 6000 Microparticle Classifier (manufactured by A.B. Bacho in Sweden and distributed by Harry W. Dietert Co., Detroit, MI) utilizes a combination of the effects of centrifugation and elutriation to separate

0.02 kgs of dust into a fine fraction and a coarse fraction. The dust particles are subjected to a centrifugal force which is opposed by a current of air. The fine fraction, composed of dust particles with a terminal velocity less than the air velocity, is blown into a collector. The remainder of the dust, the coarse fraction, is thrown by the centrifugal force into another collector.

The fine fraction of the wheat dust, corn dust, grain sorghum dust or cornstarch was further separated into eight size fractions with the microparticle classifier. The size fractions were obtained by performing a series of separations with the microparticle classifier, each with a larger air velocity. The finest size fraction was separated out of the entire fine fraction of the dust sample by the lowest air velocity. After increasing the air velocity, the rest of the fraction was divided into a fine fraction, and a coarse fraction. This was repeated until eight size fractions were obtained; however, the three size fractions with the finest particles were combined into one because there was not enough dust in each of the fractions to perform the explosion tests.

The coarse fraction of each dust sample was further divided into six size fractions with a series of sieves having Tyler mesh numbers of 65, 115, 150, 170, and 200 (corresponding openings of 208, 124, 105, 88, and 74 μm). These fractions were obtained by dividing each coarse fraction into 0.100 kg portions, which were sieved for 15 minutes on a Ro-Tap shaker (W.S. Tyler Company, Cleveland, OH). The fraction on top of the 65 mesh sieve was considered trash and discarded because it contained particles with a wide range of sizes.

Each sample of dust was divided into a total of eleven size fractions. Six were obtained from the microparticle classifier and five more from the series of sieves.

C. Determination of the Particle Size Distribution

Benzene was used as the sedimentation liquid for the corn, grain sorghum, and wheat dust; isopropyl alcohol was used for the cornstarch. The dust was initially dispersed in a feed solution consisting of the sedimentation liquid and naptha. The feed solution and dust were then placed on top of the sedimentation liquid in the tube. To decrease the settling time, the particles were centrifuged for increasing lengths of time at 600, 1200, and 1800 r.p.m. The weight percent of the total dust sample that had settled out was determined by measuring the height of the settled dust column. The diameter of the largest particles that settled out was determined from the r.p.m. of the centrifuge and the length of time it was centrifuged.

IV. RESULTS AND DISCUSSION

Table 3.1 presents the geometric mean diameter, $D_{g,3}$, and the natural logarithm of the geometric standard deviation, $\ln\sigma_{g.3}$, of the log normal approximation of the actual particle size distribution for data with $|Z| < 2$. The coefficient of determination, R^2, and the 95% confidence interval for the population correlation coefficient, ρ_r, are also presented in Table 3.1.

For each sieve classified size fraction, Table 3.2 gives the lower boundary sieve aperature, d_a^{μ}, used to obtain the size fraction and the equivalent stokes diameter, d_s^{μ}, of the aperature; the value of d_s^{μ} was obtained with the use of the shape factor of 0.9 (Heywood, 1947). In addition, the fraction of the total weight of dust in the size fraction that is contained in particles with diameters less than d_s^{μ} is given. In Table 3.3, the aperature

of the upper boundary sieve, d_a^U, of each size fraction is given with its equivalent stokes diameter, d_s^U. The fraction of the total weight of dust in the size fraction contained in particles with diameters greater than d_s^U is also presented. Table 3.4 contains the coefficients of variability of the diameters in each size distribution. The results from the analysis of variance of the coefficients of variability are given in Table 3.5. This analysis of variance is for a 2 x 2 factorial experiment in which the treatments are the type of dust and the size fraction. Each type of dust was separated into 10 size fractions by utilizing the same air velocity for the air classification and the same series of sieves for the sieve classification. Note that size fractions 1 through 6 are from the air classification and size fractions 7 through 11 are from the sieve classification.

Table 3.6 presents the mass mean diameters, D_m, of each distribution along with the natural logarithm of the geometric standard deviation, $\ln\sigma_g$, of the log normal distribution used in determining the mass mean diameters. The coefficient of determination of the distribution and the 95% confidence interval for the population correlation coefficient, ρ_r, are also presented. For each sieve separated size fraction, the aperatures of the bouning sieves with their geometric mean are presented. In addition, the equivalent stokes diameters of each geometric mean are presented; the equivalent stokes diameter was determined with the use of a shape factor of 0.9 (Heywood, 1947). The mass mean diameters of each size fraction for grain sorghum dust, corn dust, and wheat dust are presented.

In Table 3.8, the values of $D_{a,2}$ from two log normal approximations of the actual particle size distribution and one piecewise log normal approximation of the actual distribution are presented for each size fraction of each type of dust. One log normal approximation was determined with only those

data having $|Z| < 2$ and the other with data having $|Z| < 3$. The coefficients of variability between each log normal approximation and the piecewise log normal approximation are also presented. Table 3.9 contains the values of

$$D_{a,2}^2 \left(\frac{N_{tot}}{W_{tot}}\right)\frac{6}{\pi \rho_d}$$

calculated from a log normal approximation of the actual particle size distribution and from the piecewise log normal approximation of each size fraction. Note that the coefficient of variability between the two values of this quantity is also presented for each size fraction.

In Table 3.10, the values of $D_{a,3}$, from two log normal approximations of the actual particle size distribution and one piecewise log normal are present for each size fraction. Note that the two log normal approximations are the same as those used in Table 3.8 for determining $D_{a,2}$. The coefficients of variability between each log normal approximation and the piecewise log normal approximation are also presented.

The weight percents of moisture, ash, protein, and starch & fiber for each size fraction are presented in Table 3.11. Table 3.12 shows the average values of the moisture content, ash content, protein content, and starch & fiber content for each dust. The standard deviation of the contents of each component among the size fractions of each kind of dust is also given in Table 3.12. The coefficient of variability of each compositional component among the size fractions of each type of dust is shown. Table 3.13 contains the average value for all types of dust, the standard deviation among these average values and the coefficient of variability among these average values for each component. Table 3.14 contains the standard deviations of moisture

content, ash content, protein content, and starch & fiber content, among the size fractions for wheat dust, corn dust, and grain sorghum dust that result when the data from size fractions 6, 5, and 4 are removed one at a time.

Figure 3.1 is an illustration of the piecewise log normal approximation of the actual distribution. Figures 3.2 through 3.44 present the particle size distribution of each size fraction. The diameter is plotted on a logarithmic axis, and the cumulative weight percent on a probability axis. The cumulative weight percent is also presented in terms of the standard normal deviate. Figures 3.45 through 3.48 are the same as Figs. 3.2 through 3.44; except, they are for corn dust, grain sorghum dust, wheat dust, and cornstarch, respectively. Figure 3.49 shows the coefficient of variability of each size fraction plotted the size fraction for all four types of dust. Figure 3.50 presents the expected particle size distributions from the perfect sieve or air classification of a sample of dust originally having a log normal particle size distribution, curve A. Three types of classification are presented:

1) particles with diameters less than D_{min} are removed, curve B

2) particles with diameters greater than D_{max} are removed, curve C, and

3) both 1 and 2 are performed, curve D.

The moisture content for corn dust, wheat dust, and grain sorghum dust is plotted against the size fraction in Fig. 3.51. The results pertaining to the correlation of ash, protein, and starch & fiber contents with the size fraction are presented in Figs. 3.52 through 3.54. In Fig. 3.53, the moisture content is plotted against the mass mean diameter for wheat dust, corn dust, and grain sorghum dust. Similar correlations between the mass mean diameter and the ash content, protein content, or the starch & fiber content are shown in Figs. 3.56 through 3.58.

A. Particle Size

1. Particle size distribution. Twenty-one of the 43 particle size distributions shown in Figs. 3.2 to 3.44 are not complete; they do not contain data at the two extreme cumulative weight percentages, 0% and 100%. However, 15 out of these 21 distributions are essentially complete because each of them spans more than 95% of the total range of cumulative weight percents. Five of these remaining incomplete distributions contain no data between the cumulative weight percents of 95% and 100%. Among these five distributions, four are from the size fractions of grain sorghum dust, MOAC-S08, MOAC-S09, MOAC-S10, and MOAC-S11, with the maximum cumulative weight percents of 93.5, 91.0, 76.5, and 48.0% respectively, and one is from a size fraction of corn dust, CNAC-S11, with the maximum cumulative weight percent of 84.2%. Only one contains no data with cumulative weight percents between 0% and 5%. This is from the size fraction of cornstarch, CSAC-S02, having the minimum weight percent of 5.4%.

Data at the upper extreme of the distributions are missing because a maximum particle diameter that can be accurately measured exists in the Whitby sedimentation method. The first cumulative weight percent measurement is recorded at the moment when particles with a diameter equal to the maximum diameter have settled to the bottom of the capillary tube. Particles with diameters larger than the maximum diameter would have already accumulated in the tube before the first reading, and this would result in the first cumulative weight percent reading of less than 100%.

It is more critical to have data in the lower end rather than in the upper end of a weight distribution. The reason is that the number of particles per unit weight of dust is larger at the lower end of the distribution than at the upper end. All of the distributions, except for the size

fraction of cornstarch, CSAC-F02, contain data with cumulative weight percents less than 1.4%.

Table 3.1 contains the parameter of the log normal approximation to each distribution for data with values of $|Z| < 2$. Only data with $|Z| > 2$ were discarded because the Whitby sedimentation method does not give accurate results for data in this region (Martin, 1980). Note that only 16 of the 43 distributions satisfy the criteria for log normality. Four of these 16 distributions are from size fractions that were sieve classified and the remainder are from size fractions that were air classified. The four sieve classified size fractions are from corn dust. The twelve air classified fractions consist of two corn dust size fractions, six cornstarch size fractions, two wheat dust size fractions and two grain sorghum dust size fractions. Four of the six size fractions of cornstarch, whose size distributions are essentially log normal, were from non-freeze dried samples (this is 2/3 of the total number of non-freeze dried size fractions) and the remaining 2 are size fractions that were freeze dried (this is 1/3 of the total freeze dried size fractions).

Even though the particle size distributions of the original dust samples of corn dust, wheat dust, grain sorghum dust, and cornstarch are approximately log normal (see Figs. 3.45-3.48), the particle size distributions of the size fractions from the sieve and air classifications are not necessarily log normal. Herdan et al. (1960) have illustrated the shape of the resultant size distributions from perfect air and sieve classifications (see Fig. 3.2). Notice that there exists a range of cumulative weight percents, W, around the cumulative weight percent of 50%, where the distribution of particle diameters is log normal (the slope of the line tangent to the distribution is constant); however, outside this range, the slope of the tangent line increases toward

infinity as the values of W approach 0% at the diameter of D_{min} and 100% at the diameter of D_{max}.

The shapes of the distributions in Figs. 3.2 through 3.44 are different from that in Fig. 3.45. The distributions in Figs. 3.2 through 3.44 can be divided into two rough categories. The first category contains those distributions that are log normal for the entire range of particle diameters; the slope of the line tangent to the distribution is constant. The second category contains those distributions in which, at the lower end, the slope of the tangent line first decreases toward zero as the particle size increases, and increases toward a constant value. As the particle size further increases toward the upper end, the slope decreases and then increases again. In the lower portion of the distribution, its shape is the result of a range of diameters with a relatively small number of particles followed by a range of smaller diameters with a relatively large number of particles. The shape of the upper portion of the distribution could be the result of a range of diameters with a relatively small number of particles followed by another range of larger diameters that contains a relatively large number of particles.

The deviations from the shape predicted by Herdan et al. (1960) in the upper end of the distribution in Figs. 3.2 through 3.44 are more pronounced for the air classified size fractions than for the sieve classified fractions. The deviations in the lower region of the distribution are more pronounced for the sieve classified size fractions than for the air classified size fractions, except for the fifth air classified size fraction. Also, the deviations that occur in the corn dust size fractions are less than those in the wheat dust and the grain sorghum dust size fraction.

The deviations in the lower portion of the distribution are more pronounced for the sieve classified size fractions. When particles are sized

by sieving, the range of particles with diameters in each size fraction should fall within the aperatures of the bounding sieves. Therefore, the weight of the particles with diameters less than the lower boundary sieve aperature and the weight of particles with diameters larger than the upper boundary sieve aperature can be estimated. However, to compare methods of sizing particles, the shape of the particles should be considered. Heywood (1947) has reported the value of the shape factor relating the sieve aperature to a stokes diameter to be approximately 0.9. Sieve openings, transformed to equivalent stokes diameters utilizing this shape factor, are shown in Table 3.4. Note that the fraction of the total weight of the dust ranges from 80% to 100% in a size fraction that is contained in particles with diameters less than the stokes equivalent diameter of the lower sieve aperature. However, the fraction of the total weight of the dust ranges from only 0.01% to 20% in the size fraction that is contained in particles with diameters larger than the stokes equivalent diameter of the upper boundary sieve aperature. Small balls of particles could be seen in the size fractions of wheat dust and grain sorghum dust. Martin (1978) found that wheat dust contains particles having diameters that range from 40 to 60 μm called tricombs. These particles can trap large quantities of small particles during the sieving operation and prevent the small diameter particles from passing through the sieve. Martin (1978) also found that grain sorghum dust contains hair-like projections. During the sieving operation, these hair-like projections can capture small diameter particles to form a ball that can not pass through the sieve.

The coefficient of variability, C.V., is calculated from each distribution. It is a measure of the variability of the particle diameters in the distribution about its mean and is defined as

$$C.V. = \frac{\left[\int_0^\infty (D-\bar{D})^2 \frac{n(D)}{N_{tot}} dD\right]^{\frac{1}{2}}}{\bar{D}} \tag{25}$$

where

$$\overline{D} = \int_0^\infty D \frac{n(D)}{N_{tot}} dD \qquad \text{(the arithmetic mean diameter)}$$

Finney (1942) has shown that when n(D) is log normally distributed, the coefficient of variability is

$$C.V. = \left[\exp\left(\ln^2 \sigma_{g,3}\right) - 1\right]^{\frac{1}{2}} \tag{26}$$

When the distribution is approximated by a piecewise log normal distribution (Fig. 3.1), it can be shown (Appendix 3) that the coefficient of variability is

$$C.V. = \left\{ \frac{\left[\sum_{i=1}^{m-1} \frac{\exp\left(\frac{q}{2}\ln^2\sigma_{g,3,i}\right)}{D_{q,3,i}^3}\left[\operatorname{erf}(x_{i+1}) - \operatorname{erf}(x_i)\right]\right]\left[\sum_{i=1}^{m-1} \frac{\exp\left(\frac{1}{2}\ln^2\sigma_{g,3,i}\right)}{D_{g,3,i}}\left[\operatorname{erf}(y_{i+1}) - \operatorname{erf}(y_i)\right]\right]}{\left[\sum_{i=1}^{m-1} \frac{\exp\left(2\ln^2\sigma_{g,3,i}\right)}{D_{g,3,i}^2}\left[\operatorname{erf}(w_{i+1}) - \operatorname{erf}(w_i)\right]\right]} - 1 \right\} \quad (27)$$

Table 3.4 shows that the coefficients of variability range from 22% for the air classified size fraction of grain sorghum dust, MOAC-S03, to 104% for the freeze dried size fraction of cornstarch, CSAC-F02. When examining the hypothesis that the size fractions are mono-disperse, the smallest coefficient of variability, 22%, is relatively large; a value of 10% is the generally accepted level of variability in an experiment.

To ascertain if there exist any significant differences between the values of the coefficient of variability for the different types of dust or for different size fractions, a two-way analysis of variance is used. The results in Table 3.5 show that significant differences at the 1% level do exist both among the types of dust and among the size fractions; however, the interactions are also significant at the 1% level. The significant interactions indicate that the type of dust has different effects on the coefficients of variability for various size fractions. Also, the effect that the

size fraction has on the coefficient of variability is not the same for every type of dust. However, a difference can still exist between the air classified size fractions and the sieve classified size fractions. Figure 3.49 shows that the values of the coefficient of variability for all the air classified size fractions, except for wheat dust, are consistently lower than those for the sieve classified size fraction.

2. Mass mean diameter. Thirteen of the mass mean diameters in Table 3.6 are from distributions which are sufficiently non-log normal that only two pairs of data points (each pair consists of two repetitions) could be used in determining the mass mean diameter. Seven of these thirteen are from the air classified size fractions, MOAC-S03, WTAC-S04, WTAC-S05, CNAC-S02, CNAC-S03, CSAC-S03, and CSAC-F01, and the remainder are from the sieve classified size fractions, MOAC-S08, MOAC-S09, MOAC-S10, MOAC-S11, WTAC-S08, and WTAC-S09.

For each type of dust, the mass mean diameters of the air classified size fractions increase with the size fraction as expected; however, the sieve classified size fractions do not. Table 3.7 shows that the mass mean diameters are consistently lower than the geometric average of the bounding sieve aperatures that have been corrected for particle shape effects. This is expected because of the large number of particles with diameters less than the lower boundary sieve aperature.

3. Mean diameter based on the external surface area. To calculate the average diameter based on external surface area, $D_{a,2}$, from the piecewise log normal approximation of the actual distribution, a complete distribution is necessary. Nineteen of the 43 distributions do not contain cumulative weight percent data at the upper extreme of 100%. For these distributions, the log normal distribution through the two largest data points was used to estimate

the actual distribution in the region having no data. Four of the 43 distributions do not have data at the lower extreme of 0%. For these distributions, a log normal distribution which contains the data with the smallest cumulative weight percent and has a geometric standard deviation, σ_g, equal to that of the log normal approximation of the entire distribution was used to estimate the actual distribution in the region where there is no data. The log normal approximation of the entire distribution is shown in Table 3.1.

Table 3.8 shows large differences between values of $D_{a,2}$, calculated by approximating the actual distribution with a log normal distribution and with a piecewise log normal distribution. For 15 size fractions, the coefficient of variability is greater than 10%, when only data with values of $|Z| < 2$ are considered in the determination of the log normal approximation. When the log normal approximation is determined using data with $|Z| < 3$, only eight size fractions have coefficients of variability larger than 10%. This indicates that the extreme lower parts of the distribution with $Z < -2$ can be important in the calculation of $D_{a,2}$; they contain a large fraction of the total number of dust particles in the size fraction. When the estimate of $D_{a,2}$ from the log normal approximation is larger than that from the piecewise log normal approximation, the log normal approximation underestimates consistently the weight percents of the fine particles. When the estimate of $D_{a,2}$ from the log normal approximation is lower than that from the piecewise log normal approximation, the log normal approximation overestimates consistently the cumulative weight percents of the fine particles.

The differences between the values of $D_{a,2}$ calculated from the piecewise log normal distribution and that from each of the log normal distribution can be attributed to differences in calculating the quantity N_{tot}/W_{tot}. This is illustrated by examining the quantity

$$D_{a,2}^2 \left(\frac{N_{tot}}{W_{tot}}\right) \frac{6}{\pi \rho_d}$$

which does not contain the quantity N_{tot}/W_{tot}. Table 3.9 shows the coefficient of variability between the value of $D_{a,2}^2(N_{tot}/W_{tot})(6/\pi\rho_d)$ calculated from the piecewise log normal distribution and that from the log normal distribution determined from data with $|Z| < 2$ for each size fraction. Note that none of the coefficients of variability are greater than 10% and only two are greater than 5%.

4. Mean diameter based on the mass. The values of the average diameter based on the mass are presented in Table 3.10. In calculating $D_{a,3}$ for an incomplete distribution, the same methods employed in the calculation of $D_{a,2}$ were also employed to calculate $D_{a,3}$. The differences between the value of $D_{a,3}$ from each log normal approximation and that from the piecewise log normal approximation are similar to those previously noted for values of $D_{a,2}$. The coefficients of variability between the value of $D_{a,3}$ from each log normal approximation and that from the piecewise log normal approximation are shown in Table 3.10. The coefficients of variability for $D_{a,3}$ are not so large as those for $D_{a,2}$; the calculation of $D_{a,3}$ involves the cube root of N_{tot}/W_{tot} as opposed to the square root in the calculation of $D_{a,2}$. The cubic root reduces the effect of the differences in N_{tot}/W_{tot} more than the square root.

A comparison between the mass mean diameter, D_m, in Table 3.2 and the values of $D_{a,3}$ for the same size fraction in Table 10 indicates that 19 of the pairs differ only by 5 μm of being identical; however, the remaining differ as much as 68 μm. Furthermore, even when two size fractions have the same mass

mean diameter (e.g., WTAC-S05 and WTAC-S10), they can have substantially different values of $D_{a,3}$. The mass mean diameter indicates that one-half of the weight of the sample is in particles with diameters less than D_m; however, it contains no information on how the weight is distributed among the particles. The mass mean diameter does not characterize the particle size distribution sufficient, because two particulate systems can have appreciably different particle size distributions and yet have identical mass mean diameters. NOte that this difficulty is a feature of any geometric mean diameter. The geometric diameter is only one of the two parameters necessary to characterize a log normal distribution. Two different log normal distributions can have the same geometric mean diameters, D_m, and yet can have different geometric standard deviations, σ_g.

B. Composition

In Table 3.12, the standard deviations of protein contents among the size fractions of grain sorghum dust, corn dust, and wheat dust range from 1.3% to 2.7% and those for the moisture contents from 1.3% to 1.5%. This indicates that the protein content and the moisture content vary only slightly among the size fractions of the same type of dust. The standard deviation of moisture contents among the size fractions for cornstarch of 3.4% indicates that their variability is larger than those of the other types of dust. The larger variability for cornstarch is the result of freeze drying some of the size fractions to improve the dispersibility. Table 3.13 indicates that the standard deviation among the average values of the moisture content for grain sorghum dust, corn dust, and wheat dust is 1.8% and that for protein content is 0.9%. The variability of protein contents and moisture contents among the different kinds of dust is approximately the same as or smaller than the variability among size fractions within each kind of dust.

The ash content and the starch & fiber content for each type of dust in Table 3.12 show more variability between size fractions than do the moisture content and the protein content. The standard deviations of the ash contents among size fractions for grain sorghum dust, corn dust, and wheat dust range from 10.6% to 18.3% and those for the starch & fiber contents from 10.0% to 14.6%. The standard deviation of the starch & fiber contents in cornstarch, 3.4%, is less than that for the other kinds of dust. In contrast, the standard deviation among the average values of the ash contents for wheat dust, grain sorghum dust, and corn dust of 2.8% and that for the starch & fiber contents of 3.7% indicate only a slight variability among the types of grain dust.

Martin et al. (1978) have shown that air classification of grain dust results in a large ash content (approximately 40%) in the residue size fraction. Figure 3.52 indicates a similar trend in ash content for the size fractions in this investigation; the residue size fractions correspond to the sixth size fraction in Fig. 3.52. The fifth size fraction of each dust contains large weight percentages of ash (approximately 25%). For the wheat dust and the grain sorghum dust, the fourth size fraction also contains a relatively large ash content (approximately 11%) when compared to the ash content of the remaining size fractions (approximately 4%).

In Figs. 3.51 and 3.52, a similar trend is noted for the moisture content and for the starch & fiber content. For these two quantities, the fourth, fifth, and sixth size fractions exhibit lower values than those of the remaining size fractions. The correlation coefficients for the correlations between the ash content and each of those two quantities are significant at the 1% level (Table 3.15). The highly significant inverse correlation between

the ash and moisture contents results from the ash material being less hygroscopic than the organic grain dust.

The starch & fiber content was obtained by subtracting the sum of the weight percents of moisture, ash and protein from 100%; the dust was assumed to contain only moisture, ash, protein, starch & fiber. Consequently, the correlations between the starch & fiber content and the ash content are significant.

The large standard deviations of the ash contents and the starch & fiber contents among the size fractions of grain sorghum dust, wheat dust, and corn dust have resulted from the large ash contents in size fractions 4, 5, and 6. The standard deviations of the moisture contents, ash contents, protein contents, and starch & fiber contents among the remaining size fractions are given in Table 3.14. For all three types of dust, the standard deviations for the ash content decrease to less than 2%, and those for the starch & fiber contents to 4.2%. For the moisture content, the standard deviations decrease to less than 1%. Note that the standard deviations of the protein contents among the size fractions exhibit essentially no change.

The correlation coefficients in Table 3.15 indicate three additional significant correlations. The correlation between the moisture content and the starch & fiber content is significant for all types of dust at the 1% level. The correlation between the protein content and either the ash content or the starch & fiber content is significant for only the wheat dust at the 5% level. The significant correlation between the moisture content and the starch & fiber content is the result of that between the moisture content and the ash content, and that between the ash content and the starch & fiber content. The partial correlation coefficient between the moisture content and

the starch & fiber content of -0.70 with the effect of ash removed indicates no significant correlation at the 5% level.

C. Correlation Between Particle Size and Composition

The contention that the composition is dependent on the particle diameter was not verified for the particle diameters ranging from 10 to 90 μm. The correlation coefficients between each of the compositional components and the mass mean diameter indicates that it is significant at the 5% level for all types of dust except wheat dust. The correlation coefficient between the mass mean diameter and the moisture content is -0.74, and that between the mass mean diameter and the ash content is 0.673. Both are significant at the 5% level. Figure 3.49 indicates that the correlation between the mass mean diameter and the ash content is significant for only wheat dust; those size fractions (4, 5, and 6) having the highest ash contents due to air classification, by coincidence, have the largest mass mean diameters. The same observation was not made for grain sorghum dust and corn dust. Therefore, the correlations for the grain sorghum dust and the corn dust are not significant at the 5% level. For wheat dust, the sieve separated size fractions do not have the largest mass mean diameters, because they contain a large number of relatively small diameter particles. This results in size fractions 4, 5, and 6, by coincidence, having the largest mass mean diameters. The high ash contents of size fractions 4, 5, and 6 indicate that most of the ash is contained in separate particles consisting entirely of ash and not in particles of grain dust. These ash particles are either distributed in a narrow size range (approximately 40 to 60 μm) or they are of higher density than the grain dust particles. The ash content of the particles of grain dust does not depend on the size of the particle.

The significant correlation between the moisture content and the mass mean diameter for wheat dust is due to the significant correlation between moisture content and ash content that was previously discussed. From Fig. 3.55, the wheat dust size fractions that contain the lowest moisture content also contain the highest ash content, which for that dust happen to have the largest mass mean diameters. Again, the grain sorghum dust and corn dust do not exhibit these trends.

V. CONCLUSIONS

Wheat dust, corn dust, and grain sorghum dust were very similar in composition and in ranges of particle diameters. Sieve classification, unless performed very carefully, can result in carry-over of large numbers of small diameter particles in these types of dust. A large portion of the ash content was contained in separate particles consisting almost entirely of ash. Thus the ash content of the dust particles appeared to be only approximately 2% and did not vary much between size fractions or types of dust. The starch & fiber content also did not appear to vary tremendously. No correlation was found between the mass mean diameter of a size fraction and its contents of moisture, ash, protein, or starch & fiber. The log normal approximation of a distribution can have the same coefficient of determination as that of another distribution; however, the deviation between the moments calculated from the actual distribution and that from each of the log normal approximations can be quite different. For a weight distribution, how well the distribution estimates the weight percent of the particles with diameters less than the mass mean diameter can be very critical when calculating moments of the distributions. It is questionable to use the mass mean diameter or geometric mean diameter as an average diameter because of its limitations in describing the particle size distribution.

REFERENCES

American Association of Cereal Chemists. 1979. Approved methods of the AACC. 12th Ed. The Association: St. Paul, Minnesota.

Finney, D.J. 1941. On the distribution of a variate whose logarithm is normally distributed. Supplement to the Journal of the Royal Statistical Society. Vol. VII, Suppl. No. 2.

Herdan, G., Smith, M.L., and Hardwick, W.H. 1960. Small particle statistics. Bulterworth and Co.

Heywood, H. 1947. Symposium on particle size analysis, London.

Martin, C.R. 1980. Personal communication.

APPENDIX 1. INTEGRATION OF EQUATION (9)

During the calculations of the average diameters a form of the integral, I, appeared several times in which

$$I = \frac{1}{\ln \sigma_{g,3,i} (\sqrt{2\pi})} \int_{D_i}^{D_{i+1}} \frac{1}{u^n} \exp\left[- \frac{\ln^2 \left(\frac{u}{D_{g,3,i}} \right)}{2 \ln^2 \sigma_{g,3,i}} \right] du \qquad \text{(A1-1)}$$

To perform this integration a variable transformation

$$Z_i' = \frac{\ln \left(\frac{u}{D_{g,3,i}} \right)}{\sqrt{2} \ln \sigma_{g,3,i}} \qquad \text{(A1-2)}$$

is performed with Eq. (A1-1) which yields

$$I = \frac{1}{\sqrt{\pi}} \left(\frac{1}{D_{g,3,i}^{n-1}} \right) \int_{Z_i'}^{Z_{i+1}'} \exp\left[-u^2 - (n-1)\sqrt{2} \ln \left(\sigma_{g,3,i} \right) u \right] du \qquad \text{(A1-3)}$$

Another variable transformation

$$y = Z_i' + (n-1) \frac{\ln \sigma_{g,3,i}}{\sqrt{2}} \qquad \text{(A1-4)}$$

with Eq. (A1-3) results in

$$I = \frac{1}{2} \frac{\exp\left[\frac{(n-1)^2}{2} \ln^2 \sigma_{g,3,i}\right]}{D_{g,3,i}^{n-1}} \left(\frac{2}{\sqrt{\pi}}\right) \int_{y_i}^{y_{i+1}} \exp(-u^2)\, du \tag{A1-5}$$

However,

$$\operatorname{erf}(x) = \frac{2}{\sqrt{\pi}} \int_0^x \exp(-u^2)\, du \tag{A1-6}$$

Therefore, Eq. (A1-5) becomes

$$I = \frac{1}{2} \frac{\exp\left[\frac{(n-1)^2}{2} \ln^2 \sigma_{g,3,i}\right]}{D_{g,3,i}^{n-1}} \left[\operatorname{erf}(y_{i+1}) - \operatorname{erf}(y_i)\right] \tag{A1-7}$$

Substituting Eq. (A1-2) into Eq. (A1-4), produces

$$y_n = \frac{\ln\left(\frac{D_n}{D_{g,3,i}}\right)}{\sqrt{2}\, \ln \sigma_{g,3,i}} + (n-1) \frac{\ln \sigma_{g,3,i}}{\sqrt{2}} \tag{A1-8}$$

for n = i, i + 1

This equation appears as Eq. (9) in the text.

APPENDIX 2. DERIVATION OF THE RATIO OF THE TOTAL WEIGHT OF SAMPLE AND THE TOTAL NUMBER OF PARTICLES, EQUATION (11)

During the derivation of the arithmetic mean diameter based on the external surface area and the arithmetic mean diameter based on the mass, an expression for W_{tot}/N_{tot} needed to be determined. W_{tot}/N_{tot} can be expressed as

$$\left(\frac{N_{tot}}{W_{tot}}\right)^{-1} = \left[\int_0^{\infty} \frac{w(x)}{\frac{\pi}{6}\rho_d x^3}\, dx\right]^{-1} \tag{A2-1}$$

An expression for w(D) was derived, which was

$$w(D) = \left\{\frac{1}{\ln \sigma_{g,3,i}\sqrt{2\pi}} \exp\left[-\frac{\ln^2\left(\frac{D}{D_{g,3,i}}\right)}{2\ln^2\sigma_{g,3,i}}\right]\frac{1}{D}\,,\ i=1,2,\cdots,m-1\right\} \tag{A2-2}$$

Substitution of Eq. (A2-2) into Eq. (A2-1) yields

$$\frac{W_{tot}}{N_{tot}} = \left\{\frac{6}{\rho_d \pi}\sum_{i=1}^{m-1}\int_{D_i}^{D_{i+1}} \frac{1}{(\ln \sigma_{g,3,i})\sqrt{2\pi}} \exp\left[-\frac{\ln^2\left(\frac{x}{D_{g,3,i}}\right)}{2\ln^2\sigma_{g,3,i}}\right]\frac{dx}{x^4}\right\}^{-1} \tag{A2-3}$$

It can be shown (see Appendix 1) that the integration of Eq. (A2-3) yields

$$\frac{W_{tot}}{N_{tot}} = \left\{ \frac{6}{\rho_d \pi} \sum_{i=1}^{m-1} \frac{1}{2} \frac{\exp\left[\ln^2 \sigma_{g,3,i}\right]}{D^3_{g,3,i}} \left[\text{erf}(X_{i+1}) - \text{erf}(X_i) \right] \right\}^{-1} \qquad \text{(A2-4)}$$

where

$$x_n = \frac{\ln\left(\frac{D_n}{D_{g,3,i}}\right)}{\sqrt{2}\ln\sigma_{g,3,i}} + 3\frac{\ln^2\sigma_{g,3,i}}{\sqrt{2}} \qquad ; n = i, i+1$$

which is Eq. (11) in the text.

APPENDIX 3. DERIVATION OF THE COEFFICIENT OF VARIABILITY, EQUATION (27)

The coefficient of variability, C.V., is defined as

$$C.V. = \frac{\left(\int_0^\infty (x-\bar{x})^2 n(x)\,dx \right)^{\frac{1}{2}}}{\bar{x}} \tag{A3-1}$$

After rearrangement, one obtains

$$C.V. = \frac{\left(\int_0^\infty x^2 n(x)\,dx - \bar{x} \int_0^\infty x\, n(x)\,dx \right)^{\frac{1}{2}}}{\bar{x}} \tag{A3-2}$$

where $\bar{x}$ is defined as

$$\bar{x} = \int_0^\infty x\, n(x)\,dx \tag{A3-3}$$

Thus,

$$C.V. = \left(\frac{\int_0^\infty x^2 n(x)\,dx - \bar{x}^2}{\bar{x}^2} \right)^{\frac{1}{2}} \tag{A3-4}$$

or

$$C.V. = \left(\frac{1}{\bar{X}^2} \int_0^\infty X^2 n(X)\, dX \; - 1 \right)^{\frac{1}{2}} \tag{A3-5}$$

The definition of $D_{a,2}$ is given by Eq. (3) in Chapter 3, i.e.,

$$D_{a,2} = \int_0^\infty X^2 \frac{N(X)}{N_{tot}}\, dX = \int_0^\infty X^2 n(X)\, dX \tag{A3-6}$$

Substitution of Eq. (A3-6) into Eq. (A3-5) yields

$$C.V. = \left(\frac{D_{a,2}^2}{\bar{X}} - 1 \right)^{\frac{1}{2}} \tag{A3-7}$$

Therefore, the fraction of the total number of particles having sizes in the range, D to D + dD, is given by

$$n(D)\, dD = \frac{W_{tot}}{N_{tot}} \frac{\omega(D)\, dD}{\frac{\pi}{6} \rho_d D^3} \tag{A3-8}$$

Substituting Eq. (A3-8) into Eq. (A3-3) gives

$$\bar{X} = \frac{W_{tot}}{N_{tot}} \sum_{i=1}^{m-1} \left\{ \frac{6}{\pi \rho_d} \int_{D_i}^{D_{i+1}} \frac{1}{\sqrt{2\pi}\, \ln \sigma_{g,3,i}} \exp\left[- \frac{\ln^2\left(\frac{X}{D_{g,3,i}}\right)}{2 \ln^2 \sigma_{g,3,i}} \right] \frac{dX}{X^3} \right\} \qquad \text{(A3-9)}$$

It is shown in Appendix 1 that the integration of Eq. (A3-9) yields

$$\bar{X} = \frac{W_{tot}}{N_{tot}} \sum_{i=1}^{m-1} \left\{ \frac{6}{\pi \rho_d} \left(\frac{1}{2}\right) \frac{\exp\left(2 \ln^2 \sigma_{g,3,i}\right)}{D_{g,3,i}^2} \left[\operatorname{erf}(w_{i+1}) - \operatorname{erf}(w_i) \right] \right\} \qquad \text{(A3-10)}$$

where

$$w_n = \frac{\ln\left(\frac{D_n}{D_{g,3,i}}\right)}{\sqrt{2}\, \ln \sigma_{g,3,i}} + \frac{2 \ln^2 \sigma_{g,3,i}}{\sqrt{2}} \qquad \text{for } n = i,\ i+1$$

The expression for $D_{a,2}$ is (see Eq. (3) in Chapter 3)

$$D_{a,2} = \frac{W_{tot}}{N_{tot}} \sum_{i=1}^{m-1} \left\{ \frac{6}{\pi \rho_d} \left(\frac{1}{2}\right) \frac{\exp\left(\frac{1}{2} \ln^2 \sigma_{g,3,i}\right)}{D_{g,3,i}} \left[\operatorname{erf}(y_{i+1}) - \operatorname{erf}(y_i) \right] \right\} \qquad \text{(A3-11)}$$

where

$$y_n = \frac{\ln\left(\frac{D_n}{D_{g,3,i}}\right)}{\sqrt{2}\, \ln \sigma_{g,3,i}} + \frac{\ln^2 \sigma_{g,3,i}}{\sqrt{2}} \qquad ;\ n = i,\ i+1$$

Substitution of Eqs. (A3-11) and (A3-10) into Eq. (A3-7) yields

$$C.V. = \left\{ \frac{\sum_{i=1}^{m-1} \frac{\exp\left(\frac{1}{2}\ln^2\sigma_{g,3,i}\right)}{D_{g,3,i}} \left[\operatorname{erf}(y_{i+1}) - \operatorname{erf}(y_i) \right]}{\frac{W_{tot}}{N_{tot}} \frac{6}{\pi \rho_d} \left(\frac{1}{2}\right) \left[\sum_{i=1}^{m-1} \frac{\exp\left(2\ln^2\sigma_{g,3,i}\right)}{D_{g,3,i}^2} \left[\operatorname{erf}(X_{i+1}) - \operatorname{erf}(X_i) \right] \right]^2} - 1 \right\}^{\frac{1}{2}} \qquad \text{(A3-12)}$$

The expression for W_{tot}/N_{tot} is (Appendix 2)

$$\frac{W_{tot}}{N_{tot}} = \left\{ \frac{6}{\pi \rho_d} \sum_{i=1}^{m-1} \left(\frac{1}{2}\right) \frac{\exp\left(\frac{9}{2}\ln^2\sigma_{g,3,i}\right)}{D_{g,3,i}^3} \left[\operatorname{erf}(X_{i+1}) - \operatorname{erf}(X_i) \right] \right\}^{\frac{1}{2}} \qquad \text{(A3-13)}$$

where

$$x_n = \frac{\ln\left(\frac{D_n}{D_{g,3,i}}\right)}{\sqrt{2}\ln\sigma_{g,3,i}} + \frac{9}{\sqrt{2}}\ln^2\sigma_{g,3,i} \qquad ; n = i,\ i+1$$

Substituting Eq. (A3-13) into Eq. (A3-12) results in

C.V.

$$= \left\{ \frac{\left[\sum_{i=1}^{m-1} \frac{\exp\left(\frac{9}{2} \ln^2 \sigma_{g,3,i}\right)}{D_{g,3,i}^3} \left\{ \operatorname{erf}(X_{i+1}) - \operatorname{erf}(X_i) \right\} \right] \left[\sum_{i=1}^{m-1} \frac{\exp\left(\frac{1}{2} \ln^2 \sigma_{g,3,i}\right)}{D_{g,3,i}} \left\{ \operatorname{erf}(y_{i+1}) - \operatorname{erf}(y_i) \right\} \right]}{\left[\sum_{i=1}^{m-1} \frac{\exp\left(2 \ln^2 \sigma_{g,3,i}\right)}{D_{g,3,i}^2} \left\{ \operatorname{erf}(w_{i+1}) - \operatorname{erf}(w_i) \right\} \right]^2} - 1 \right\}^{\frac{1}{2}} \qquad \text{(A3-14)}$$

which is the Eq. (27) in Chapter 3.

As the entire distribution tends toward a log normal distribution, one obtains

$$\begin{aligned} \sigma_{g,3,i} &\to \sigma_{g,3} \\ D_{g,3,i} &\to D_{g,3} \end{aligned} \qquad i = 1,2,3,\ldots,m-1$$

Consequently Eq. (A3-14) becomes

$$C.V. = \left\{ \exp\left(\ln^2 \sigma_{g,3}\right) \frac{\left[\operatorname{erf}(X_m) - \operatorname{erf}(X_1) \right] \left[\operatorname{erf}(y_m) - \operatorname{erf}(y_1) \right]}{\left[\operatorname{erf}(w_m) - \operatorname{erf}(w_1) \right]^2} - 1 \right\}^{\frac{1}{2}} \qquad \text{(A3-15)}$$

In addition, as the distribution approaches a log normal distribution, a distribution defined over the interval $[0,\infty]$, the

$$D_m \to \infty \tag{A3-16}$$

$$D_1 \to 0 \tag{A3-17}$$

Carrying out the limits in Eqs. (A3-16) and (A3-17) on Eqs. (A3-10), (A3-11) and (A3-13) for w_n, y_n, and x_n, respectively, we find that

$$w_m, y_m, x_n \to +\infty \tag{A3-18}$$

$$w_1, y_1, x_1 \to -\infty \tag{A3-19}$$

After performing the limits in Eqs. (A3-18) and (A3-19) on Eq. (A3-15) we obtain

$$C.V. = \left\{ \exp\left(\ln^2 \sigma_{g,3} \right) \frac{[1-(-1)][1-(-1)]}{[1-(-1)]^2} - 1 \right\}^{\frac{1}{2}} \tag{A3-20}$$

or

$$C.V. = \left\{ \exp\left(\ln^2 \sigma_{g,3} \right) - 1 \right\}^{\frac{1}{2}} \tag{A3-21}$$

Note that Eq. (A3-21) is identical to Eq. (27) in Chapter 3 which is the coefficient of variability derived for a log normal distribution.

Table 3.1 Log Normal Representation of the Particle Size Distribution for $|Z| < 2$

Sample Identification	Coefficient of Determination	Geometric Mean Diameter $D_{g,3,\mu m}$	Natural Log of the Geometric Standard Deviation $\ln\sigma_{g,3}$	95% Confidence Interval	
WTAC-S01*	0.979	17.2	0.640	0.962	0.997
WTAC-S02*	0.970	16.8	0.393	0.898	0.998
WTAC-S03*	0.991	21.3	0.380	0.967	0.999
WTAC-S04*	0.914	24.4	0.389	0.770	0.992
WTAC-S05*	0.981	30.6	0.286	0.914	0.999
WTAC-S06*	0.948	42.2	0.286	0.857	0.995
WTAC-S07**	0.930	28.5	0.534	0.852	0.992
WTAC-S08**	0.936	32.2	0.520	0.848	0.993
WTAC-S09**	0.974	29.1	0.505	0.944	0.997
WTAC-S10**	0.938	23.5	0.749	0.889	0.991
MOAC-S01*	0.952	10.6	0.620	0.861	0.996
MOAC-S02*	0.968	14.2	0.498	0.931	0.996
MOAC-S03*	0.957	22.0	0.332	0.810	0.998
MOAC-S04*	0.994	27.3	0.325	0.973	1.000
MOAC-S05*	0.983	33.3	0.326	0.953	0.999
MOAC-S06*	0.956	49.4	0.341	0.906	0.995
MOAC-S07**	0.883	41.6	0.450	0.760	0.986
MOAC-S08**	0.818	48.4	0.480	0.838	0.977
MOAC-S09**	0.844	45.9	0.705	0.730	0.977
MOAC-S10**	0.863	61.4	0.848	0.761	0.980
MOAC-S11**	0.785	125.0	1.088	0.636	0.968
CNAC-S01*	0.953	11.2	0.513	0.887	0.995
CNAC-S02*	0.977	14.1	0.340	0.830	0.999
CNAC-S03*	0.955	17.6	0.354	0.802	0.998
CNAC-S04*	0.990	20.4	0.360	0.966	0.999
CNAC-S05*	0.903	25.6	0.421	0.693	0.993

Table 3.1 (continued)

Sample Identification	Coefficient of Determination	Geometric Mean Diameter $D_{g,3,\mu m}$	Natural Log of the Geometric Standard Deviation $\ln\sigma_{g,3}$	95% Confidence Interval	
CNAC-S06*	0.988	42.2	0.359	0.973	0.999
CNAC-S07**	0.993	23.5	0.507	0.985	0.999
CNAC-S08**	0.995	23.9	0.556	0.989	0.999
CNAC-S09**	0.990	25.5	0.552	0.977	0.999
CNAC-S10**	0.993	33.5	0.628	0.985	0.999
CNAC-S11**	0.914	50.0	0.677	0.821	0.990
CSAC-S02*	0.976	18.7	0.552	0.960	0.996
CSAC-S03*	0.957	18.2	0.391	0.908	0.995
CSAC-S04*	0.986	22.1	0.368	0.996	0.999
CSAC-S05*	0.989	22.6	0.376	0.974	0.999
CSAC-S06*	0.996	35.3	0.277	0.968	1.000
CSAC-F01*	0.952	24.0	0.474	0.906	0.994
CSAC-F02*	0.981	22.8	0.620	0.947	0.998
CSAC-F03*	0.931	26.3	0.513	0.890	0.989
CSAC-F04*	0.986	21.5	0.429	0.969	0.998
CSAC-F05*	0.955	21.5	0.467	0.924	0.993
CSAC-F06*	0.989	16.6	0.368	0.976	0.999

Table 3.2 The Amount of Weight in Particles with Diameters Less Than the Lower Boundary Sieve Aperatures

Size Fraction	Sieve Aperature d_a, μm	Stokes Equivalent Diameter of d_a d_s, μm	Weight Percent Less Than d_s		
			Grain Sorghum Dust %	Wheat Dust %	Corn Dust %
7	61	55	60	92	95
8	74	67	62	88	98
9	88	79	80	99	98
10	105	95	> 70	100	> 84
11	124	112	> 50		> 84

Table 3.3 The Amount of Weight in Particles with Diameters Greater Than the Upper Boundary Sieve Aperatures

Size Fraction	Sieve Aperature d_a, μm	Stokes Equivalent Diameter of d_a d_s, μm	Weight Percent Less Than d_s		
			Grain Sorghum Dust %	Wheat Dust %	Corn Dust %
7	74	67	18	3	2
8	88	79	15	5	0.5
9	105	95	< 10	< 0.01	< 2
10	124	112	< 20	< 0.01	< 16
11	208	188			< 16

Table 3.4 The Spread of the Particle Size Distributions

Sample Identification	Coefficients of Variability	
	Equation (27) %	Equation (26) %
MOAC-S01	42	68
MOAC-S02	53	53
MOAC-S03	22	34
MOAC-S04	28	33
MOAC-S05	34	34
MOAC-S06	42	35
MOAC-S07	65	47
MOAC-S08	74	51
MOAC-S09	67	80
MOAC-S10	70	103
MOAC-S11	98	150
WTAC-S01	55	71
WTAC-S02	55	41
WTAC-S03	67	39
WTAC-S04	85	40
WTAC-S05	47	29
WTAC-S06	35	29
WTAC-S07	65	57
WTAC-S08	59	56
WTAC-S09	54	54
WTAC-S10	60	87

Table 3.4 (continued)

Sample Identification	Coefficients of Variability	
	Equation (27) %	Equation (26) %
CNAC-S01	43	55
CNAC-S02	45	35
CNAC-S03	31	36
CNAC-S04	36	37
CNAC-S05	51	44
CNAC-S06	36	37
CNAC-S07	47	54
CNAC-S08	46	60
CNAC-S09	46	60
CNAC-S10	56	69
CNAC-S11	58	76
CSAC-S02	42	60
CSAC-S03	36	41
CSAC-S04	41	38
CSAC-S05	49	39
CSAC-S06	27	28
CSAC-F01	39	50
CSAC-F02	104	76
CSAC-F03	43	55
CSAC-F04	41	45
CSAC-F05	41	49
CSAC-F06	34	38

Table 3.5 The Results from the Analysis of Variance of the Coefficients of Variability for the Size Fractions

Source of Variation	Degrees of Freedom	Sum of Squares	Mean Square	F
Treatment				
Dust	2	2194.26	1097.13	60.41**
Size Fraction	9	4823.30	535.92	29.51**
Interactions				
D x S	18	6508.23	361.57	19.91**
Error	30	544.94	18.16	
Total	59	14070.73		

** Significant at the 1% level.

Table 3.6 Results from the Mass Mean Diameter Determination

Sample Identification	Coefficient of Determination	Geometric Mean Diameter $D_{g,3,\mu m}$	Natural Log of the Geometric Standard Deviation $\ln\sigma_{g,3}$	No. of Data Points	95% Confidence Interval	
MOAC-S01	0.992	10.0	0.534	8	0.964	1.000
MOAC-S02	0.990	14.9	0.389	6	0.953	0.999
MOAC-S03*	0.969	22.4	0.256	4	0.435	1.000
MOAC-S04	0.994	27.3	0.325	6	0.973	1.000
MOAC-S05	0.983	33.3	0.326	8	0.953	0.999
MOAC-S06	0.985	51.4	0.296	8	0.957	0.999
MOAC-S07	0.991	49.9	0.306	6	0.957	1.000
MOAC-S08*	0.999	62.8	0.222	4	0.972	1.000
MOAC-S09*	0.998	64.4	0.232	4	0.939	1.000
MOAC-S10*	0.997	71.5	0.286	4	0.916	1.000
MOAC-S11*	0.987	89.4	0.382	4	0.708	1.000
WTAC-S01	0.979	17.2	0.640	14	0.962	0.997
WTAC-S02	0.999	16.5	0.363	6	0.995	1.000
WTAC-S03	0.991	21.3	0.380	8	0.967	0.999
WTAC-S04*	0.903	27.4	0.260	4	0.126	0.999
WTAC-S05*	0.993	31.9	0.241	4	0.834	1.000
WTAC-S06	0.998	43.9	0.235	6	0.991	1.000
WTAC-S07	0.994	34.2	0.344	6	0.970	1.000
WTAC-S08*	0.960	36.4	0.419	4	0.321	1.000
WTAC-S09	0.996	31.3	0.589	8	0.988	1.000
WTAC-S10*	0.952	31.7	0.543	4	0.230	1.000
CNAC-S01*	0.998	11.2	0.378	4	0.962	1.000
CNAC-S02*	1.000	13.8	0.308	4	0.990	1.000
CNAC-S03	0.995	16.9	0.314	6	0.964	1.000
CNAC-S04	0.990	20.4	0.360	8	0.996	0.999
CNAC-S05*	0.996	29.4	0.265	4	0.915	1.000

Table 3.6 (continued)

Sample Identification	Coefficient of Determination	Geometric Mean Diameter $D_{g,3,\mu m}$	Natural Log of the Geometric Standard Deviation $\ln\sigma_{g,3}$	No. of Data Points	95% Confidence Interval	
CNAC-S06	0.988	42.2	0.359	10	0.973	0.999
CNAC-S07	0.993	23.5	0.507	10	0.985	0.999
CNAC-S08	0.995	23.9	0.556	10	0.989	0.999
CNAC-S09	0.990	25.5	0.552	12	0.977	0.999
CNAC-S10	0.993	33.5	0.628	10	0.985	0.999
CNAC-S11*	0.996	60.3	0.375	4	0.908	1.000
CSAC-S02	0.987	17.7	0.469	10	0.971	0.999
CSAC-S03*	0.880	18.6	0.358	10	0.236	0.999
CSAC-S04	0.986	22.1	0.368	10	0.966	0.999
CSAC-S05	0.989	22.6	0.376	12	0.974	0.999
CSAC-S06	0.996	35.3	0.277	8	0.968	1.000
CSAC-F01*	0.827	22.4	0.426	10	0.409	0.998
CSAC-F02	0.991	22.8	0.552	6	0.957	1.000
CSAC-F03	0.990	24.6	0.427	14	0.980	0.999
CSAC-F04	0.986	21.5	0.429	10	0.969	0.998
CSAC-F05	0.992	20.1	0.396	12	0.981	0.999
CSAC-F06	0.989	16.6	0.368	12	0.976	0.999

* Only two pairs of data utilized.

Table 3.7 Comparison of the Geometric Mean Diameter of the Boundary Sieve Aperatures to the Mass Mean Diameters

Size Fraction	Sieve Aperature		Geometric Mean of Sieve Aperature d_a, µm	Stokes Equivalent Diameter of d_a µm[a]	Weight Percent Less Than d_s		
	Lower µm	Upper µm			Grain Sorghum Dust %	Wheat Dust %	Corn Dust %
7	61	74	67	60	50	34	24
8	74	88	81	73	63	36	24
9	88	105	96	86	64	31	26
10	105	124	114	103	72	32	34
11	124	208	161	145	89	--	60

Table 3.8 Comparison of Values of $D_{a,2}$

Sample Identification	Piecewise Log Normal Approximation Value of $D_{a,2}$ µm	Log Normal Approximation |Z| < 2 $D_{a,2}$ µm	Coefficient of Variability	Log Normal Approximation |Z| < 3 $D_{a,2}$ µm	Coefficient of Variability
MOAC-S01	7	5	23	4	30
MOAC-S02	9	9	0	8	7
MOAC-S03	21	18	12	12	39
MOAC-S04	24	22	5	21	8
MOAC-S05	27	27	0	26	3
MOAC-S06	39	39	0	39	0
MOAC-S07	19	28	28	22	11
MOAC-S08	19	31	32	23	12
MOAC-S09	16	17	6	17	6
MOAC-S10	17	15	10	15	10
MOAC-S11	17	11	27	11	27
WTAC-S01	9	8	13	7	16
WTAC-S02	10	12	12	10	4
WTAC-S03	13	16	16	12	2
WTAC-S04	12	18	29	13	8
WTAC-S05	22	26	12	22	0
WTAC-S06	36	36	0	36	0
WTAC-S07	14	16	29	14	0
WTAC-S08	18	19	4	18	0
WTAC-S09	17	18	1	18	1
WTAC-S10	8	8	0	8	0
CNAC-S01	8	7	9	6	16
CNAC-S02	10	11	9	9	5
CNAC-S03	14	14	0	13	4
CNAC-S04	16	16	0	15	3
CNAC-S05	18	18	0	18	0

Table 3.8 (continued)

Sample Identification	Piecewise Log Normal Approximation Value of $D_{a,2}$ µm	Log Normal Approximation |Z| < 2 $D_{a,2}$ µm	Coefficient of Variability	Log Normal Approximation |Z| < 3 $D_{a,2}$ µm	Coefficient of Variability
CNAC-S06	33	33	0	33	0
CNAC-S07	15	14	4	14	4
CNAC-S08	15	13	9	13	9
CNAC-S09	15	14	8	14	8
CNAC-S10	17	15	8	17	0
CNAC-S11	26	20	18	20	18
CSAC-S01	17	15	6	16	2
CSAC-S02	17	9	44	9	44
CSAC-S03	12	10	13	11	8
CSAC-S04	15	13	6	13	10
CSAC-S05	17	17	0	17	0
CSAC-S06	16	17	4	15	6
CSAC-S07	31	30	1	29	4
CSAC-F01	13	12	8	11	9
CSAC-F04	17	16	4	16	4
CSAC-F05	16	15	5	15	5
CSAC-F06	15	14	5	14	5
CSAC-F07	13	13	0	13	0

Table 3.9 Comparison of Values of $D_{a,2}^2(N_{tot}/W_{tot})(6/\rho_d\pi)$

Sample Identification	Piecewise Log Normal Approximation	Log Normal Approximation $\|Z\| < 2$	Coefficient of Variability
MOAC-S01	0.1092	0.1139	3
MOAC-S02	0.0763	0.0795	3
MOAC-S03	0.0442	0.0481	6
MOAC-S04	0.0375	0.0386	2
MOAC-S05	0.0311	0.0316	1
MOAC-S06	0.0209	0.0215	2
MOAC-S07	0.0290	0.0266	2
MOAC-S08	0.0250	0.0232	5
MOAC-S09	0.0288	0.0279	2
MOAC-S10	0.0245	0.0233	4
MOAC-S11	0.0170	0.0148	10
WTAC-S01	0.0711	0.0713	0
WTAC-S02	0.0671	0.0641	3
WTAC-S03	0.0513	0.0506	1
WTAC-S04	0.0437	0.0442	1
WTAC-S05	0.0352	0.0341	2
WTAC-S06	0.0240	0.0247	2
WTAC-S07	0.0399	0.0405	1
WTAC-S08	0.0352	0.0356	1
WTAC-S09	0.0384	0.0390	1
WTAC-S10	0.0585	0.0564	3
CNAC-S01	0.1010	0.1016	0
CNAC-S02	0.0789	0.0753	3
CNAC-S03	0.0622	0.0604	2
CNAC-S04	0.0520	0.0524	1
CNAC-S05	0.0410	0.0427	3
CNAC-S06	0.0253	0.0253	0
CNAC-S07	0.0475	0.0483	1

Table 3.9 (continued)

Sample Identification	Piecewise Log Normal Approximation	Log Normal Approximation $\|Z\| < 2$	Coefficient of Variability
CNAC-S08	0.0486	0.0489	0
CNAC-S09	0.0488	0.0457	5
CNAC-S10	0.0364	0.0363	0
CNAC-S11	0.0238	0.0252	4
CSAC-S01	0.0483	0.0466	3
CSAC-S02	0.0580	0.0577	0
CSAC-S03	0.0623	0.0624	0
CSAC-S04	0.0573	0.0595	3
CSAC-S05	0.0478	0.0484	1
CSAC-S06	0.0476	0.0475	0
CSAC-S07	0.0291	0.0295	1
CSAC-F04	0.0446	0.0434	2
CSAC-F05	0.0502	0.0510	1
CSAC-F06	0.0531	0.0519	2
CSAC-F07	0.0636	0.0644	1

Table 3.10 Comparison of Values of $D_{a,3}$

Sample Identification	Piecewise Log Normal Approximation Value of $D_{a,3}$ μm	Log Normal Approximation |Z| < 2 $D_{a,3}$ μm	Coefficient of Variability	Log Normal Approximation |Z| < 3 $D_{a,3}$ μm	Coefficient of Variability
MOAC-S01	8	6	16	6	16
MOAC-S02	10	10	10	10	0
MOAC-S03	21	19	10	14	32
MOAC-S04	25	23	4	23	4
MOAC-S05	29	28	1	28	1
MOAC-S06	42	42	0	42	0
MOAC-S07	23	31	21	25	7
MOAC-S08	25	34	24	27	8
MOAC-S09	21	22	4	22	4
MOAC-S10	23	21	6	21	6
MOAC-S11	26	21	15	21	15
WTAC-S01	11	9	10	9	10
WTAC-S02	12	13	10	11	4
WTAC-S03	15	17	11	14	3
WTAC-S04	15	19	19	15	2
WTAC-S05	24	27	9	23	2
WTAC-S06	38	37	1	37	1
WTAC-S07	17	19	6	17	3
WTAC-S08	21	21	0	21	0
WTAC-S09	20	20	0	20	0
WTAC-S10	11	10	4	10	4
CNAC-S01	8	8	0	7	10
CNAC-S02	11	12	7	10	3
CNAC-S03	15	15	0	14	1
CNAC-S04	17	17	0	17	1
CNAC-S05	20	20	0	20	0

Table 3.10 (continued)

Sample Identification	Piecewise Log Normal Approximation Value of $D_{a,3}$ µm	Log Normal Approximation |Z| < 2 $D_{a,3}$ µm	Log Normal Approximation |Z| < 2 Coefficient of Variability	Log Normal Approximation |Z| < 3 $D_{a,3}$ µm	Log Normal Approximation |Z| < 3 Coefficient of Variability
CNAC-S06	35	5	0	35	0
CNAC-S07	17	16	3	16	3
CNAC-S08	16	15	6	15	6
CNAC-S09	17	16	5	16	5
CNAC-S10	20	19	5	20	0
CNAC-S11	30	25	14	25	14
CSAC-S01	18	17	3	18	0
CSAC-S02	18	11	34	11	34
CSAC-S03	13	12	9	13	0
CSAC-S04	15	14	6	14	6
CSAC-S05	18	18	0	18	2
CSAC-S06	18	18	0	16	5
CSAC-S07	32	31	1	31	1
CSAC-F04	19	18	4	19	0
CSAC-F05	17	16	3	16	3
CSAC-F06	16	16	2	16	1
CSAC-F07	14	14	2	14	3

Table 3.11 The Composition of Each Size Fraction

Identification Number	Moisture	Weight Percent, %		Starch and Fiber
		Ash	Protein	
CNAC-S01	11.7	2.20	6.7	79.40
CNAC-S02	12.1	1.31	4.8	81.79
CNAC-S03	12.1	1.35	4.6	81.95
CNAC-S04	11.9	6.43	6.9	74.77
CNAC-S05	11.3	14.13	8.5	66.07
CNAC-S06	7.3	46.27	6.1	40.33
CNAC-S07	12.4	3.94	7.7	75.96
CNAC-S08	12.6	3.37	6.9	77.13
CNAC-S09	12.5	3.25	6.8	77.45
CNAC-S10	12.6	3.39	7.5	76.51
CNAC-S11	12.5	3.84	8.4	75.26
WTAC-S01	10.4	5.19	6.7	77.71
WTAC-S02	11.8	9.06	12.1	67.04
WTAC-S03	11.0	6.97	8.5	73.53
WTAC-S04	9.0	14.96	11.1	64.94
WTAC-S05	8.8	24.99	12.7	53.51
WTAC-S06	6.8	44.83	14.0	34.37
WTAC-S07	10.6	6.79	11.9	70.71
WTAC-S08	10.8	5.95	9.4	73.85
WTAC-S09	10.3	5.24	6.3	78.16
MOAC-S01	10.0	7.14	10.0	72.86
MOAC-S02	10.3	5.14	6.5	78.06
MOAC-S03	11.4	4.49	4.3	79.81
MOAC-S04	10.1	11.74	6.0	72.16
MOAC-S05	10.2	22.78	8.7	58.32
MOAC-S06	7.7	30.09	8.3	44.91
MOAC-S07	11.1	9.73	9.7	69.47
MOAC-S08	11.6	6.25	8.1	74.05

Table 3.11 (continued)

Identification Number	Moisture	Weight Percent, %		Starch and Fiber
		Ash	Protein	
MOAC-S09	12.0	5.52	7.3	75.18
MOAC-S10	12.1	5.82	7.3	74.78
CSAC-S02	11.3	0.00	0.0	88.70
CSAC-S03	10.6	0.00	0.0	89.40
CSAC-S04	9.9	0.00	0.0	90.10
CSAC-S05	8.9	0.00	0.0	91.10
CSAC-S06	9.0	0.00	0.0	91.00
CSAC-F01	4.0	0.00	0.0	96.00
CSAC-F02	4.0	0.00	0.0	96.00
CSAC-F03	14.9	0.00	0.0	85.10
CSAC-F04	12.2	0.00	0.0	87.80
CSAC-F05	12.1	0.00	0.0	87.90

Table 3.12 The Mean, Standard Deviation, and Coefficient of Variability of Moisture, Ash, Protein or Starch & Fiber Content among the Size Fractions within Each Dust

Composition Component	Sample Identification	Number of Samples	Mean $\bar{x}$(%)	Standard Deviation (%)	Coefficient of Variability (%)
Moisture	Wheat	9	9.9	1.5	15
	Grain Sorghum	11	10.8	1.3	12
	Corn	11	11.7	1.5	13
	Cornstarch	9	9.9	3.4	34
Ash	Wheat	9	13.8	13.3	97
	Grain Sorghum	11	11.4	10.6	93
	Corn	11	8.1	13.1	162
Protein	Wheat	9	10.3	2.7	26
	Grain Sorghum	11	7.8	1.8	23
	Corn	11	6.8	1.3	19
Starch and Fiber	Wheat	9	66.0	14.1	21
	Grain Sorghum	11	70.0	10.0	14
	Corn	11	73.3	11.7	16
	Cornstarch	9	90.1	3.4	4

Table 3.13 The Mean, Standard Deviation, and Coefficient of Variability of Moisture, Ash, Protein or Starch & Fiber Content among the Average Values for Each Dust

Composition Component	Number of Samples	Mean $\bar{x}$(%)	Standard Deviation (%)	Coefficient of Variability (%)
Moisture	4	10.6	0.86	8
Ash	5	11.1	2.84	26
Protein	3	8.3	1.80	22
Starch & Fiber	4	75.0	10.60	14

Table 3.14 The Effect of Removing Separation Numbers 4, 5, and 6 in the Standard Deviation of the Composition Components among the Size Fractions for Each Type of Grain Dust Samples

Composition Component	Type of Dust	Number of Samples	Sample Removed			
			None	6	6,5	6,5,4
Moisture	Wheat	9	1.51	1.0	0.8	0.5
	Grain Sorghum	11	1.30	0.8	0.8	0.8
	Corn	11	1.53	0.4	0.3	0.3
	Means		0.80	0.9	0.8	0.8
Ash	Wheat	9	13.32	6.9	3.4	1.4
	Grain Sorghum	11	10.60	5.5	2.3	1.6
	Corn	11	13.14	3.7	1.6	1.1
	Means		2.84	2.6	2.4	2.1
Protein	Wheat	9	2.70	2.5	2.4	2.5
	Grain Sorghum	11	1.80	1.9	2.0	2.0
	Corn	11	1.27	1.3	1.3	1.3
	Means		1.80	1.5	1.4	1.3
Starch and Fiber	Wheat	9	14.10	8.1	5.0	4.2
	Grain Sorghum	11	10.00	5.9	3.3	3.4
	Corn	11	11.74	4.5	2.7	2.6
	Means		3.70	3.4	2.8	2.5

Table 3.15 Simple Correlation Coefficients for the Correlation between Compositional Components

Correlation	Correlation Coefficients, r			
	Grain Sorghum Dust	Wheat Dust	Corn Dust	Cornstarch
Ash and Moisture	-0.83**	-0.91**	-0.97**	--
Ash and Starch & Fiber	-0.98**	-0.99**	-0.99**	--
Moisture and Starch & Fiber	0.76**	0.85**	0.94**	1.0**
Protein and Ash	--	0.72*	--	--
Protein and Starch & Fiber	--	-0.82**	--	--

* Significant at the 5% level.

** Significant at the 1% level.

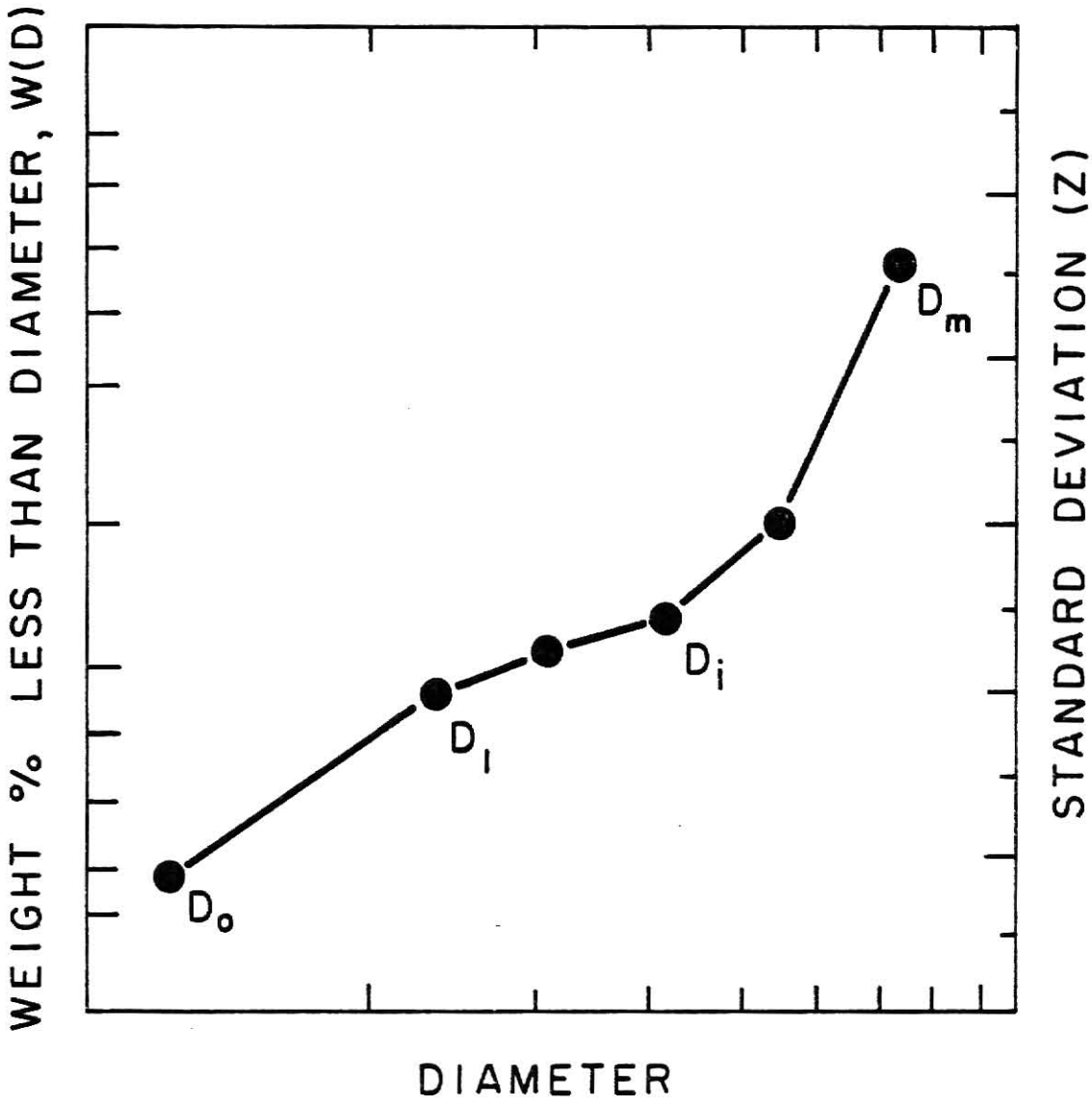

Fig. 3.1 The Piecewise Log Normal Approximation of the Particle Size Distribution

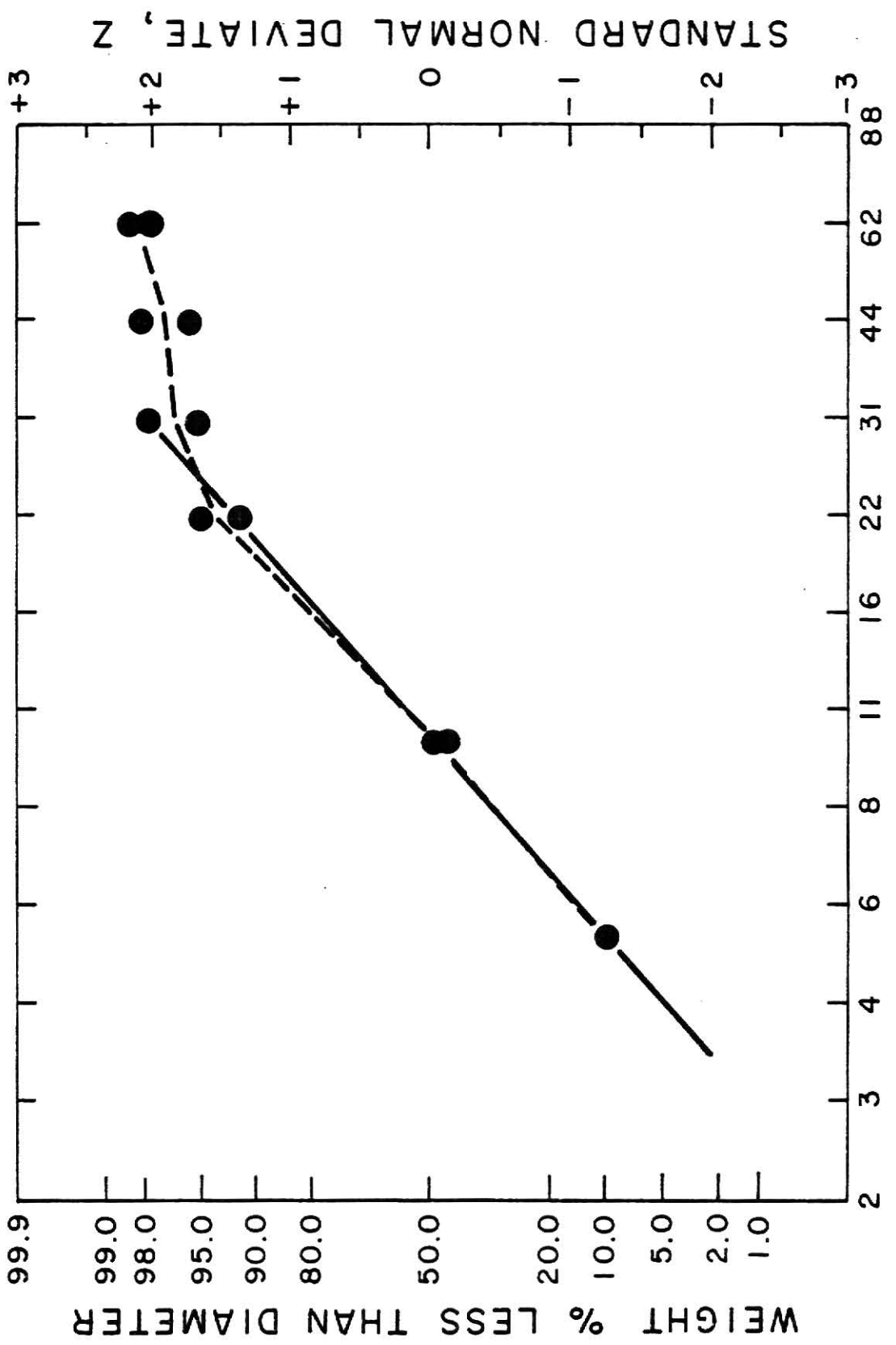

Fig. 3.2 Particle Size Distribution of Grain Sorghum Dust, MOAC-SOI

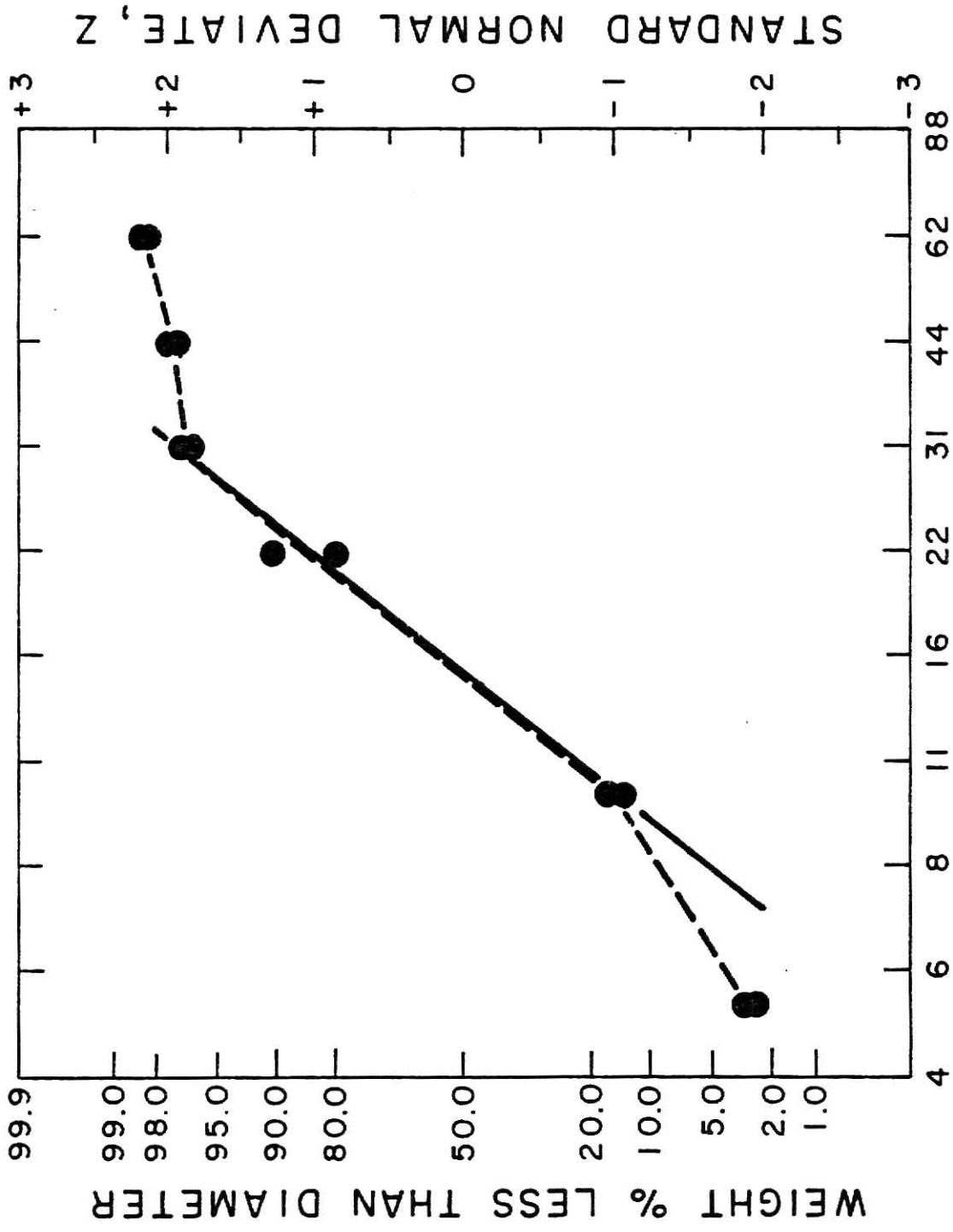

Fig. 3.3 Particle Size Distribution of Grain Sorghum Dust, MOAC-SO2

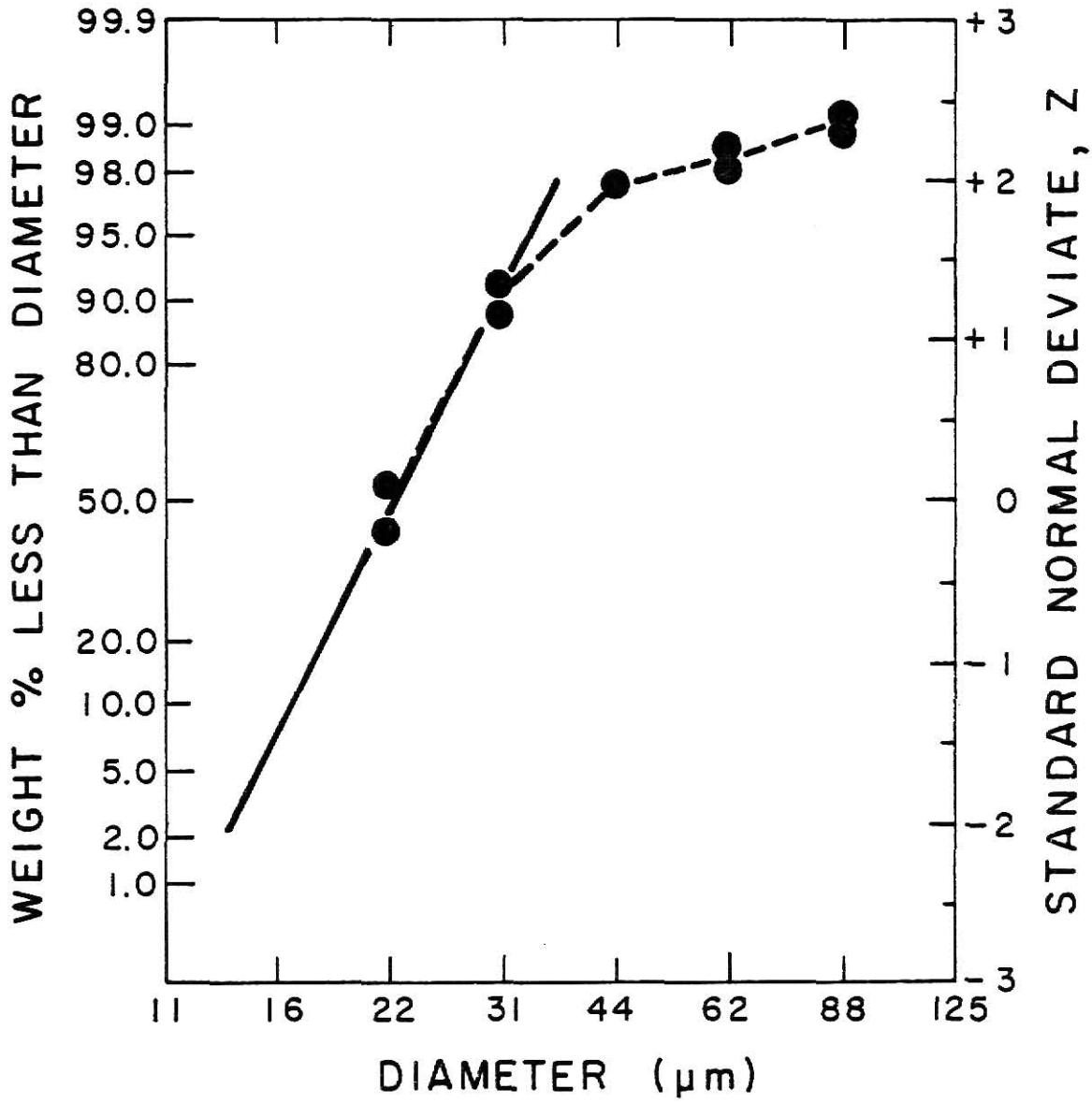

Fig. 3.4 Particle Size Distribution of Grain Sorghum Dust, MOAC-SO3

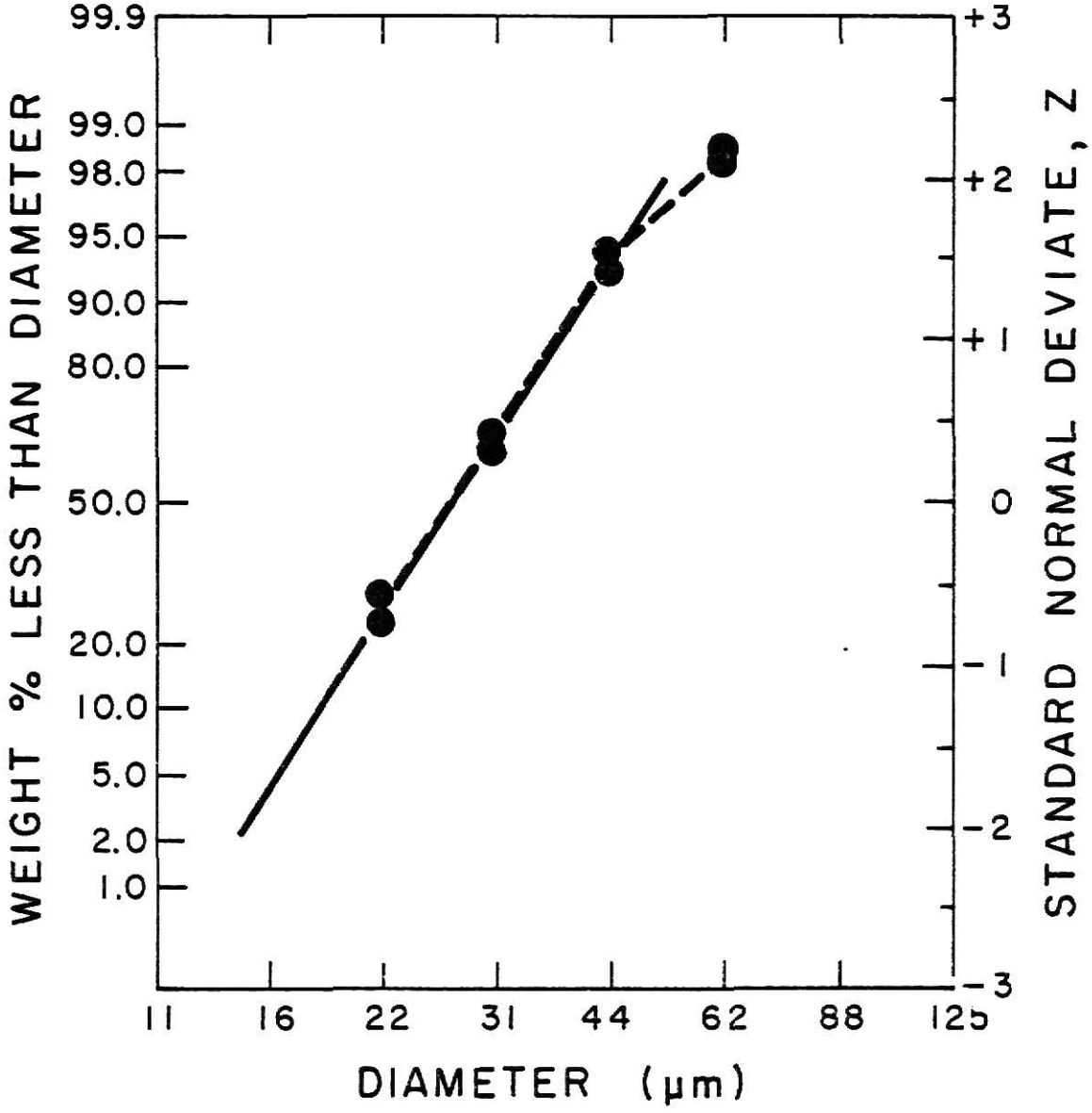

Fig. 3.5 Particle Size Distribution of Grain Sorghum Dust, MOAC-SO4

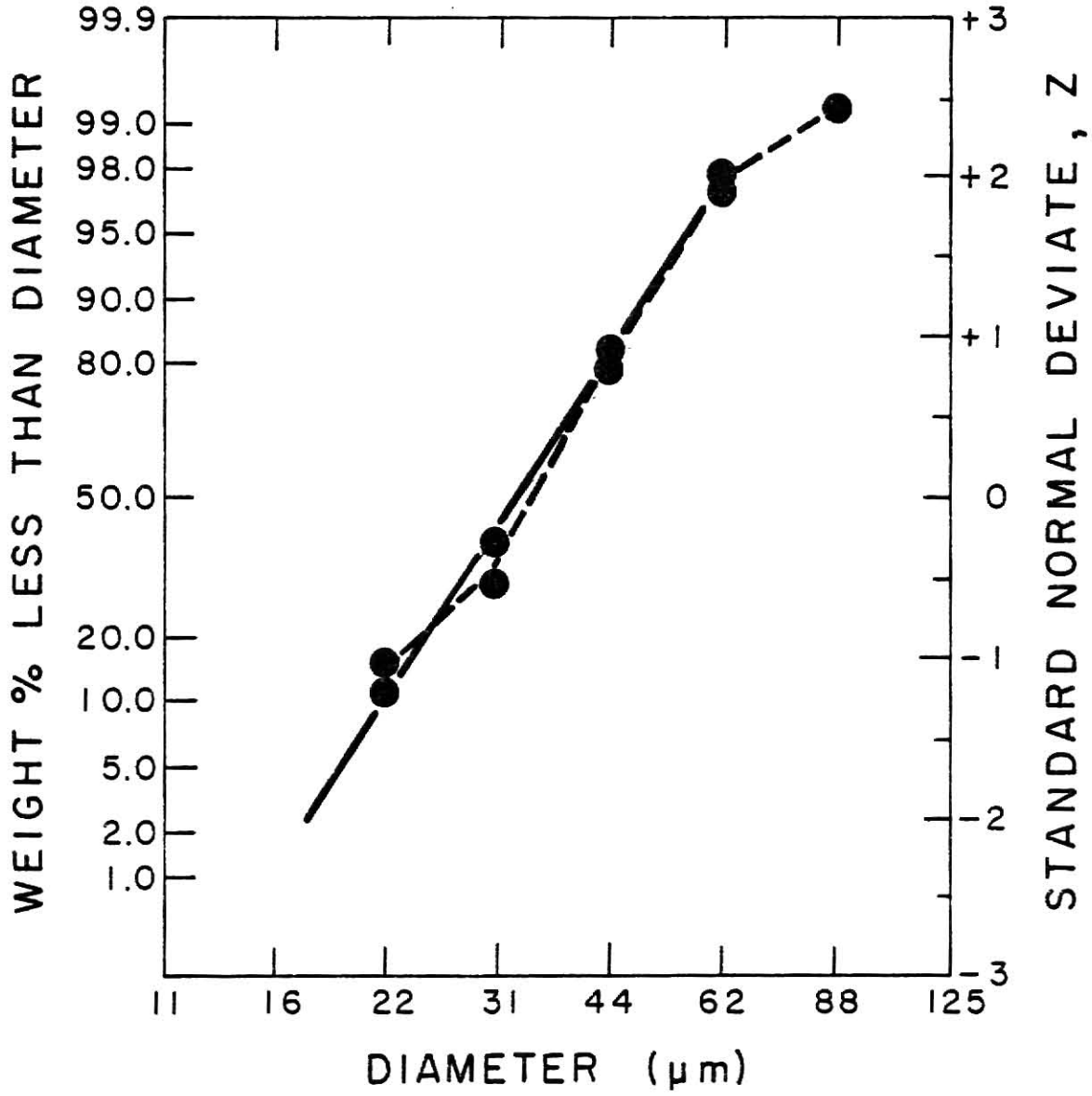

Fig. 3.6 Particle Size Distribution of Grain Sorghum Dust, MOAC-SO5

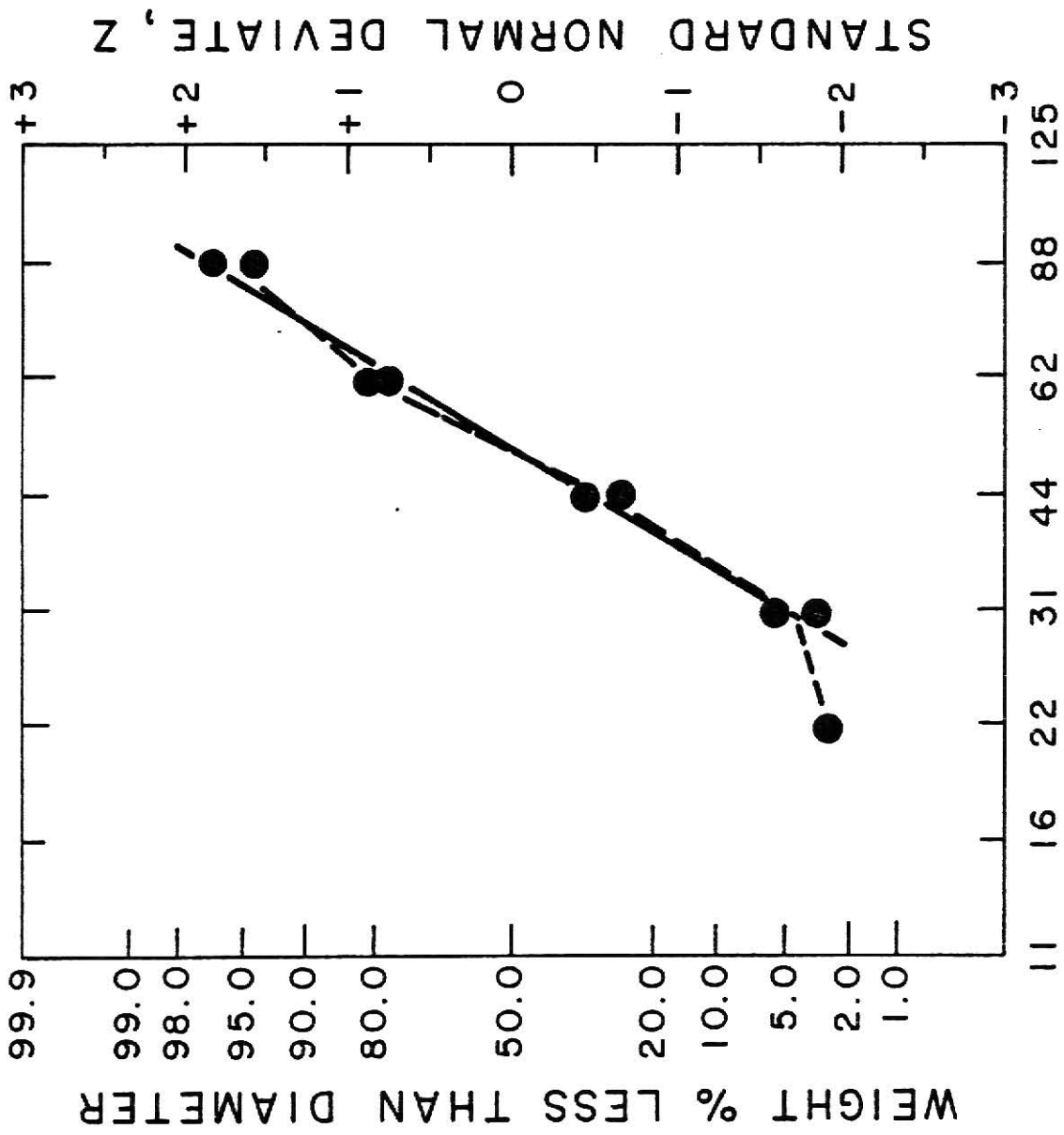

Fig. 3.7 Particle Size Distribution of Grain Sorghum Dust MOAC-S06

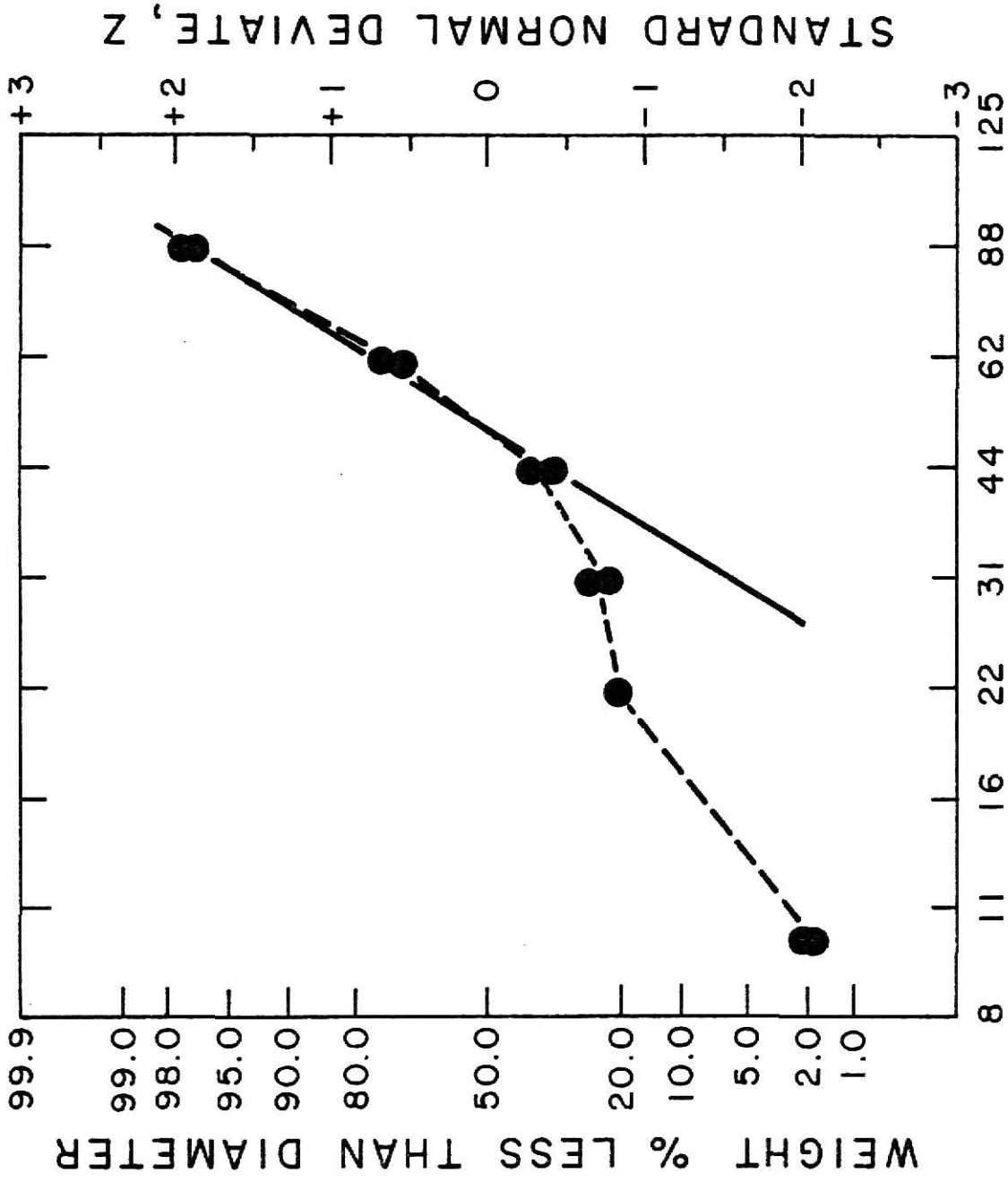

Fig. 3.8 Particle Size Distribution of Grain Sorghum Dust, MOAC-S07

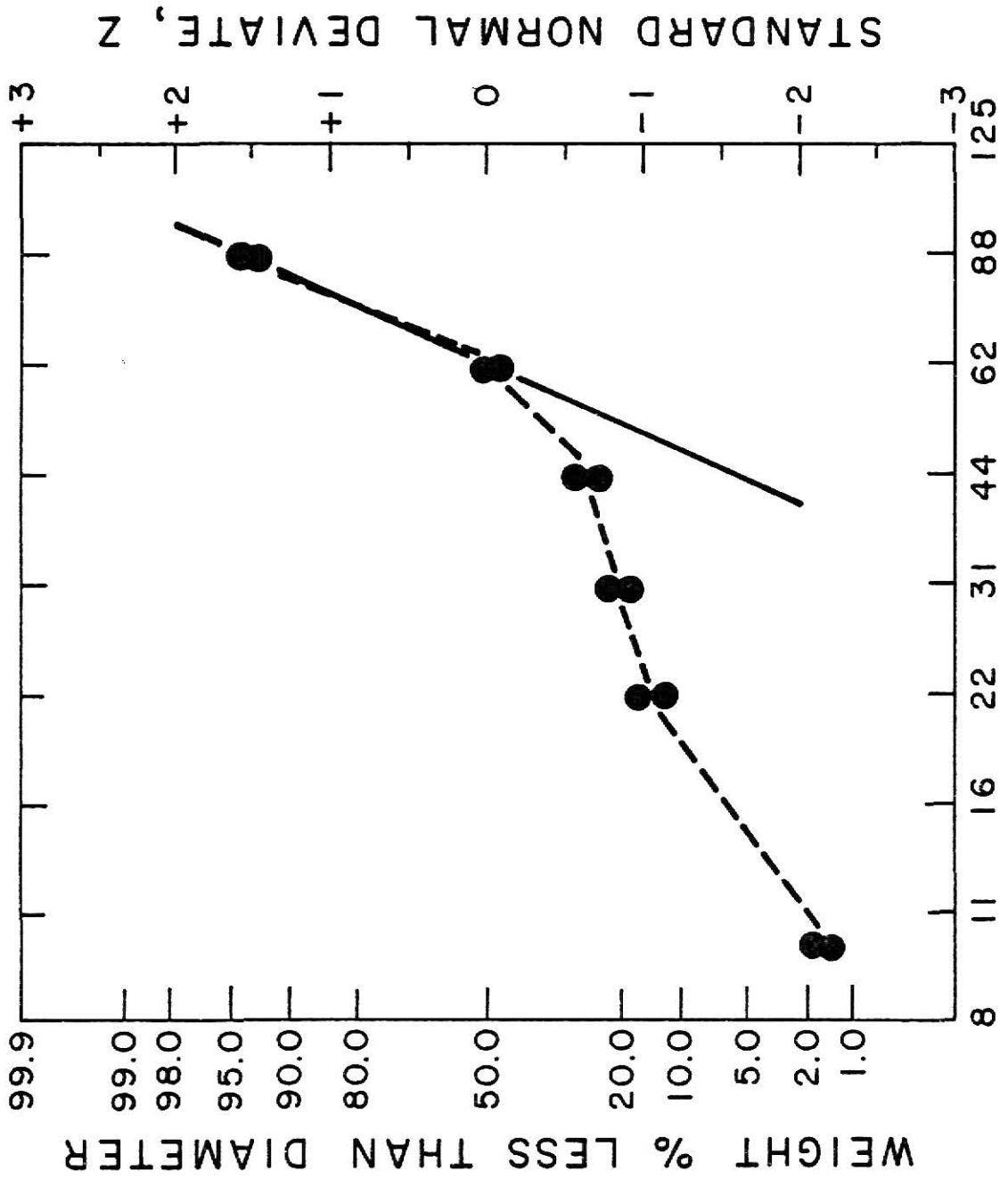

Fig. 3.9 Particle Size Distribution of Grain Sorghum Dust, MOAC-S08

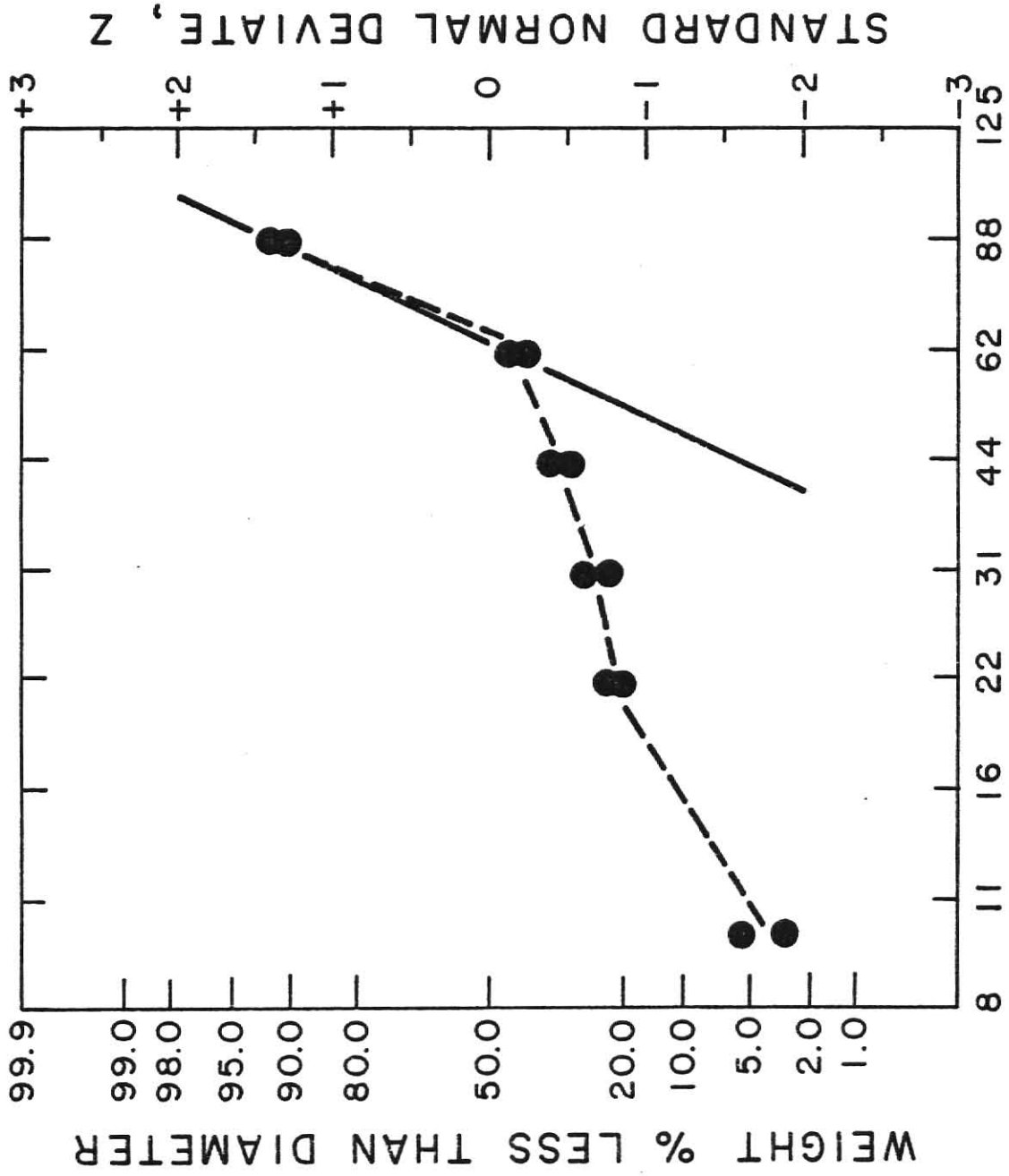

Fig. 3.10 Particle Size Distribution of Grain Sorghum Dust, MOAC-S09

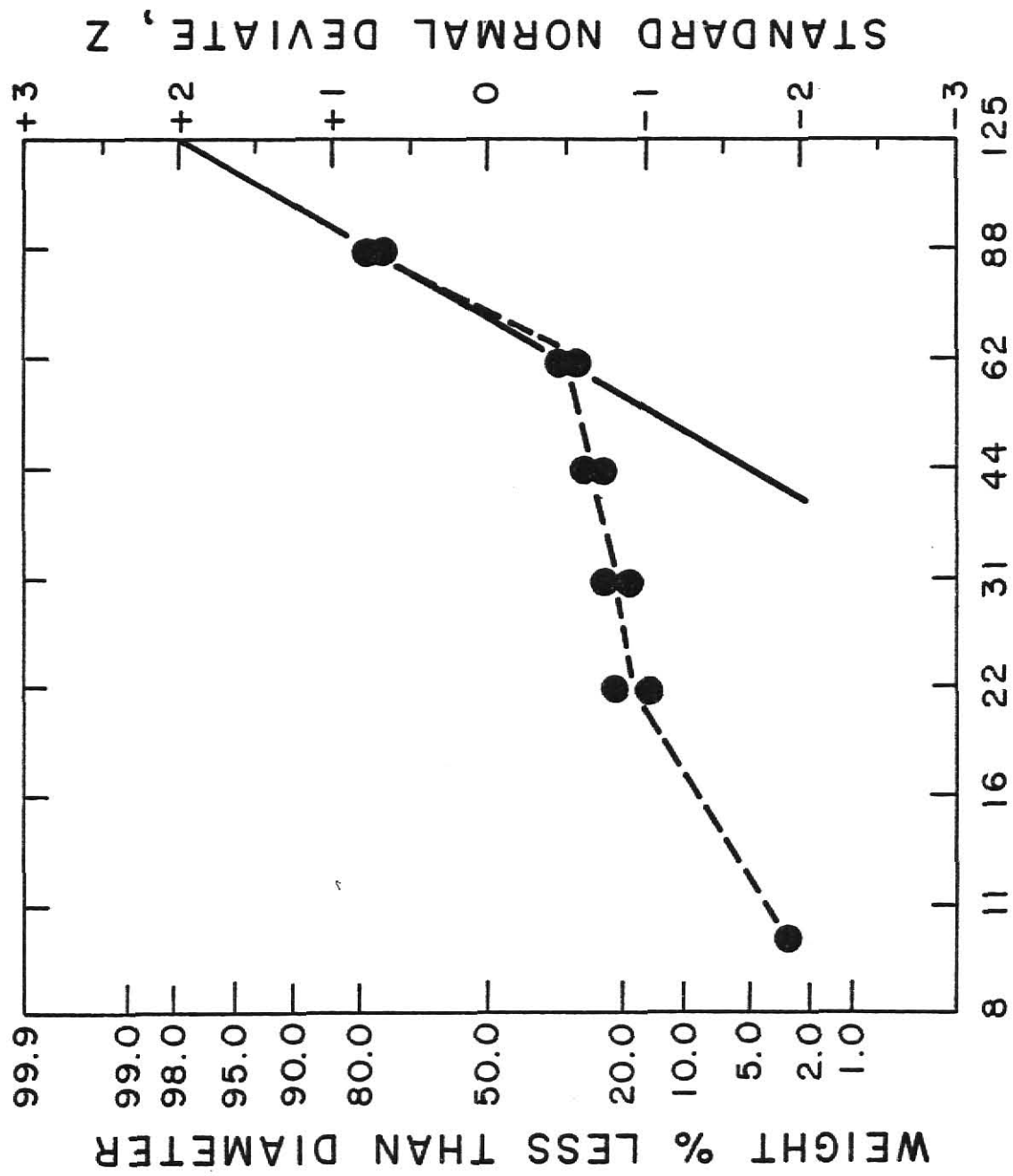

Fig. 3.11 Particle Size Distribution of Grain Sorghum Dust, MOAC-S10

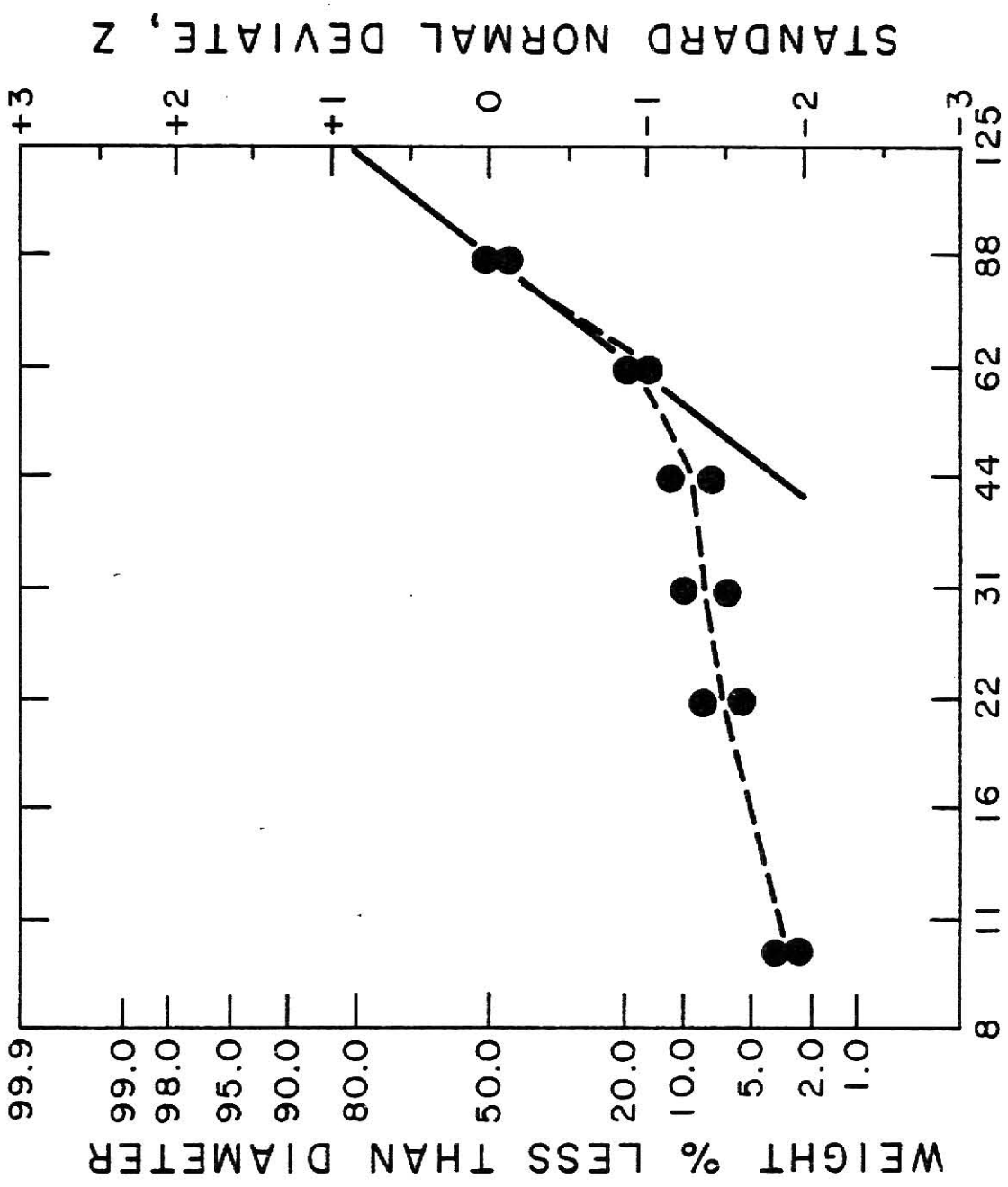

Fig. 3.12 Particle Size Distribution of Grain Sorghum Dust, MOAC-S11

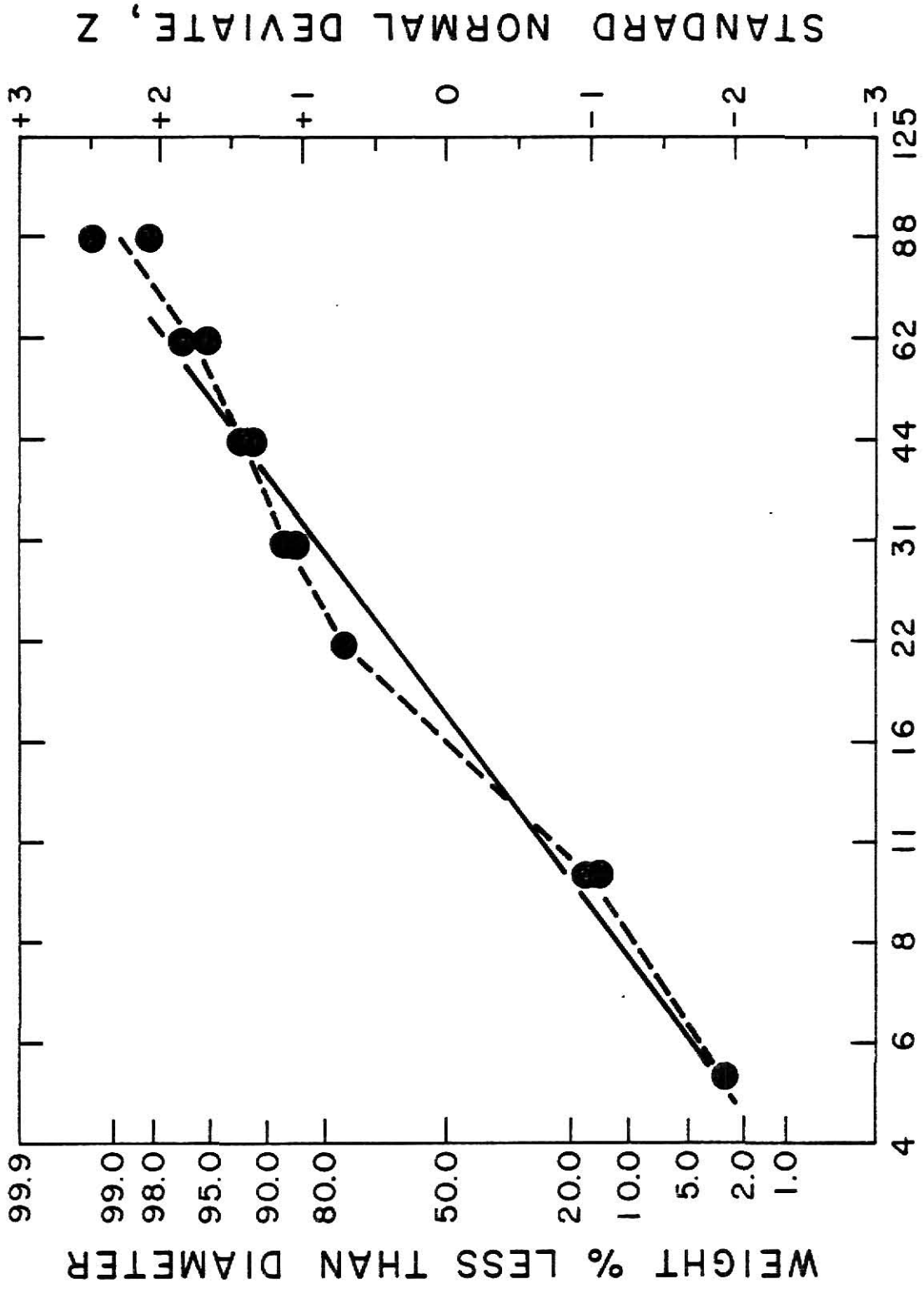

Fig. 3.13 Particle Size Distribution of Wheat Dust, WIAC-SOl

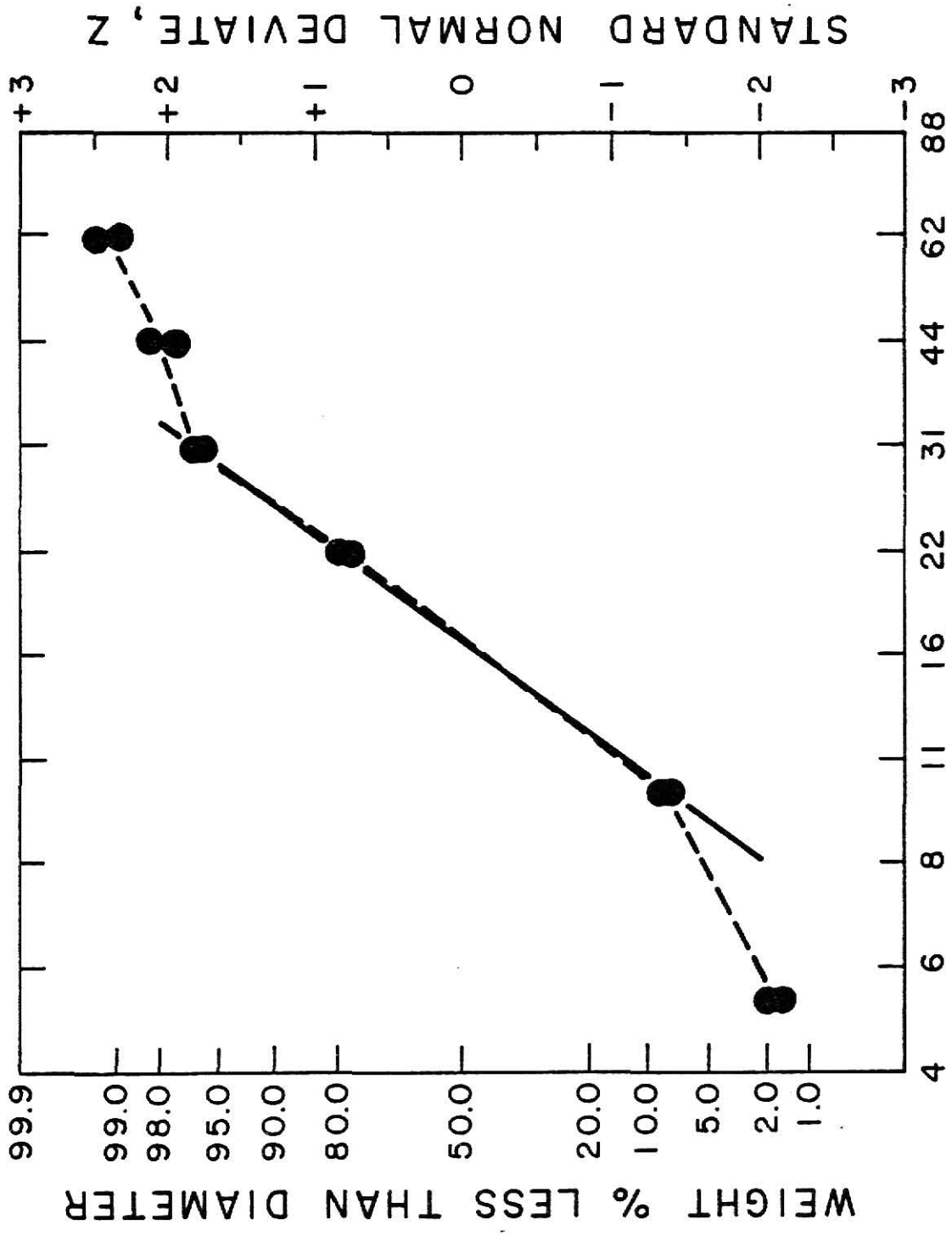

Fig. 3.14 Particle Size Distribution of Wheat Dust, WTAC-S02

KEDO

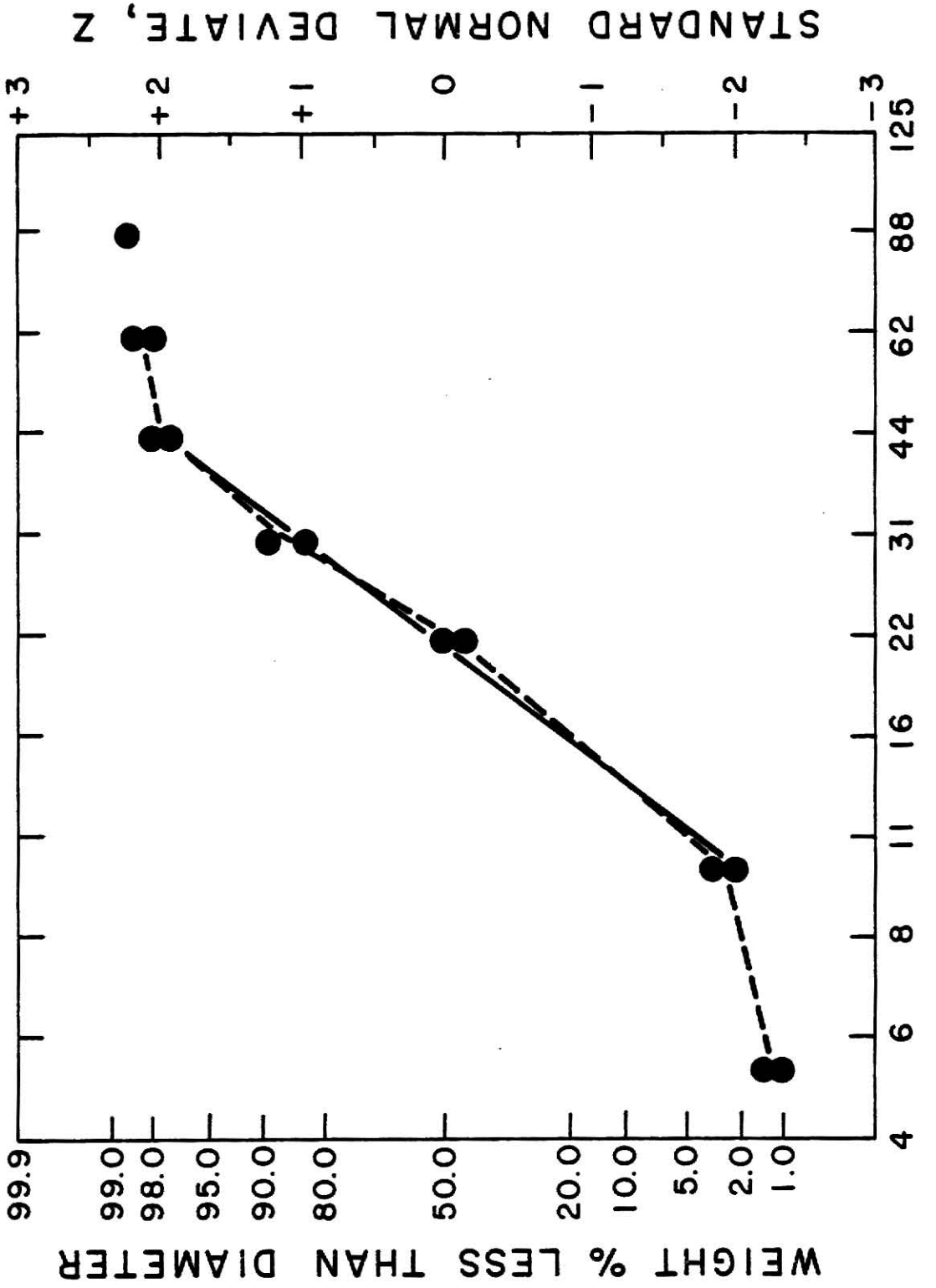

Fig. 3.15 Particle Size Distribution of Wheat Dust, WTAC-S03

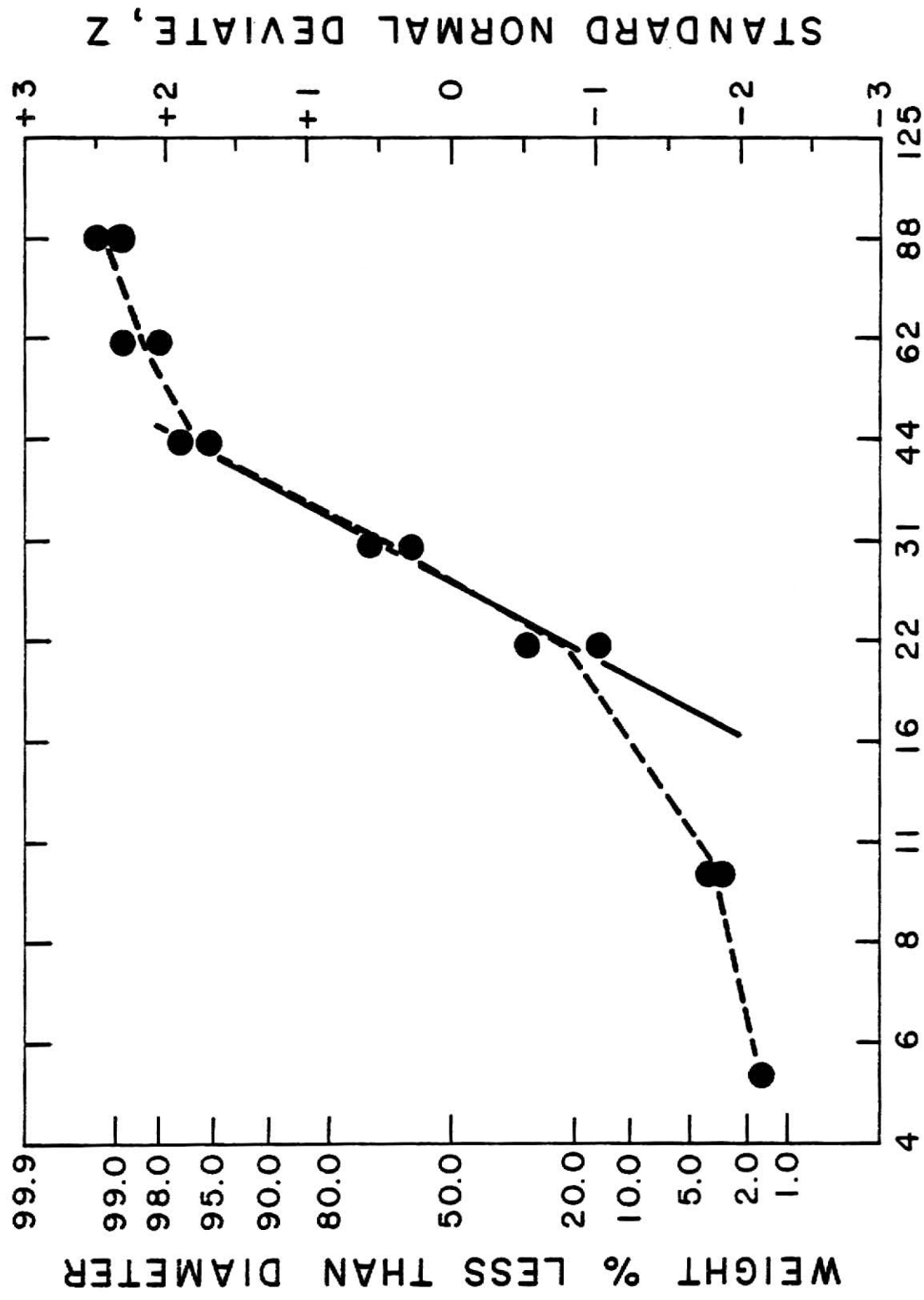

Fig. 3.16 Particle Size Distribution of Wheat Dust, WTAC-S04

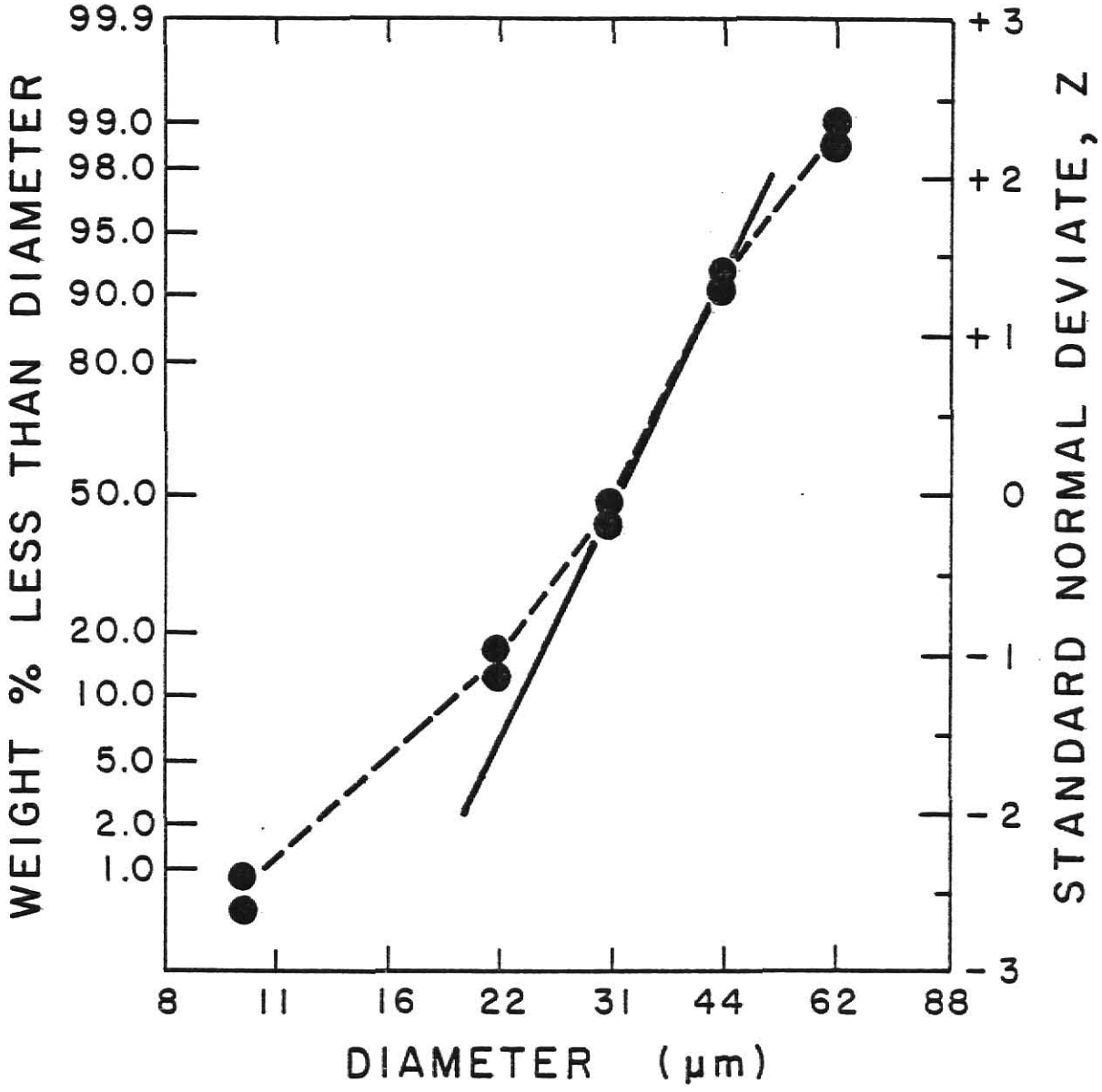

Fig. 3.17 Particle Size Distribution of Wheat Dust, WTAC-S05

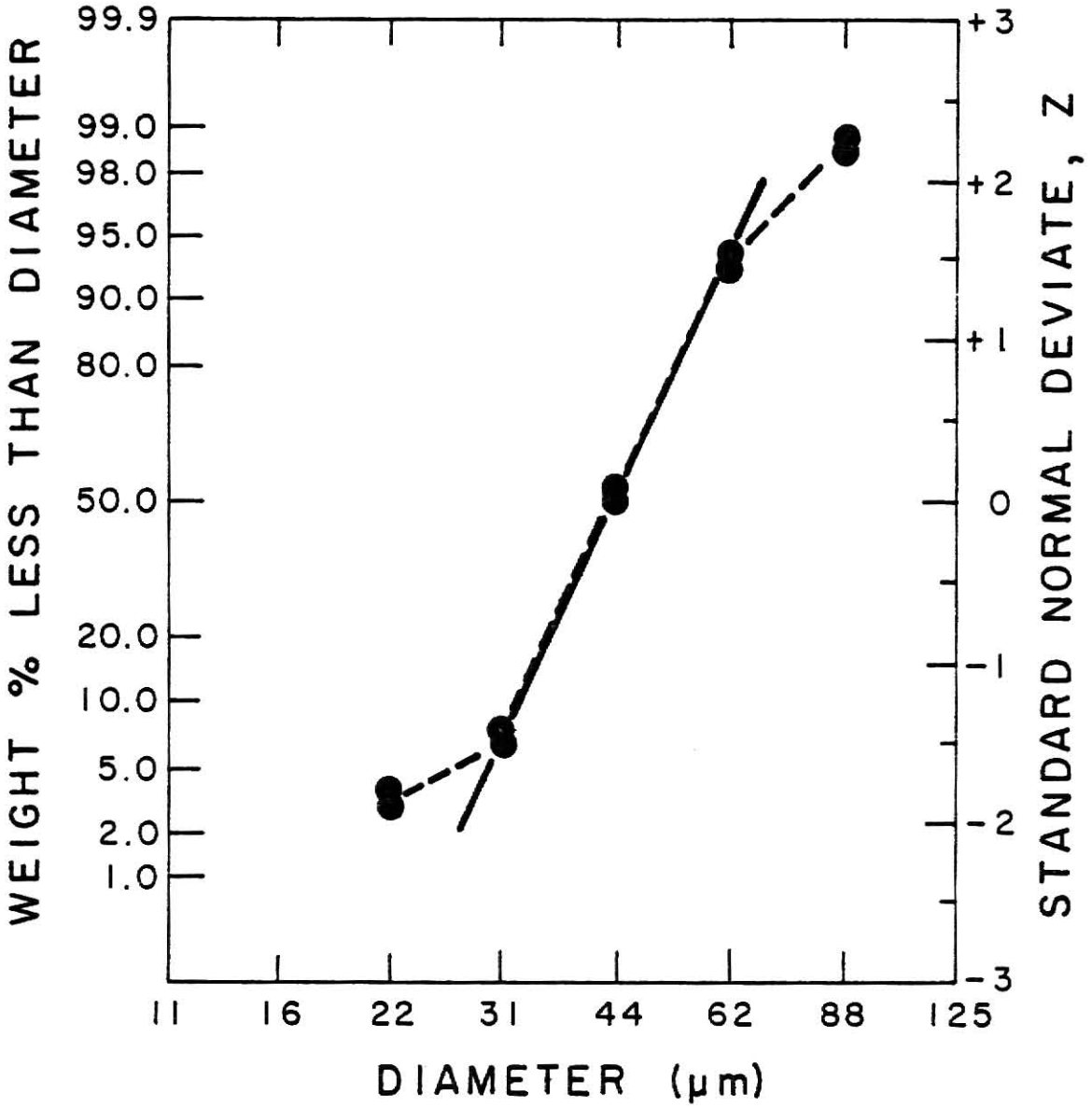

Fig. 3.18 Particle Size Distribution of Wheat Dust, WTAC-S06

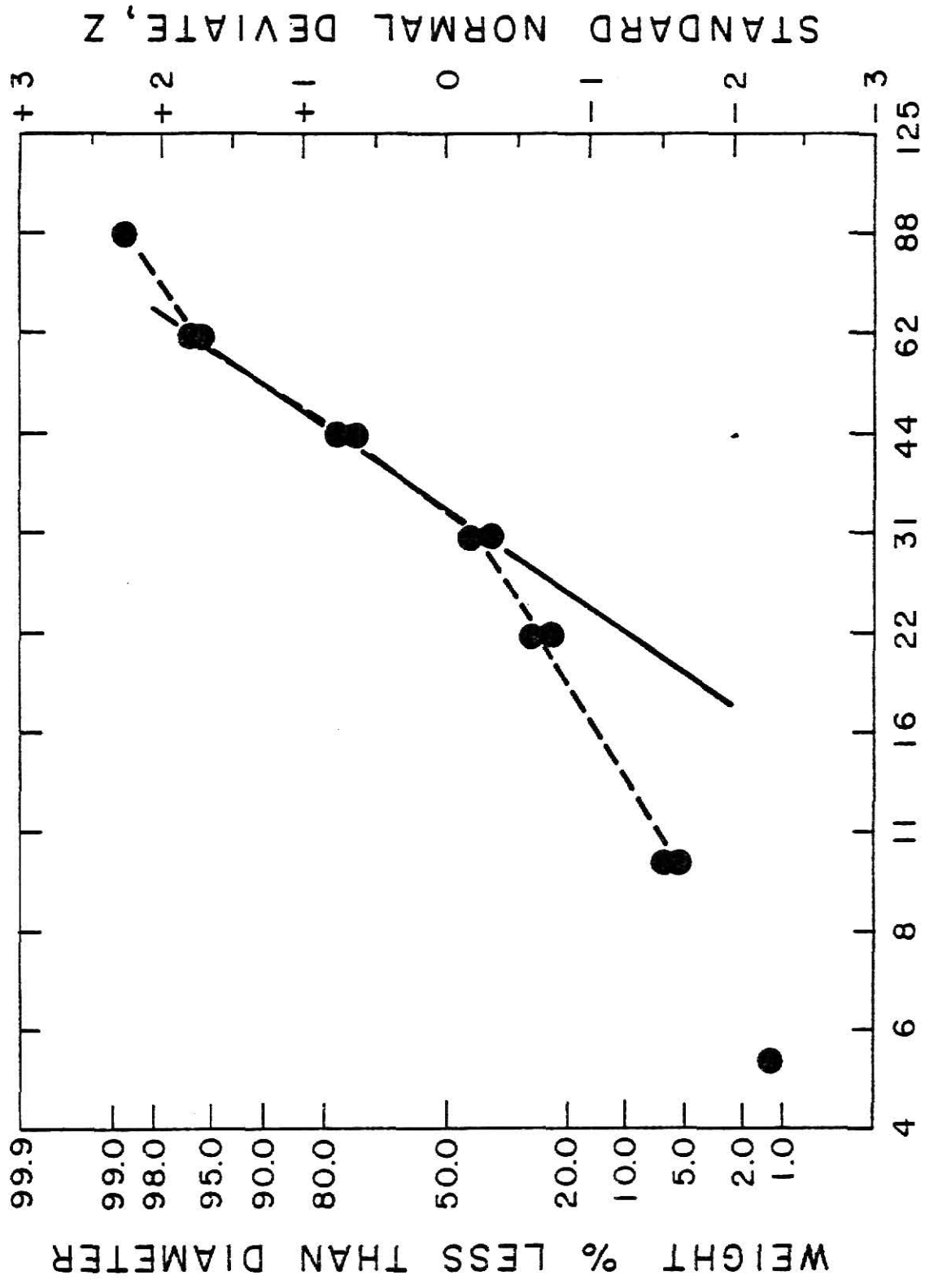

Fig. 3.19 Particle Size Distribution of Wheat Dust, WTAC-S07

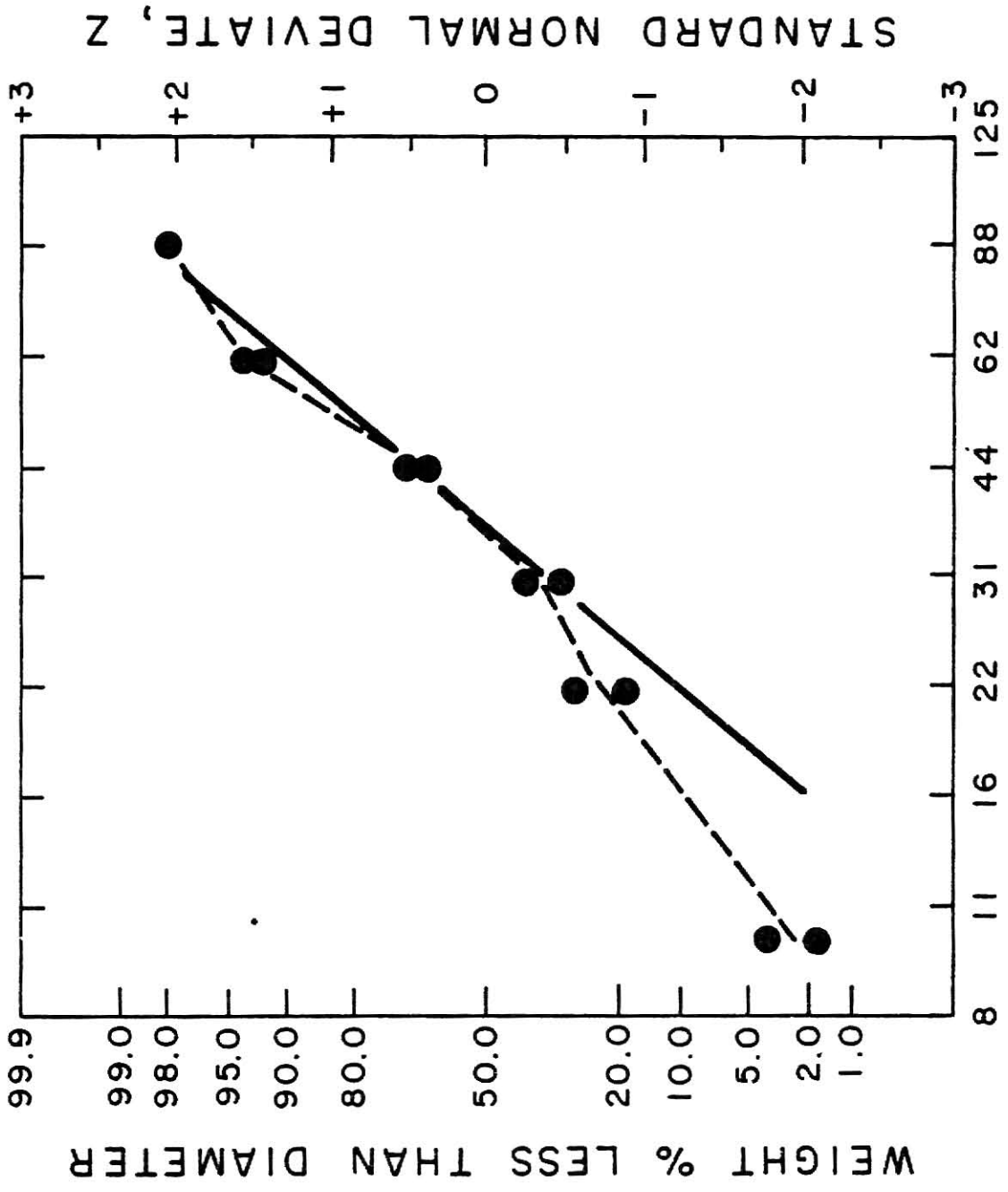

Fig. 3.20 Particle Size Distribution of Wheat Dust, WTAC-S08

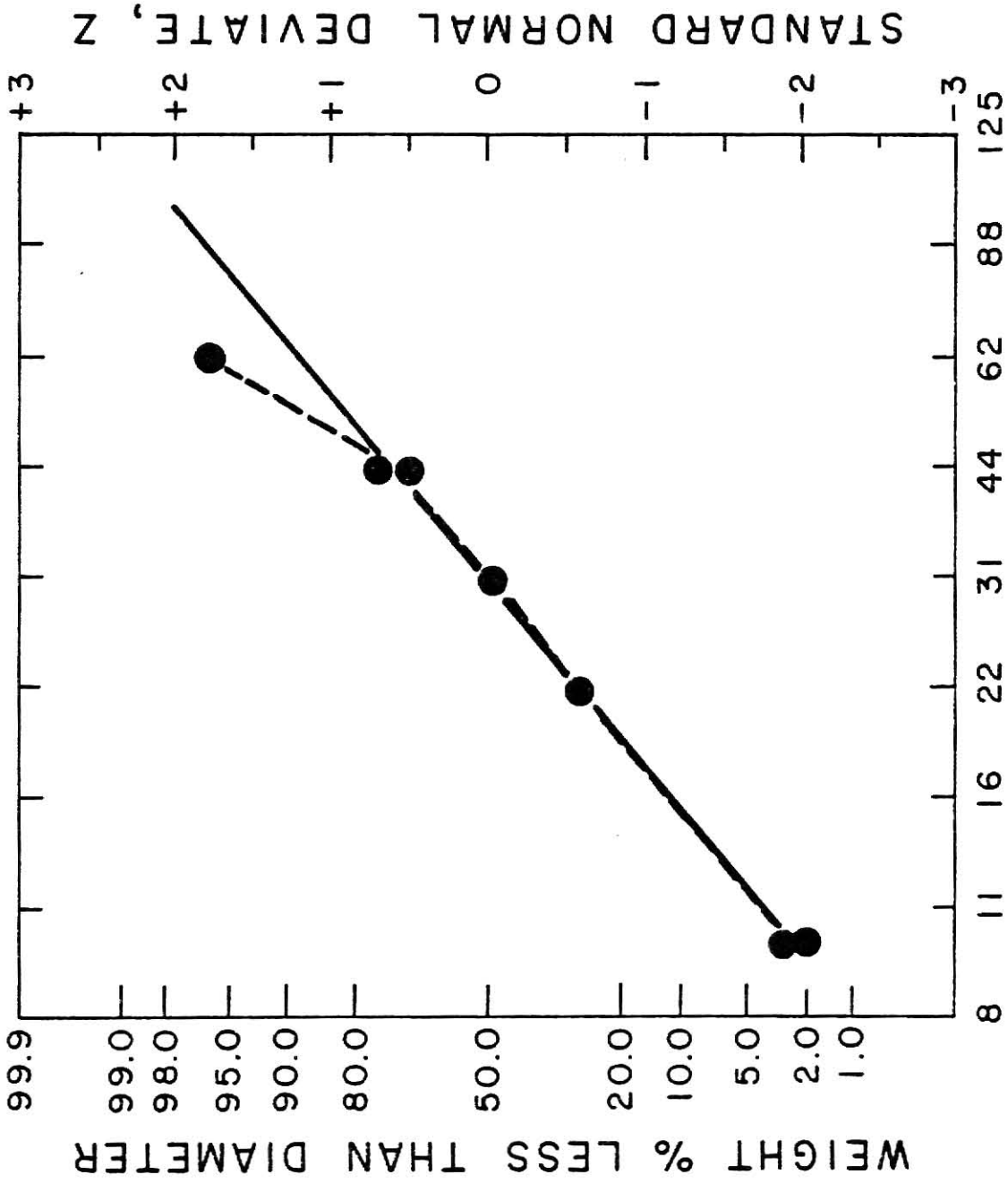

Fig. 3.21 Particle Size Distribution of Wheat Dust, WTAC-S09

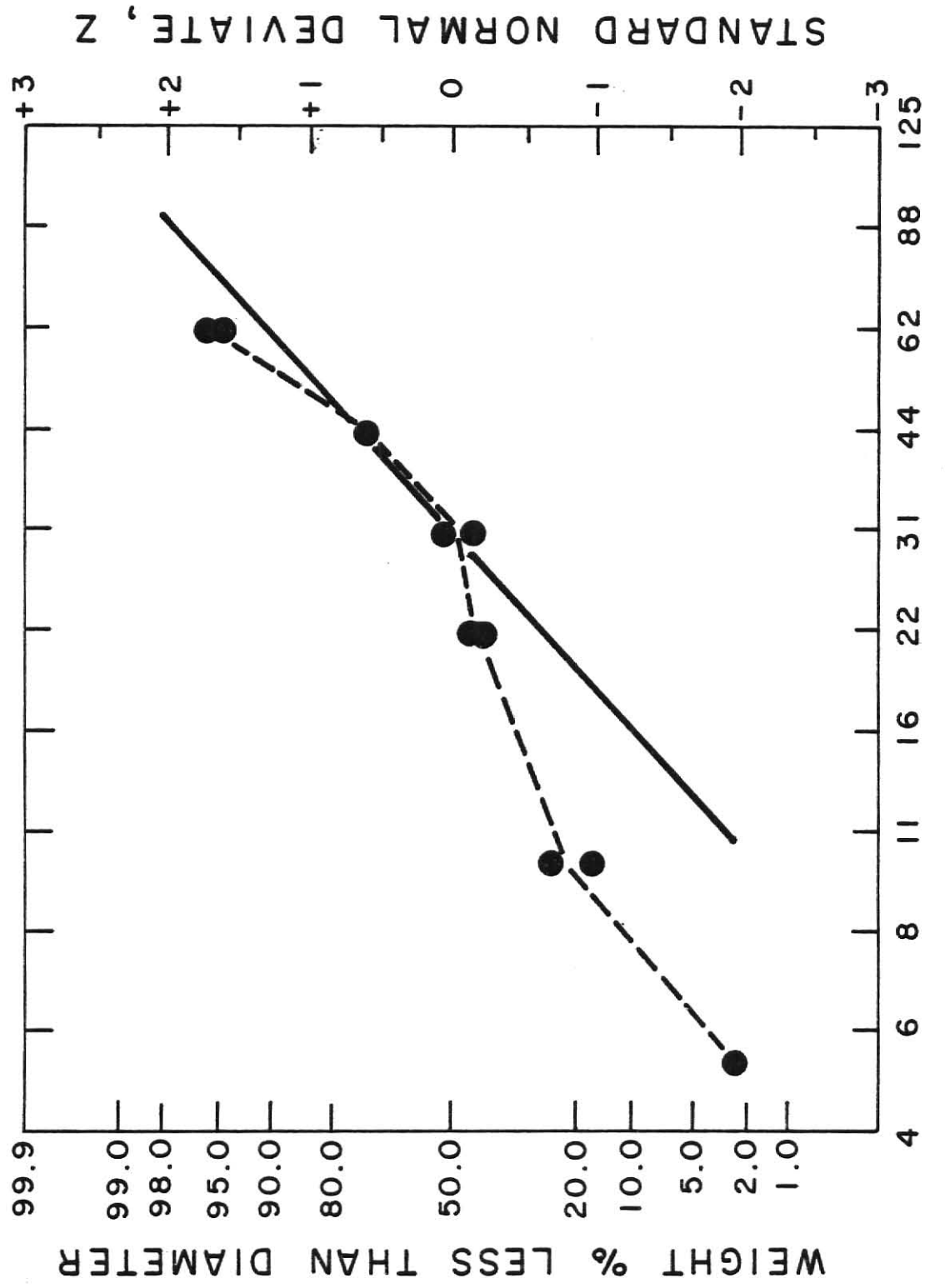

Fig. 3.22 Particle Size Distribution of Wheat Dust, WTAC-S10

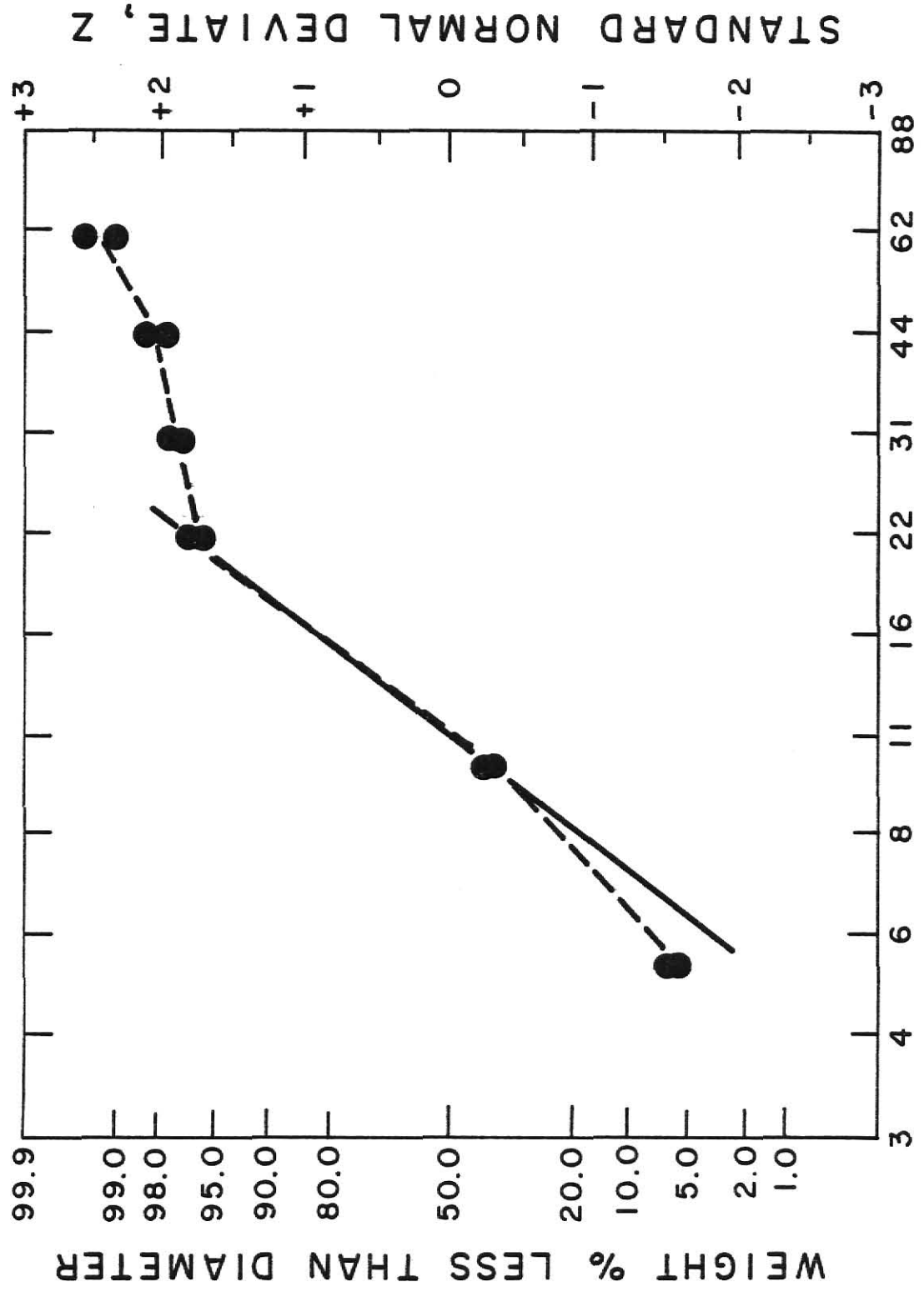

Fig. 2.23 Particle Size Distribution of Corn Dust, CNAC-S01

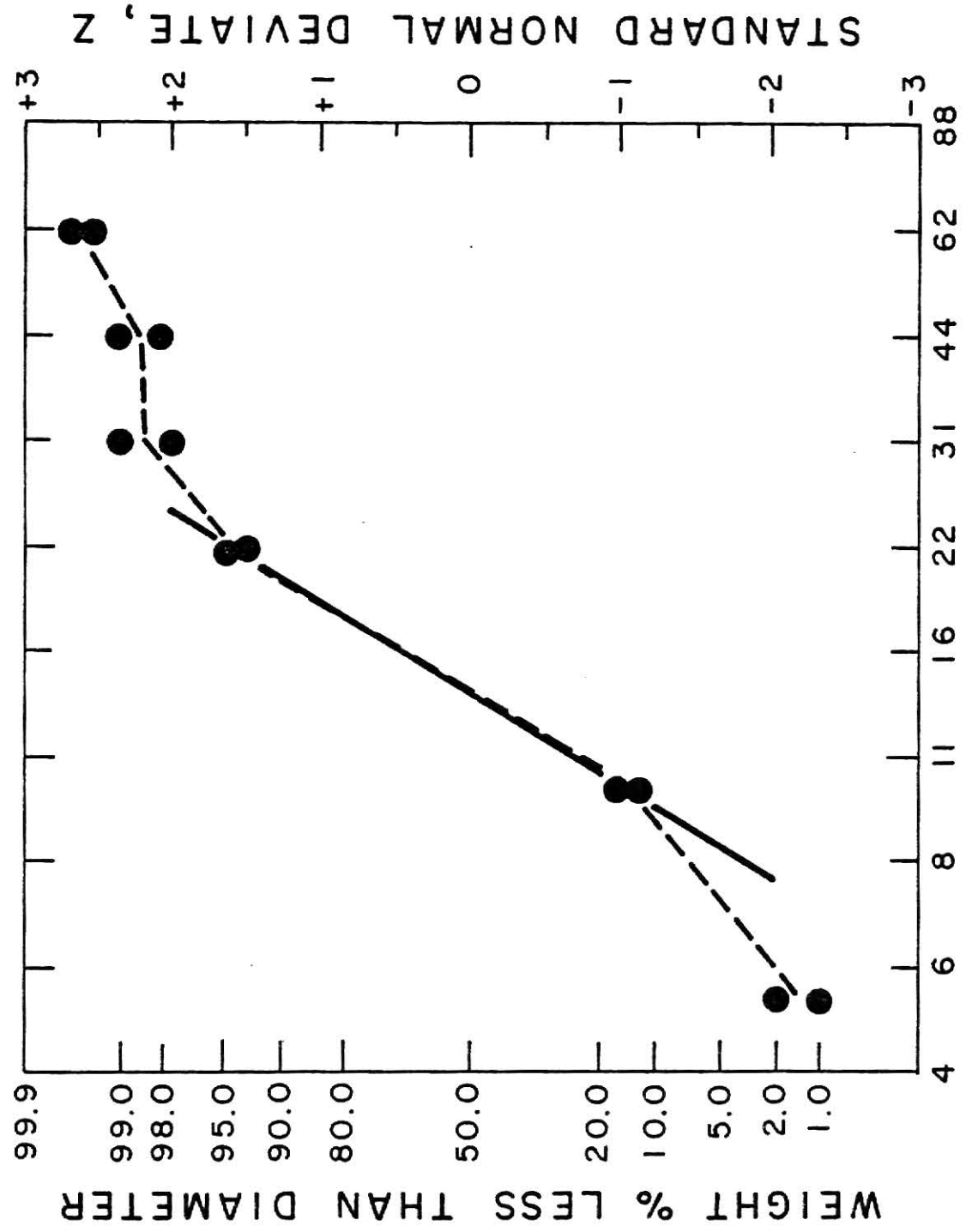

Fig. 3.24 Particle Size Distribution of Corn Dust, CNAC-S02

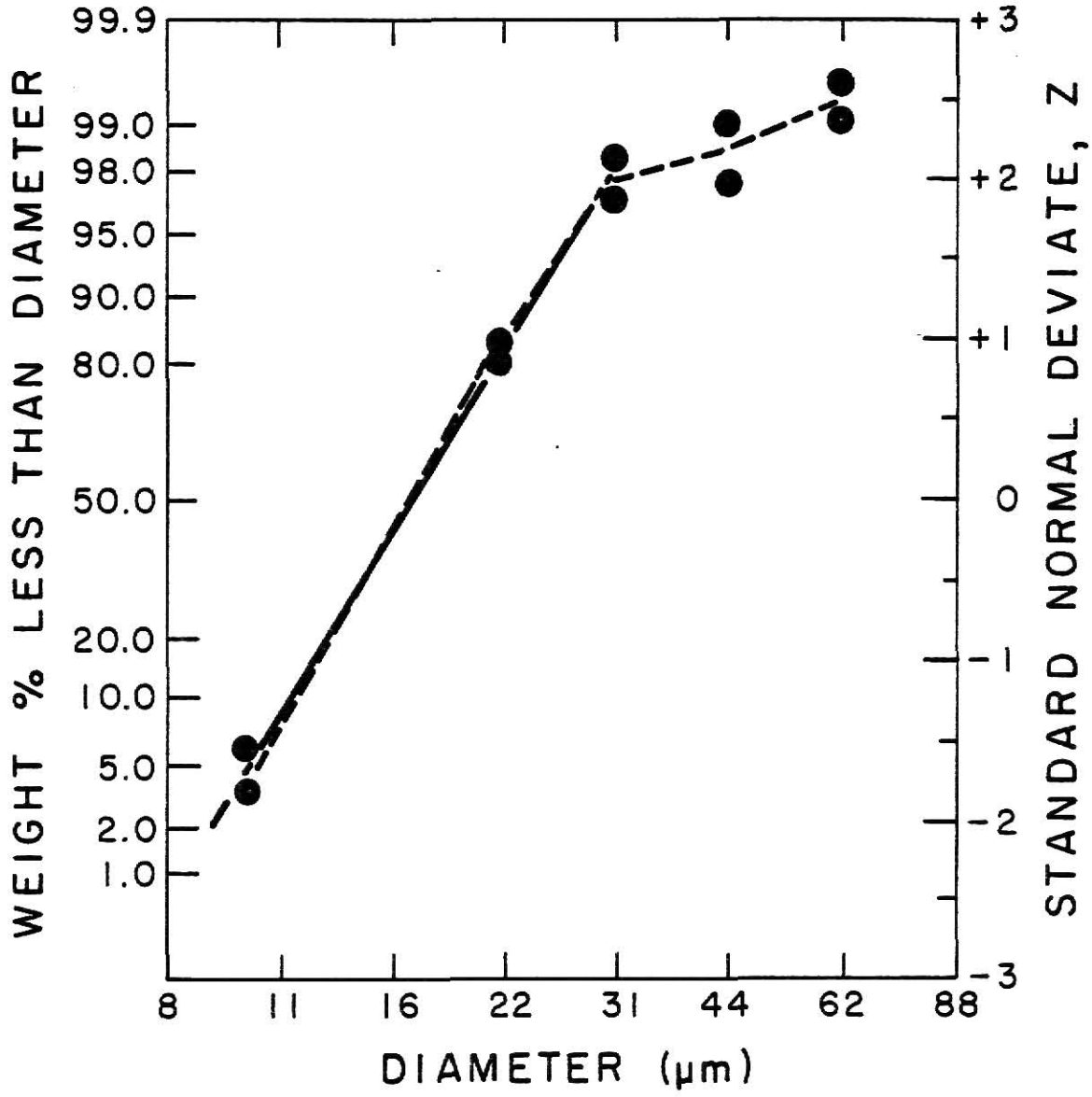

Fig. 3.25 Particle Size Distribution of Corn Dust, CNAC-S03

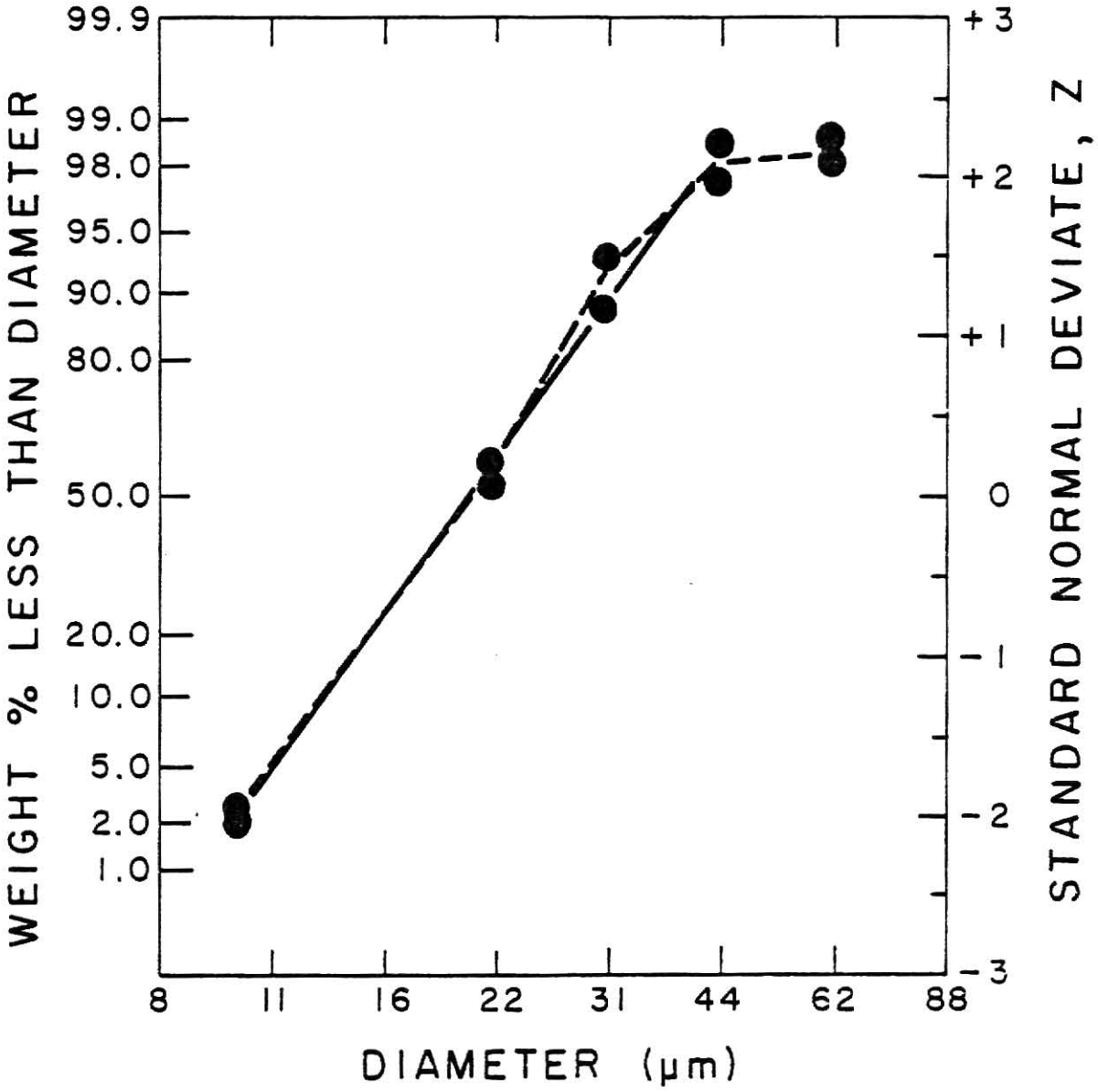

Fig. 3.26 Particle Size Distribution of Corn Dust, CNAC-S04

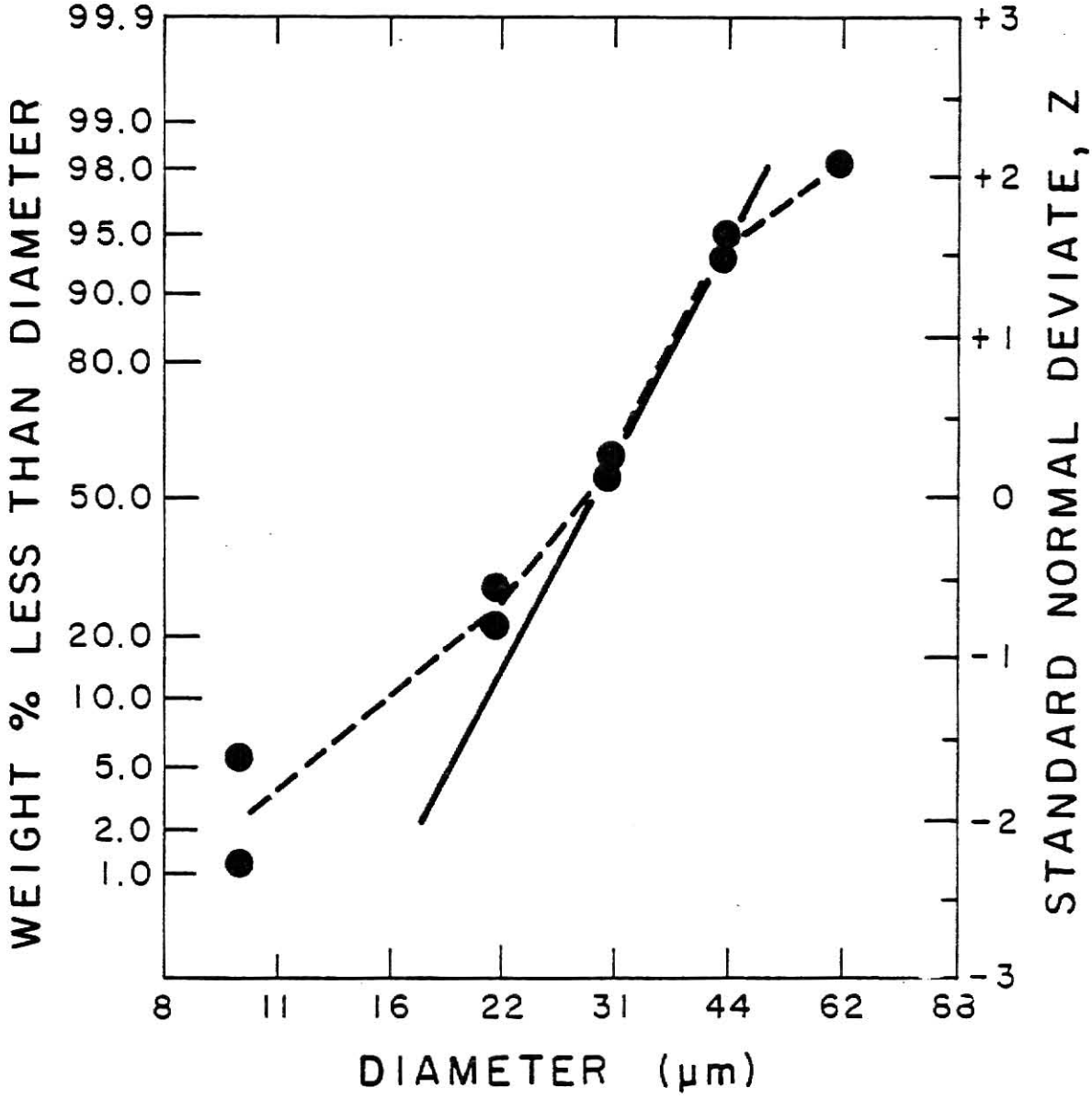

Fig. 3.27 Particle Size Distribution of Corn Dust, CNAC-S05

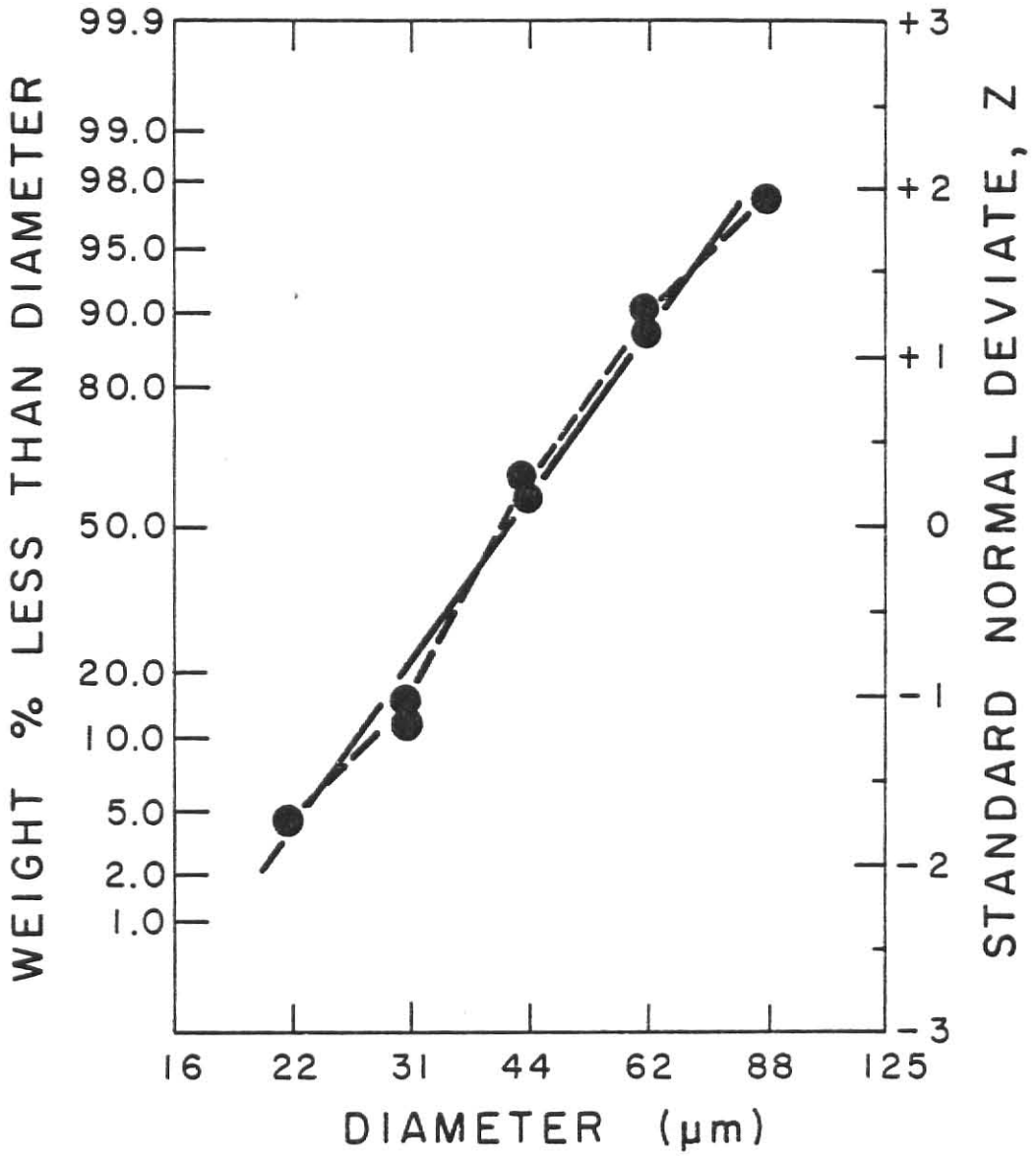

Fig. 3.28 Particle Size Distribution of Corn Dust, CNAC-S06

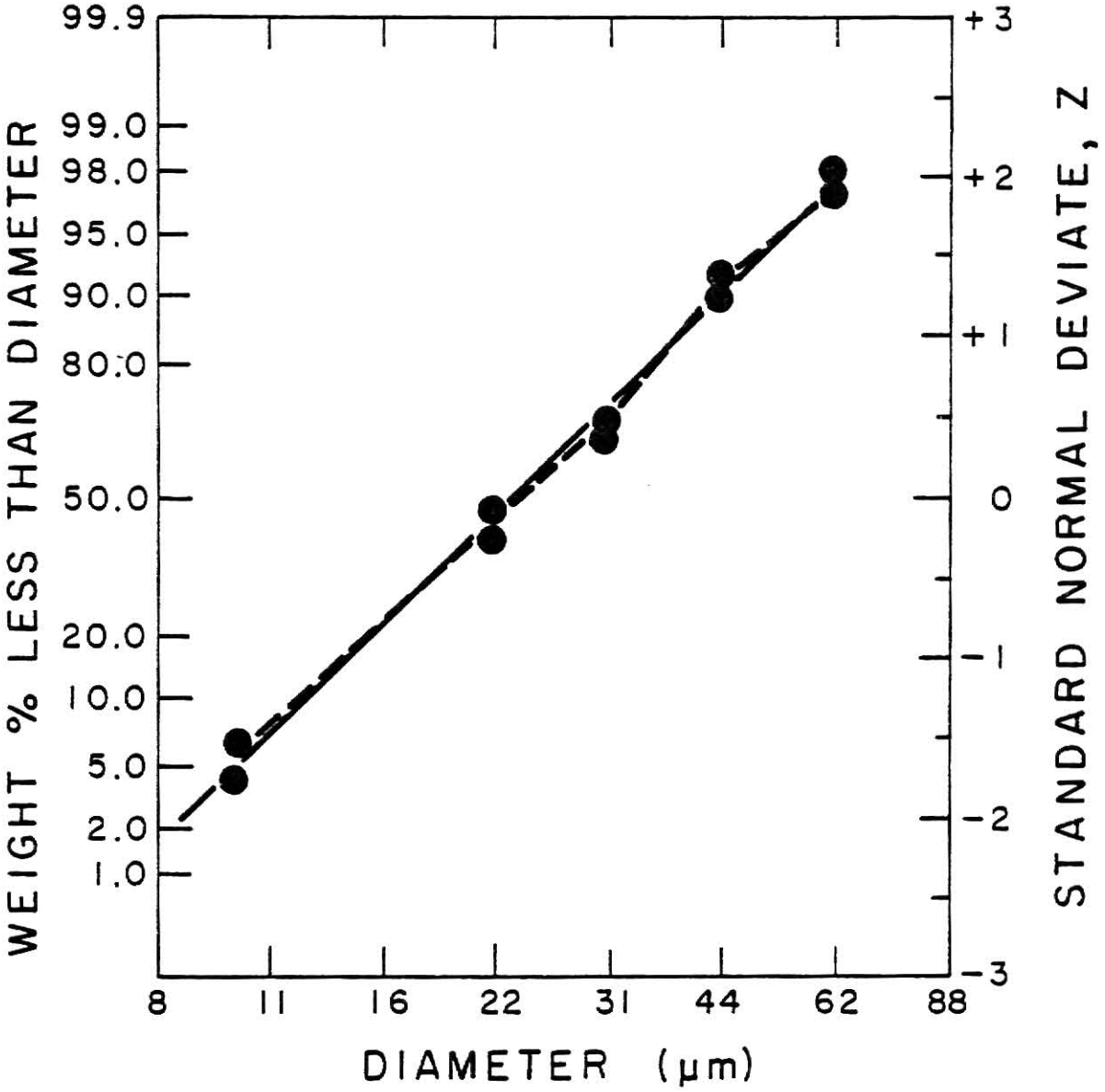

Fig. 3.29 Particle Size Distribution of Corn Dust, CNAC-S07

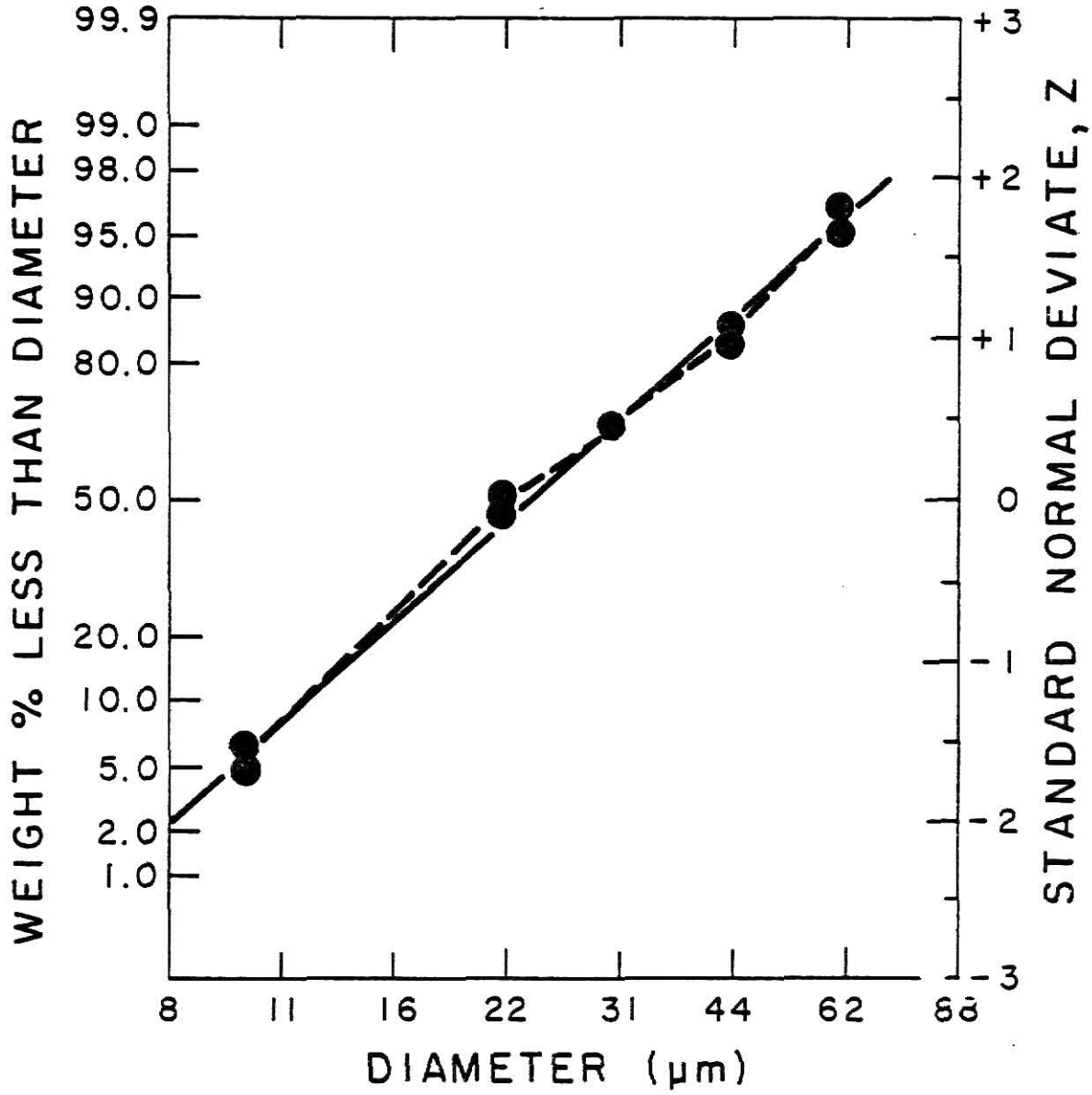

Fig. 3.30 Particle Size Distribution of Corn Dust, CNAC-S08

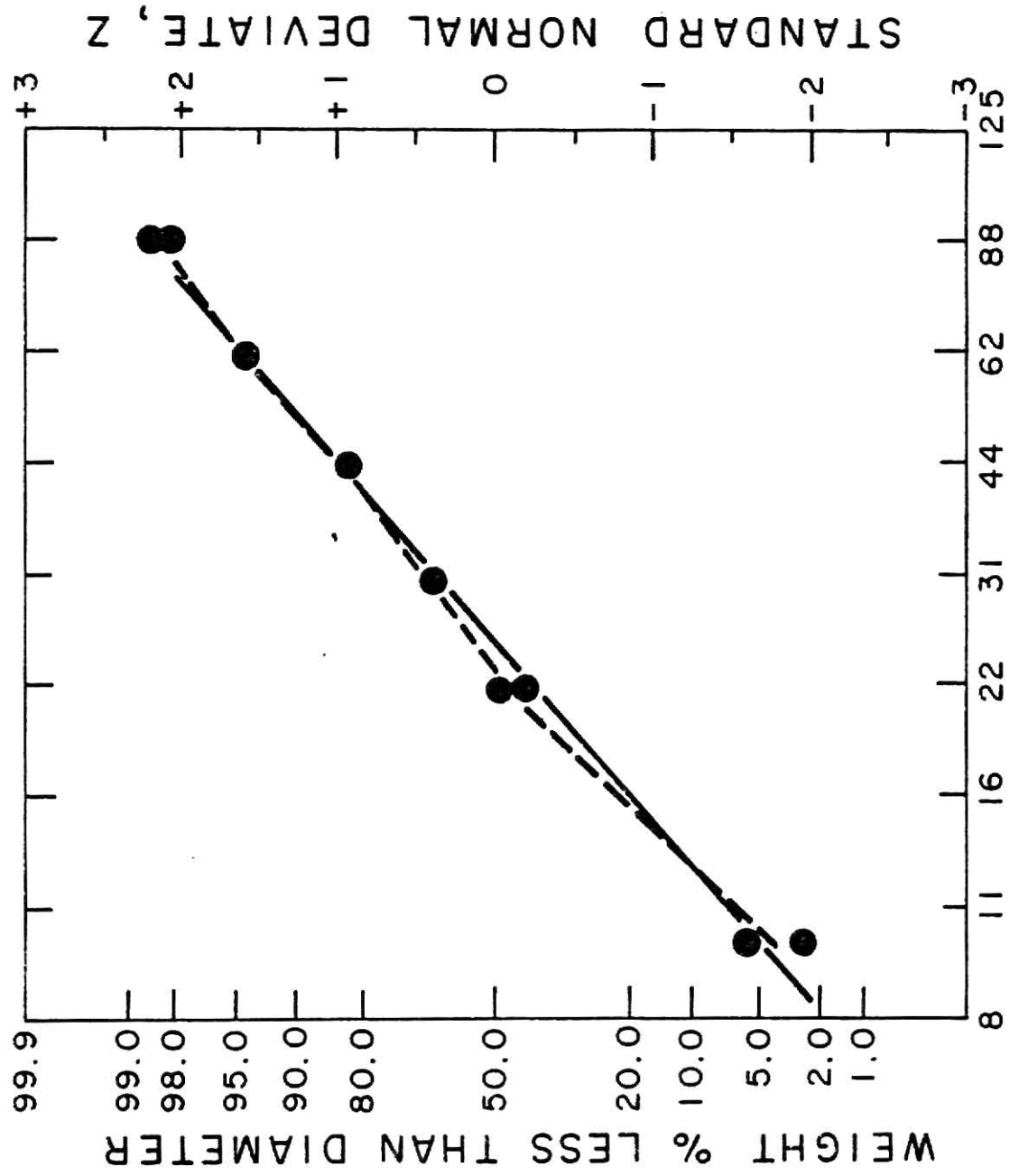

Fig. 3.31 Particle Size Distribution of Corn Dust, CNAC-S09

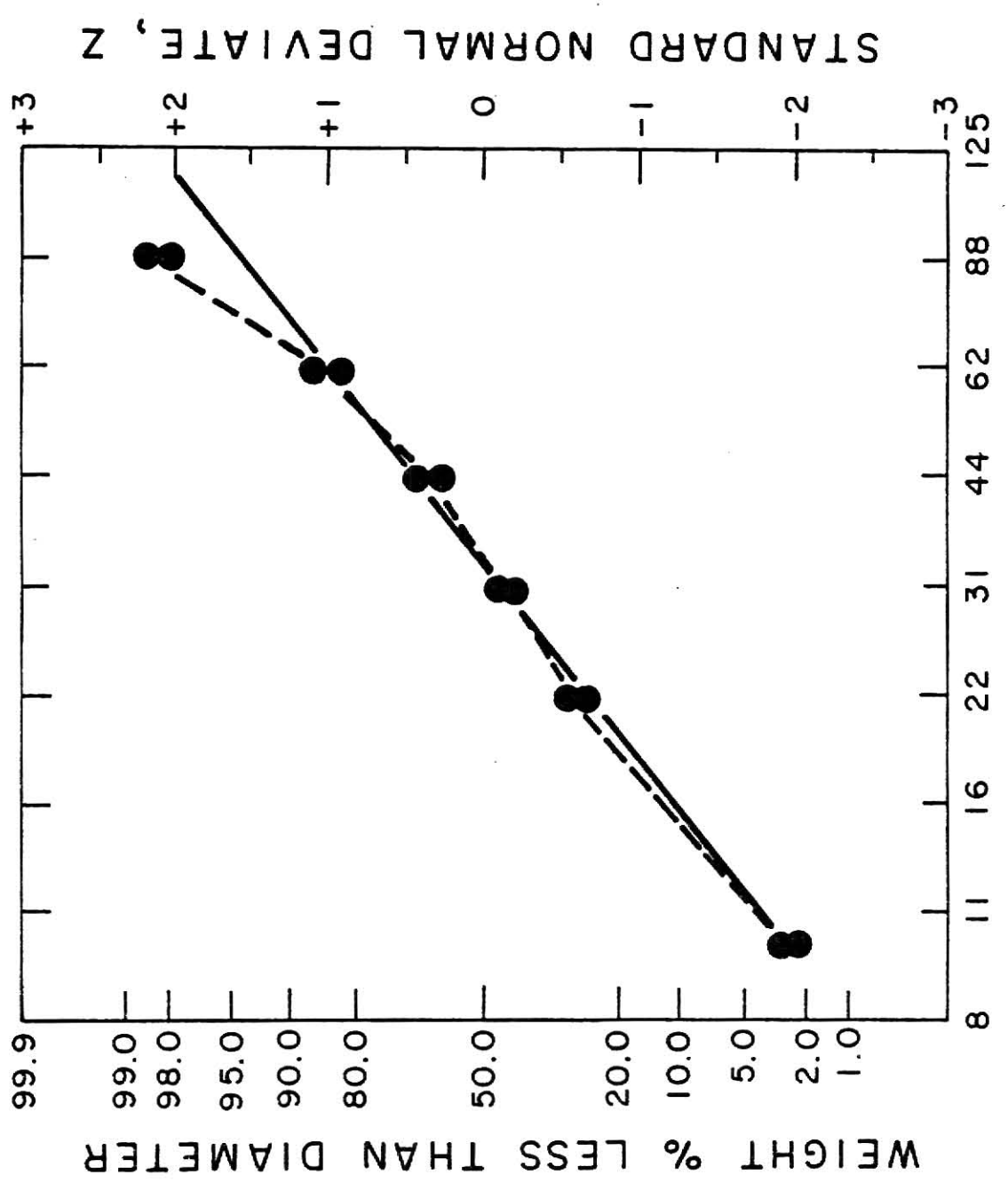

Fig. 3.32 Particle Size Distribution of Corn Dust, CNAC-S10

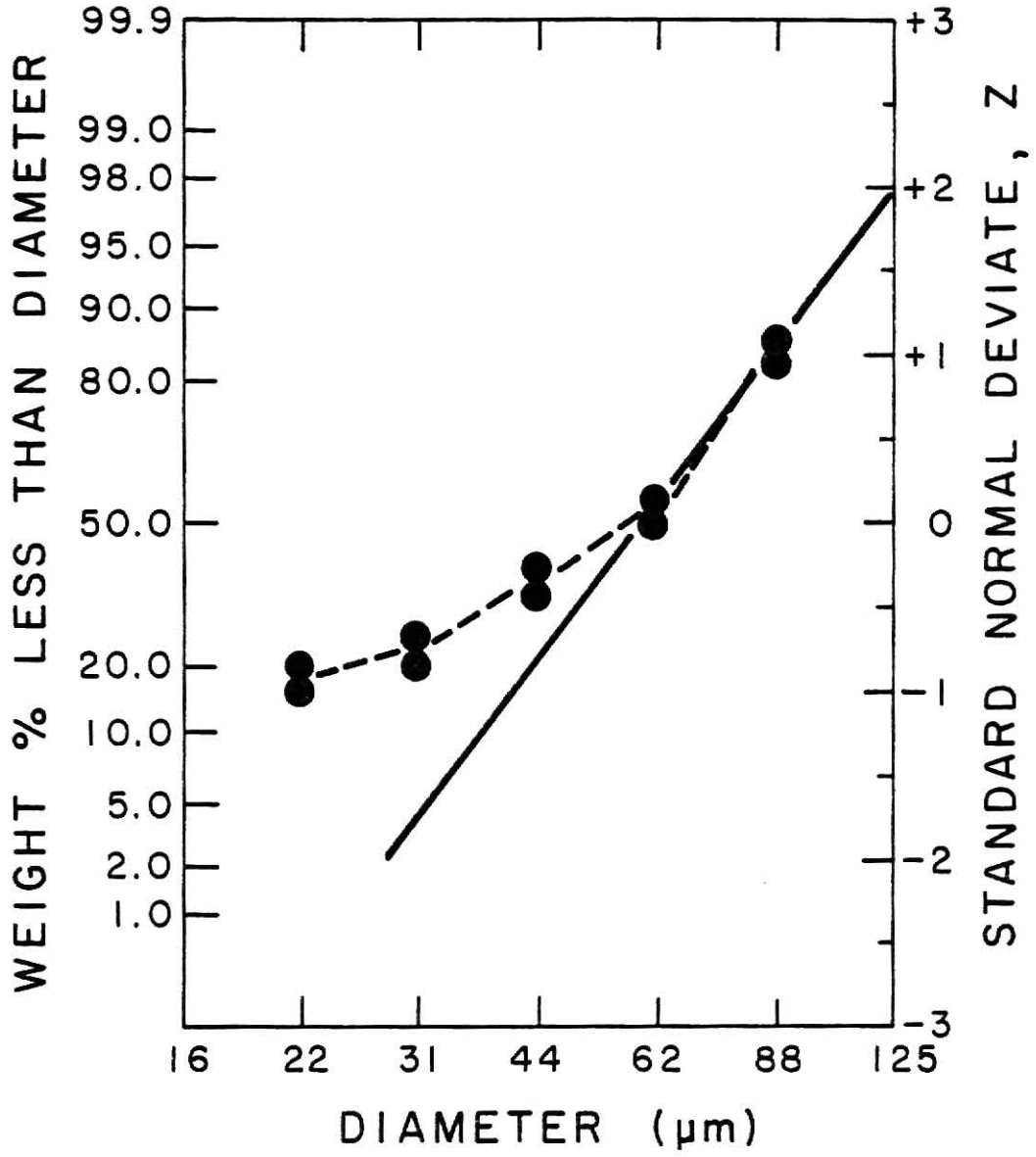

Fig. 3.33 Particle Size Distribution of Corn Dust, CNAC-S11

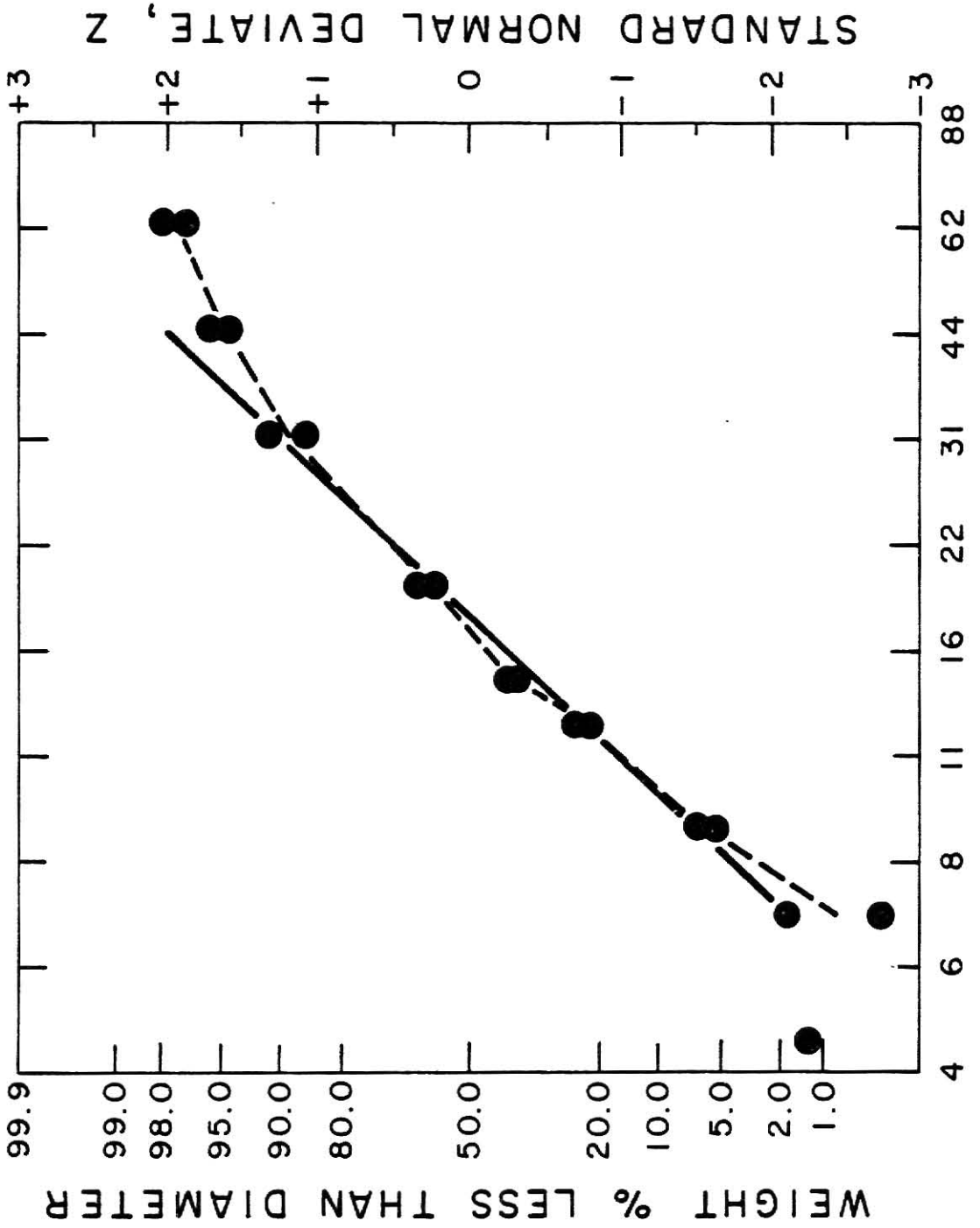

Fig. 3.34 Particle Size Distribution of Cornstarch, CSAC-SO2

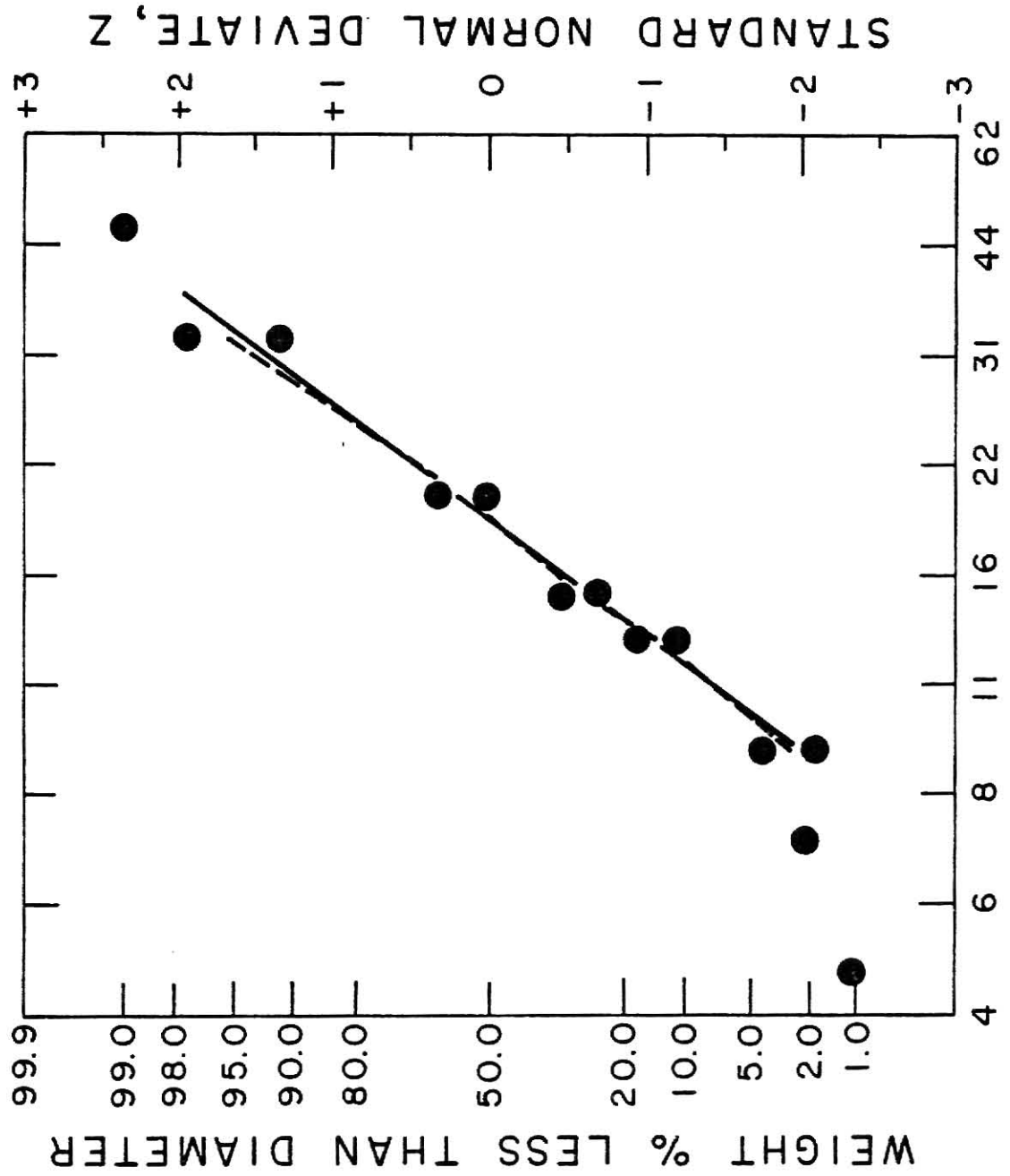

Fig. 3.35 Particle Size Distribution of Cornstarch, CSAC-S03

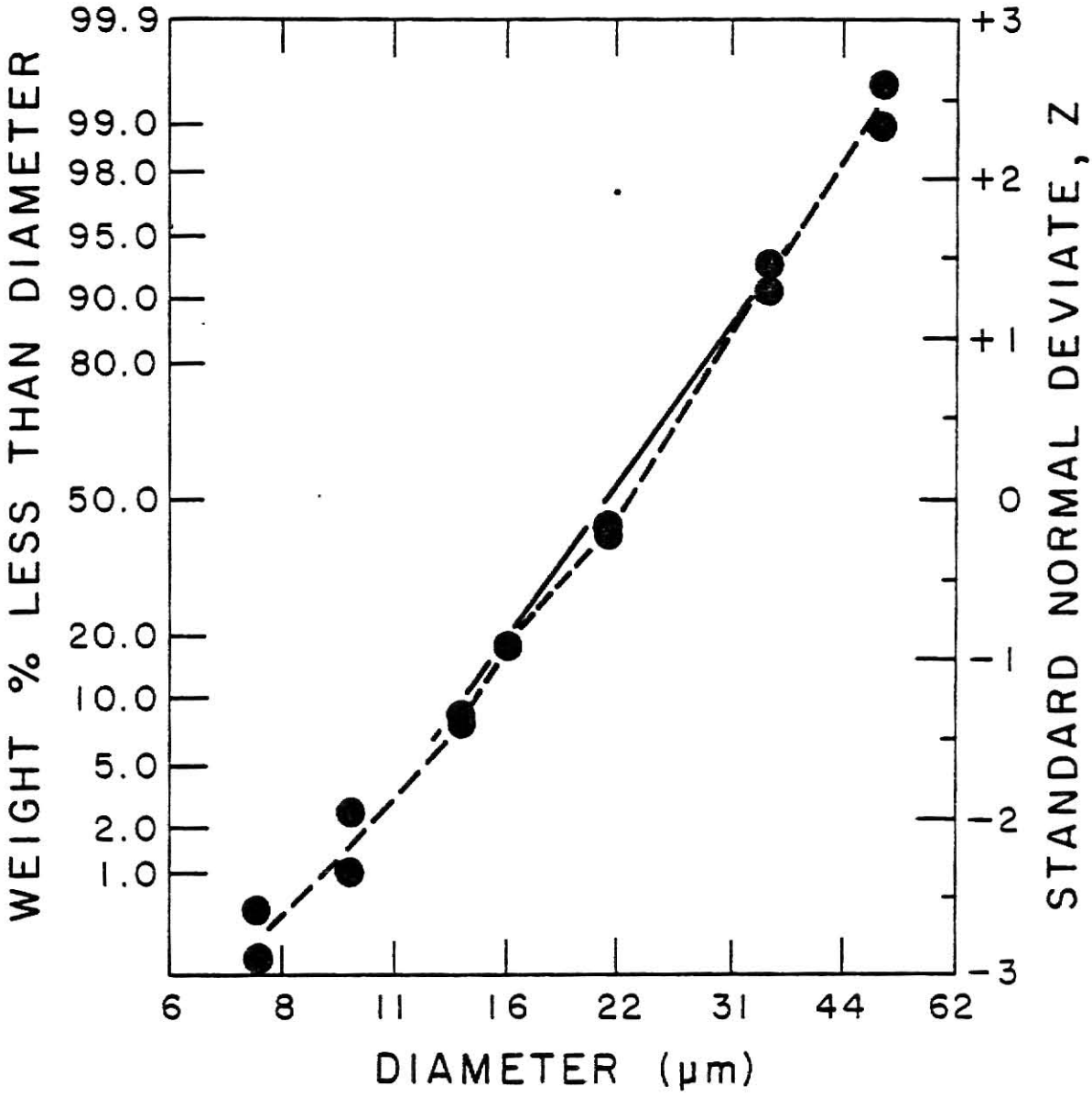

Fig. 3.36 Particle Size Distribution of Cornstarch, CSAC-S04

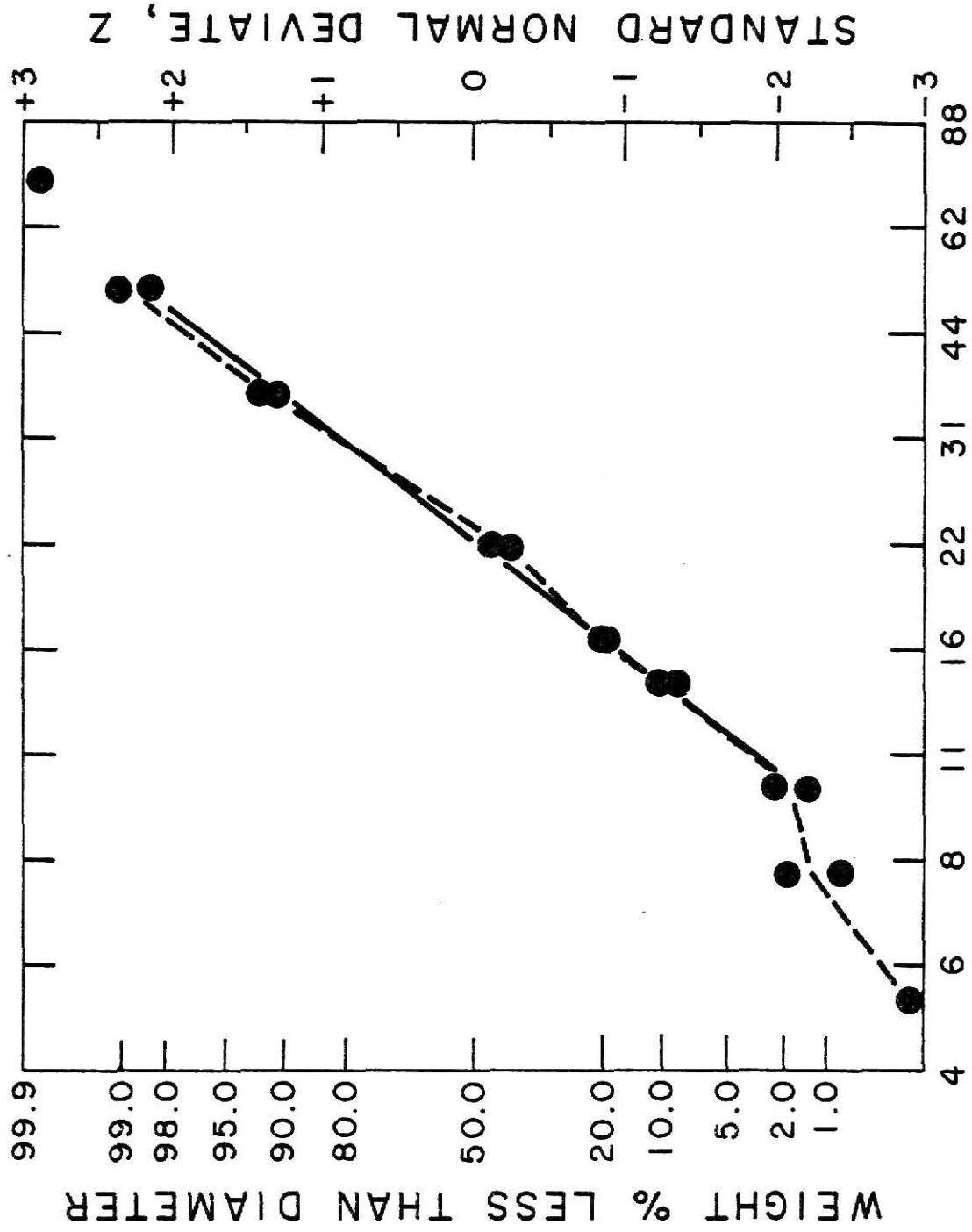

Fig. 3.37 Particle Size Distribution of Cornstarch, CSAC-S05

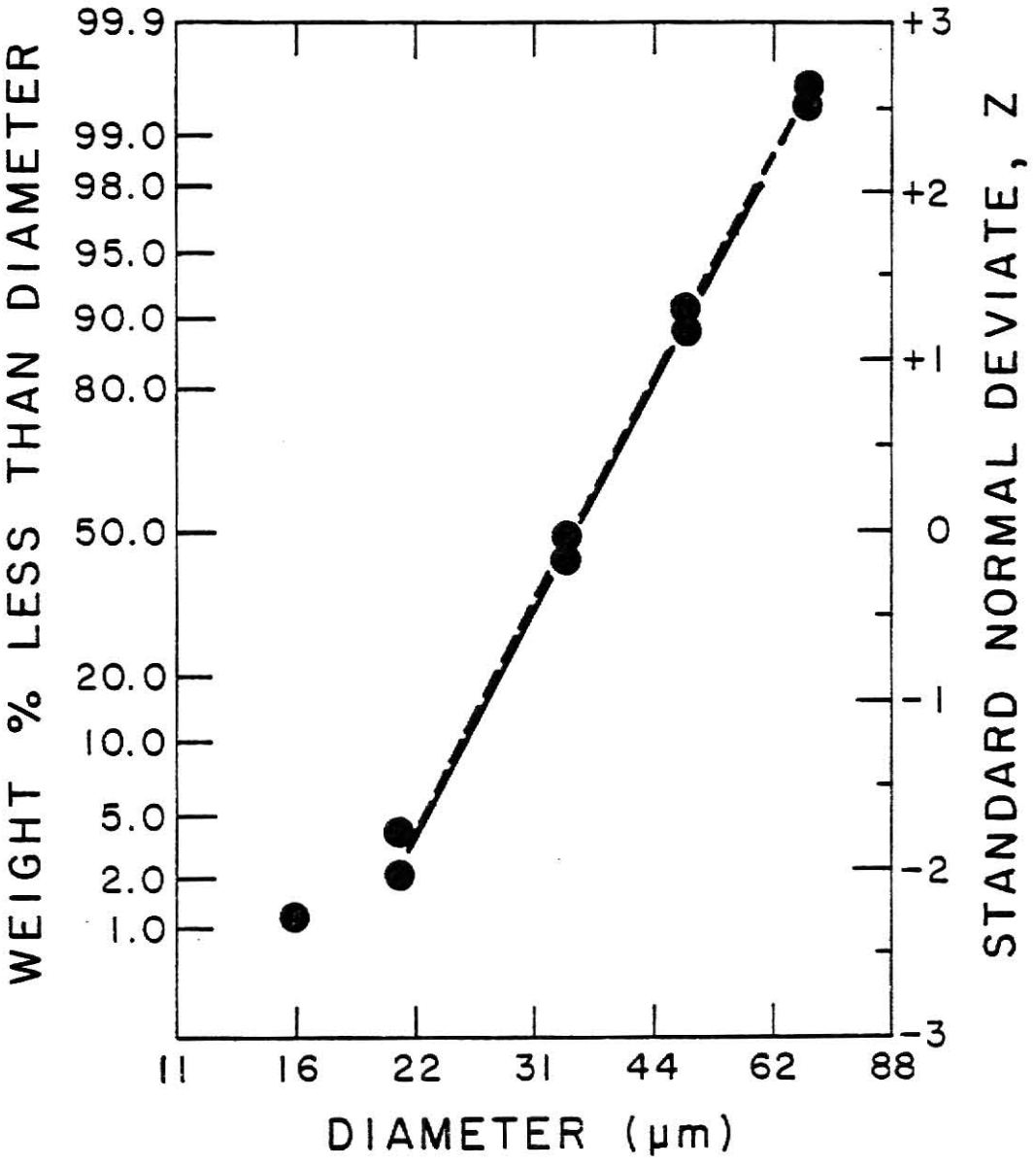

Fig. 3.38 Particle Size Distribution of Cornstarch, CSAC-S06

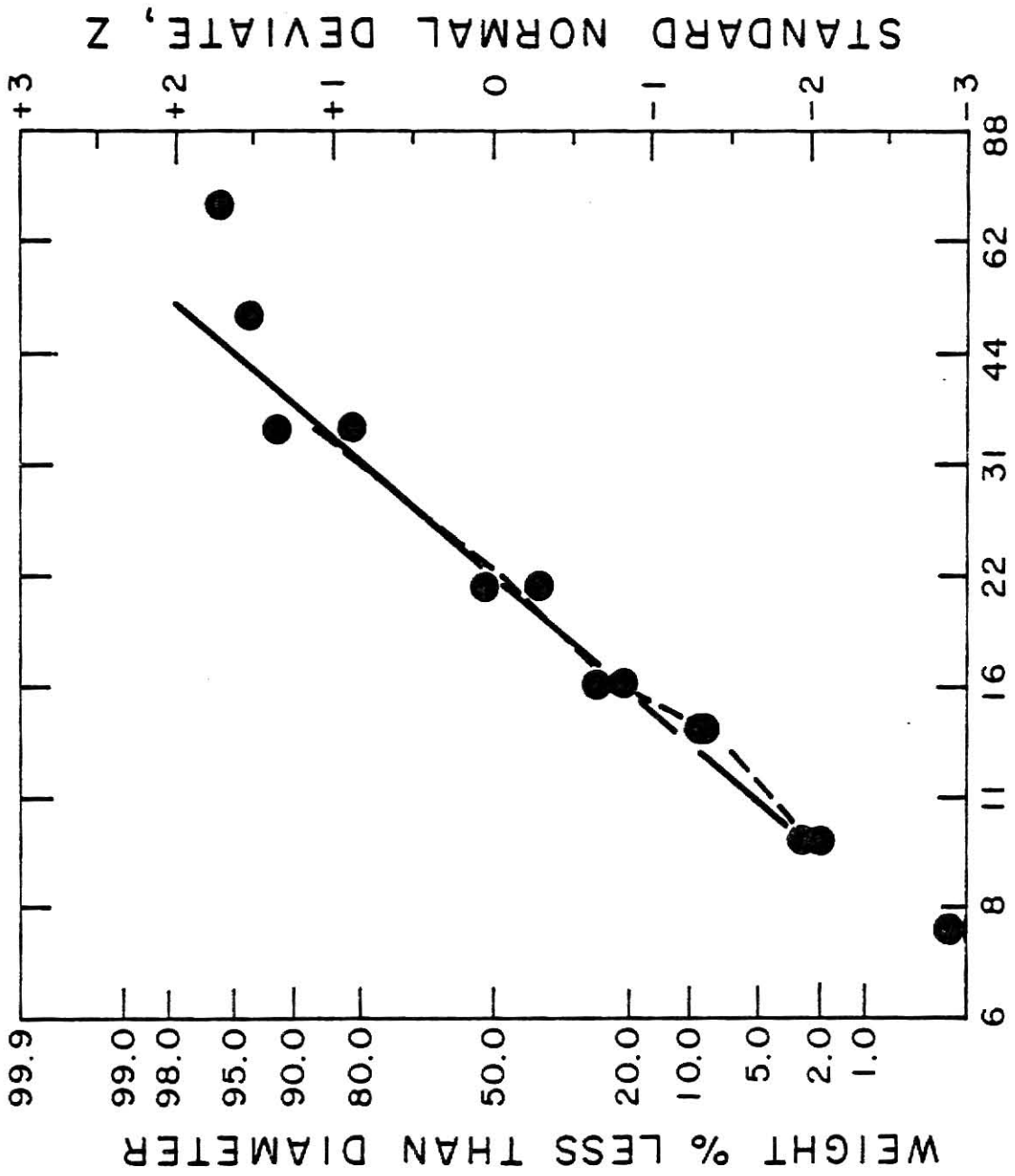

Fig. 3.39 Particle Size Distribution of Cornstarch, CSAC-F01

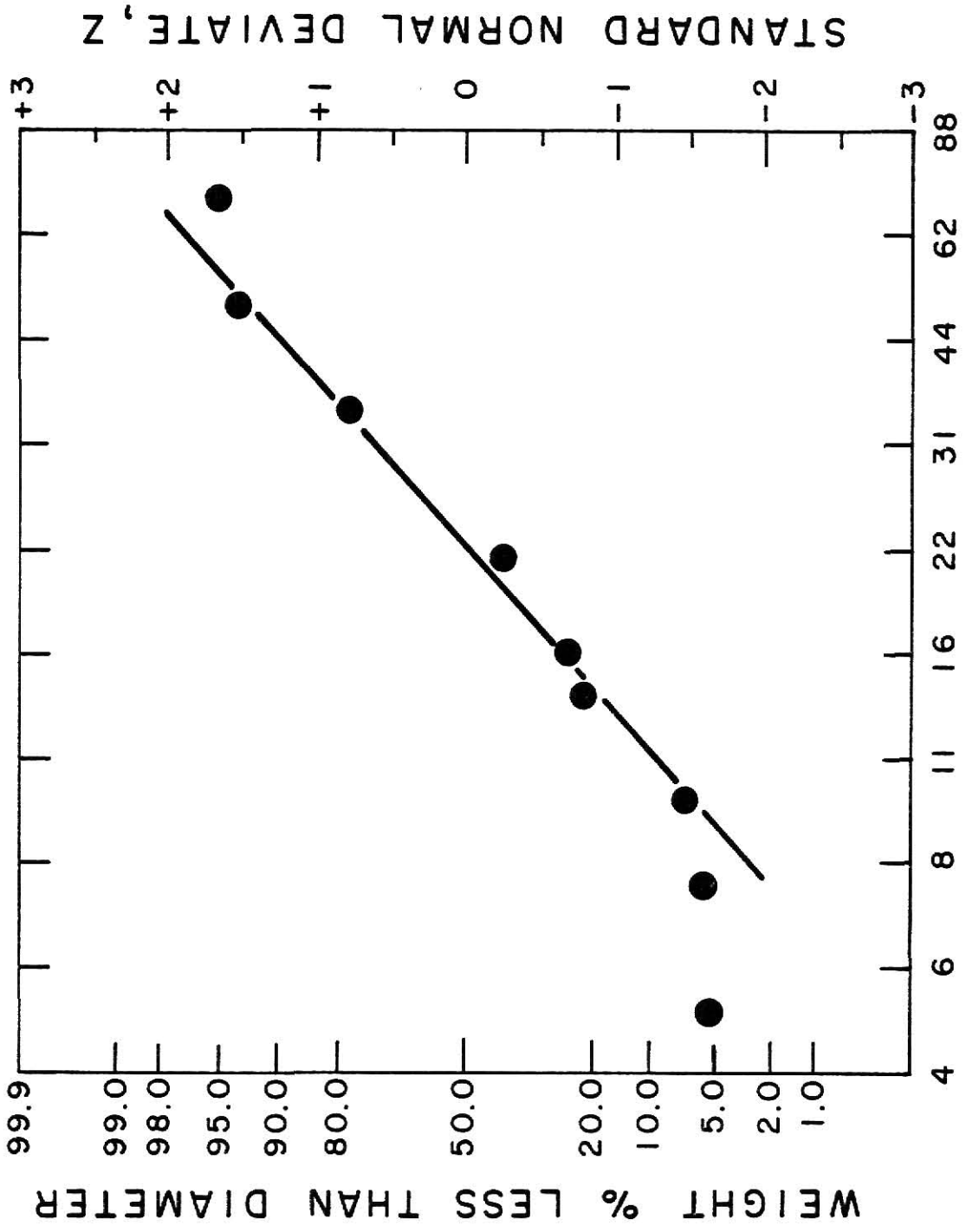

Fig. 3.40 Particle Size Distribution of Cornstarch, CSAC-F02

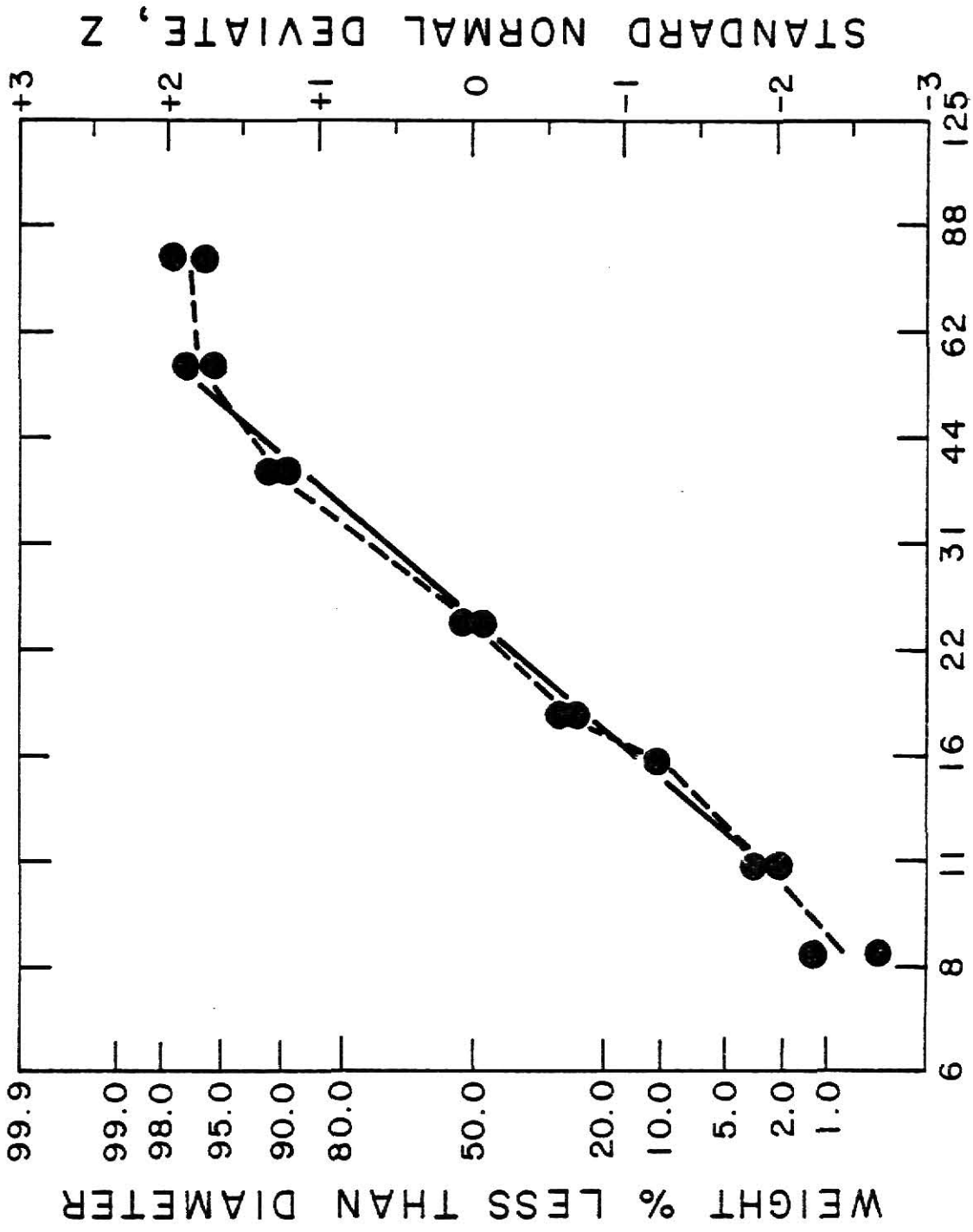

Fig. 3.41 Particle Size Distribution of Cornstarch, CSAC-F03

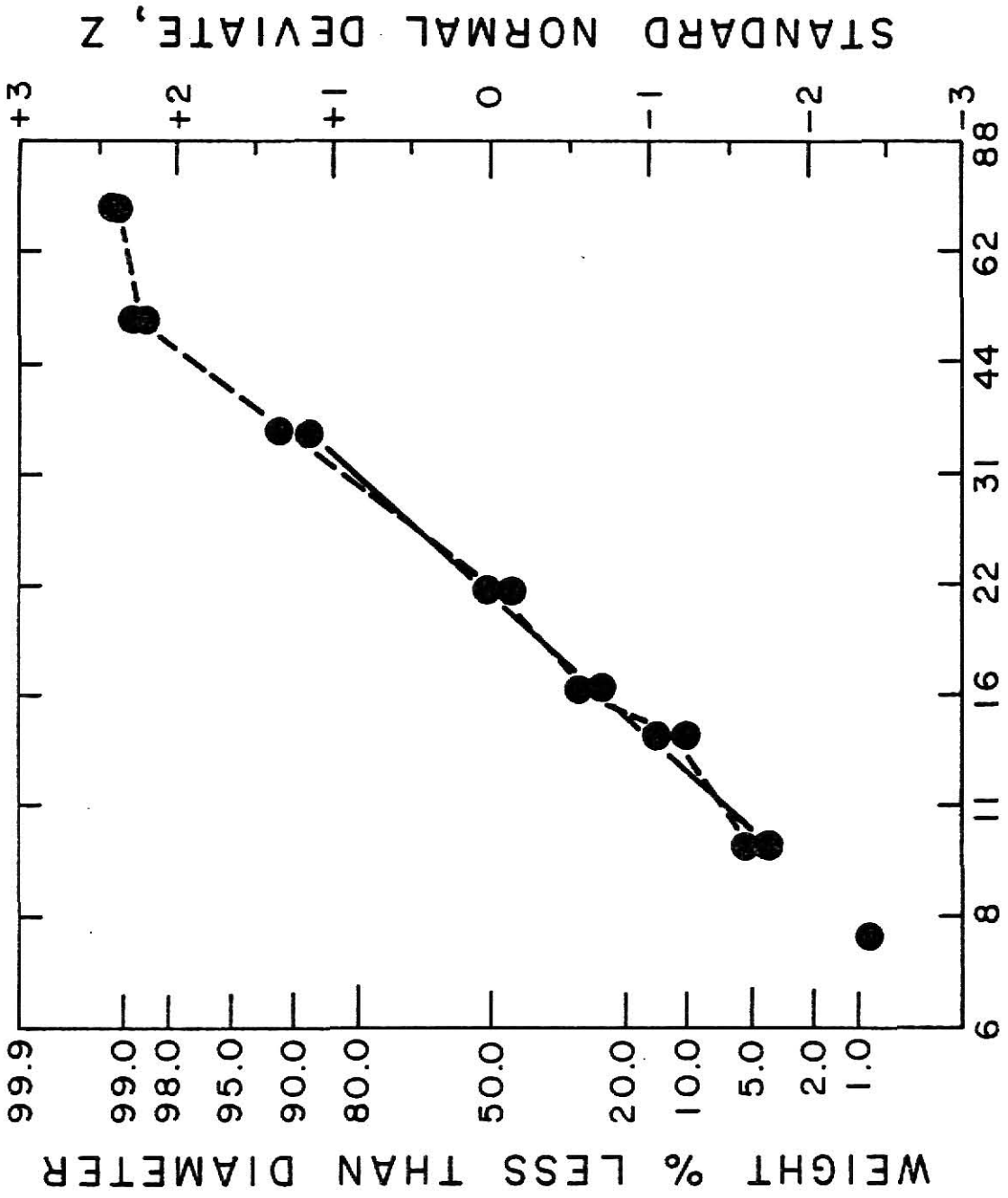

Fig. 3.42 Particle Size Distribution of Cornstarch, CSAC-F04

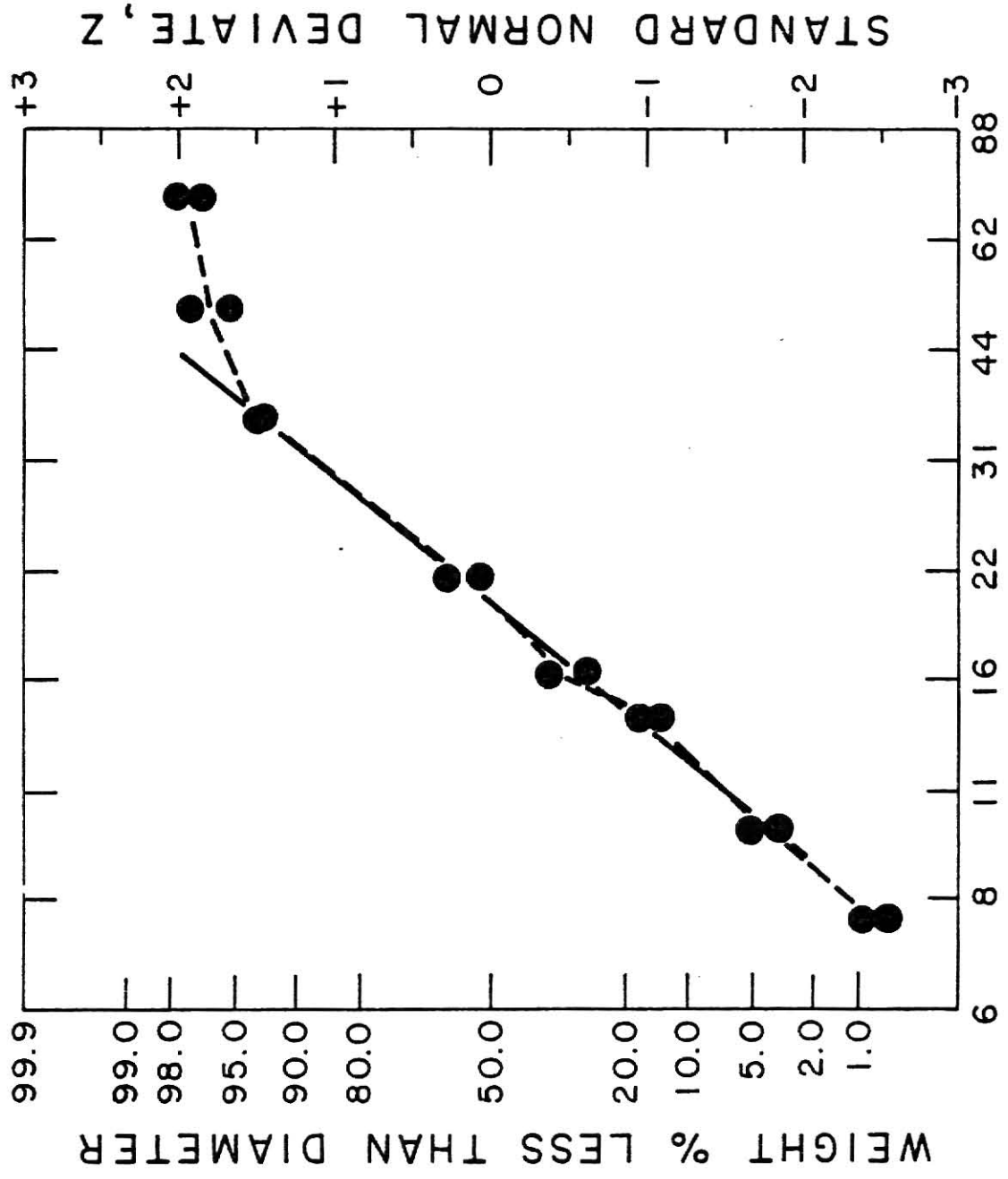

Fig. 3.43 Particle Size Distribution of Cornstarch, CSAC-F05

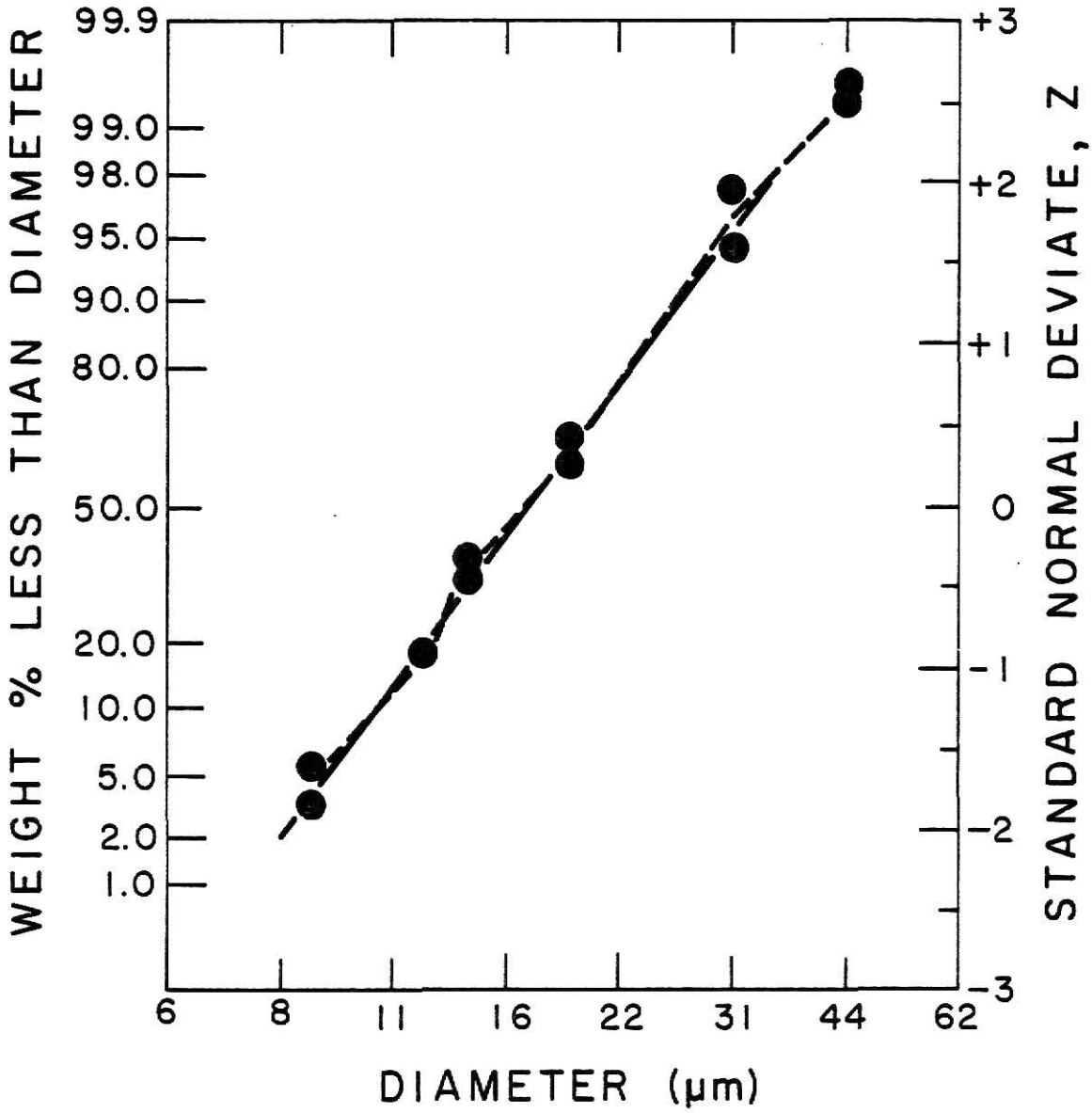

Fig. 3.44 Particle Size Distribution of Cornstarch, CSAC-F06

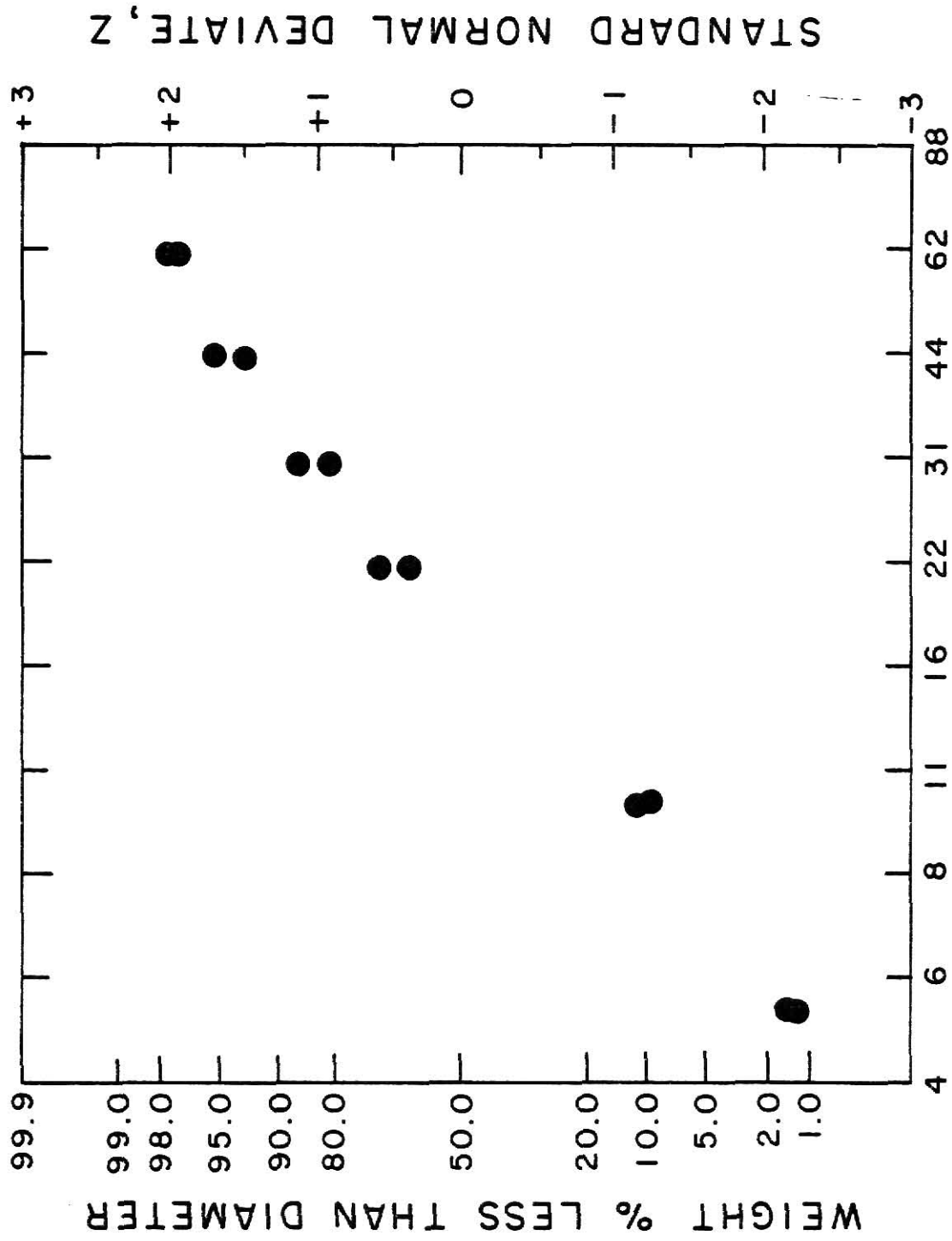

Fig. 3.45 Particle Size Distribution of Corn Dust

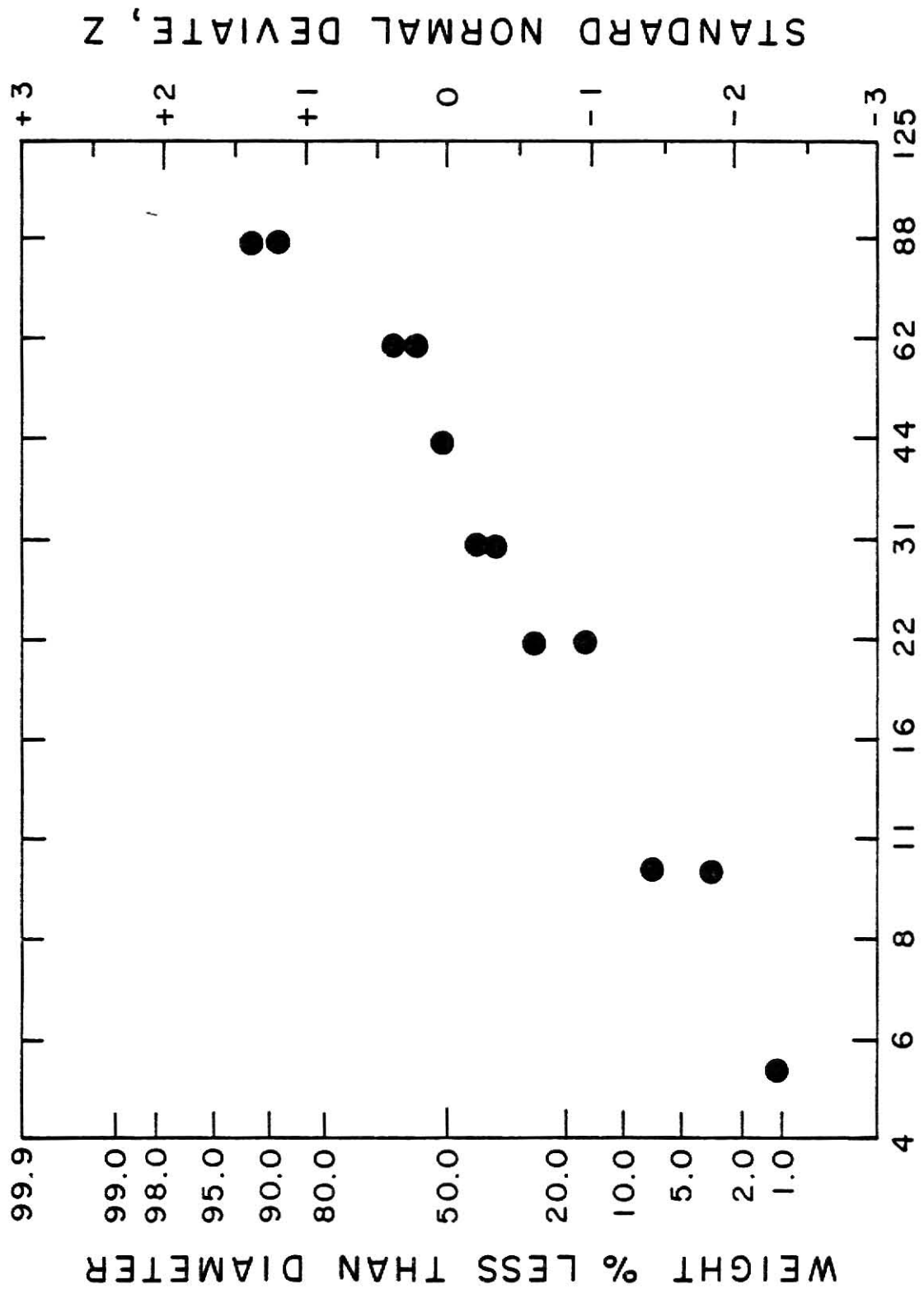

Fig. 3.46 Particle Size Distribution of Grain Sorghum Dust

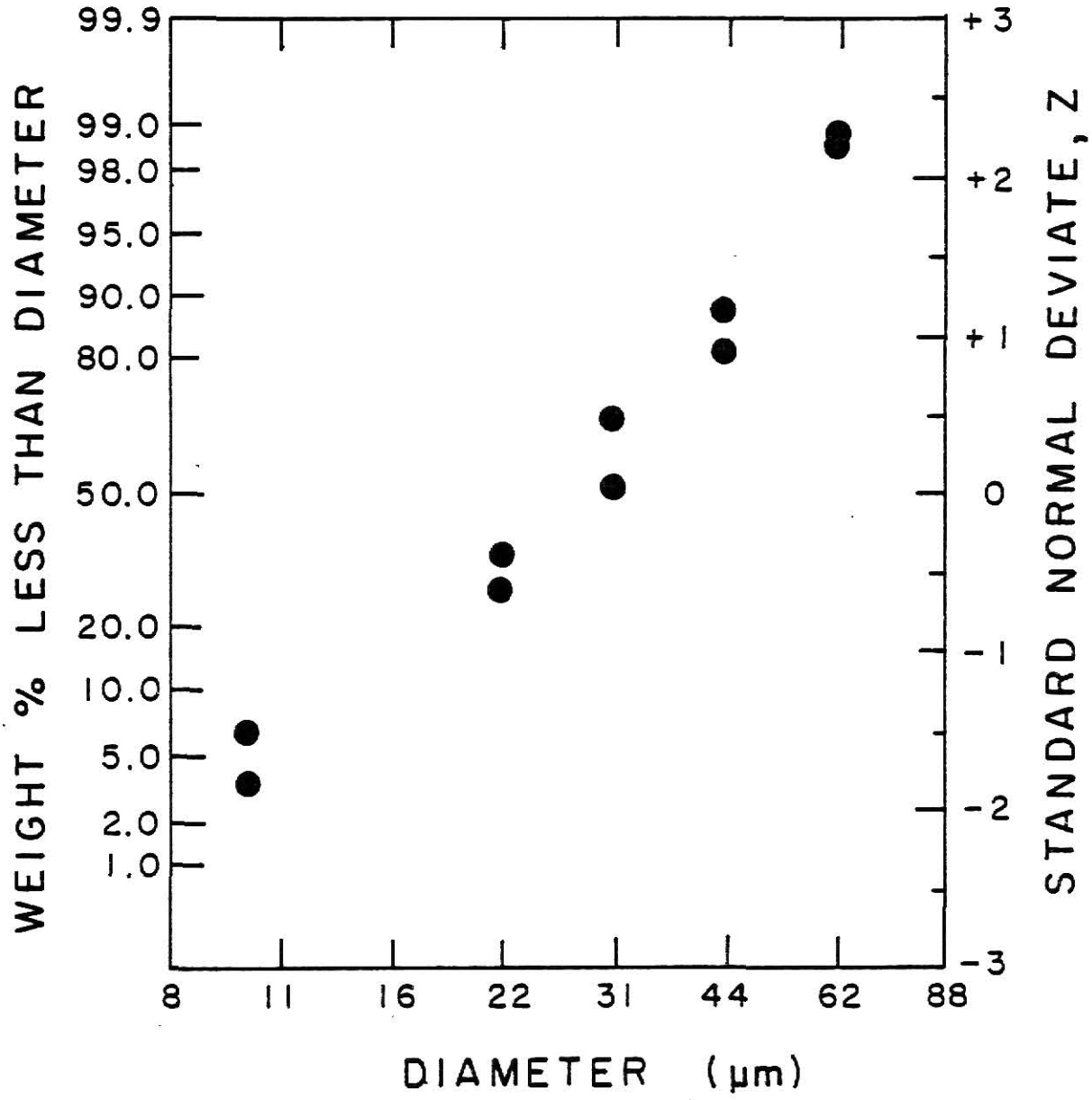

Fig. 3.47 Particle Size Distribution of Wheat Dust

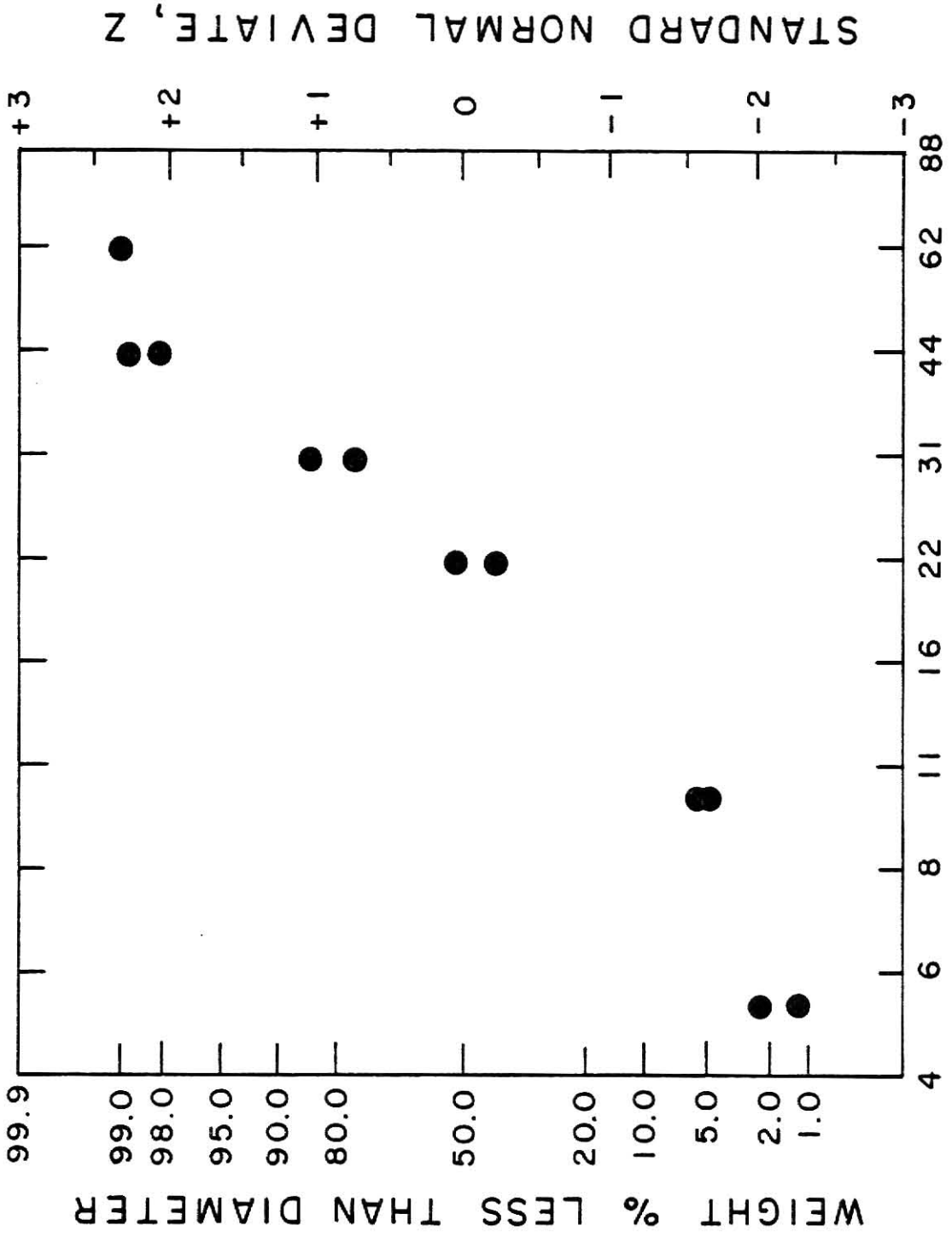

Fig. 3.48 Particle Size Distribution of Cornstarch

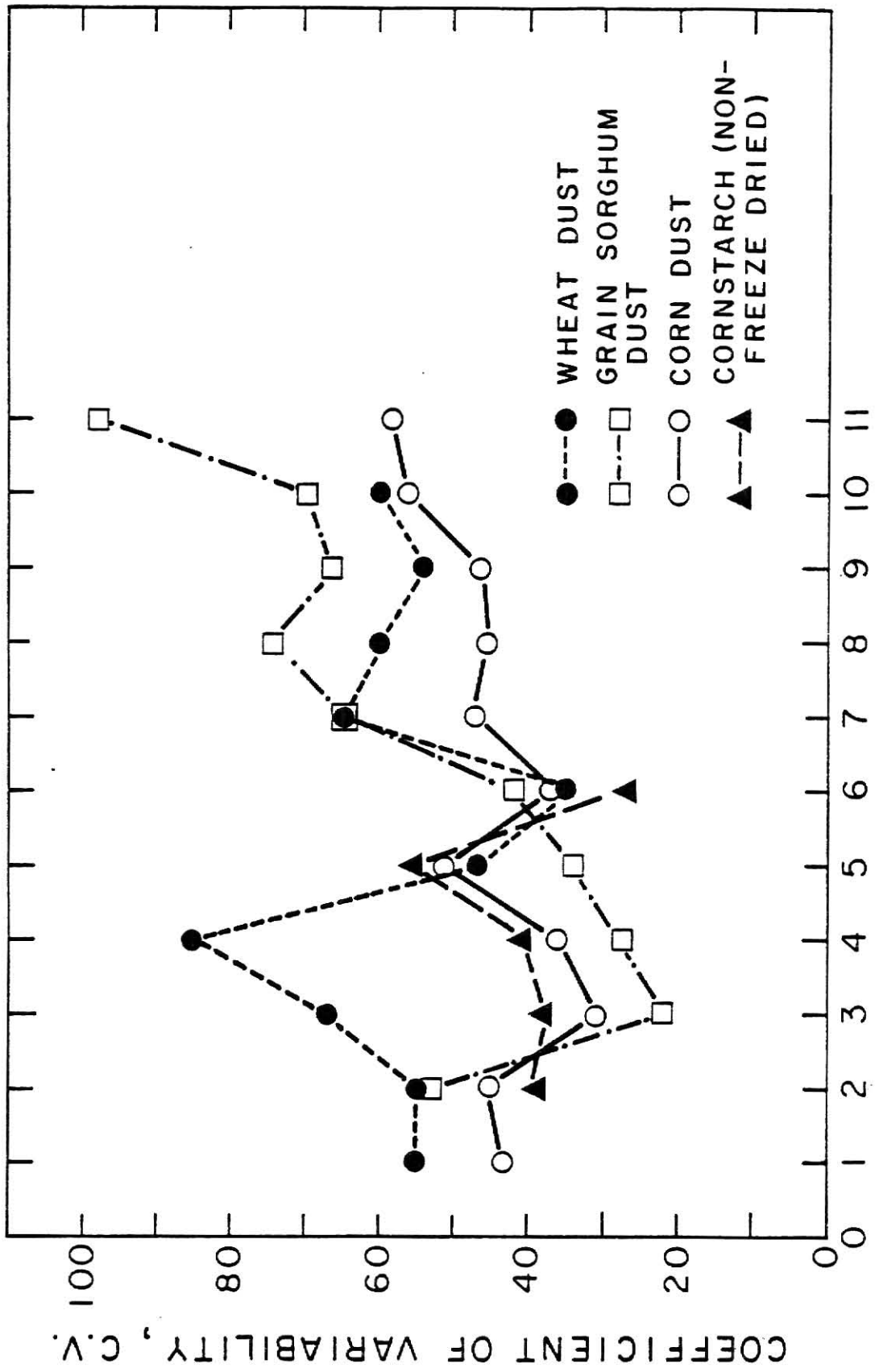

Fig. 3.49 Correlation Between the Coefficient of Variability and the Size Fraction

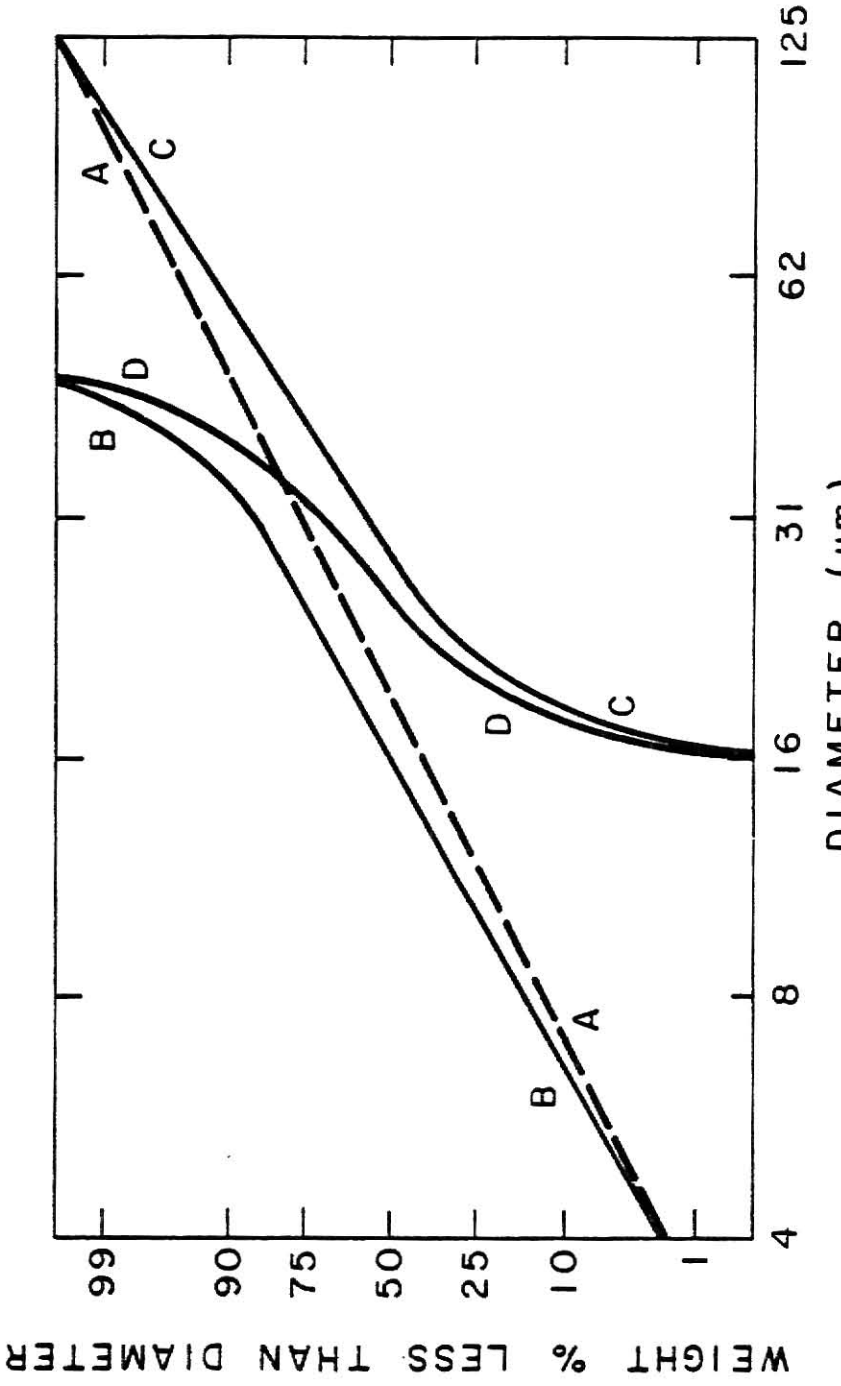

Fig. 3.50 Particle Size Distribution Expected from Perfect Air or Sieve Classification of a Dust with a Log Normal Particle Size Distribution, A, Herdan et al. (1960)

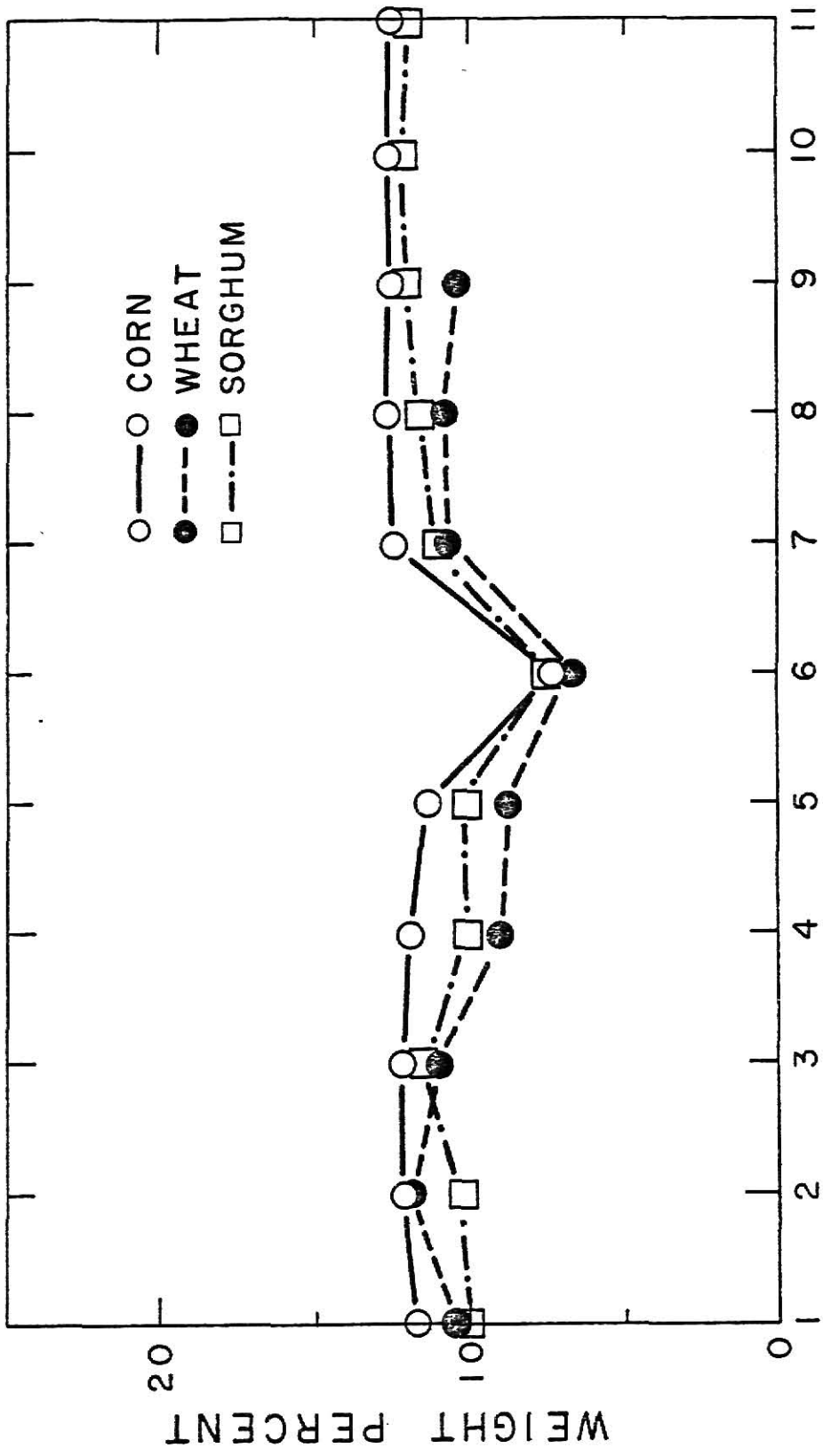

Fig. 3.51 Comparison of the Moisture Contents of Each Size Fraction

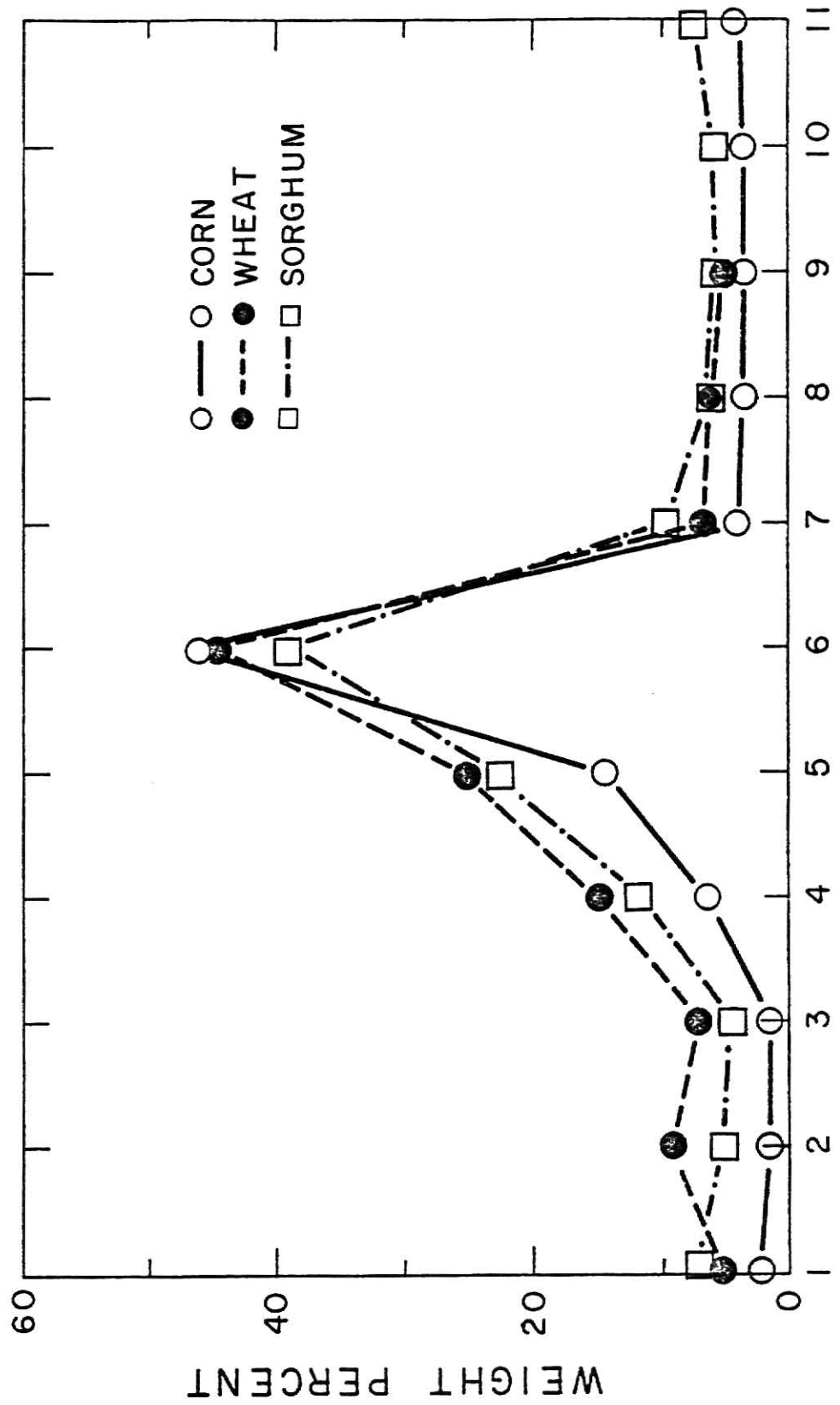

Fig. 3.52 Comparison of the Ash Content of Each Size Fraction

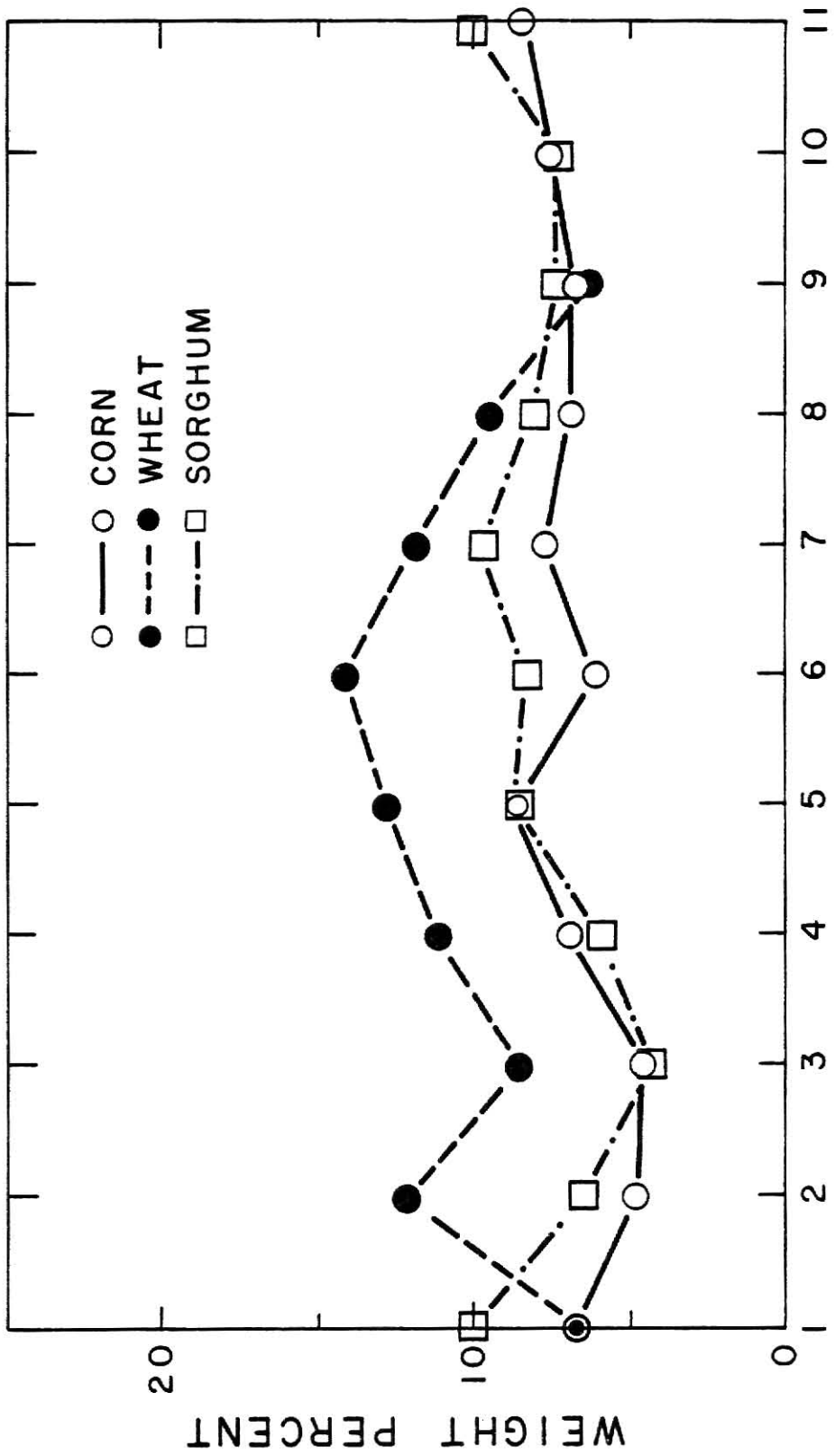

Fig. 3.53 Comparison of the Protein Contents of Each Size Fraction

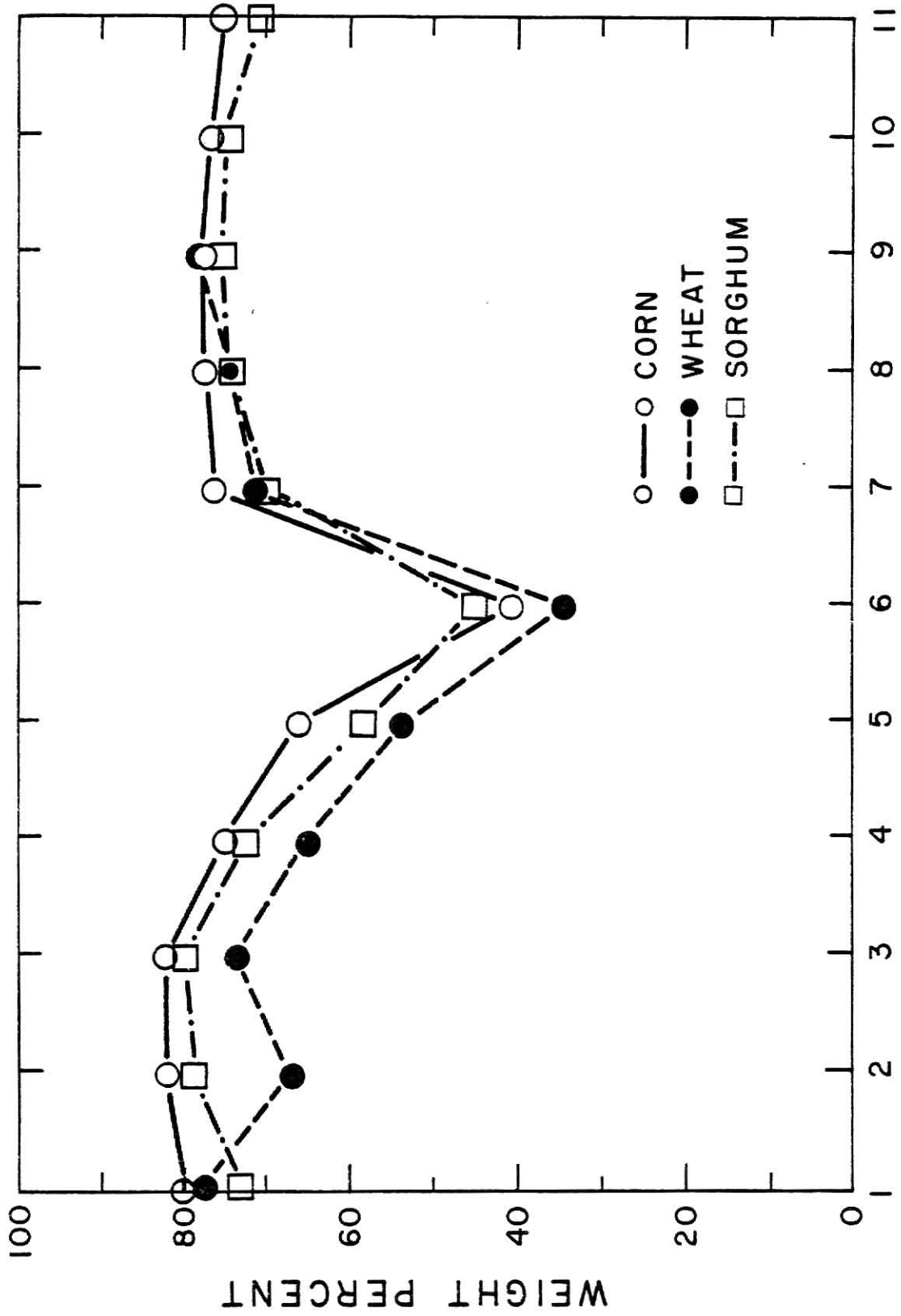

Fig. 3.54 Comparison of the Starch and Fiber Contents for Each Size Fraction

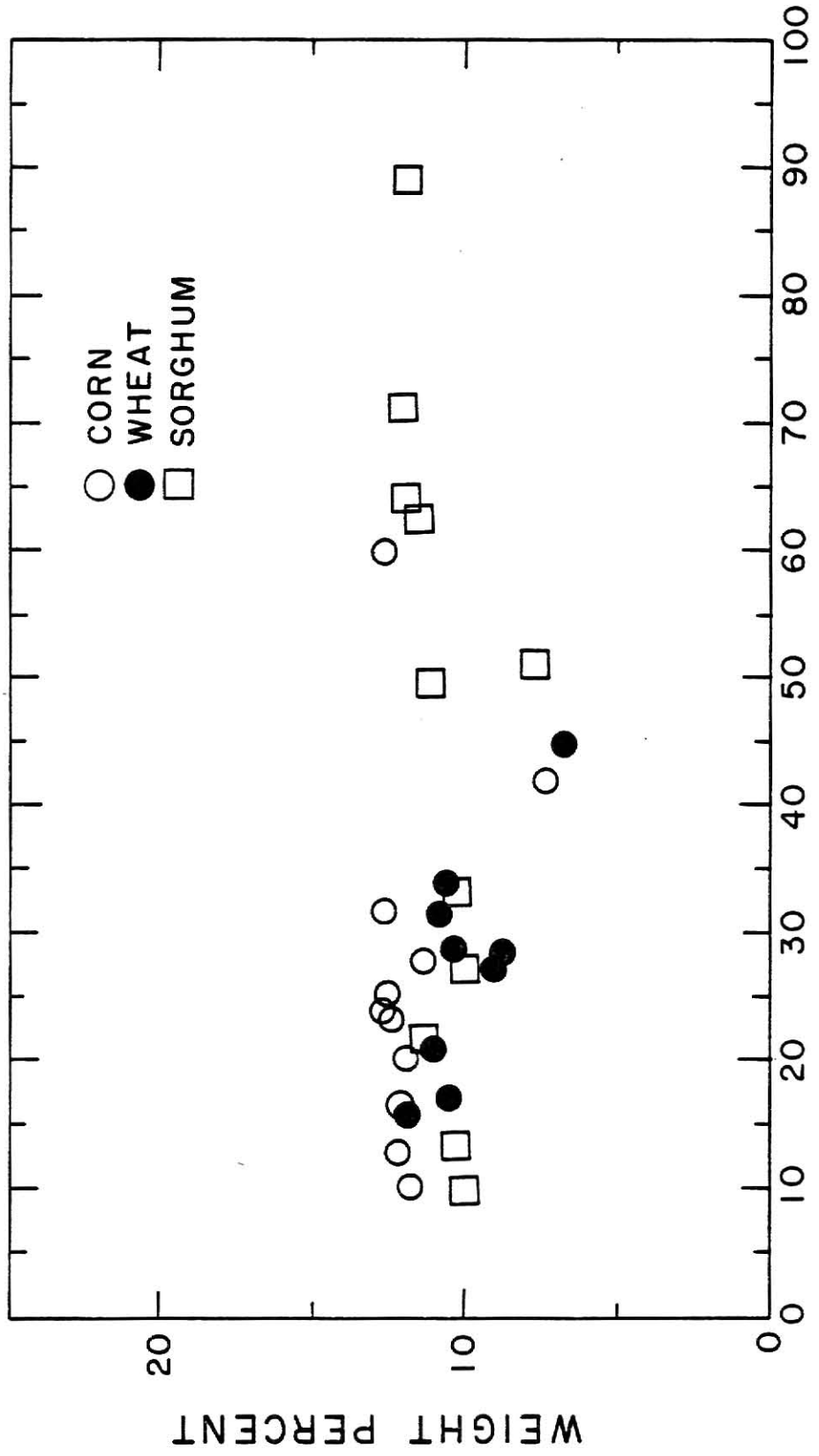

Fig. 3.55 Correlation Between Moisture Content and Mass Mean Diameter

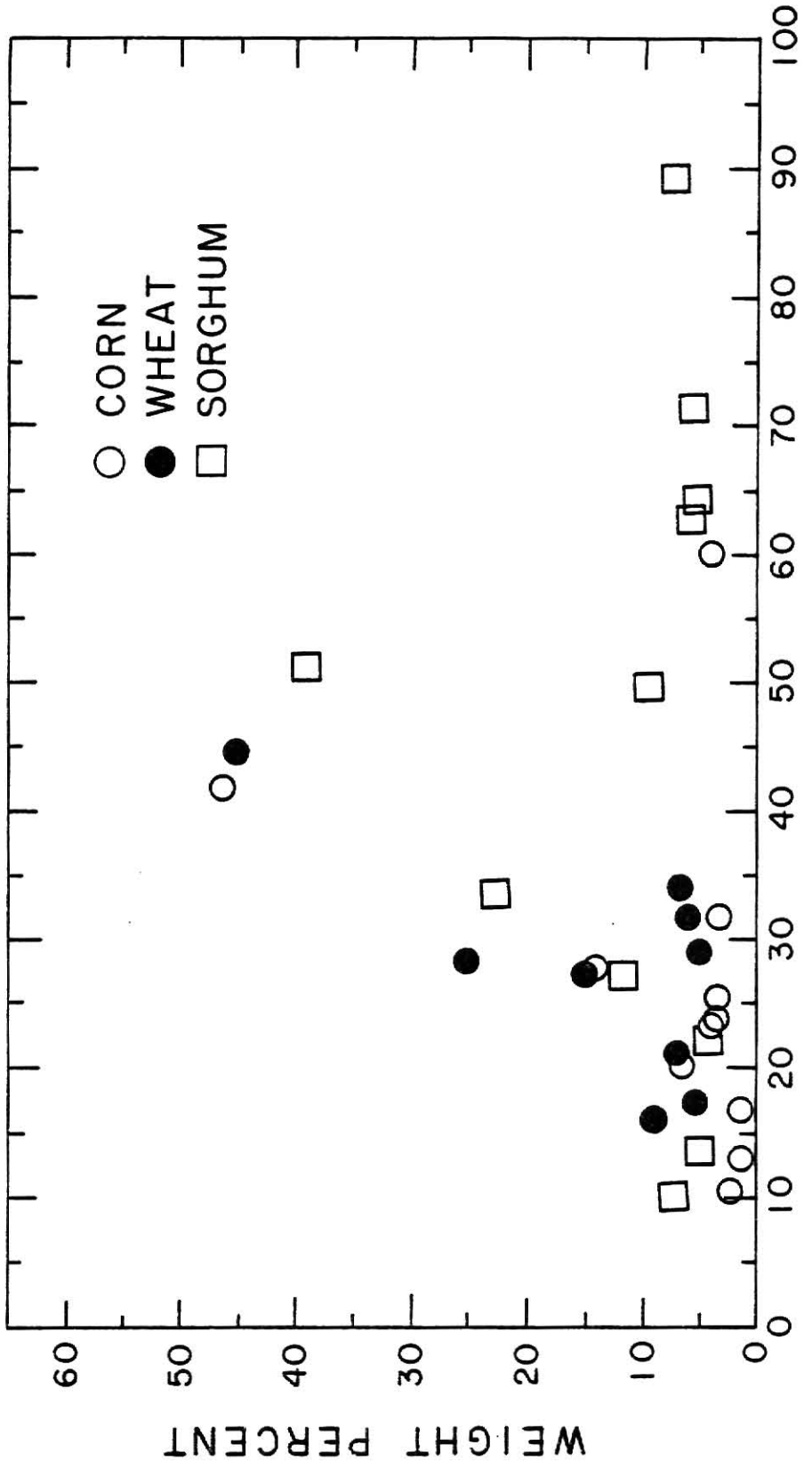

Fig. 3.56 Correlation Between the Ash Content and Mass Mean Diameter

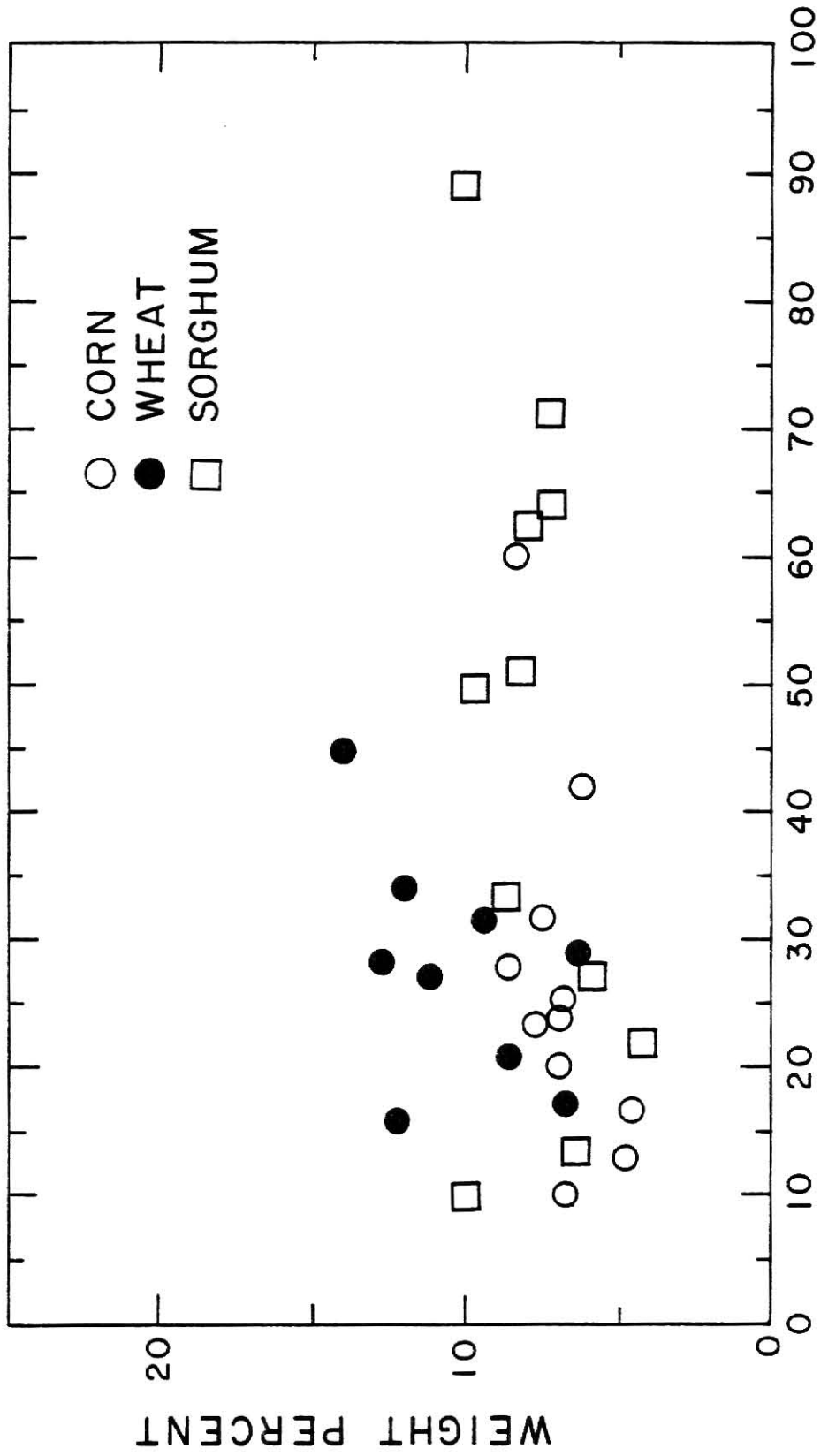

Fig. 3.57 Correlation Between the Protein Content and the Mass Mean Diameter

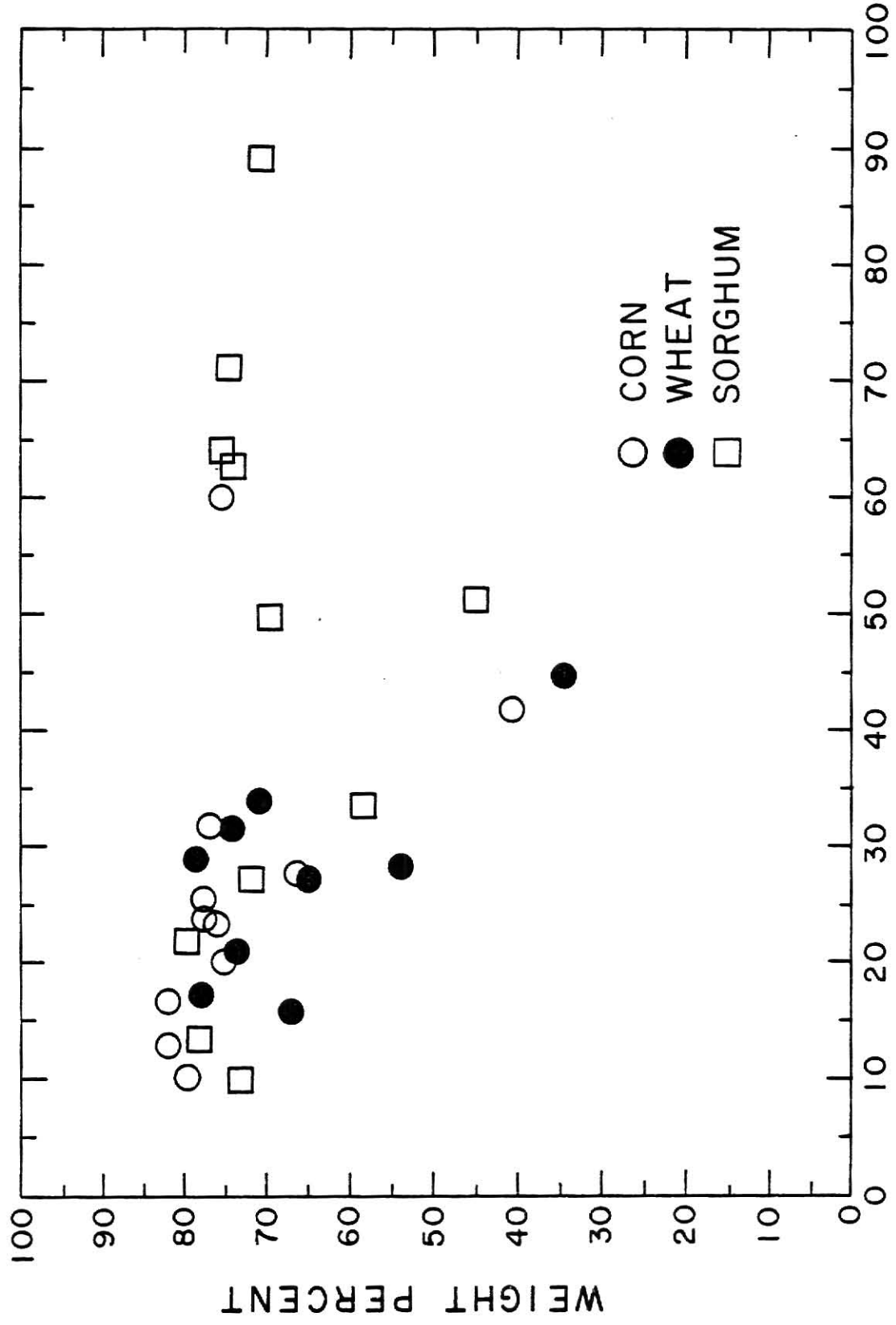

Fig. 3.58 Correlation Between the Starch and Fiber Content and Mass Mean Diameter

CHAPTER 4

MINIMUM EXPLOSIBLE CONCENTRATION AS AFFECTED BY PARTICLE SIZE AND COMPOSITION

I. INTRODUCTION

A dust explosion involves two major phases, namely, the ignition and propagation phases. The minimum explosible concentration is the smallest concentration of dust (mass of dust per unit volume of the dust and air mixture) that will lead to an explosion. To determine the minimum explosible concentration, basically one identifies the smallest amount of dust which, upon ignition, will give rise to a maximum explosion pressure that exceeds a fixed limit (e.g., rupture a paper diaphragm). The minimum explosible concentration is one quantity used to characterize the ignition phase of an explosion. The propagation phase is characterized by three quantities, the maximum explosion pressure, the maximum rate of pressure rise, and the average rate of pressure rise; a study of which is the subject of Chapter 5.

II. THEORETICAL DERIVATION OF CORRELATION MODELS

The system under consideration can be modeled as a mixture of dust and air inside a closed vessel. Two phases, a solid or dust phase and a gas phase, are assumed to exist in the system. The dust phase plays the role of a heat source and the gas phase a heat sink. Each phase is assumed to be at a constant temperature, even though the explosion occurs in a turbulent environment. When radiation is neglected, the energy balance for the dust phase is

$$\int_0^\infty \rho_d C_{p,d}\left(\frac{dT}{dt}\right)\left[\frac{\pi}{6}\left(\frac{D}{D_o}\right)^3 D_o^3 n(D_o)\right] dD_o$$

$$= \int_0^\infty h(T_g - T)\pi\left(\frac{D}{D_o}\right)^2 D_o^2 n_o(D_o)\, dD_o$$

$$+ (-\Delta H)\int_0^\infty (-r_d'')\pi\left(\frac{D}{D_o}\right)^2 D_o^2 n_o(D_o)\, dD_o \qquad (1)$$

$$+ S_v h_d (T_o - T) + r_w(\Delta H_w)$$

where

$C_{p,d}$ = specific heat capacity of the dust

D = particle diameter at time t

D_o = particle diameter at time equal to zero

ρ_d = density of the dust

h = heat transfer coefficient between the dust and the air

h_d = heat transfer coefficient between the dust phase and the vessel (probably a function of the concentration)

ΔH = heat of combustion of dust

ΔH_w = heat of vaporization of water

$n_o(\chi)$ = number distribution of particle diameter, χ, at time equal to zero

r_w = rate of water evaporation

$-r_d''$ = reaction (combustion) rate of dust based on the external surface area

S_v = surface area of the vessel

t = time

T = temperature of the dust phase

T_g = temperature of the air

T_o = temperature of the vessel

$\frac{D}{D_o}$ is a function of D_o and t, i.e., $\frac{D}{D_o} = f(D_o, t)$ and $\frac{D}{D_o}$ is defined to be equal to 0 when $D_o = 0$, i.e., $\frac{D}{D_o} = 0$ if $D_o = 0$.

The energy balance for air phase gives

$$\rho_a C_{p,a} V_v \frac{dT_s}{dt} = -\int_0^\infty h(T_g - T)\pi\left(\frac{D}{D_o}\right)^2 D_o^2 n_o(D_o)\, dD_o + S_v h_a (T_o - T_g) \qquad (2)$$

where

ρ_a = density of air

$C_{p,a}$ = heat capacity of air

V_v = vessel volume

h_a = heat transfer coefficient between the air and the vessel

The mass balance for oxygen yields

$$\frac{dN_{O_2}}{dt} = \nu_{O_2} \frac{dN_d}{dt} = \int_0^\infty \frac{\nu_{O_2}}{M_d} (-r_d')\left(\frac{D}{D_o}\right)^2 D_o^2 n_o(D_o)\, dD_o \qquad (3)$$

where

N_{O_2} = total number of moles of oxygen

ν_{O_2} = number of moles of oxygen used per mole of dust

M_d = molecular weight of dust

N_d = number of moles of dust

With an expression for (D/D_o) and that for $(-r_d'')$ in hand, in principal, this set of equations could be solved numerically. For simplicity, one can assume that the particles are of constant size with a burned layer; thus, D/D_o remains constant at unity. The difference between the density and the specific heat capacity the ash layer and those of the dust are assumed to be negligible. Furthermore, it is assumed that the heat loss from the air to the vessel would be small. The determination of minimum explosible concentration is usually performed at a low pressure and of low temperature environment With these assumptions, Eqs. (1), (2) and (3) become, respectively,

$$N_{tot}\rho_d C_{p,d}\frac{dT}{dt}\left(\frac{\pi}{6}D_{a,3}^{\circ 3}\right) = N_{tot}^{\circ} h (T_s - T)\pi D_{a,2}^{\circ 2} + (-\Delta H)\int_0^{\infty}(-r_d'')D_0^2 n_0(D_0)dD_0 + s_v h_d (T_0 - T) + r_w(-\Delta H_w) \quad (4)$$

$$\rho_a C_{p,a} V_v \frac{dT_g}{dt} = -N_{tot}^{\circ}(T_s - T)\pi D_{a,2}^{\circ 2} \quad (5)$$

and

$$\frac{dN_{O_2}}{dt} = \frac{\nu_{O_2}}{M_d} \int_0^\infty (-r_2'') D_o^2 n_o(D_o) dD_o \tag{6}$$

where

$D^o_{a,3}$ = mean diameter based on weight at time zero

$D^o_{a,2}$ = mean diameter based on area at time zero

N^o_{tot} = total number of particles at time zero

Assuming that the air behaves ideally, and that the total number of moles of gas is constant, the expression relating the air temperature to the pressure is obtained as

$$T_g = \frac{V_v P}{n_o R} \tag{7}$$

where

P = pressure

n_o = total number of moles of gas at time zero

The definition of $D^o_{a,3}$ is

$$D^o_{a,3} = \left(\frac{1}{N^o_{tot}} \int_0^\infty D_o^3 n_o(D_o) dD_o \right)^{\frac{1}{3}} \tag{8}$$

or

$$\rho_d \frac{\pi}{6} D_{a,3}^{o\,3} = \frac{W_{tot}^o}{N_{tot}^o} \tag{9}$$

where

W_{tot}^o = total weight of dust initially present at time zero

Therefore, N_{tot}^o is

$$N_{tot}^o = \frac{W_{tot}^o}{\rho_d \frac{\pi}{6} D_{a,3}^{o\,3}} \tag{10}$$

Substituting Eqs. (7) and (10) into Eqs. (4), (5) and (6) yields, respectively,

$$W_{tot}^o C_{p,d} \frac{dT}{dt} = \frac{6 W_{tot}^o}{\rho_d} \left(\frac{V_r h}{n_o R}\right)\left(P - \frac{n_o R T}{V_r}\right) \frac{D_{a,2}^{o\,2}}{D_{a,3}^{o\,3}}$$

$$+ (-\Delta H) \int_0^\infty (-r_d'') D_o^2 n_o(D_o)\, dD_o$$

$$+ \frac{S_v L_d V_r}{n_o R} \left(P_o - \frac{n_o R T}{V_r}\right) \frac{D_{a,2}^2}{D_{a,3}^2} \tag{11}$$

$$\rho_a C_{p,a} \frac{V_v^2}{n_o R} \frac{dP}{dt} = \frac{6 W^o_{tot}}{\rho_d} \left(\frac{h V_v}{n_o R}\right)\left(P - \frac{n_o R T}{V_v}\right) \frac{D^{o\,2}_{a,2}}{D^{o\,3}_{a,3}} \tag{12}$$

and

$$\frac{d N_{O_2}}{dt} = \frac{\nu'_{O_2}}{M_d} \int_0^\infty (-r''_d)\, D_o^2\, n_o(D_o)\, d D_o \tag{13}$$

where

P_o = the initial pressure of the air

The maximum explosion pressure, P_{max}, occurs when

$$\frac{dP}{dt} = 0$$

Therefore, from Eq. (12), one obtains

$$P_{max} = \frac{n_o R T_{max}}{V_v}$$

where

T_{max} = temperature of the dust when $P = P_{max}$

Substituting this equation into Eq. (11) gives

$$W^{\circ}_{tot}\, C_{p,d}\, \frac{dT}{dt} = -\rho_a C_{p,a} \frac{V_r^2}{n_o R} \frac{dP}{dt} + (-\Delta H) \int_0^{\infty} (-r_d'')\, D_o^2\, n_o(D_o)\, dD_o$$

$$+ \frac{S_r h_d V_r}{n_o R} \left(P_o - \frac{n_o R T}{V_r} \right) + r_w (-\Delta H_w) \qquad (14)$$

Integration of this equation from time equal to zero to the time when P_{max} occurs, t_{max}, yields

$$W^{\circ}_{tot}\, C_{p,d}\, (T_{max} - T_o) = -\frac{\rho_a C_{p,a} V_r^2}{n_o R} (P_{max} - P_o)$$

$$+ (-\Delta H) \int_0^{t_{max}} \int_0^{\infty} (-r_d'')\, D_o^2\, n_o(D_o)\, dD_o\, dt$$

$$+ \frac{S_r h_d V_r}{n_o R} \int_0^{t_{max}} \left[\left(\frac{n_o R T}{V_r} \right) - P_o \right] dt \qquad (15)$$

$$+ (-\Delta H_w) \int_0^{t_{max}} r_w\, dt$$

or

$$C_{min}\, c_{p,d}\, (P_{max} - P_o) = -\rho_a\, c_{p,a}\, (P_{max} - P_o) + \frac{(-\Delta H)}{V_v^2} \int_0^{t_{max}} \int_0^{\infty} (-r_d'')\, D_o^2\, n_o(D_o)\, d D_o\, dt + \frac{S_v}{V_v} L_d n_o R \int_0^{t_{max}} \left[\left(\frac{n_o R T}{V_v} \right) - P_o \right] dt - \frac{\Delta H_w n_o R}{V_v^2} \int_0^{t_{max}} r_w\, dt \qquad (16)$$

where

C_{min} = minimum concentration

As a first approximation, one can assume that the rate of reaction is controlled by the rate of adsorption of oxygen; thus,

$$-r_d'' = \int_0^{t_{max}} \int_0^{\infty} K\, P_{O_2}\, D_o^2\, n_o(D_o)\, d D_o\, dt \qquad (17)$$

where

K = proportionally constant (function of temperature)

P_{O_2} = partial pressure of oxygen

However, K is a function of temperature. Equation (17) can be rewritten as

$$(-r_d'') = \frac{W_{tot}^{\circ}}{\rho_d \frac{\pi}{6}} \bar{K} P_{O_2} \frac{D_{a,2}^{\circ 2}}{D_{a,2}^{\circ 3}} \tag{18}$$

where $\bar{K}$ is an average value of K; it is not a function of temperature. The expression for the integral of the heat loss due to water evaporation can be approximated as

$$(-\Delta H_\omega) \int_0^{t_{max}} r_\omega \, dt \doteq - W_{tot}^{\circ} X_m^{\circ} \Delta H_\omega \tag{19}$$

where

X_m° = the weight fraction of water initially in the dust if one assumes that all the water is evaporated during the explosion

Substituting Eqs. (18) and (19) into Eq. (16) yields

$$C_{min} C_{p,d} (P_{max} - P_o) = - \rho_a C_{p,a} (P_{max} - P_o) + \frac{6(-\Delta H) n_3 R}{\rho_d V_v \pi} C_{min} \bar{K} P_{O_2} \frac{D_{a,2}^{\circ 2}}{D_{a,3}^{\circ 3}}$$

$$- L - C_{min} X_m^{\circ} \frac{\Delta H_\omega}{V_v} \tag{20}$$

or

$$C_{min} C_{p,d} = -\rho_a c_{p,a} + \frac{6(-\Delta H)\, n_o R}{\rho_d V_v \pi (P_{max} - P_o)} \bar{K} P_{o_2} \left[C_{min} \frac{D_{a,2}^{o\,2}}{D_{a,3}^{o\,3}} \right]$$

$$- \frac{L}{(P_{max} - P_o)} - \frac{\Delta H_w}{V_o (P_{max} - P_o)} \left[C_{min} X_m^o \right] \qquad (21)$$

where

$$L = \frac{S_v}{L_v} h_a n_o R \int_o^{t_{max}} \left[\left(\frac{n_o R T}{V_v} \right) - P_o \right] dt$$

The heat capacity of the dust can be approximated as

$$C_{p,d} = C_{p,m} X_m^o + C_{p,a} X_a^o + C_{p,p} X_p^o + C_{p,s} X_s^o \qquad (22)$$

where

$C_{p,m}$ = heat capacity of water

$C_{p,a}$ = heat capacity of ash

$C_{p,p}$ = heat capacity of protein

$C_{p,s}$ = heat capacity of starch & fiber

X_a^o = weight fraction of ash initially present in dust

X_p^o = weight fraction of protein initially present in dust

X_s^o = weight fraction of starch & fiber initially present in dust

Since the starch & fiber content is obtained by difference, Eq. (22) becomes

$$C_{p,d} = (C_{p,m} - C_{p,s})X_m^o + (C_{p,a} - C_{p,s})X_a^o + (C_{p,p} - C_{p,s})X_p^o + C_{p,s} \tag{23}$$

Combining this equation with Eq. (20), one obtains

$$C_{min}\left[(C_{p,m} - C_{p,s})X_m^o + (C_{p,a} - C_{p,s})X_a^o + (C_{p,p} - C_{p,s})X_p^o + C_{p,s}\right] = -\rho_a C_{p,a} + \frac{6(-\Delta H)\eta_o R}{\rho_d V_v \pi (P_{max} - P_o)} \bar{K} P_{o_2}\left[C_{min}\frac{D_{a,2}^{o\,2}}{D_{a,3}^{o\,3}}\right] - \frac{L}{(P_{max} - P_o)} - \frac{\Delta H_w}{V_v (P_{max} - P_o)}\left[C_{min} X_m^o\right] \tag{24}$$

or

$$\frac{1}{C_{min}} = -AX_m^o - BX_a^o - CX_p^o - D + E\frac{D_{a,2}^{o\,2}}{D_{a,3}^{o\,3}} \tag{25}$$

where

$$A = \left[(C_{P,m} - C_{P,s}) + \frac{\Delta H_v}{V_v (P_{max} - P_0)} \right] \Big/ \left[\rho_a C_{P,a} + \frac{L}{(P_{max} - P_0)} \right]$$

$$B = (C_{P,a} - C_{P,s}) \Big/ \left[\rho_a C_{P,a} + \frac{L}{(P_{max} - P_0)} \right]$$

$$C = (C_{P,p} - C_{P,s}) \Big/ \left[\rho_a C_{P,a} + \frac{L}{(P_{max} - P_0)} \right]$$

$$D = C_{P,s} \Big/ \left[\rho_a C_{P,a} + \frac{L}{(P_{max} - P_0)} \right]$$

$$E = \frac{6(-\Delta H) n_0 R}{\rho_d V_v \pi (P_{max} - P_0)} \cdot \frac{\bar{K} P_{0_2}}{\left[\rho_a C_{P,a} + \frac{L}{(P_{max} - P_0)} \right]}$$

Alternatively, the term

$$(-\Delta H) \int_0^{t_{max}} \int_0^{\infty} (-r_d'') D_0^2 n_0(D_0) \, d D_0 \, dt$$

can be approximated as

$$(-\Delta H) C_{min} V_v$$

Thus Eq. (25) becomes

$$\frac{1}{C_{min}} = -A X_m^0 - B X_a^0 - C X_p^0 - D + E'' \qquad (26)$$

where

$$E'' = \left[\frac{(-\Delta H)\, n_o R}{V_v (P_{max} - P_o)}\right] \Big/ \left[P_a C_{p,a} + \frac{L}{(P_{max} - P_o)}\right]$$

III. EXPERIMENTAL DETERMINATION OF MINIMUM EXPLOSIBLE CONCENTRATION

The material and methods employed are outlined here.

A. Sample Preparation

Samples of dust from three grains (corn, wheat, and grain sorghum) were collected from the dust removal systems in three commercial elevators, and cornstarch was purchased in bulk from a mill. Each dust sample was separated into several size fractions by sieve separation and by air classification. The particle size distribution and average particle diameter were determined for each size fraction. The contents of moisture, ash, protein, and starch & fiber in each fraction were also determined. A detailed description is given in Chapter 3.

The dust samples were stored in a refrigerator at 3°C (37°F). The samples were allowed to equilibrate with the temperature and humidity of the laboratory air for at least 16 hours prior to the tests. The temperature and humidity of the laboratory were continuously monitored by a hygro-thermograph recorder (Belfort Instrument Company, Baltimore, MD).

B. Hartmann Explosion Test

1. Apparatus. Photographs of the explosion apparatus are shown in Figs. 4.1 and 4.2. A schematic of the apparatus is presented in Fig. 4.3.

The design of the explosion chamber is the same as that of a standard Hartmann apparatus (Dorsett et al., 1960), except for the four light emitting

diode (LED) and phototransistor (PT) pairs which function in the infrared spectral region (LED and PT are Spectronics SE-140-3 and Spectronics SD-1440-3, respectively). Figure 4.4 is a schematic diagram of an LED. The diagram for a PT is identical except an PT is used instead of an LED. A diagram of the circuitry for the pairs is in Fig. 4.5. All of the pairs are mounted on the outside surface of the Lucite explosion chamber (see Fig. 4.3), and the light passes through the chamber walls to reach the dust. The lowest phototransistor was positioned above the electric spark to remove the effect of the light from the spark. When the dust is dispersed in the explosion chamber, the intensity of the light received by the PT in each pair decreases as the concentration increases. This decrease in light intensity results in a corresponding decrease in the output voltage of the PT. The PT output voltage signal is measured as a function of time with a Tektronix 5112 dual beam oscilloscope (Tektronix Inc., Beaverton, OR). The signal traces on the oscilloscope screen were photographed with a Tektronix series 125 camera.

The timing circuitry (see Fig. 4.3) controls the length of time between the initiation of the electric spark and the dispersion of the dust. The circuitry initiates the spark by closing a relay that connects a 120 V ac line voltage to a luminous tube transformer (Jefferson Electric Co., Bellwook, IL). The transformer steps up the line voltage to 12 kV and 30 ma. The output from the transformer is connected across the electrodes (see Fig. 4.3). The dust is dispersed when the circuitry opens the solenoid valve which allows the compressed air in the dispersion air cylinder to flow into the explosion chamber.

A paper diaphragm that is mounted on top of the explosion chamber is filter paper (Whatmann 42 ashless) with a diameter of 0.09 m. The diaphragm is for determining the occurrence of an explosion, which is generally defined

to have occurred if there is sufficient pressure built up during the test to rupture the diaphragm (Dorsett et al., 1960).

2. Procedure. Prior to the explosion, a specified amount of dust was weighed and placed into the dust cup (Fig. 4.3), and the explosion chamber was attached on the top of the dust cup with T-bolts and wing nuts. The high voltage electrical leads from the transformer were attached to the electrodes. The distance between the electrode tips inside the explosion chamber was measured with a square rod having sides of 4.8 mm (3/16") and a length of 0.3 m (12"). The paper diaphragm was mounted on top of the explosion chamber, and the air dispersion cylinder (see Fig. 4.3) was pressurized to 1.4 bar (20 psig). The timing circuitry was programmed to simultaneously open the solenoid valve and initiate the electric spark. The photograph film was initially exposed by the PT output traces for 100% transmission when the LED in each pair was on and for 0% transmission when the LED in each pair was off.

After these pre-explosion preparations the timing circuit was initiated. After the explosion, the camera shutter was closed and the photograph removed. The condition of the diaphragm (whether it was ruptured or not) was recorded.

C. Determination of the Minimum Explosible Concentration

The concentration was calculated by dividing the mass of dust placed in the dust cup (the loading) by the volume of the explosion chamber. The minimum loading was determined by repeatedly performing explosion tests with varying loadings until the smallest loading that yielded four consecutive positive explosion tests (the paper diaphragm ruptures) was found.

1. Procedure for determining the minimum loading. A flow diagram of the procedure is presented in Figs. 4.6a and 4.6b. A preliminary explosion test

was performed with an amount of dust estimated to be approximately the minimum loading. Depending on the result of this test, one of two paths described below was followed.

If the result of the preliminary test was positive (an explosion), a two series of explosion tests were performed. In the first series each succeeding loading was decreased by an increment of 0.5×10^{-3} kg until one of the tests yielded a negative result. The dust loading in the initial test of the second series was of 0.5×10^{-3} kg larger than the loading in the final test of the first series. The succeeding loadings in the second series were increased by 0.5×10^{-3} kg increments until one of the tests yielded a negative result.

If the result of the preliminary test was negative, a series of explosion tests were performed, in which each succeeding loading was increased by 0.5×10^{-3} kg until one of the tests yielded a positive result. The initial test of this series was performed with a dust loading of 0.5×10^{-3} kg smaller than the loading in the final test of the first series. The succeeding loadings in the second series were decreased by 0.5×10^{-3} kg increments until one of the tests yielded a positive result.

The smallest loading, which yielded two consecutive positive results, was determined. The test performed with this loading was the initial test for a third series of tests. In the series the succeeding dust loadings were incrementally decreased by 0.2×10^{-3} kg until the smallest loading was found that yielded four consecutive positive explosion tests. Finally, this loading was decreased by 0.1×10^{-3} kg and a series of explosion tests performed with it. If the series of tests yielded four consecutive positive results then this was the minimum loading; otherwise, the loading 0.1×10^{-3} kg larger was the minimum loading.

2. Calculation of the minimum explosible concentration from the minimum loading. Dorsett et al. (1960) determined the minimum loading with the electrodes at two different heights, 63 mm and 114 mm, from the bottom of the explosion chamber. The arithmetic average of the minimum loadings at the two electrode heights was taken as the final minimum loading of the sample to compensate for the spatial non-uniformity of the dust suspension in the explosion chamber during the explosion. The minimum explosible concentration was calculated by dividing the arithmetic average of the minimum loading by the total volume of the explosion chamber. This method of calculating the minimum explosible concentration assumes that the dust is uniformly suspended within the explosion chamber at the time of the explosion.

In this study, the minimum loading was determined with the electrodes only at a height of 63 mm from the bottom of the explosion chamber. The minimum explosible concentration was calculated by dividing the minimum loading by the total volume of the explosion chamber. This was done to reduce the amount of sample used because of the limited amount of sample in some of the size fractions. The distribution of the suspended dust within the explosion chamber was also monitored by the PT-LED pairs.

IV. RESULTS AND DISCUSSION

The results from the determinations of the minimum explosible concentration are given in Table 4.1. The order in which the tests were performed is indicated by the Test No. The coefficient of variability between repetitions and the number of degrees of freedom for each coefficient are presented in Table 4.2 for wheat dust, corn dust, grain sorghum dust, and cornstarch. In Table 4.3, the simple correlation coefficients between the minimum explosible concentration, C_{min}, and the mass mean diameter, D_m, are presented

for grain sorghum dust, corn dust, wheat dust, and cornstarch. The partial correlation coefficients when the moisture content, ash content, protein content, or starch & fiber content are fixed are also presented in Table 4.3. Table 4.4 contains the simple correlation coefficients between $1/C_{min}$ and the content of each component (moisture, ash, protein, or starch & fiber) for grain sorghum dust, corn dust, wheat dust, and cornstarch. The partial correlation coefficients when the specific external surface area, S_{ext}, is fixed are also presented. Table 4.5 contains similar information as Table 4.3 except that the correlation is between $1/C_{min}$ and S_{ext} instead of between C_{min} and D_m. For corn dust and grain sorghum dust, Table 4.6 contains the slopes and the intercepts for the regressions of S_{ext} on $1/C_{min}$ when the regression is constrained to pass through the origin. The results of the F-test, degrees of freedom and the coefficient of determination, R^2, are also presented for each regression in Table 4.6. Table 4.7 contains similar information as Table 4.4 except that the correlations are between $1/C_{min}$ and the content of each component instead of between C_{min} and each component. The slope, intercept, results of the F-test, degrees of freedom, and coefficient of determination, R^2, of the regression of the ash content on $1/C_{min}$ are presented in Table 4.8 for those size fractions of wheat dust with the ash content greater than 10%. In addition, the same quantities for the regression of moisture content on $1/C_{min}$ are presented in Table 4.8 for cornstarch, corn dust, and grain sorghum dust. Note that for the grain sorghum dust, the data for the size fraction with the highest ash content are not included in the regression. In Table 4.9, the results of the F-test, the coefficient of determination, R^2, and the residual degrees of freedom for the multilinear regression of the variables shown in the Table on $1/C_{min}$ are presented for corn dust, grain sorghum dust, wheat dust, cornstarch, and the combination of all four of the

dusts. The values of the coefficients of the dependent variables and of the constant are also presented in Table 4.9. The ignition delays are presented in Table 4.10 with the corresponding sample identification and minimum explosible concentration.

The minimum explosible concentration, C_{min}, is plotted against the mass mean diameter, D_m, in Figs. 4.7, 4.8, 4.9, and 4.10 for grain sorghum dust, corn dust, wheat dust, and cornstarch, respectively. In Figs. 4.11, 4.12, and 4.13, C_{min} is plotted against the ash content for grain sorghum, corn, and wheat dust, respectively. In Fig. 4.14, C_{min} is plotted against the moisture content for grain sorghum dust and corn dust. Similar correlations for wheat dust and cornstarch are presented in Figs. 4.15 and 4.16, respectively. In Figs. 4.17, 4.18, and 4.19, C_{min} is plotted against the protein content for grain sorghum, corn, and wheat dust, respectively. Figs. 4.20, 4.21, 4.22, and 4.23 present the correlation between C_{min} and the starch & fiber content for grain sorghum dust, corn dust, wheat dust, and cornstarch, respectively. The results of the correlations and regressions between the reciprocal of the minimum explosible concentration, $1/C_{min}$, and the specific external surface area, S_{ext}, ash content, moisture content, protein content, or starch & fiber content are presented in Figs. 4.24 through 4.40.

Figure 4.41 presents the percent transmission plotted against time from the output of the four phototransistors, PT, shown in Fig. 4.3. The relative position of each trace among the four traces in Fig. 4.41 corresponds to the relative position of the PT among the four PTs (e.g., the bottom trace is from the bottom PT in Fig. 4.3).

A. Effect of Particle Size and Composition

1. Mass mean diameter. Figures 4.7 and 4.8 show definitely that an inverse relationship exists between the minimum explosible concentration, C_{min}, and the mass mean diameter, D_m, for grain sorghum dust and corn dust. The correlation coefficients between C_{min} and D_m are significant at the 1% level for these types of dust (Table 4.7). For wheat dust, the correlation is significant at the 5% level (Fig. 4.9). For cornstarch, however, the correlation is not significant at the 5% level (Fig. 4.10).

The effect of particle size, i.e., the mass mean diameter, on C_{min} can not be examined apart from the effect of composition. In Table 4.3, the partial correlation coefficients are used to indicate the effect of the content of each component on these correlations.

When the ash content is fixed, the partial correlation coefficients between C_{min} and D_m remain essentially unchanged from the simple correlation between these two attributes for grain sorghum dust and corn dust. For wheat dust, however, the partial correlation coefficient is insignificant at the 5% level.

When the moisture content is fixed, the partial correlation coefficient between C_{min} and D_m again remains essentially unchanged from the simple correlation between these two attributes for grain sorghum dust (Table 4.3). The partial correlation coefficient for corn dust is significant at the 5%, instead of the 1%, level. For wheat dust, the partial correlation coefficient is insignificant at the 5% level; the ash content and the moisture content are highly correlated. For cornstarch, the partial correlation coefficient is much larger than the simple correlation coefficient; however, it is still insignificant at the 5% level. Note that mass mean diameters for cornstarch range from 17 to 35 μm, which is the smallest range among all types of dust.

Therefore, a correlation between C_{min} and D_m would be more difficult to detect for cornstarch than for other types of dust.

When the protein content is fixed, the partial correlation coefficient between C_{min} and D_m also remains essentially unchanged for grain sorghum dust. The partial correlation for corn dust is only significant at the 5% instead of the 1% level. For wheat, the partial correlation is still not significant at the 5% level, when the protein content is fixed.

When the starch & fiber content is fixed, the partial correlation coefficient between C_{min} and D_m for grain sorghum dust again remains essentially unchanged, and that for wheat dust again is insignificant at the 5% level. Note that these partial correlation coefficients are essentially the same as those with the ash content fixed. For corn dust, the partial correlation coefficient is significant at the 5% level while the simple correlation coefficient is significant at the 1% level. The ash and protein contents of the cornstarch are negligibly small; thus, the total content of each size fraction is assumed to consist of two parts: the moisture content and the starch & fiber content. The starch & fiber content, therefore, is the difference between total content and the moisture content. For cornstarch, the partial correlation coefficient with the starch & fiber content fixed is exactly the same as that with the moisture content fixed.

The correlation between C_{min} and D_m for grain sorghum dust, corn dust, wheat dust, or cornstarch is affected differently when the moisture, ash, protein, or starch & fiber content is removed. The correlation for grain sorghum dust remains essentially unchanged when the content of each component is fixed. For corn dust, fixing the ash content does not greatly alter the correlation. No data for C_{min} exists for the size fractions with the highest contents, 5 and 6 (see Table 4.1); an insufficient quantity of dust in these

size fractions rendered the determination of C_{min} impossible. The ash contents of the remaining size fractions range from 1.3% to 6.4%. For wheat dust, when the moisture content, protein content, or starch & fiber content is fixed, the resultant partial correlation coefficients are different from the simple correlation coefficients. The partial correlation coefficients, however, are still insignificant at the 5% level. A correlation is more difficult to detect for wheat dust than for the other kinds of dust; wheat dust contains the smallest amount of data.

The total number of degrees of freedom for each dust is too small to detect effectively correlations between C_{min} and D_m, and the resultant partial correlation coefficients are difficult to interpret. The table of these correlations is given in the Appendix.

2. Composition. The ash content varies more than the moisture, protein, or starch & fiber content among the size fractions for corn dust, grain sorghum dust, and wheat dust. In spite of this, the simple and partial correlation coefficients for corn dust listed in Table 4.4 indicate that no significant relationship exists between the ash content and C_{min} at the 5% level. Since a sufficient quantity of dust was not available in the size fractions with the highest ash contents, the determination of C_{min} was impossible for these size fractions. The ash content ranges only from 1.3% to 6.4% among these size fractions for which C_{min} was determined. The ash content of grain sorghum dust varies widely from 4.5% to 39.5%. For grain sorghum dust, however, the correlation coefficients and the partial correlation coefficients between the C_{min} and the ash content also indicate no significant correlation at the 5% level. The correlation coefficient for wheat dust shows a significant correlation at the 5% level. This is expected

because of the large range of the ash contents, 6.0 to 48%. While three data points with high ash contents are available for wheat dust, only two are available for grain sorghum dust; for grain sorghum dust, the amount of dust in the third size fraction was not sufficient to perform a determination of C_{min}. When the mass mean diameter is fixed, the partial correlation coefficient between the C_{min} and the ash content indicates no significant correlation at the 5% level.

The correlation coefficients between the minimum explosible concentration and the moisture content for grain sorghum dust, corn dust, wheat dust, and cornstarch are given in Table 4.4. The simple correlation coefficient for grain sorghum dust shows no significant correlation at the 5% level. This is expected because of the small range of moisture contents, from 7.7% to 12.1%. The simple correlation coefficient for corn dust is significant at the 1% level (Fig. 4.14). Note that for corn dust, the moisture content ranges only from 11.3% to 12.6%. When the mass mean diameter is fixed, the resultant partial correlation coefficient is significant at the 5% level. For cornstarch, the simple and partial correlation coefficients (with the mass mean diameter fixed) between C_{min} and moisture content are significant at the 1% level. The range of the moisture contents, between 4.0% and 14.9%, for this dust is the largest among all four types of dusts (Fig. 4.16). The correlation coefficients for wheat dust are insignificant at the 5% level.

The correlation coefficients between the minimum explosible concentration and the protein content are shown in Table 4.4. The simple correlation coefficients for grain sorghum dust, corn dust, and wheat dust are insignificant at the 5% level (see Figs. 4.17, 4.18, and 4.19, respectively). The partial correlation coefficients with the mass mean diameter fixed are also insignificant at the 5% level for all three types of dust.

The correlation coefficients between the minimum explosible concentration and the starch & fiber content are given in Table 4.4. They are insignificant at the 5% level for grain sorghum dust and corn dust (Figs. 4.20 and 4.21, respectively). When the mass mean diameter is fixed the partial correlation coefficients are also insignificant at the 5% level. For the wheat dust, the simple correlation coefficient is significant at the 5% level (Fig. 4.22); however, with the mass mean diameter fixed, the partial correlation coefficient is insignificant at the 5% level. The correlation for cornstarch is significant at the 1% level (Fig. 4.23). Note that this correlation is the same as that between the C_{min} and the moisture content except that the former is a negative correlation. The ash and protein contents of the cornstarch are negligibly small; thus, the total content of each size fraction is assumed to consist of two parts, the moisture content and the starch & fiber content. The starch & fiber content, therefore, is the difference between total content and the moisture content.

B. Correlations Utilizing a Simple Model

1. Specific external surface area. Equation (25) indicates that the reciprocal of the minimum explosible concentration, C_{min}, can be correlated linearly as a function of the specific external surface area, S_{ext}. In Table 4.5, the correlation coefficients between Y_{min} and S_{ext} are significant at the 1% level for both grain sorghum dust and corn dust (Figs. 4.24 and 4.25, respectively). For both wheat dust (Fig. 4.26) and cornstarch (Fig. 4.27), however, the correlation coefficients are insignificant at the 5% level. Note that cornstarch contains the smallest range of particle specific surface area, 0.13×10^3 to 0.283×10^3 m^2/kg, and the largest range of moisture contents, 4% to 14.9%. Figure 4.24 shows definitely that the

correlation between $1/C_{min}$ and specific external surface area for grain sorghum dust is non-linear at the larger specific external surface areas. This could have resulted from agglomeration of the smaller particles with diameters of approximately between 8 μm and 12 μm or due to inaccuracy in the model; however, the correlation coefficient is significant at the 1% level.

The particle correlation coefficients; determined by fixing the content of each component one at a time, were calculated. Note that the simplified model, Eq. (25), suggests a possible linear correlation between the $1/C_{min}$ and the content of each component. When the moisture content is fixed, the partial correlation coefficients between the $1/C_{min}$ and the specific external surface area are shown in Table 4.5 for grain sorghum dust, corn dust, wheat dust, and cornstarch. The simple and partial correlation coefficients are essentially the same for grain sorghum dust and corn dust. The partial correlation coefficients for wheat dust and for cornstarch are not significant at the 5% level.

The partial correlation coefficients for the same correlation with the ash content fixed are also given in Table 4.5 for grain sorghum dust, corn dust, and wheat dust. The ash content in cornstarch is insignificant. For grain sorghum dust and corn dust, the partial correlation coefficients are essentially the same as their respective simple correlation coefficients. The partial correlation coefficient for corn dust is larger than the simple correlation coefficient by 0.01. The partial correlation coefficient for wheat dust again indicates no significant correlation at the 5% level.

When the protein content is fixed, there are no significant changes in the correlations for any dust (see Table 4.5). For example, the partial correlation coefficient for grain sorghum dust is larger than its respective correlation coefficient by 0.02.

For all types of dust except cornstarch, the partial correlation coefficients between the $1/C_{min}$ and the specific external surface area with the starch & fiber content fixed are essentially the same as those with the ash content fixed. This is expected; the correlation coefficients between the ash content and the starch & fiber content are highly significant for grain sorghum dust, corn dust, and wheat dust.

The correlations between the $1/C_{min}$ and the specific external surface area are substantially different for grain sorghum dust, corn dust, wheat dust, and cornstarch. The correlation coefficients between the $1/C_{min}$ and the specific external surface area are significant for grain sorghum dust and corn dust. These correlations are not significantly altered by fixing the content of any component. The partial correlation coefficients with the contents of all four composition components fixed have also been determined (see Appendix); it has been found that they are difficult to interpret and that resultant number of degrees of freedom, ranging from 2 to 5, are too small to detect significant correlations effectively. The insignificant simple and partial correlations for wheat dust are not unexpected. Wheat dust along with cornstarch have smaller ranges of the specific external surface area, 0.15 x 10^3 m^2/kg, than do grain sorghum dust and corn dust, 0.4 x 10^3 and 0.34 x 10^3 m^2/kg, respectively. The wheat dust also has the smallest number minimum explosible concentration data among all types of dust, and three of these contain large quantities of ash material, 15 to 45%. The combination of these factors makes it difficult to detect a significant correlation between $1/C_{min}$ and specific external surface area difficult for wheat dust. The cornstarch has a small range of specific external surface area, as expected, and has the largest range of moisture contents, 4 to 15%. Thus, the correlation between the $1/C_{min}$ and the specific external surface area is also difficult to detect.

If the effects of the content of any component on $1/C_{min}$ are small or are random with respect to the specific external surface area, then the model (Eq. 25) would predict a linear relationship between the $1/C_{min}$ and the specific external surface area.

The experimental data indicate that the model must be constrained to pass through the origin. The result of the regression of S_{ext} on $1/C_{min}$ are shown in Table 4.6. The F-tests for both regression are significant at the 1% level and the coefficients of determination are 0.94 for the corn dust and 0.86 for the grain sorghum dust.

For the specific external surface area (the particle size) to be a major factor, the value of C_{min} (0.055 kg/m^3) obtained by Jacobson et al. (1961) should be in the range of C_{min} obtained in this study. The smallest value of C_{min} from this study, however, is 0.15 kg/m^3 for the size fraction of grain sorghum dust having a mass mean diameter of 10 μm. This is 2.7 times higher than that reported by Jacobson et al. (1961) for grain dust. Even though the correlations are significant, the discrepancies between the values of C_{min} obtained in this investigation and those obtained by Jacobson et al. (1961) are difficult to explain.

2. Composition. According to the model, Eq. (25), the reciprocal of the minimum explosible concentration, C_{min}, should be linearly correlated with the weight fractions of each composition component. The simple correlation coefficients and partial correlation coefficients with the specific external surface area, S_{ext}, fixed between $1/C_{min}$ and the ash content are shown in Table 4.7 for grain sorghum dust, corn dust, and wheat dust. These coefficients are insignificant at the 5% level. In Fig. 4.28 for wheat dust, however, for ash contents greater than approximately 15%, $1/C_{min}$ decreases as

the ash content increases. Note that the size fraction with the highest ash content, 45%, exhibits the lowest value of $1/C_{min}$. Figure 4.29 for grain sorghum dust, contains only one data point with an ash content greater than 15%. The value of $1/C_{min}$ for this data point is relatively low. For wheat dust, a linear regression of ash content on $1/C_{min}$ is presented in Table 4.8 in which only data from the three size fractions with the highest ash contents are included. Extrapolation of the resultant regression equation to the ash content at which $1/C_{min}$ becomes zero (i.e., C_{min} approaches infinity) yields a value of approximately 73%. Jacobson et al. (1961) reported a value of 85%; this value is for dry dust and was obtained from a different apparatus than that used in this study. The apparatus used by Jacobson et al. (1961), however, also utilizes an electric spark as the ignition source.

The simple and partial correlation coefficients between the $1/C_{min}$ and the moisture content are shown in Table 4.7 for corn dust, cornstarch, grain sorghum dust, and wheat dust. The simple correlation coefficients for corn dust and cornstarch are significant at the 1% level, Figs. 4.31 and 4.33, respectively. When the specific external surface area is fixed, the partial correlation coefficients for both types of dust remain significant at the 1% level. The simple and partial correlation coefficients for grain sorghum dust are not significant at the 5% level; however, a significant correlation appears to exist in Fig. 4.31 if the data containing the highest ash content are excluded. When the ash content is fixed, the partial correlation coefficient between the $1/C_{min}$ and the moisture content is -0.95 with 7 degrees of freedom. This coefficient is significant at the 1% level. For wheat dust, the simple and partial correlation coefficients with the specific external surface area fixed are not significant at the 5% level.

Table 4.8 presents the regressions of moisture content on $1/C_{min}$ for corn dust, cornstarch, and grain sorghum dust. For corn dust and cornstarch, the extrapolation of the regression equations to the moisture contents above which no explosion can occur has yielded values of 13.2 and 15.8%, respectively. These moisture contents are consistent with an average value of 15% reported by Eckhoff (1976). When the relationships for corn dust and cornstarch are extrapolated to a moisture content of zero, they predict minimum explosible concentrations of 0.02 and 0.038 kg/m^3, respectively. Jacobson et al. (1961) report values of C_{min} ranging from 0.04 to 0.055 kg/m^3 for dry cornstarch and a value of 0.055 kg/m^3 for dry grain dust. For grain sorghum dust, the data with the highest ash content is not included in the determination of the regression in Table 4.8. The moisture content above which no explosion can occur is 13.3% and the minimum explosible concentration for a moisture content of zero is 0.043 kg/m^3.

The simple and partial correlation coefficients between the $1/C_{min}$ and the protein content are presented in Table 4.7 for grain sorghum, corn, and wheat dust. These coefficients indicate no significant correlations at the 5% level. These relationships are presented in Figs. 4.34, 4.35, and 4.36 for grain sorghum, corn, and wheat dust, respectively. Insignificant correlations are expected because of the small range of protein contents for each dust. Unless the effect of protein is very marked, one would not expect to see significant correlations.

The simple and partial correlation coefficients between the $1/C_{min}$ and the starch & fiber content are presented in Table 4.7 for grain sorghum dust, corn dust, wheat dust, and cornstarch. These coefficients for wheat, grain sorghum, and corn dust are not significant at the 5% level (Figs. 4.37, 4.38, and 4.39). For cornstarch, however, the simple and partial correlation

coefficients with the specific external surface area fixed are both significant at the 1% level (Fig. 4.40). Note that these coefficients are the same as those for the correlation between moisture content and $1/C_{min}$; except the former are negative. For cornstarch, the starch & fiber content is the difference between the total content and the moisture content. Thus the significant correlation between the $1/C_{min}$ and the starch & fiber content could be the result of the correlation between the $1/C_{min}$ and the moisture content. Note that none of the remaining types of dust show a significant correlation between $1/C_{min}$ and the starch & fiber content; however, both grain sorghum dust and corn dust, as well as cornstarch, exhibit significant correlations between the $1/C_{min}$ and the moisture content.

3. Combined effects of specific external surface area and composition. The synergistic effects of the specific external surface area and the composition can be analyzed by means of the simplified models, Eq. (25) and (26). These models have been fitted to the experimental data. The results are presented in Table 4.9. Only those variables that significantly contribute to the regression at the 5% level are included in the models. Not all the variables in the models can be utilized in the analysis because the total number of data per type of dust is too small.

For corn dust, the experimental data can be described with an R^2 of 0.95 when the specific external surface area, S_{ext}, and the ash content are the only two variables included in the first model, Eq. (25). The minimum explosible concentrations from this model are 3 to 10 times larger than those obtained by Jacobson et al. (1961). The second model in Eq. (26) describes the data with an R^2 of 0.90 when only the ash and moisture contents are considered in the model. By extrapolating this model to a moisture content of

zero, it predicts the minimum explosible concentration to be 0.020 kg/m^3 on an ash-free basis; Jacobson et al. (1961) reported 0.055 kg/m^3 for grain dust. For an average ash content for corn dust of 8.17, this model predicts C_{min} to be 0.033 kg/m^3 on a moisture-free basis. For corn dust, it also predicts the moisture content below which no explosion will take place for a given ash content. For the range of ash contents of corn dust, 1.3 to 6.4%, such moisture contents range between 11.5 and 13%. Eckhoff (1976) reported that moisture contents above approximately 15% showed essentially no pressure rise. His values ranged from approximately 10 to 16% for four dusts tested (the range of ash content is unknown).

For grain sorghum dust, the second model characterizes the data better than the first. This model predicts the data with an R^2 of 0.91. For an ash content of 39.1%, this model predicts the minimum explosible concentration on a moisture-free basis to be 0.055 kg/m^3, and for an ash content of 4.5%, 0.035 kg/m^3. These values are of the same order of magnitude as the values of 0.055 kg/m^3 reported by Jacobson et al. (1961). The moisture content, above which no explosion can occur, is predicted to range from 8.8% for an ash content of 39.9% to 13.2% for an ash content of 4.4%.

For wheat dust, the first model gives the only significant regression with an F-value of 5.5 (the F-test value of 5.41 is significant at the 3% level). Again, with this model, it is difficult to reconcile the values reported by Jacobson et al. (1961) with the experimental data obtained in this work. However, it is more difficult to identify the relationship among the variables for wheat dust than for any other dust.

For cornstarch, the second model shows a significant regression at the 1% level with an R^2 value of 0.73. For cornstarch, the coefficient of determination, R^2, is lower than those of the other dusts; the coefficient of

variability between repetitions is 30.8% (Table 4.2). The coefficients of variability for corn dust, grain sorghum dust, and wheat dust are 18, 8, and 5%, respectively. When this is extrapolated to a moisture content of zero, the model predicts a value of 0.038 kg/m^3 for the minimum explosible concentration. Jacobson et al. (1961) reported values ranging from 0.040 kg/m^3 to 0.055 kg/m^3. The present prediction is slightly lower than those obtained by Jacobson et al. (1961). The model also predicts the moisture content above which no explosion can occur to be 15.8% which essentially is in agreement with the value reported by Eckhoff (1976).

For a combination of all types of dust, the first model gives no significant regression at the 5% level (see Table 4.9). The second model yields a significant regression at the 5% level with an R^2 of 0.83 (see Table 4.9). This model predicts the minimum explosible concentration of 0.039 kg/m^3 on a moisture-free, ash-free, and protein-free basis. Jacobson et al. (1961) reported values of 0.04 to 0.055 kg/m^3 for cornstarch and 0.045 kg/m^3 for wheat starch. For the average values of the ash content and the protein content for all dusts, 11.1 and 8.3%, respectively, the model predicts a minimum explosible concentration of 0.048 kg/m^3 for a moisture content of zero. Jacobson et al. (1961) reported a value of 0.055 kg/m^3 for dry grain dust. On an ash-free and protein-free basis, the second model predicts the maximum moisture content to be 15.8% above which no explosion can occur. By extrapolation, Eckhoff (1976) showed the maximum moisture content to be approximately 16.3% for cornstarch. At the largest ash and protein contents of 48% and 14%, respectively, the maximum moisture content was found to be 7.2%.

Examination of the data given in Table 4.9 indicates that a large ash content (approximately 25%) is necessary to significantly increase the minimum explosible concentration. For moisture and protein contents within the ranges

of the present study, the model predicts that the ash content, above which no explosion can occur, ranges from 30 to above 100%. The model is applicable for an ash content below 100%. However, as the ash content approaches 100%, the heat liberated from the particles of combustible dust approaches zero.

In summary, one can state that the moisture content is the major factor which influences the minimum explosible concentration; the ash content becomes a significant factor only when it exceeds approximately 25%. The effect of protein content is minimal at the levels encountered in this investigation. The particle size seems to have a slight effect; however, its role has yet to be fully explored.

C. Ignition Delay

The photograph of the phototransistor, PT, and the output voltage in Fig. 4.41 indicates that the variation of the light intensity before the arrival of the dust was insignificant. A series of short bursts of light can be observed in the photograph after the arrival of the dust at the bottom phototransistor. This light could have resulted from the ignition of single particles or groups of particles that failed to ignite the entire dust cloud.

Many of the photographs taken for concentrations at which the explosions occurred show a large and extended light source. The explosions did not occur prior to these bursts of light. This light source could possibly be interpreted as the result of an explosion. The time between the arrival of the dust at the lowest PT and the reception of this intense light source in the experiment is termed the ignition delay. This delay is closely associated with that reported by Eckhoff (1977) for the Hartmann explosion chamber for measuring the maximum explosion pressure, the maximum rate of pressure rise, and the average rate of pressure rise. Table 4.11 lists the ignition delays

ranging from 152 to 466 msec for wheat dust, 40 to 490 msec for grain sorghum dust, 14 to 137 msec for corn dust, and 0 to 134 msec for cornstarch. The concentration at the electrodes is a function of time because of the transitory nature of the dust cloud. Lee et al. (1980) have observed that for cornstarch and lycopodium, the concentration of dust reaches a maximum within approximately 20 msec from the arrival of the dust at the electrodes, and then decreases immediately. The reduction in the concentration of dust could be due to the effects of its dispersion into the explosion chamber; some adheres to the walls of the vessel, some escapes from the hole in the paper diaphragm or other cracks, and some settles out of the suspension. A similar observation can be made in Fig. 4.41. No quantitative statement can be made of the significance of the delay time; however, when the delay times are larger than the time to reach the initial peak concentration, it can not be ascertained which dust particles are involved in the explosion. To define the minimum explosible concentration for a particular type of dust, it would be desirable to have the explosion occur at the initial peak concentration. Then, the entire distribution of particles, not just a particular portion, will be involved in the explosion. This could severely alter the effect of particle size on the minimum explosible concentration for dust that is not easily ignitable.

V. CONCLUSIONS

The minimum explosible concentrations of all types of dust studied are similar. Ranking the dusts in decreasing order of their explosibility yields cornstarch, corn dust, grain sorghum dust, and wheat dust. The values of C_{min} for grain sorghum dust and corn dust are similar. Particles with smaller diameters have lower values of C_{min} than those with larger diameters. The

moisture content appears to be an important factor; for cornstarch, C_{min} ranges from 0.04 kg/m^3 to 0.31 kg/m^3 for moisture contents ranging from 4% to 14.9%. The ash content appears to become an important factor for values greater than approximately 25%.

Two models were developed that linearly correlate $1/C_{min}$ as a function of S_{ext}, ash content, moisture content, and protein content. The important variables that effect C_{min} appear to be the ash content and the moisture content. Extrapolation of the models to a moisture content necessary to obtain an inert dust sample yields a value of 15.8% for cornstarch; Eckhoff (1976) reported a value of 16.3% for cornstarch. Similar extrapolations for the remaining dusts yields values of moisture content that range from 13 to 15% depending on the ash content. For wheat dust, extrapolation of the models to an ash content necessary for an inert dust sample yields a value of 73%.

There appears to be a long ignition delay, approximately 100-200 msec, for most types of dust studied. This could alter the effect of S_{ext} on C_{min}.

REFERENCES

Dorsett, H.G., Jr., Jacobson, M., Nagy, J., and Williams, R.P. 1960. Laboratory equipment and test procedures for evaluating explosibility of dusts. U.S. Department of the Interior, Bureau of Mines, Report of Investigations, RI-5624.

Eckhoff, R.K. 1976. A study of selected problems related to the assessment of ignitability and explosibility of dust clouds. A.S. John Greigs Boktrykkeri. Bergen, Norway.

Eckhoff, R.K. 1977. The use of the Hartmann bomb for determining K_{st} values of explosible dust clouds. Staub Reinhaltung der Luft 37(3):110-112.

Jacobson, M., Cooper, A.R., and Ball, F.J. 1961. Explosibility of agricultural dust. U.S. Department of the Interior, Bureau of Mines, Report of Investigations, RI-5753.

Lee, R.S., Aldis, D.F., Garrett, D.W., and Lai, F.S. 1980. Improved diagmostics for the determination of minimum explosible concentration, minimum ignition energy, and minimum ignition temperature of grain dusts. Submitted to Cereal Chemistry for publication.

APPENDIX. PARTIAL CORRELATION COEFFICIENTS BETWEEN C_{min} AND D_m, AND C_{min} AND S_{ext} WITH ALL THE CONTENTS OF MOISTURE, ASH, PROTEIN, AND STARCH & FIBER FIXED

Correlation	Type of Dust	Degrees of Freedom	Correlation Coefficient
		d.f.	r
C_{min} and D_m	Grain Sorghum	5	0.77*
	Corn	4	0.71
	Wheat	3	0.82
$1/C_{min}$ and S_{ext}	Grain Sorghum	5	0.67
	Corn	4	0.91*
	Wheat	3	0.79

*Significant at the 5% level

Table 4.1 Results from the Minimum Explosible Concentration Experiments

Test No.	Sample Identification	Minimum Explosible Concentration kg/m^3
1	CNAC-S07	0.29
2	CNAC-S02	0.20
3	CNAC-S08	0.46
4	CNAC-S10	0.54
5	CNAC-S09	0.47
6	CNAC-S11	0.53
7	CNAC-S04	0.26
8	CNAC-S07	0.31
9	CNAC-S03	0.26
10	CNAC-S08	0.33
11	CNAC-S02	0.22
12	CNAC-S09	0.28
13	CNAC-S01	0.16
14	CNAC-S10	0.50
15	CNAC-S11	0.49
16	WTAC-S07	0.30
17	WTAC-S04	0.29
18	WTAC-S08	0.32
19	WTAC-S03	0.29
20	WTAC-S05	0.36
21	WTAC-S06	0.57
22	WTAC-S09	0.41
23	WTAC-S10	0.36
24	WTAC-S04	0.25
25	WTAC-S03	0.29
26	WTAC-S06	0.54
27	WTAC-S05	0.35
28	WTAC-S07	0.30
29	WTAC-S08	0.30

Table 4.1 (continued)

Test No.	Sample Identification	Minimum Explosible Concentration kg/m^3
30	WTAC-S09	0.38
31	WTAC-S10	0.37
32	MOAC-S03	0.20
33	MOAC-S02	0.17
34	MOAC-S04	0.24
35	MOAC-S08	0.35
36	MOAC-S07	0.31
37	MOAC-S02	0.19
38	MOAC-S09	0.43
39	MOAC-S10	0.49
40	MOAC-S07	0.28
41	MOAC-S04	0.25
42	MOAC-S08	0.33
43	MOAC-S03	0.23
44	MOAC-S09	0.37
45	MOAC-S01	0.15
46	MOAC-S06	0.37
47	MOAC-S11	0.73
48	CSAC-F01	0.05
49	CSAC-S06	0.16
50	CSAC-F02	0.05
51	CSAC-S05	0.12
52	CSAC-S02	0.16
53	CSAC-S04	0.15
54	CSAC-S03	0.17
55	CSAC-F02	0.04
56	CSAC-S03	0.15
57	CSAC-S04	0.15
58	CSAC-S02	0.15
59	CSAC-S05	0.13

Table 4.1 (continued)

Test No.	Sample Identification	Minimum Explosible Concentration kg/m^3
60	CSAC-S06	0.20
61	CSAC-F01	0.04
62	CSAC-F04	0.10
63	CSAC-F06	0.14
64	CSAC-F03	0.14
65	CSAC-F05	0.15
66	CSAC-F05	0.11
67	CSAC-F06	0.16
68	CSAC-F04	0.11
69	CSAC-F05	0.12
70	CSAC-F03	0.31

Table 4.2 The Coefficients of Variability between Repetitions for Minimum Explosible Concentration

Type of Dust	Degrees of Freedom	Coefficient of Variability %
Wheat	6	4.7
Grain Sorghum	4	8.2
Corn	4	17.9
Cornstarch	9	30.8

Table 4.3 The Results of Simple and Partial Correlation between the Minimum Explosible Concentration and the Mass Mean Diameter

The Variable That is Fixed	Grain Sorghum Dust		Corn Dust		Wheat Dust		Cornstarch	
	Correlation Coefficient r	Degrees of Freedom d.f.	Correlation Coefficient r	Degrees of Freedom d.f.	Correlation Coefficient r	Degrees of Freedom d.f.	Correlation Coefficient r	Degrees of Freedom d.f.
None	0.93**	8	0.85**	7	0.76*	6	0.27	8
Moisture	0.92**	7	0.80*	6	0.65	5	0.60	7
Ash	0.93**	7	0.84**	6	0.56	5	--	--
Protein	0.92**	7	0.74*	6	0.73	5	--	--
Starch	0.93**	7	0.78*	6	0.57	5	-0.60	7

* Significant at the 5% level.

** Significant at the 1% level.

Table 4.4 The Results of the Simple and Partial Correlation between Each Composition Variable and the Minimum Explosible Concentration

Variable Correlate With C_{min}	Variable Whose Effect is Removed	Grain Sorghum Dust		Corn Dust		Wheat Dust		Cornstarch	
		Correlation Coefficient r	Degrees of Freedom d.f.	Correlation Coefficient r	Degrees of Freedom d.f.	Correlation Coefficient r	Degrees of Freedom d.f.	Correlation Coefficient r	Degrees of Freedom d.f.
Ash	None	0.05	8	0.28	7	0.76*	6		
	Mass Mean	0.00	7	0.03	6	0.58	5		
Moisture	None	0.39	8	0.86**	7	-0.61	6	0.82**	8
	Mass Mean	-0.09	7	0.81*	6	-0.40	5	0.88**	7
Protein	None	0.37	8	0.63	7	0.30	6		
	Mass Mean	0.08	7	0.11	6	0.11	5		
Starch	None	-0.18	8	-0.57	7	-0.71*	6	-0.82**	8
	Mass Mean	-0.00	7	-0.16	6	-0.47	5	-0.88**	7

* Significant at the 5% level.

** Significant at the 1% level.

Table 4.5 The Results of the Simple and Partial Correlation between $1/C_{min}$ and the Specific External Surface Area, $D^2_{a,2}/D^3_{a,3}$

The Variable That is Fixed	Grain Sorghum Dust		Corn Dust		Wheat Dust		Cornstarch	
	Correlation Coefficient r	Degrees of Freedom d.f.	Correlation Coefficient r	Degrees of Freedom d.f.	Correlation Coefficient r	Degrees of Freedom d.f.	Correlation Coefficient r	Degrees of Freedom d.f.
None	0.93**	8	0.97**	7	0.51	6	0.03	8
Moisture	0.93**	7	0.95**	6	0.22	5	0.30	7
Ash	0.93**	7	0.98**	6	0.09	5	--	7
Protein	0.95**	7	0.96**	6	0.55	5		
Starch	0.92**	7	0.96**	6	0.15	5		

* Significant at the 5% level.

** Significant at the 1% level.

Table 4.6 The Results of the Regression of the Specific External Surface Area, S_{ext}, on $1/C_{min}$

Type of Dust	F-test	Residue Degrees of Freedom	Coefficient of Determination R^2	Intercept	Slope
Corn	107.6**	8	0.94	--	14.09
Grain Sorghum	13.4**	9	0.86	--	17.16

Table 4.7 The Results of the Simple and Partial Correlation between Each Composition Variable and $1/C_{min}$

Variable Correlate With $1/C_{min}$	Variable Whose Effect is Removed	Grain Sorghum Dust		Corn Dust		Wheat Dust		Cornstarch	
		Correlation Coefficient r	Degrees of Freedom d.f.	Correlation Coefficient r	Degrees of Freedom d.f.	Correlation Coefficient r	Degrees of Freedom d.f.	Correlation Coefficient r	Degrees of Freedom d.f.
Moisture	None	-0.34	8	-0.91**	7	0.48	6	-0.86**	8
	Specific Surface Area	-0.32	7	-0.84**	6	0.13	5	-0.87**	7
Ash	None	-0.19	8	-0.36	7	-0.65	6		
	Specific Surface Area	0.15	7	0.60	6	-0.47	5		
Protein	None	-0.18	8	-0.53	7	-0.17	6		
	Specific Surface Area	-0.61	7	0.27	6	0.30	5		
Starch	None	0.29	8	0.57	7	0.59	6	0.86**	8
	Specific Surface Area	0.007	7	-0.46	6	0.38	5	0.87**	7

* Significant at the 5% level. ** Significant at the 1% level.

Table 4.8 The Results of the Regression of the Moisture Content or the Ash Content on $1/C_{min}$

Composition Component	Type of Dust	F-test	Residual Degrees of Freedom	Coefficient of Determination R^2	Slope	Intercept
Ash	Wheat	21.07	1	0.98	-0.0626	4.5512
Moisture	Corn-starch	11.10**	8	0.73	-1.6470	26.0200
	Corn	16.20**	7	0.82	-3.8540	50.7700
	Grain Sorghum	9.40*	7	0.73	-1.7540	23.2800

Table 4.9 Results of the Multilinear Regression Analysis for $1/C_{min}$

Type of Dust	Independent Variables in the Regression	F-test	Coefficient of Determination R^2	Residual Degrees of Freedom	Constant	Specific External Surface Area S_{ext}	Coefficients		
							Moisture	Ash	Protein
Corn	SSA, ASH	69.0**	0.95	7	--	13.22	--	0.08370	--
	Const., Ash, Mois.	17.6**	0.90	6	50.210	--	-3.743	-2.47950	--
Grain Sorghum	Const., Ash Mois.	24.0**	0.91	7	29.650	--	-2.154	-0.26800	--
Wheat	Const., Ash Protein	4.1	0.71	5	1.898	--	--	-0.05746	0.1871
	SSA, Ash, Protein	5.5*	0.77	5	--	6.71	--	-0.05010	0.2440
Corn-starch	Const., Mois.	11.0**	0.73	8	26.020	--	-1.647	--	--
All Dusts	Const., Mois. Ash, Prot.	39.8**	0.83	32	25.730	--	-1.629	-0.20100	-0.3093
	SSA, Mois., Ash, Protein	1.6	0.22	32	--	--	--	--	--

Table 4.10 Ignition Delay Times

Sample Identification	Minimum Explosible Concentration	Ignition Delay msec
CNAC-S01	0.16	94
CNAC-S02	0.22	29
CNAC-S02	0.22	83
CNAC-S03	0.26	123
CNAC-S03	0.26	72
CNAC-S08	0.33	137
CNAC-S09	0.28	14
CNAC-S10	0.50	98
WTAC-S03	0.29	152
WTAC-S03	0.29	221
WTAC-S04	0.25	239
WTAC-S04	0.29	253
WTAC-S05	0.36	181
WTAC-S05	0.35	217
WTAC-S06	0.57	> 412
WTAC-S06	0.54	> 376
WTAC-S07	0.30	> 329
WTAC-S07	0.30	> 289
WTAC-S08	0.30	> 466
WTAC-S08	0.32	> 325
WTAC-S09	0.41	278
WTAC-S09	0.38	260
WTAC-S10	0.37	347
WTAC-S10	0.36	> 231
MOAC-S01	0.15	137
MOAC-S02	0.17	40
MOAC-S02	0.19	94
MOAC-S03	0.20	177

Table 4.10 (continued)

Sample Identification	Minimum Explosible Concentration	Ignition Delay msec
MOAC-S03	0.23	> 108
MOAC-S06	0.37	412
MOAC-S07	0.31	> 318
MOAC-S07	0.33	> 470
MOAC-S08	0.35	> 94
MOAC-S09	0.43	> 390
MOAC-S10	0.49	> 477
CSAC-S01	0.05	14
CSAC-S01	0.04	22
CSAC-S02	0.05	~0
CSAC-S02	0.04	36
CSAC-S03	0.16	29
CSAC-S03	0.15	--
CSAC-S04	0.29	134
CSAC-S04	0.15	54
CSAC-S05	0.15	87
CSAC-S05	0.15	83
CSAC-S06	0.12	25
CSAC-S06	0.13	22
CSAC-S07	0.16	76
CSAC-S07	0.20	130

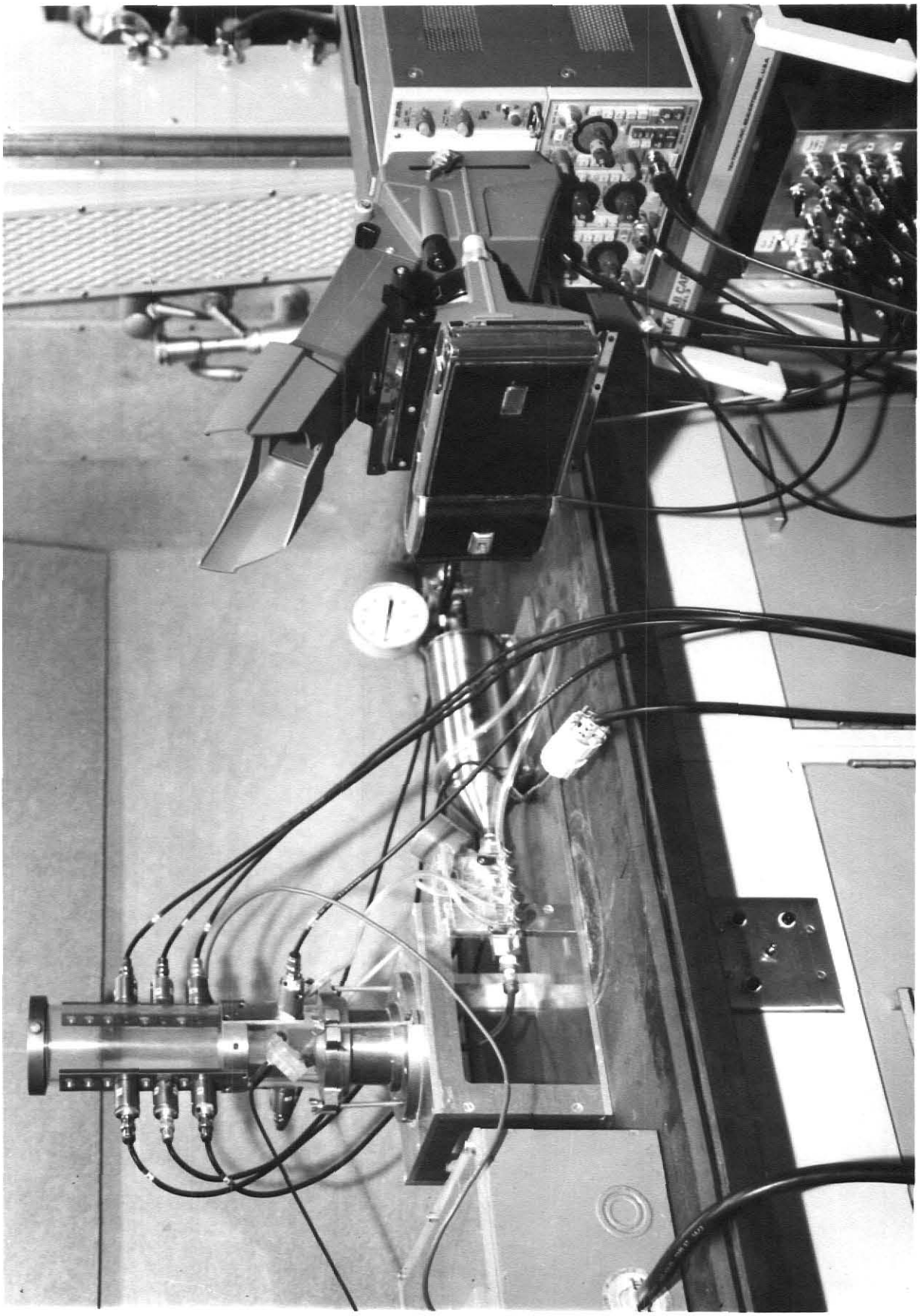

Fig. 4.1 Photograph of the Hartmann Apparatus Used to Determine the Minimum Explosible Concentration

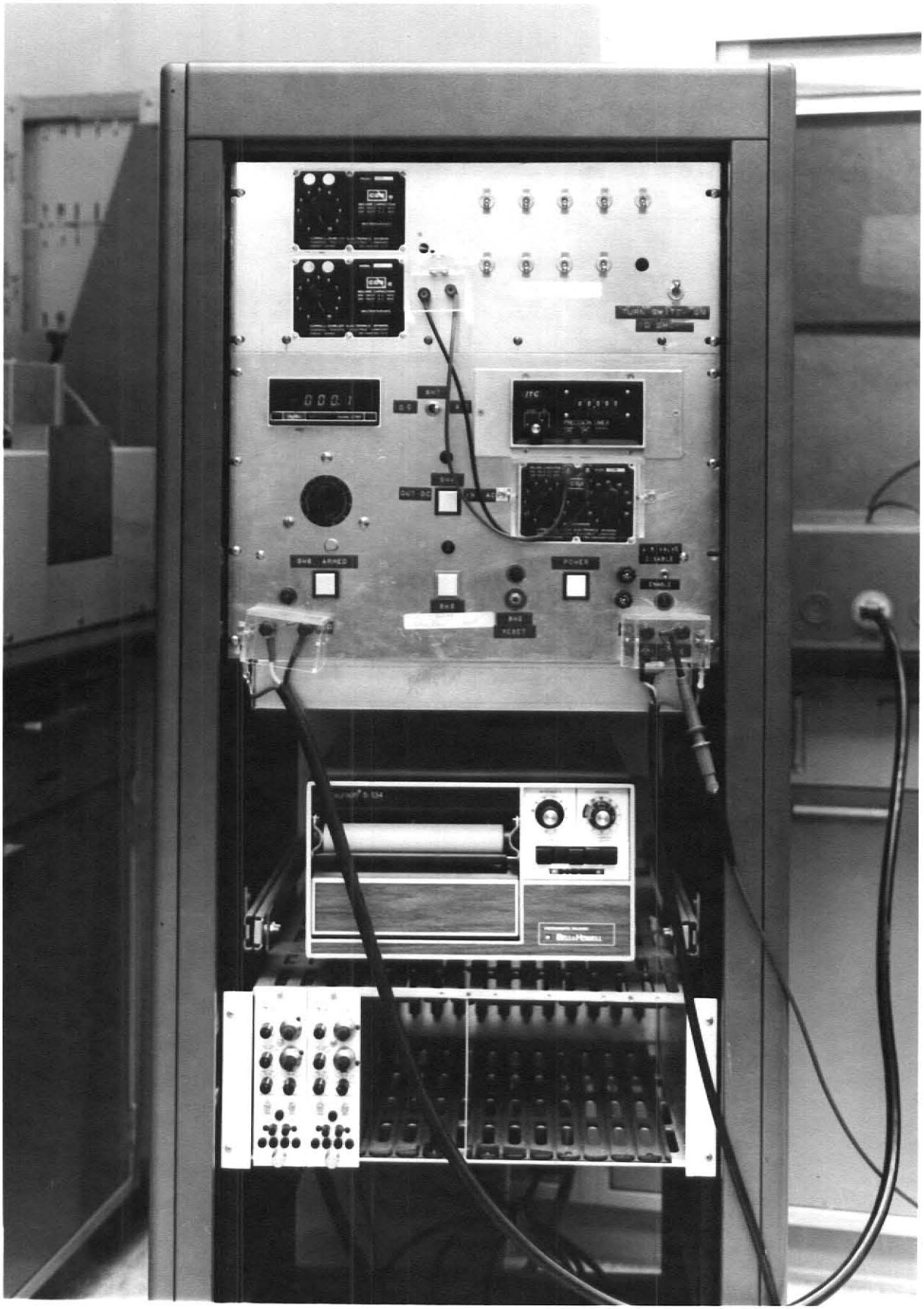

Fig. 4.2 Photograph of the Ignition Timing Circuitry

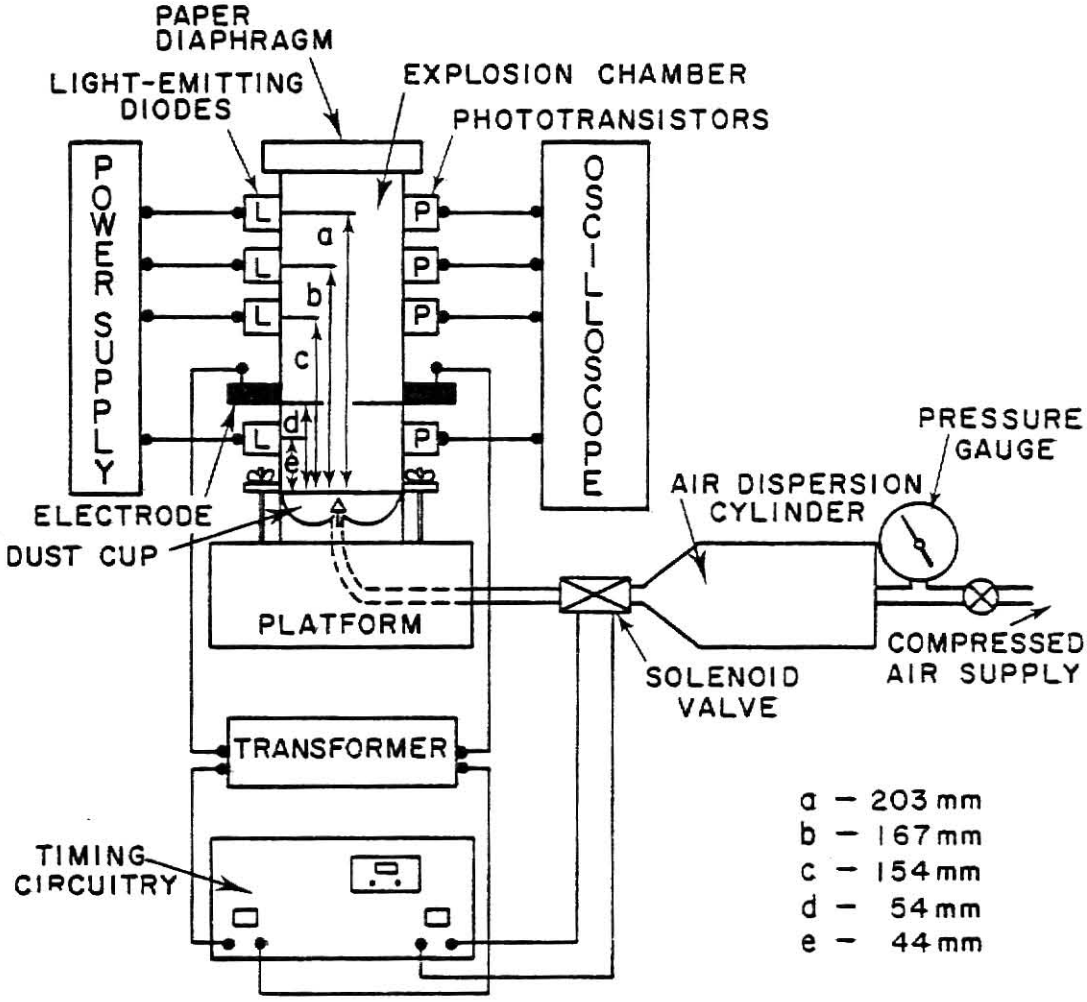

Fig. 4.3 Schematic Diagram of the Entire Experimental Apparatus

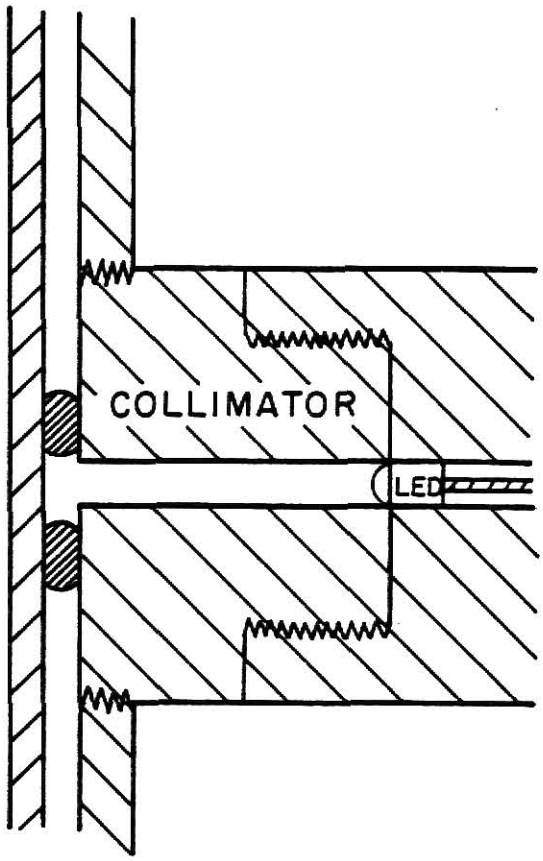

Fig. 4.4 Schematic Diagram of a Light-Emitting Diode (LED)

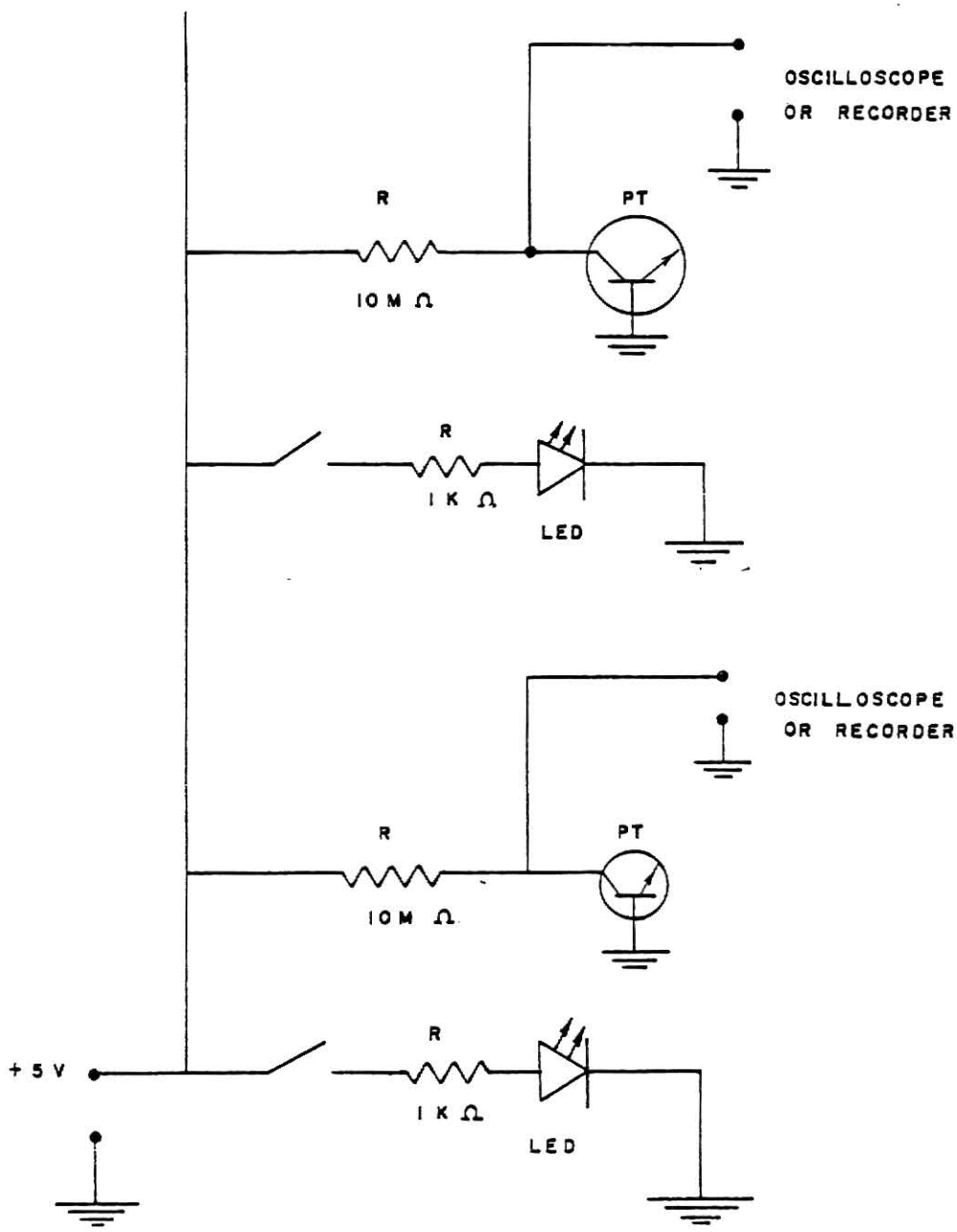

Fig. 4.5 Schematic Diagram of the Electrical Circuitry for the Light-Emitting Diodes and Phototransistors

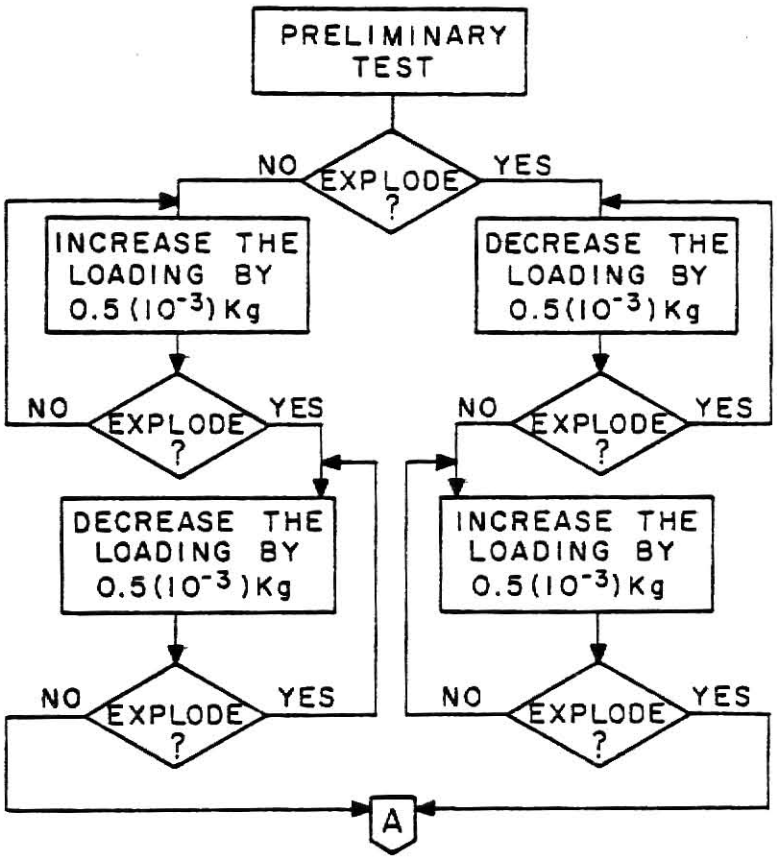

Fig. 4.6a Logic Diagram of the Procedure Used to Determine the Minimum Explosible Concentration

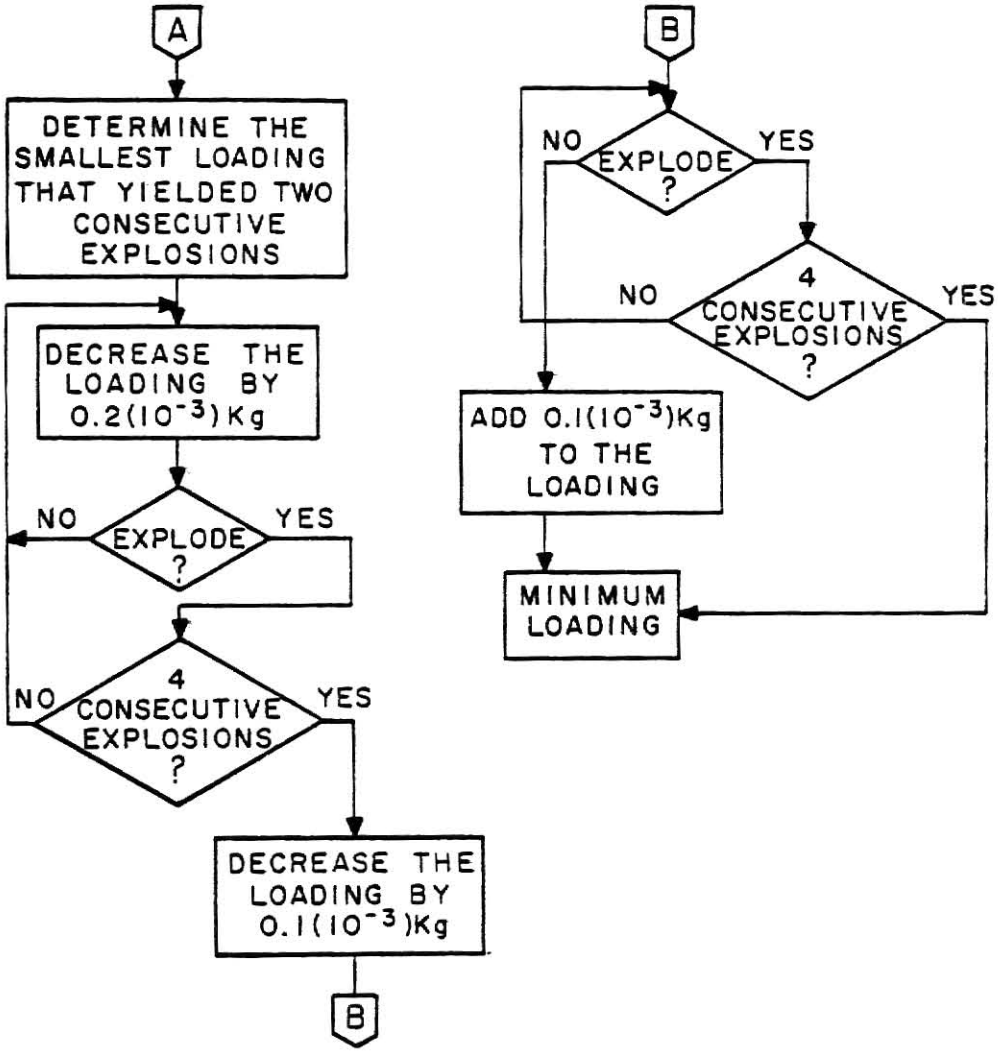

Fig. 4.6b Logic Diagram of the Procedure Used to Determine the Minimum Explosible Concentration

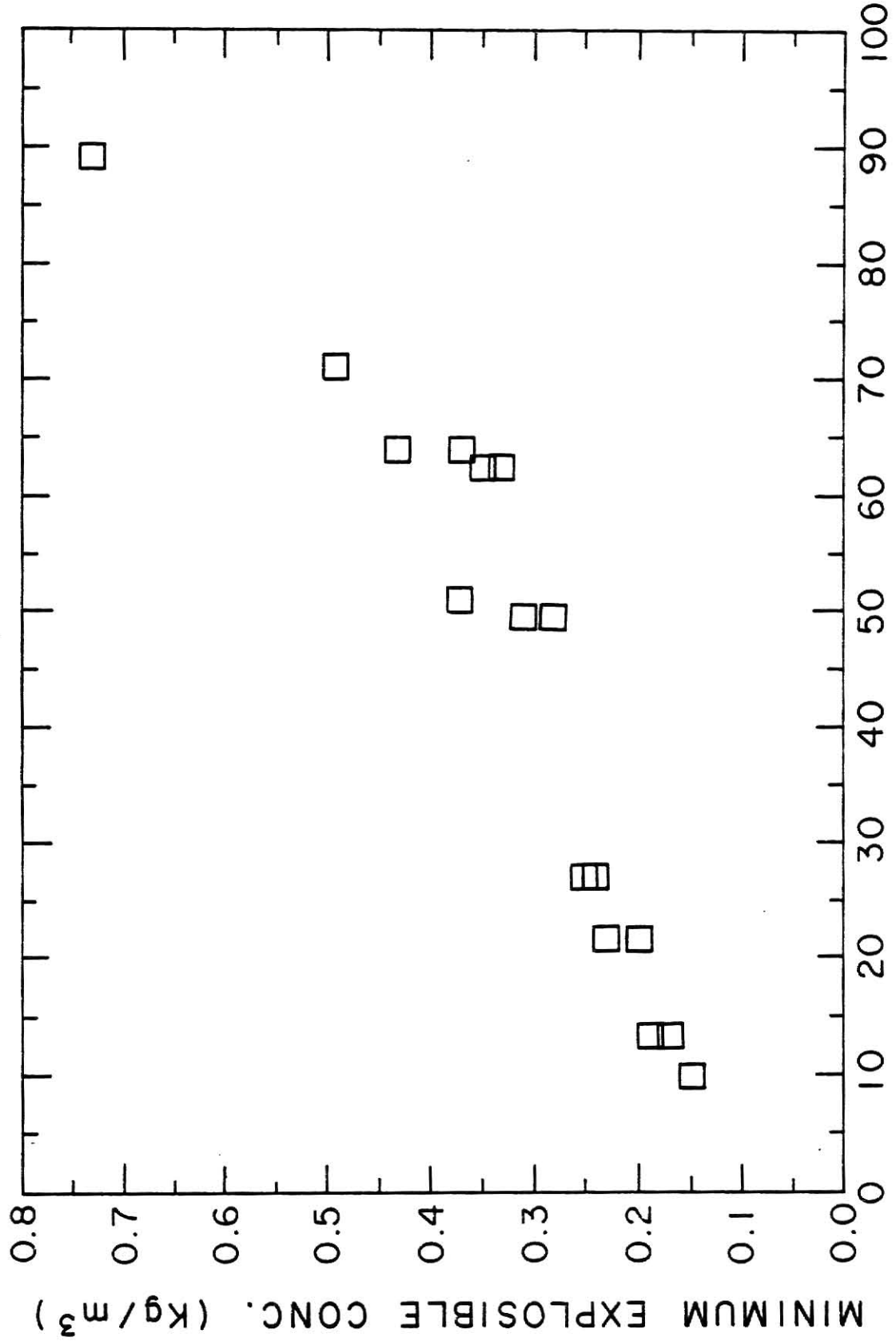

Fig. 4.7 The Relationship between the Minimum Explosible Concentration and the Mass Mean Diameter for Grain Sorghum Dust

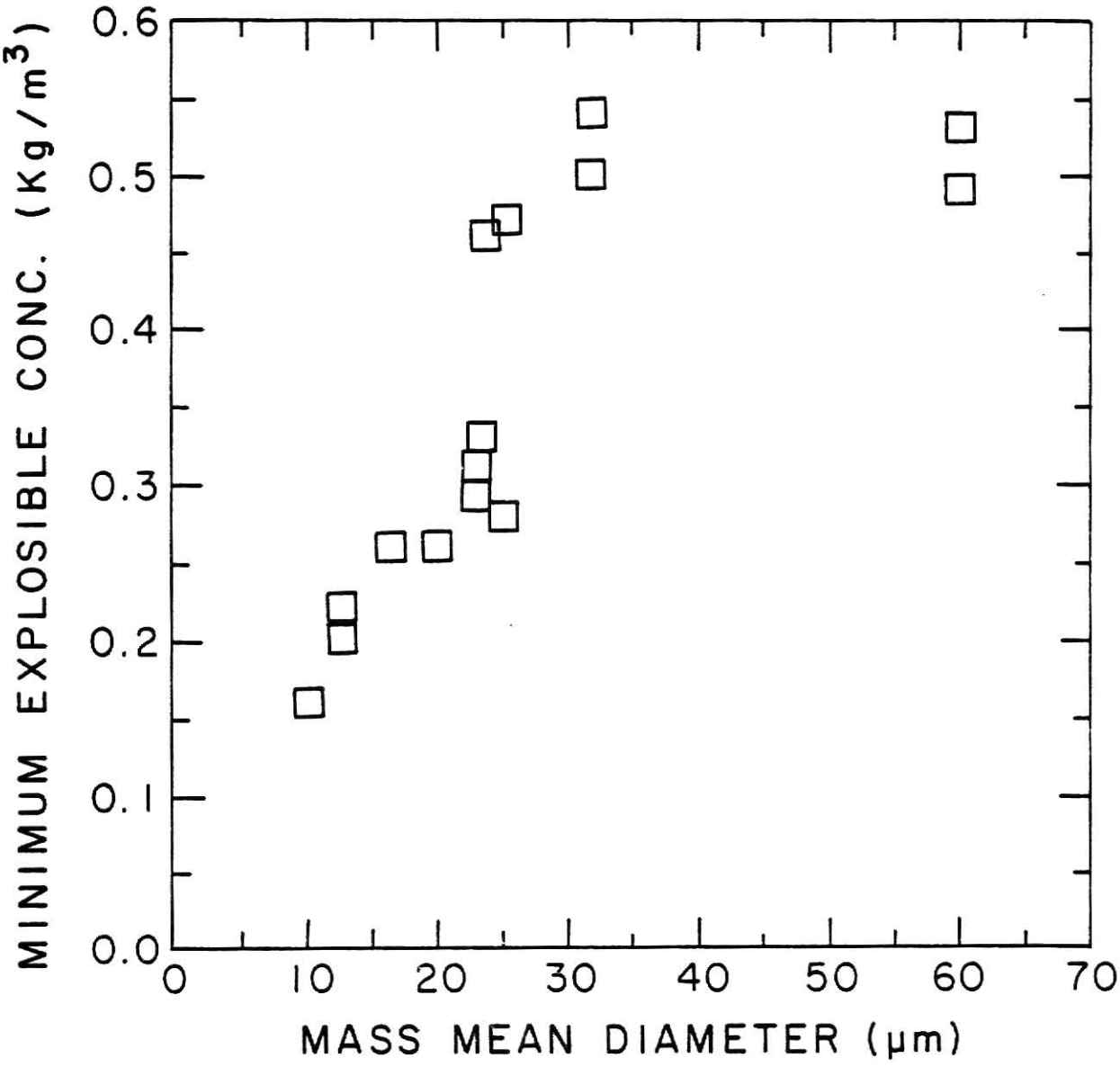

Fig. 4.8 The Relationship between the Minimum Explosible Concentration and the Mass Mean Diameter for Corn Dust

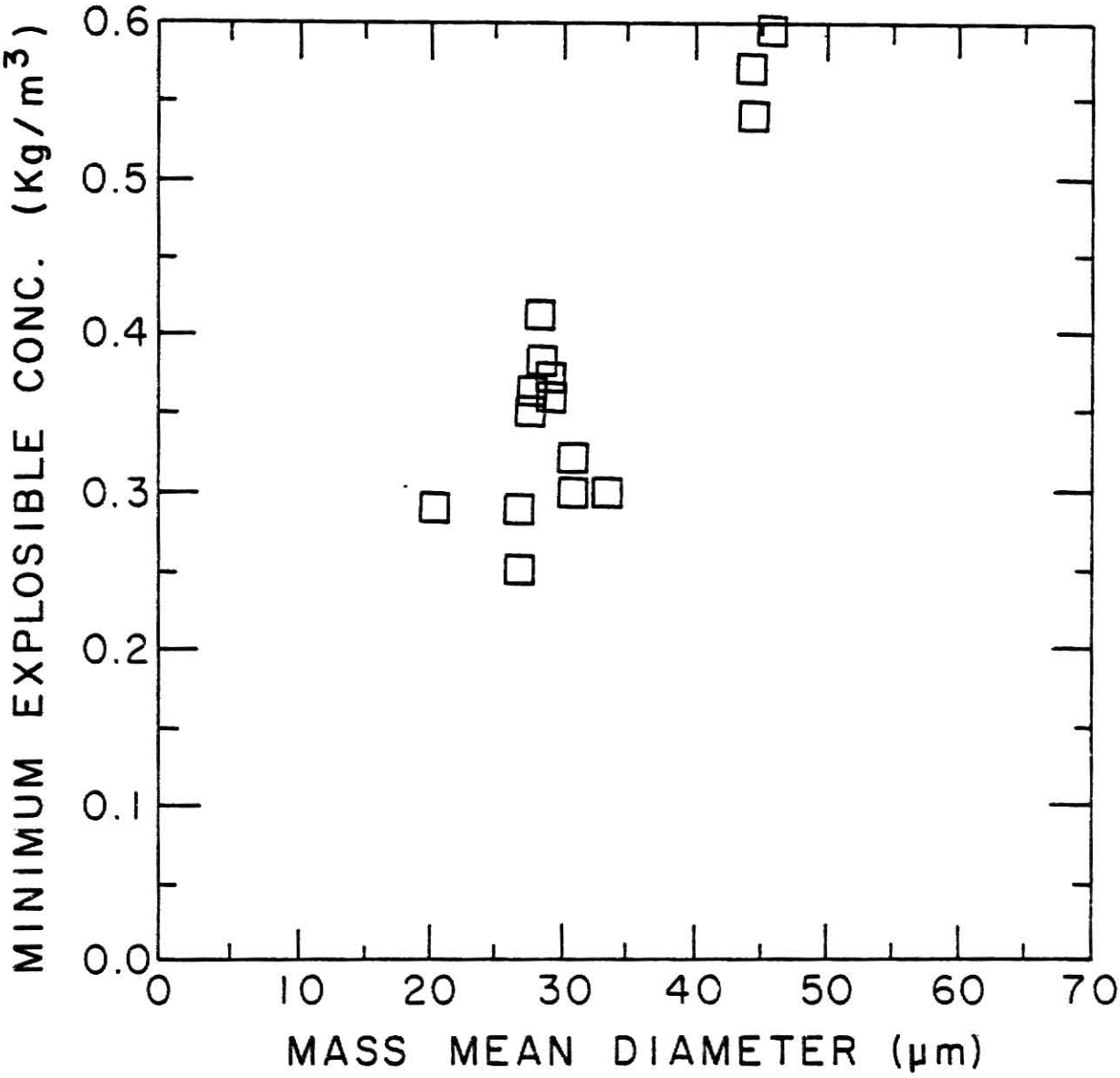

Fig. 4.9 The Relationship between the Minimum Explosible Concentration and the Mass Mean Diameter for Wheat Dust

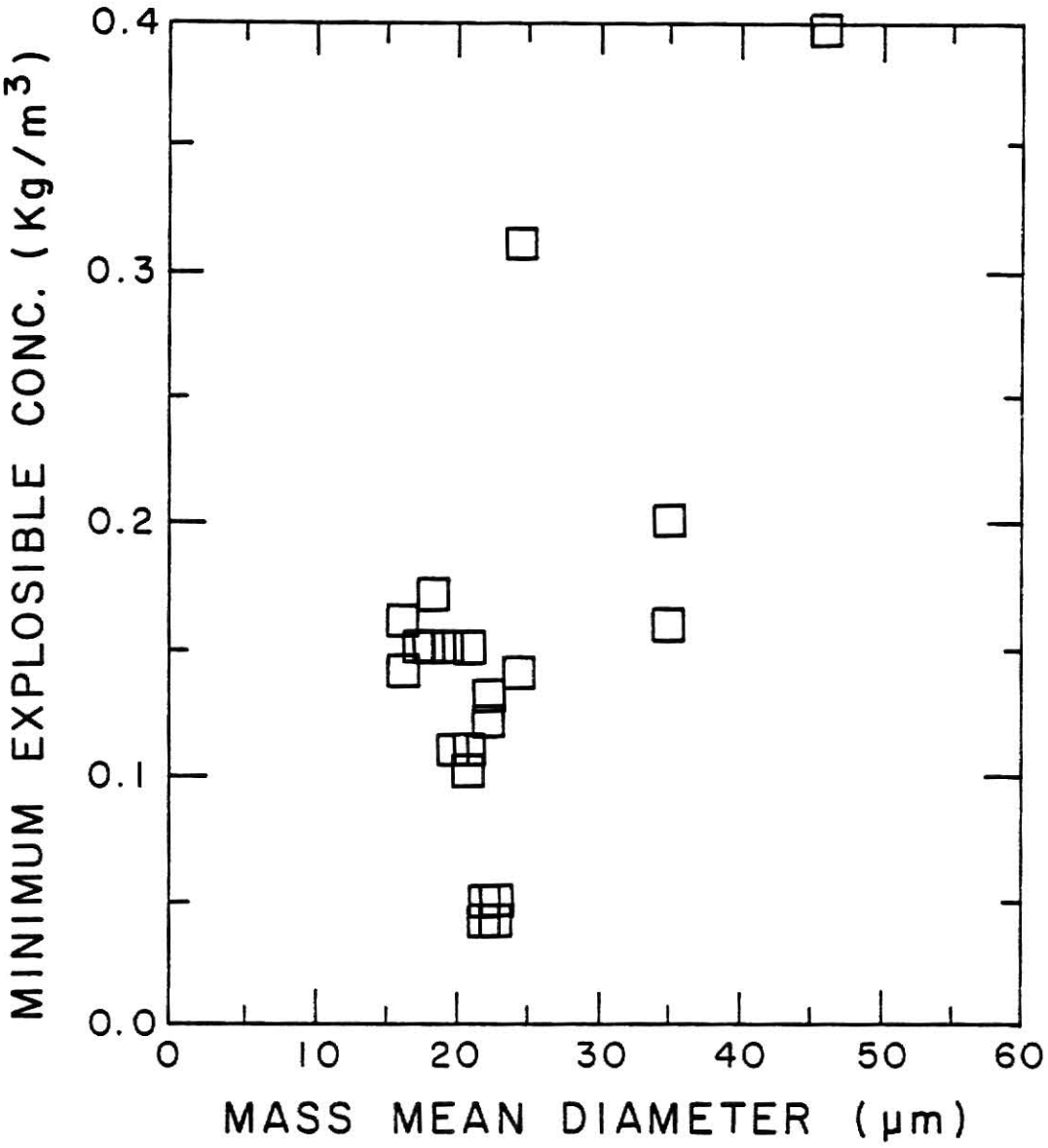

Fig. 4.10 The Relationship between the Minimum Explosible Concentration and the Mass Mean Diameter for Cornstarch

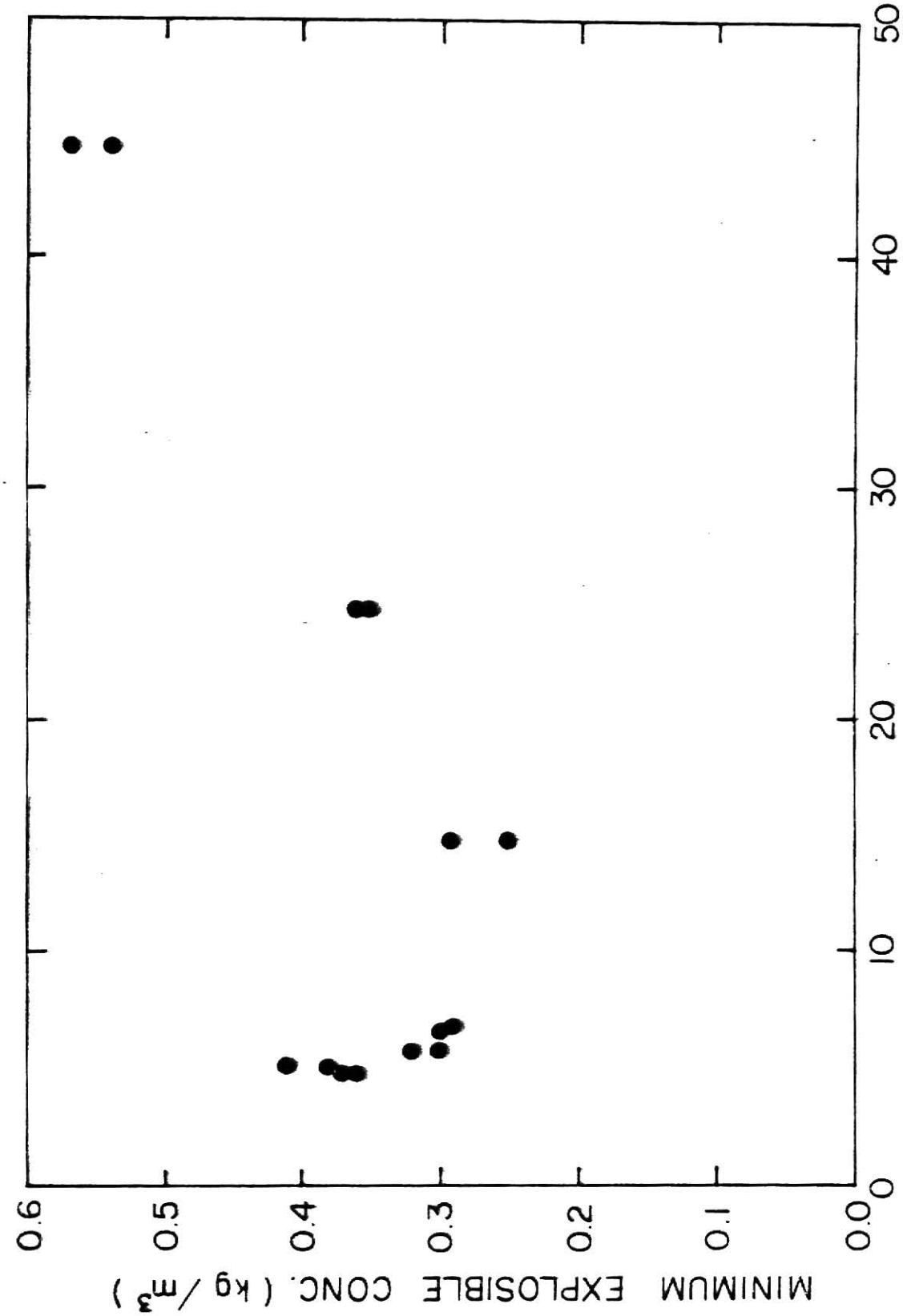

Fig. 4.11 The Relationship between the Minimum Explosible Concentration and the Ash Content for Wheat Dust

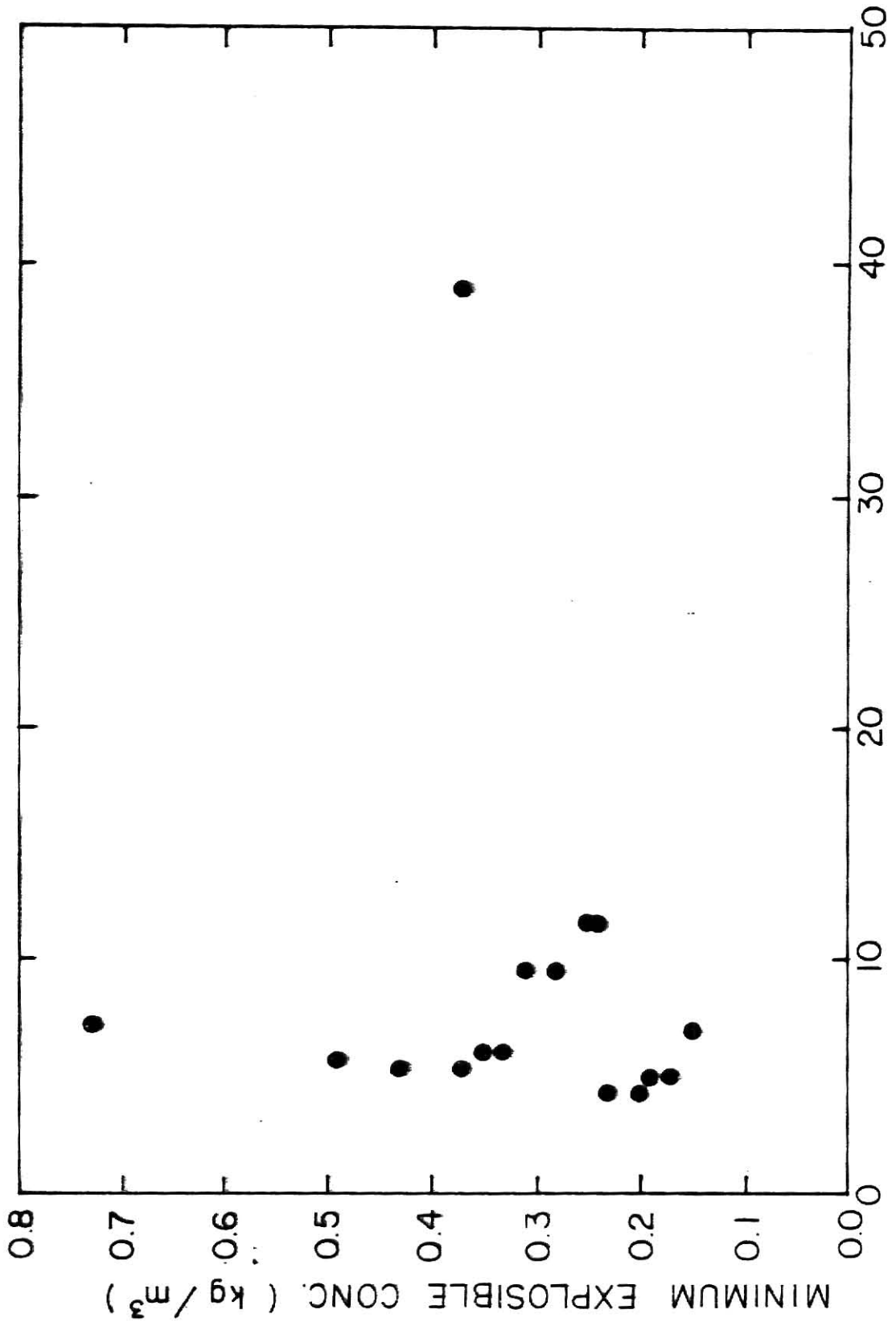

Fig. 4.12 The Relationship between the Minimum Explosible Concentration and the Ash Content for Grain Sorghum Dust

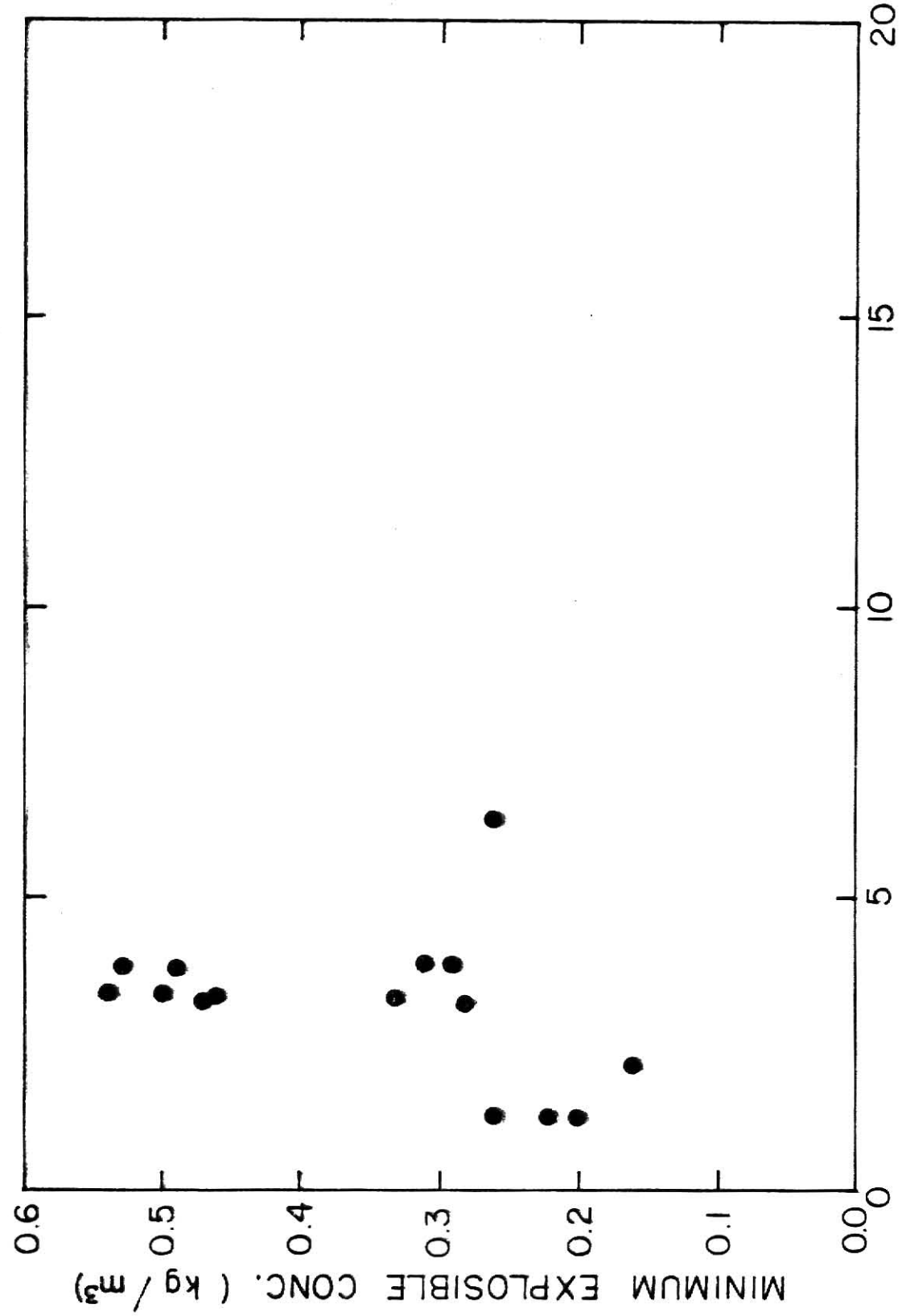

Fig. 4.13 The Relationship between the Minimum Explosible Concentration and the Ash Content for Corn Dust.

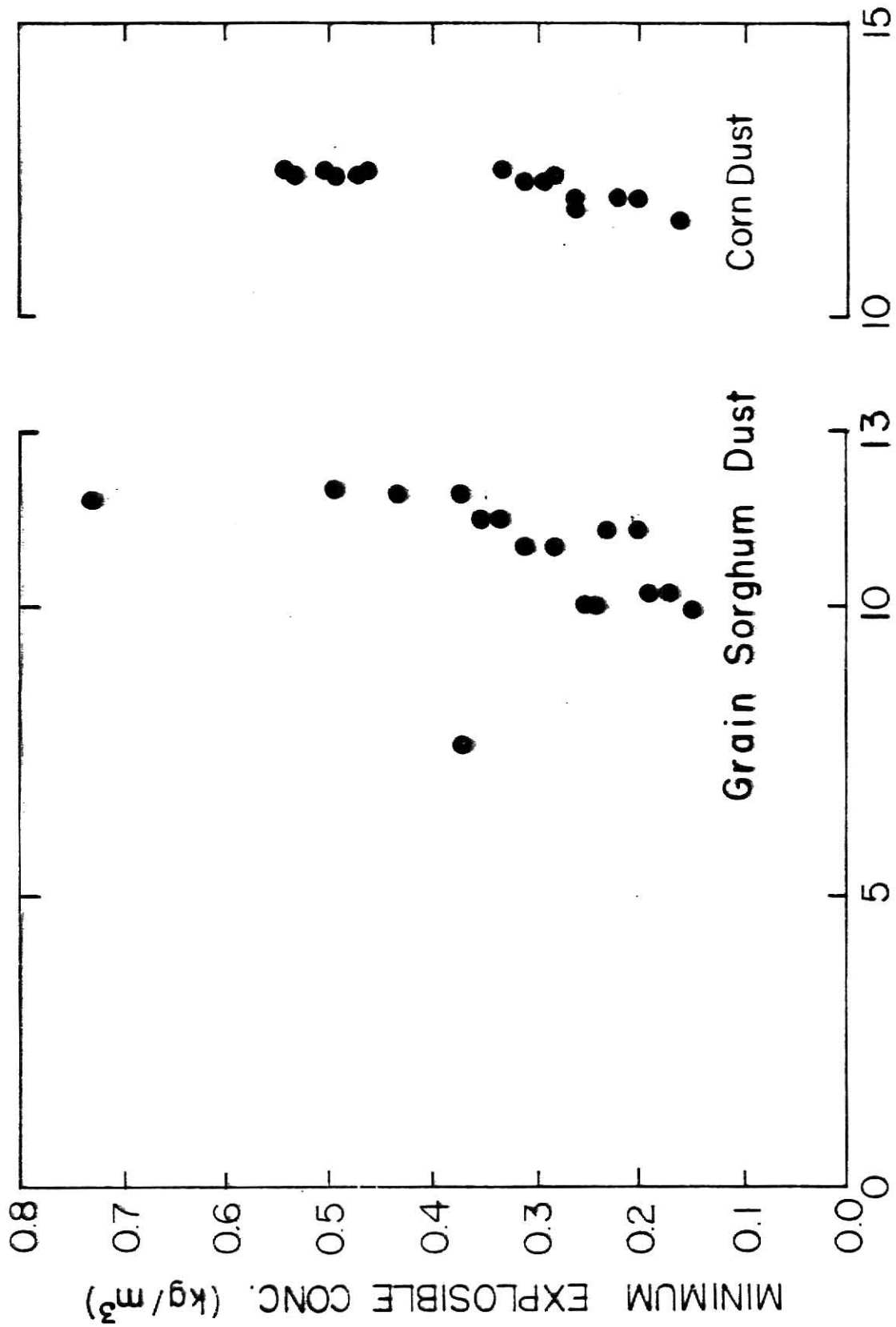

Fig. 4.14 The Relationship between the Minimum Explosible Concentration and the Moisture Content for Grain Sorghum Dust and Corn Dust

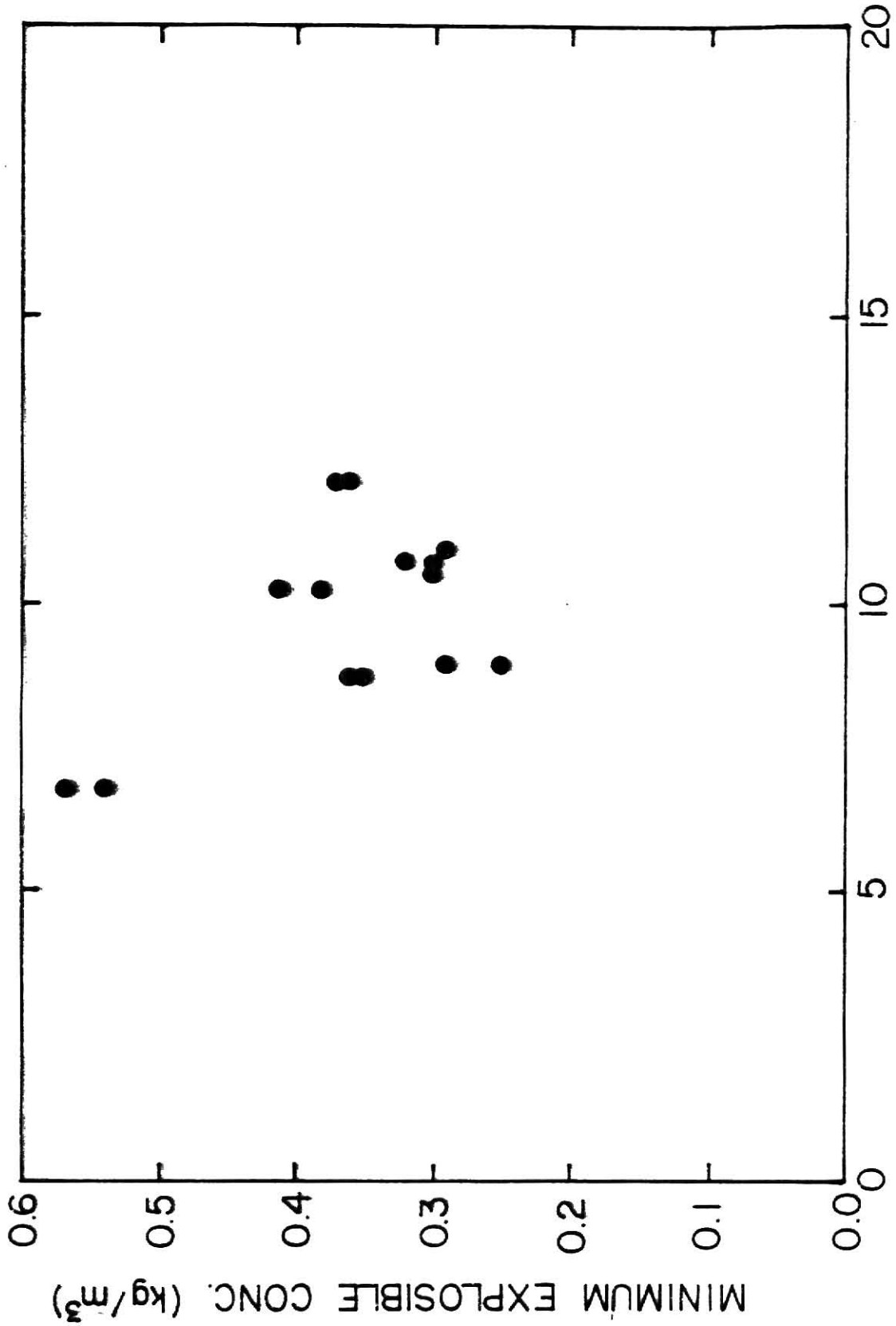

Fig. 4.15 The Relationship between the Minimum Explosible Concentration and the Moisture Content for Wheat Dust

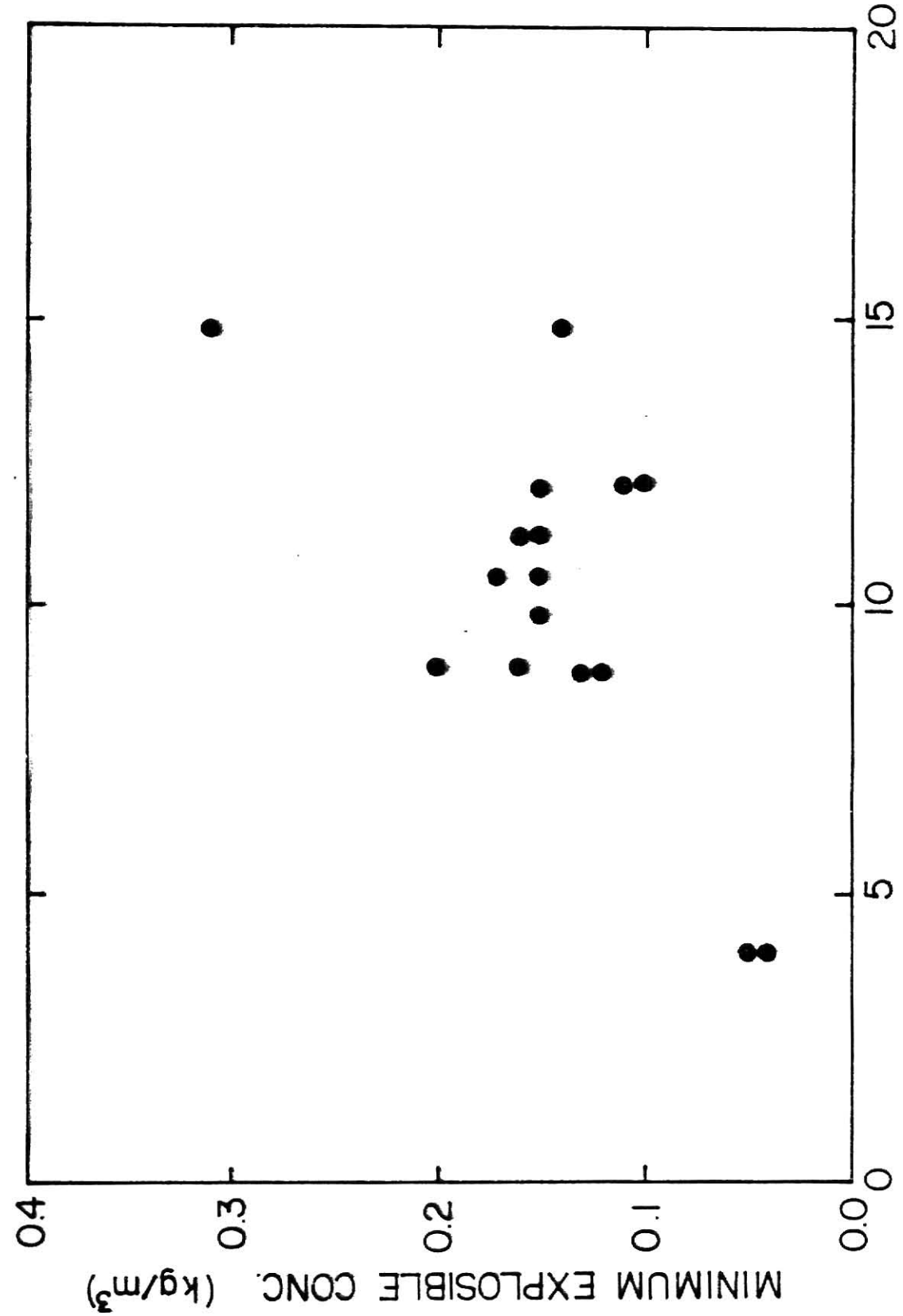

Fig. 4.16 The Relationship between the Minimum Explosible Concentration and the Moisture Content for Cornstarch

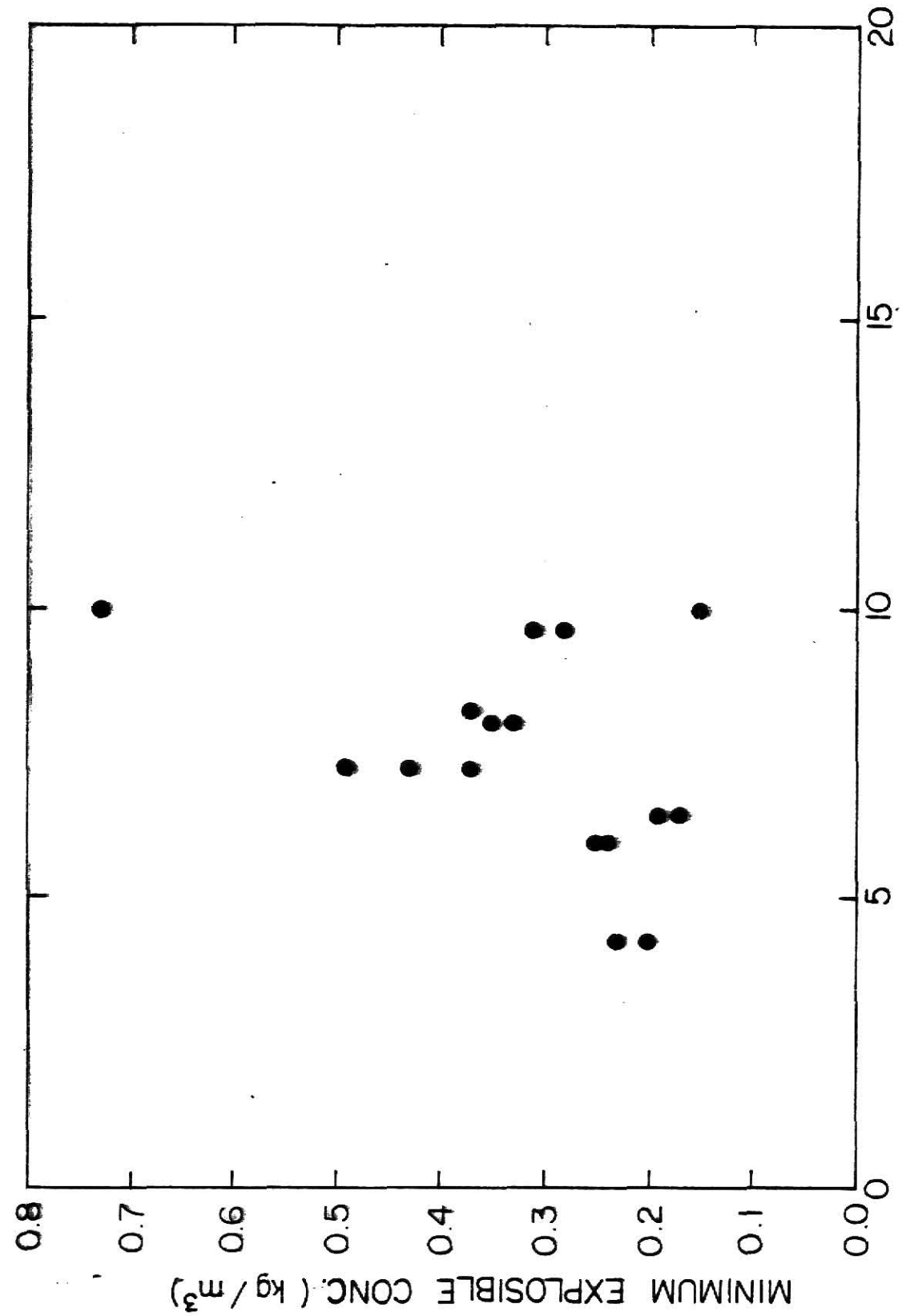

Fig. 4.17 The Relationship between the Minimum Explosible Concentration and the Protein Content for Grain Sorghum Dust

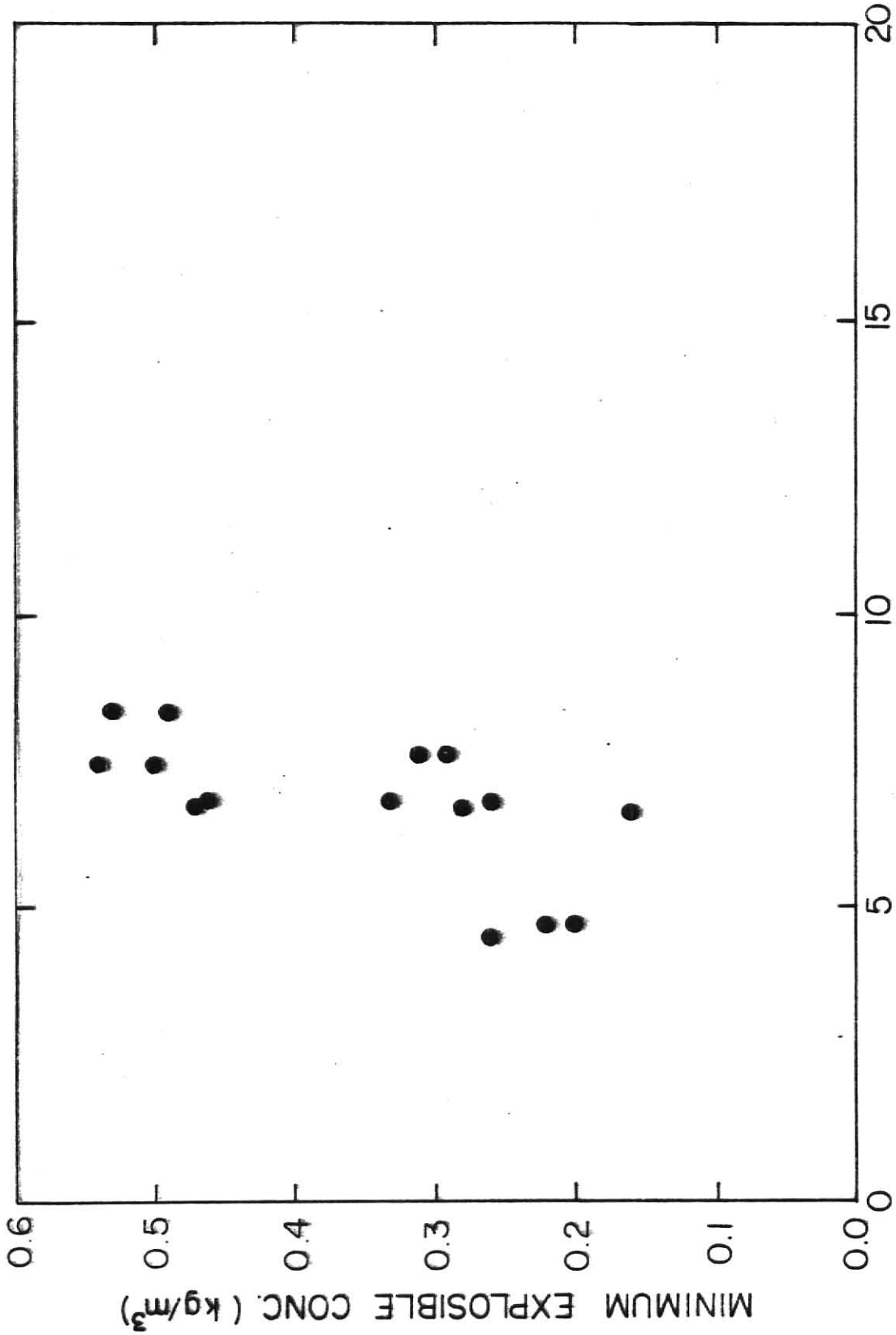

Fig. 4.18 The Relationship between the Minimum Explosible Concentration and the Protein Content for Corn Dust

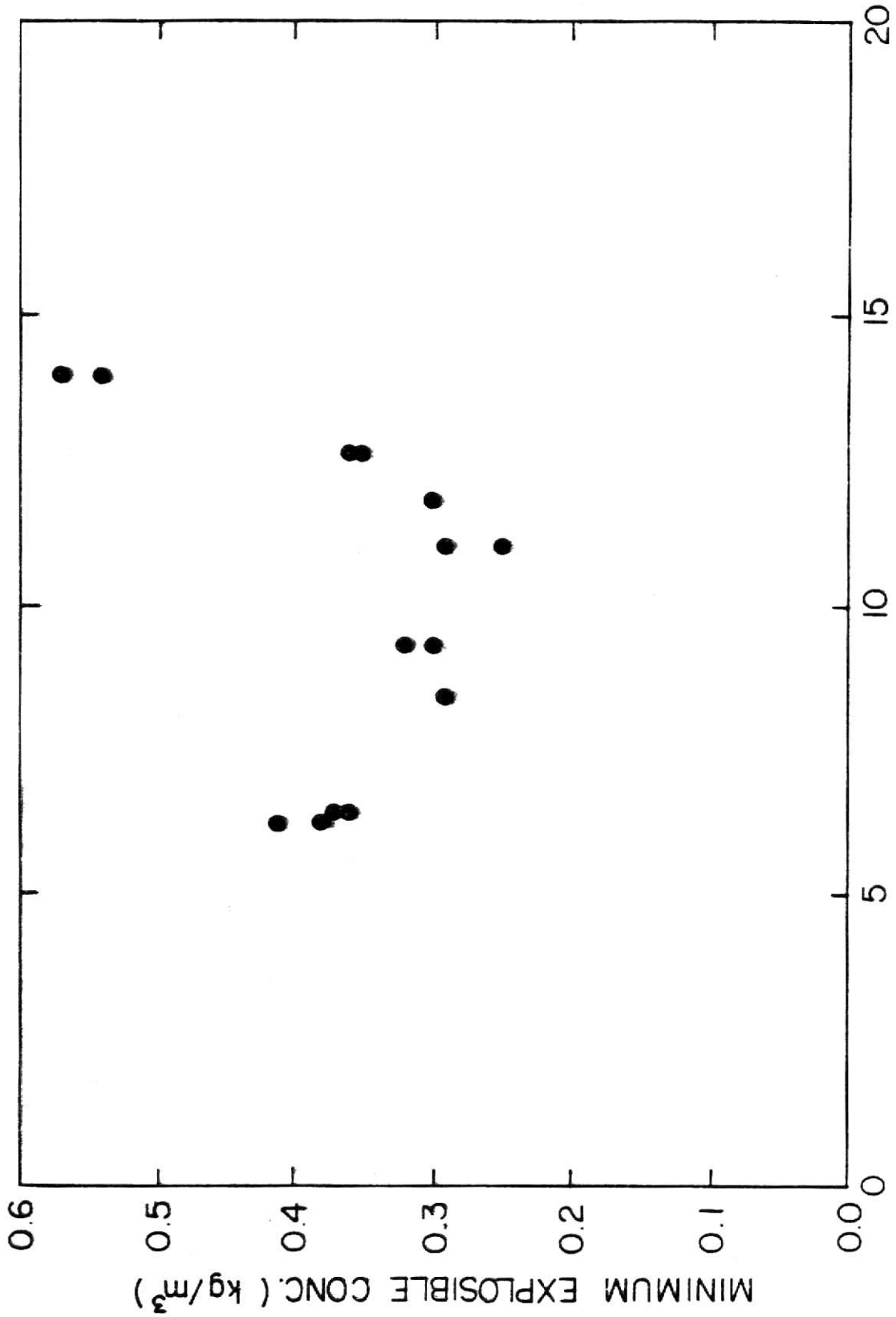

Fig. 4.19 The Relationship between the Minimum Explosible Concentration and the Protein Content for Wheat Dust

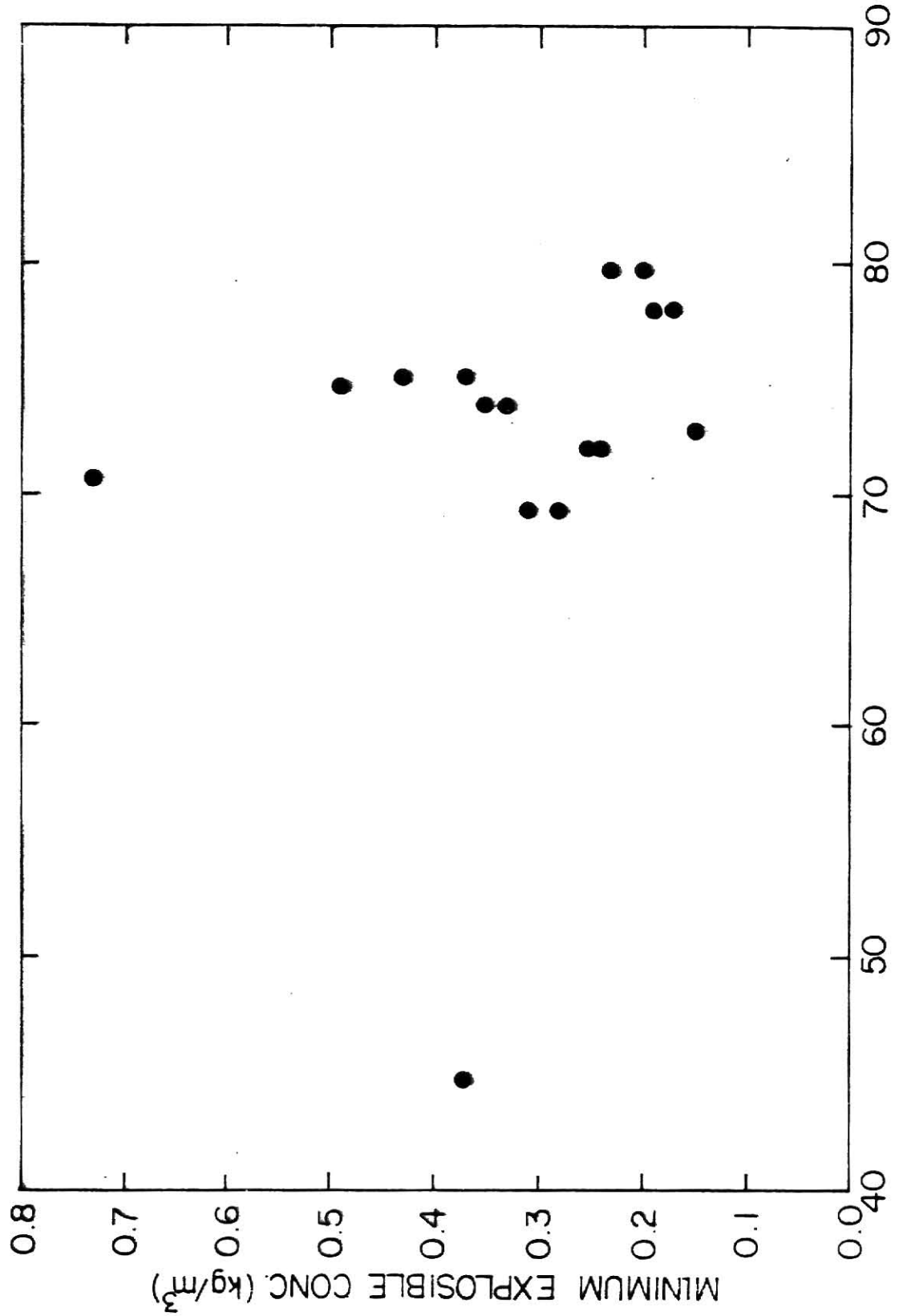

Fig. 4.20 The Relationship between the Minimum Explosible Concentration and the Starch and Fiber Content for Grain Sorghum Dust

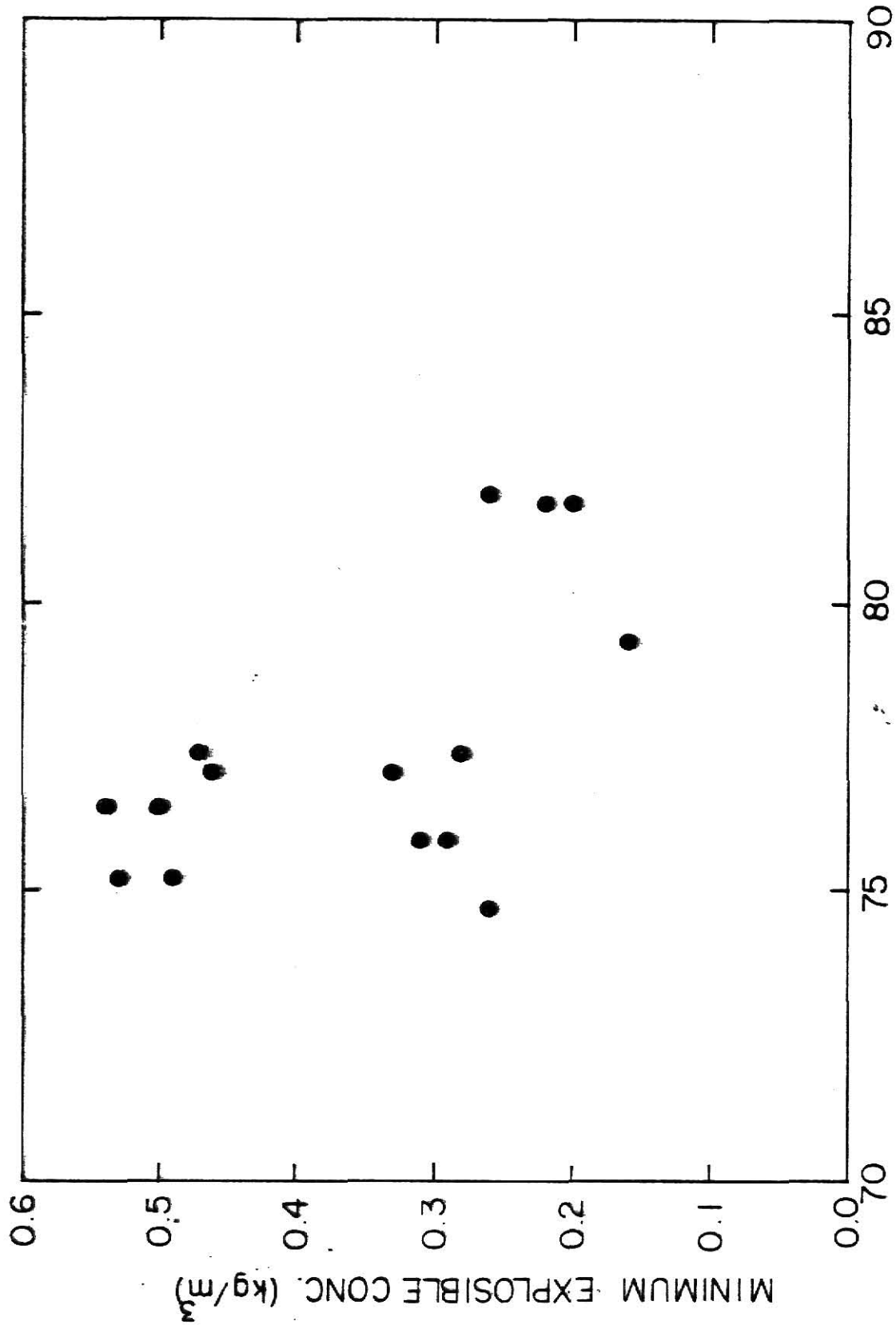

Fig. 4.21 The Relationship between the Minimum Explosible Concentration and the Starch and Fiber Content for Corn Dust

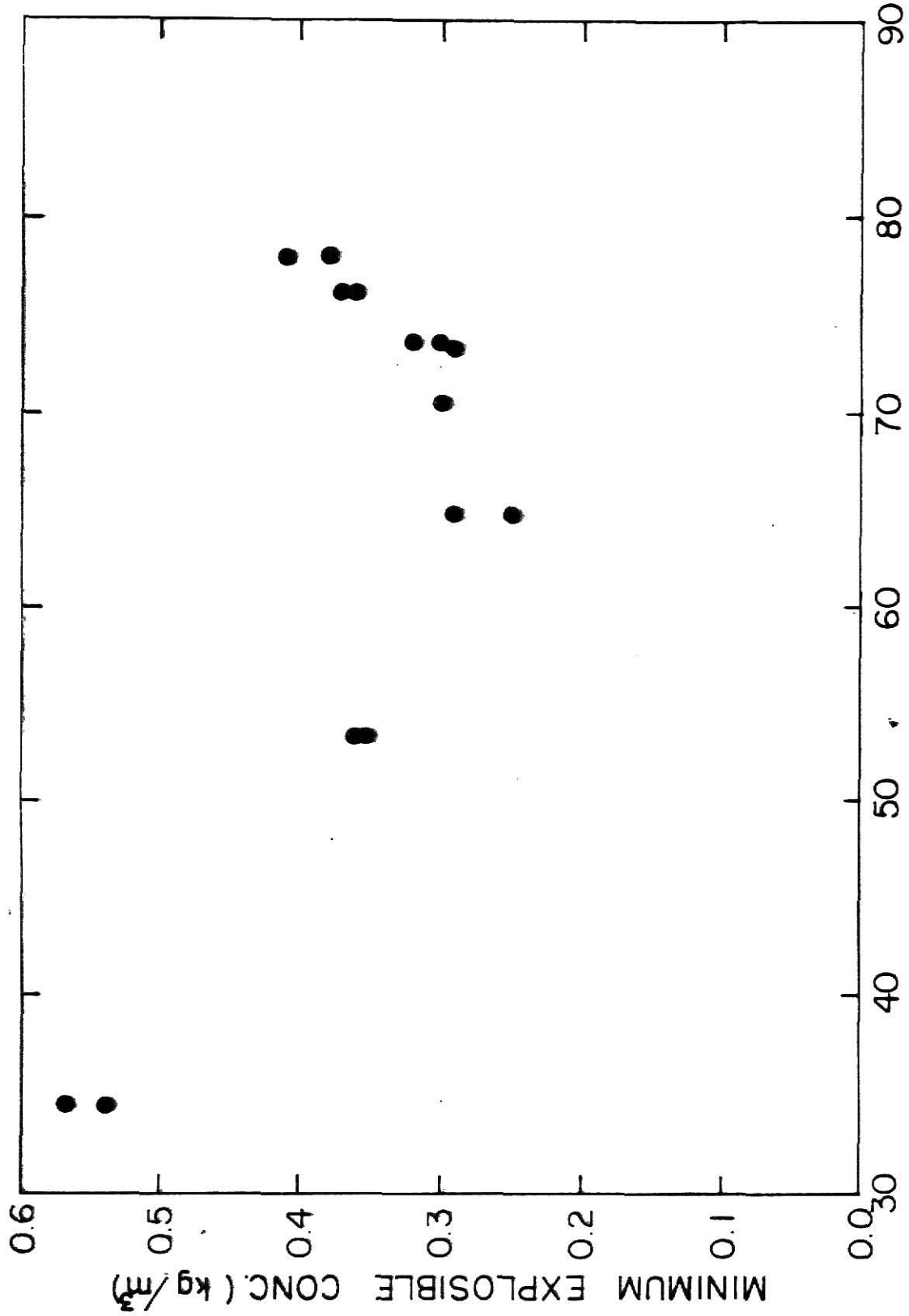

Fig. 4.22 The Relationship between the Minimum Explosible Concentration and the Starch and Fiber Content for Wheat Dust

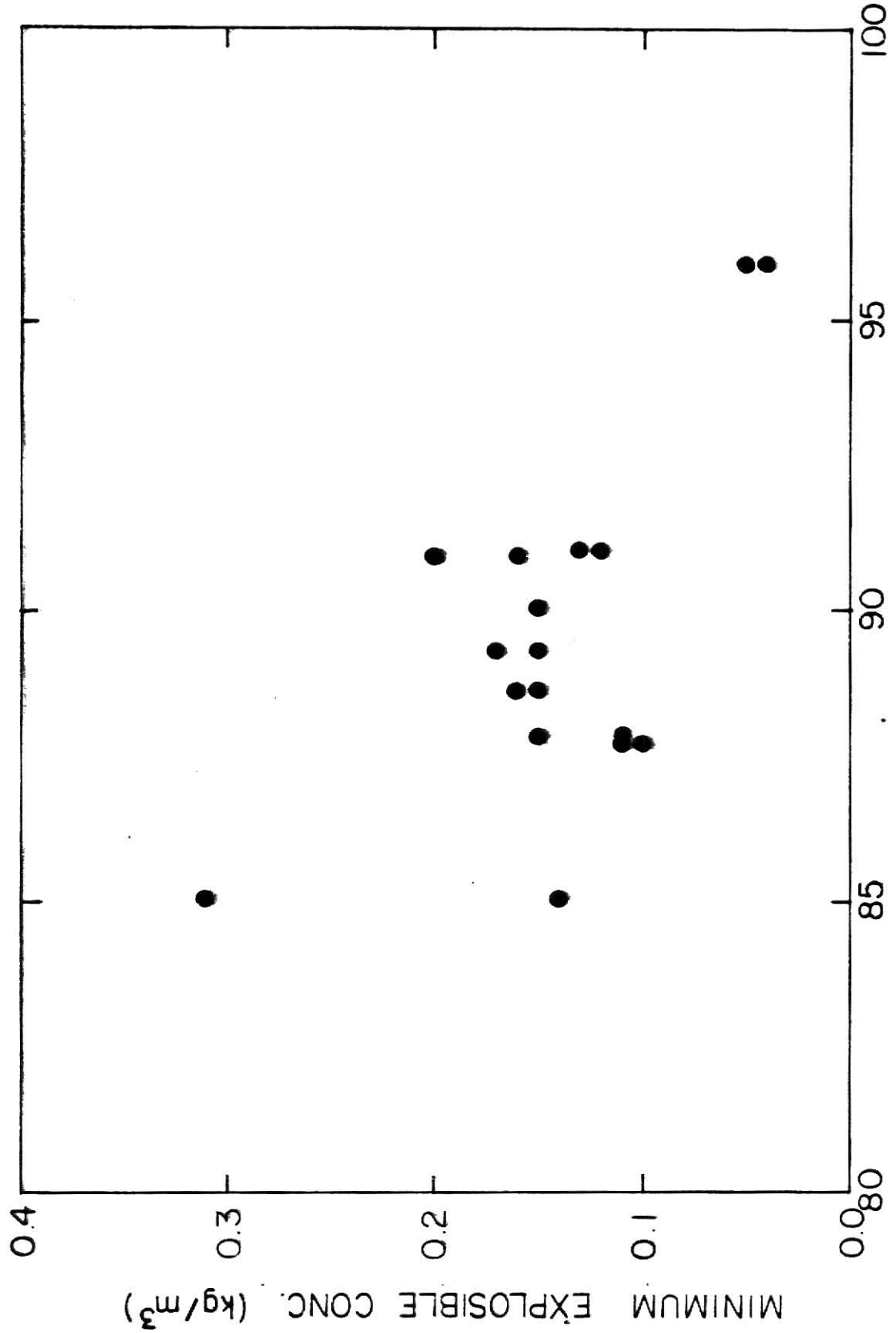

Fig. 4.23 The Relationship between the Minimum Explosible Concentration and the Starch and Fiber Content for Cornstarch

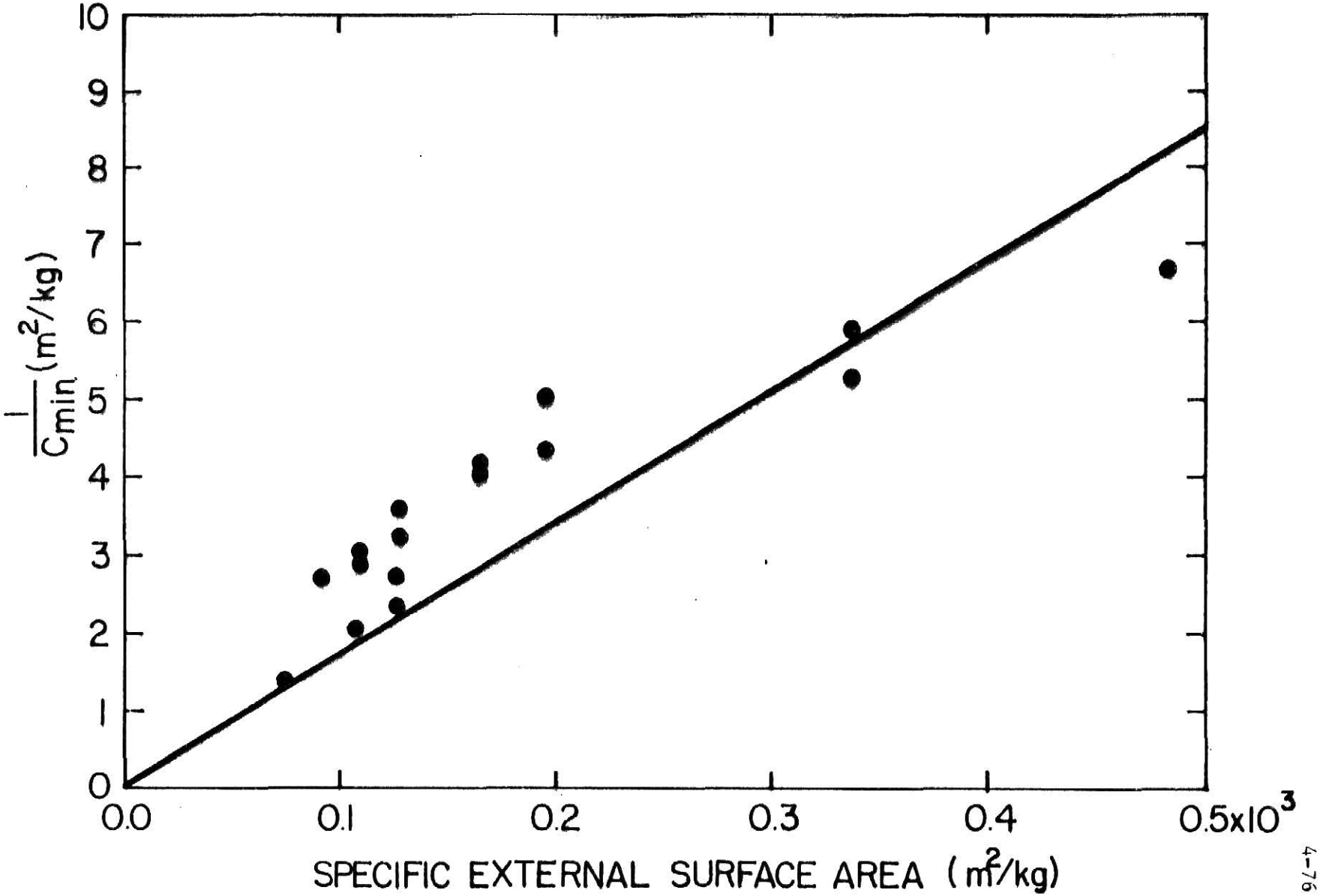

Fig. 4.24 The Relationship between the Reciprocal of the Minimum Explosible Concentration and the Specific External Surface Area for Grain Sorghum Dust

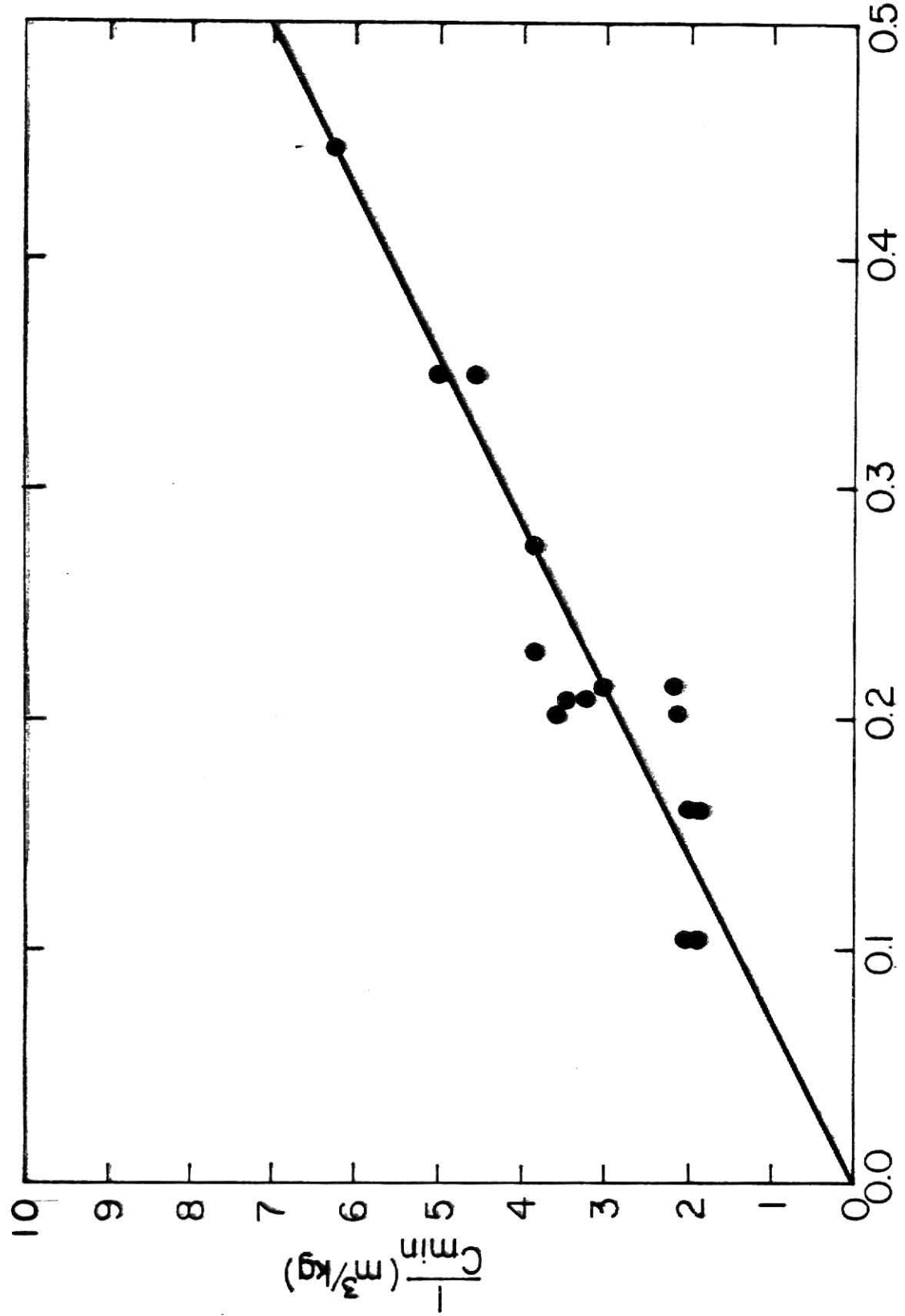

Fig. 4.25 The Relationship between the Reciprocal of the Minimum Explosible Concentration and the Specific External Surface Area for Corn Dust

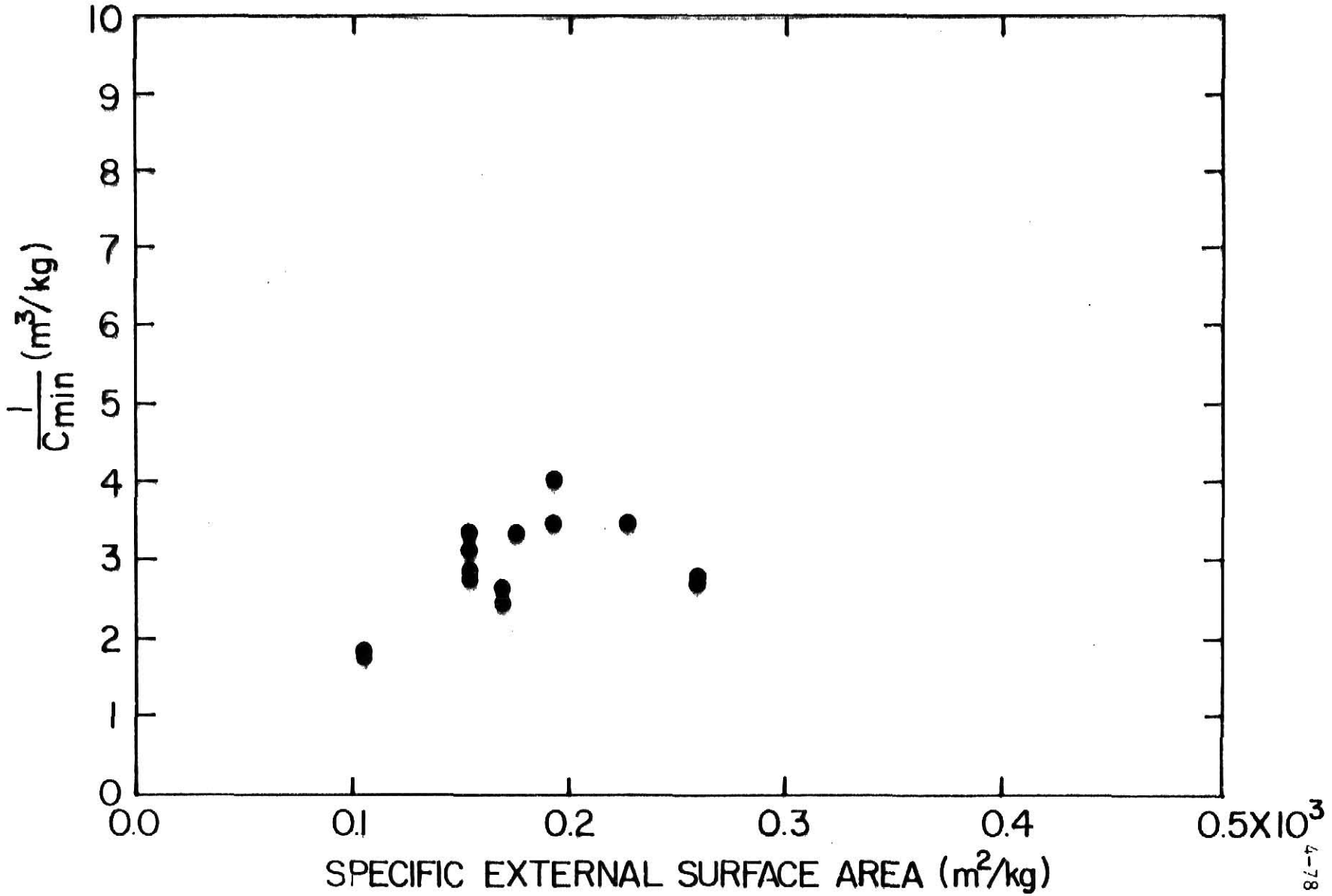

Fig. 4.26 The Relationship between the Reciprocal of the Minimum Explosible Concentration and the Specific External Surface Area for Wheat Dust

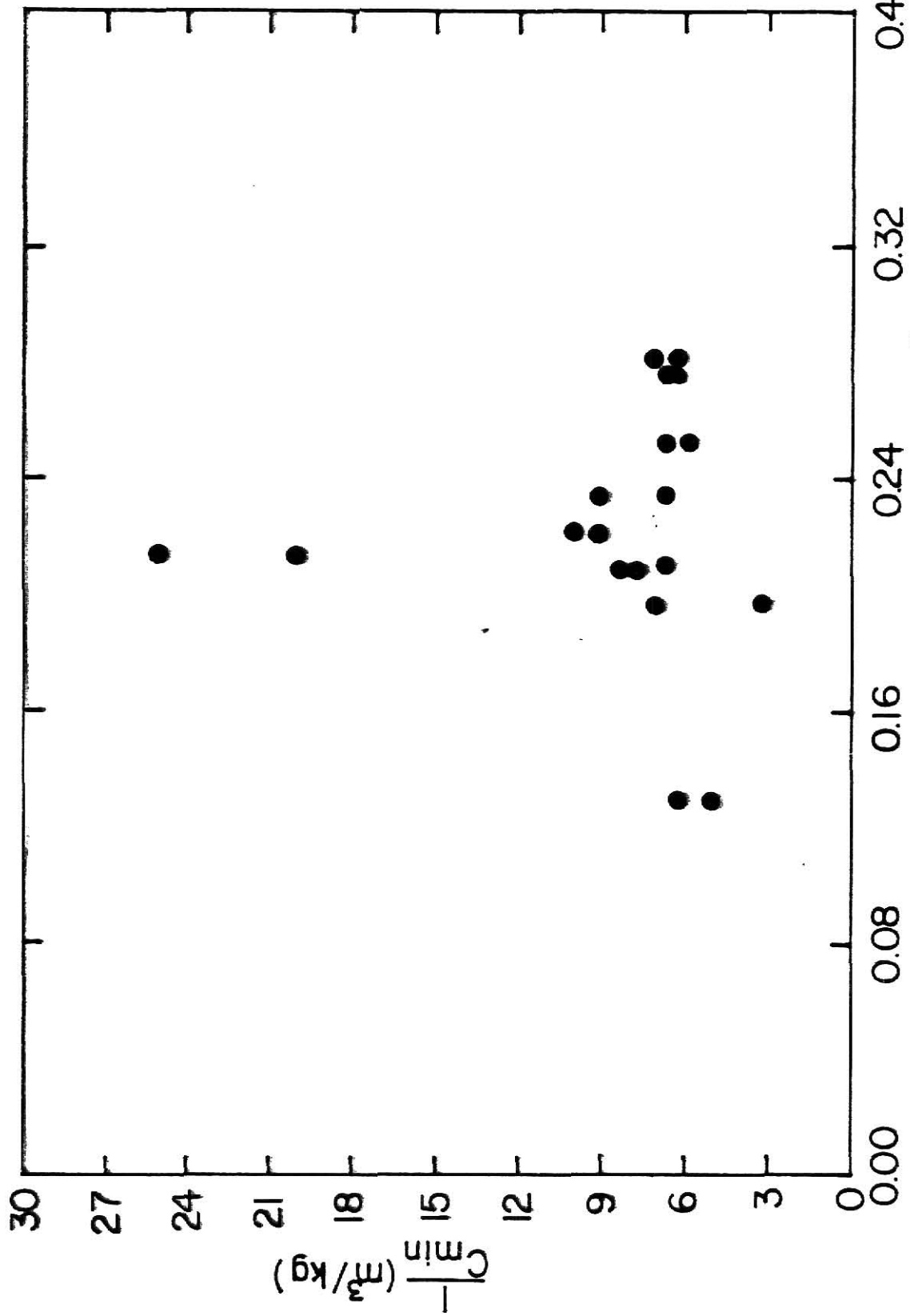

Fig. 4.27 The Relationship between the Reciprocal of the Minimum Explosible Concentration and the Specific External Surface Area for Cornstarch

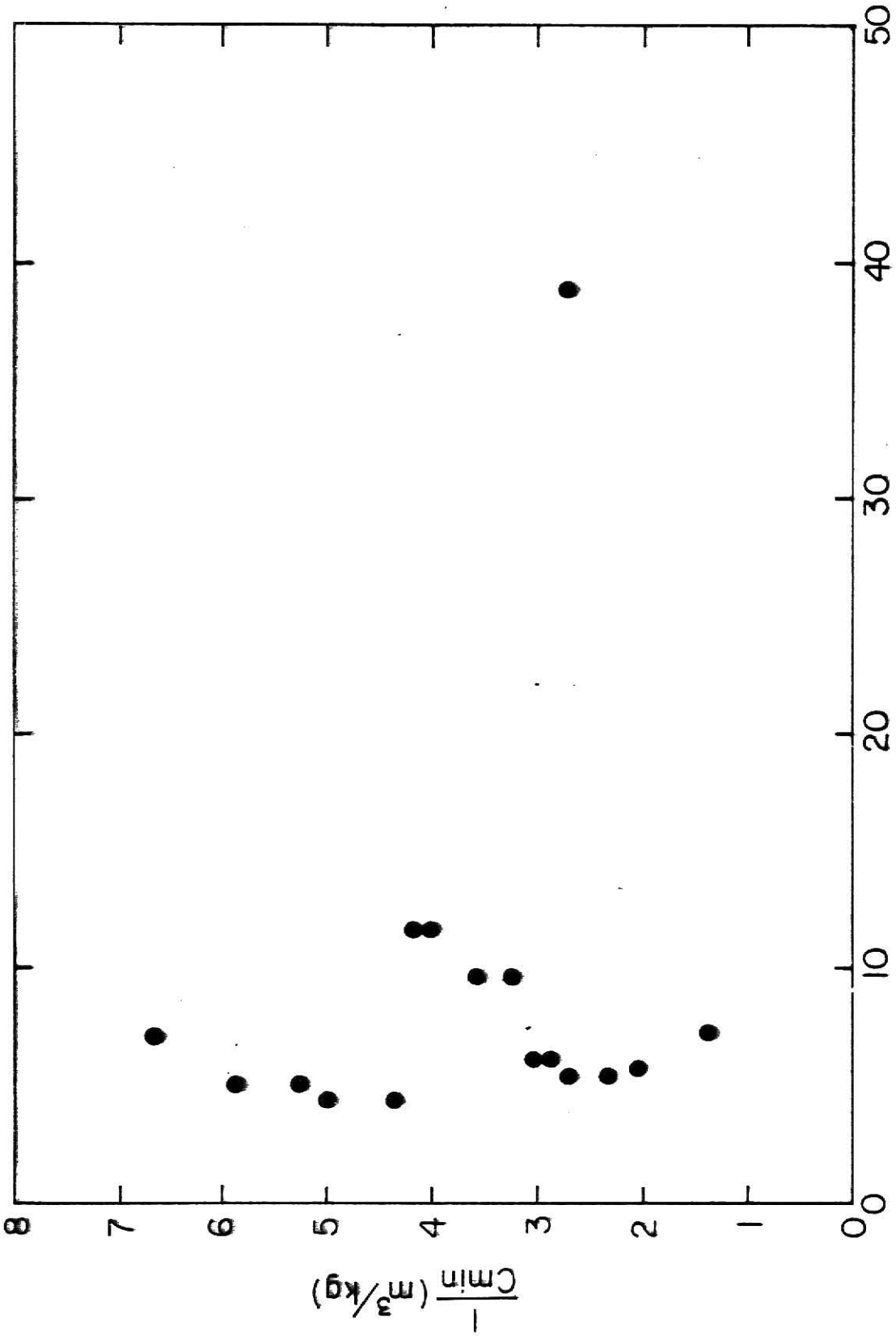

Fig. 4.28 The Relationship between the Reciprocal of the Minimum Explosible Concentration and the Ash Content for Wheat dust

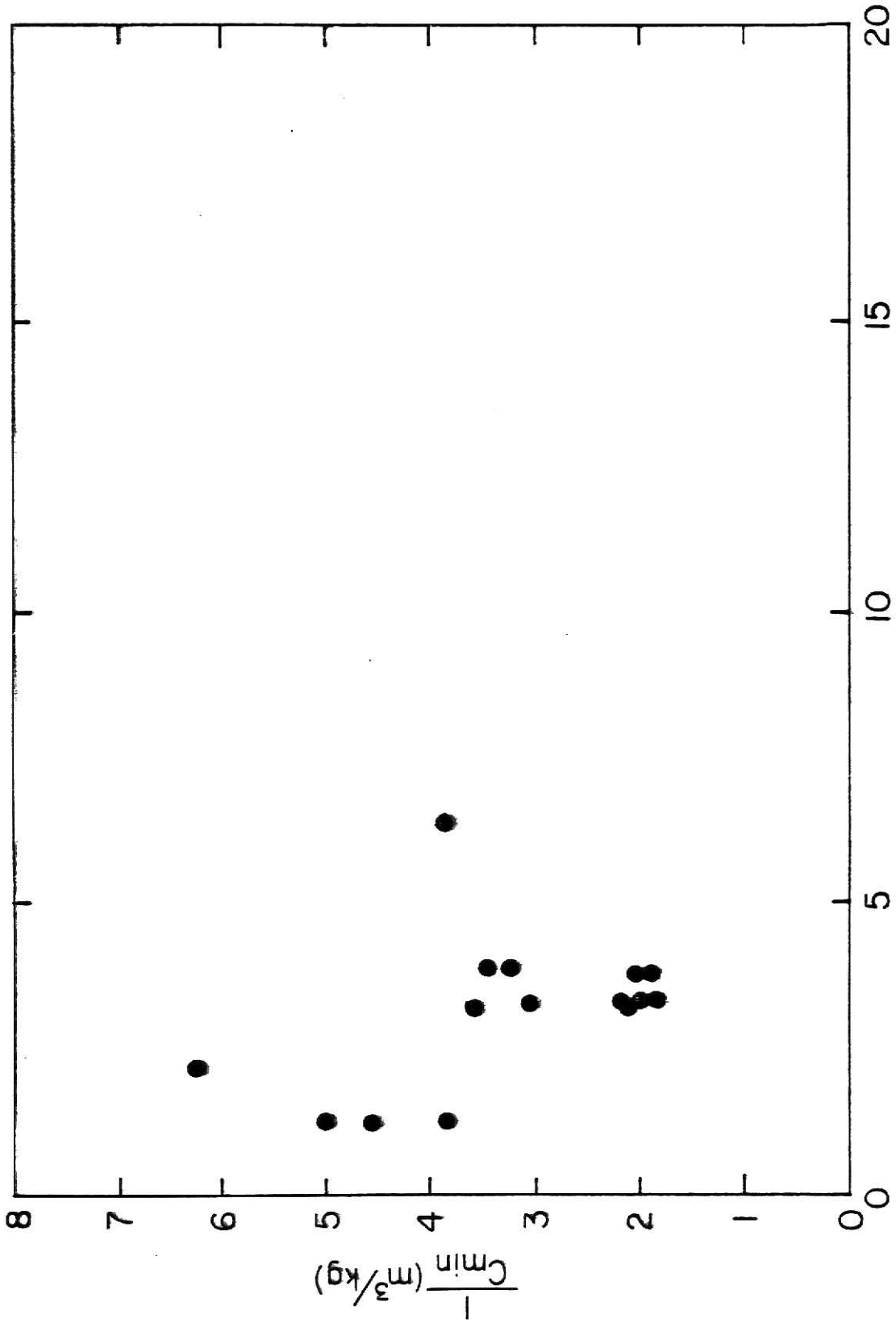

Fig. 4.29 The Relationship between the Reciprocal of the Minimum Explosible Concentration and the Ash Content for Grain Sorghum Dust

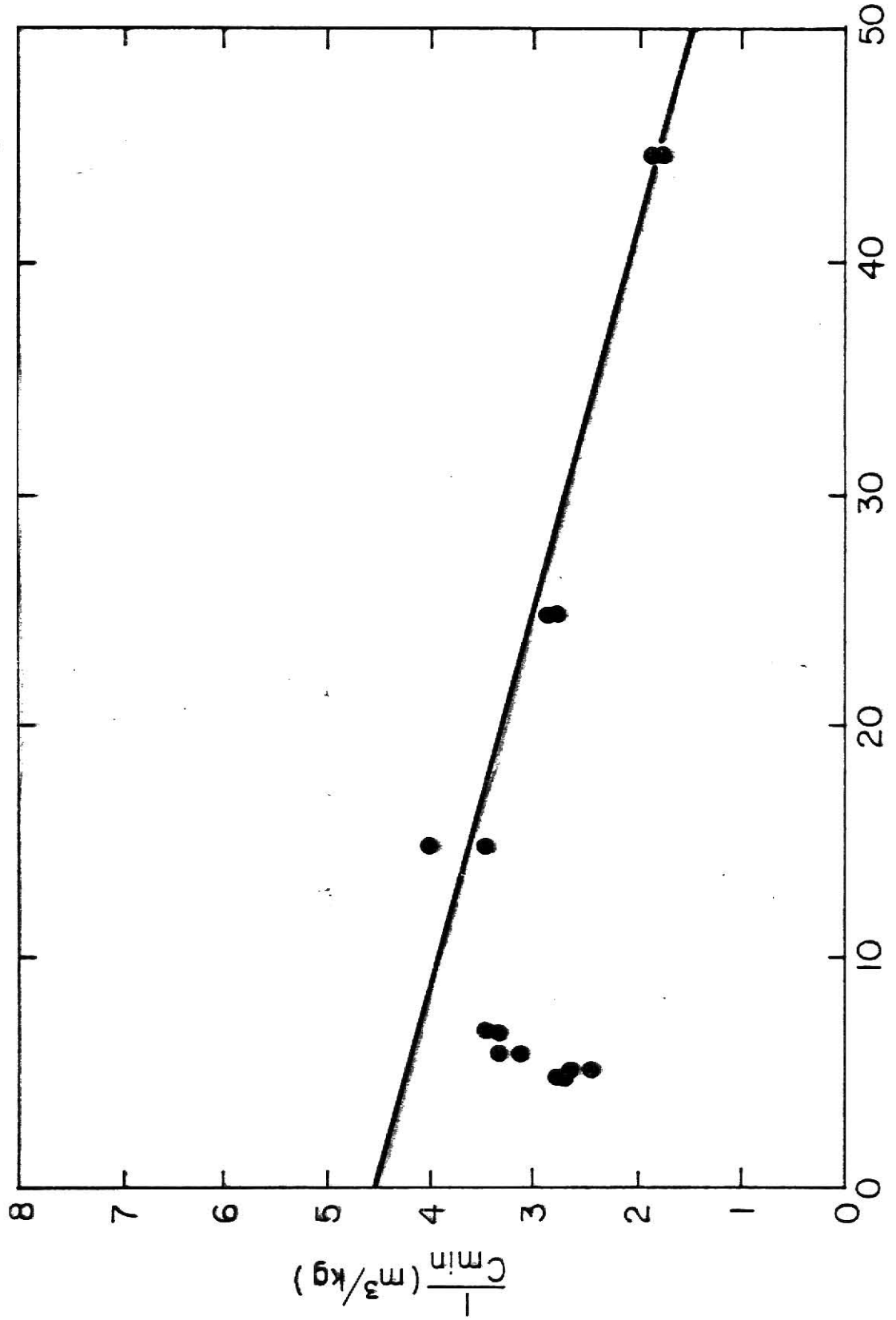

Fig. 4.30 The Relationship between the Reciprocal of the Minimum Explosible Concentration and the Ash Content for Corn Dust

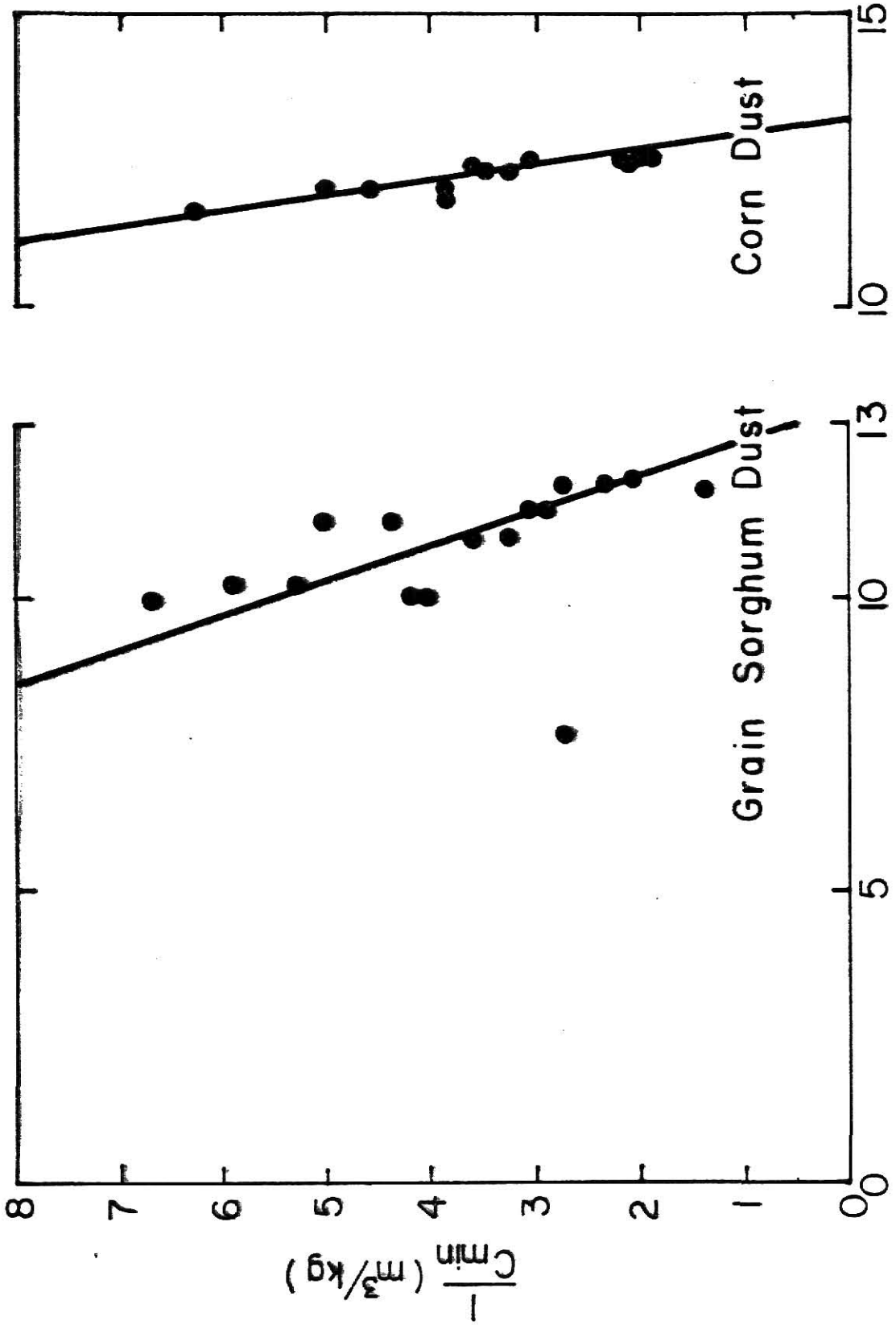

Fig. 4.31. The Relationship between the Reciprocal of the Minimum Explosible Concentration and the Ash Content for Grain Sorghum and Corn Dust

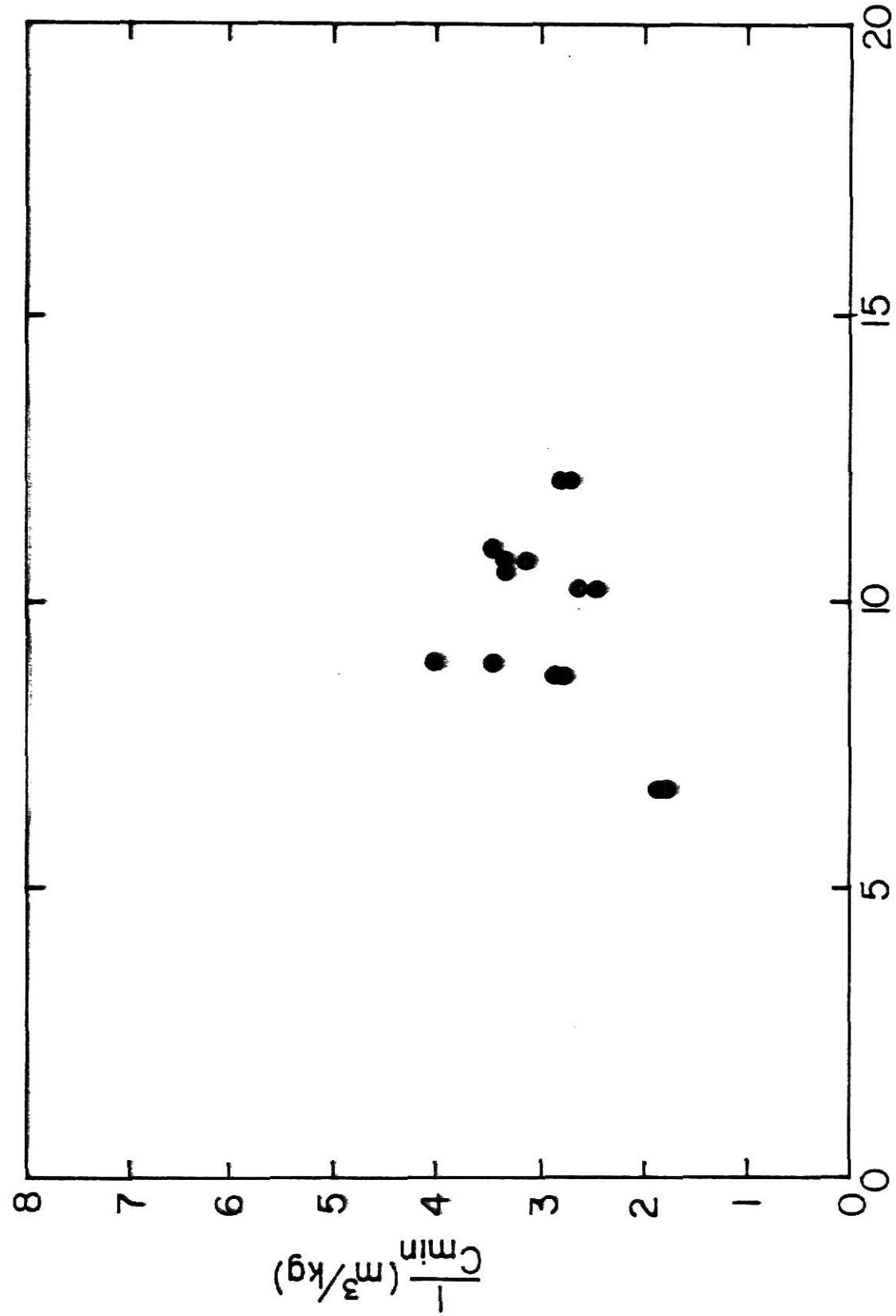

Fig. 4.32 The Relationship between the Reciprocal of the Minimum Explosible Concentration and the Moisture Content for Wheat Dust

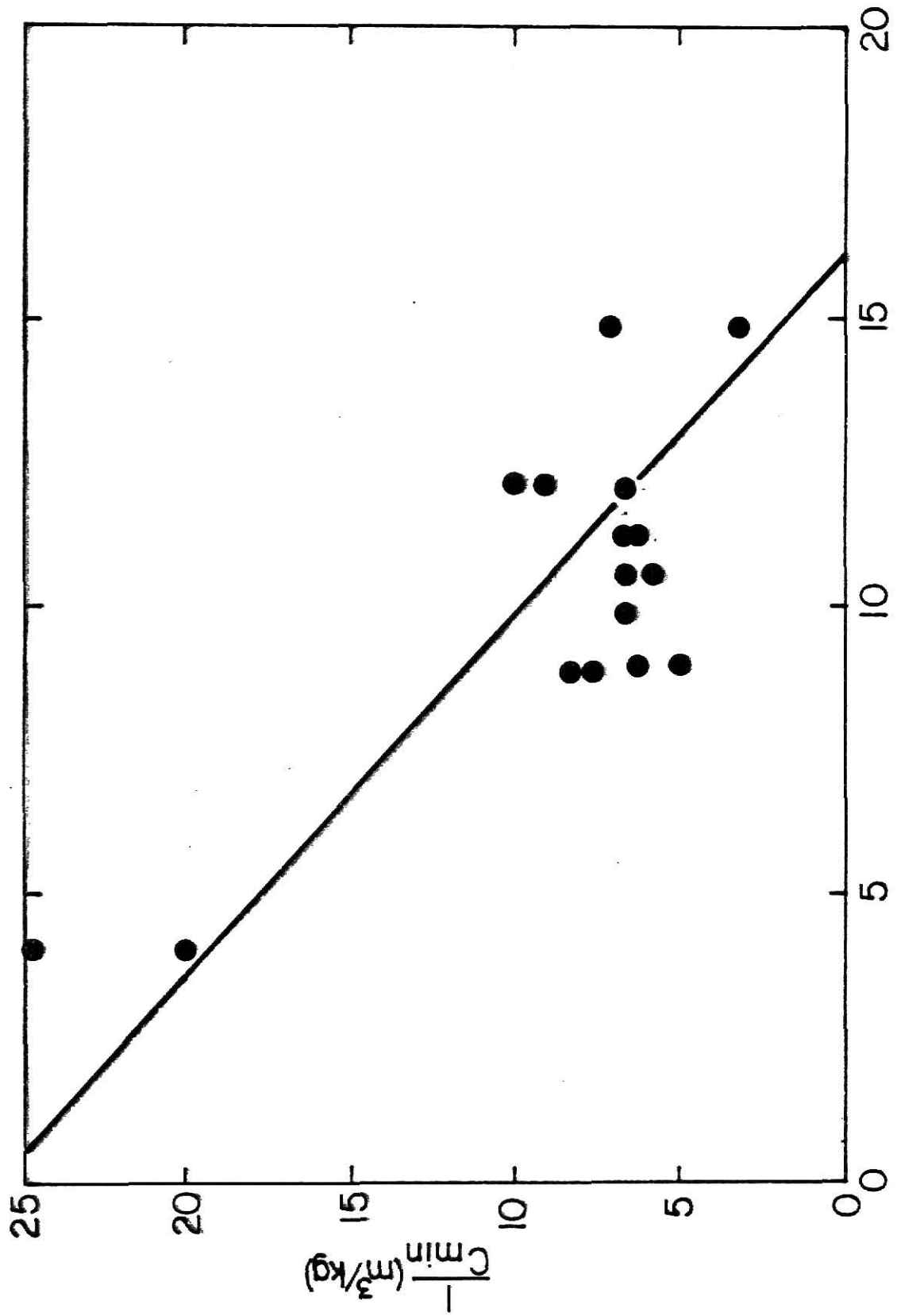

Fig. 4.33 The Relationship between the Reciprocal of the Minimum Explosible Concentration and the Moisture Content for Cornstarch

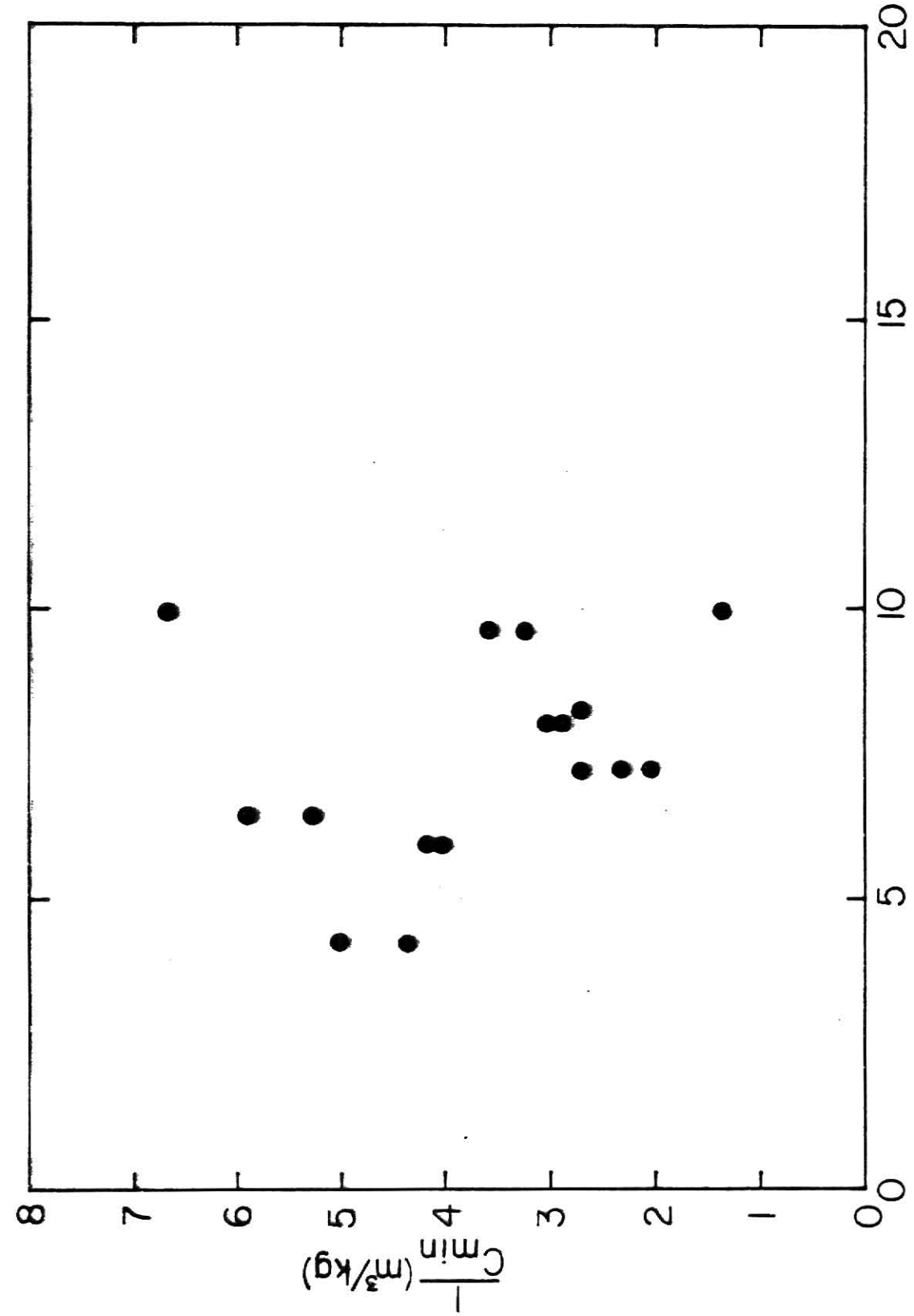

Fig. 4.34 The Relationship between the Reciprocal of the Minimum Explosible Concentration and the Protein Content for Grain Sorghum Dust

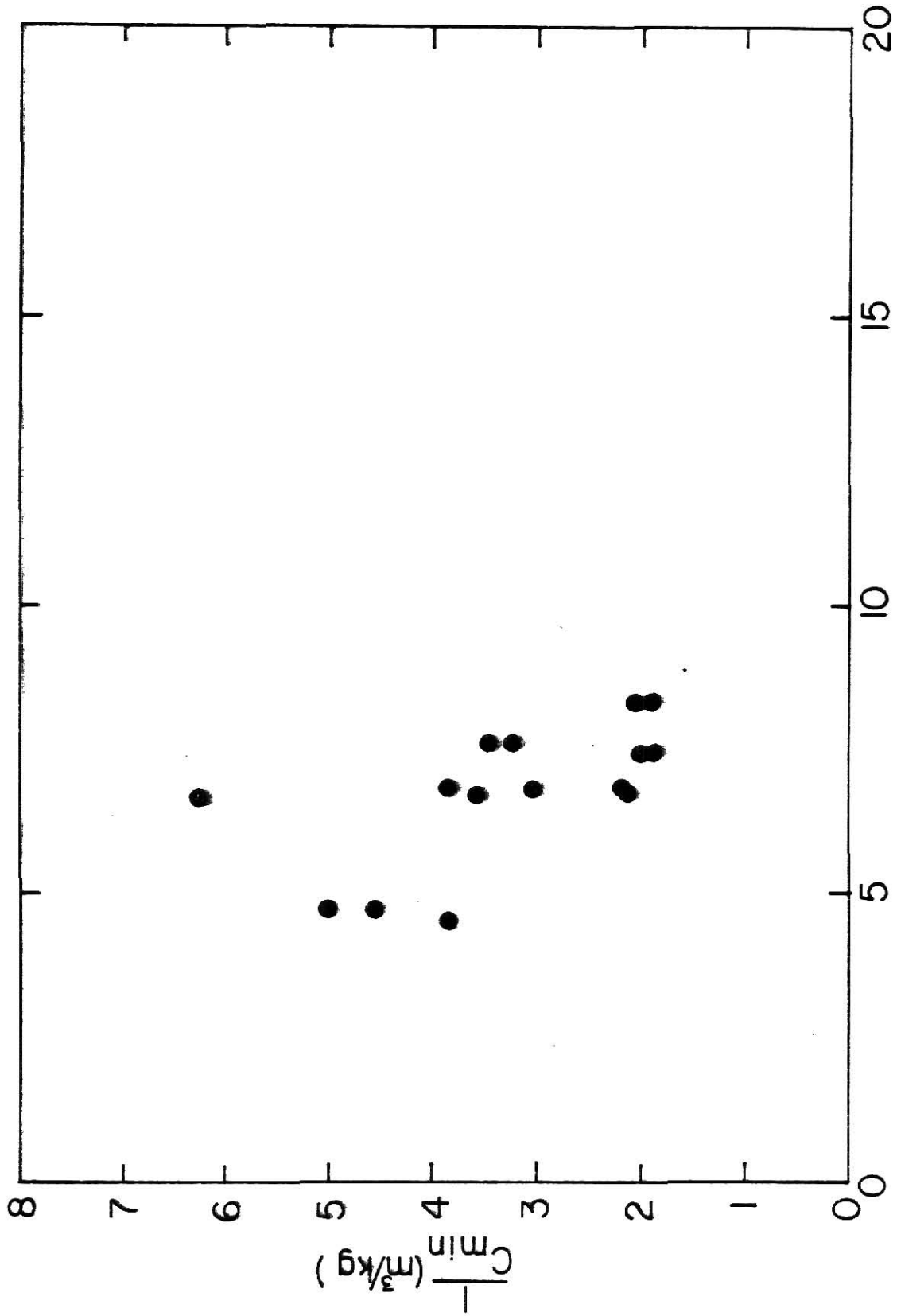

Fig. 4.35 The Relationship between the Reciprocal of the Minimum Explosible Concentration and the Protein Content for Corn Dust

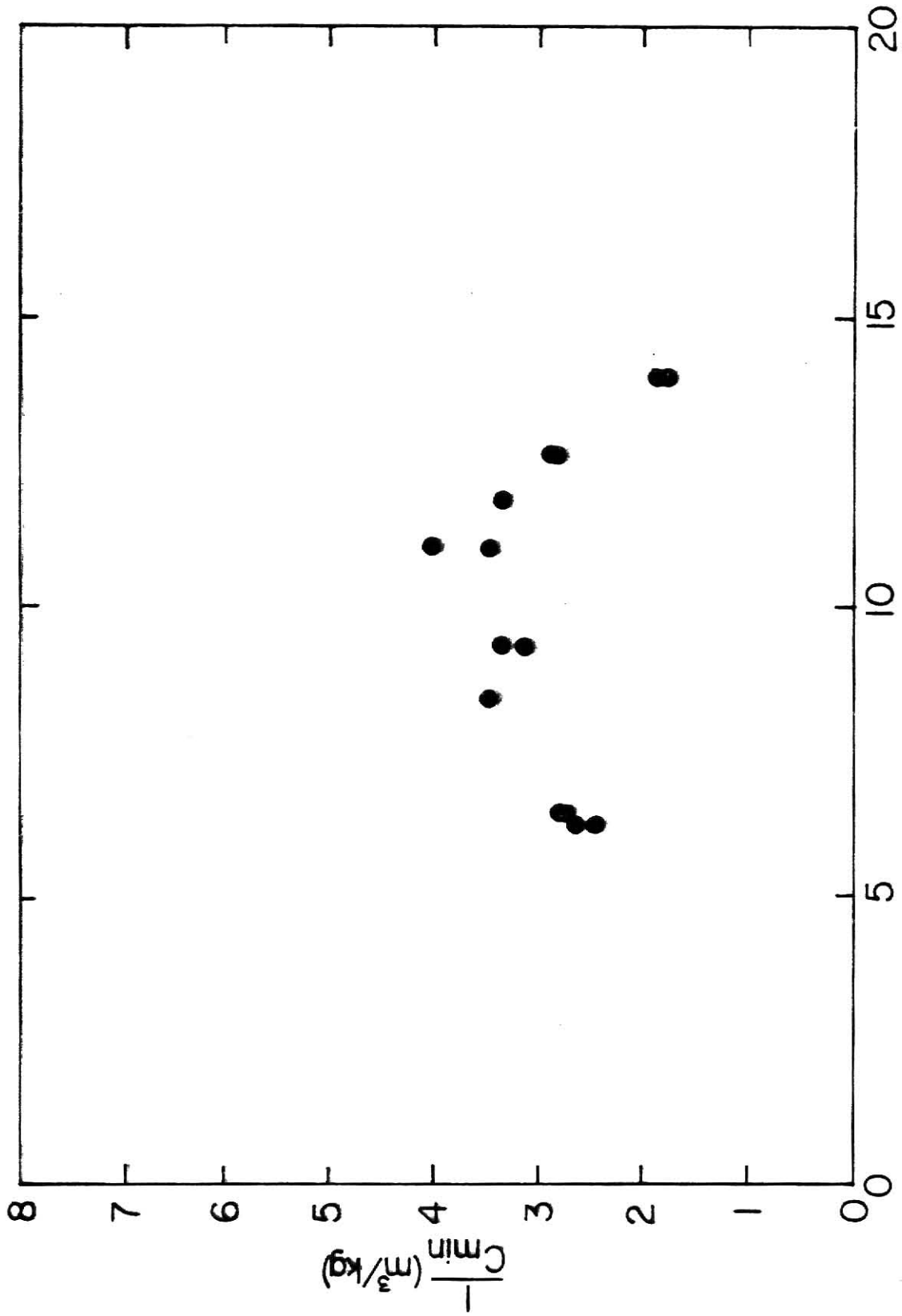

Fig. 4.36 The Relationship between the Reciprocal of the Minimum Explosible Concentration and the Protein Content for Wheat Dust

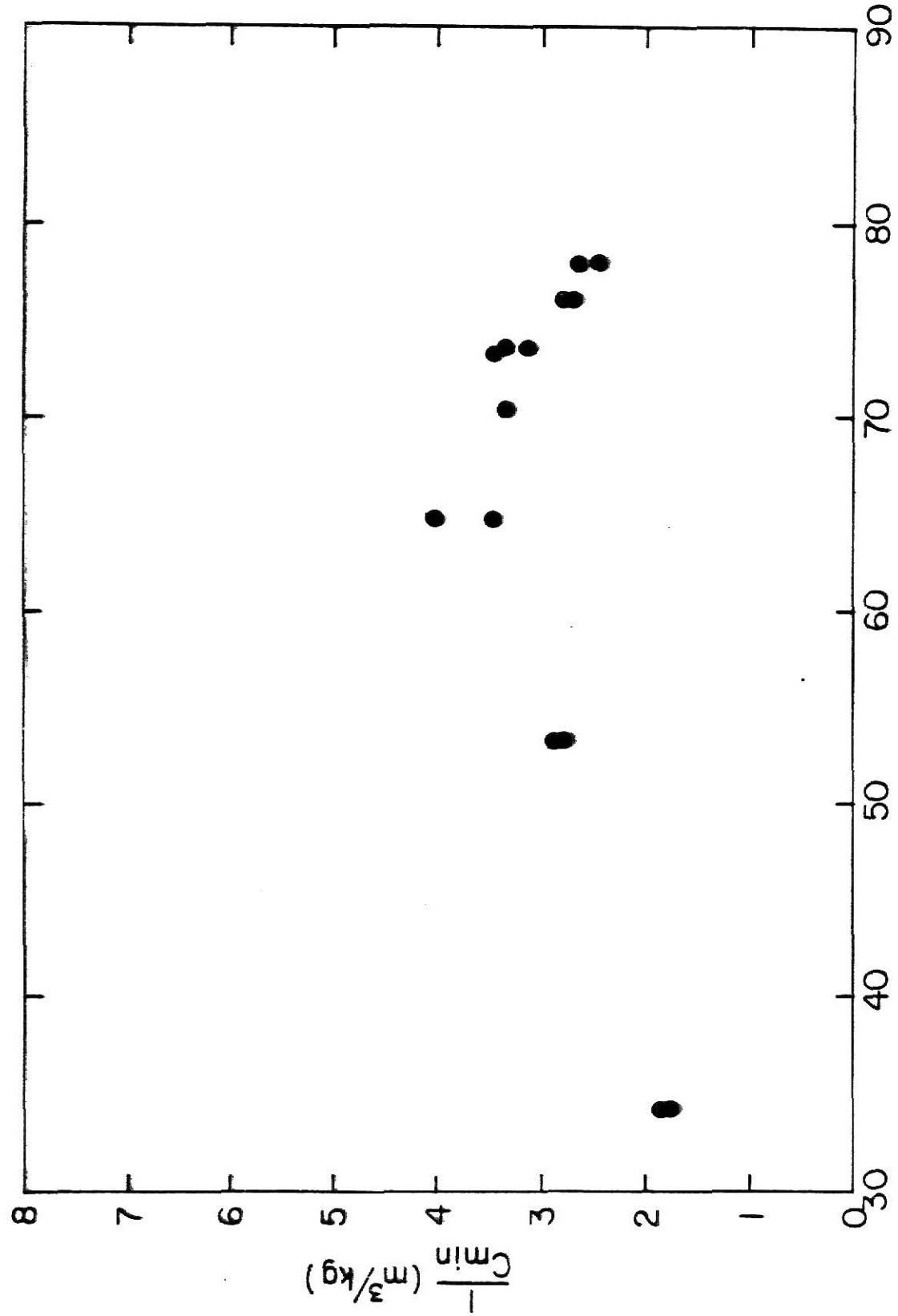

Fig. 4.37 The Relationship between the Reciprocal of the Minimum Explosible Concentration and the Starch and Fiber Content for Wheat Dust

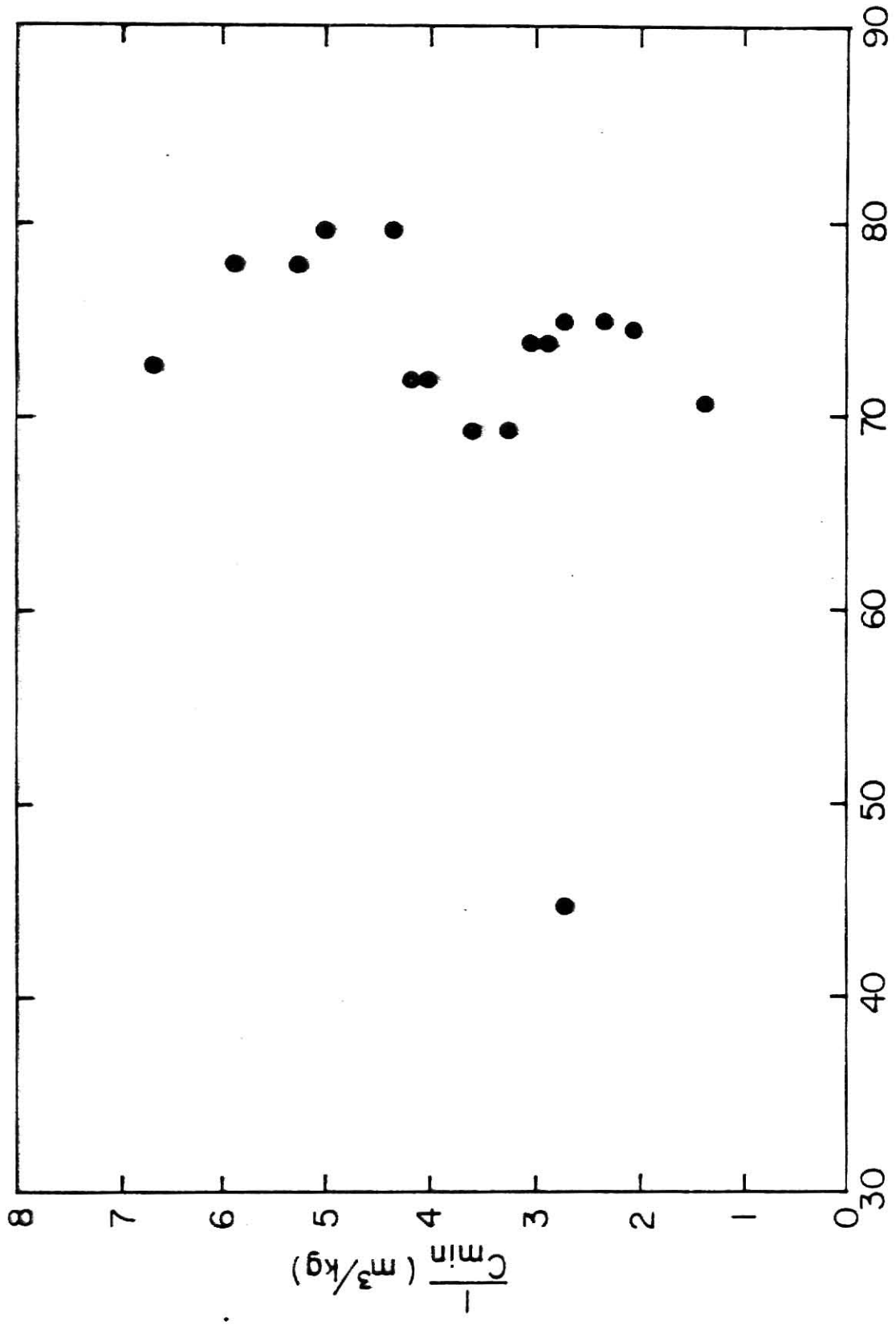

Fig. 4.38 The Relationship between the Reciprocal of the Minimum Explosible Concentration and the Starch and Fiber Content for Grain Sorghum Dust

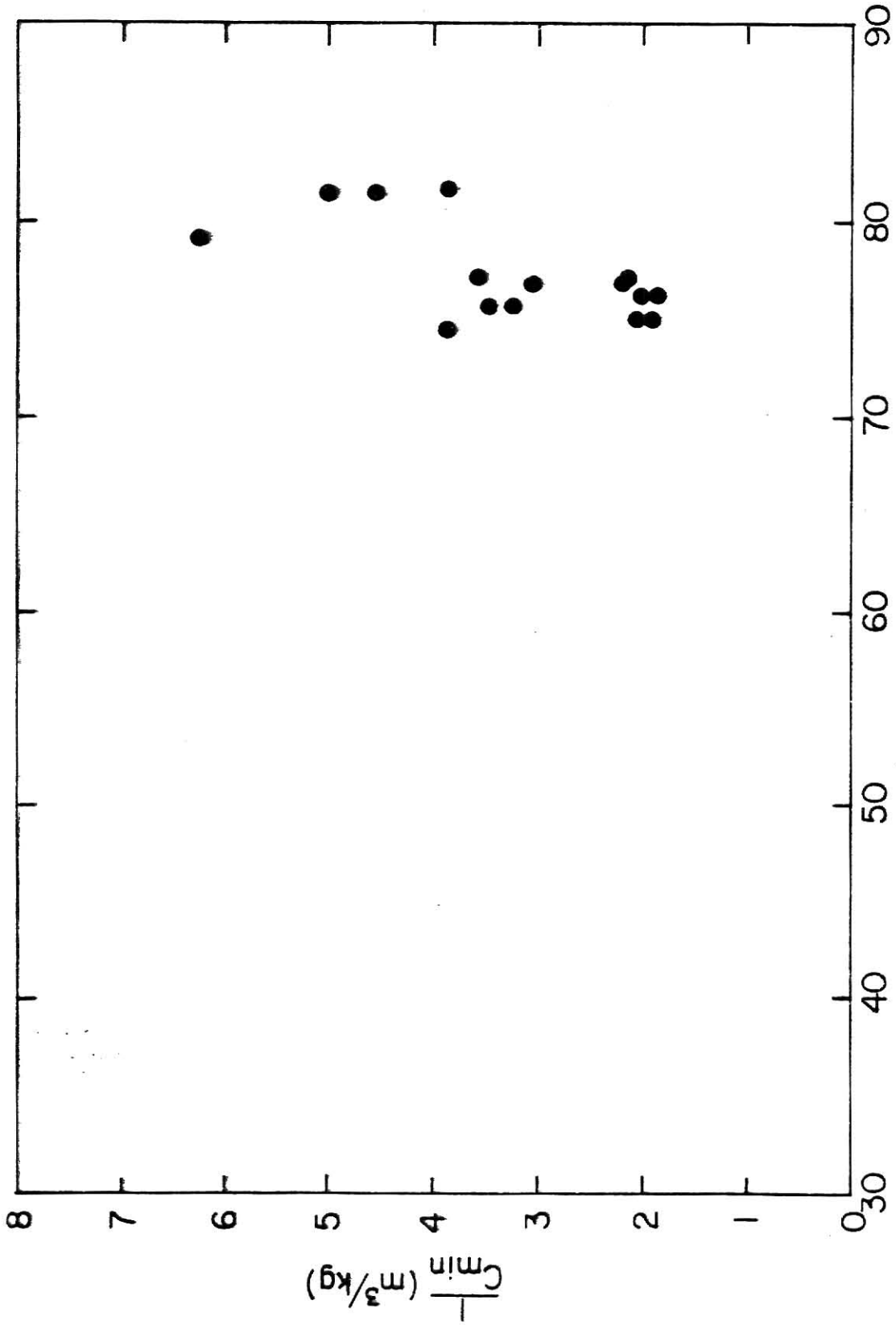

Fig. 4.39 The Relationship between the Reciprocal of the Minimum Explosible Concentration and the Starch and Fiber Content for Corn Dust

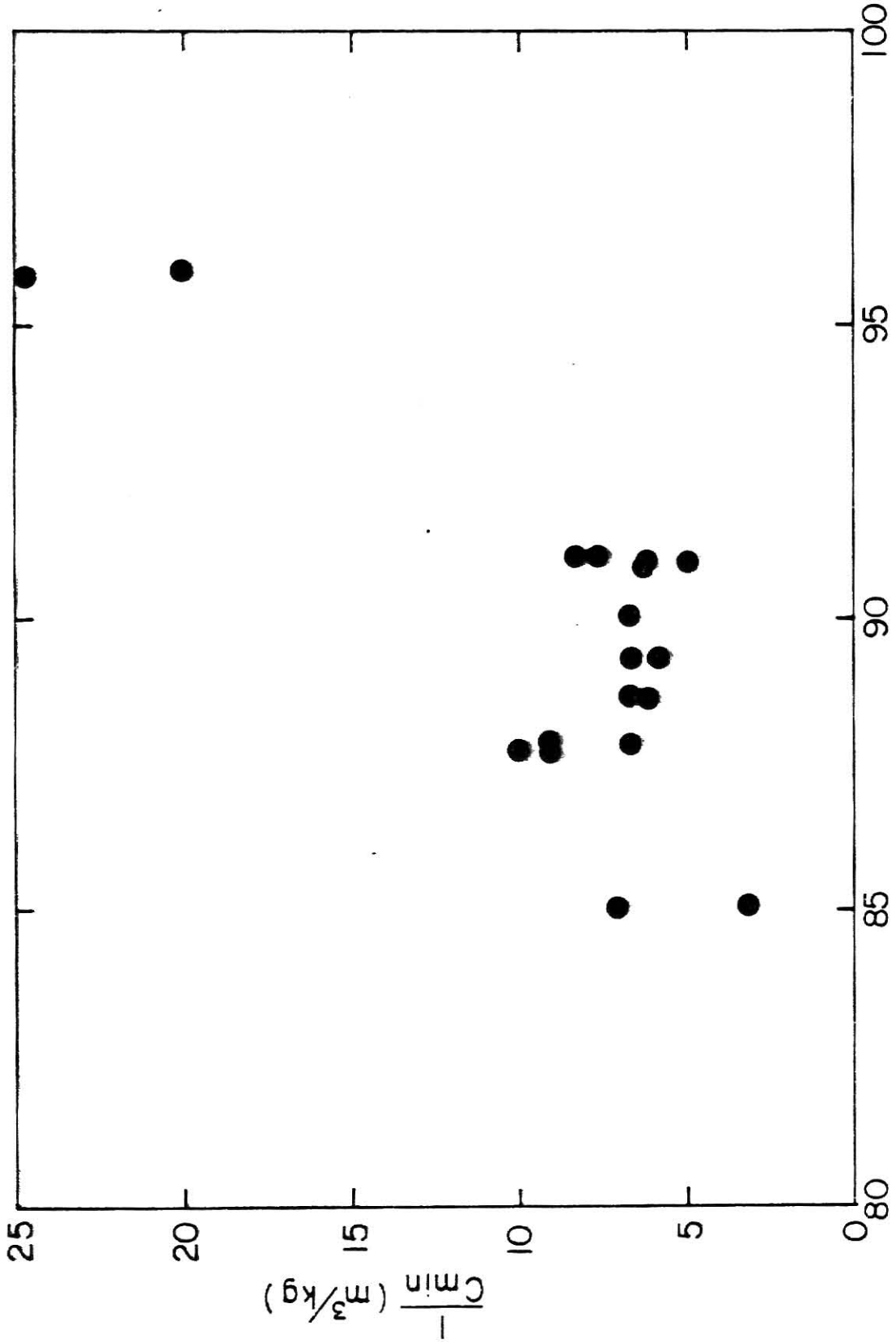

Fig. 4.40 The Relationship between the Reciprocal of the Minimum Explosible Concentration

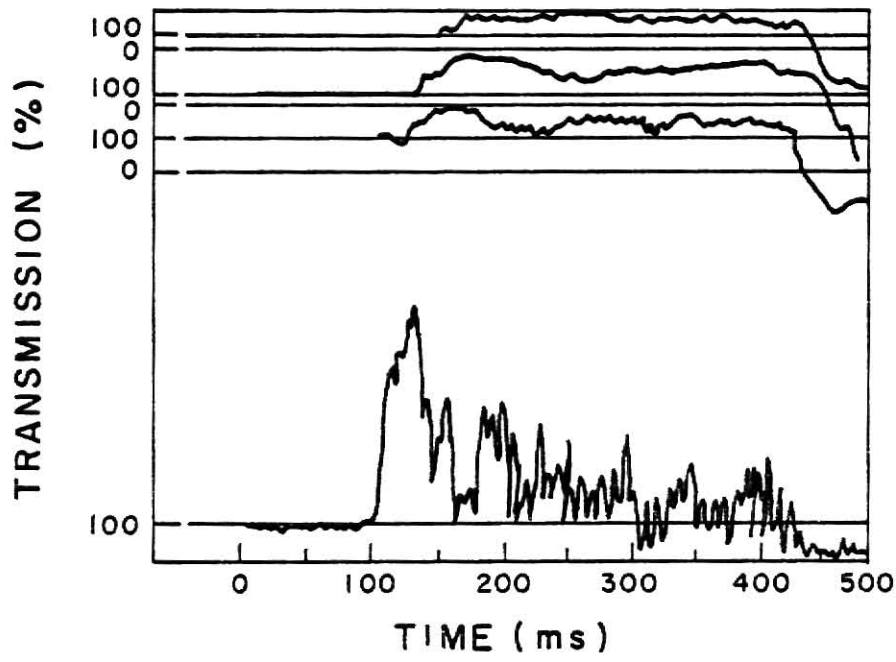

Fig. 4.41 A Photograph of the Oscilloscope Trace of the Output Voltage from the Phototransistor During an Explosion Test of Wheat Dust

CHAPTER 5

MAXIMUM EXPLOSION PRESSURE, MAXIMUM RATE OF PRESSURE RISE, AND AVERAGE RATE OF PRESSURE RISE AS AFFECTED BY PARTICLE SIZE AND COMPOSITION

I. INTRODUCTION

There are two major phases in a dust explosion, the ignition phase and the propagation phase. The maximum explosion pressure, the maximum rate of pressure rise, and the average rate of pressure rise are quantities that characterize the propagation phase of an explosion. These three quantities are the major factors on which the extent of damage from an explosion of a dust cloud depends.

The objectives of this work were to determine the maximum explosion pressure, the maximum rate of pressure rise, and the average rate of pressure rise for the dust in several size fractions and to correlate these three quantities with the average particle diameter and composition of each fraction. In addition, the effect of dust concentration on these quantities was studied for each fraction. Finally, the results of this study were compared with those from 0.19 m^3 spherical apparatus.

II. DERIVATION OF CORRELATION MODELS

The pressure tests of the Hartmann apparatus can be modeled as a two-phase system enclosed in a constant volume vessel. The two phases consist of a dust phase and a gaseous phase. Each of these phases is assumed to be homogeneous within itself. By neglecting energy transport by radiation, the energy balance for the dust phase is

$$\int_0^\infty \rho_d C_{p,d} \frac{dT}{dt}\left[\frac{\pi}{6}\left(\frac{D}{D_o}\right)^3 D_o^3 n_o(D_o)\, dD_o\right]$$

$$= \int_0^\infty h(T_g - T)\,\pi\left(\frac{D}{D_o}\right)^2 D_o^2 n_o(D_o)\, dD_o + (-\Delta H)\int_0^\infty (-r_d'')\,\pi\left(\frac{D}{D_o}\right) n(D_o)\, dD_o$$

$$+ S_v h_d (T_o - T) - r_w \Delta H_w \qquad (1)$$

where

t = time

T = temperature of the dust phase

D_o = particle diameter at time equal to zero

D = particle diameter at time t

ρ_d = density of the dust

$C_{p,d}$ = specific heat capacity of the dust

$n_o(D)$ = number distribution of particle diameter, D, at time equal to zero

$-r_d''$ = reaction rate of dust based on external surface area

S_v = surface area of the vessel

h_d = heat transfer coefficient between the dust phase and the vessel (probably a function of the concentration)

T_o = temperature of the vessel

ΔH = heat of combustion of dust

h = heat transfer coefficient between the dust and the air

T_g = temperature of the air

r_w = rate of water evaporation

ΔH_w = heat of vaporization of water

D/D_o is a function of D_o and t, i.e.,

$$\frac{D}{D_o} = f(D_o, t)$$

It is defined to be equal to 0 when $D_o = 0$, i.e., $D/D_o = 0$ if $D_o = 0$. The energy balance for the gaseous phase gives

$$\rho_a C_{p,a} V_v \frac{dT_g}{dt} = -\int_0^\infty h (T_g - T) \pi \left(\frac{D}{D_o}\right)^2 D_o^2 n_o(D_o) dD_o \qquad (2)$$

$$+ S_v h_a (T_o - T_g)$$

where

ρ_a = density of air

$C_{p,a}$ = heat capacity of air

V_v = vessel volume

h_a = heat transfer coefficient between the air and the vessel

The mass balance for oxygen yields

$$\frac{dN_{O_2}}{dt} = \nu_{O_2} \frac{dN_d}{dt} \int_0^\infty \pi \frac{\nu_{O_2}}{M_d} (-r_d'') \left(\frac{D}{D_o}\right)^2 D_o \, n_o(D_o) dD_o \qquad (3)$$

where

N_{O_2} = total number of moles of oxygen

O_2 = number of moles of oxygen consumed per mole of dust

M_d = molecular weight of the dust

N_d = number of moles of dust

For simplicity, one can assume that the particles are a constant size with a burned layer. The heat capacity and density of the dust are assumed to be constant as the reaction proceeds. Therefore, Eqs. (1), (2), and (3) become, respectively,

$$N^\circ_{tot}\,\rho_d\,c_{p,d}\,\frac{dT}{dt}\left(\frac{\pi}{6}\right)D^{\circ\,3}_{a,3} = N^\circ_{tot}\,L\,(T_g - T)\,\pi\,D^{\circ\,2}_{a,2} + (-\Delta H)\,\pi\int_0^\infty (-r_d'')\,D_o^2\,n_o(D_o)\,dD_o + S_v\,h_d\,(T_o - T) - r_\omega\,\Delta H_\omega \tag{4}$$

$$\rho_a\,c_{p,a}\,V_v\,\frac{dT_g}{dt} = -N^\circ_{tot}\,h\,(T_g - T)\,\pi\,D^{\circ\,2}_{a,2} + S_v\,h_a\,(T_o - T_g) \tag{5}$$

and

$$\frac{dN_{o_2}}{dt} = \frac{\nu_{o_2}}{M_d} \int_0^\infty \pi (-r_d'') D_o^2 n_o(D_o) dD_o \tag{6}$$

where

N^o_{tot} = total number of particles at time zero

$D^{o^2}_{a,2}$ = mean diameter based on area at time zero

$D^{o^3}_{a,3}$ = mean diameter based on weight at time zero

From the definition of $D^{o^3}_{a,3}$, it can be shown that

$$N^o_{tot} = \frac{W^o_{tot}}{\rho_d \frac{\pi}{6} D^{o^3}_{a,3}} \tag{7}$$

where

w^o_{tot} = total weight of dust initially present at time zero

Assuming that the gas phase behaves ideally and that the total number of moles of gas is constant, the expression relating the air temperature to the pressure is obtained as

$$T_g = \frac{V_v P}{\tilde{n} R} \tag{8}$$

where

P = pressure

R = gas constant

$\tilde{n}$ = total number of moles of gas at time zero

By substituting Eq. (7) into Eqs. (4), (5), and (6), one obtains, respectively,

$$W_{tot} C_{p,d} \frac{dT}{dt} = \frac{6 W_{tot}^{\circ}}{\rho_d} \frac{V_v h}{\tilde{n}} \left(P - \frac{\tilde{n} R T}{V}\right) \frac{D_{a,2}^{\circ 2}}{D_{a,3}^{\circ 3}}$$

$$+ (-\Delta H) \pi \int_0^{\infty} (-r_d'') D_o^2 n_o(D_o) \, d D_o$$

$$+ \left(\frac{S_v}{V_v}\right) \frac{h_d V_v^3}{\tilde{n} R} \left(P_o - \frac{\tilde{n} R T}{V_v}\right) - r_w \Delta H_w \qquad (9)$$

$$\rho_a C_{p,a} \frac{V_v^2}{\tilde{n} R} \frac{dP}{dt} = - \frac{6 C^{\circ}}{\rho_d} \frac{L V_v^2}{\tilde{n} R} \left(P - \frac{\tilde{n} R T}{V_v}\right) \frac{D_{a,2}^{\circ 2}}{D_{a,3}^{\circ 3}}$$

$$- \frac{S_v}{V_v} h_a \frac{V_v^2}{\tilde{n} R} (P - P_o) \qquad (10)$$

and

$$\frac{dN_{O_2}}{dt} = \frac{\nu_{O_2}}{M_d}\pi\int_0^\infty (-\dot{G}'')\, D_o^2\, n_o(D_o)\, dD_o \tag{11}$$

The maximum rate of pressure rise occurs when

$$\frac{d^2P}{dt^2} = 0 \tag{12}$$

Differentiating Eq. (10) with respect to t, one obtains

$$\rho_a C_{p,a}\frac{V_v^2}{\tilde{n}R}\frac{d^2P}{dt^2} = -\frac{6C^\circ}{\rho_d}\frac{LV_v^2}{\tilde{n}R}\left[\frac{dP}{dt} - \frac{\tilde{n}R}{V_v}\left(\frac{dT}{dt}\right)\right]\frac{D_{a,2}^{\circ 2}}{D_{a,3}^{\circ 3}} \cdot$$

$$- \frac{S_v}{V_v} L_a \frac{V_v^2}{\tilde{n}R}\frac{dP}{dt} \tag{13}$$

Therefore, at the time when the maximum rate of pressure rise occurs, one has

$$\left(\frac{dT}{dt}\right)_{max} = \frac{V_v}{\tilde{n}R}\left\{1 + \frac{\rho_d}{6C^\circ}\left(\frac{S_v}{V_v}\right)\left(\frac{h_a}{h}\right)\left(\frac{D_{a,2}^{\circ 2}}{D_{a,3}^{\circ 3}}\right)\right]\left(\frac{dP}{dt}\right)\Big|_{max} \tag{14}$$

Eliminating the first term on the right hand sides of Eqs. (9) and (10), one finds

$$C^{\circ} C_{p,d} V_v \frac{dT}{dt} = - \rho_a C_{p,a} \frac{V_v^2}{\hat{n} R} \frac{dP}{dt} + (-\Delta H)\pi \int_0^{\infty} (-r_d'') D_0^2 n_0(D_0)\, dD_0$$

$$- r_w \Delta H_w - \frac{S_v}{V_v} h_d \frac{V_v^2}{\hat{n} R} \left(\frac{\hat{n} R T}{V_v} - P_0 \right)$$

$$- \frac{S_v}{V_v} h_a \frac{V_v^2}{\hat{n} R} (P - P_0) \qquad (15)$$

Substituting $(dT/dt)_{tmax}$ from Eq. (14) into Eq. (15) yields

$$C^{\circ} C_{p,d} \left[1 + \frac{\rho_d}{C^{\circ}} \left(\frac{S_v}{V_v} \right) \left(\frac{h_a}{h} \right) \frac{D_{a,3}^{\circ 3}}{D_{a,2}^{\circ 2}} \right] \left(\frac{dP}{dt} \right)_{max}$$

$$= - \rho_a C_{p,a} \left(\frac{dP}{dt} \right)_{max} + \left[\frac{(-\Delta H) \hat{n} R}{V_v^3} \pi \int_0^{\infty} (-r_d'') D_0^2 n_0(D_0)\, dD_0 \right] \Bigg|_{t_{max}}$$

$$- \frac{\hat{n} R}{V_v^2} (r_w \Delta H_w) \Big|_{t_{max}} - \frac{S_v}{V_v} \left[h_d \left(\frac{\hat{n} R T}{V_v} - P_0 \right) - h_a (P - P_0) \right] \Bigg|_{t_{max}} \qquad (16)$$

or

$$\left(\frac{dP}{dt}\right)_{max}$$

$$= \frac{\left[\frac{(-\Delta H)\tilde{n}R}{V_v^2}\pi\int_0^{\infty}(-r_d'')D_0^2 n_0(D_0)dD_0 - \frac{\tilde{n}R}{V_v^2}(r_w\Delta H_v) - \frac{S_v}{V_v}\left[h_d\left(\frac{\tilde{n}RT}{V_v}-P_0\right)+h_a(P-P_0)\right]\right]_{t_{max}}}{\left[C^0 C_{p,d} + P_a C_{p,a} + \frac{C_{p,d}\rho_d}{6}\left(\frac{S_v}{V_v}\right)\left(\frac{h_a}{h}\right)\frac{D_{a,3}^{0\,3}}{D_{a,2}^{0\,2}}\right]_{t_{max}}} \qquad (17)$$

The maximum explosion pressure occurs when

$$\frac{dP}{dt} = 0 \qquad (18)$$

that is, when the rate of heat transfer into the gas phase from the dust is equal to that from the gas phase. From Eq. (10), this condition occurs when

$$0 = -\frac{6C^0 h}{\rho_d}\left(P_{max} - \frac{\tilde{n}RT_{max}}{V_v}\right)\frac{D_{a,2}^{0\,2}}{D_{a,3}^{0\,3}} - \frac{S_v}{V_v}h_a\left(P_{max} - P_0\right) \qquad (19)$$

This equation can be rewritten as

$$\frac{\tilde{n}RT_{max}}{V_v} = P_{max}\left[1 + \frac{S_v}{V_v}\left(\frac{h_a}{h}\right)\left(\frac{\rho_d}{6C^0}\right)\frac{D_{a,3}^{0\,3}}{D_{a,2}^{0\,2}}\right] - \frac{S_v}{V_v}\left(\frac{h_a}{h}\right)\left(\frac{\rho_d}{6C^0}\right)\frac{D_{a,3}^{0\,3}}{D_{a,2}^{0\,2}}P_0 \qquad (20)$$

Integrating Eq. (15) from time zero to the time when the condition in Eq. (18) is satisfied, one obtains

$$C^{\circ}\rho_d C_{p,d}\left(\frac{\hat{n}RT_{max}}{V_v}-P_0\right)=-\rho_a C_{p,a}(P_{max}-P_0)-\frac{\tilde{n}R}{V_v^2}\int_0^{t'_{max}} r_w \Delta H_w dt$$

$$+\frac{\hat{n}R(-\Delta H)}{V_v^2}\pi\int_0^{t'_{max}}\int_0^{\infty}(-r_d'')D_0^2 n_0(D_0)dD_0 dt$$

$$-\frac{S_v}{V_v}\left[L_d\int_0^{t'_{max}}\left(\frac{\hat{n}RT}{V_v}-P_0\right)dt+h_a\int_0^{t_{max}}(P-P_0)dt\right] \tag{21}$$

where

t'_{max} = time necessary to realize the maximum pressure

Substituting Eq. (20) into Eq. (21) gives

$$P_{max}-P_0 = \frac{\left\{\frac{\hat{n}R(-\Delta H)}{V_v^2}\pi\int_0^{t'_{max}}\int_0^{\infty}(-r_d'')D_0^2 n_0(D_0)dD_0 dt-\frac{\tilde{n}R}{V_v^2}\int_0^{t'_{max}} r_w\Delta H_w dt-\frac{S_v}{V_v}\left[L_d\int_0^{t'_{max}}\left(\frac{\hat{n}RT}{V_v}-P_0\right)dt+h_a\int_0^{t_{max}}(P-P_0)dt\right]\right\}}{\left[\rho_a C_{p,a}+C^{\circ}C_{p,d}+\left(\frac{S_v}{V_v}\right)\left(\frac{h_a}{h}\right)\frac{\rho_d}{6}C_{p,d}\left(\frac{D_{a,3}^{0\,3}}{D_{a,2}^{0\,2}}\right)\right]} \tag{22}$$

The average rate of pressure rise is defined as

$$\left(\frac{dP}{dt}\right)_{AVG}=\frac{P_{max}-P_0}{t'_{max}} \tag{23}$$

Substituting, $P_{max}-P_o$ from Eq. (22) into Eq. (23) yields

$$\left(\frac{dP}{dt}\right)_{avg} = \left\{\frac{\tilde{n} R(-\Delta H)}{V_v^2}\left(\frac{1}{t'_{max}}\int_0^{t'_{max}}\int_0^{\infty}(-r_d'')\, D_o^2\, n_o(D_o)\, dD_o\, dt\right)\right.$$

$$\left. - \frac{S_v}{V_v}\left[h_a \frac{1}{t'_{max}}\int_0^{t'_{max}}\left(\frac{\tilde{n} RT}{V_v} - P_o\right) dt + L_a \frac{1}{t'_{max}}\int_0^{t'_{max}}(P - P_o)\, dt\right]\right\}$$

$$\left\{\rho_a C_{p,a} + C^{\circ} \rho_{p,d} + \frac{S_v}{V_v}\left(\frac{h_a}{h}\right)\frac{\rho_d}{6} C_{p,d}\left(\frac{D_{a,3}^{\circ 3}}{D_{a,2}^{\circ 2}}\right)\right\} \qquad (24)$$

Essenhigh et al. (1965) showed that for particles less than 100 μm, the rate is desorption controlled at temperatures less than 10000K and adsorption controlled at high temperatures. Therefore, the expression for $(-r_d'')$ is

$$-r_d'' = \frac{K_1 K_2 P_{O_2}}{K_2 + K_1 P_{O_2}} \qquad (25)$$

where

K_1, K_2 = functions of temperature only

P_{O_2} = partial pressure of oxygen

For simplicity, let B_p defined to be

$$B_p \equiv \frac{\tilde{n} R(-\Delta H)}{V_v^2}\pi \int_0^t \int_0^{\infty} (-r_d'')\, D_o^2\, n_o(D_o)\, dD_o\, dt \qquad (26)$$

Hence

$$B_p = \frac{6C^\circ}{\rho_d} \frac{\tilde{n} R(-\Delta H)}{V_v} \frac{D_{a,2}^{\circ 2}}{D_{a,3}^{\circ 3}} \int_0^t \frac{K_1 K_2 P_{O_2}}{K_2 + K_1 P_{O_2}} dt \tag{27}$$

or

$$B_p = \frac{6C^\circ}{\rho_d} \frac{\tilde{n} R(-\Delta H)}{V_v} \left(\frac{D_{a,2}^{\circ 2}}{D_{a,3}^{\circ 3}} \right) f(T, t, P_{O_2}) \tag{28}$$

Then the expression for the maximum presure rise, Eq. (22), can be simplified as

$$P_{max} - P_o = \frac{B_p|_{t'_{max}} - \frac{\tilde{n} R}{V_v^2} \int_0^{t'_{max}} r_w \Delta H_w dt - \frac{S_v}{V_v} \left[h_d \int_0^{t'_{max}} \left(\frac{\hat{n} RT}{V_v} - P_o \right) dt + L_a \int_0^{t_{max}} (P - P_o) dt \right]}{\left[\rho_a c_{p,a} + C^\circ c_{p,d} + \left(\frac{S_v}{V_v} \right) \left(\frac{h_a}{h} \right) \frac{\rho_d}{6} c_{p,d} \left(\frac{D_{a,3}^{\circ 3}}{D_{a,2}^{\circ 2}} \right) \right]} \tag{29}$$

The maximum rate of pressure rise in Eq. (17) becomes

$$\left(\frac{dP}{dt}\right)_{max} = \frac{\left.\frac{d(B_P)}{dt}\right|_{t'_{max}}}{\left\{ C_o C_{P,d} + \rho_a C_{P,a} + \frac{C_{P,d}\rho_d}{6}\left(\frac{S_v}{V_v}\right)\left(\frac{h_a}{h}\right)\left(\frac{D_{a,3}^{o3}}{D_{a,2}^{o2}}\right)\right\}\Big|_{t'_{max}}}$$

$$- \left\{ \frac{\hat{n} R (r_\omega \Delta H_\omega) - \frac{S_v}{V_v}\left[L_d \left(\frac{\hat{n} RT}{V_v} - P_o\right) - h_a (P - P_o)\right]}{\left[C^\circ C_{P,d} + \rho_a C_{P,a} + \frac{C_{P,d}\rho_d}{6}\left(\frac{S_v}{V_v}\right)\left(\frac{h_a}{h}\right)\left(\frac{D_{a,3}^{o3}}{D_{a,2}^{o2}}\right)\right]} \right\}\Bigg|_{t'_{max}} \qquad (30)$$

and the average rate of pressure rise in Eq. (24) gives

$$\left(\frac{dP}{dt}\right)_{avg} = \frac{\frac{1}{t'_{max}} B_P \Big|_{t'_{max}}}{\left[C^\circ C_{P,d} + \rho_a C_{P,a} + \frac{C_{P,d}\rho_d}{6}\left(\frac{S_v}{V_v}\right)\left(\frac{h_a}{h}\right)\left(\frac{D_{a,3}^{o3}}{D_{a,2}^{o2}}\right)\right]}$$

$$- \left\{ \frac{\frac{\hat{n} R}{V_v}\left(\frac{1}{t'_{max}}\int_0^{t'_{max}} r_\omega \Delta H_\omega \, dt - \left(\frac{1}{t'_{max}}\right)\frac{S_v}{V_v}\left[h_d \int_0^{t'_{max}} \left(\frac{\hat{n} RT}{V_v} - P_o\right) dt + h_a \int_0^{t'_{max}} (P - P_o)\, dt\right]\right.}{\left[\rho_a C_{P,a} + C^\circ C_{P,d} + \frac{C_{P,d}\rho_d}{6}\left(\frac{S_v}{V_v}\right)\left(\frac{h_a}{h}\right)\left(\frac{D_{a,3}^{o3}}{D_{a,2}^{o2}}\right)\right]} \right\} \qquad (31)$$

The expression for the rate of oxygen consumption becomes

$$\frac{dN_{O_2}}{dt} = \frac{\nu_{O_2}}{M_d}\left(\frac{V_v^2}{\hat{n} R (-\Delta H)}\right)\left(\frac{dB_P}{dt}\right) \qquad (32)$$

III. EXPERIMENTAL DETERMINATION OF EXPLOSION CHARACTERISTICS

The maximum explosion pressure, maximum rate of pressure rise, and average rate of pressure rise were measured for wheat, grain sorghum, and corn dust. Cornstarch was also included as a reference. All samples were measured in a Hartmann apparatus. Autolyzed yeast extract was also tested to compare it with the result obtained independently by a 0.19 m^3 spherical bomb.

A. Equipment and Apparatus

Photographs of the apparatus are shown in Figs. 5.1 and 5.2. The schematic diagram of the apparatus is given in Fig. 5.3.

The design of the explosion chamber is the same as that of a standard Hartmann pressure apparatus (Dorsett et al., 1960), except for the sampling valve attached to the side of the chamber (see Fig. 5.3), which could be used to remove a sample of the post explosion gases.

The length of time between the ignition of the electric spark and the dispersion of the dust was controlled with the timing circuitry shown in Figs. 5.2 and 5.3. A detailed description of the design is given in Chapter 4.

The pressure inside the explosion chamber was measured with a pressure transducer (Bell & Howell Type No. CEC-402). This transducer has a pressure range of 0 to 17.2 bars (0-250 psig), and a flat frequency response up to 1000 Hz, which corresponds to a time constant of approximately 1 ms. The transducer is connected to a bridge network (Bell & Howell 8-115 Signal Conditioner; Pasadena, CA) that produces an output electrical voltage proportional to the pressure in the explosion chamber.

A Tetronix 5112 dual beam oscilloscope (Tetronix Inc.; Beaverton, OR) was employed to measure the output voltage from the signal conditioner as a

function of time. The signal trace on the oscilloscope screen was photographed with a Tetronix series 125 camera.

B. Sample Preparation

Dust samples were collected from the dust removal systems in three commercial elevators, and cornstarch was purchased in bulk from a mill. Each dust sample was divided into several size fractions by sieve separation and by air classification. The particle size distribution and average particle diameter were determined for each size fraction. The moisture content, ash content, protein content, and starch & fiber content in each fraction were also determined. A detailed description is given in Chapter 3.

The dust samples were stored in a refrigerator at 3°C (37°F). The samples to be used were allowed to equilibrate with the temperature and humidity of the laboratory air for at least 10 hrs prior to the experiment. The temperature and humidity of the laboratory were continuously monitored by a hygro-thermograph recorder (Belfort Instrument Company; Baltimore, MD).

C. PROCEDURE

The transducer was calibrated with the pressure gauge that was mounted on the dispersion air cylinder. Compressed air was allowed to pressurize the air dispersion cylinder and explosion chamber simultaneously. Starting at atmospheric pressure, the pressure was increased by an increment of 0.7 bar (10 psig) each time until it reached 10.3 bar (150 psig). At each increment, the pressure of the air dispersion cylinder indicated by the gauge and the corresponding output voltage from the signal conditioner were recorded. To ensure that the transducer and the pressure gauge were measuring the same pressure, the solenoid valve was held open and the air was allowed to stop flowing before any voltages or pressures were recorded.

Prior to the explosion, a specified amount of dust was weighed and placed into the dust cup (Fig. 5.3), and the explosion chamber was attached on top of the dust cup with T-bolts and wing nuts. The high voltage electrical leads from the transformer were attached to the electrodes. A square rod, having sides of 4.8 mm (3/16") and a length of 0.3 m (12"), was used to check the distance between the electrode tips inside the explosion chamber. After the pressure transducer was securely mounted in place (see Fig. 5.3), the air dispersion cylinder was pressurized to 6.9 bars (100 psig). The photograph film was initially exposed by the signal conditioner trace for atmospheric pressure indicated by the baseline shown in Fig. 5.4. The timing circuitry was programmed to simultaneously open the solenoid valve and ignite the electric spark. The camera shutter was opened again, so that the film could be exposed a second time by the explosion pressure trace.

After these pre-explosion preparations, the timing circuitry was initiated. After the explosion, the camera shutter was closed and the photograph removed.

The pressure history is characterized by the maximum explosion pressure, the maximum rate of pressure rise and the average rate of pressure rise as functions of concentration. When the pressure history of a dust sample is determined with a Hartmann explosion apparatus, the pressure tests are usually performed with five specific concentrations of dust (Dorsett et al., 1960). The five concentrations are 0.1, 0.2, 0.5, 1.0, and 2.0 kg/m^3 (1 kg/m^3 = 1 oz/ft^3). The concentration is defined as the total mass of dust placed in the explosion chamber divided by the chamber volume.

In this study, the pressure history was determined for each size fraction of each dust sample. Two replications of the explosion test were performed at each concentration, when enough sample was available.

A typical trace of pressure as a function of time for a dust explosion is shown in Fig. 5.4. The maximum explosion pressure is generally defined as the difference between the maximum pressure attained, B (see Fig. 5.4), and the pressure rise resulting from the dispersion air, A, (Dorsett, 1960).

The maximum rate of pressure rise is, in general, defined as the largest slope of the line tangent to the pressure-versus-time trace. In Fig. 5.4, this slope is shown as D/E. In this work the slope was obtained graphically.

The average rate of pressure rise is defined as the maximum explosion pressure divided by the estimated time between the ignition of the explosion and the attainment of the maximum pressure. The average rate of pressure rise is B/C in Fig. 5.4.

IV. RESULTS AND DISCUSSION

The maximum explosion pressure, P_{max}, the maximum rate of pressure rise, $(dP/dt)_{max}$, and the average rate of pressure rise, $(dP/dt)_{ave}$, are presented in Table 5.1 for five levels of concentration for each size fraction of grain sorghum dust, corn dust, wheat dust, and cornstarch. The corresponding sample identification and concentration are also presented. Note that the values of P_{max}, $(dP/dt)_{max}$, and $(dP/dt)_{ave}$ are tabulated according to chronological order in performing the experiments. In Table 5.2, the coefficients of variability of P_{max}, $(dP/dt)_{max}$, and $(dP/dt)_{ave}$ between replications are given for each level of concentration of grain sorghum dust, corn dust, wheat dust, or cornstarch. This table also contains the coefficients of variability of P_{max}, $(dP/dt)_{max}$, and $(dP/dt)_{ave}$ by pooling the data of all concentration levels for each type of dust.

Table 5.3 contains the ash contents in wheat dust, grain sorghum dust, and corn dust necessary for a completely inert dust sample. In this table,

the results from the three levels of concentration, 0.5, 1.0, and 2.0 kg/m^3, are presented. These were determined from the regressions of the ash content on P_{max}, $(dP/dt)_{max}$, or $(dP/dt)_{ave}$ for the three size fractions, 4, 5, and 6, with the highest ash contents. These three size fractions spanned over a wide range of the ash content from approximately 10 to 50%. In Table 5.4, the number of data, the coefficient of determination, R^2, the slope, and the intercept of the regression of the specific external surface area, S_{ext}, on P_{max} are presented for grain sorghum dust at three concentrations, 2.0, 1.0, and 0.5 kg/m^3. The range of S_{ext} included in each regression is also given. For each regression, the specific external surface area, below which no explosion can occur, is also presented with its corresponding particle diameter, $\overline{D}_1$, estimated from the relationship

$$\overline{D}_1 = \frac{\sigma}{\rho_s S_{ext}}$$

Similarly, the results of the regression of S_{ext} on $(dP/dt)_{max}$ are given in Table 5.5. In addition, Table 5.5 contains regressions for grain sorghum dust with four levels of concentration, 2.0, 1.0, 0.5, and 0.2 kg/m^3, and for corn dust with three levels of concentration, 2.0, 1.0, and 0.5 kg/m^3. Table 5.6 contains the results of the regression of S_{ext} on $(dP/dt)_{ave}$. In Table 5.7, the coefficient of determination, R^2, the slope, the intercept, and the total number of data are presented so that the experimental data at each level of concentration can be compared to those predicted by the model of Eckhoff (1976).

The concentration, P_{max}, $(dP/dt)_{max}$, and $(dP/dt)_{ave}$ obtained in the explosion test of autolyzed yeast extract are presented in Table 5.8 using a spherical explosion chamber with a volume of 0.19 m^3 (Fenwal) and a cylindrical

Hartmann apparatus with a volume of 0.00123 m^3 (USGMRL). Note that the results are tabulated according to chronological order for performing the explosion tests. In Table 5.9, the results of an analysis of variance for P_{max} is shown. The data for P_{max} in Table 5.8 are in the form of a 2 x 2 factorial experiment with the concentration and the apparatus as treatments.

Figures 5.5 through 5.8 present P_{max} plotted against the mass mean diameter, D_m, for grain sorghum dust, corn dust, wheat dust, and cornstarch, respectively. Each figure shows the relationship at four levels of concentration, 2.0, 1.0, 0.5, and 0.2 kg/m^3. Similarly, P_{max} is plotted against S_{ext} in Figs. 5.9 through 5.12 for the four types of dust. The maximum explosion pressure is plotted against the moisture content at the four highest levels of the concentration in Figs. 5.13, 5.14, 5.15, and 5.16 for cornstarch, wheat dust, corn dust, and grain sorghum dust, respectively. The relationships between P_{max} and ash content are shown in Figs. 5.17, 5.18, and 5.19, for wheat dust, corn dust, and grain sorghum dust, respectively. Each figure presents the relationship at the four highest levels of the concentration. The correlations between P_{max} and the protein content are presented in Figs. 5.20, 5.21, and 5.22, for wheat dust, corn dust, and grain sorghum dust, respectively. The maximum explosion pressure is plotted against the starch & fiber content in Figs. 5.23, 5.24, 5.25, and 5.26, for cornstarch, wheat dust, corn dust, and grain sorghum dust, respectively.

The results pertaining to $(dP/dt)_{max}$ are presented and correlated in Figs. 5.27 through 5.48. These results are compared to those predicted by Eckhoff's model in Figs. 5.49 through 5.53. The results pertaining to $(dP/dt)_{ave}$ are presented and correlated in Figs. 5.54 through 5.75.

Figure 5.76 presents the coefficients of variability of P_{max} between replications plotted against the concentration for the cylindrical Hartmann

apparatus with a volume of 0.00123 m^3 and for the spherical apparatus with a volume of 0.19 m^3. The maximum explosion pressure in each apparatus is plotted against the concentration in Fig. 5.77. Similarly, the coefficients of variability are plotted against the concentration. Figure 5.78 is the same as Fig. 5.76 except that the coefficients of variability are for $(dP/dt)_{max}$ instead of P_{max}. The relation between the $(dP/dt)_{max}$ and the volume of the explosion chamber is given according to the cubic law (Bartknecht, 1978):

$$K_{st} = \left(\frac{dP}{dt}\right)_{max} \cdot V^{1/3}$$

where

K_{st} = constant

V = volume of the explosion chamber

The values of K_{st} for the cylindrical Hartmann apparatus are plotted against those for the spherical apparatus. The regression line of K_{st} for the spherical apparatus on K_{st} for the Hartmann apparatus is shown in Fig. 5.79; a similar correlation experimentally determined by Bartknecht (1978) is also shown for comparison. Figure 5.80 is identical to Fig. 5.76 except that the coefficients of variability are for $(dP/dt)_{ave}$ instead of for $(dP/dt)_{max}$. The quantity $K_{st,ave} = (dP/dt)_{ave} \cdot V^{1/3}$ for the cylindrical Hartmann apparatus is plotted against that for the spherical apparatus. The regression line of $K_{st,ave}$ for the spherical apparatus on $K_{st,ave}$ for the Hartmann apparatus is also shown. The same experimentally determined correlation by Bartknecht (1978), shown in Fig. 5.79, is also reproduced in Fig. 5.80.

A. Maximum Explosion Pressure

1. Effect of particle size

a. Mass mean diameter

Figure 5.5 shows the relationship between the maximum explosion pressure, P_{max}, and the mass mean diameter, D_m, for grain sorghum dust. It includes four levels of dust concentration, 0.2, 0.5, 1.0, and 2.0 kg/m^3. The maximum explosion pressures for the size fraction with the three highest ash contents are represented by circles. Note that these values are relatively low.

As the mass mean diameter decreases from 89 µm to approximately 60 µm, P_{max} increases for all levels of concentration. The higher the concentration, the higher the P_{max}. As the particle diameter decreases from 60 to 15 µm, P_{max} remains essentially constant (approximately 6.0 ± 0.3 bar) at the two higher concentrations (1.0 and 2.0 kg/m^3). At the two lower concentrations (0.2 and 0.5 kg/m^3), P_{max} continues to increase as D_m decreases. At the concentration of 0.5 kg/m^3, the slope decreases slightly, whereas for the 0.2 kg/m^3 concentration, the slope continues to increase. As the particle diameter further decreases from 15 to 10 µm, P_{max} decreases sharply for the concentrations of 0.5 and 2.0 kg/m^3; however, for the concentration of 0.2 kg/m^3, P_{max} continues to increase. For the concentration of 1.0 kg/m^3, there is a sharp increase from 6.3 to 7.8 bar. Note that at the concentration of 0.5 kg/m^3, P_{max} reaches the maximum value of nearly 5.9 bar. This value approximates to the constant value attained when the dust concentration is 1.0 or 2.0 kg/m^3. The maximum explosion pressure at the lowest concentration continues to increase throughout the entire range of D_m; it never reaches a value in the range of 5.9 to 6.0 bar but only reaches approximately 4.8 bar. Note that when the concentration is 0.2 or 0.5 kg/m^3, it has a more pronounced effect on P_{max} than when it is 1.0 or 2.0 kg/m^3. The effect of concentration

on P_{max} is also a function of D_m. At a value of D_m equal to 89 μm, P_{max} is zero for the concentration 0.2 kg/m^3 and approximately 0.5 bar for the concentration of 0.5 kg/m^3. At D_m equal to 50 μm, however, P_{max} is 0.5 and 3.6 bar for the concentrations of 0.2 and 0.5 kg/m^3, respectively. At the two lower concentrations, P_{max} becomes essentially zero for particles with diameters larger than 89 μm. The minimum explosible concentration appears to be a function of D_m.

Figure 5.6, which is for corn dust, shows the same relationship as Fig. 5.5 which is for grain sorghum dust. The data for samples with high ash contents are given with circles. For corn dust, the range of particle diameters is between only 10 μm and 60 μm. At the two higher concentrations, P_{max} remains essentially constant at 5.5 ± 0.5 bar, as does the grain sorghum dust. For corn dust, however, there is no sharp decrease for values of D_m less than 15 μm. For the concentration of 0.5 kg/m^3, P_{max} increases slightly as D_m decreases to 15 μm; however, the decrease is not so drastic as that for grain sorghum dust. For D_m less than 15 μm, P_{max} decreases sharply, as does the grain sorghum dust. For these three concentrations, the curves are not so smooth as those for grain sorghum dust. For the concentration of 0.2 kg/m^3, except for some variability, P_{max} continuously increases as D_m decreases, as does the grain sorghum dust. Again, the slope is not so steep as that for grain sorghum dust. The effect of the concentration again is dependent on the particle size and diminishes at high concentrations. In general, the values of P_{max} for grain sorghum dust are slightly higher than those for corn dust.

Figure 5.7 indicates that no clear relationship can be identified between P_{max} and D_m at any level of concentration. The range of mass mean diameters is smaller for wheat dust than for either corn or grain sorghum dust. Note that for corn dust and grain sorghum dust, a range of D_m exists in which P_{max}

is independent of D_m. For wheat dust, all the values of D_m are in this range. The effect of the concentration is essentially the same as that for the other types of dust. The maximum explosion pressure at 0.2 kg/m^3, the lower concentration, is much lower than that for corn dust or grain sorghum dust; 0.2 kg/m^3 is near the minimum explosible concentration. At the other concentrations, however, P_{max} is essentially the same as that for corn dust. The effect of the concentration can be very severe at concentrations near the minimum explosible concentration.

In Fig. 5.8, note that for the three highest levels of concentration, the relationship between P_{max} and D_m for cornstarch is essentially the same as that for wheat dust, except that variability is more pronounced for the former; the coefficient of variability between replications is larger for cornstarch than for all other types of dust (Table 5.2). The variability of P_{max} is also due to that in the moisture content. Except for a concentration of 0.2 kg/m^3, P_{max} is essentially the same as that for corn or wheat dust.

b. Specific external surface area

It has been shown in Section II that P_{max} is a function of the specific external surface area, S_{ext}, according to Eq. (29). For grain sorghum dust, P_{max} exhibits linear relationships on S_{ext} for S_{ext} up to approximately 0.11 m^2/g, except for the lowest concentrations (see Table 5.5 and Fig. 5.9). The values of the coefficient of determination, R^2, are 0.88, 0.78, and 0.95 for concentrations of 2.0, 1.0, and 0.5 kg/m^3, respectively. However, deviations from linearity become more pronounced of the upper 1/3 of the total range of P_{max}. The slope changes very sharply at pressures close to the maximum, as if the reaction was abruptly stopped by a limitation of a reactant such as oxygen. Hertzberg et al. (1979) showed that 90% or more of the oxygen

in the closed vessel is consumed by the explosion of 22 μm coal dust at 0.2 and 0.5 kg/m^3. In addition, Eq. 5.32 indicates that the rate of oxygen consumption is proportional S_{ext}. At this stage it is unclear why P_{max} increases abruptly for the largest S_{ext} when the concentration is 1.0 kg/m^3.

At the lowest concentration, (0.2 kg/m^3), the relationship is sufficiently non-linear throughout the entire range of specific external surface area; however, P_{max} never becomes independent of S_{ext} as in the case of the three higher concentrations. Note that P_{max} also never attains a value so large as those for the three higher concentrations.

The relationship between P_{max} and S_{ext} for corn dust is presented in Table 5.10 for the four levels of concentration, 0.2, 0.5, 1.0, and 2.0 kg/m^3. For the three higher concentrations, P_{max} does not appear to depend on S_{ext}. Note that the lowest value of S_{ext} is 0.11 m^2/g. For grain sorghum dust, P_{max} is also essentially independent of S_{ext} for values of S_{ext} greater than 0.13 m^2/g. For the lowest concentration, P_{max} depends more profoundly on S_{ext} than at any higher concentration. The samples with the three highest ash contents are represented by circled points.

Figure 5.11 exhibits a relationship between P_{max} and S_{ext} for wheat dust. Note that for all concentrations, the dust samples with the smallest values of S_{ext} also have the highest ash contents. A sufficiently linear correlation cannot be obtained if these data are excluded.

For cornstarch, Fig. 5.12 also exhibits essentially no correlation between P_{max} and S_{ext}, except at the two lower concentrations; variability is excessive due to the large range of moisture contents. Another reason for the lack of correlation might be that cornstarch contains the smallest range of particle sizes.

2. Effect of composition

a. Moisture content

The maximum explosion pressure is plotted against the moisture content for cornstarch, wheat dust, corn dust, and grain sorghum dust in Figs. 5.13, 5.14, 5.15, and 5.16, respectively. Each figure contains four levels of concentration, 0.2, 0.5, 1.0, and 2.0 kg/m^3. For cornstarch, Fig. 5.13 shows that P_{max} increases as the moisture content decreases. The maximum explosion pressure and the moisture content appear to be correlated quadratically. The effect of moisture content on P_{max} varies with concentration. The higher the concentration, the less the effect of moisture content; at a concentration of 0.2 kg/m^3, P_{max} is reduced by 2.4 bar over the entire range of moisture contents, whereas at any other concentration, the reduction is about 1.7 to 1.9 bar. The condition of $P_{max} = 0$ is reached at a higher moisture content at higher concentration. At the dust concentration of 0.2 kg/m^3, P_{max} becomes zero at a moisture content of approximately 16%; however, at higher dust concentration, P_{max} becomes zero at a moisture content around 20% or higher.

It can be seen in Fig. 5.14 that the correlation between P_{max} and the moisture content for wheat dust is opposite to that for cornstarch. For wheat dust, the ash content increases as the moisture content decreases, and this increase in ash content causes P_{max} to decrease. The samples with the highest ash content are identified by circles in Fig. 5.14. If those samples are removed it becomes difficult to observe a clear correlation between P_{max} and the moisture content.

Similarly, it becomes difficult to observe definite correlation between P_{max} and the moisture content for corn dust if the data from the samples with high ash contents are removed as shown in Fig. 5.15. In the case of cornstarch, the concentration stratifies the values of P_{max} into groups. The

maximum explosion pressures for concentrations of 1.0 and 2.0 kg/m^3 are essentially identical. It is difficult to observe a relationship between P_{max} and the moisture content in Fig. 5.16 for grain sorghum dust. In contrast to corn dust, the concentration seems to be a minor effect; the values of P_{max} for the different concentrations are not stratified.

b. Ash content

The maximum explosion pressure is plotted against the ash content for wheat dust, corn dust, and grain sorghum dust in Figs. 5.17, 5.18, and 5.19, respectively. Each figure presents four levels of concentration, 0.2, 0.5, 1.0, and 2.0 kg/m^3. In Fig. 5.17, it is difficult to detect any correlation between P_{max} and the ash content for wheat dust, at ash contents below approximately 10%. For ash contents above 10%, P_{max} decreases with increasing ash content. The rate of this decrease is greater for the 0.5 kg/m^3 concentration than for either the 1.0 or the 2.0 kg/m^3 concentration. Note that the minimum explosible concentration is approximately 0.2 kg/m^3 for all ash contents. For ash contents greater than 10%, a regression of P_{max} on the ash content was performed. The results of the regressions, as shown in Table 5.3, indicate that at the concentration of 0.5 kg/m^3, an ash content of 56% is necessary to result in no explosion, whereas a larger ash content is necessary at the higher concentrations. Note that an ash content greater than 100% is not possible.

The correlations between P_{max} and the ash content for corn dust in Fig. 5.18 are similar to those for wheat dust. For corn dust, it is difficult again to observe any correlation at ash contents below approximately 6%. Table 5.3 also presents results from the regression of P_{max} and ash contents greater than 6% for corn dust. The table indicates that no explosion can

occur for ash contents above 52 and 54% for concentrations of 0.5 and 1.0 kg/m^3, respectively. Again, the higher concentrations show less effect of ash content on P_{max} than the lower concentrations.

The correlations between P_{max} and the ash content for grain sorghum dust in Fig. 5.19 are also similar to those for wheat dust. At ash contents below 12%, any correlation between P_{max} and the ash content are difficult to detect for grain sorghum dust. Table 5.3 indicates that the ash contents above which no explosion can occur are essentially the same as those for wheat dust.

c. Protein content

The maximum explosion pressure is plotted against the protein content for wheat dust, corn dust, and grain sorghum dust in Figs. 5.20, 5.21, and 5.22, respectively. In Fig. 5.20, there appears to be an inverse correlation between P_{max} and the protein content for wheat dust. This correlation is due to the significant correlation between the ash content and the protein content. Note that the size fractions with the three highest protein contents also contain the highest ash contents. The samples from the size fractions with the three highest ash contents are again identified by circles. When those samples are excluded, a correlation between P_{max} and the protein content is difficult to observe. Note that the samples with the second smallest protein content also have the smallest mass mean diameter.

For corn dust, a correlation between P_{max} and the protein content is difficult to detect for the two lower concentrations, as can be seen in Fig. 5.21; however, an inverse correlation is observed. The samples from the samples with the three highest ash contents are identified with circles. Note that again the concentration stratifies the values of P_{max} into groups. In Fig. 5.22, a correlation between P_{max} and the protein content is hard to

detect for grain sorghum dust at any level of concentration. Any stratification due to concentration is essentially absent. For grain sorghum dust, the protein content appears to be a minor effect.

d. Starch & fiber content

The maximum explosion pressure is plotted against the starch & fiber content for cornstarch, wheat dust, corn dust, and grain sorghum dust in Figs. 5.23, 5.24, 5.25, and 5.26, respectively. For cornstarch, Fig. 5.23 shows that as the starch & fiber content decreases, P_{max} decreases. Note that the contents of ash and protein are negligibly small for cornstarch. Cornstarch is assumed, therefore, to consist of only moisture, starch and fiber. This correlation must be the negative of that between P_{max} and the moisture content.

Figure 5.24 presents the correlation between P_{max} and the starch & fiber content for wheat dust. Again, as the starch & fiber content decreases, P_{max} decreases. Note that the three size fractions with the lowest starch & fiber contents also contain the highest ash content; the data from these size fractions are identified by circles in Fig. 5.24. The correlation between P_{max} and the starch & fiber contents could be the result of the correlation between the ash content and P_{max}; when the circled data are excluded, the correlation between P_{max} and the starch & fiber content is difficult to detect. A similar trend can be observed in Fig. 5.25 for corn dust and in Fig. 5.26 for grain sorghum dust.

For wheat, corn, or grain sorghum dust, it is difficult to ascertain if P_{max} is directly correlated to the starch & fiber content or if the correlation between P_{max} and the starch & fiber content is the result of that between P_{max} and the ash content. Similarly, for cornstarch, it is difficult

to ascertain if P_{max} is directly correlated to the starch & fiber content or if this correlation is the result of that between P_{max} and the moisture content. If P_{max} is directly correlated to the starch & fiber content, then it becomes difficult to explain why a reduction in the starch & fiber content due to an increase in moisture content is more effective in reducing P_{max} than a decrease in starch & fiber content due to an increase in the ash content. In addition, low correlation at low ash or moisture contents is explainable whereas the low correlation at high starch & fiber content is not. The starch & fiber content of the dust particles themselves might not vary widely; from Chapter 3, it appears that a large percentage of the ash is contained in separate ash particles and not in the grain dust particles themselves. It appears, therefore, that a correlation between P_{max} and the moisture content is more easily explained than that between P_{max} and the starch & fiber content.

B. Maximum Rate of Pressure Rise

1. Effect of particle size

a. Mass mean diameter

Figure 5.27 shows the correlation between the maximum rate of pressure rise, $(dP/dt)_{max}$, and the mass mean diameter, D_m, at concentration levels of 2.0, 1.0, 0.5, and 0.2 kg/m^3 for grain sorghum dust. This figure indicates an inverse relationship between $(dP/dt)_{max}$ and D_m for all concentrations. The slope of the curves is significantly greater for D_m between approximately 15 to 50 μm than for D_m between 50 to 89 μm. For all but the lowest concentration of 0.2 kg/m^3, the effect of particle size becomes less significant for diameters less than approximately 15 μm; the slope of the curve approaches to zero or negative. This observation could be interpreted as the result of increase agglomeration at the higher concentrations or variability in the

experiment. At D_m of 50 μm, the values of $(dP/dt)_{max}$ are approximately 60, 55, 40, and 5 bar/s for concentrations of 2.0, 1.0, 0.5, and 0.2 kg/m^3, respectively. Than at D_m of approximately 22 μm, the values of $(dP/dt)_{max}$ are 202, 114, 110, and 90 bar/s for concentrations of 0.5, 0.2, 1.0, and 2.0 kg/m^3, respectively. Finally, at D_m of 10 μm, the values of $(dP/dt)_{max}$ are 382, 310, and 180 bar/s for concentrations of 0.2, 0.5, and 1.0 kg/m^3, respectively. Thus, at particle diameter less than approximately 15 μm, the lowest concentration immediately above the minimum explosible concentration can be the most hazardous.

As the particle size increases, $(dP/dt)_{max}$ approaches zero more quickly for the lower concentrations. However, as the particle diameter decreases, the lowest concentration yields the largest values of $(dP/dt)_{max}$. The value of D_m for a concentration of 0.2 kg/m^3, for which $(dP/dt)_{max}$ is less than 10 bar/s, is approximately 50 μm, that for a concentration of 0.5 kg/m^3, approximately 89 μm, and those for concentrations of 1.0 and 2.0 kg/m^3 are larger than 89 μm. Note that at a D_m of 89 μm, all four concentrations show values of $(dP/dt)_{max}$ below 20 bar/s.

The correlation between $(dP/dt)_{max}$ and D_m for corn dust is shown in Fig. 5.28. It can be seen that trends are similar to those for the grain sorghum dust; however, the curves are not as smooth. The coefficient of variability between replications is 4% for grain sorghum dust and 53% for corn dust. The data points for size fractions with ash contents greater than 15% are indicated with circles. At the concentrations of 2.0 kg/m^3, the effect of D_m is insignificant. The values of $(dP/dt)_{max}$ and each D_m are essentially the same as those for the grain sorghum dust.

The correlation between $(dP/dt)_{max}$ and D_m for wheat dust in Fig. 5.29 is similar to that for corn dust; however, the values of $(dP/dt)_{max}$ are below

120 bar/s whereas for corn dust and grain sorghum dust, the values of $(dP/dt)_{max}$ are as high as 380 bar/s. In contrast to grain sorghum dust and corn dust, $(dP/dt)_{max}$ for the concentration of 0.2 kg/m^3 for wheat dust never rose above a value of 10 bar/s. For wheat dust, a concentration of 0.2 kg/m^3 is close to the minimum explosible concentration for all particle sizes. The lowest diameter was 21 μm, so that one does not observe the decrease in slope at the smallest value of D_m noted for corn dust and grain sorghum dust.

The correlation between $(dP/dt)_{max}$ and D_m for cornstarch is shown in Fig. 5.30. There is essentially no relationship between $(dP/dt)_{max}$ and D_m for any value of concentration. The range of diameters is the smallest of the four types of dust, 17 μm to 35 μm, and the range of moisture contents is the largest, 4% to 14.9%.

b. Specific external surface area

It has been shown that the maximum rate of pressure rise, $(dP/dt)_{max}$, is a function of the specific external surface area, S_{ext}, according to Eq. (5.30). The resultant correlations based on Eq. (5.30) for grain sorghum dust, corn dust, wheat dust, and cornstarch are shown in Figs. 5.31, 5.32, 5.33, and 5.34, respectively. Each includes four levels of concentration.

In Fig. 5.31, the correlation for grain sorghum dust is approximately linear for specific ranges of S_{ext}. For the lowest concentration, 0.2 kg/m^3, the relationship is linear with an R^2 of 0.92 (Table 5.6) for the entire range of specific external surface areas in this investigation. Through extrapolation, this relationship indicates that the largest diameter particle which yields a significant value of $(dP/dt)_{max}$ is approximately 45 μm.

For the three largest concentrations (0.5, 1.0, and 2.0 kg/m^3), the correlation between $(dP/dt)_{max}$ and S_{ext} is linear for values of S_{ext} up to

0.345, 0.745, and 0.168 m^2/g, respectively (Table 5.6). The coefficients of correlation are 0.92, 0.89, and 0.80 for concentrations of 0.5, 1.0, and 2.0 kg/m^3, respectively. For values of S_{ext} above these, the slope of the correlation decreases toward zero or becomes negative. This decrease in slope could be the result of factors such as radiation, agglomeration, or an oxygen limiting condition. At the high concentrations, the decrease in the partial pressure of oxygen could not be taken into account by the simple correlation. From Eq. (5.32), the rate at which oxygen is consumed increases with increasing S_{ext}. By extrapolation, the largest diameters for which an explosion can occur are 46, 69, and 64 μm for concentrations of 0.5, 1.0, and 2.0 kg/m^3, respectively. Note that the slopes of the regression lines in Table 5.6 increase as the concentration decreases except for the lowest concentration of 0.2 kg/m^3.

In Fig. 5.32, a similar relationship is observed for corn dust; however, there is more variability in the data as indicated by the R^2 values in Table 5.6. The coefficient of variability between replications for corn dust is 53% whereas for grain sorghum dust it is 40% (Table 5.2). The slopes are slightly higher for corn dust than those for grain sorghum dust. Note that the range of external specific surface areas included in the regression is very similar to those for grain sorghum dust.

For wheat dust in Fig. 5.33, there might possibly be a similar relationship as for the case of grain sorghum dust when the data with the highest ash content are discarded. The range of specific external surface area is too small and there is too much variability to be able to observe effectively any relationship that might exist.

For cornstarch, there is essentially no observable relationship (Fig. 5.34). This may be due to the small range of specific external surface

areas examined and the variability due to the moisture contents.

2. Effect of composition

a. Moisture content

The correlations between the maximum rate of pressure rise, $(dP/dt)_{max}$, and the moisture content for cornstarch, grain sorghum dust, corn dust, and wheat dust, are shown in Figs. 5.35, 5.36, 5.37, and 5.38, respectively. For cornstarch, there appears to be a correlation in which the value of $(dP/dt)_{max}$ decreases as the moisture content increases (Fig. 5.35). For each concentration, a regression of $(dP/dt)_{max}$ on the moisture content was performed; the results are presented in Table 5.4. Note that the slope of the regression lines decreases as the concentration decreases except for the lowest concentration of 0.2 kg/m^3. The maximum rate of pressure rise approaches zero for moisture contents ranging between 14.6 to 20%, depending on the concentration. The higher the concentration, the larger the moisture content to cause $(dP/dt)_{max}$ to approach zero.

It is difficult to observe any relationship between $(dP/dt)_{max}$ and the moisture content for grain sorghum dust, as shown in Fig. 5.36. However, the moisture content above which no explosion occurs appears to range from approximately 13 to 15%. Below the moisture content of approximately 11.2%, there is much variability in the maximum rate of pressure rise. At the moisture content of 10%, $(dP/dt)_{max}$ ranges from approximately 70 to 380 bar/s. The circled data with the lowest moisture content have very low values of $(dP/dt)_{max}$; these data come from size fractions that contain 39.1%. In Fig. 5.37, a relationship for corn dust similar to that for grain sorghum dust is observed; however, there is more variability at the higher moisture contents. The wheat dust shows a relationship that is opposite to those shown by

the other types of dust (Fig. 5.38). As the moisture content decreases, $(dP/dt)_{max}$ decreases. This relationship is the result of highly significant inverse correlation between ash content and moisture content. The data from size fractions containing the three highest ash contents are identified by circles. Note that a correlation is difficult to observe for the remaining uncircled data. Grain sorghum dust and corn dust also exhibited little correlation for moisture contents below 10%.

The correlations between $(dP/dt)_{max}$ and the moisture content for all four types of dust exhibit increased variability in $(dP/dt)_{max}$ for moisture contents below approximately 11%. For cornstarch, grain sorghum dust, or corn dust, the values of $(dP/dt)_{max}$ were relatively low with little variability for the moisture content above a certain value. For the four levels of concentration, this moisture content ranged from 13 to 20%.

b. Ash content

The correlations between the maximum rate of pressure rise and ash content for wheat dust, grain sorghum dust, and corn dust are shown in Figs. 5.39, 5.40, and 5.41, respectively. For all three types of dust, as the ash content increases, the maximum rate of pressure rise decreases. For ash contents below approximately 11%, it does not appear to be a major effect. In addition, the effect on $(dP/dt)_{max}$ of ash is more pronounced for the lower concentrations than for the higher concentrations. The data from size fractions with ash contents greater than 11% were linearly extrapolated to ash contents corresponding to $(dP/dt)_{max} = 0$ (Table 5.3). For wheat dust, Table 5.3 indicates ash contents of 49, 79, and 86%, for concentrations of 0.5, 1.0, and 2.0 kg/m^3, respectively. Note that the higher the dust concentration, the higher the ash content necessary to reduce $(dP/dt)_{max}$ to zero.

For corn dust, the values of ash content at which the value of $(dP/dt)_{max}$ is zero are 48%, 45%, and 68%, for concentrations of 0.5, 1.0, and 2.0 kg/m^3, respectively, and those for grain sorghum dust are 42 and 74% for concentrations of 0.5 and 1.0 kg/m^3, respectively.

c. Protein content

The correlations between the maximum rate of pressure rise and the protein content for wheat dust, corn dust, and grain sorghum dust are shown in Figs. 5.42, 5.43, and 5.44, respectively. For grain sorghum dust, it is difficult to detect any correlation. A correlation between $(dP/dt)_{max}$ and the protein content is also difficult to detect for corn dust. Note that the data from size fractions with protein contents above 8% also contain ash contents greater than 16% and mass mean diameters greater than 60 μm. Consequently, these data have relatively low values of $(dP/dt)_{max}$. For wheat dust there appears to be an inverse correlation between $(dP/dt)_{max}$ and the protein content. For wheat dust, however, a significant correlation exists between the ash and protein contents. The data in Fig. 5.42 that are circled are from size fractions that contain the two highest ash contents. When those data are excluded, it is again difficult to detect a relationship between $(dP/dt)_{max}$ and the protein content. In addition, the data with the highest $(dP/dt)_{max}$ is from a size fraction with the smallest mass mean diameter or largest external specific surface area.

d. Starch & fiber content

The relationships between the maximum rate of pressure rise and starch & fiber content for cornstarch, wheat dust, grain sorghum dust, and corn dust are shown in Figs. 5.45, 5.46, 5.47, and 5.48, respectively. For cornstarch and wheat dust, there appear to be significant correlations. However, it was

found that the starch & fiber content is highly correlated to the ash content for wheat dust, corn dust, and grain sorghum dust and to the moisture content for cornstarch. The data from size fractions with ash contents greater than 11% are identified with circles. Note that for wheat dust, corn dust, and grain sorghum dust a correlation between $(dP/dt)_{max}$ and the starch & fiber content is difficult to observe if these data are removed. Whether the reduction in $(dP/dt)_{max}$ for all types of dust is due to a reduction in the starch & fiber content or an increase in the ash content or the moisture content is difficult to determine. It appears, however, that a reduction in the starch & fiber content due to moisture is more effective than that due to ash. This is difficult to explain if the reduction in $(dP/dt)_{max}$ is due to a reduction in starch & fiber content. In addition, a large percentage of the ash content appears to be contained in separate ash particles and not in the grain dust particles themselves. Thus, the starch & fiber content of the grain dust particles might vary only slightly between size fractions. This could eliminate the effect of starch & fiber content on $(dP/dt)_{max}$.

3. Combined effect of particle size and composition

The correlations between $(dP/dt)_{max}$ and that particle size for grain sorghum dust are more distinct than those for the other types of dust; however, the correlations between $(dP/dt)_{max}$ and each of the composition components exhibit the most random variability. In contrast, the correlations between $(dP/dt)_{max}$ and the moisture content are noticeable for cornstarch; on the other hand, it is difficult to detect any other correlations for cornstarch. For wheat dust, the correlations between $(dP/dt)_{max}$ and the ash content are the only observable correlations. Corn dust exhibits the best correlation between $(dP/dt)_{max}$ and the particle size; however, there is more variability

than in the case of grain sorghum dust. For the composition components, the correlations for corn dust exhibit less variability than in the case of grain sorghum dust.

4. Comparison of the experimental data with those predicted by Eckhoff's model

Eckhoff (1976) presented an approximate correlation between the maximum rate of pressure rise, and the specific external surface area and composition. The expression is

$$\left(\frac{dP}{dt}\right)_{max} = \left(840 \cdot \frac{z}{100} + 460\right) S \left(1 + \frac{y}{15}\right) \cdot C$$

where

z = percent of starch & fiber content

y = weight percent of moisture

s = specific external surface area, m^2/g

c = conversion factor, 0.978989 (bar/s)/(kp/cm^2s)

This equation was used to predict the values of $(dP/dt)_{max}$ obtained in this investigation. The experimental values of $(dP/dt)_{max}$ are plotted against those predicted by the model in Figs. 5.49, 5.50, 5.51, 5.52, and 5.53 for concentrations of 2.0, 1.0, 0.5, 0.2, and 0.1 kg/m^3, respectively. The equation predicts the values of $(dP/dt)_{max}$ at the highest concentration, than those at the lower concentrations; the coefficients of determination are 0.72, 0.63, 0.67, 0.71, and 0.001 for concentrations of 2.0, 1.0, 0.5, 0.2, and

0.1 kg/m^3, respectively (see Table 5.11). Note that the values of R^2 at each concentration is significant at the 1% level. For a concentration of 2.0 kg/m^3 the prediction equation underestimates the experimental data by less than 58, 47, 26, and 11 bar/s for cornstarch, corn dust, grain sorghum dust, and wheat dust, respectively. For a concentration of 0.5 kg/m^3, the equation underestimates the maximum rate of pressure rise by as much as 480, 256, 191, and 32 bar/s for the cornstarch, corn dust, grain sorghum dust, and wheat dust, respectively.

The model does not contain a concentration dependence which can be quite complex. However, the model should be made to yield the worst possible case, i.e., low concentration. In addition, the lower concentrations are encountered earlier and more frequently than the higher concentrations in industry.

C. Average Rate of Pressure Rise

1. Effect of particle size

a. Mass mean diameter

The correlations between the average rate of pressure rise, $(dP/dt)_{ave}$ and the mass mean diameter are shown in Figs. 5.54, 5.55, 5.56, and 5.57 for grain sorghum dust, corn dust, wheat dust, and cornstarch, respectively. Each figure presents four levels of concentration, 0.2, 0.5, 1.0, and 2.0 kg/m^3. For grain sorghum dust, (Fig. 5.54), the relationship at each level of concentration is very similar to that observed for $(dP/dt)_{max}$, except that the values of $(dP/dt)_{ave}$ are approximately 1/2 to 1/3 of those for the maximum rate of pressure rise. As D_m decreases from 89 to 50 μm, the values of $(dP/dt)_{ave}$ for the two higher concentrations (1.0 and 2.0 kg/m^3) are larger and increase faster than those for the two lower concentrations (0.2 and 0.5 kg/m^3). As D_m decreases from approximately 50 to 20 μm, the rate at which

$(dP/dt)_{ave}$ rises with D_m decreases sharply for the two higher concentrations, and the values of $(dP/dt)_{ave}$ become smaller than those for the two lower concentrations. As D_m further decreases from 20 to 15 μm, the rate at which $(dP/dt)_{ave}$ rises with D_m for the 0.5 kg/m^3 concentration falls becomes smaller than that for the 0.2 kg/m^3 concentration. Finally, as D_m decreases from 15 to 10 μm the values of $(dP/dt)_{ave}$ for the 1.0 and 0.5 kg/m^3 concentrations decrease sharply; however, the value of $(dP/dt)_{ave}$ for the lowest concentration, 0.2 kg/m^3, continues to increase and attains the highest value of $(dP/dt)_{ave}$ for all four concentrations. The effect of particle size seems to diminish with decreasing mass mean diameter. This is similar to that noted for the maximum explosion pressure. Note that the average rate of pressure rise is the maximum explosion pressure divided by the time necessary to reach the maximum. As the maximum explosion pressure for the three highest concentrations increases and reaches a constant value, the time necessary to realize the maximum explosion pressure continues to decrease; the rate at which it decreases becomes less until it also reaches a constant value. This could be the result of an oxygen limiting condition or increasing agglomeration.

In Fig. 5.55 for corn dust, similar trends can be observed; nevertheless, there is more variability in the data, especially at the two lowest concentrations. The coefficient of variability between replications is 56% for corn dust and only 27% for grain sorghum dust. Note that the coefficient of variability between replications for corn dust is much larger than for grain sorghum dust at concentrations of 0.2 and 0.1 kg/m^3. The points that are circled come from size fractions that also contain high ash contents. The mass mean diameter ranges only to 60 μm. The values of $(dP/dt)_{ave}$ for corn dust are essentially the same as those for grain sorghum dust.

In Fig. 5.56 it is difficult to observe a correlation between $(dP/dt)_{ave}$ and D_m for wheat dust. The circled data again come from size fractions that contain high ash contents. Note that the range of mass mean diameters for wheat dust is smaller than that for grain sorghum dust or corn dust. The values of $(dP/dt)_{ave}$ are approximately 1/3 of those for grain sorghum dust and corn dust. The values of $(dP/dt)_{ave}$ for the lowest concentration are 5 to 30 times smaller than those for grain sorghum dust or corn dust. Dust can become hazardous for concentrations just over their minimum values especially at small mass mean diameters, (10 to 40 μm).

In Fig. 5.57, a correlation between $(dP/dt)_{ave}$ and D_m is difficult to observe for cornstarch. This could be due to the small range of mass mean diameters and the large range of moisture contents. The largest values of $(dP/dt)_{ave}$ for grain sorghum dust and corn dust are 128 and 138 bar/s, respectively; that for cornstarch is 245 bar/s.

b. Specific external surface area

It has been shown that the average rate of pressure rise, $(dP/dt)_{ave}$, can be correlated with the specific external surface area, S_{ext}, according to Eq. (5.31). In Fig. 5.58, the correlation for grain sorghum dust is reasonably linear up to a value of 0.340 m^2/g. For values of S_{ext} larger than 0.340 $m^2 g$, the slopes decrease sharply to a negative value for concentrations of 1.0 and 0.5 kg/m^3. Prior to this value of S_{ext}, the slope for the concentration of 0.5 kg/m^3 decreases. The coefficients of determination, R^2, and the range of external specific surface area used in the linear regression are given in Table 5.8 for all four levels of concentration. The coefficients of determination range from 0.87 to 0.95 for all concentration. The correlation for the lowest concentration (0.2 kg/m^3) is linear for the entire range of

S_{ext} in this investigation with the highest value of R^2. Except for the lowest level of concentration, the slopes of the regression lines increase with decreasing concentration. In addition, the diameters above which no explosion can occur increase with increasing concentration. The decrease in slope of the correlation at the highest values of S_{ext} is consistent with that observed for $(dP/dt)_{max}$. This could be the result of increased agglomeration at small particle diameters, increased radiation at high temperatures and concentrations or an oxygen limiting condition at high concentrations and conversion. Hertzberg et al. (1979) showed that 90% or more of the oxygen in the closed vessel is consumed for concentrations of approximately 0.200 to 0.500 kg/m^3. Note that the average rate is by definition related to P_{max}. The maximum explosion pressure also showed a linear relation; however, the slope decreased significantly from values of S_{ext} lower than those in the case of $(dP/dt)_{ave}$.

In Fig. 5.59, the correlations between $(dP/dt)_{ave}$ and S_{ext} for corn dust are similar to those for grain sorghum dust for concentrations of 0.2, 0.5, and 1.0 kg/m^3. The average rate of pressure rise for corn dust shows more variability than those for grain sorghum dust; the coefficients of determination for corn dust are smaller than those for grain sorghum dust. This variability appears to be random with respect to the linear relationship. In Table 5.2, the coefficient of variability of $(dP/dt)_{ave}$ between replications for corn dust is larger than that for grain sorghum dust. The highest did not show much change over the range of specific external surface areas. Again, the correlations for the concentrations of 1.0 and 0.5 kg/m^3 exhibit a sharp decrease in slope at values of the specific external surface area above 0.34 whereas those for the concentration of 0.2 kg/m^3 increase throughout the entire range of S_{ext}.

The correlation between $(dP/dt)_{ave}$ and S_{ext} is presented in Fig. 5.60 for wheat dust. The data from the size fractions with the three highest ash contents are identified by circles. For all four concentrations, a correlation is difficult to observe when these data are excluded. The combination of variability and the smallest range of S_{ext} for all types of dust, 0.154 to 0.228 m^2/g causes the determination of any relationship difficult. The coefficient of variability between trials for wheat dust is 33% (Table 5.2).

In Fig. 5.61, it is also difficult to observe a correlation between $(dP/dt)_{ave}$ and S_{ext} for cornstarch. The variability in the determination of $(dP/dt)_{ave}$, the variability of moisture content among the size fractions and the small range of S_{ext} cause the determination of a relationship to be difficult. The coefficient of variability between replications for cornstarch is 27% (see Table 5.3).

2. Effect of composition

a. Moisture content

The relationships between $(dP/dt)_{ave}$ and the moisture content are shown in Figs. 5.62, 5.63, 5.64, and 5.65 for cornstarch, grain sorghum dust, corn dust, and wheat dust, respectively. For cornstarch, there definitely exists a relationship between $(dP/dt)_{ave}$ and the moisture content. This relationship, for all concentrations, is also very similar to that for $(dP/dt)_{max}$. As the moisture content decreases, $(dP/dt)_{ave}$ increases. The correlation appears to be reasonably linear with some variability. By extrapolation of the regression line (see Table 5.4), the moisture contents above which no explosion is possible are 14.6, 17.3, 22.2, and 14.6% for concentrations of 0.2, 0.5, 1.0, and 2.0 kg/m^3, respectively. It appears that the effect of moisture content is more pronounced at the lower concentrations. For moisture contents below

approximately 11%, the two lower concentrations become more hazardous than the two higher ones.

For grain sorghum dust, it is difficult to observe a correlation between the moisture content and $(dP/dt)_{ave}$ (see Fig. 5.63). At moisture contents above 11.5%, it appears that $(dP/dt)_{ave}$ is consistently low (less than 20 bar/s) whereas at moisture contents below 11.5% there is considerable variability, i.e., at a moisture content of 10% $(dP/dt)_{ave}$ ranges from 40 to 128 bar/s. This could indicate that the moisture content at high levels (approximately 13 to 15%) becomes a controlling variable. This observation is consistent with what Eckhoff (1976) found and with what was found in this investigation for cornstarch. There appears to be little difference between concentration levels.

In Fig. 5.64, the correlations for corn dust are similar to those for grain sorghum dust. The three data points that are circled come from size fractions with high ash content.

For wheat dust, the correlation in Fig. 5.65 appears to be opposite to those observed for the other types of dust. For wheat dust, this correlation can be explained by the highly significant inverse correlation between ash content and moisture content. Note that the nine circled data points are those from size fractions that contain ash contents greater than approximately 15%. When these data are excluded, a correlation between moisture content and $(dP/dt)_{ave}$ becomes difficult to observe. The highest moisture contents of approximately 11% are below the moisture contents for which a moisture effect is observed for corn dust or grain sorghum dust. Again, there seems to be little difference between the values of $(dP/dt)_{ave}$ and the concentrations except for the lowest concentration; the lowest concentration is close to the minimum explosible concentration.

b. Ash content

The correlations between the ash content and the average rate of pressure rise are presented in Figs. 5.66, 5.67, and 5.68 for wheat dust, corn dust, and grain sorghum dust, respectively. Again, the relationship for all three types of dust is very similar to those for $(dP/dt)_{max}$. As the ash content decreases, $(dP/dt)_{ave}$ decreases for all types of dust. At a concentration of 0.5 kg/m^3, the ash content for wheat dust appears to be the dominate variable for values above approximately 8%. At concentrations of 0.5 and 1.0 kg/m^3, the ash content for wheat dust appears to become a dominant variable for values above approximately 8 and 15%, respectively. At a concentration of 2.0 kg/m^3, the ash content appears to be a dominant variable for values greater than 15%. For each type of dust, the data with the ash contents greater than approximately 8% have been linearly extrapolated for the purpose of estimating the ash contents corresponding to the condition of $(dP/dt)_{AUC} = 0$ (see Table 5.3). The table also indicates that it takes a higher ash content to cause $(dP/dt)_{ave}$ to become zero at a higher dust concentration than at a lower concentration. In Fig. 5.67, similar correlations are observed for corn dust. The correlation between ash content and $(dP/dt)_{ave}$ is difficult to observe for ash contents below approximately 6% to 10%, depending on the dust concentration. The ash content has a more pronounced effect on $(dP/dt)_{ave}$ for corn dust than for wheat dust. In Fig. 5.68, similar correlations are also observed for grain sorghum dust. It is difficult to identify a correlation for ash contents less than approximately 10%. The ash contents necessary to cause $(dP/dt)_{ave}$ to become zero are between those for corn dust and wheat dust (Table 5.3).

c. Protein content

The correlations between the protein content and $(dP/dt)_{ave}$, for wheat dust, corn dust, and grain sorghum dust are shown in Figs. 5.69, 5.70, and 5.71, respectively. For wheat dust there appears to be an inverse correlation between protein content and $(dP/dt)_{ave}$. This correlation is due again to the significant inverse correlation between protein and ash contents. The data with the highest protein content come from size fractions that also contain the highest ash content. When these data are eliminated, a correlation is difficult to detect at the two highest concentrations; however, a slight correlation may be observed for the concentration of 0.5 kg/m^3. Again no correlation is indicated by the data for corn dust at the two highest concentrations, whereas at the two lowest concentrations there may be a slight inverse correlation. The protein content does not appear to have a major effect. A correlation between $(dP/dt)_{ave}$ and the protein content in grain sorghum is difficult to detect at any level of concentration.

d. Starch & fiber content

The correlations between the starch & fiber content and $(dP/dt)_{ave}$ are given in Figs. 5.72, 5.73, 5.74, and 5.75 for cornstarch, wheat dust, corn dust, and grain sorghum dust, respectively. One can observe a definite correlation between $(dP/dt)_{ave}$ and starch & fiber content for cornstarch in Fig. 5.72. This correlation is the negative of the correlation between $(dP/dt)_{ave}$ and moisture content for cornstarch (Fig. 5.62). The contents of ash and protein are negligibly small in cornstarch. Thus, the cornstarch is assumed to consist only of moisture and starch & fiber. In Fig. 5.73, there also appears to be a direct correlation between $(dP/dt)_{ave}$ and the starch & fiber content for wheat dust. Note that a significant correlation exists

between the ash content and the starch & fiber content for wheat dust. The three data that are circled come from the three size fractions that contain ash contents significantly larger than the remaining size fractions. Without these data, a correlation between the starch & fiber content and $(dP/dt)_{ave}$ is difficult to observe. The data from the size fractions with ash contents are also identified with circles in Fig. 5.74 for corn dust and in Fig. 5.75 for grain sorghum dust. When these are excluded, a correlation between $(dP/dt)_{ave}$ and the starch & fiber content is difficult to detect for either corn or wheat dust.

The significant correlations between the starch & fiber content and the ash content, and the starch & fiber and moisture contents make it difficult to determine if the decrease in the value of $(dP/dt)_{ave}$ is due to an increase in ash or moisture content or a decrease in starch & fiber content. To prove the hypothesis that the decrease in starch & fiber content causes the decrease in $(dP/dt)_{ave}$, one must explain why a decrease in the starch & fiber content due to an increase in the moisture content is more effective in preventing explosion than that due to an increase in the ash content. Also note that for both ash content and moisture content, the effect on $(dP/dt)_{ave}$ appears to become dominant as the content increases; as the ash or moisture content decreases, the effect of other variables causes the variability in $(dP/dt)_{ave}$ to increase. This observation is not true for the starch & fiber content. It is possible ash is not uniformly distributed in all the grain dust particles in a sample. The starch & fiber content varies between 70 and 85% for those size fractions that do not contain the highest quantities of ash material. A correlation between $(dP/dt)_{ave}$ and the ash content or $(dP/dt)_{ave}$ and the moisture content appears to be more plausible than that between $(dP/dt)_{ave}$ and the starch & fiber content.

D. Comparison of Explosion Characteristics Between Hartmann Apparatus and 0.19 m^3 Spherical Apparatus

To evaluate the performance of the Hartmann apparatus constructed specifically for the present work, the data obtained with it were compared with those obtained from experiments conducted by Fenwal, Inc. (Ashland, MA) with a 0.19 m^3 spherical apparatus. A series of explosion tests yielding maximum explosion pressures, maximum rates of pressure rise, and average rates of pressure rise were performed on samples of an identical powder, Autolyzed Yeast Extract. Both the precision and accuracy of the two types of apparatus were compared.

The results from the explosion tests are tabulated in Table 5.8. The test number indicates the sequence in which the tests were performed. The explosion tests were performed at 6 different levels of concentration, and the number of replications at each concentration ranged from one to four.

1. Maximum explosion pressure

For the maximum explosion pressure, the pooled standard deviation between trails was 0.435 bars for the Hartmann apparatus and 0.554 bars for the 0.19 m^3 spherical apparatus. A two-tailed F-test was performed to examine the equality of the variances from the two types of apparatus. The F value of 1.62 was not significant even for $\alpha = 0.50$; the larger variance contained 8 degrees of freedom and the smaller variance contained 6 degrees of freedom. Figure 5.76 presents the coefficients of variability between trials plotted against the concentration for each apparatus. The coefficients of variability for the 0.19 m^3 apparatus are larger than those for the Hartmann apparatus, except for the concentrations of 0.5 and 1.1 kg/m^3.

The average maximum explosion pressures from both types of apparatus and the coefficient of variability between them are plotted against the

concentration in Fig. 5.77. The values of the coefficient of variability are less than 10% except for 0.3 kg/m^3 where it is 17%. To statistically determine if there exists a significant difference between the maximum pressures obtained from the two types of apparatus, an analysis of variance for a 2 x 2 factorial experiment with two replications per treatment combination was performed. The treatments were the type of apparatus (the Hartmann and the 0.19 m^3 apparatus) and the level of concentration. If a level of concentration contained more than two replications (see Table 5.8), then two replications were selected at random. The results of the analysis are given in Table 5.9. The table indicates that no significant difference exists between the two types of apparatus at the 1% level of significance; the interactions are also insignificant. However, the effect of the concentration is significant at the 1% level.

To compare the values of $(dP/dt)_{max}$ from the two apparatus, the previously mentioned cubic law, which is

$$K_{st} = \left(\frac{dP}{dt}\right)_{max} \cdot V^3 , \qquad (1)$$

can be utilized. Figure 5.78 presents the coefficient of variability between replication of K_{st} for each apparatus, plotted against the concentration. The coefficients of variability for the 0.19 m^3 apparatus are consistently higher than those for the Hartmann apparatus, except for the concentration at 1.1 kg/m^3. The two highest coefficients of variability for the Hartmann apparatus are 23% and 27%; for the 0.19 m^3 apparatus, three of the coefficients are greater than or equal to 40%.

The values of K_{st} for the Hartmann apparatus are plotted against those for the 0.19 m^3 spherical apparatus in Fig. 5.79. If the two types of

apparatus yielded the same K_{st} values for a given concentration, then all points would lie around the line of "consistency of measured values" with a slope of 1; however, the regression line for the experimental data has a slope of 0.356 with a r^2 of 0.909. This slope is significantly different from 1 at the 95% confidence level. The 95% confidence interval ranges from -0.026 to 0.756, which does not contain 1. Bartknecht (1978) experimentally demonstrated that the Hartmann apparatus consistently yields values of K_{st} that are lower than those from apparatus with explosion chambers having a volume of 0.02 m^2 or larger. The slope of the regression line obtained by him was 0.35 instead of 1. This value falls within the 95% confidence interval.

2. Average rate of pressure rise

To compare the average rates of pressure rise, a quantity similar to K_{st} is defined with the following equation:

$$K_{st,ave} = \left(\frac{dP}{dt}\right)_{ave} \cdot V^{1/3}$$

where

$\left(\frac{dP}{dt}\right)_{ave}$ = average rate of pressure rise

Figure 5.84 presents the coefficients of variability between trials of $K_{st,ave}$ for each apparatus plotted against the concentration. Again, the coefficients of variability for the Hartmann apparatus are consistently lower than those for the 0.19 m^3 apparatus.

Figure 5.81 presents the values of $K_{st,ave}$ plotted in the same format as those of the K_{st} in Fig. 5.79. The regression line through the experimental data has a slope of 0.458 with an r^2 of 0.963. The 95% confidence interval

for this value of the slope ranges from 0.103 to 0.813, which contains 0.35 (the value of the slope reported by Bartknecht (1978)).

V. CONCLUSIONS

The smallest size fraction of grain sorghum dust yielded the largest maximum explosion pressure, P_{max}, of 7.8 bar at a concentration of 1.0 kg/m^3. At the highest dust concentration of 2.0 kg/m^3, the highest value of P_{max} ranged from approximately 6.0 to 6.5 bar for corn dust, wheat dust, and cornstarch.

For grain sorghum dust and corn dust, P_{max} remained essentially constant at 6.0 bar as the mass mean diameter decreased from approximately 50 m to 15 m for the concentrations of 1.0 and 2.0 kg/m^3. At a concentration of 0.5 kg/m^3, P_{max} increased with decreasing diameter until values of approximately 6.0 bar for grain sorghum dust and 4.7 for corn dust were attained at a diameter of 15 μm. Below a diameter of approximately 15 μm, P_{max} remained essentially constant or decreased for these three concentrations except in the case of grain sorghum dust at a concentration of 1.0 kg/m^3. For a concentration of 0.2 kg/m^3, P_{max} increased for all diameters; it never attained a value of 6.0 bar.

A model has been developed, which correlates P_{max} with the specific external surface area, S_{ext}. The data for grain sorghum dust were fitted to the model. The resultant correlation shows sufficient linearity up to a certain S_{ext}, depending on the concentration; above this point, P_{max} rapidly approaches a constant value. The coefficients of determination, R^2, for grain sorghum dust are, 0.95, 0.78, and 0.88 for the concentrations of 0.5, 1.0, and 2.0 kg/m^3, respectively.

The maximum explosion pressure is also linearly correlated with the ash content for values above approximately 10% for grain sorghum dust, wheat dust, and corn dust. The maximum explosion pressure is quadratically correlated with the moisture content for cornstarch. Moisture contents ranging from approximately 16% to greater than 20% cause P_{max} to become zero. For both grain sorghum dust and corn dust, the correlations between P_{max} and the moisture content indicate that moisture content becomes the dominating variable that suppresses P_{max} for values above approximately 11%.

For all size fractions of grain sorghum dust and corn dust, the maximum rate of pressure rise, $(dP/dt)_{max}$, attained values as high as approximately 380 bar/s. The values for wheat dust were approximately 1/2 of those for grain sorghum dust. For low moisture contents of approximately 4%, $(dP/dt)_{ave}$ for cornstarch attained values as high as 680 bar/s.

For the concentrations of 0.5, 1.0, and 2.0 kg/m^3 for grain sorghum dust and corn dust, $(dP/dt)_{max}$ increased as the mass mean diameter decreased to approximately 15 μm. Below 15 μm, $(dP/dt)_{max}$ decreased sharply for these three concentrations. At a concentration of 0.2 kg/m^3, $(dP/dt)_{max}$ increased for the entire range of D_m.

For diameters below approximately 20 μm, the highest values of $(dP/dt)_{max}$ were obtained at the concentration of 0.5 kg/m^3. For D_m below approximately 15 μm, the highest values of $(dP/dt)_{max}$ were obtained at a concentration of 0.2 kg/m^3.

A model has been developed to correlate $(dP/dt)_{max}$ with the specific external surface area, S_{ext}. As in the case of P_{max}, the data for grain sorghum dust and corn dust were fitted to the model; the resultant correlation exhibits linearity up to certain values of S_{ext}. For grain sorghum dust, the coefficients of determination obtained are 0.92, 0.92, 0.90 and 0.80 for

concentrations of 0.2, 0.5, 1.0, and 2.0 kg/m^3, respectively. At the lowest concentration, the correlation is linear for the entire range of S_{ext}.

For all types of dust, the correlation between $(dP/dt)_{max}$ and the ash content is similar to that between P_{max} and the ash content. These correlations indicate that ash contents above approximately 50% are necessary to cause $(dP/dt)_{max}$ to become zero. The higher the dust concentration, the higher the ash content necessary to cause $(dP/dt)_{max}$ to become zero. The correlations between $(dP/dt)_{max}$ and the moisture content are also similar to those between P_{max} and the moisture content. For cornstarch, however, the correlations appear to be linear. The coefficients of determination are 0.94, 0.64, 0.56, and 0.78, for dust concentrations of 0.2, 0.5, 1.0, and 2.0 kg/m^3, respectively. From the extrapolation of these regression equations, the moisture contents that cause $(dP/dt)_{max}$ to approach zero are 14.6, 16.3, 17.9, and 18.6%, for concentrations of 0.2, 0.5, 1.0, and 2.0 kg/m^3, respectively.

The values of $(dP/dt)_{ave}$ for all types of dust were 1/2 to 1/3 of the values of $(dP/dt)_{max}$. A model which correlates $(dP/dt)_{ave}$ to S_{ext} has also been developed. As in the case of $(dP/dt)_{max}$, the correlations are linear up to specific values of S_{ext} with coefficients of determination of 0.95, 0.88, 0.94, and 0.87 for concentrations of 0.2, 0.5, 1.0, and 2.0 kg/m^3. Similar observations were made from the correlations between $(dP/dt)_{ave}$ and particle size (D_m or S_{ext}) and between $(dP/dt)_{ave}$ and each composition component as were made from identical correlations for $(dP/dt)_{max}$.

REFERENCES

Bartknecht, W. 1978. Gas, vapor and dust explosions. Preprints of International Symposium on Grain Elevator Explosions. National Academy of Sciences, Washington, D.C.

Dorsett, H.G., Jr., Jacobson, M., Nagy, J., and Williams, R.P. 1960. Laboratory equipment and test procedures for evaluating explosibility of dusts. U.S. Department of the Interior, Bureau of Mines, Report of Investigations, RI-5624.

Eckhoff, R.K. 1976. A study of selected problems related to the assessment of ignitability and explosibility of dust clouds. A.S. John Greigs Boktrykkeri. Bergen, Norway.

Essenhigh, R.H., Froberg, R., and Howard, J.B. 1965. Combustion behavior of small particles. Industrial and Engineering Chemistry 57(9):32-43.

Hertzberg, M., Cashdollar, K., and Obferman, J. 1979. The flammability of coal dust-air mixtures. U.S. Department of the Interior, Bureau of Mines, Report of Investigations, RI-8360.

Table 5.1 The Results of the Maximum Explosion Pressure, the Maximum Rate of Pressure Rise, and the Average Rate of Pressure Rise from the Hartmann Pressure Tests

Sample Identification	Test No.	Concentration kg/m^3	Maximum Pressure bar	Maximum Rate of Pressure Rise bar/s	Average Rate of Pressure Rise bar/s
CNAC-S02	1	0.2	3.5	128	52
	2	0.1	1.7	81	33
	3	2.0	5.9	53	25
CNAC-S03	4	0.2	3.4	116	42
	5	0.5	4.7	164	49
	6	1.0	5.8	155	47
	7	2.0	5.8	37	21
CNAC-S04	8	0.2	2.3	33	13
	9	0.5	4.2	94	29
	10	2.0	5.7	72	32
CNAC-S07	11	0.2	1.7	17	11
	12	1.0	5.7	76	38
	13	2.0	5.2	31	17
CNAC-S08	14	0.5	4.6	97	30
CNAC-S10	15	0.2	2.3	40	17
CNAC-S09	16	0.2	2.6	52	19
	17	1.0	5.0	50	24
CNAC-S01	18	0.2	4.4	381	127
	19	1.0	6.1	121	45
	20	0.1	0.7	22	11
	21	2.0	5.9	86	60
CNAC-S11	22	0.5	5.2	68	24
	23	2.0	6.1	44	26
	24	1.0	5.7	68	24
CNAC-S06	25	0.5	0.5	4	2
	26	1.0	0.8	6	3
CNAC-S05	27	0.5	3.9	65	27
	28	1.0	5.8	71	40
CNAC-S06	29	2.0	4.4	31	14

Table 5.1 (continued)

Sample Identification	Test No.	Concentration kg/m^3	Maximum Pressure bar	Maximum Rate of Pressure Rise bar/s	Average Rate of Pressure Rise bar/s
MOAC-S03	30	0.5	5.5	202	82
	31	1.0	6.0	137	45
	32	0.2	0.7	13	6
	33	2.0	6.1	59	31
	34	0.1	1.3	27	14
MOAC-S02	35	0.5	6.6	383	126
	36	1.0	6.3	206	75
	37	0.2	4.0	172	88
	38	2.0	6.9	98	56
MOAC-S08	39	0.5	3.3	22	11
	40	2.0	5.9	39	20
	41	1.0	5.0	33	17
MOAC-S04	42	0.5	5.1	136	44
	43	0.2	3.6	110	54
	44	1.0	6.5	122	56
	45	2.0	5.8	58	27
	46	0.1	0.3	6	5
MOAC-S07	47	0.5	4.2	55	22
	48	1.0	6.3	79	39
	49	0.2	0.5	2	1
	50	2.0	6.2	64	28
MOAC-S01	51	0.1	0.2	7	8
	52	0.5	5.0	308	91
	53	1.0	7.6	180	63
	54	0.2	5.0	361	158
	55	0.2	4.6	402	94
MOAC-S06	56	0.5	2.0	12	7
	57	1.0	4.2	48	21
MOAC-S09	58	0.5	2.1	14	7
	59	1.0	4.9	42	17

Table 5.1 (continued)

Sample Identification	Test No.	Concentration kg/m^3	Maximum Pressure bar	Maximum Rate of Pressure Rise bar/s	Average Rate of Pressure Rise bar/s
	60	2.0	5.3	28	15
MOAC-S11	61	0.5	0.2	2	1
	62	2.0	1.3	8	4
MOAC-S10	63	0.5	2.7	18	7
	64	1.0	3.8	25	11
WTAC-S03	65	0.5	4.3	65	21
	66	1.0	5.6	76	25
	67	2.0	5.3	36	15
WTAC-S10	68	0.5	2.9	36	11
WTAC-S04	69	0.5	3.8	57	20
	70	1.0	4.0	43	17
	71	0.2	0.3	3	2
WTAC-S09	72	0.5	4.6	50	24
	73	0.2	1.8	11	6
	74	2.0	6.0	46	23
WTAC-S05	75	0.5	3.2	37	13
	76	1.0	4.7	54	23
	77	0.2	0.8	8	4
	78	2.0	5.2	48	17
WTAC-S08	79	1.0	4.3	35	12
	80	0.2	0.8	6	2
WTAC-S06	81	0.5	0.4	3	2
	82	1.0	4.1	31	13
	83	2.0	5.1	37	18
WTAC-S07	84	0.5	3.4	23	15
	85	1.0	5.9	61	28
	86	2.0	6.0	55	22
WTAC-S03	87	0.5	4.7	113	37
	88	1.0	6.0	129	49
	89	2.0	6.2	67	26

Table 5.1 (continued)

Sample Identification	Test No.	Concentration kg/m^3	Maximum Pressure bar	Maximum Rate of Pressure Rise bar/s	Average Rate of Pressure Rise bar/s
WTAC-S04	90	2.0	5.0	52	24
	91	0.5	3.8	64	18
	92	1.0	4.5	63	25
	93	0.2	0.4	3	2
	94	2.0	5.4	84	42
WTAC-S05	95	0.5	2.5	36	17
	96	1.0	4.4	84	43
	97	0.2	0.0	0	0
	98	2.0	4.4	44	18
WTAC-S06	99	0.5	1.7	13	6
	100	1.0	2.9	27	14
	101	2.0	4.5	41	17
WTAC-S07	102	0.2	0.3	3	2
	103	0.5	3.7	37	16
	104	1.0	4.6	44	21
	105	0.2	0.2	1	1
	106	2.0	5.7	52	24
WTAC-S08	107	0.5	4.8	56	29
	108	0.2	0.8	5	3
	109	2.0	5.3	54	26
	110	1.0	4.7	44	22
	111	0.5	4.7	66	31
	112	2.0	4.8	38	17
WTAC-S09	113	0.5	3.8	43	20
	114	1.0	5.3	59	29
	115	0.2	0.5	4	2
	116	2.0	5.1	45	23
	117	1.0	4.7	64	25
WTAC-S10	118	1.0	4.6	36	20
	119	2.0	5.2	41	25

Table 5.1 (continued)

Sample Identification	Test No.	Concentration kg/m^3	Maximum Pressure bar	Maximum Rate of Pressure Rise bar/s	Average Rate of Pressure Rise bar/s
	120	1.0	4.6	56	23
	121	2.0	4.8	39	19
CNAC-S02	122	2.0	4.7	40	23
CNAC-S01	123	0.5	3.9	133	67
	124	0.2	3.5	365	143
	125	2.0	5.8	50	29
	126	0.5	4.2	167	68
	127	1.0	5.0	188	44
	128	0.1	0.9	49	20
CNAC-S02	129	1.0	5.3	214	70
CNAC-S03	130	1.0	5.7	201	81
	131	0.2	3.1	253	108
CNAC-S04	132	0.5	3.9	94	51
	133	1.0	5.5	158	54
	134	2.0	5.9	104	52
CNAC-S07	135	0.5	4.8	147	58
	136	1.0	4.6	103	33
	137	0.2	1.6	31	17
CNAC-S08	138	1.0	6.4	144	73
	139	2.0	5.1	50	27
	140	0.2	2.3	68	30
CNAC-S02	141	0.5	4.2	280	81
CNAC-S09	142	0.5	3.6	87	33
	143	1.0	4.9	128	45
	144	0.2	3.1	79	38
	145	2.0	4.9	55	27
CNAC-S10	146	0.5	3.9	60	33
	147	1.0	5.5	103	51
	148	2.0	5.2	71	34
CNAC-S11	149	0.5	2.8	22	12

Table 5.1 (continued)

Sample Identification	Test No.	Concentration kg/m^3	Maximum Pressure bar	Maximum Rate of Pressure Rise bar/s	Average Rate of Pressure Rise bar/s
	150	2.0	5.1	37	20
CNAC-S02	151	1.0	5.4	189	56
	152	0.2	3.2	187	80
CNAC-S03	153	0.5	4.5	216	98
	154	2.0	4.9	60	29
CNAC-S04	155	0.2	3.6	452	184
	156	1.0	5.4	214	55
CNAC-S07	157	0.5	4.4	178	53
	158	2.0	4.8	51	26
CNAC-S08	159	0.5	3.6	83	41
	160	1.0	5.3	121	43
	161	2.0	4.6	48	21
	162	0.2	2.2	49	27
CNAC-S09	163	2.0	5.0	74	31
	164	0.5	3.8	264	88
CNAC-S10	165	0.5	3.5	59	29
	166	1.0	4.7	55	28
	167	2.0	5.1	77	38
CNAC-S11	168	1.0	5.2	86	33
CNAC-S02	169	0.5	5.0	379	128
CSAC-S02	170	0.1	0.2	8	4
	171	0.1	0.5	19	12
CSAC-S04	172	0.2	2.0	141	71
	173	1.0	4.7	180	86
	174	2.0	5.0	93	42
	175	1.0	6.5	269	117
	176	2.0	6.1	193	84
CSAC-S01	177	0.5	4.5	614	237
	178	0.2	3.4	400	180
	179	2.0	6.0	213	84

Table 5.1 (continued)

Sample Identification	Test No.	Concentration kg/m^3	Maximum Pressure bar	Maximum Rate of Pressure Rise bar/s	Average Rate of Pressure Rise bar/s
	180	0.1	1.5	114	49
	181	1.0	5.3	314	130
CSAC-S07	182	0.5	4.5	130	71
	183	1.0	5.0	122	51
	184	2.0	5.4	71	48
CSAC-S05	185	2.0	5.9	126	67
	186	0.5	4.0	203	61
	187	1.0	5.0	206	81
	188	0.1	1.3	51	26
	189	0.2	2.5	128	69
CSAC-S06	190	0.5	3.9	319	140
	191	0.2	2.5	204	89
	192	1.0	5.4	160	85
	193	2.0	5.8	116	67
	194	0.1	1.7	76	37
CSAC-S03	195	0.5	3.7	261	117
	196	1.0	5.1	360	84
	197	0.2	2.9	239	123
	198	2.0	5.2	113	40
CSAC-S02	199	0.5	4.1	468	187
	200	1.0	5.5	555	179
	201	0.2	2.8	354	150
	202	2.0	6.0	210	97
CSAC-S01	203	0.1	0.4	32	16
	204	1.0	5.3	473	101
	205	2.0	5.7	234	78
	206	0.2	2.7	333	180
	207	0.5	4.0	727	248
CSAC-S02	208	2.0	6.1	167	105
	209	1.0	5.0	417	102

Table 5.1 (continued)

Sample Identification	Test No.	Concentration kg/m^3	Maximum Pressure bar	Maximum Rate of Pressure Rise bar/s	Average Rate of Pressure Rise bar/s
	210	0.5	3.9	201	140
	211	0.2	3.1	370	194
CSAC-S03	212	0.2	1.8	117	70
	213	0.5	3.4	291	148
	214	1.0	4.5	402	128
	215	2.0	4.7	102	50
CSAC-S06	216	0.5	3.4	180	103
	217	0.2	2.4	194	63
	218	1.0	4.9	206	66
	219	0.1	1.8	129	63
	220	2.0	5.2	141	50
CSAC-S07	221	0.5	4.3	149	76
	222	1.0	5.0	115	63
	223	2.0	5.1	62	39
CSAC-S05	224	0.5	3.9	279	121
	225	0.2	2.4	168	91
	226	1.0	4.5	165	42
	227	0.1	1.5	87	47
	228	2.0	5.4	113	60
CSAC-S04	229	0.5	3.9	230	104
	230	0.5	3.5	183	80
	231	0.2	1.7	102	60
CSAC-F04	232	1.0	3.7	119	55
	233	0.2	0.8	14	8
	234	2.0	4.2	57	26
	235	0.5	2.6	52	29
	236	0.2	0.0	0	0
	237	0.5	2.3	57	34
CSAC-F05	238	0.5	3.5	172	85
	239	1.0	4.0	179	69

Table 5.1 (continued)

Sample Identification	Test No.	Concentration kg/m^3	Maximum Pressure bar	Maximum Rate of Pressure Rise bar/s	Average Rate of Pressure Rise bar/s
	240	0.1	1.2	48	28
	241	0.2	2.0	124	50
	242	2.0	5.1	88	45
CSAC-F06	243	0.5	3.6	128	65
	244	0.2	0.0	0	0
	245	1.0	4.6	162	57
	246	2.0	4.6	79	41
CSAC-F07	247	0.5	3.5	230	121
	248	1.0	5.2	258	102
	249	2.0	5.0	101	43
CSAC-F04	250	1.0	3.6	61	36
CSAC-F07	251	0.2	2.2	61	51
	252	0.1	0.0	0	0
CSAC-F04	253	2.0	4.1	45	22
CSAC-F05	254	0.5	4.0	257	100
	255	1.0	4.4	170	67
	256	0.2	0.8	20	9
	257	0.1	0.0	0	0
	258	2.0	4.6	80	37
CSAC-F06	259	0.5	3.5	158	69
	260	2.0	4.7	100	34
	261	0.2	2.2	64	27
	262	1.0	3.8	110	65
CSAC-F07	263	0.1	1.7	76	41
	264	0.2	2.7	196	98
	265	0.5	4.0	317	116
	266	1.0	4.8	267	69
MOAC-S03	267	0.5	5.2	198	90
	268	1.0	5.8	86	40
	269	0.2	4.0	210	99

Table 5.1 (continued)

Sample Identification	Test No.	Concentration kg/m^3	Maximum Pressure bar	Maximum Rate of Pressure Rise bar/s	Average Rate of Pressure Rise bar/s
	270	2.0	5.6	53	25
MOAC-S02	271	0.5	5.2	224	94
	272	1.0	5.7	221	83
	273	0.2	4.3	224	93
	274	0.1	1.3	27	13
	275	2.0	5.6	67	55
MOAC-S08	276	0.5	2.8	17	9
	277	1.0	5.2	49	19
	278	2.0	5.5	28	17
	279	0.2	1.2	7	4
MOAC-S04	280	0.5	5.0	138	50
	281	1.0	5.4	50	26
	282	2.0	6.0	77	40
	283	0.2	1.8	174	16
MOAC-S07	284	0.5	3.7	27	15
	285	1.0	5.0	33	20
	286	2.0	6.2	54	30
MOAC-S11	287	0.5	0.8	3	3
	288	1.0	2.4	14	7
	289	2.0	1.8	9	6

Table 5.2 The Coefficients of Variability between Replications

Type of Dust	Concentration kg/m^3	Degrees of Freedom	Coefficient of Variability		
			P_{max} bar	$(dP/dt)_{max}$ bar/s	$(dP/dt)_{ave}$ bar/s
Grain Sorghum	2.0	6	8	22	15
	1.0	5	10	32	27
	0.5	6	12	40	22
	0.2	4	38	37	55
	0.1	--	--	--	--
	All	21	16	40	27
Corn	2.0	9	9	26	32
	1.0	9	9	26	29
	0.5	9	16	36	40
	0.2	7	15	76	78
	0.1	1	25	54	41
	All	35	12	53	56
Wheat	2.0	8	9	22	15
	1.0	8	10	32	27
	0.5	7	12	40	22
	0.2	5	38	37	55
	0.1	--	--	--	--
	All	28	12	32	33
Cornstarch	2.0	10	7	22	20
	1.0	11	10	22	29
	0.5	11	7	30	18
	0.2	10	33	33	29
	0.1	6	69	75	76
	All	48	14	30	27

Table 5.3 The Minimum Ash Contents for a Dust Sample Completely Inert to Explosion

Explosion Characteristic	Concentration kg/m^3	Ash Content, %		
		Wheat Dust	Grain Sorghum Dust	Corn Dust
Maximum Explosion Pressure	0.5	56	58	52
	1.0	> 100	> 100	54
	2.0	> 100	--	> 100
Maximum Rate of Pressure Rise	0.5	49	42	48
	1.0	79	74	45
	2.0	86	--	68
Average Rate of Pressure Rise	0.5	54	44	30
	1.0	92	67	48
	2.0	83	--	65

Table 5.4 Results of the Regression of Moisture Content on the Explosion Characteristic $(dP/dt)_{max}$ and $(dP/dt)_{ave}$ for Cornstarch

Explosion Characteristic	Concentration kg/m^3	Coefficient of Determination R^2	Degrees of Freedom d.f.	Slope (bar/s)/%	Intercept bar/s	Moisture Content for Complete Inerting %
$(dP/dt)_{max}$	2.0	0.78	8	-13.5660	251.58	18.6
	1.0	0.56	8	-28.9300	517.61	17.9
	0.5	0.64	8	-38.3600	624.70	16.3
	0.2	0.94	7	-34.2030	499.30	14.6
$(dP/dt)_{ave}$	2.0	0.84	8	- 5.9870	113.79	19.0
	1.0	0.56	8	- 6.6672	148.03	22.2
	0.5	0.74	8	-14.6040	252.24	17.3
	0.2	0.90	7	-16.3132	238.98	14.6

Table 5.5 The Results of the Regression Analysis for the Linear Portion of the Relationship between P_{max} and the Specific External Surface Area

Type of Dust	Concentration kg/m^3	Number of Data	Coefficient of Determination R^2	Slope $(bar/s)/(m^2/g)$	Intercept bar/s	The Particle Size Above Which No Explosion Occurs		Range of Specific Surface Areas	
						Specific Surface Area m^2/g	Diameter D_m µm	Lower	Upper
								m^2/g	
Grain Sorghum	2.0	4	0.88	78.01	-3.9690	0.051	76	0.076	0.130
	1.0	6	0.78	49.12	-0.9271	0.019	205	0.076	0.130
	0.5	6	0.95	48.30	-2.6360	0.055	71	0.076	0.168

Table 5.6 The Results of the Regression Analysis for the Linear Portion of the Relationship between $(dP/dt)_{max}$ and the Specific External Surface Area

Type of Dust	Concentration kg/m^3	Number of Data	Coefficient of Letermination R^2	Slope $(bar/s)/(m^2/g)$	Intercept bar/s	The Particle Size Above Which No Explosion Occurs		Range of Specific Surface Areas	
						Specific Surface Area m^2/g	Diameter μm	Lower	Upper
								m^2/g	
Grain Sorghum	2.0	5	0.80	641.00	-38.72	0.0640	64	0.760	0.168
	1.0	8	0.89	760.40	-42.95	0.0565	69	0.760	0.345
	0.5	9	0.92	1282.70	-109.22	0.0852	46	0.760	0.345
	0.2	6	0.92	926.92	-80.20	0.0865	45	0.760	0.486
Corn	1.0	9	0.70	848.10	-59.50	0.0701	55	0.106	0.277
	0.5	10	0.83	1181.00	-120.90	0.1024	38	0.106	0.351
	0.2	8	0.70	1072.00	-138.40	0.1291	30	0.160	0.450

Table 5.7 Comparison of the Experimental Data to that Predicted by Eckhoff's Model

Concentration kg/m^3	Coefficient of Determination R^2	Slope	Intercept	Total Number of Data n
2.0	0.720**	0.935	14.90	34
1.0	0.630**	1.961	7.65	38
0.5	0.670**	2.570	-18.60	38
0.2	0.710**	2.300	-36.00	28
0.1	0.001	-0.002	44.50	11

* Significant at the 5% level.

** Significant at the 1% level.

Table 5.8 The Results of the Regression Analysis of the Linear Portion of the Relationship between $(dP/dt)_{ave}$ and the Specific External Surface Area

Type of Dust	Concentration kg/m^3	Number of Data	Coefficient of Determination R^2	Slope $(bar/s)/(m^2/g)$	Intercept bar/s	The Particle Size Above Which No Explosion Occurs		Range of Specific Surface Areas	
						Specific Surface Area m^2/g	Diameter	Lower m^2/g	Upper m^2/g
Grain Sorghum	2.0	7	0.87	173.8	-2.176	0.0125	310	0.076	0.34
	1.0	9	0.94	271.1	-10.990	0.0405	96	0.076	0.34
	0.5	9	0.88	468.6	-37.520	0.0800	49	0.076	0.34
	0.2	6	0.95	329.5	-26.860	0.0810	48	0.110	0.49
Corn	1.0	9	0.72	279.7	-13.196	0.0800	83	0.106	0.35
	0.5	10	0.87	378.4	-32.800	0.0870	45	0.106	0.35
	0.2	8	0.67	379.0	-41.700	0.1100	35	0.160	0.45

Table 5.9 Comparison of the Data from Explosion Tests of Autolyzed Yeast Extract Performed in a 0.19 m^3 Spherical Explosion Apparatus and a 1.25 x 10^{-3} m^3 Cylindrical Hartmann Explosion Apparatus

Apparatus	Test No.	Conc. kg/m^3	Maximum Explosion Pressure bar	Maximum Rate of Pressure Rise bar/s	Average Rate of Pressure Rise bar/s
Spherical	1	0.3	4.0	11	5
Explosion	2	0.5	6.1	44	22
Chamber	3	0.7	7.4	59	25
with 0.19 m^3	4	0.9	7.8	96	37
(Fenwal)	5	1.1	7.7	50	23
	6	0.9	7.1	52	17
	7	1.1	7.0	46	19
	8	0.7	7.8	132	43
	9	0.9	7.4	50	19
	10	0.6	7.5	125	42
	11	0.5	5.4	28	14
	12	0.6	6.1	24	12
	13	0.7	7.0	52	19
	14	0.7	8.1	66	27
Cylindrical	1	0.5	6.0	136	60
Hartmann	2	0.3	5.2	103	39
Apparatus with	3	0.7	7.4	143	66
1.25 x 10^{-3} m^3	4	0.6	6.1	138	73
(USGMRL)	5	1.1	7.3	108	55
	6	0.9	7.0	112	58
	7	0.3	5.0	74	31
	8	0.7	7.5	148	76
	9	0.6	6.0	141	58
	10	0.5	5.0	100	47
	11	0.9	7.0	96	49
	12	1.1	6.2	85	37

Table 5.10 Analysis of Variance of the Maximum Explosion Pressure Data

Source of Variation	Degrees of Freedom	Sum of Squares	Mean Square	F
Treatment				
Concentration (C)	4	9.11	2.28	6.61**
Apparatus (A)	1	0.85	0.85	2.46
Interactions				
C x A	4	0.35	0.09	0.25
Error	10	3.45	0.35	
Total	19	13.76		

** Significant at the 1% level.

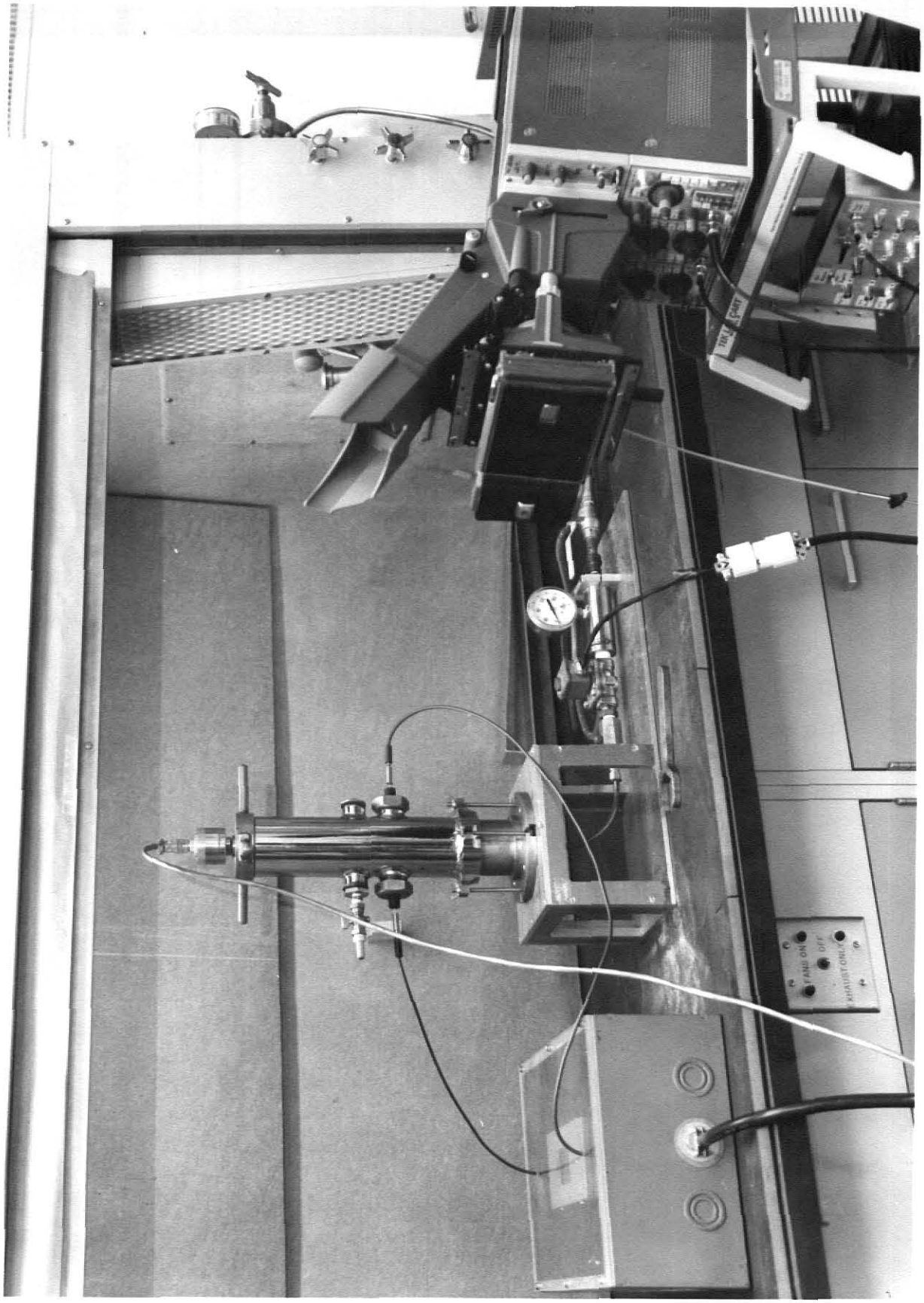

Fig. 5.1 Photograph of the Hartmann Apparatus for Determining P_{max}, $(dP/dt)_{max}$, $(dP/dt)_{ave}$

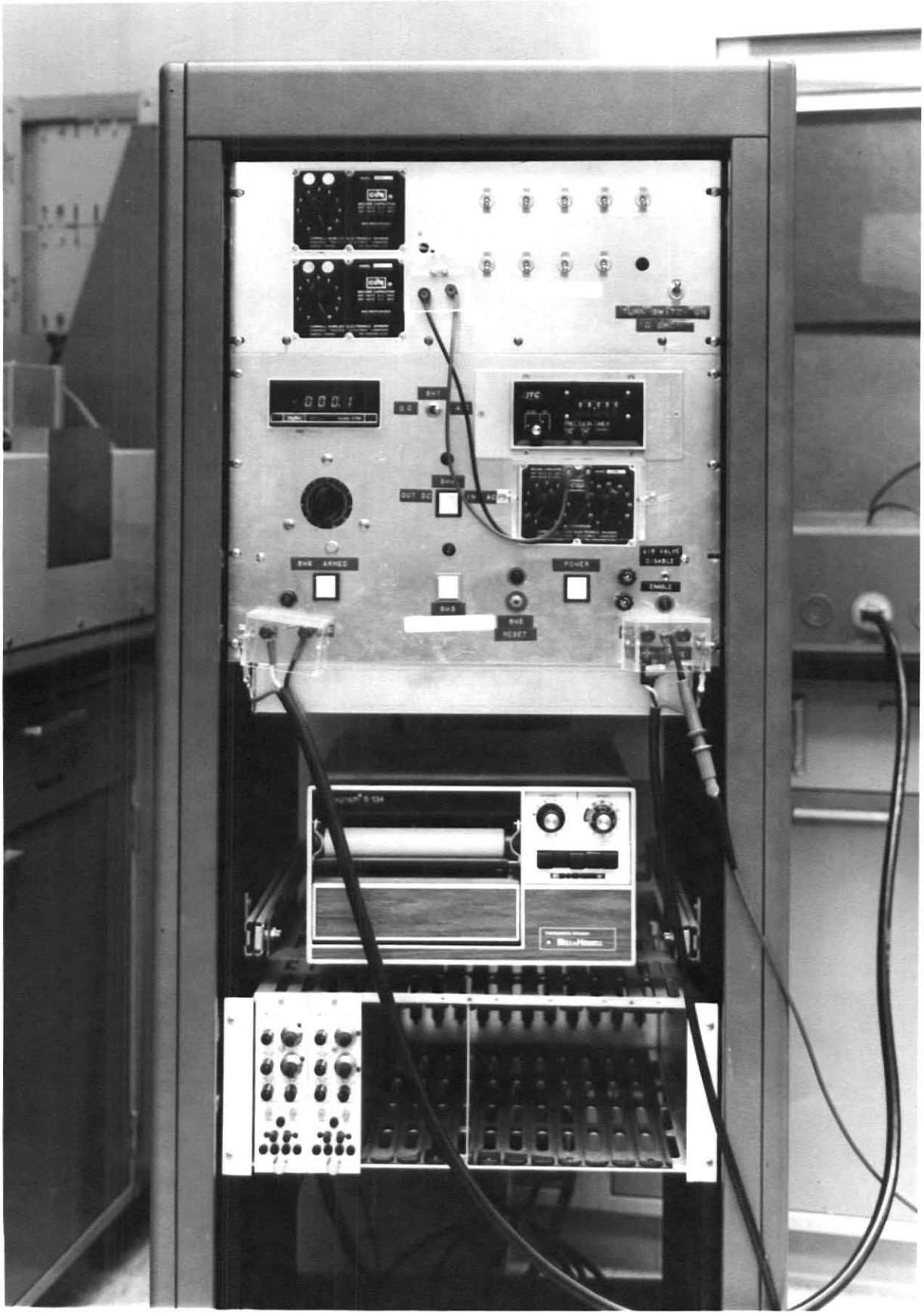

Fig. 5.2 Photograph of the Ignition Timing Circuitry

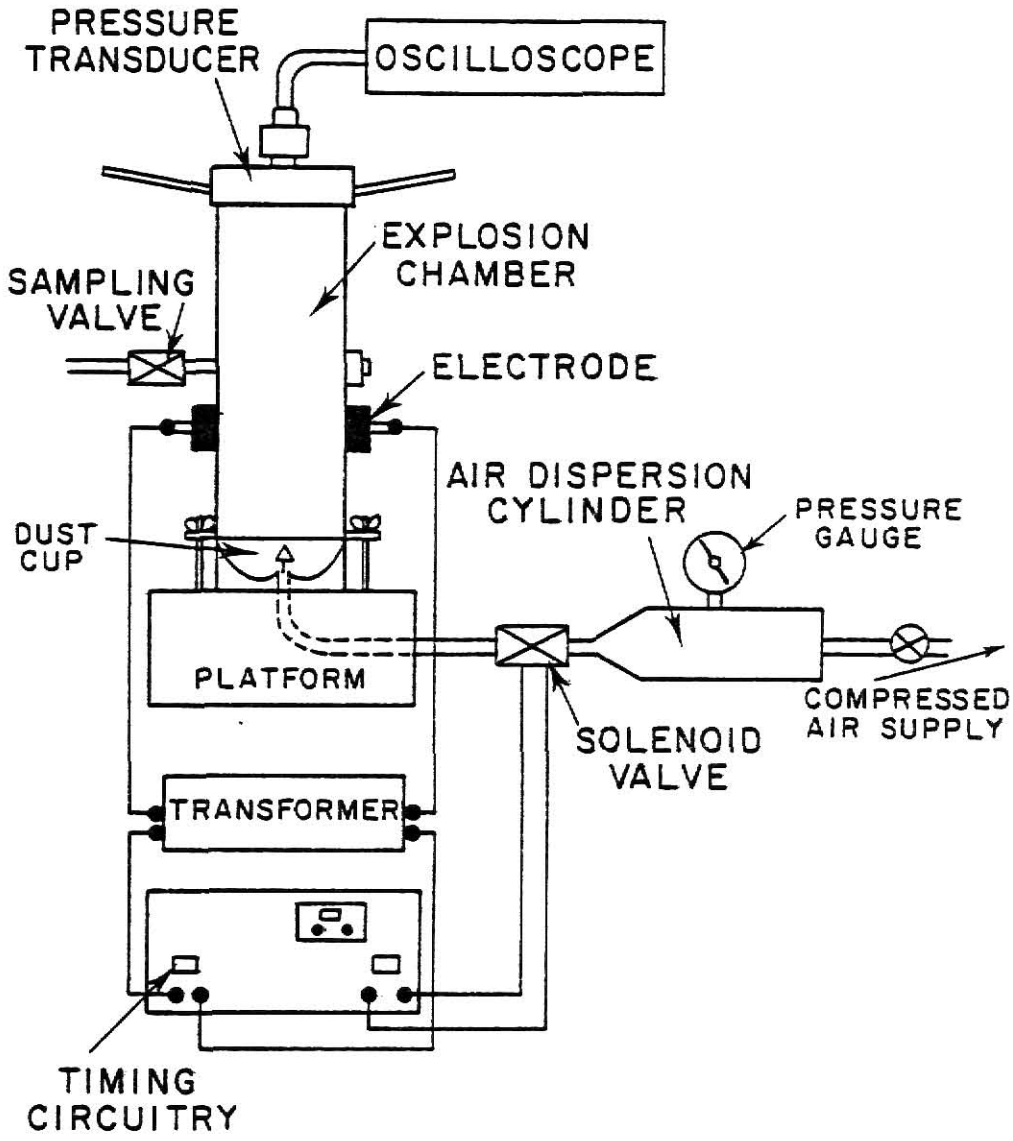

Fig. 5.3 Schematic Diagram of the Entire Experimental Apparatus

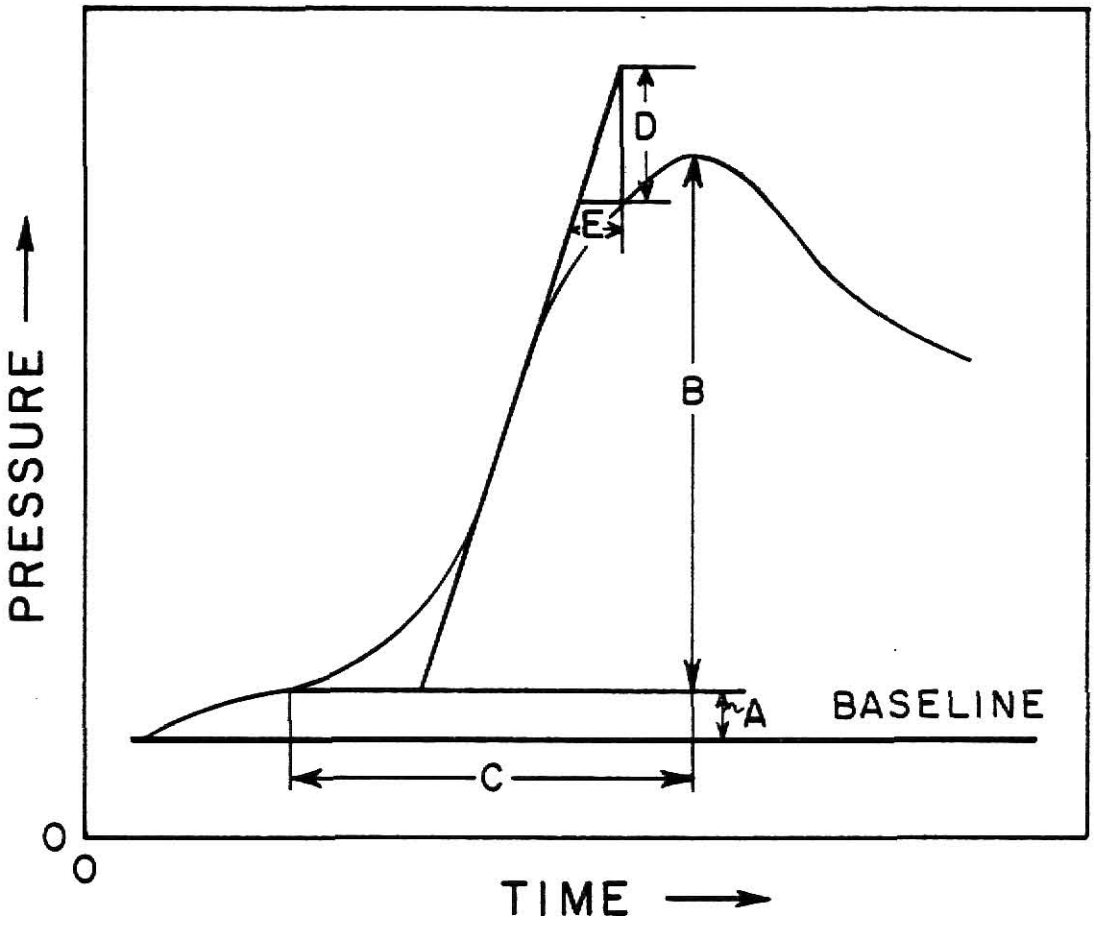

Fig. 5.4 An Illustration of the Pressure Characteristics P_{max}, $(dP/dt)_{max}$, $(dP/dt)_{ave}$

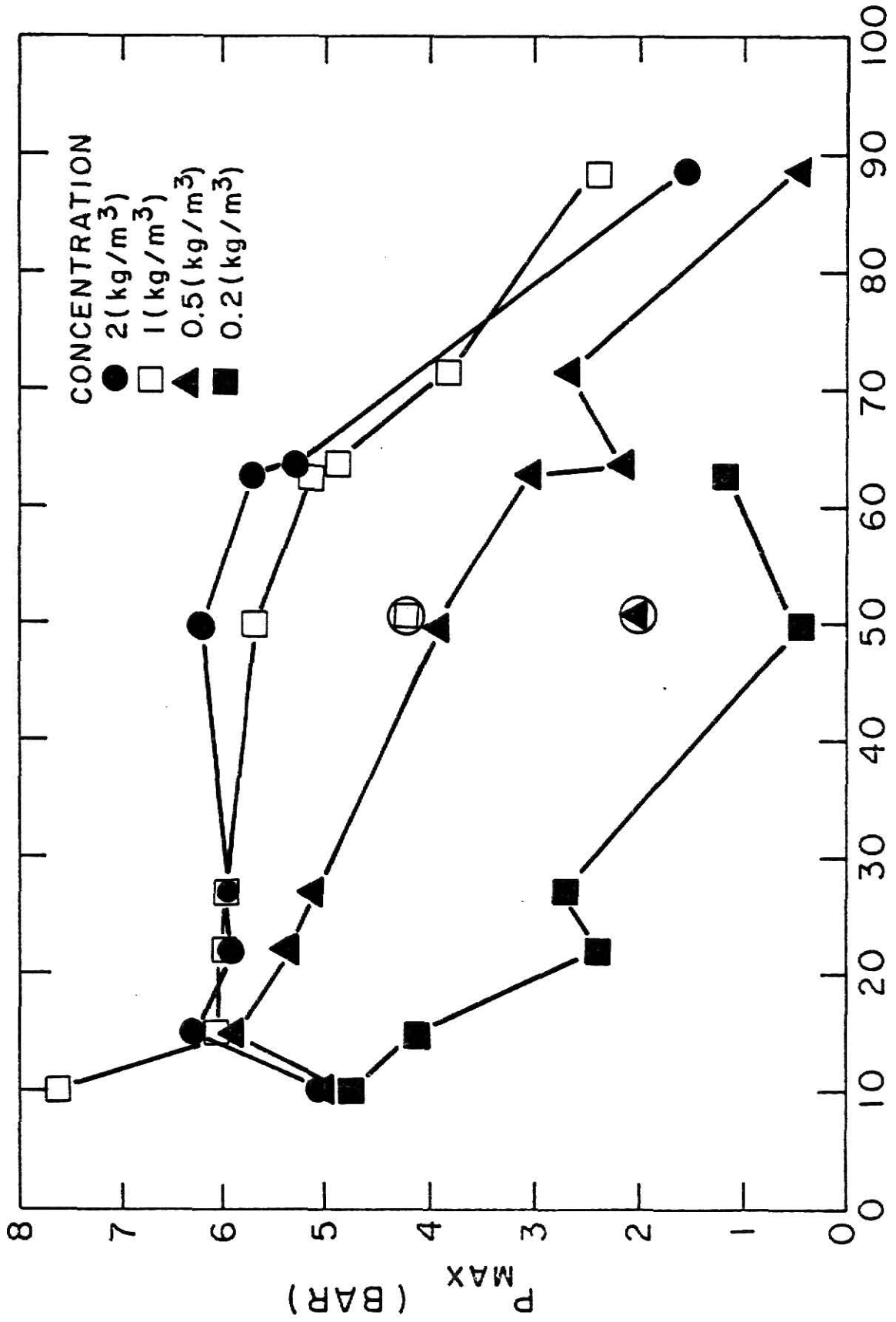

Fig. 5.5 The Relationship between the Maximum Explosion Pressure and the Mass Mean Diameter for Grain Sorghum Dust

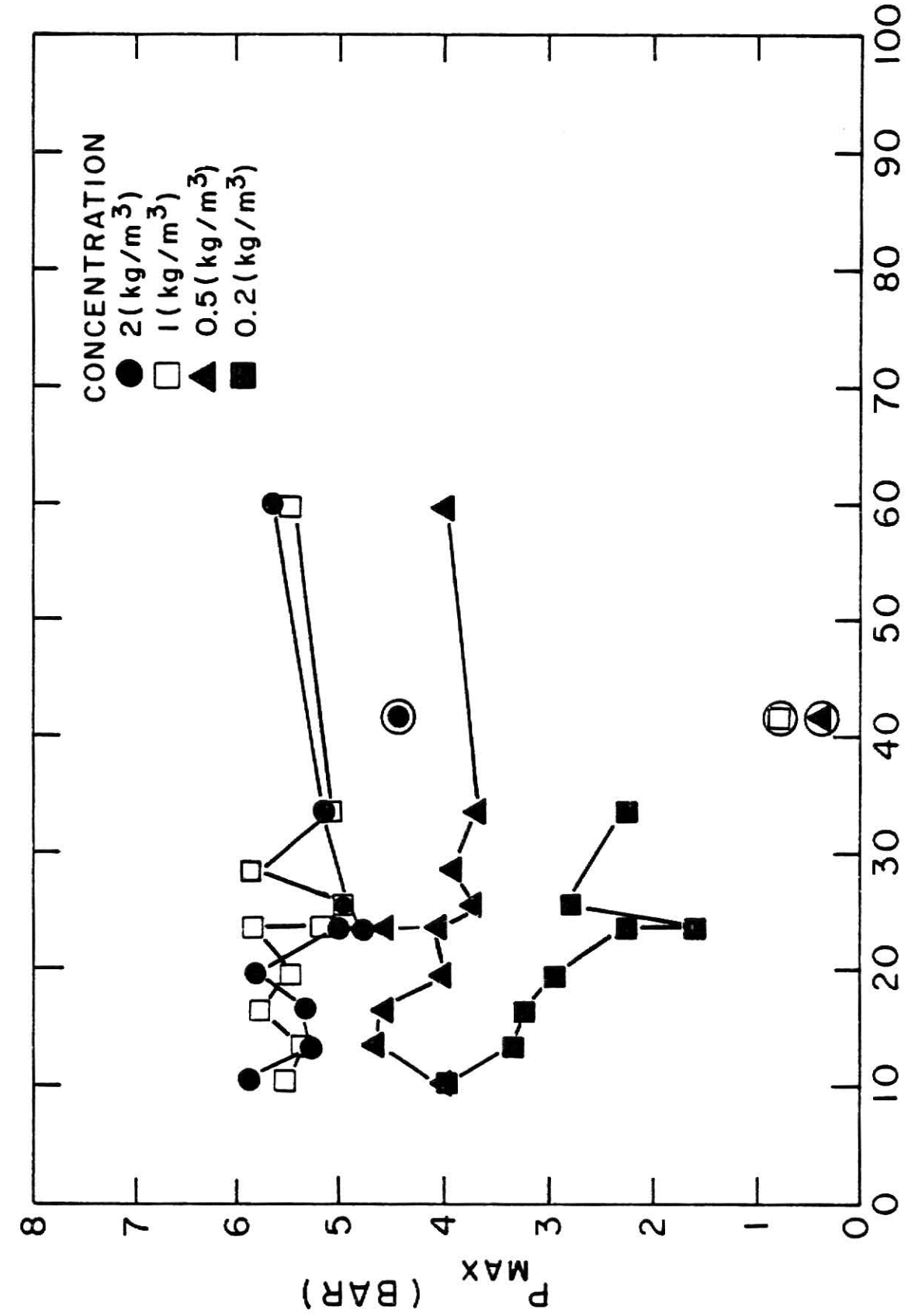

Fig. 5.6 The Relationship between the Maximum Explosion Pressure and the Mass Mean Diameter for Corn Dust

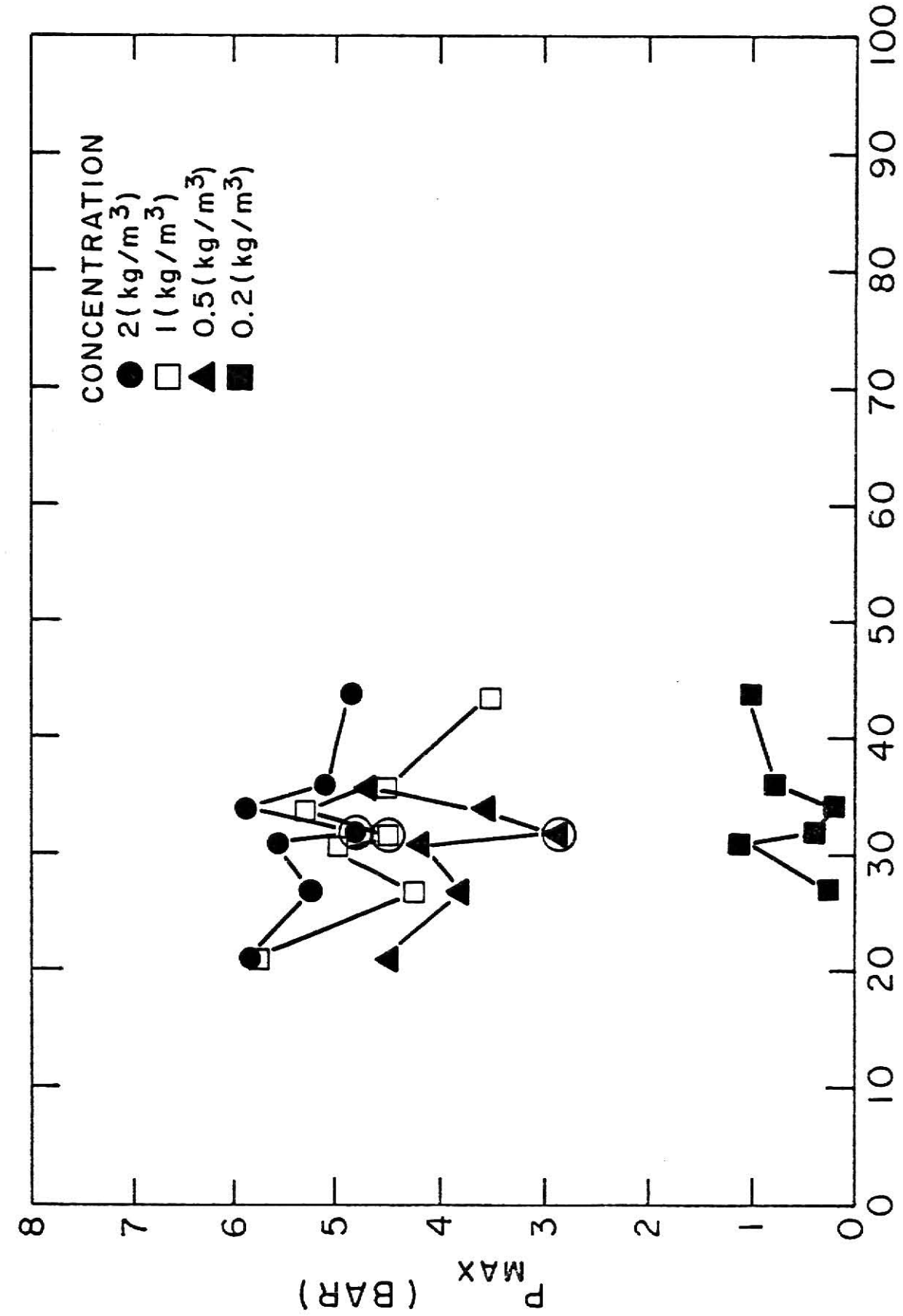

Fig. 5.7 The Relationship between the Maximum Explosion Pressure and the Mass Mean Diameter for Wheat Dust

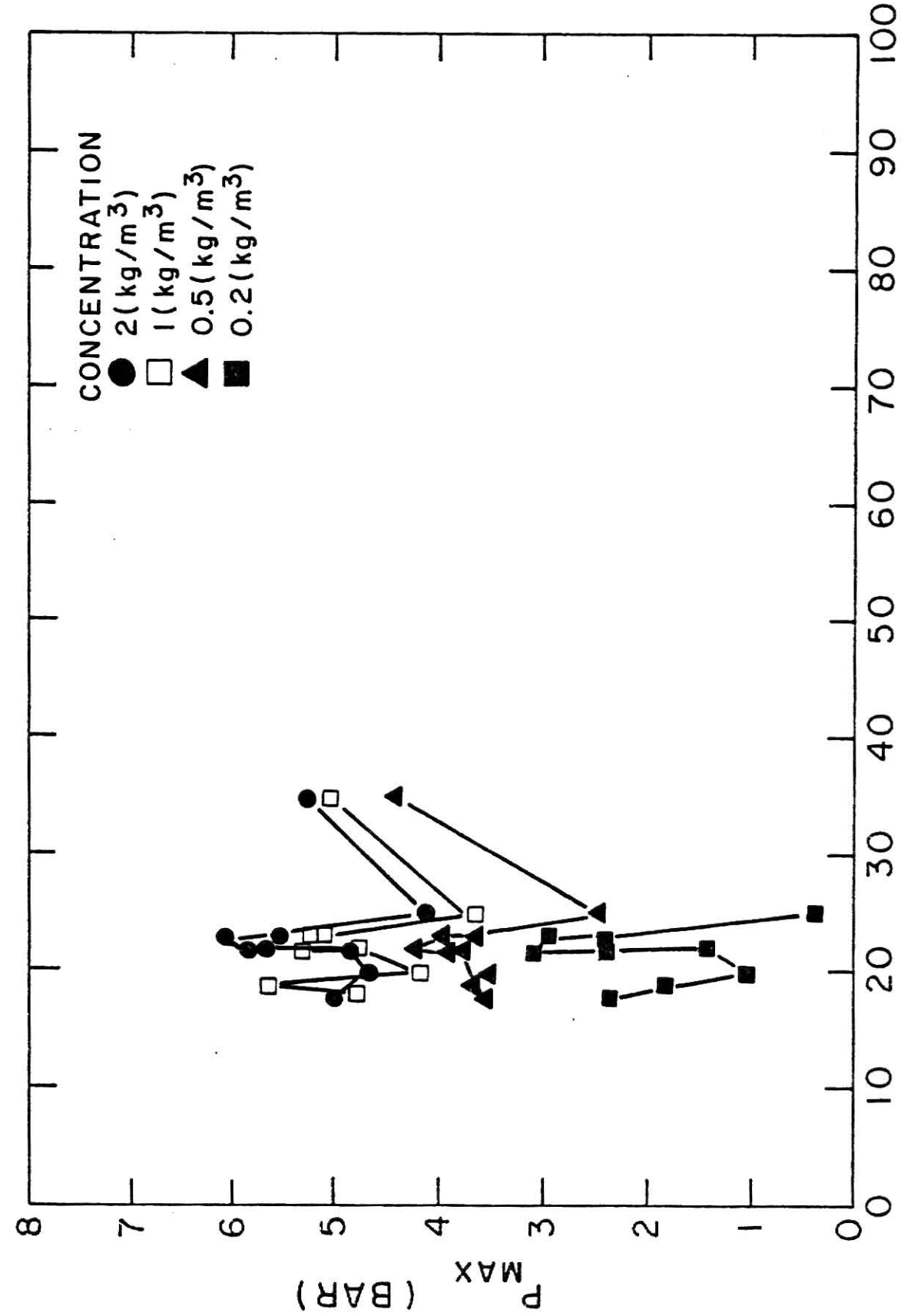

Fig. 5.8 The Relationship between the Maximum Explosion Pressure and the Mass Mean Diameter for Cornstarch

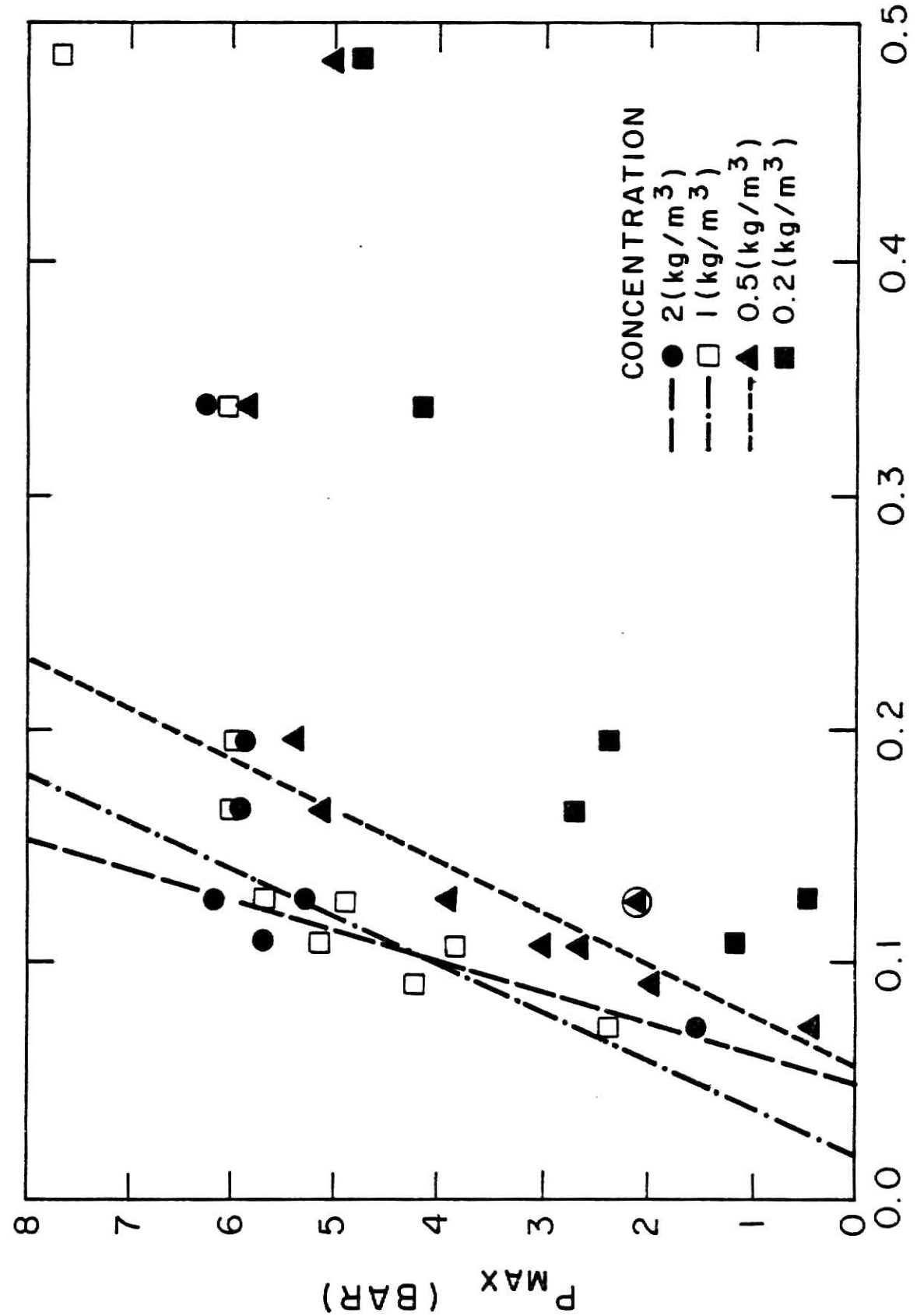

Fig. 5.9 The Relationship between the Maximum Explosion Pressure and the Specific External Surface Area for Grain Sorghum Dust

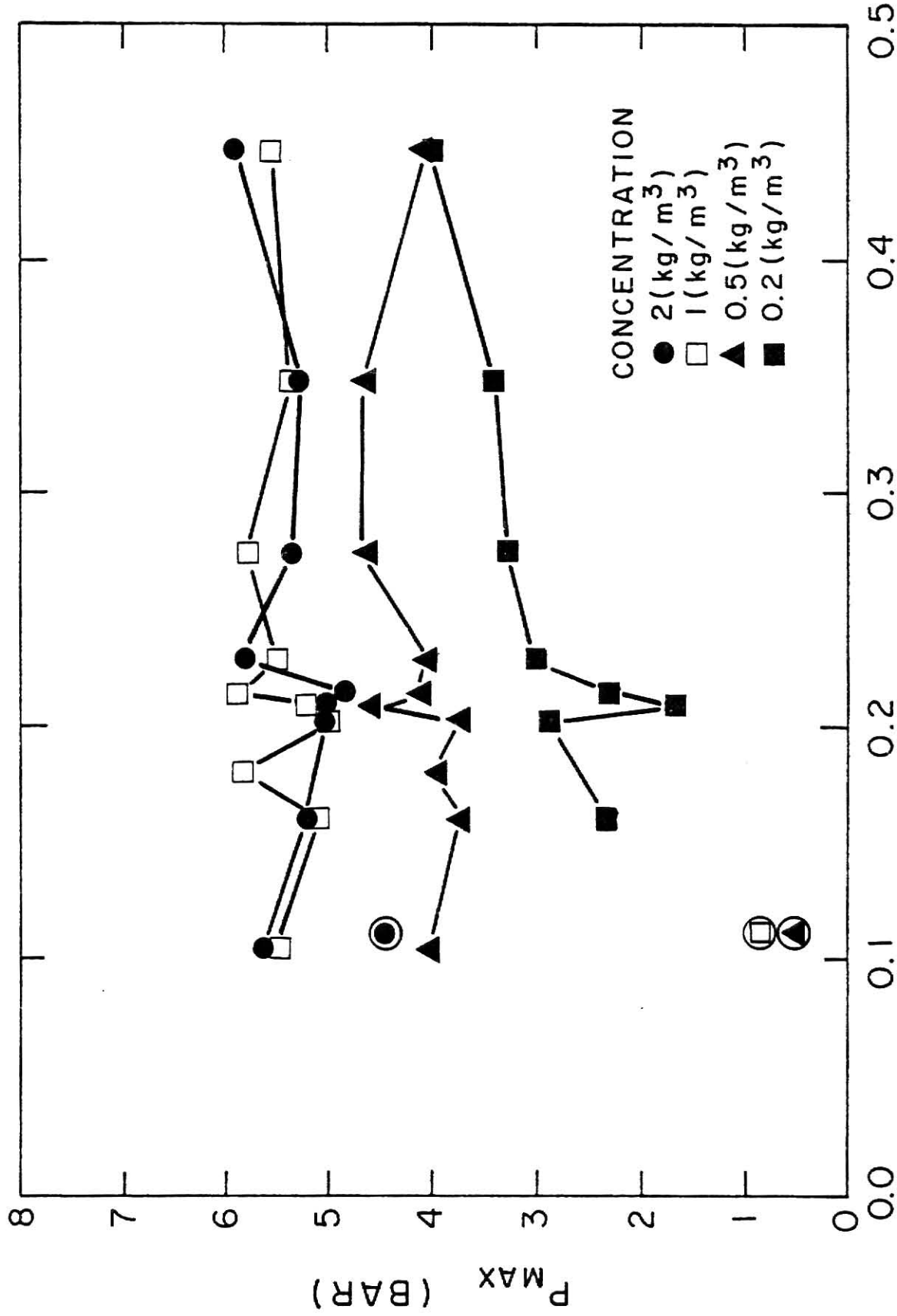

Fig. 5.10 The Relationship between the Maximum Explosion Pressure and the Specific External Area for Corn Dust

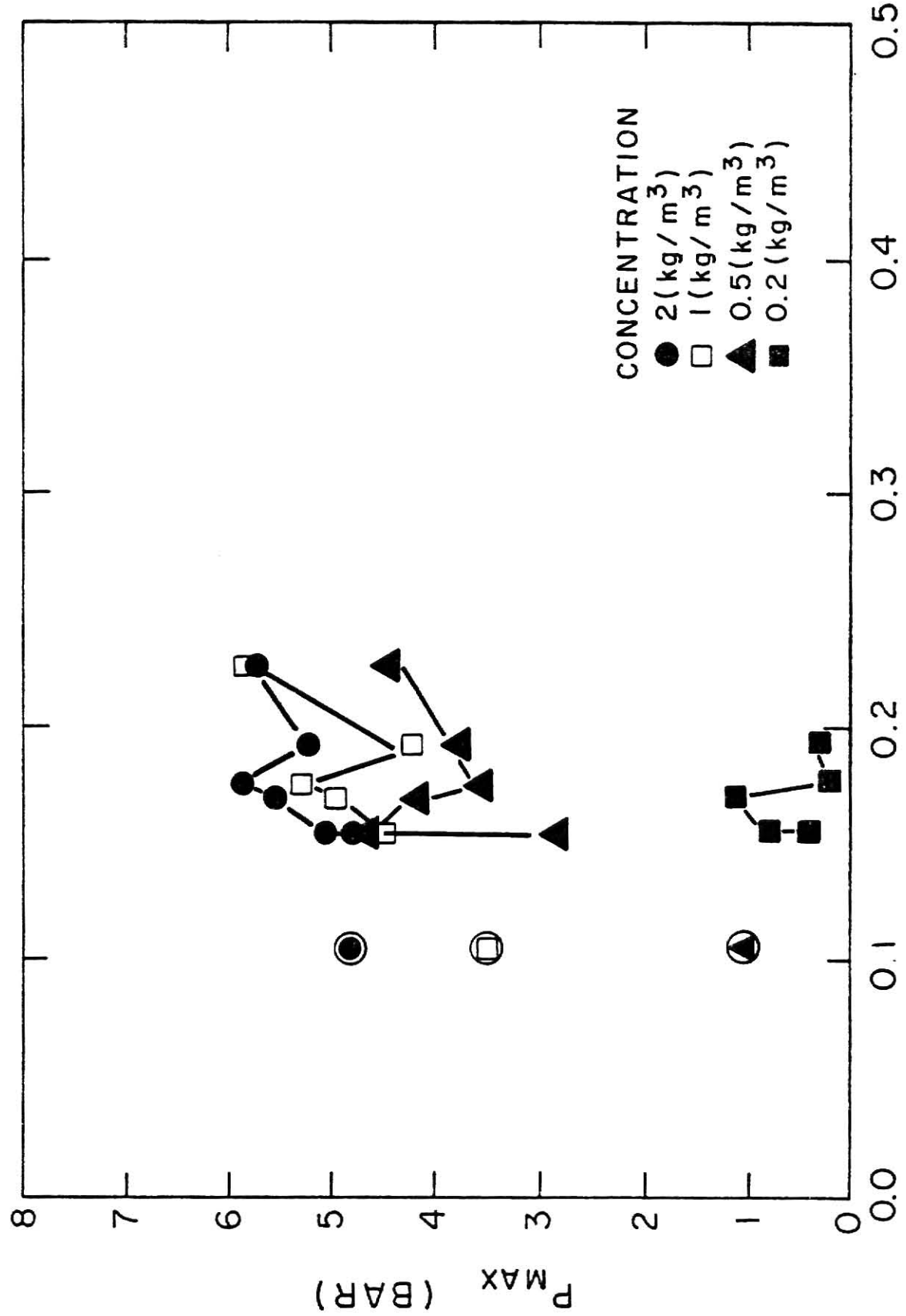

Fig. 5.11 The Relationship between the Maximum Explosion Pressure and the Specific External Area for Wheat Dust

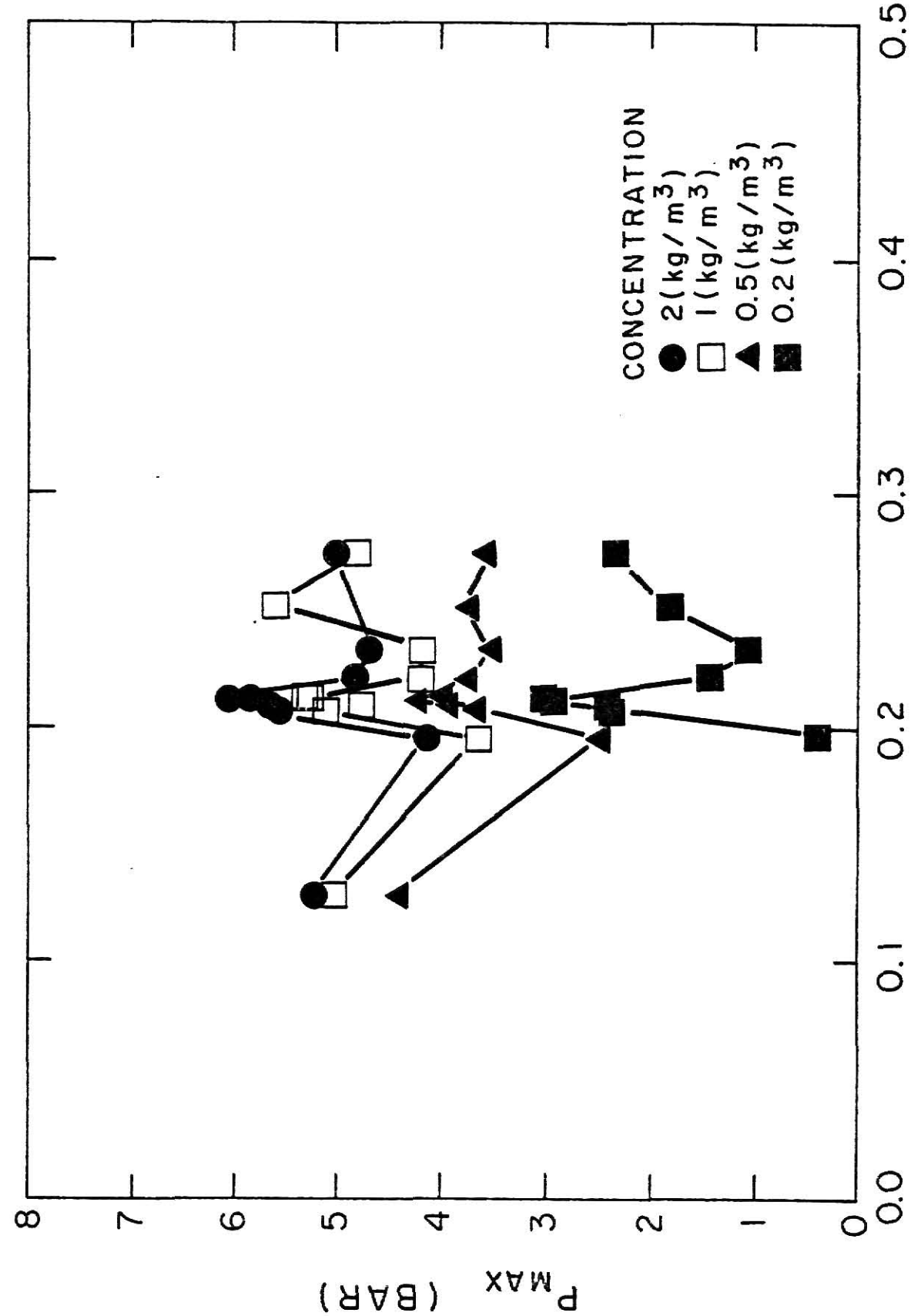

Fig. 5.12 The Relationship between the Maximum Explosion Pressure and the Specific External Area for Cornstarch

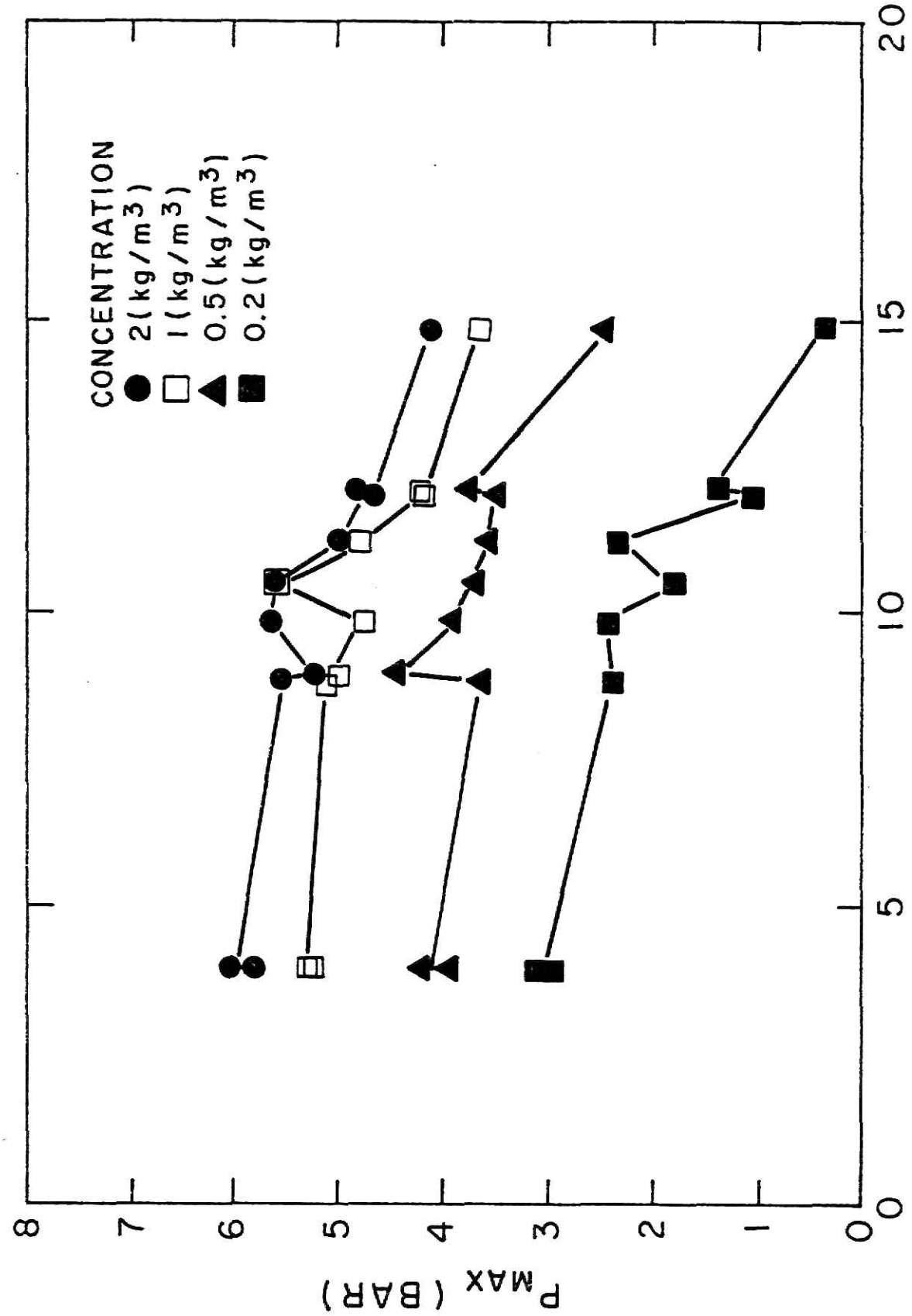

Fig. 5.13 The Relationship between the Maximum Explosion Pressure and the Moisture Content for Corn Starch

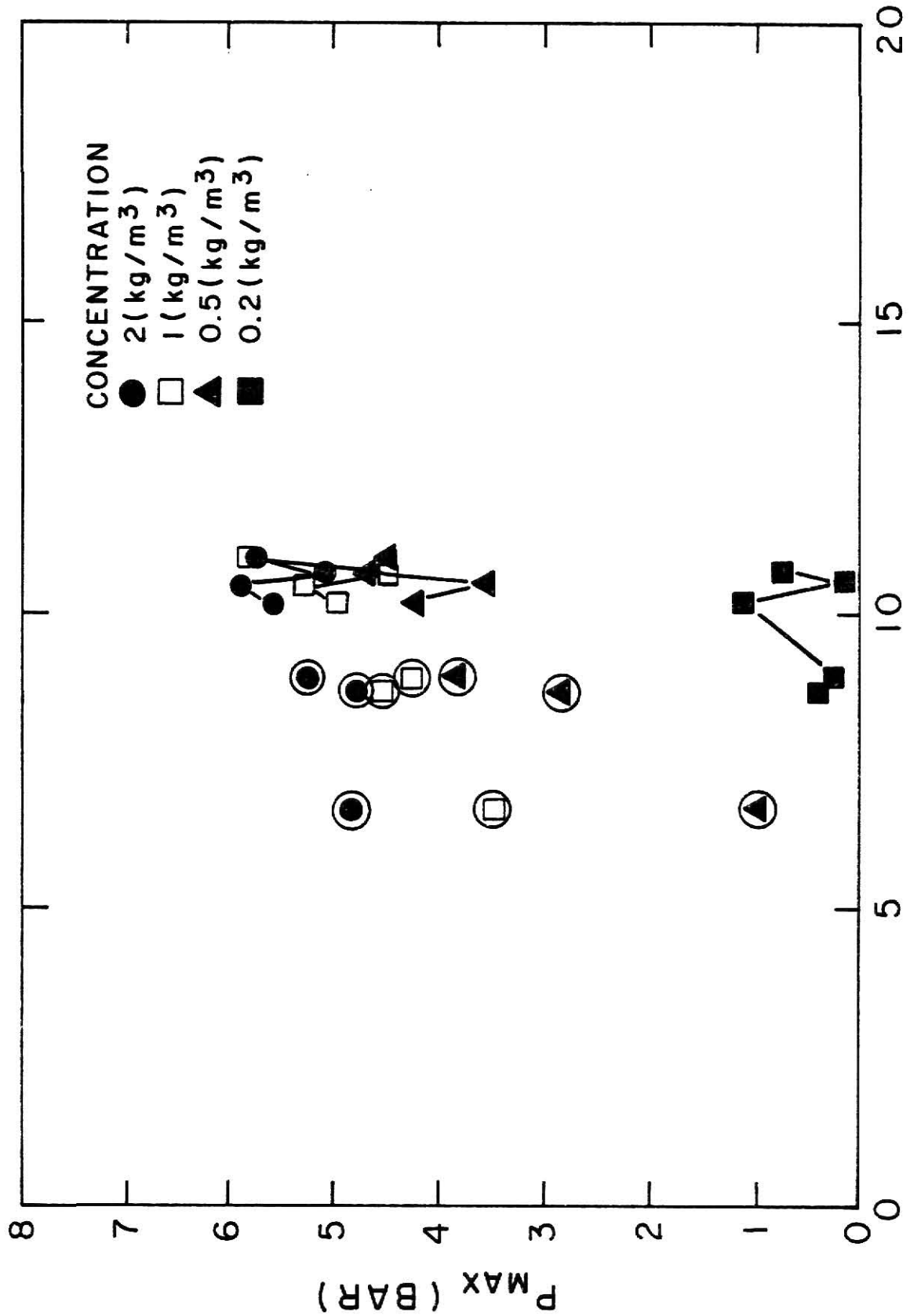

Fig. 5.14 The Relationship between the Maximum Explosion Pressure and the Moisture Content for Wheat Dust

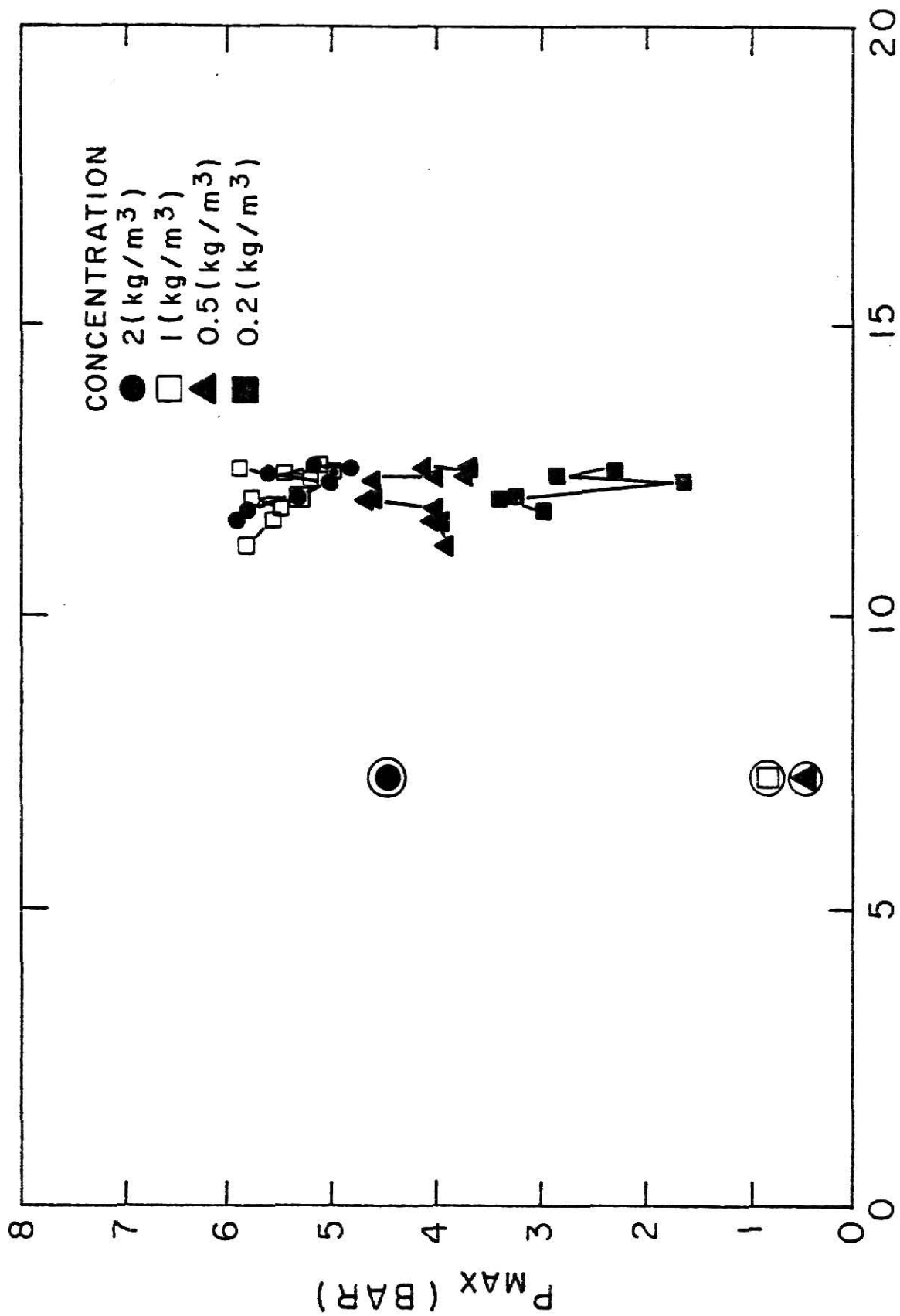

Fig. 5.15 The Relationship between the Maximum Explosion Pressure and the Moisture Content for Corn Dust

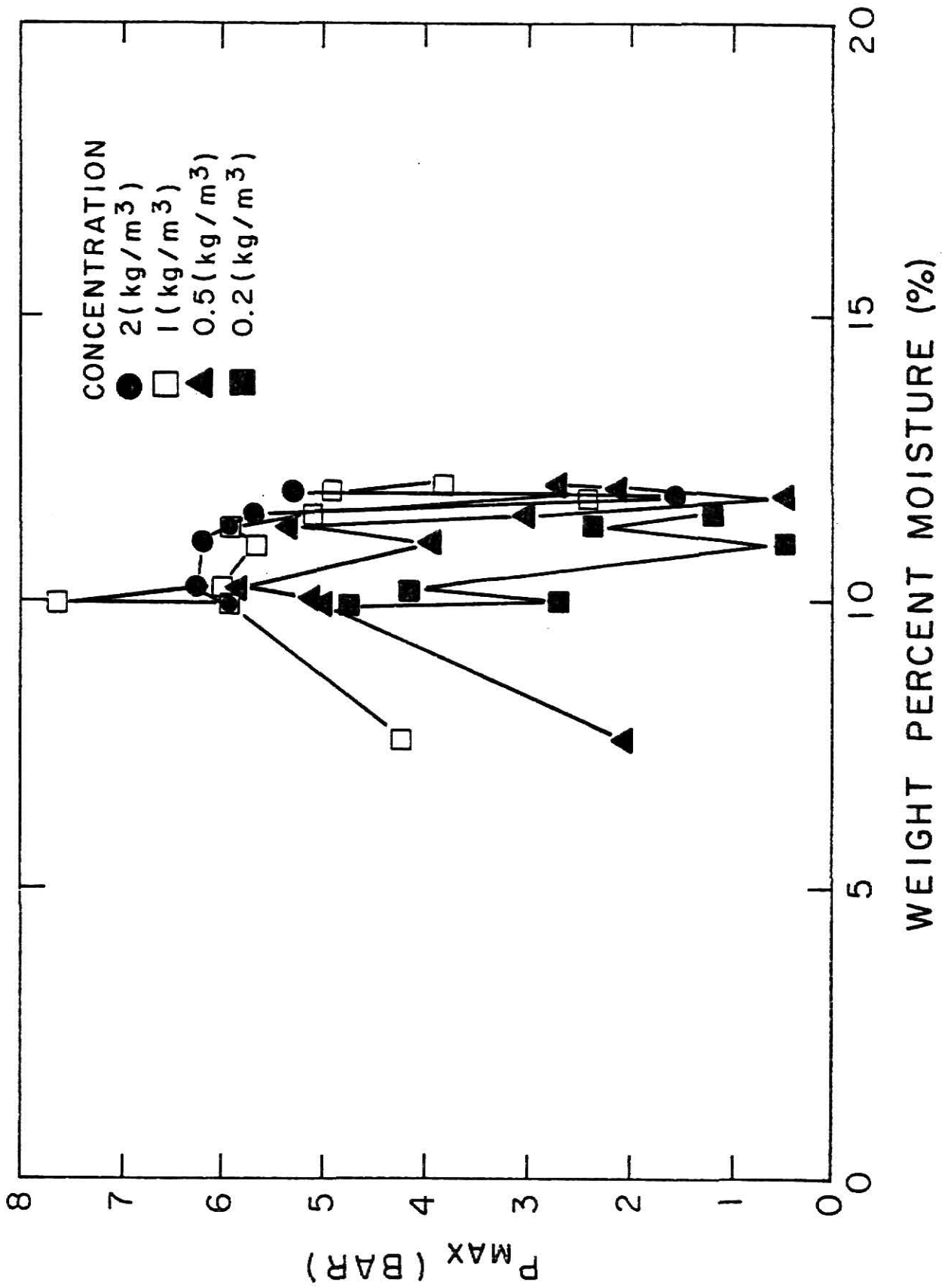

Fig. 5.16 The Relationship between the Maximum Explosion Pressure and the Moisture Content for Grain Sorghum Dust

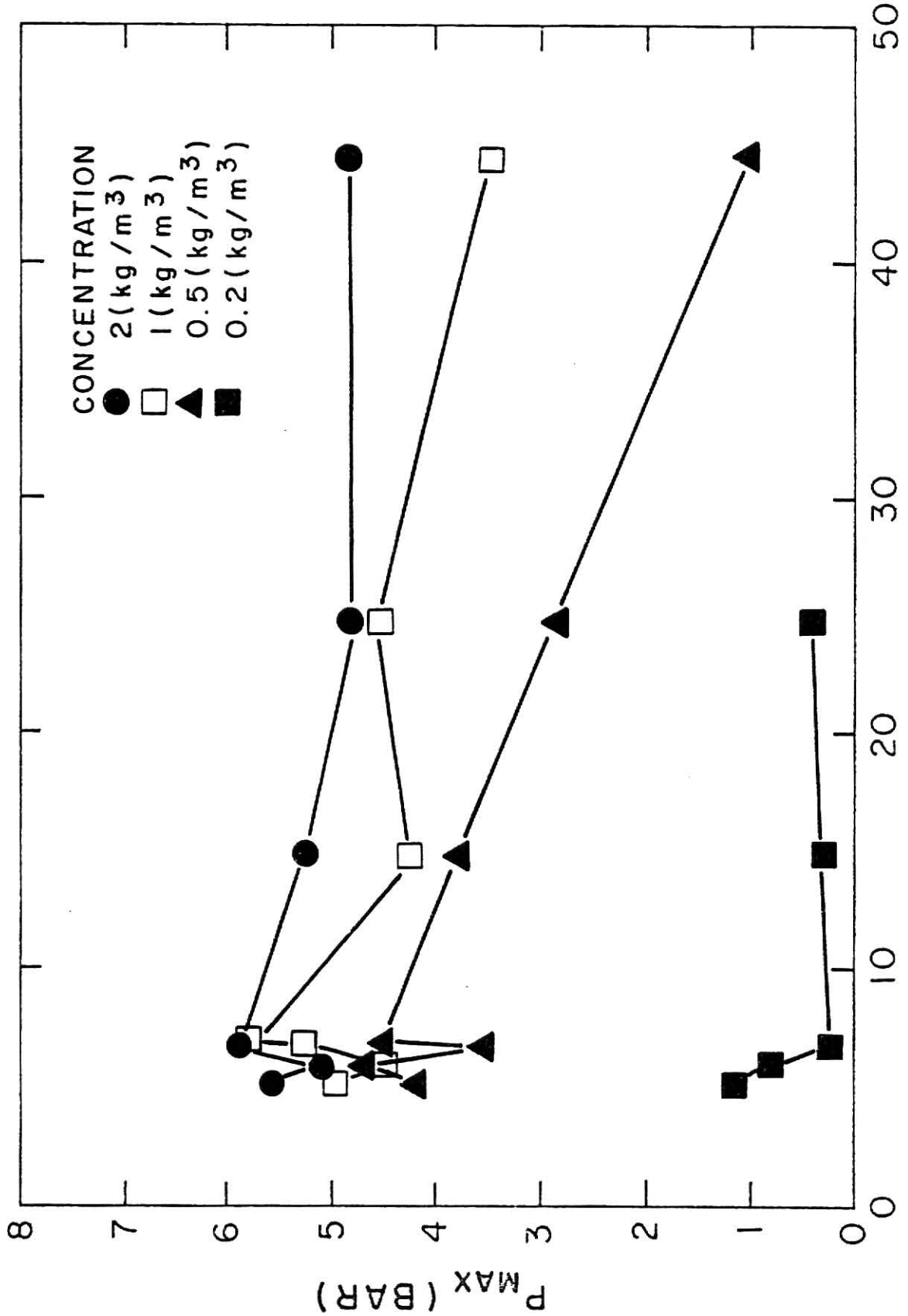

Fig. 5.17 The Relationship between the Maximum Explosion Pressure and the Ash Content for Wheat Dust

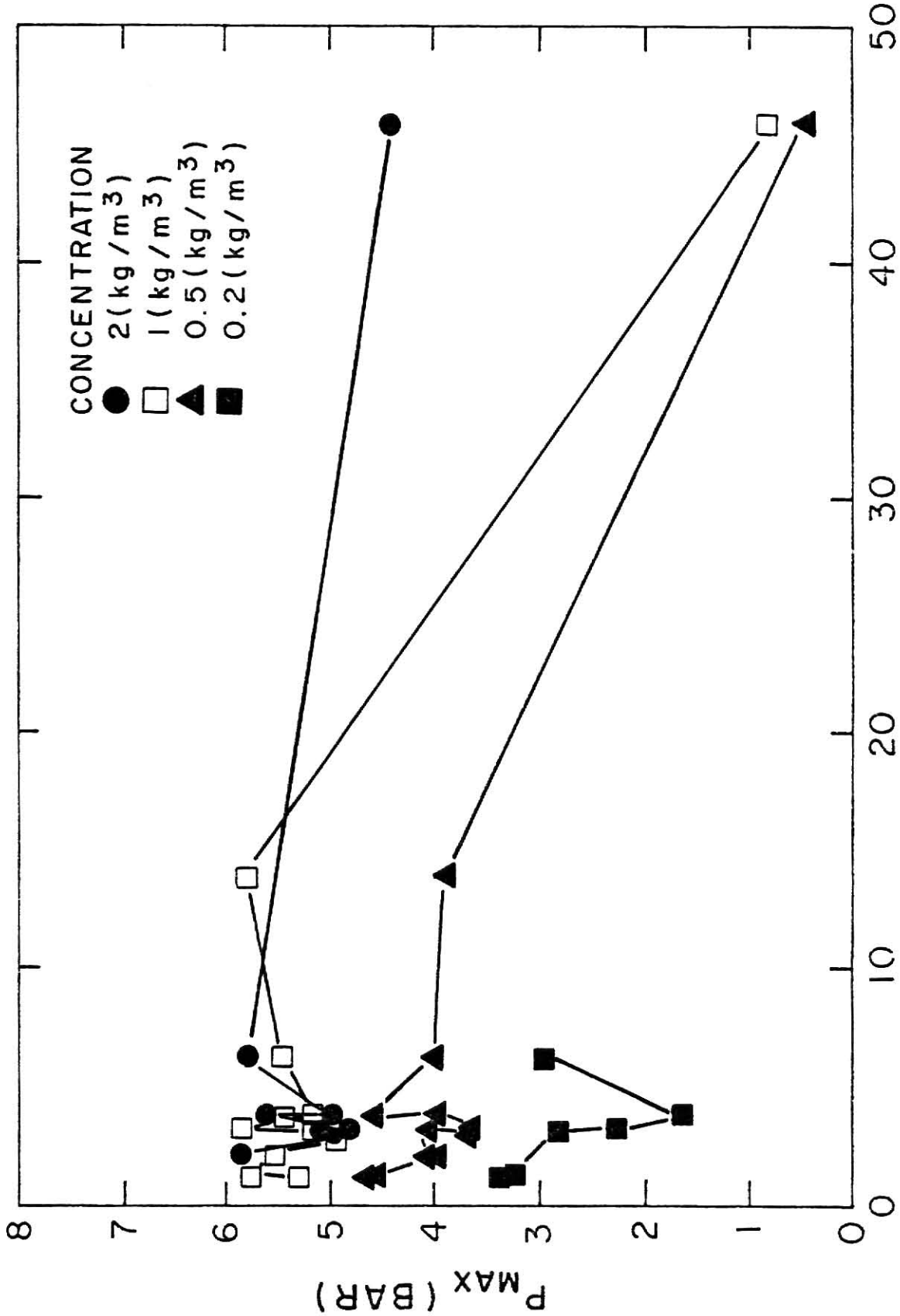

Fig. 5.18 The Relationship between the Maximum Explosion Pressure and the Ash Content for Corn Dust

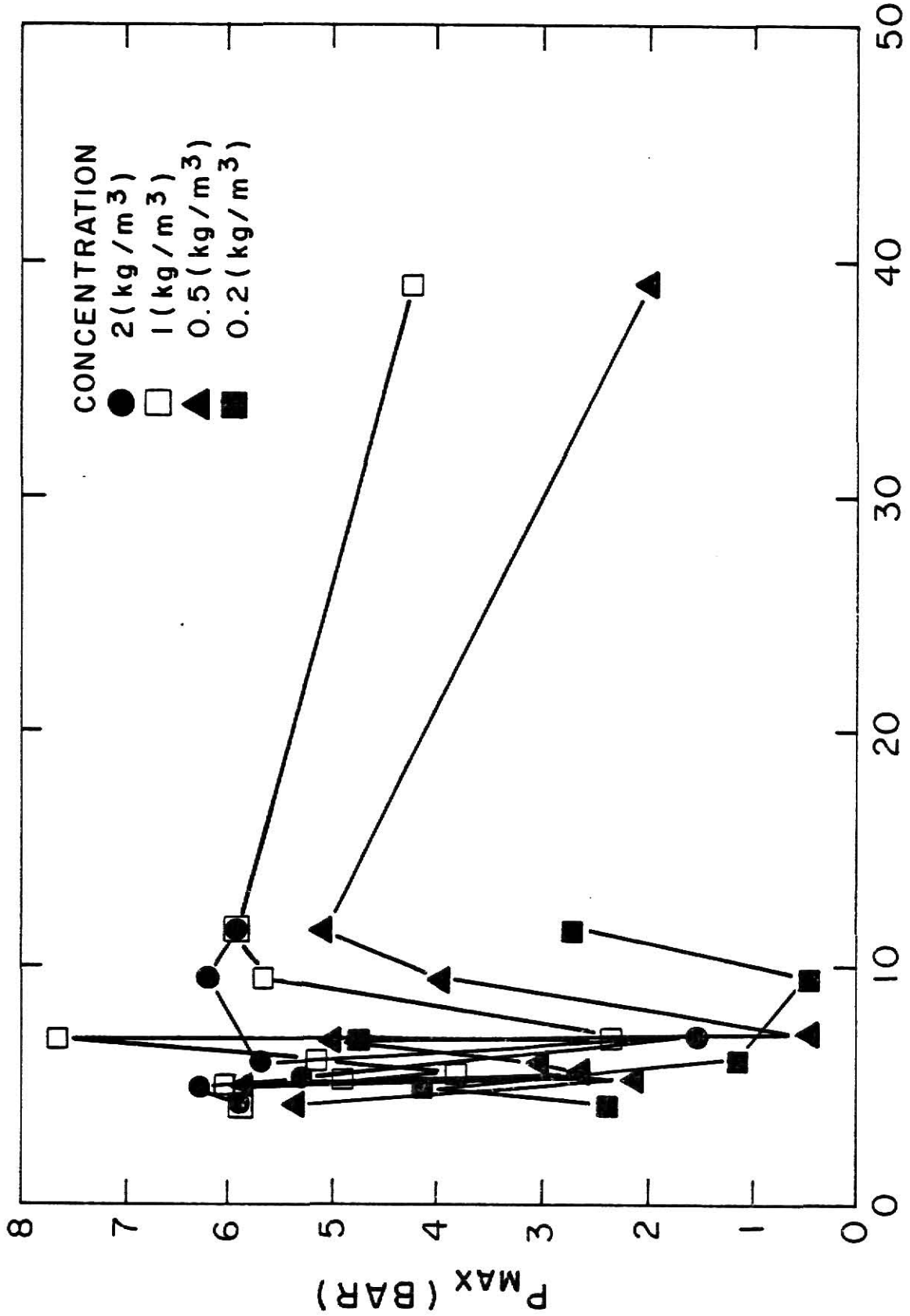

Fig. 5.19 The Relationship between the Maximum Explosion Pressure and the Ash Content for Grain Sorghum Dust

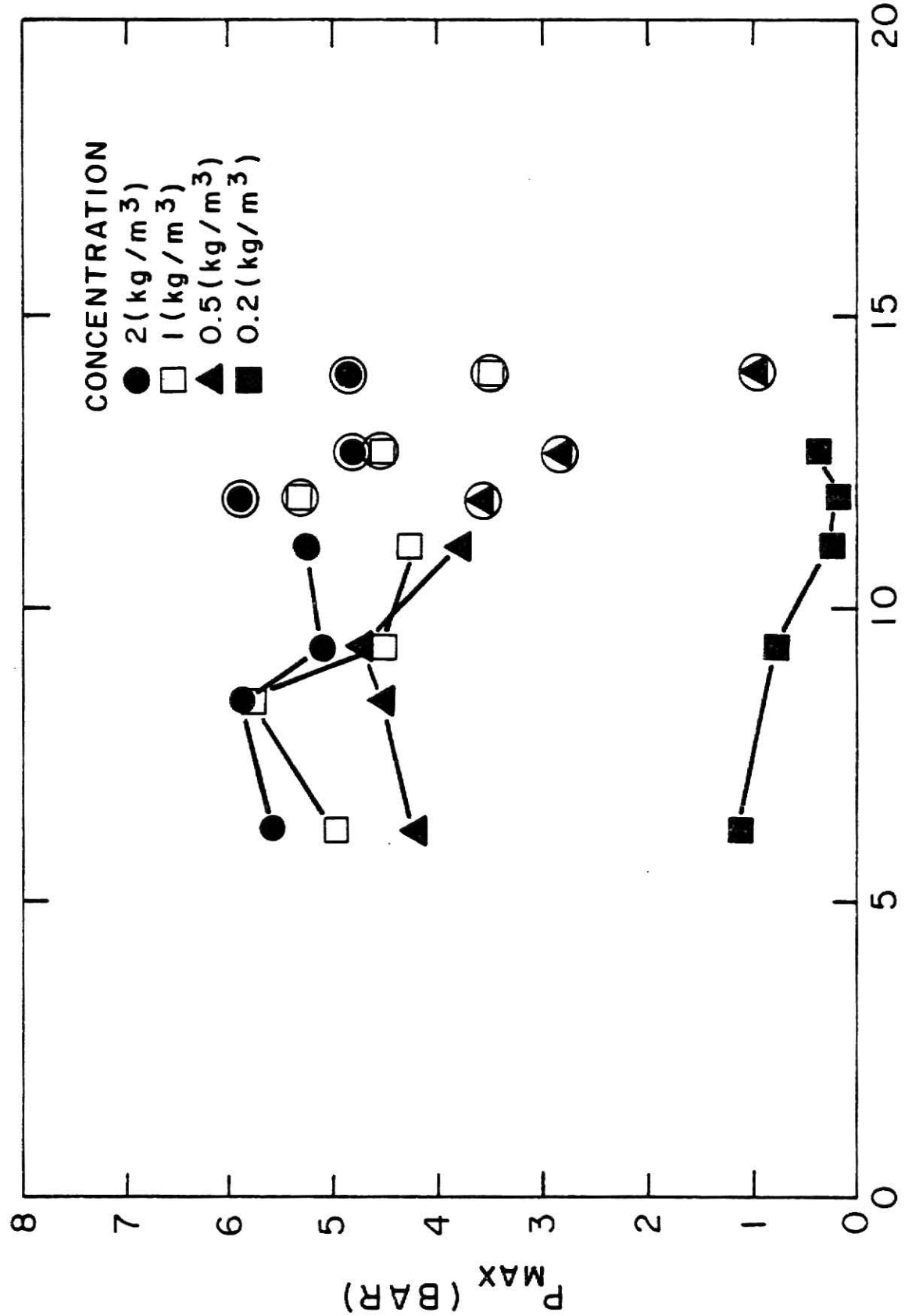

Fig. 5.20 The Relationship between the Maximum Explosion Pressure and the Protein Content for Wheat Dust

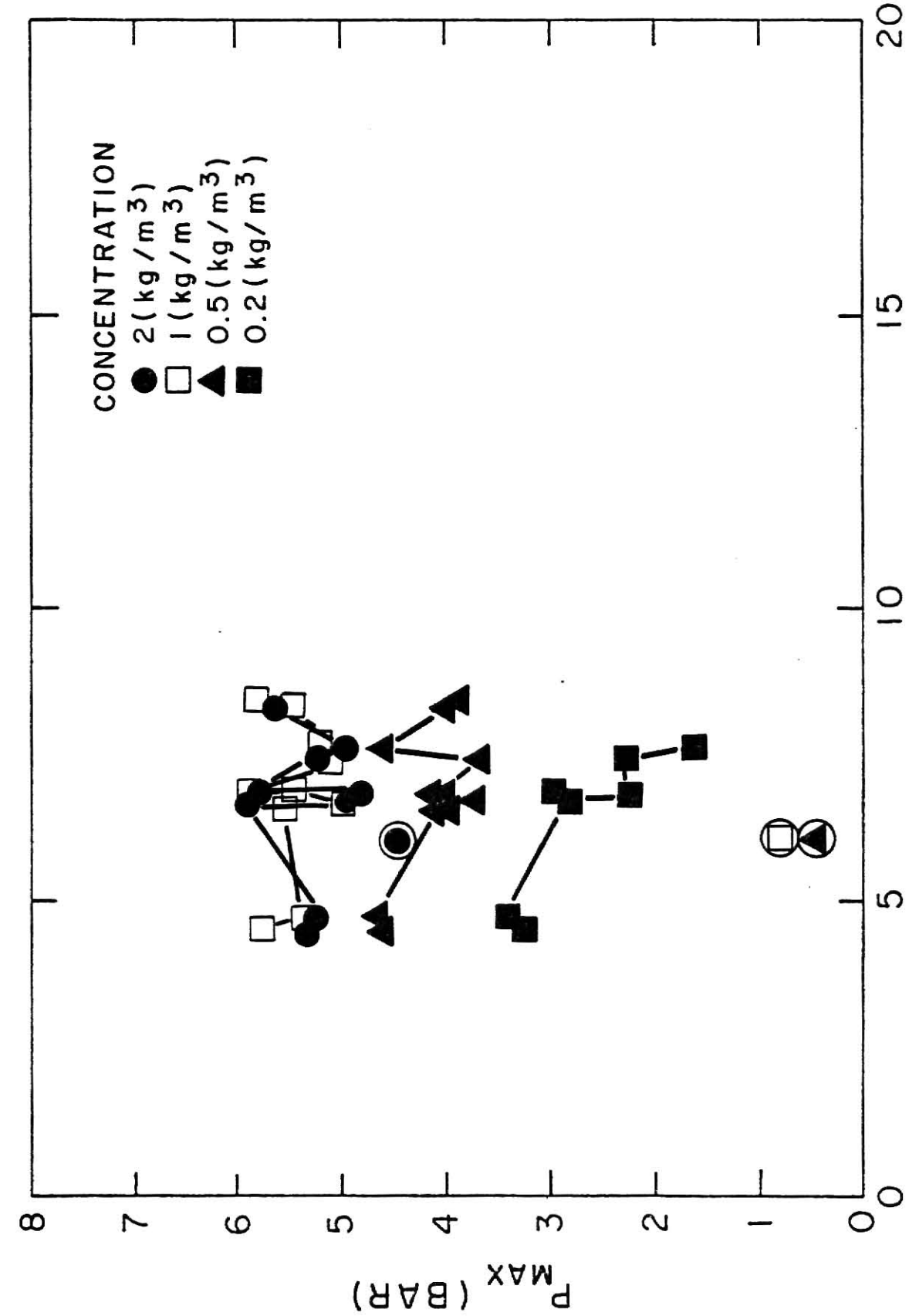

Fig. 5.21 The Relationship between the Maximum Explosion Pressure and the Protein Content for Corn Dust

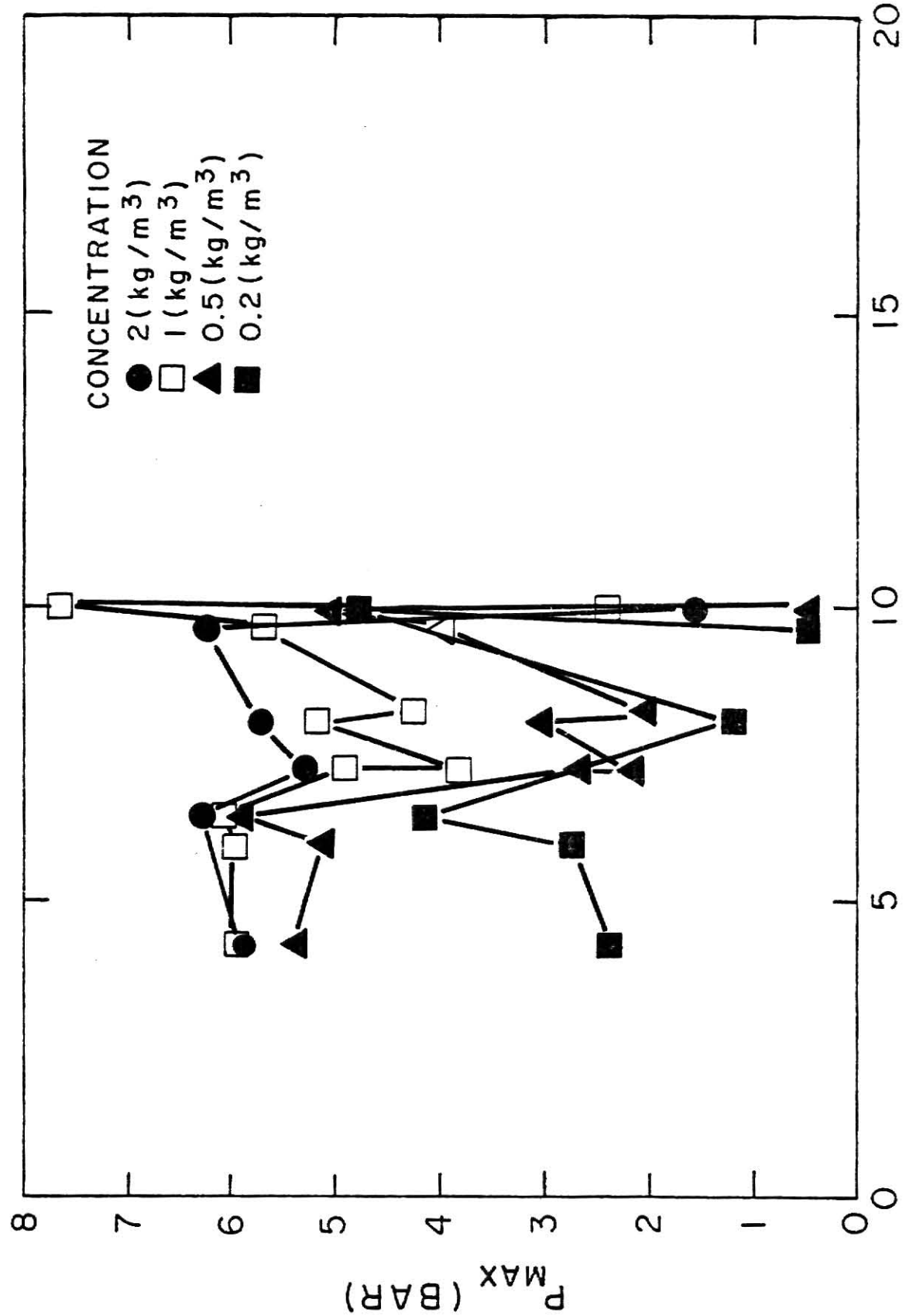

Fig. 5.22 The Relationship between the Maximum Explosion Pressure and the Protein Content for Grain Sorghum Dust

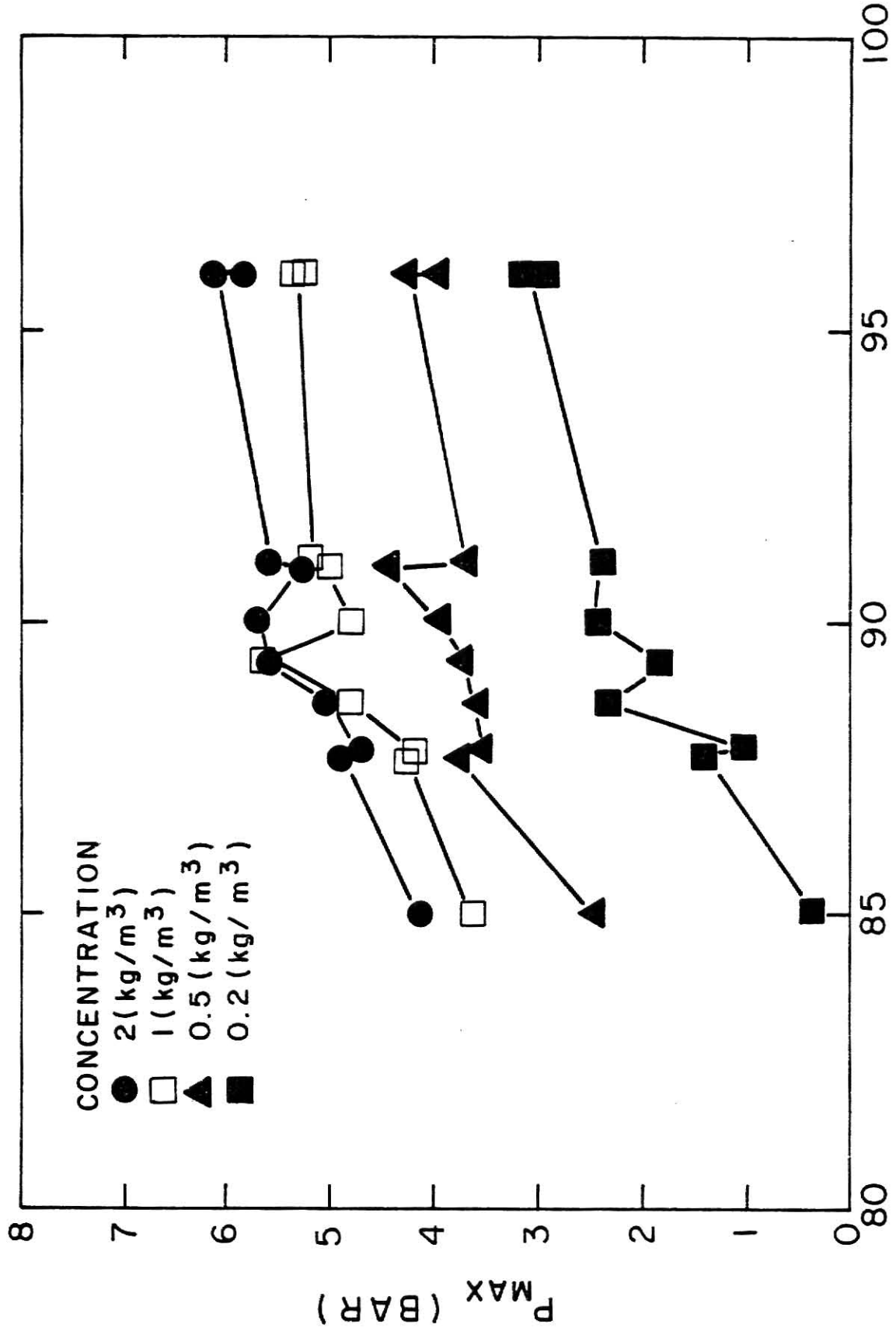

Fig. 5.23 The Relationship between the Maximum Explosion Pressure and the Starch and Fiber Content for Cornstarch

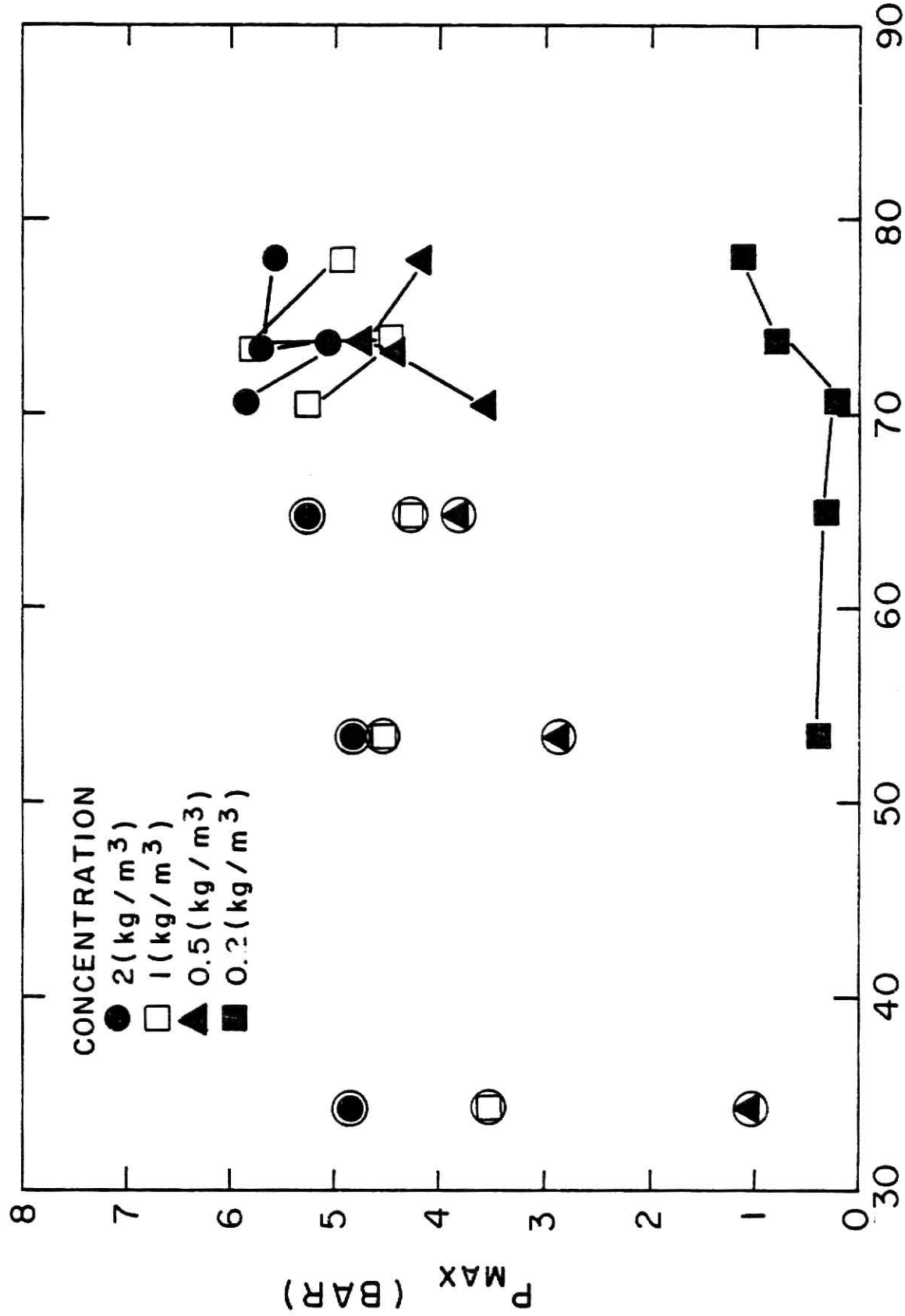

Fig. 5.24 The Relationship between the Maximum Explosion Pressure and the Starch and Fiber Content for Wheat Dust

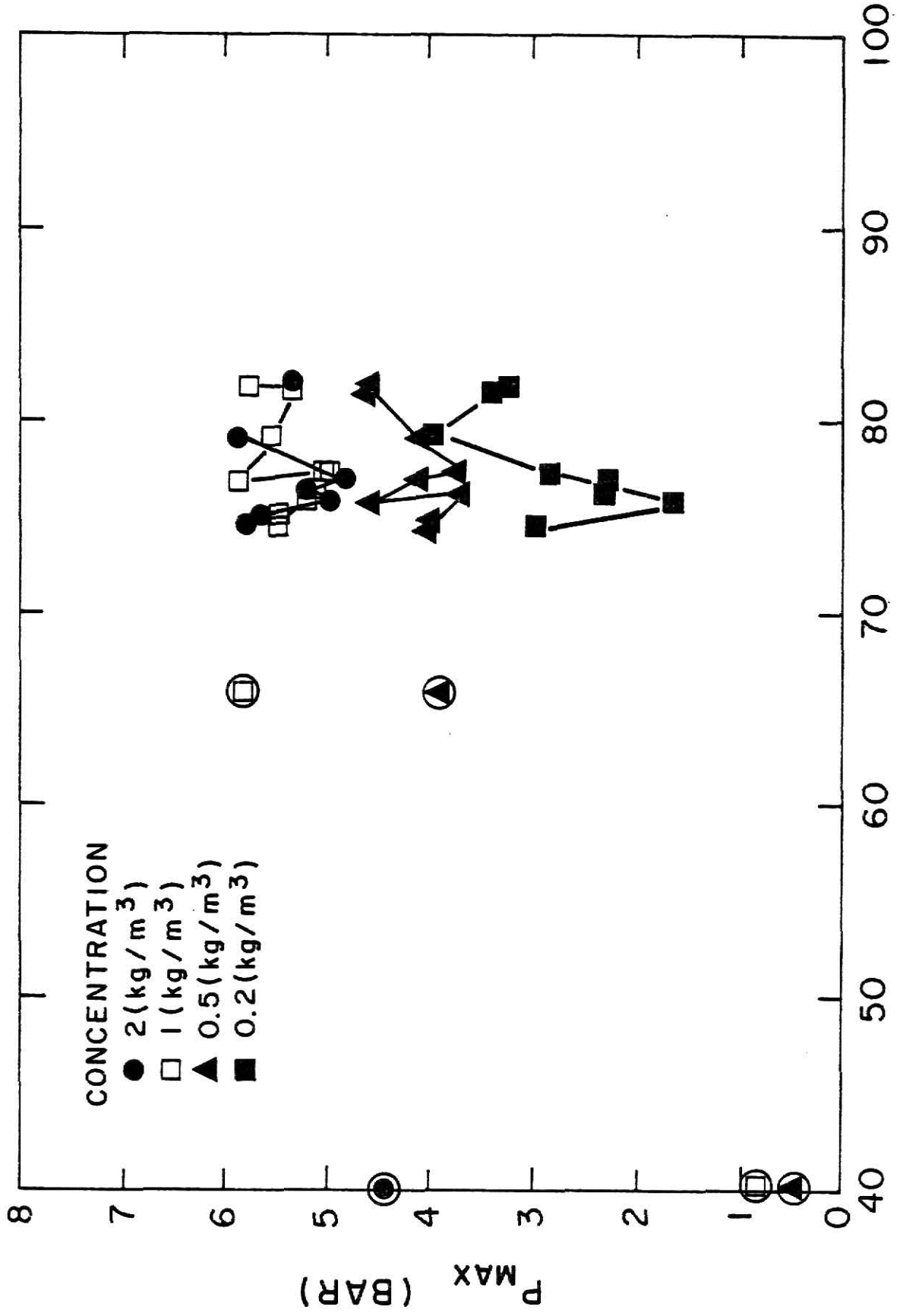

Fig. 5.25 The Relationship between the Maximum Explosion Pressure and the Starch and Fiber Content for Corn Dust

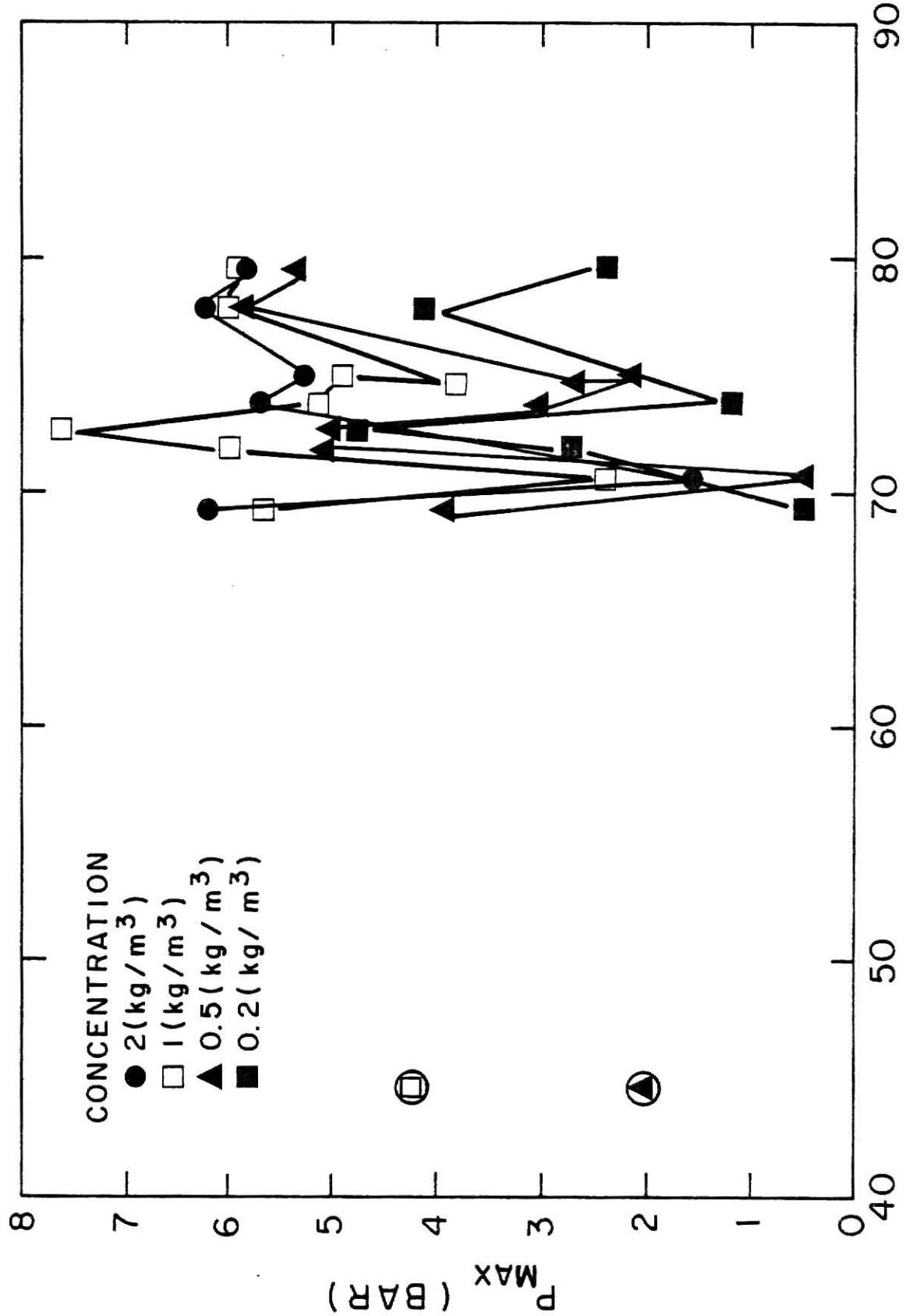

Fig. 5.26 The Relationship between the Maximum Explosion Pressure and the Starch and Fiber Content for Grain Sorghum Dust

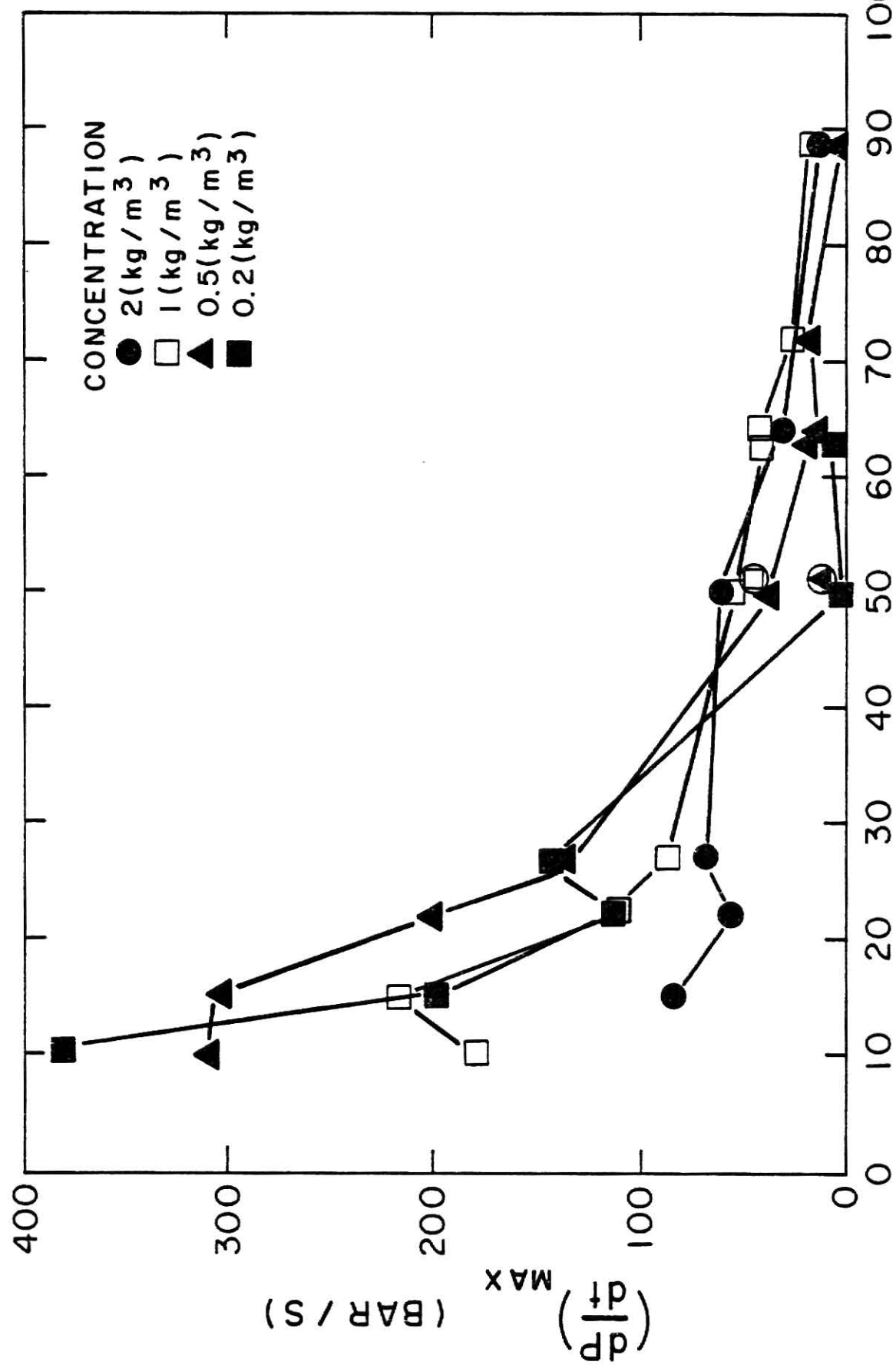

Fig. 4.27 The Relationship between the Maximum Rate of Pressure Rise and the Mass Mean Diameter for Grain Sorghum Dust

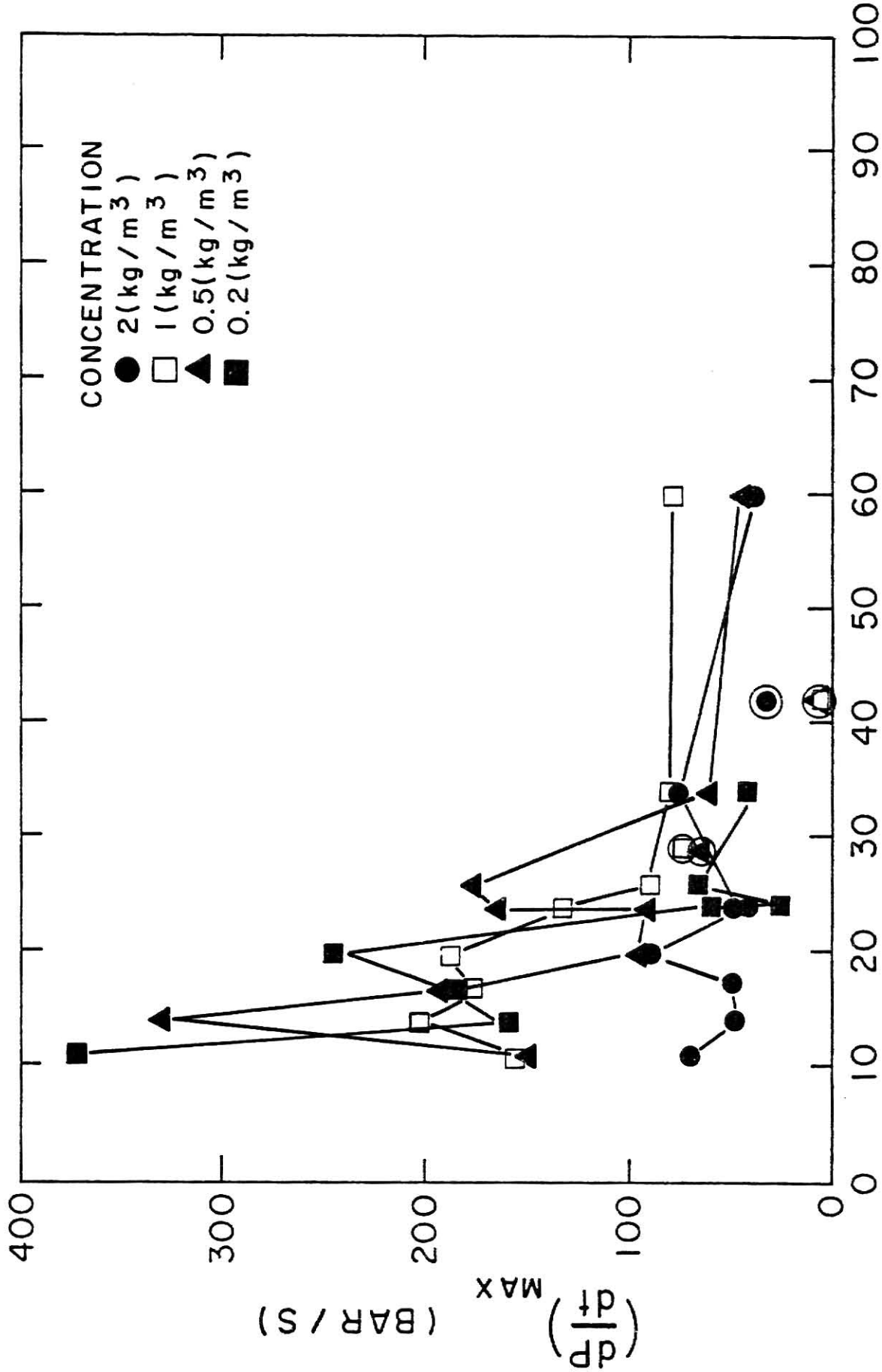

Fig. 5.28 The Relationship between the Maximum Rate of Pressure Rise and the Mass Mean Diameter for Corn Dust

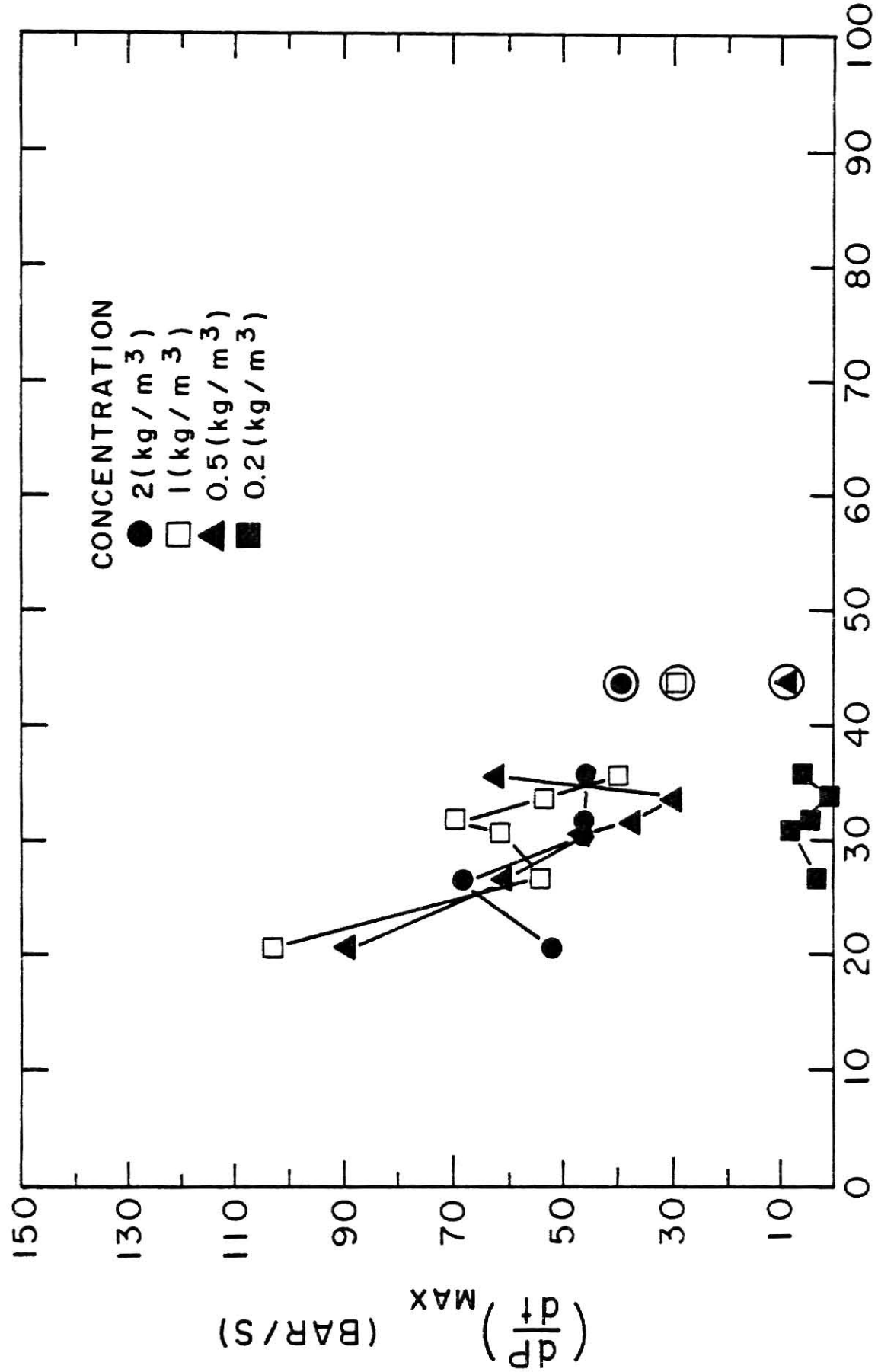

Fig. 5.29 The Relationship between the Maximum Rate of Pressure Rise and the Mass Mean Diameter for Wheat Dust

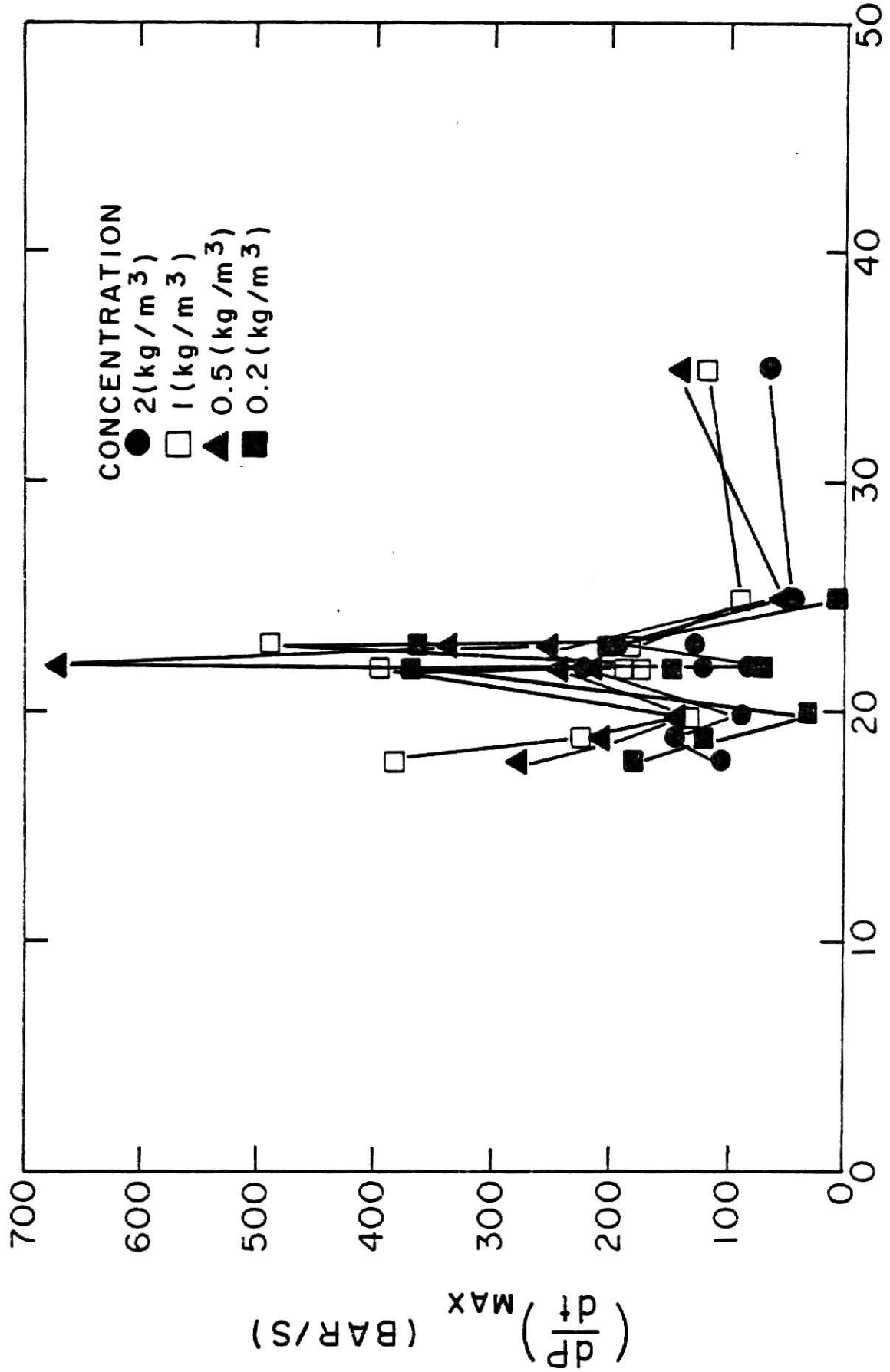

Fig. 5.30 The Relationship between the Maximum Rate of Pressure Rise and the Mass Mean Diameter for Cornstarch

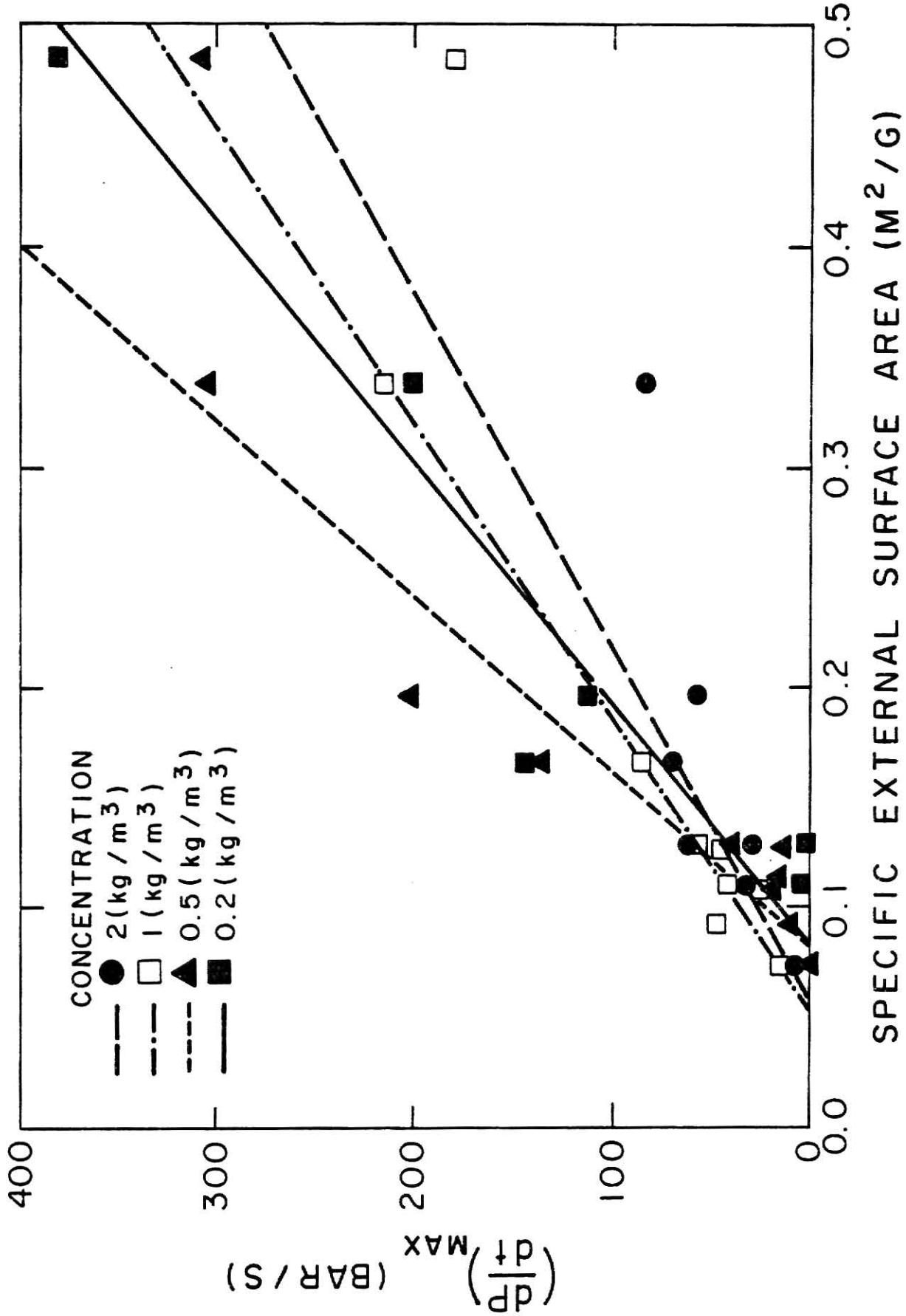

Fig. 5.31 The Relationship between the Maximum Rate of Pressure Rise and the Specific External Surface Area for Grain Sorghum Dust

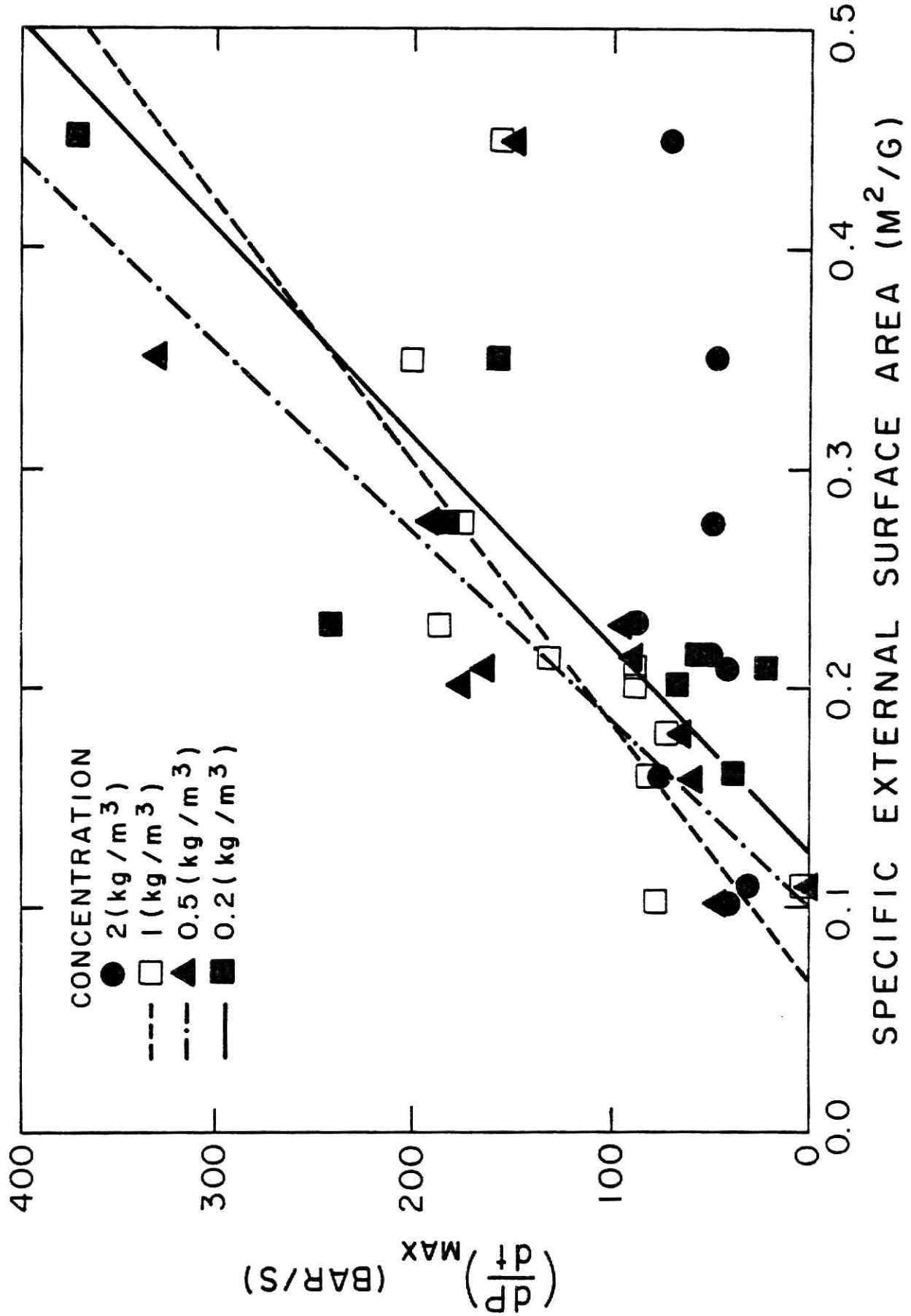

Fig. 5.32 The Relationship between the Maximum Rate of Pressure Rise and the Specific External Surface Area for Corn Dust

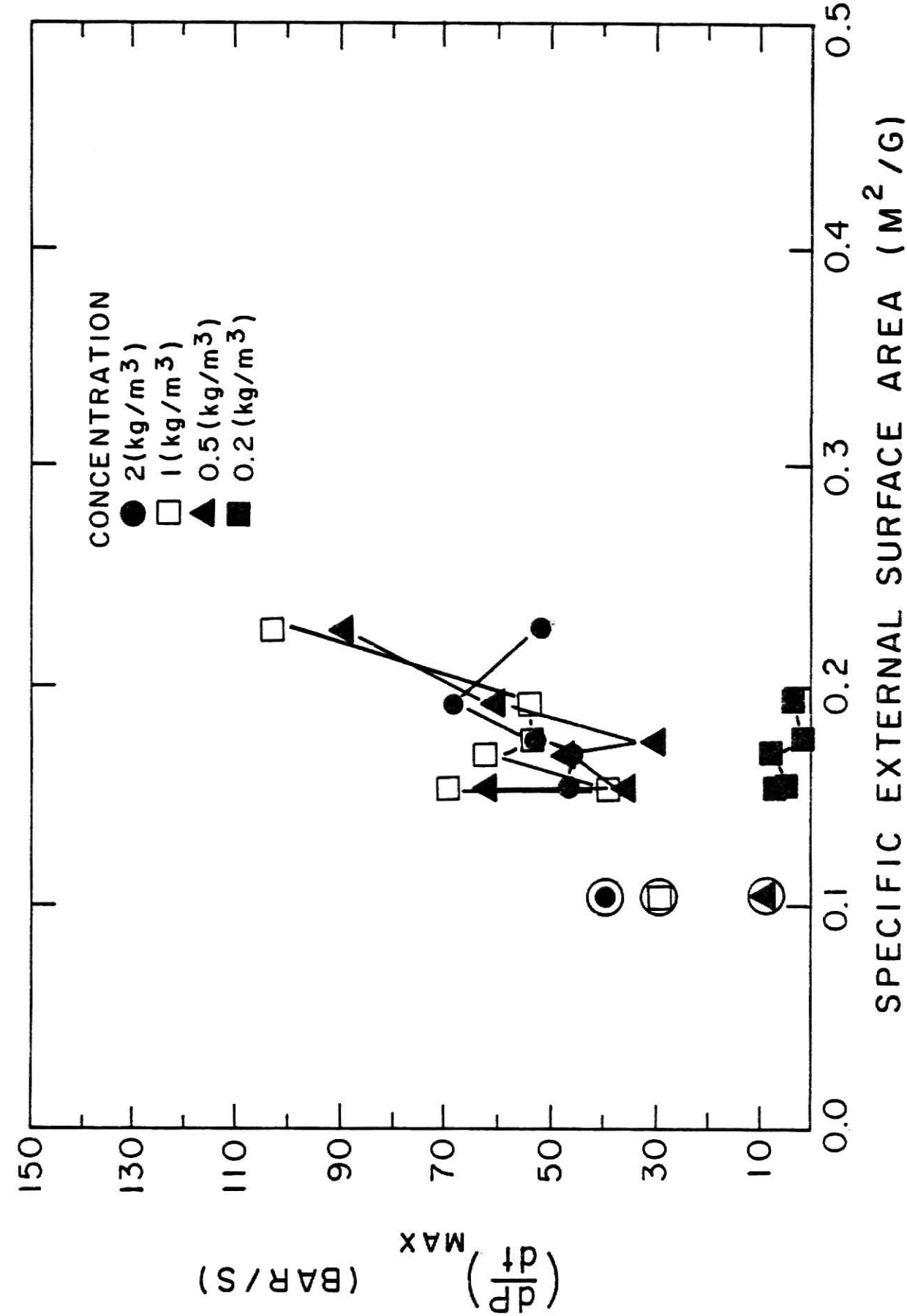

Fig. 5.33 The Relationship between the Maximum Rate of Pressure Rise and the Specific External Surface Area for Wheat Dust

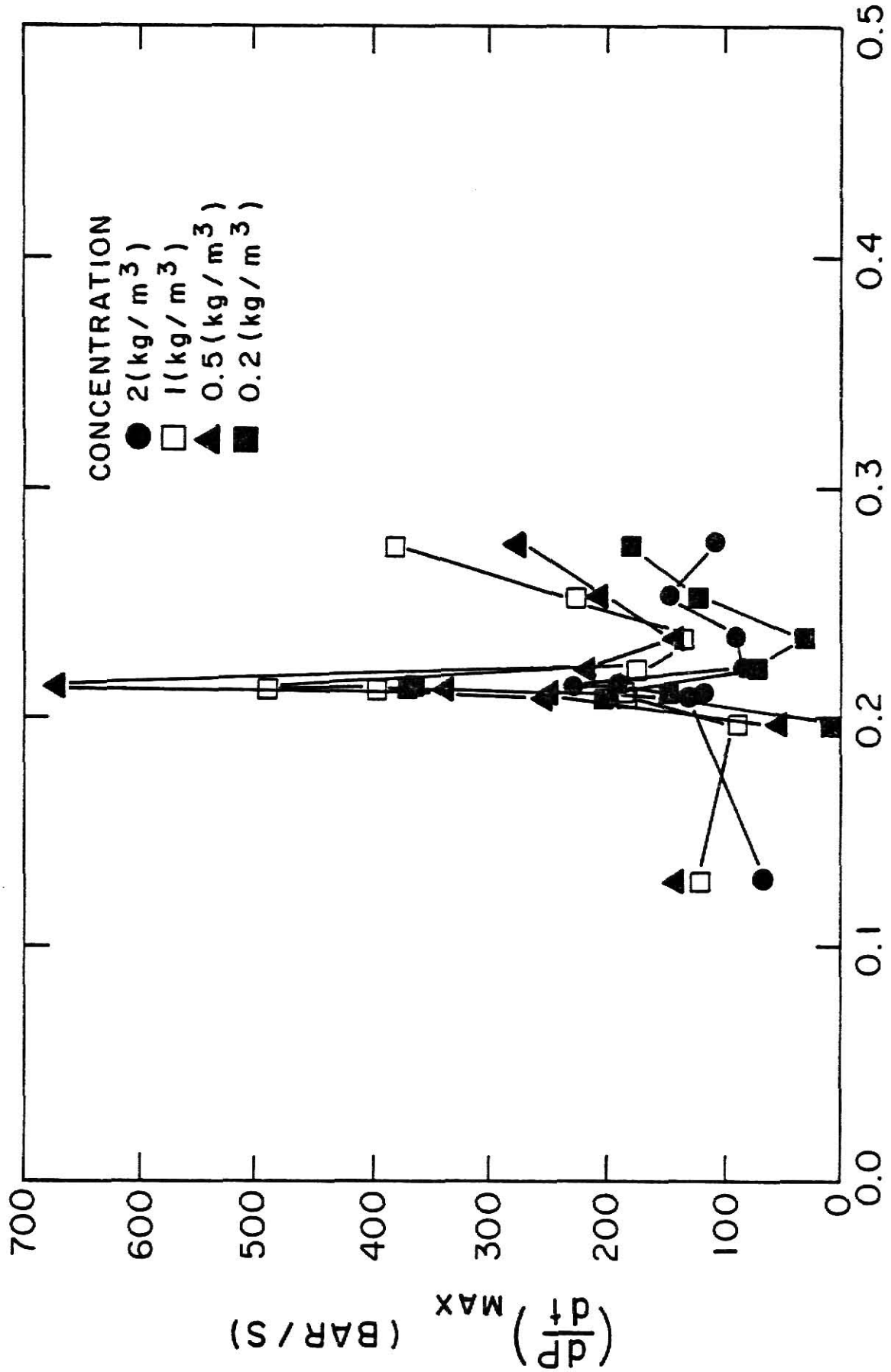

Fig. 5.34 The Relationship between the Maximum Rate of Pressure Rise and the Specific External Surface Area for Cornstarch

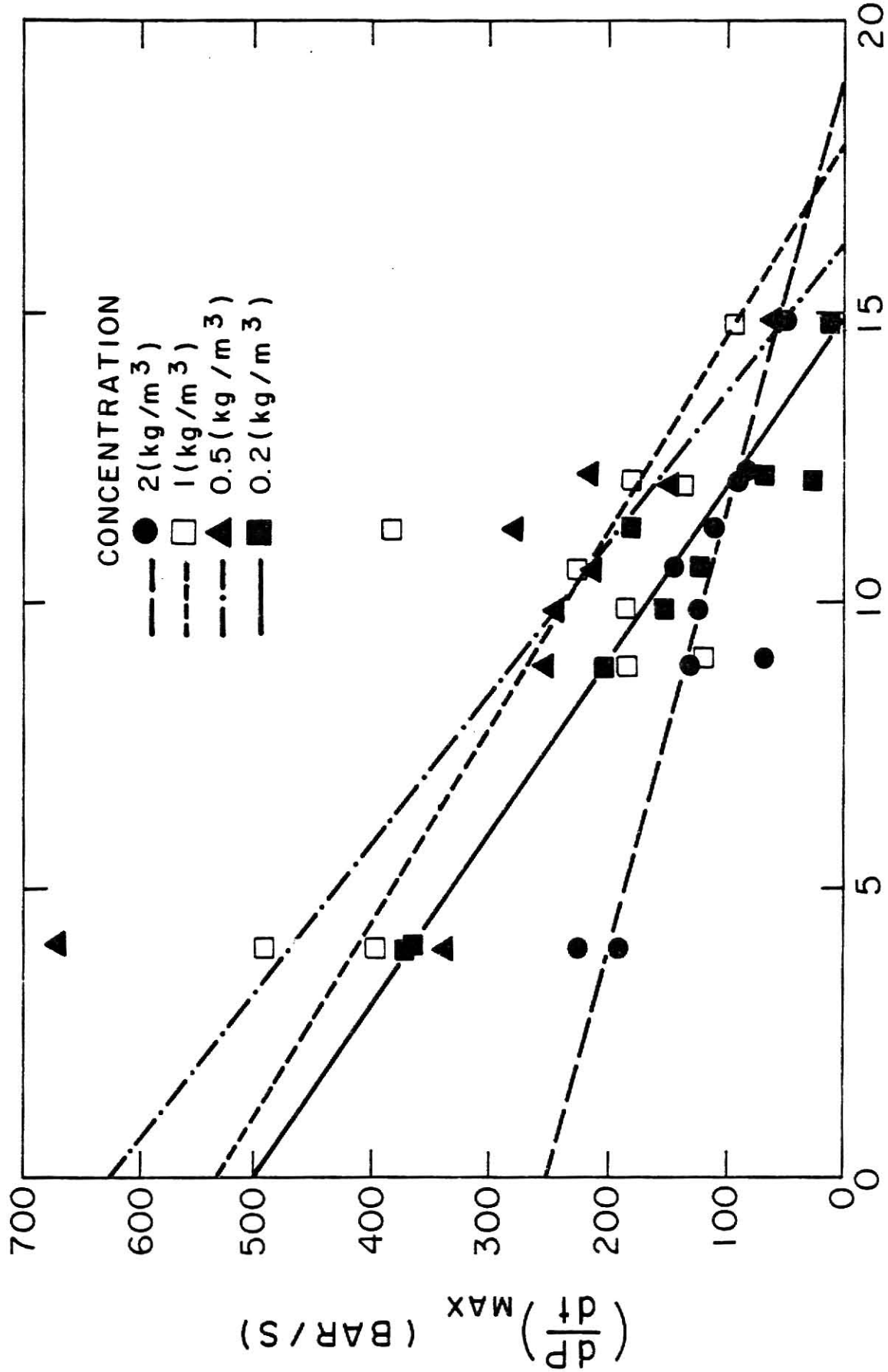

Fig. 5.35 The Relationship between the Maximum Rate of Pressure Rise and the Moisture Content for Cornstarch

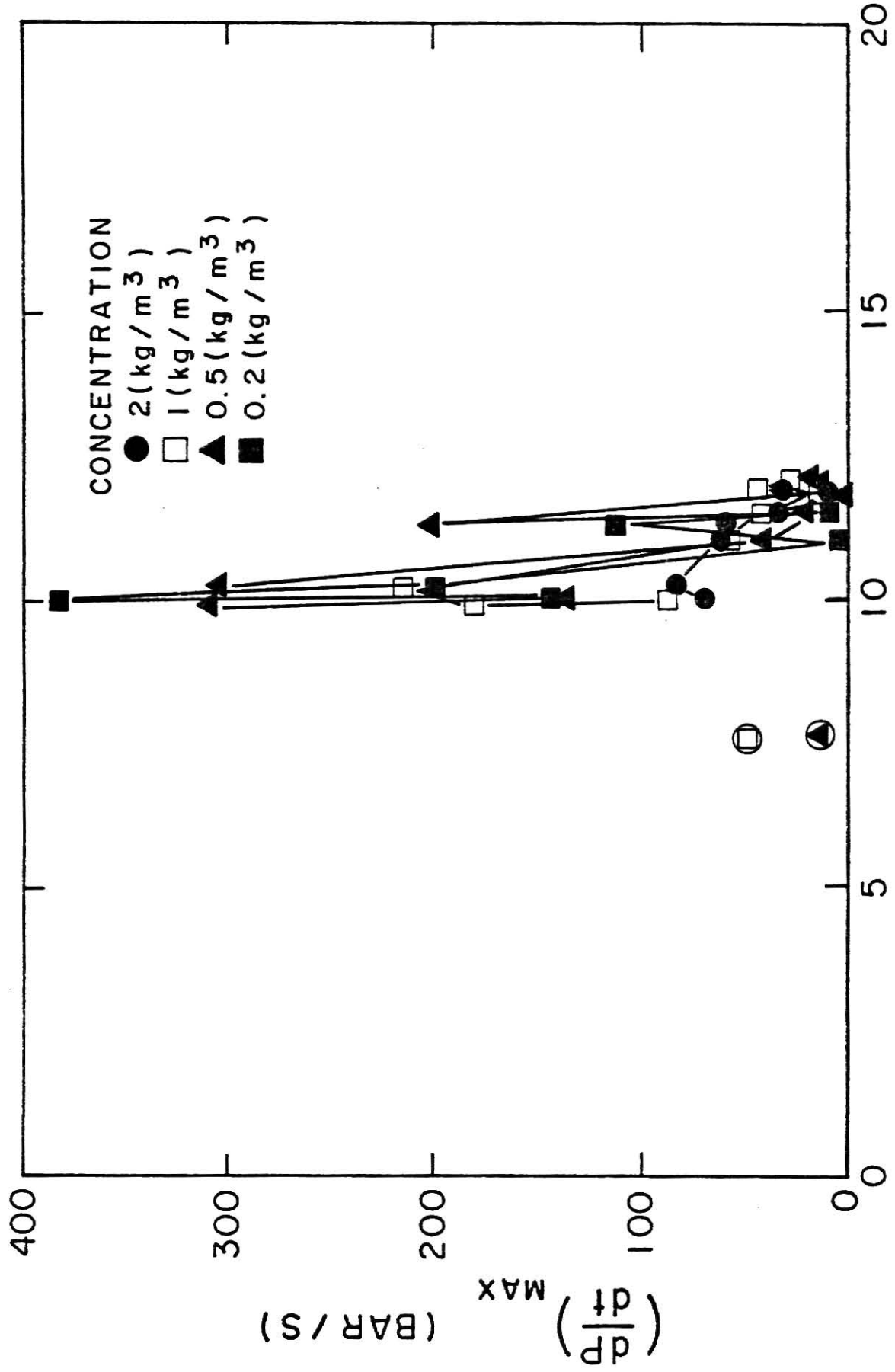

Fig. 5.36 The Relationship between the Maximum Rate of Pressure Rise and the Moisture Content for Grain Sorghum Dust

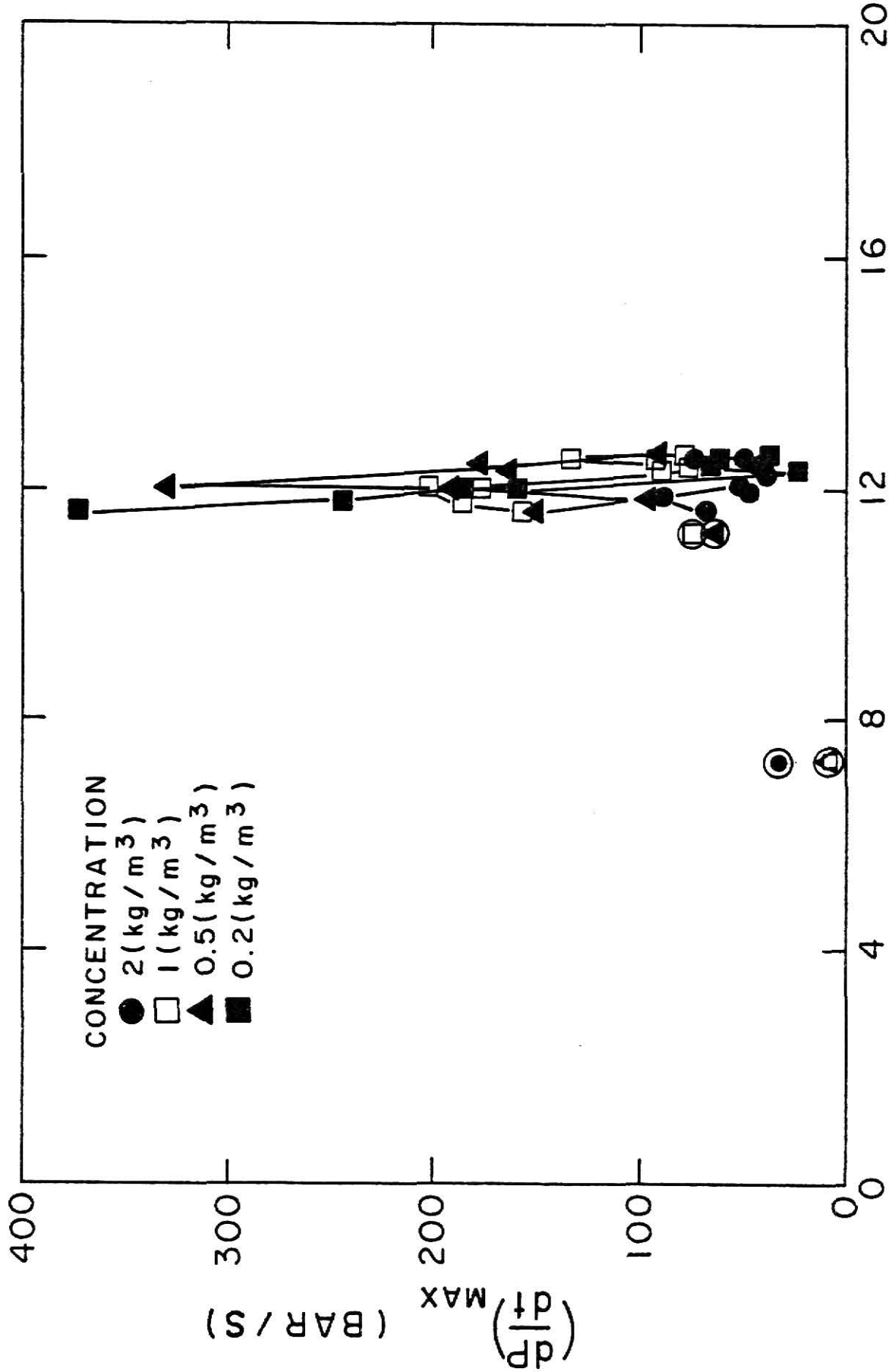

Fig. 5.37 The Relationship between the Maximum Rate of Pressure Rise and the Moisture Content for Corn Dust

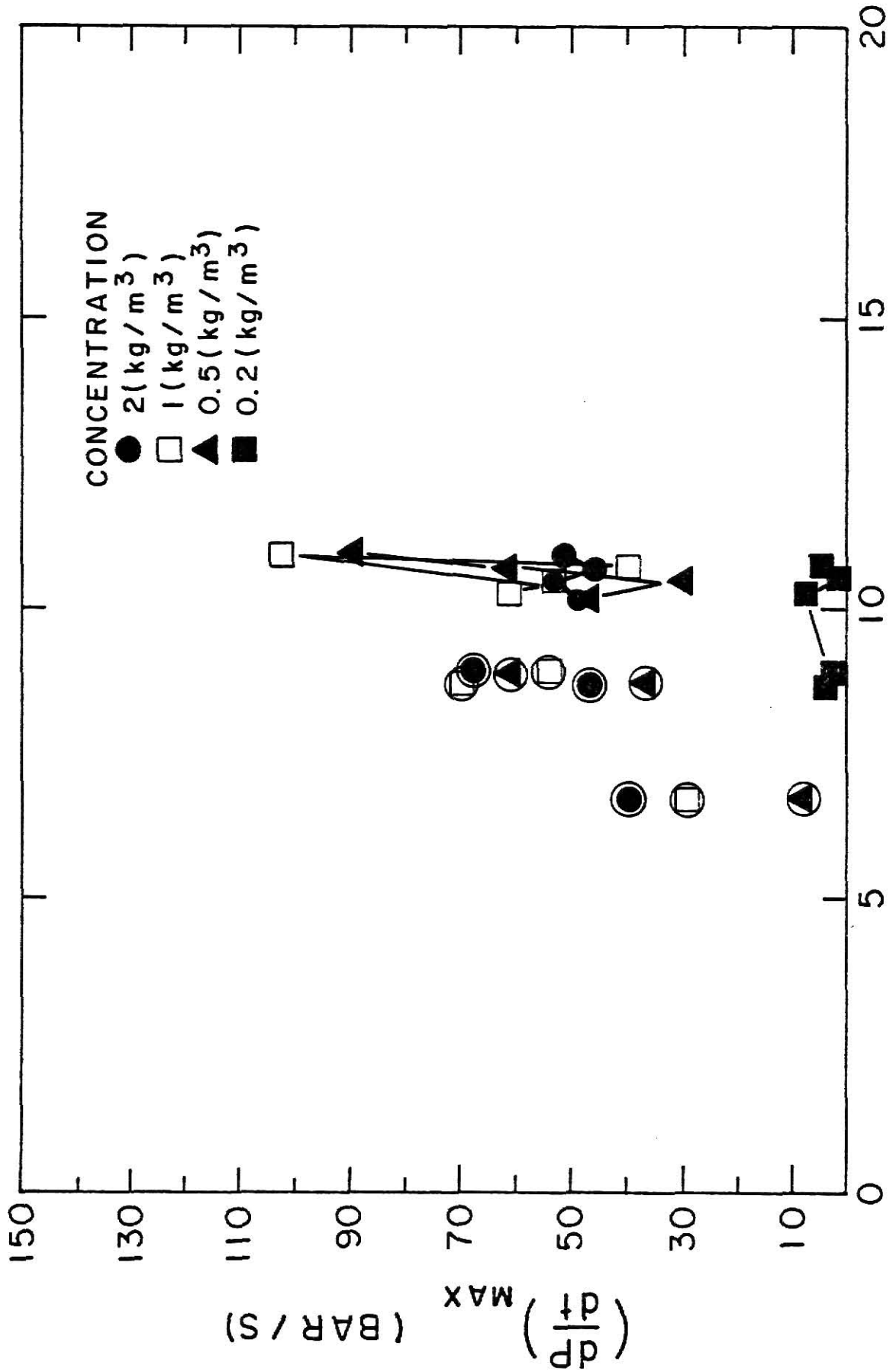

Fig. 5.38 The Relationship between the Maximum Rate of Pressure Rise and the Moisture Content for Wheat Dust

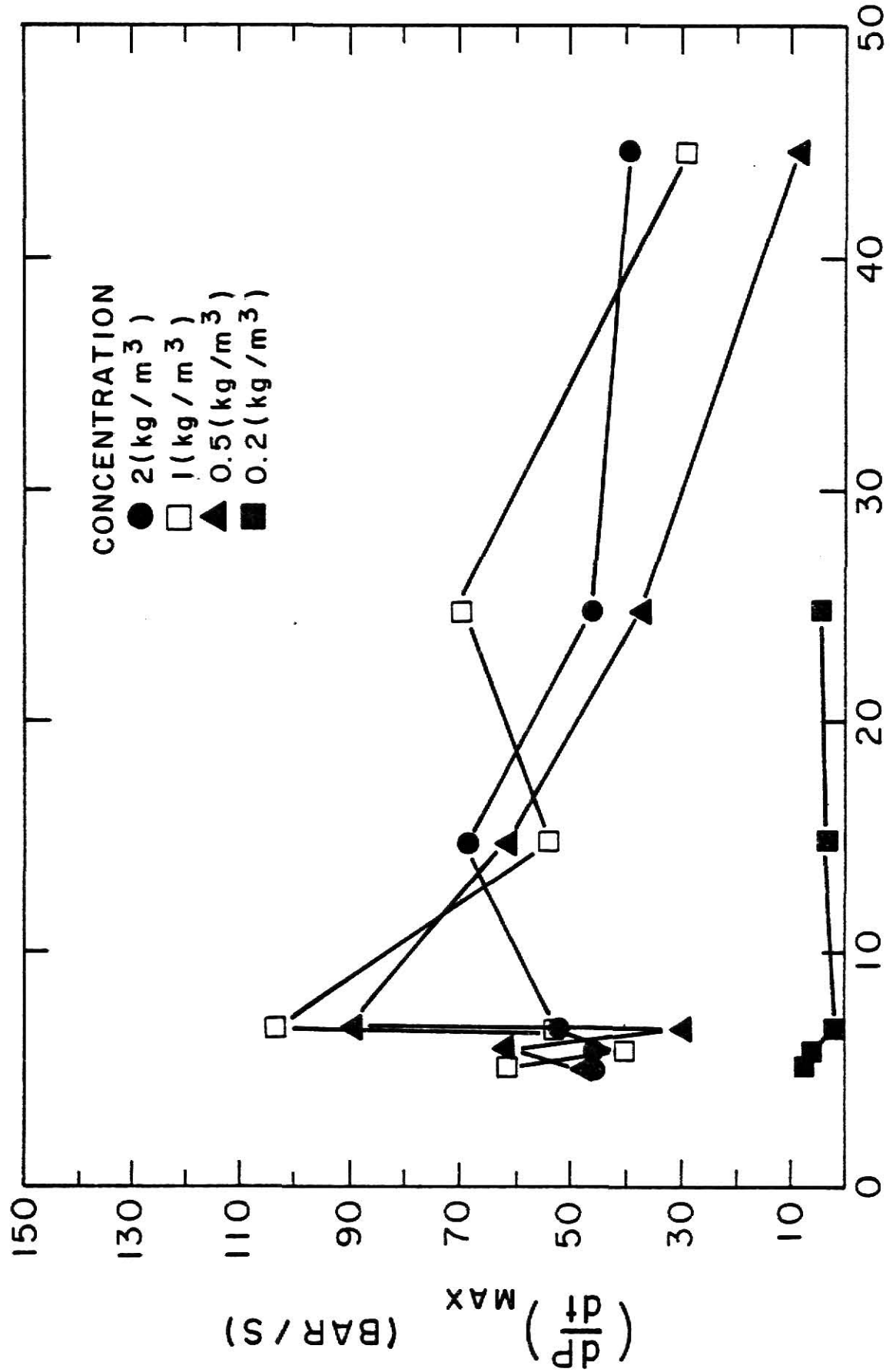

Fig. 5.39 The Relationship between the Maximum Rate of Pressure Rise and the Ash Content for Wheat Dust

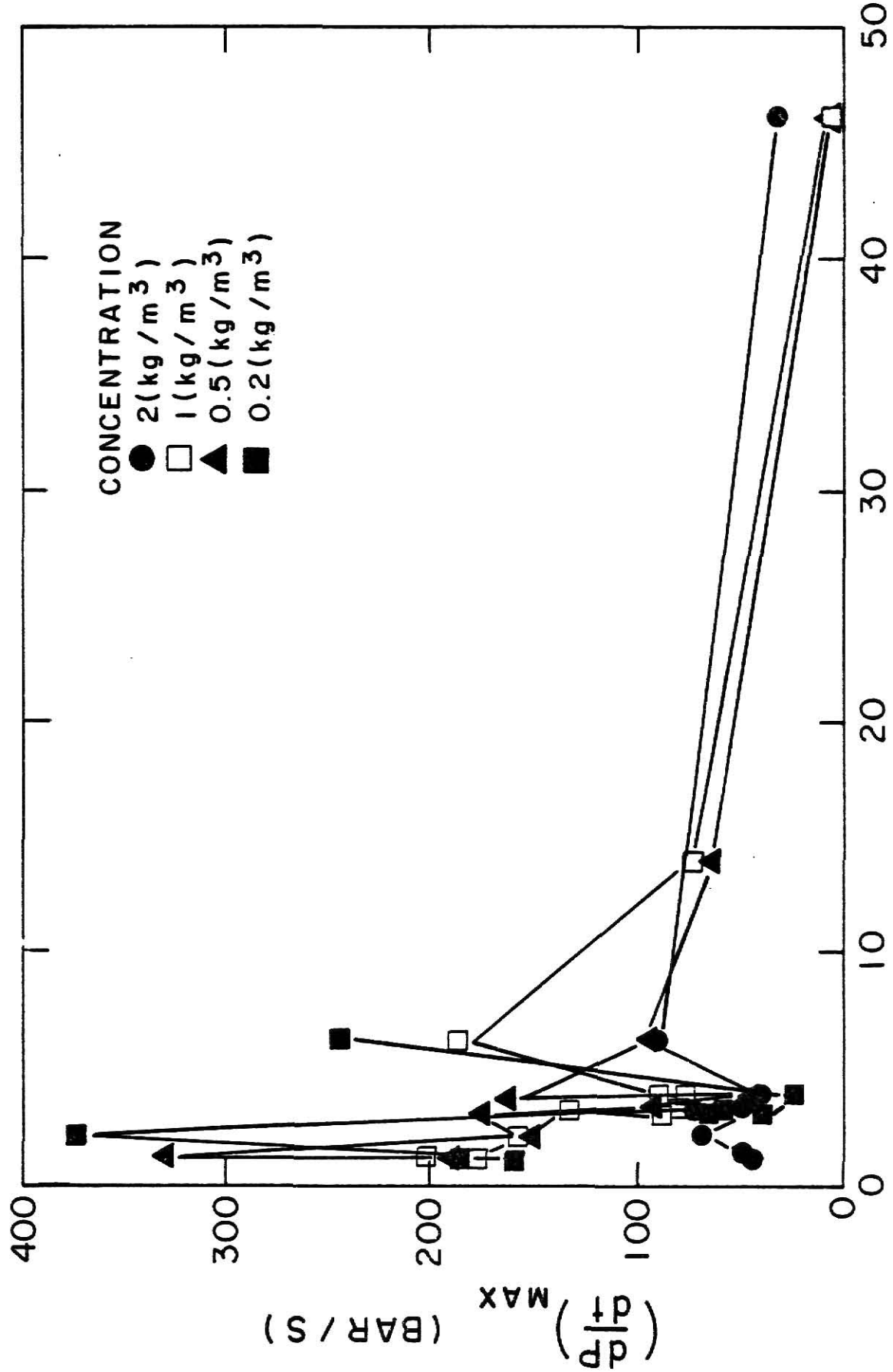

Fig. 5.40 The Relationship between the Maximum Rate of Pressure Rise and the Ash Content for Corn Dust

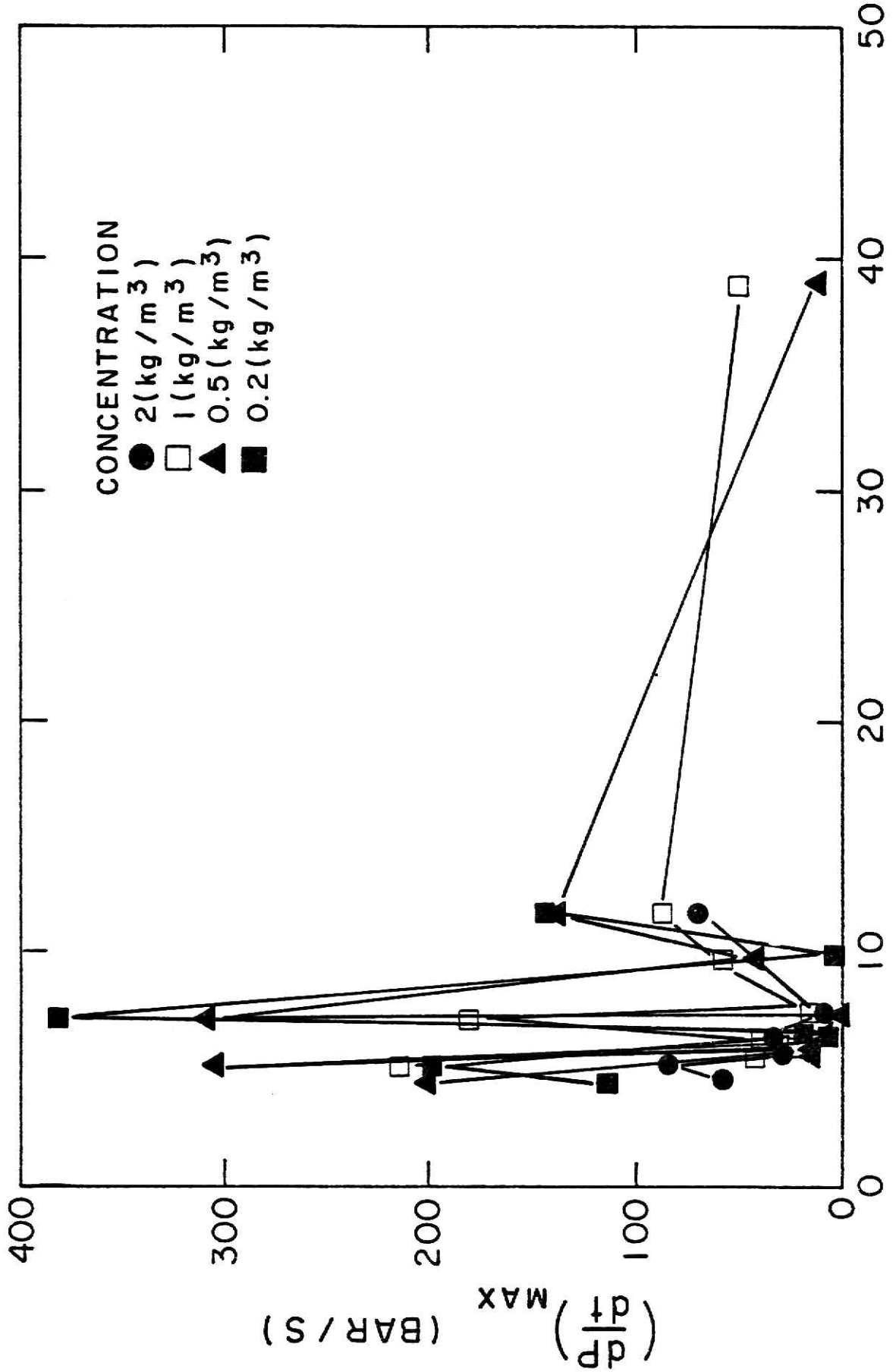

Fig. 5.41 The Relationship between the Maximum Rate of Pressure Rise and the Ash Content for Grain Sorghum Dust

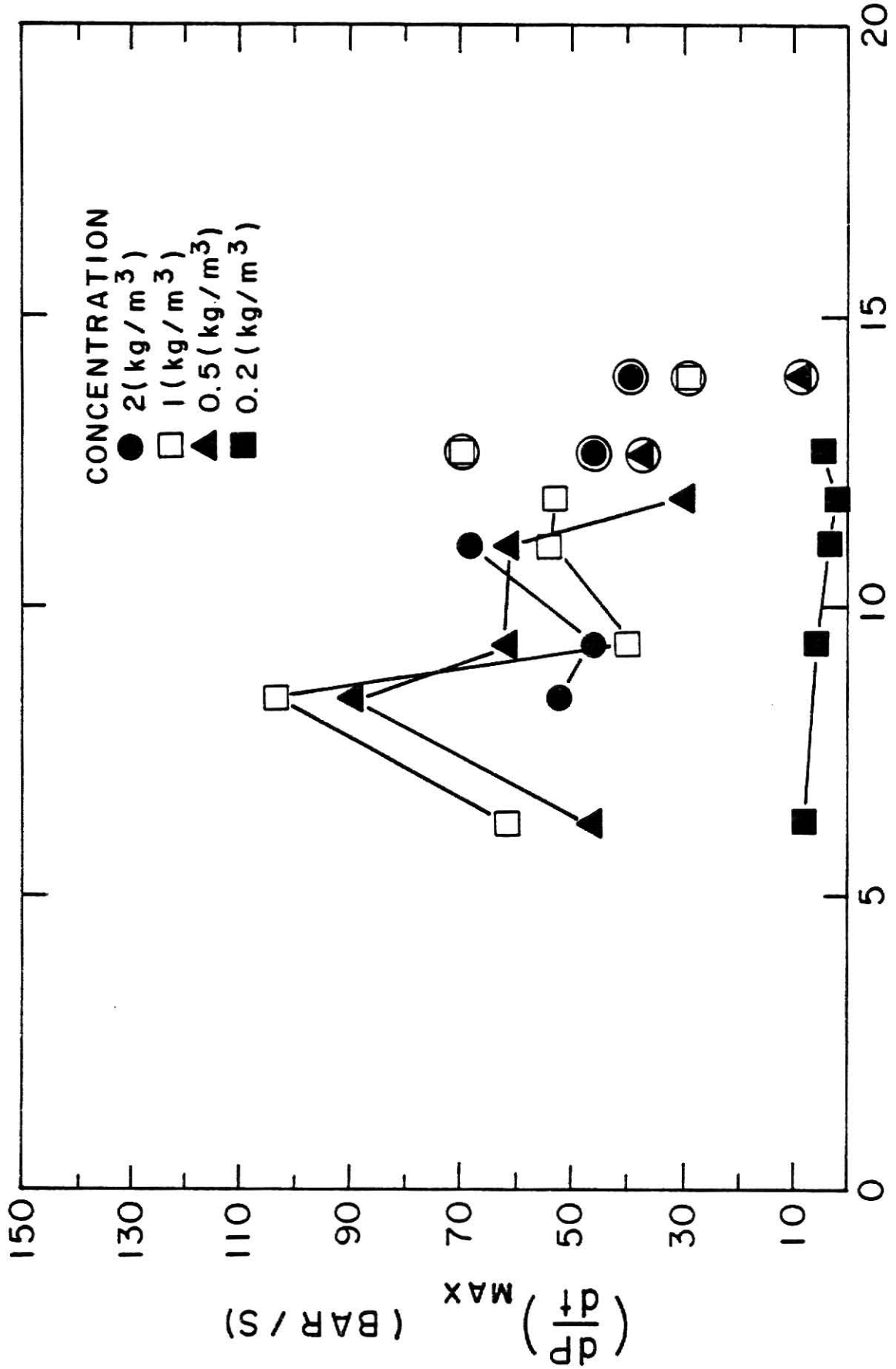

Fig. 5.42 The Relationship between the Maximum Rate of Pressure Rise and the Protein Content for Wheat Dust

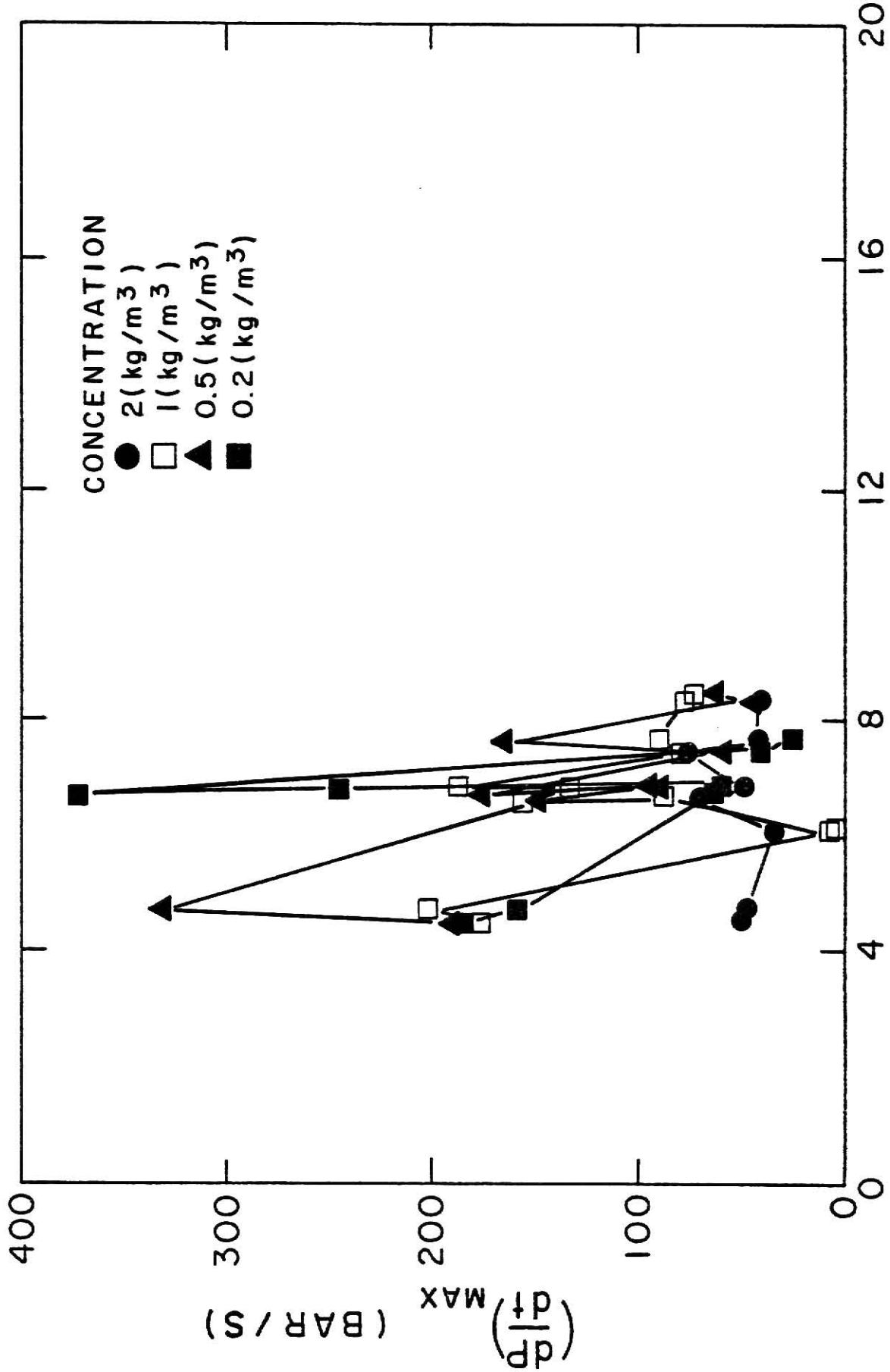

Fig. 5.43 The Relationship between the Maximum Rate of Pressure Rise and the Protein Content for Corn Dust

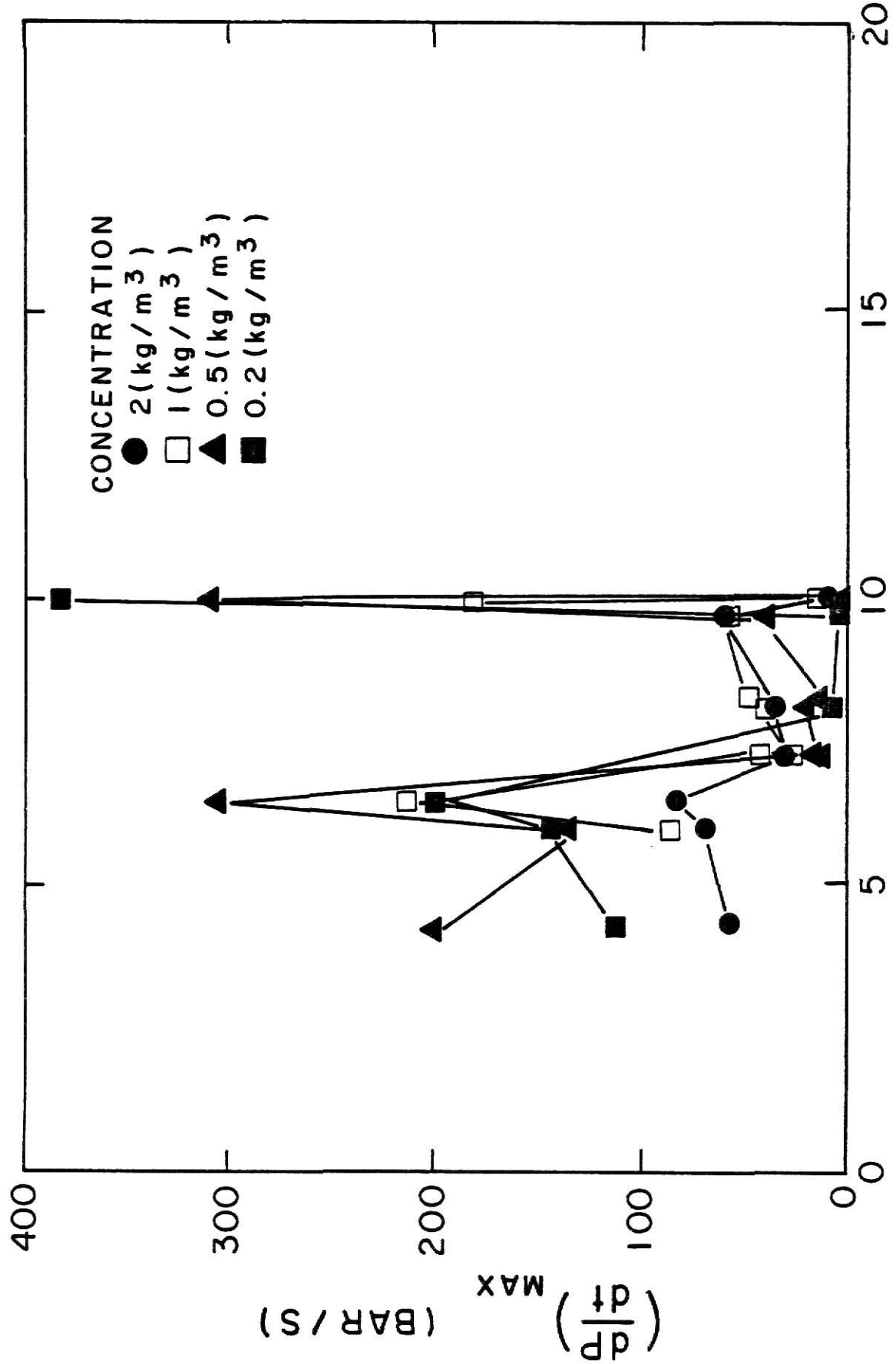

Fig. 5.44 The Relationship between the Maximum Rate of Pressure Rise and the Protein Content for Grain Sorghum Dust

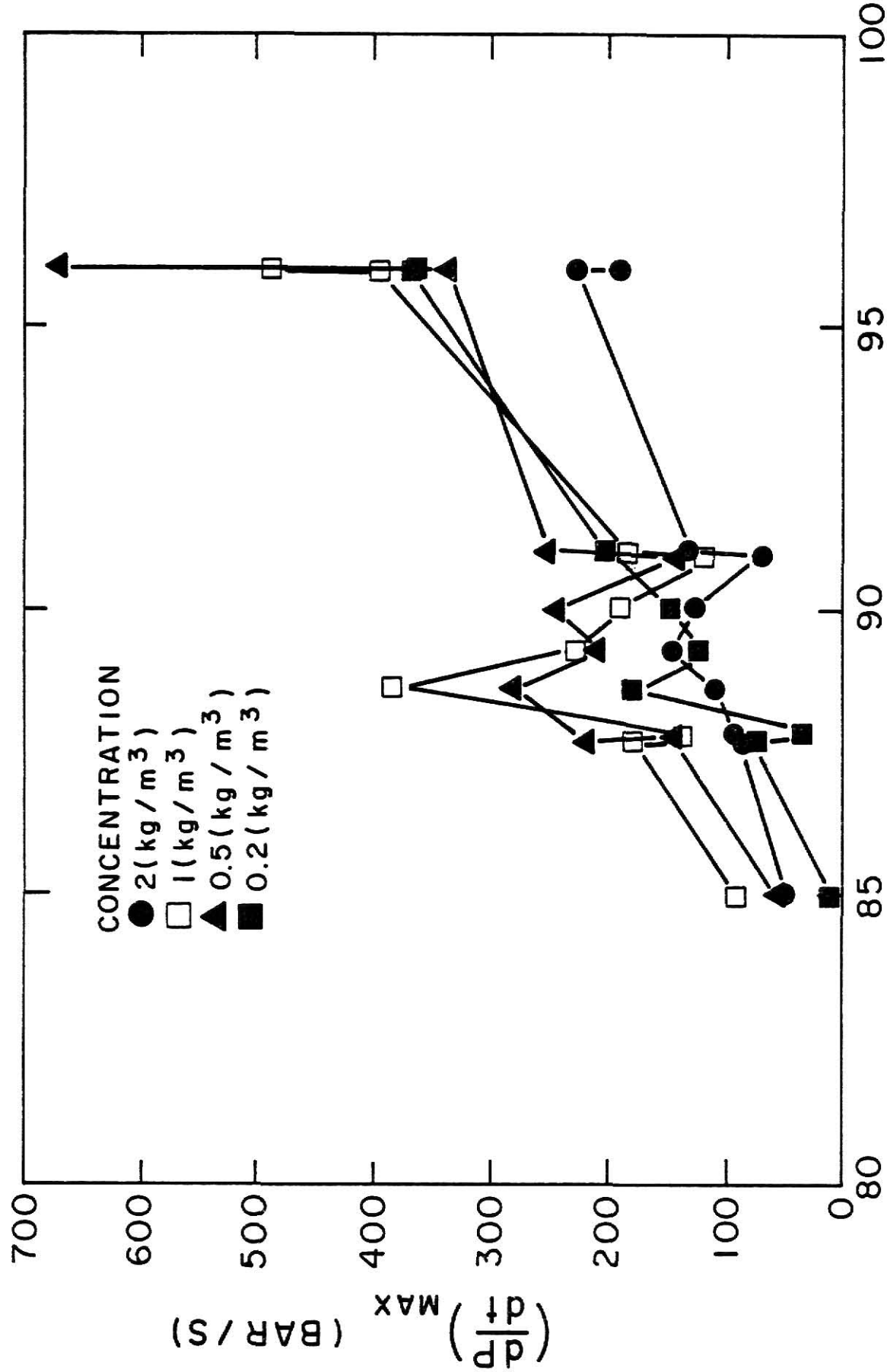

Fig. 5.45 The Relationship between the Maximum Rate of Pressure Rise and the Starch and Fiber Content for Cornstarch

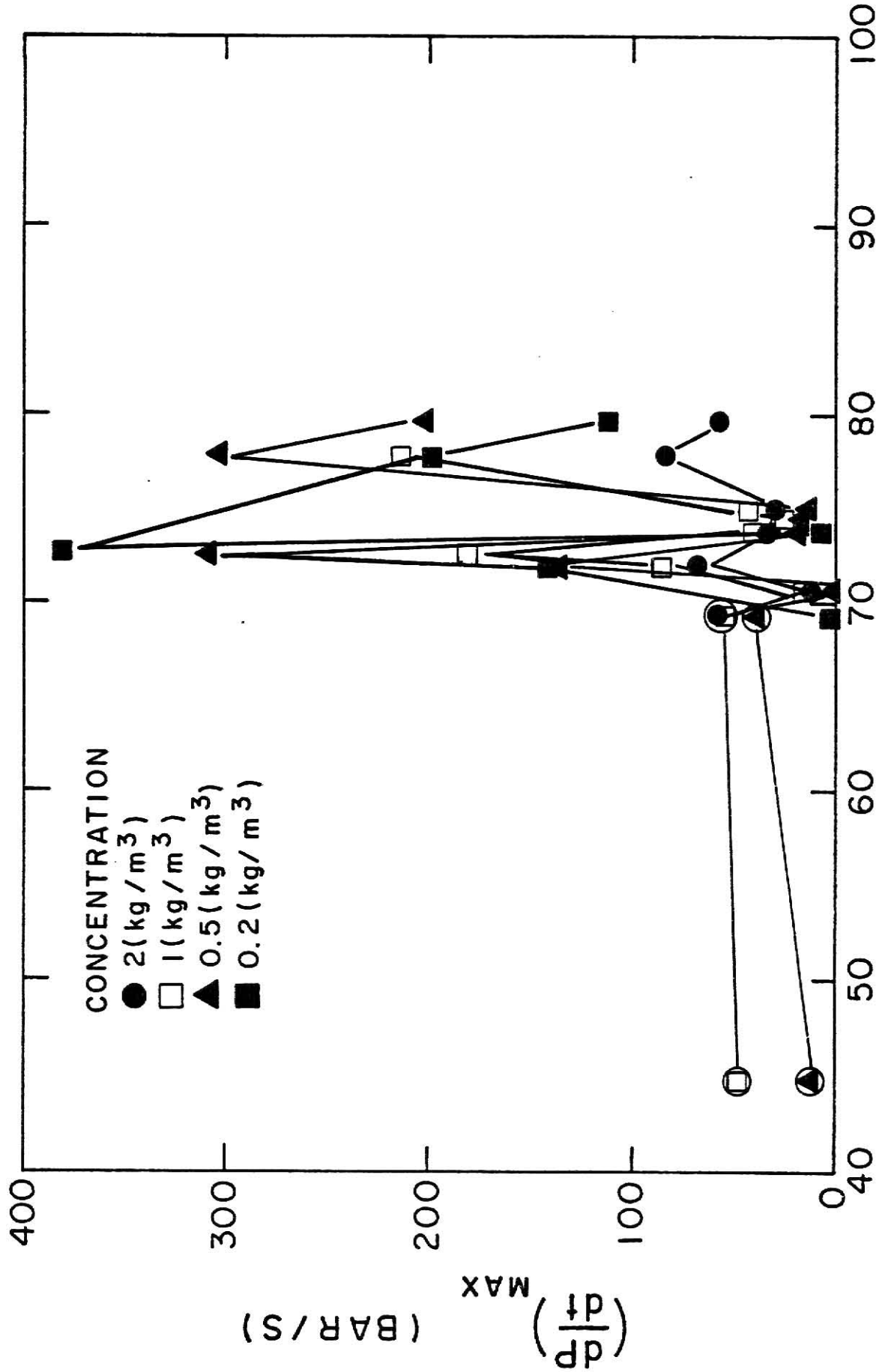

Fig. 5.46 The Relationship between the Maximum Rate of Pressure Rise and the Starch and Fiber Content for Wheat Dust

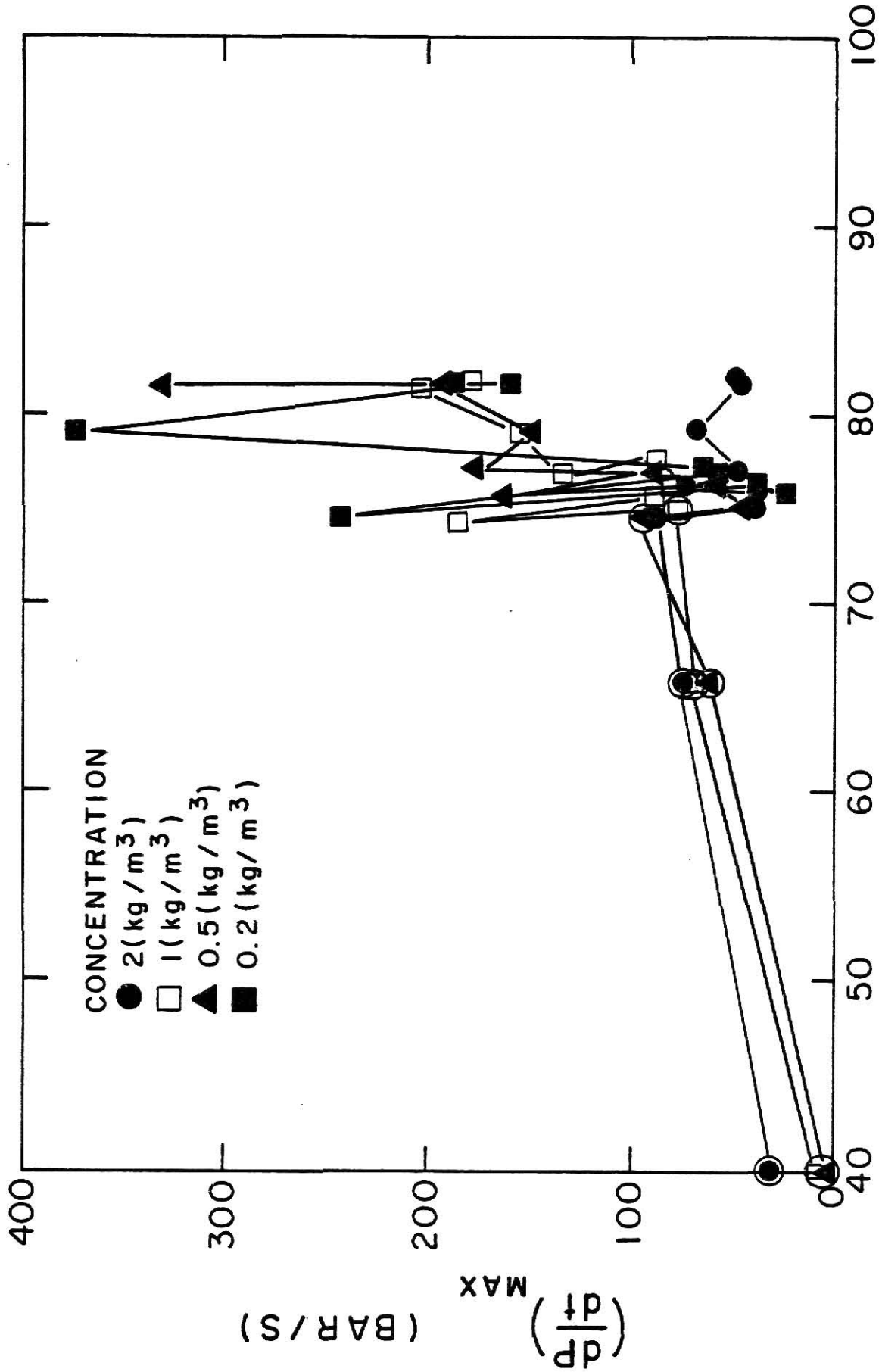

Fig. 5.47 The Relationship between the Maximum Rate of Pressure Rise and the Starch and Fiber Content for Grain Sorghum Dust

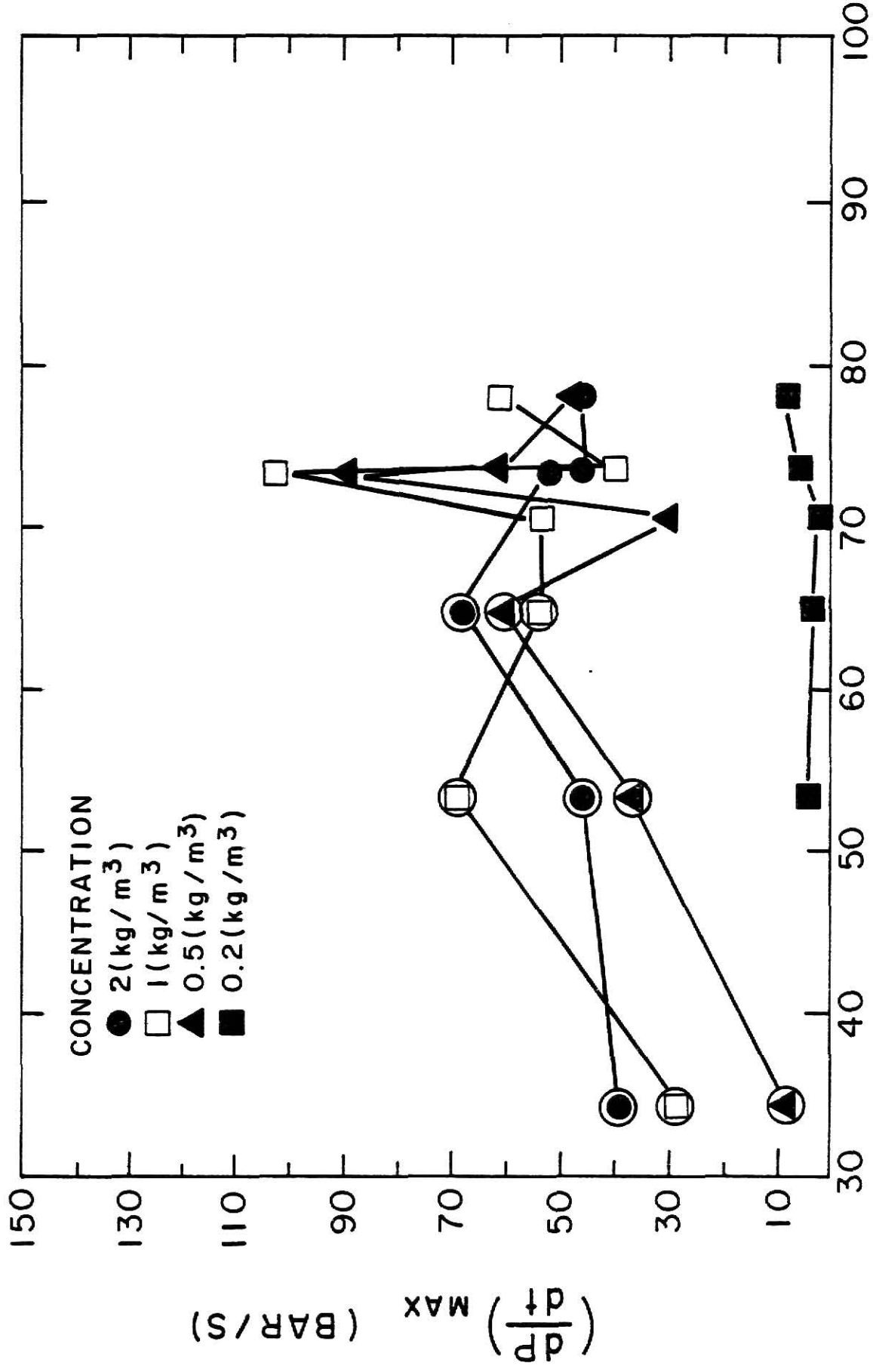

Fig. 5.48 The Relationship between the Maximum Rate of Pressure Rise and the Starch and Fiber Content for Corn Dust

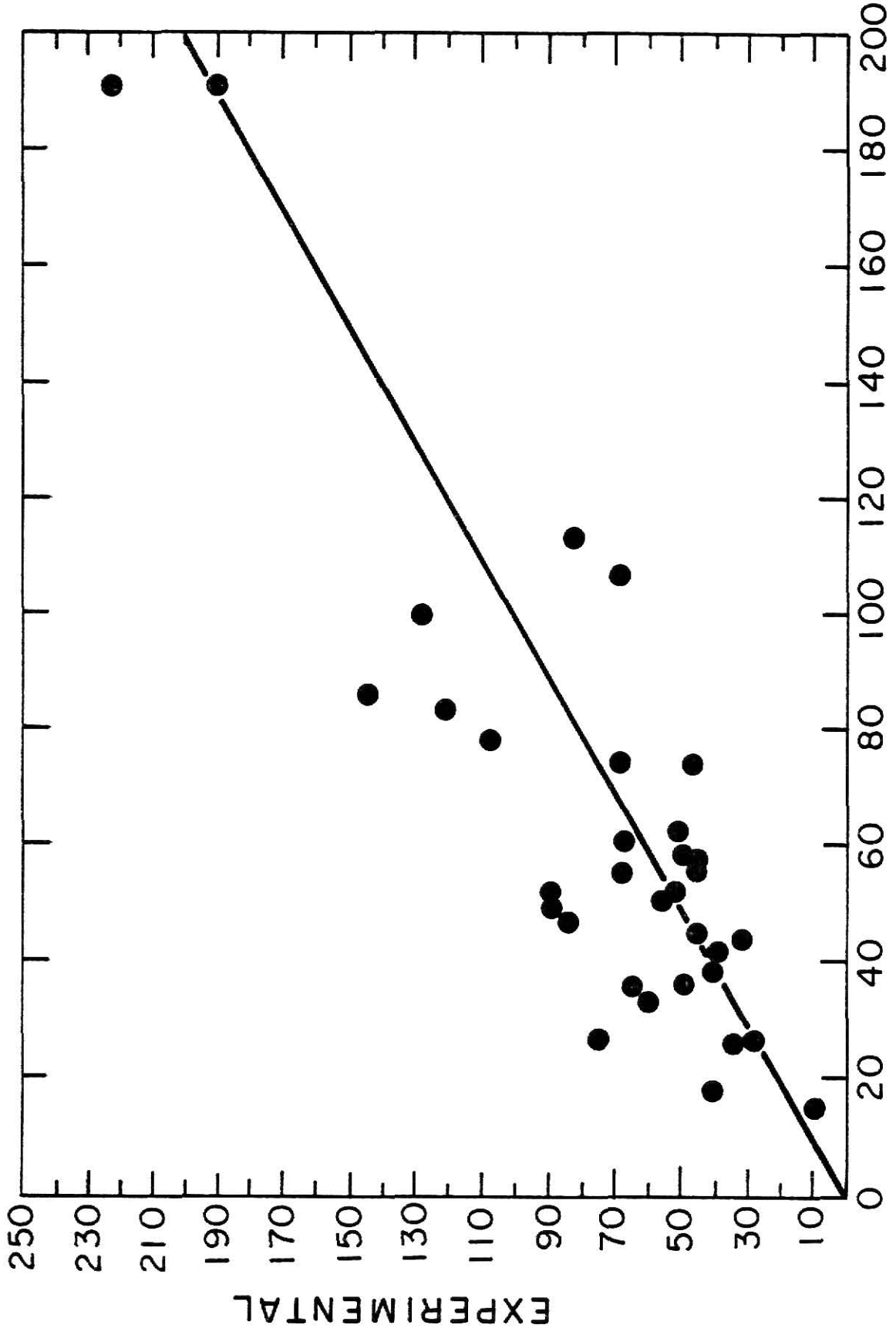

Fig. 5.49 The Comparison between the Experimentally Determined Values of the Maximum Rate of Pressure Rise and Those Predicted by Eckhoff's Model for Concentration 2.0 kg/m^3

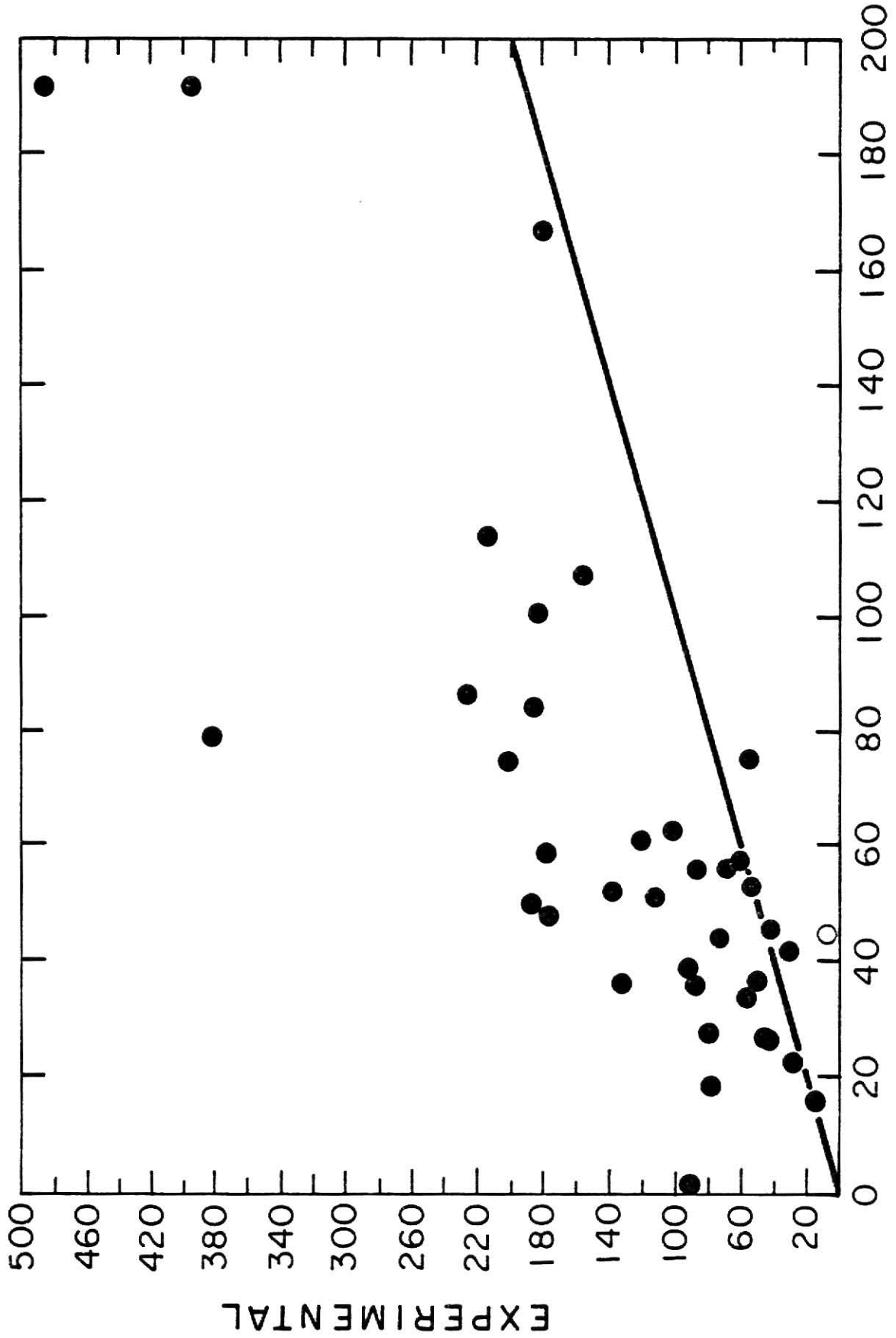

Fig. 5.50 The Comparison between the Experimentally Determined Values of the Maximum Rate of Pressure Rise and Those Predicted by Eckhoff's Model for Concentration of 1.0 kg/m^3

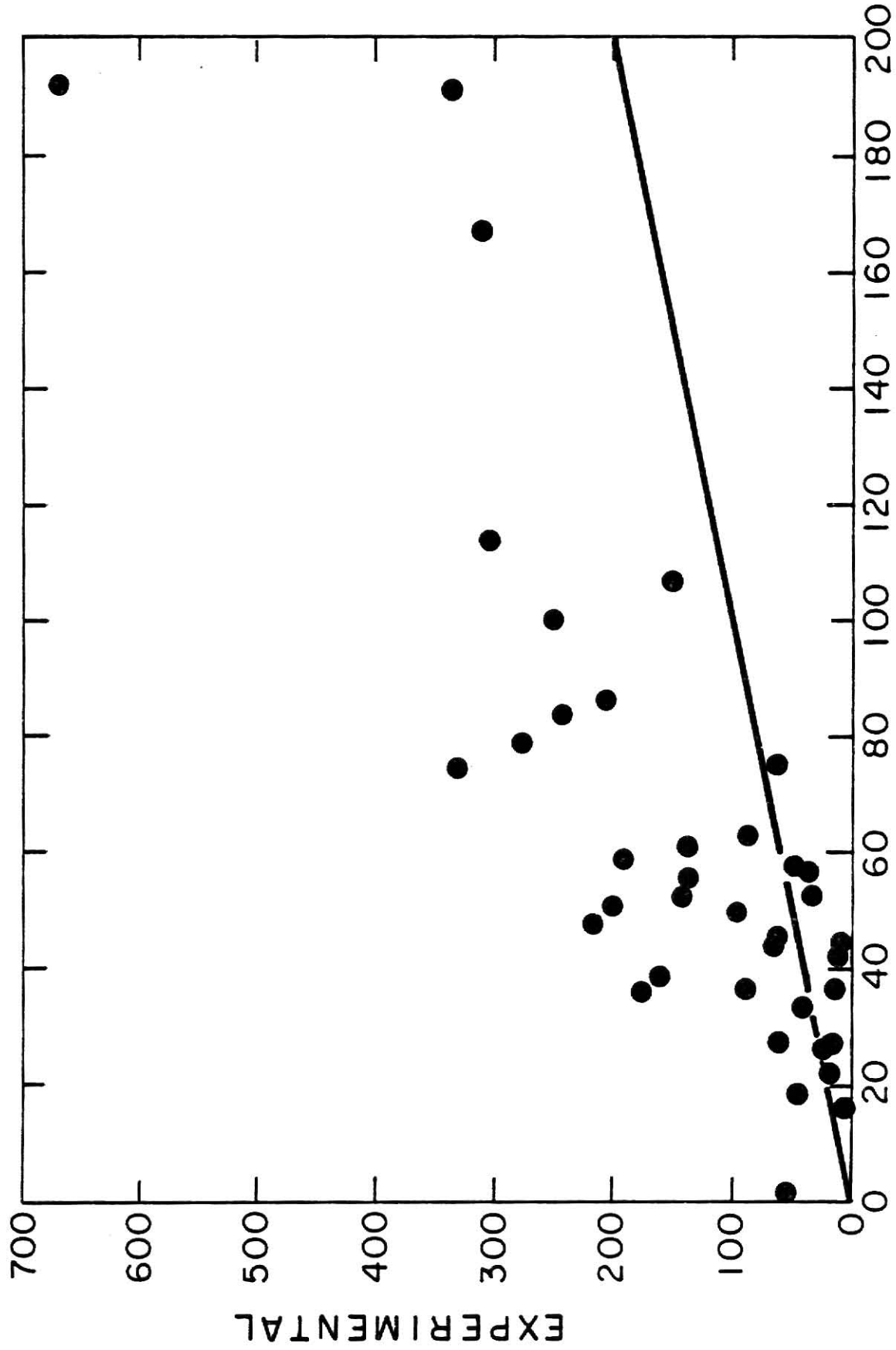

Fig. 5.51 The Comparison between the Experimentally Determined Values of the Maximum Rate of Pressure Rise and Those Predicted by Eckhoff's Model for Concentration of 0.5 kg/m^3

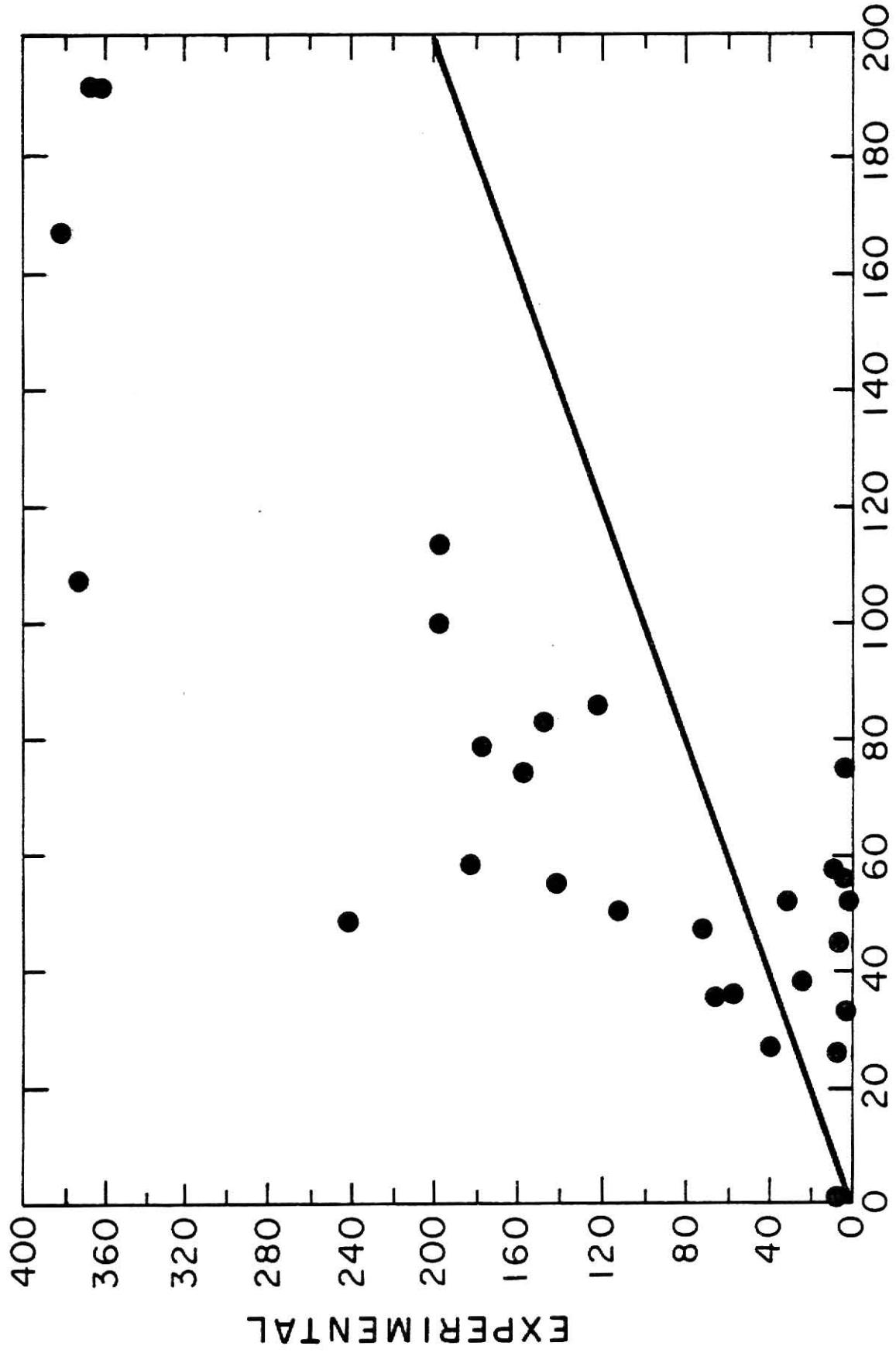

Fig. 5.52 The Comparison between the Experimentally Determined Values of the Maximum Rate of Pressure Rise and Those Predicted by Eckhoff's Model for Concentration of 0.2 kg/m^3

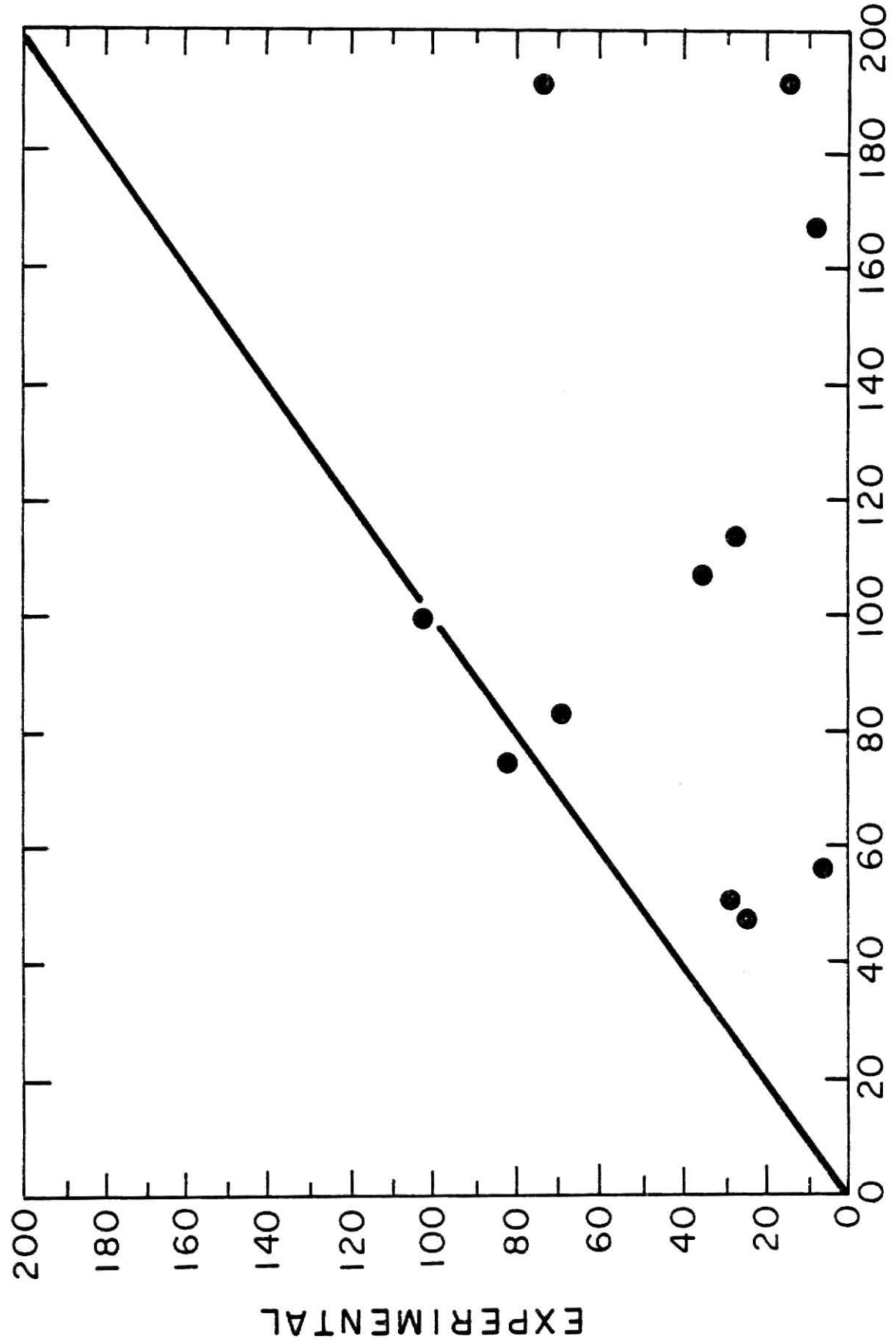

Fig. 5.53 The Comparison between the Experimentally Determined Values of the Maximum Rate of Pressure Rise and Those Predicted by Eckhoff's Model for Concentration of 0.1 kg/m^3

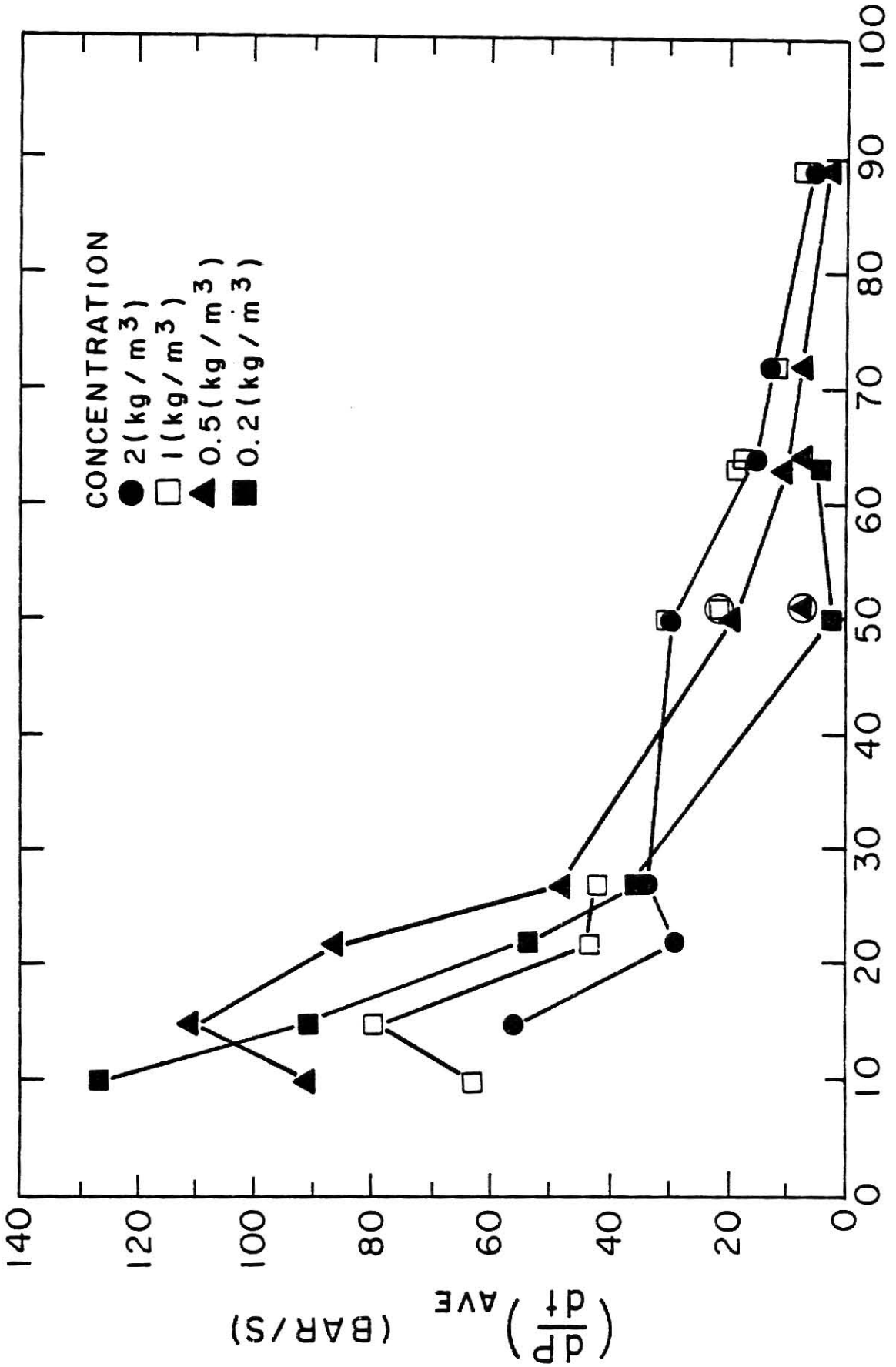

Fig. 5.54 The Relationship between the Average Rate of Pressure Rise and the Mass Mean Diameter for Grain Sorghum Dust

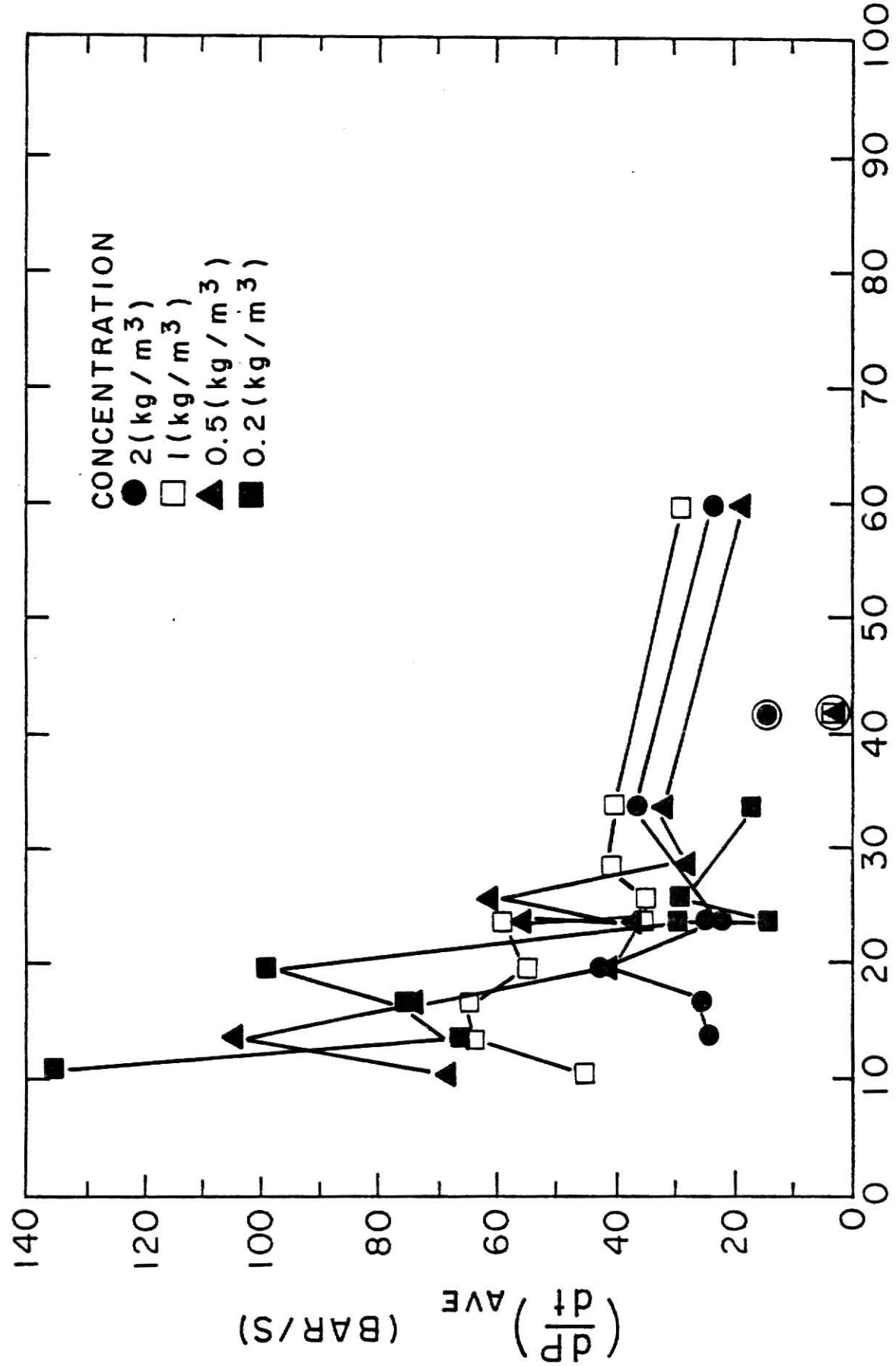

Fig. 5.55 The Relationship between the Average Rate of Pressure Rise and the Mass Mean Diameter for Corn Dust

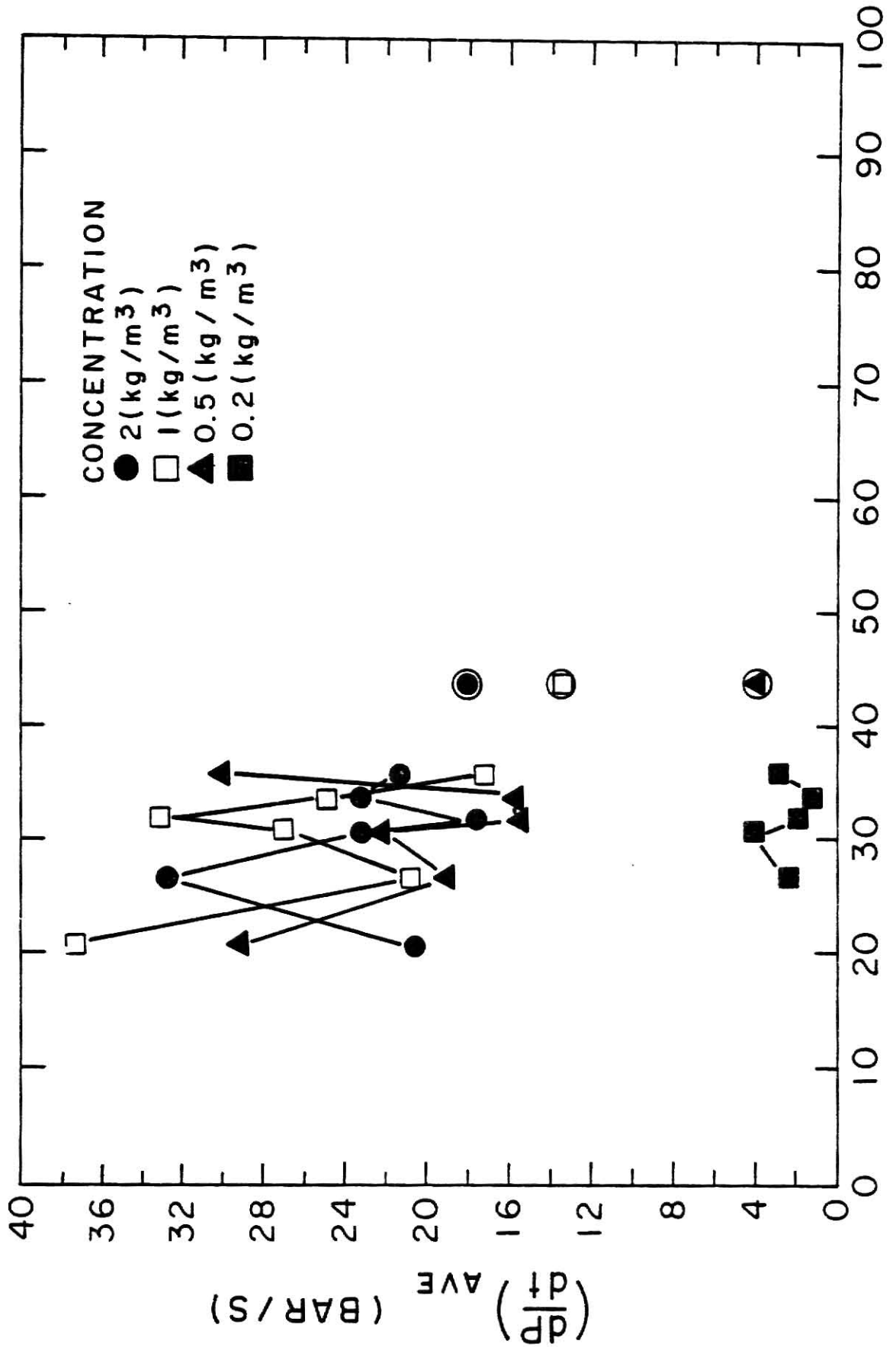

Fig. 5.56 The Relationship between the Average Rate of Pressure Rise and the Mass Mean Diameter for Wheat Dust

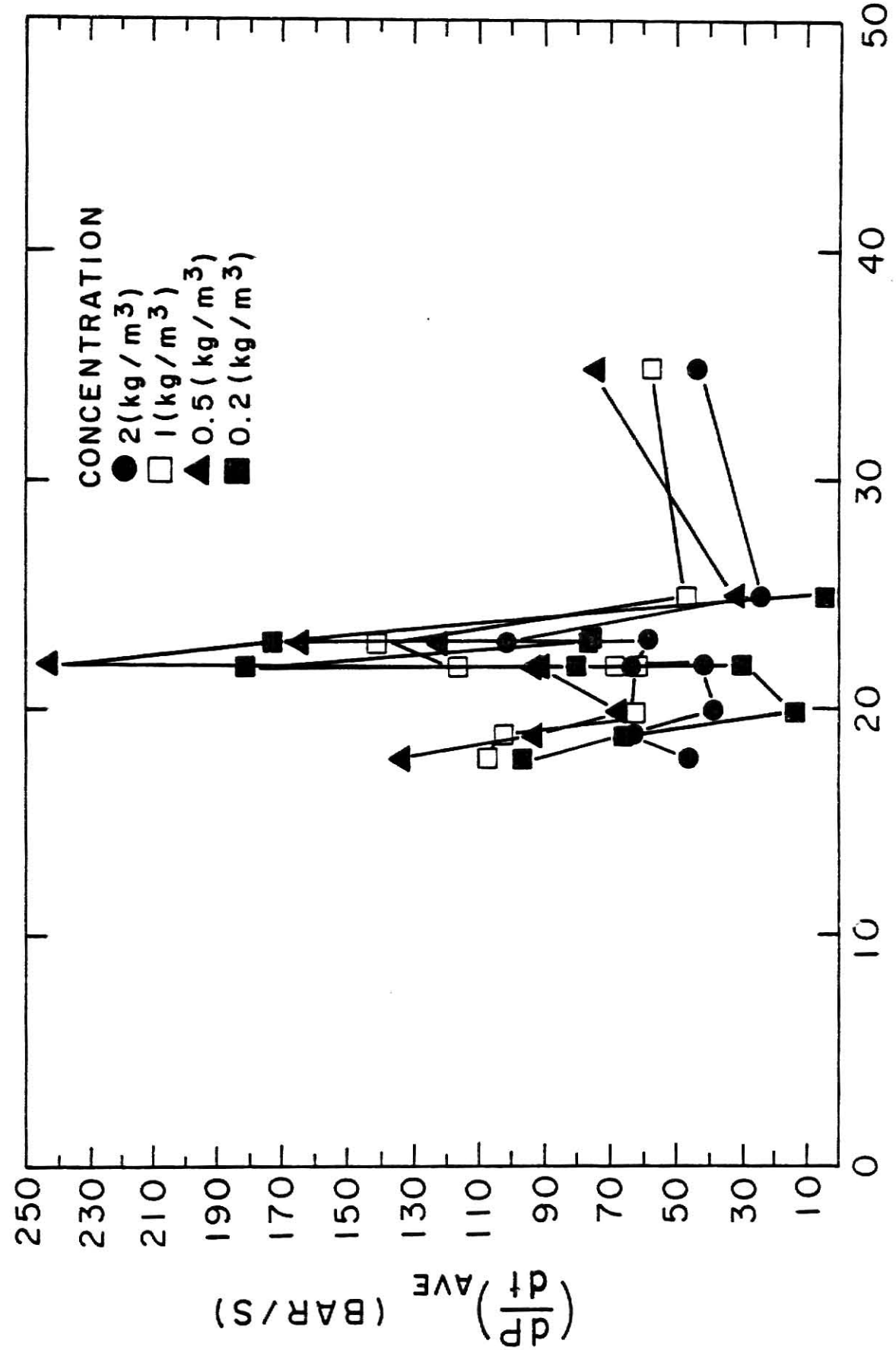

Fig. 5.57 The Relationship between the Average Rate of Pressure Rise and the Mass Mean Diameter for Cornstarch

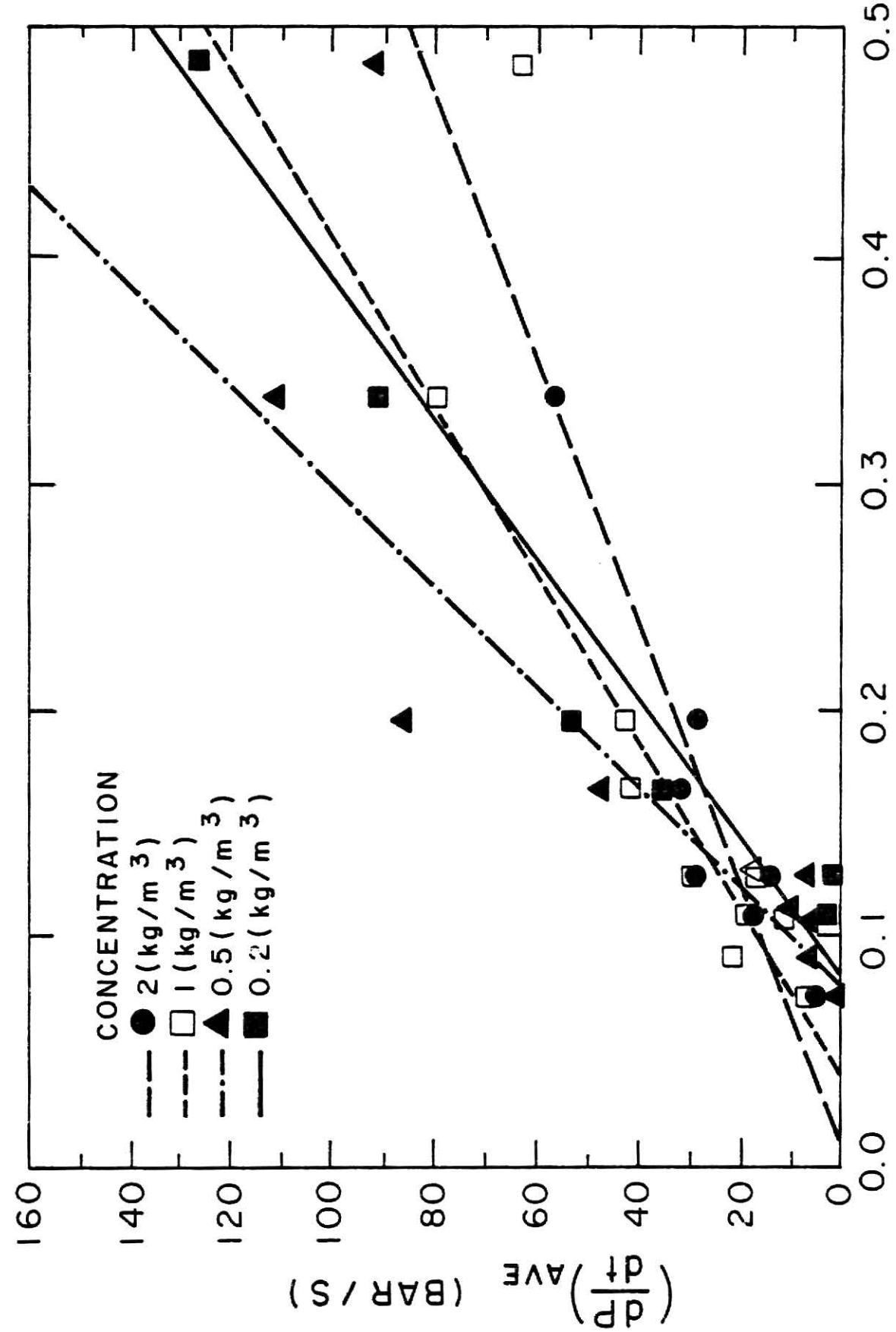

Fig. 5.58 The Relationship between the Average Rate of Pressure Rise and the Specific External Surface Area for Grain Sorghum Dust

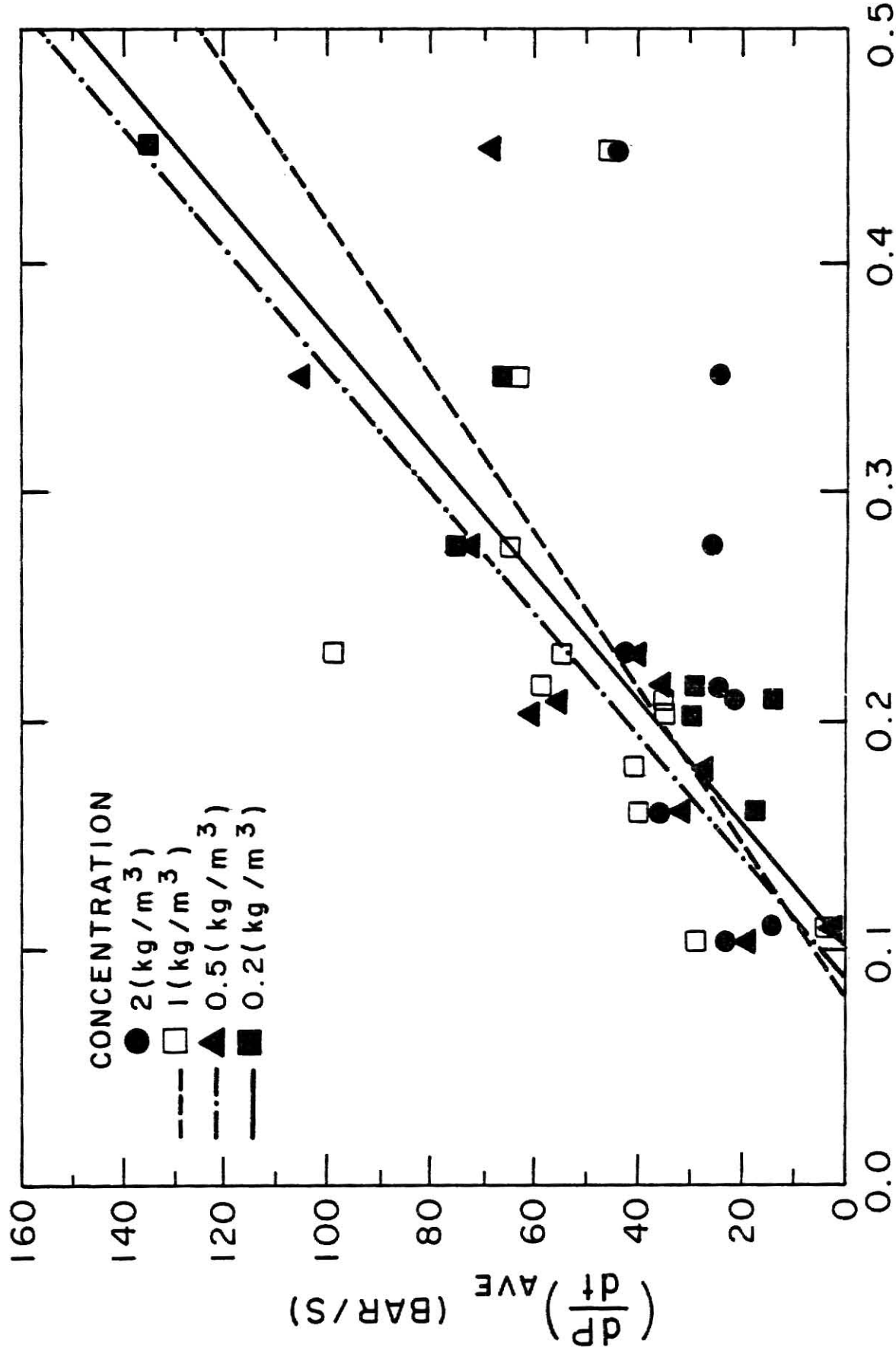

Fig. 5.59 The Relationship between the Average Rate of Pressure Rise and the Specific External Surface Area for Corn Dust

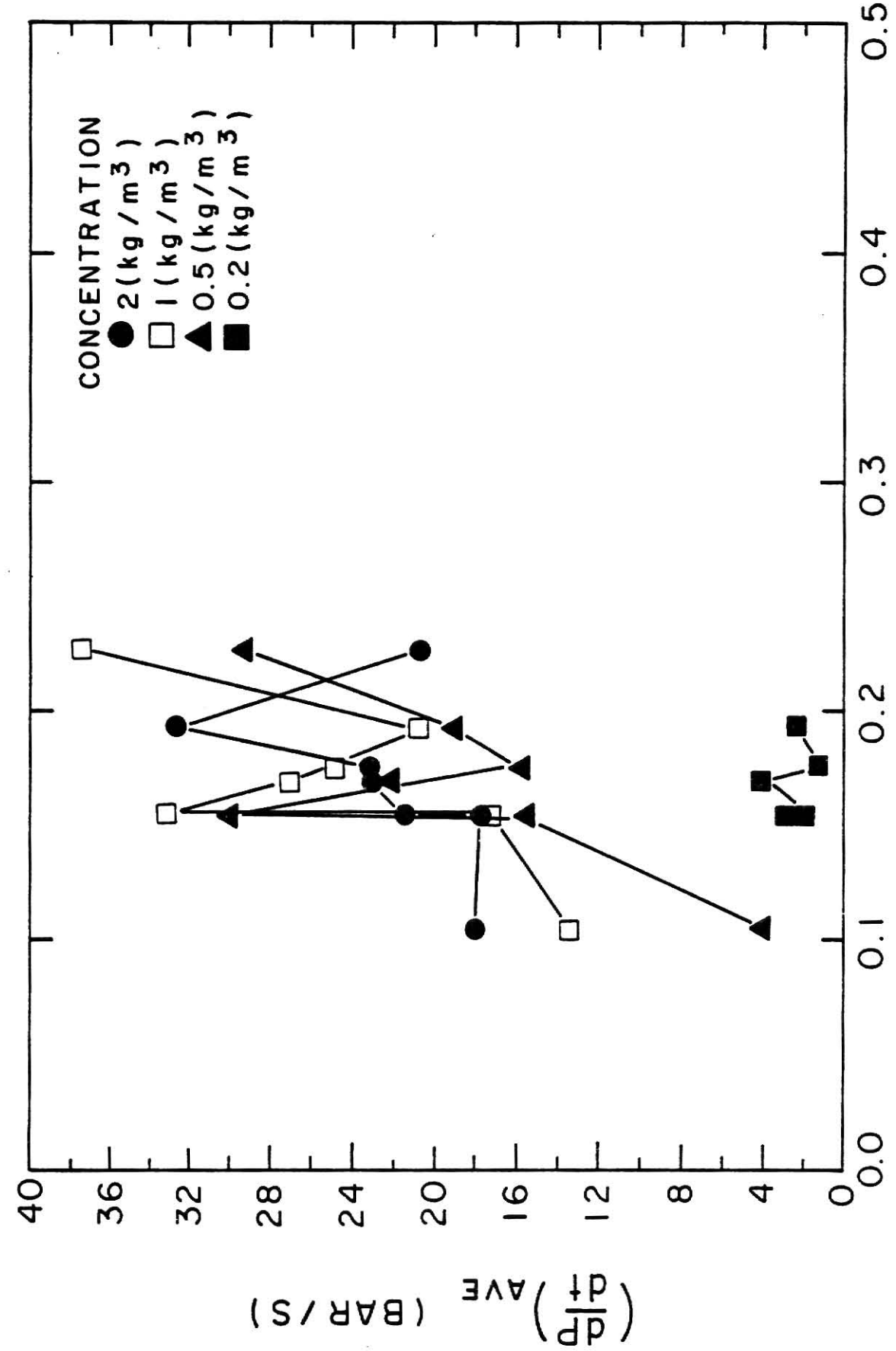

Fig. 5.60 The Relationship between the Average Rate of Pressure Rise and the Specific External Surface Area for Wheat Dust

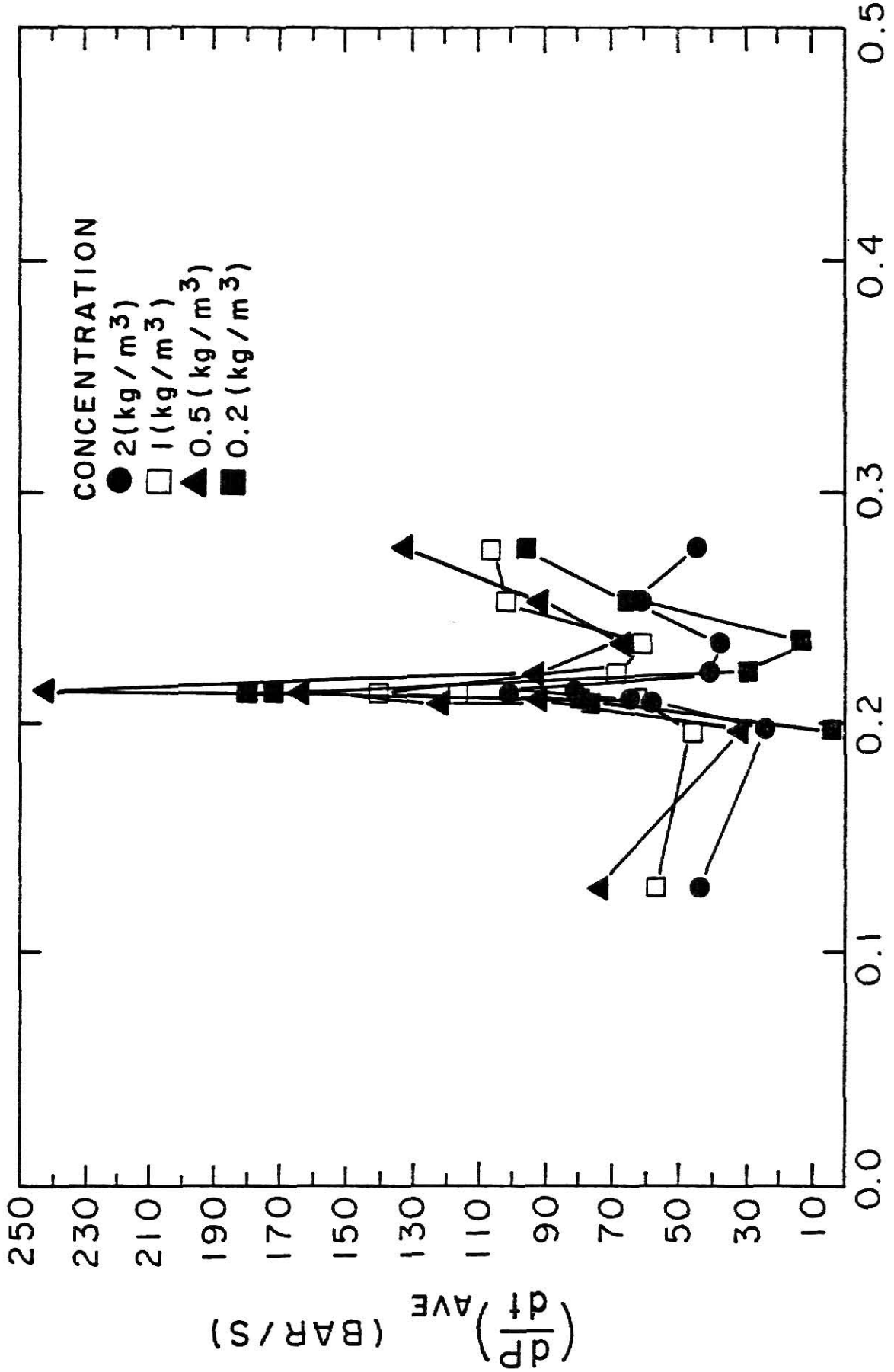

Fig. 5.61 The Relationship between the Average Rate of Pressure Rise and the Specific External Surface Area for Cornstarch

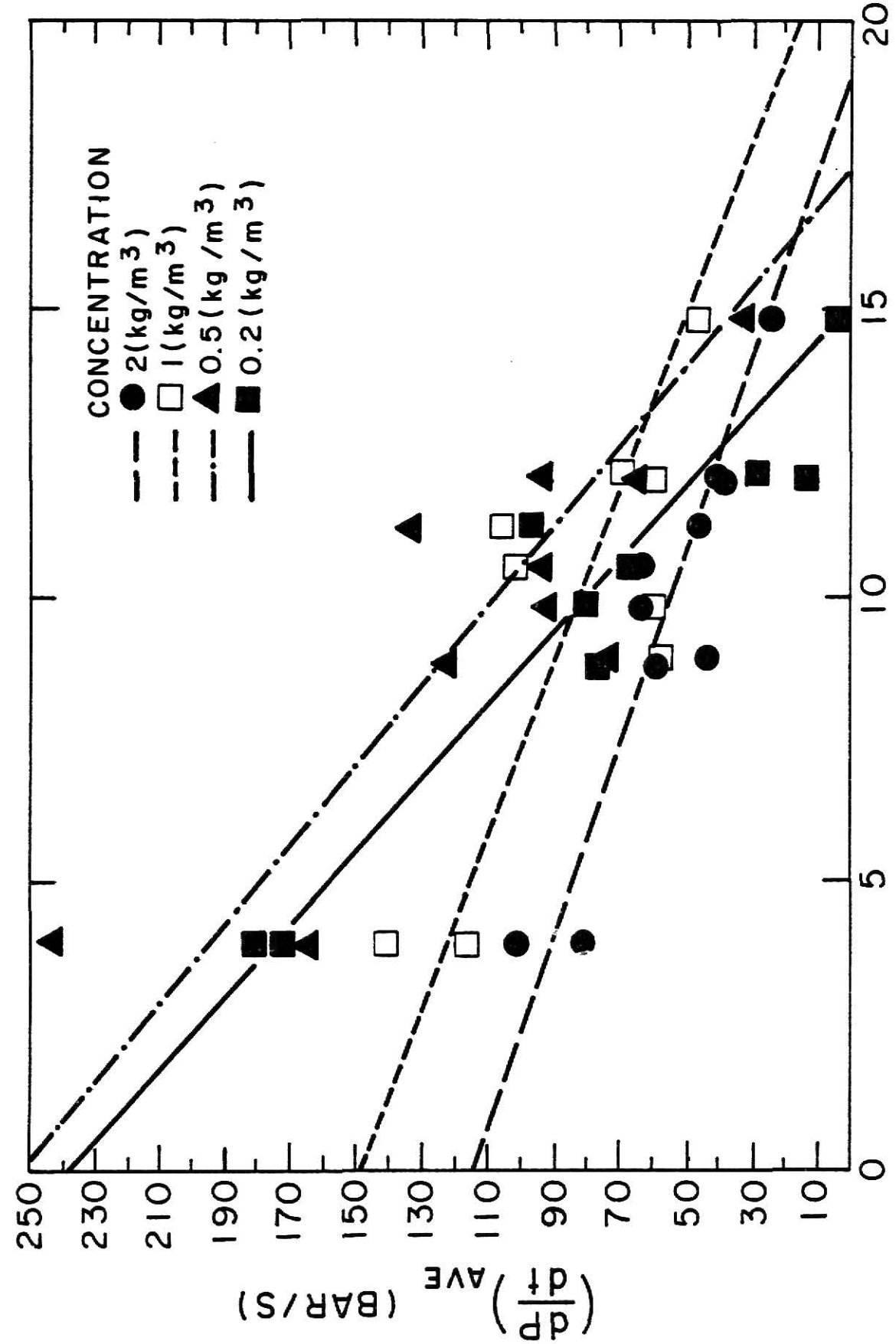

Fig. 5.62 The Relationship between the Average Rate of Pressure Rise and the Moisture Content for Cornstarch

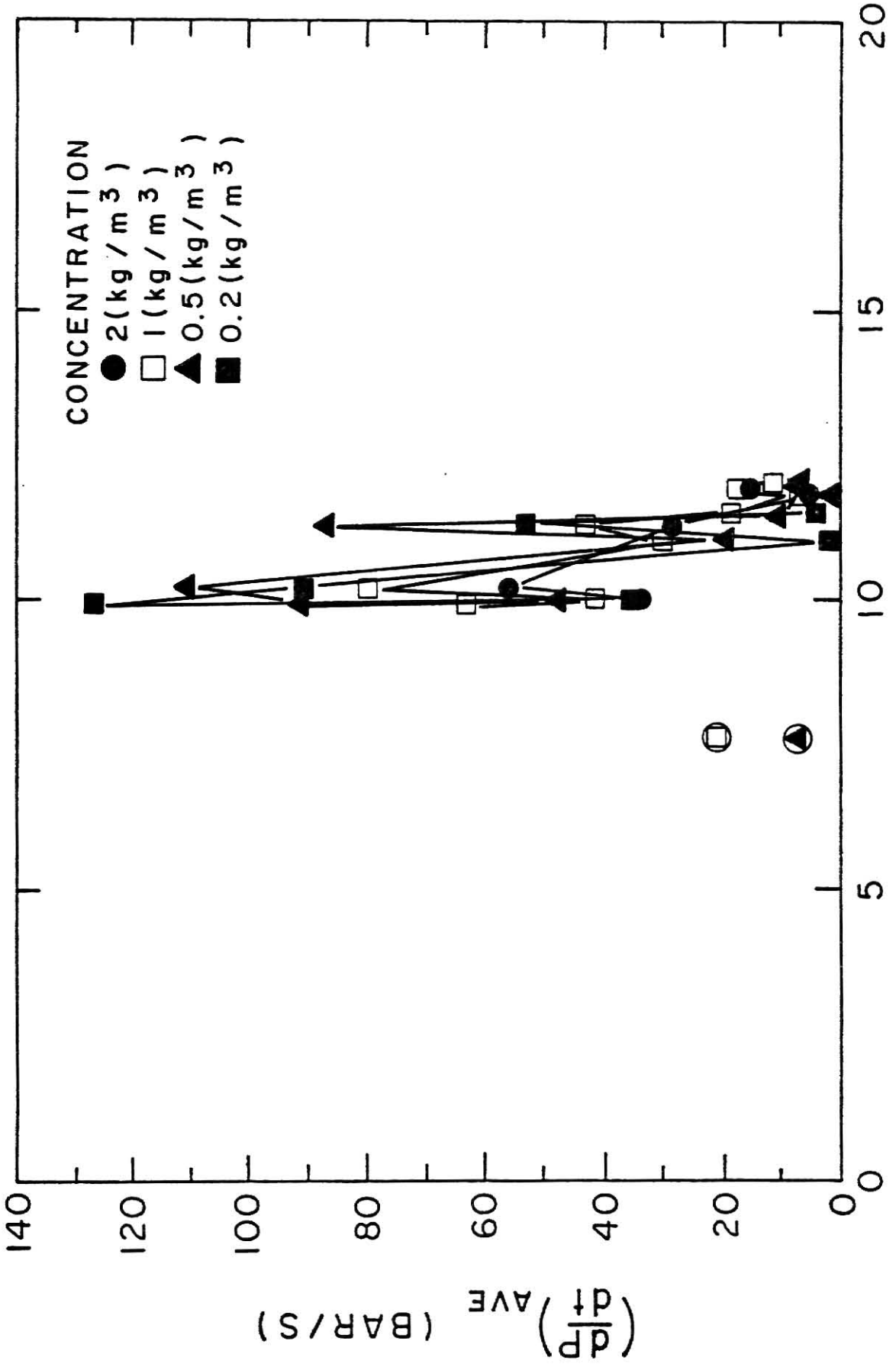

Fig. 5.63 The Relationship between the Average Rate of Pressure Rise and the Moisture Content for Grain Sorghum Dust

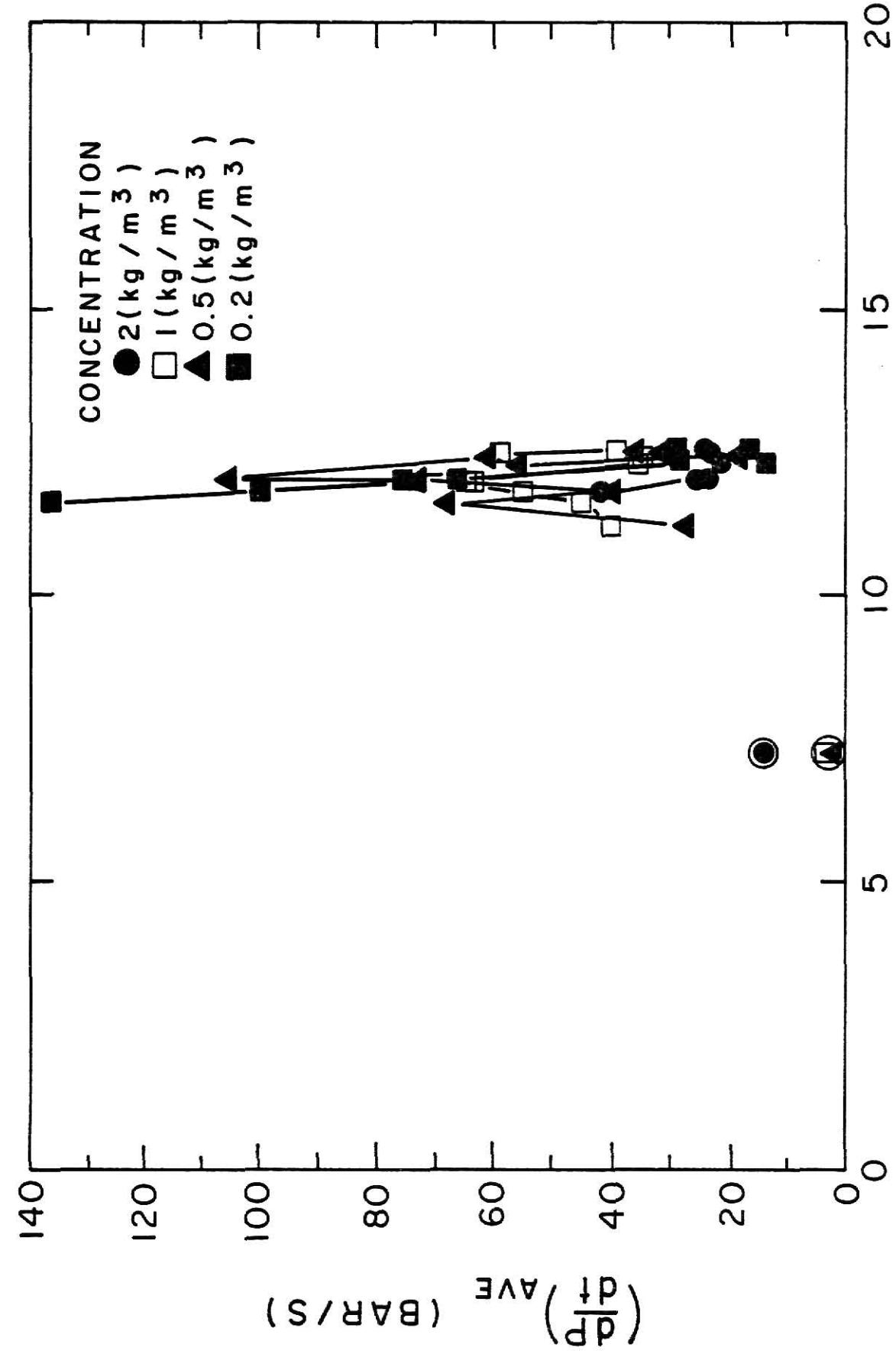

Fig. 5.64 The Relationship between the Average Rate of Pressure Rise and the Moisture Content for Corn Dust

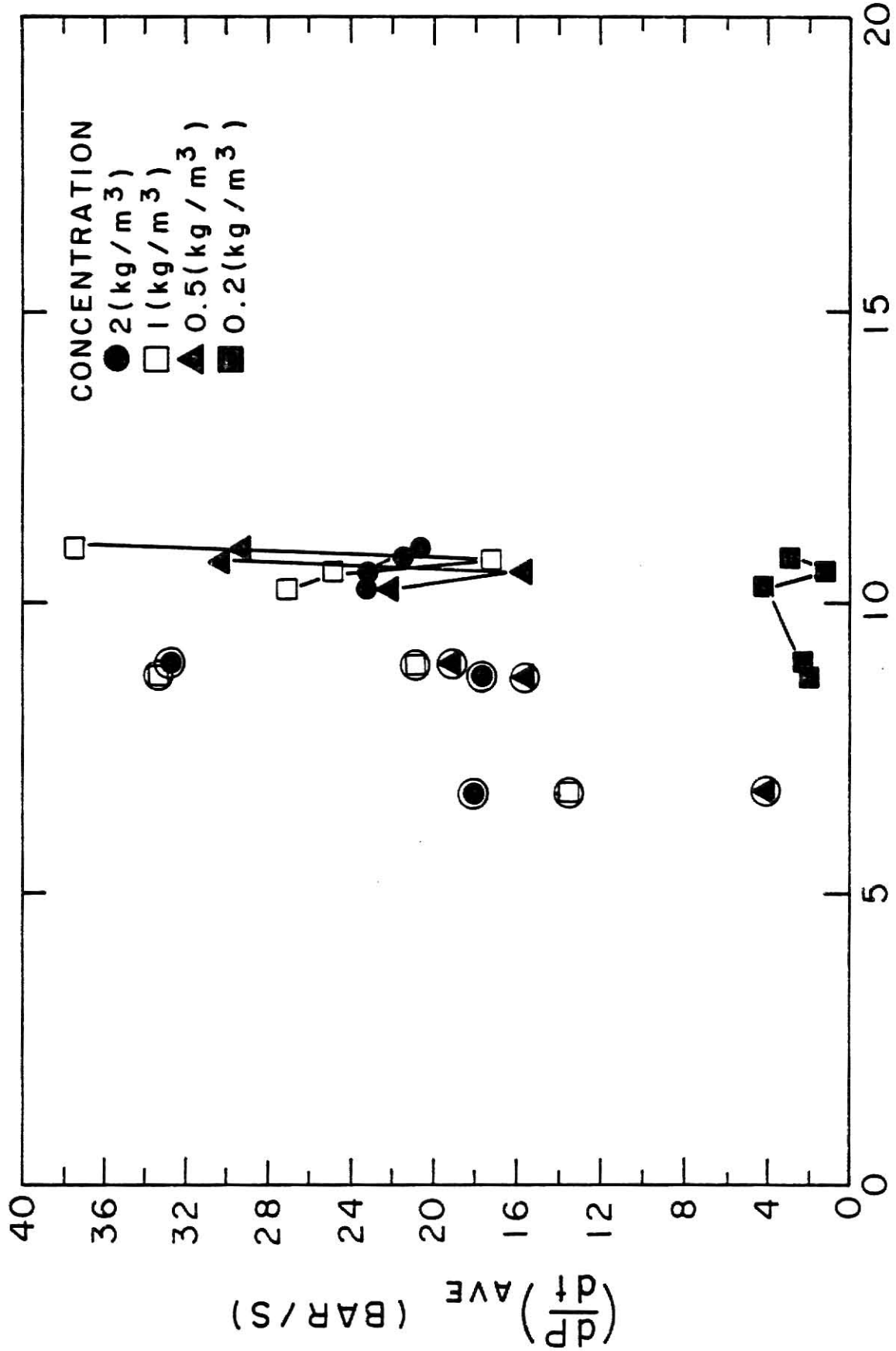

Fig. 5.65 The Relationship between the Average Rate of Pressure Rise and the Moisture Content for Wheat Dust

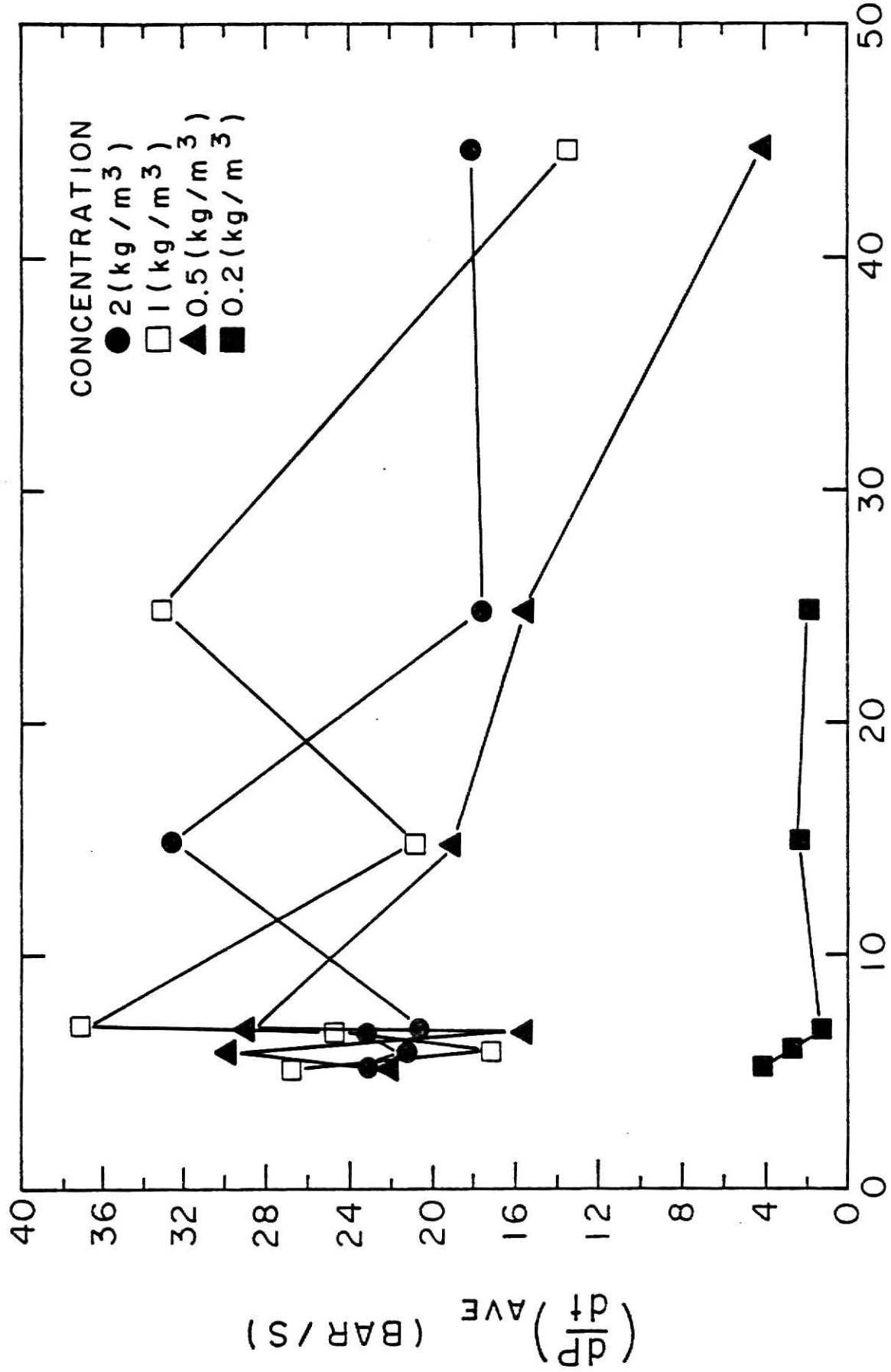

Fig. 5.66 The Relationship between the Average Rate of Pressure Rise and the Ash Content for Wheat Dust

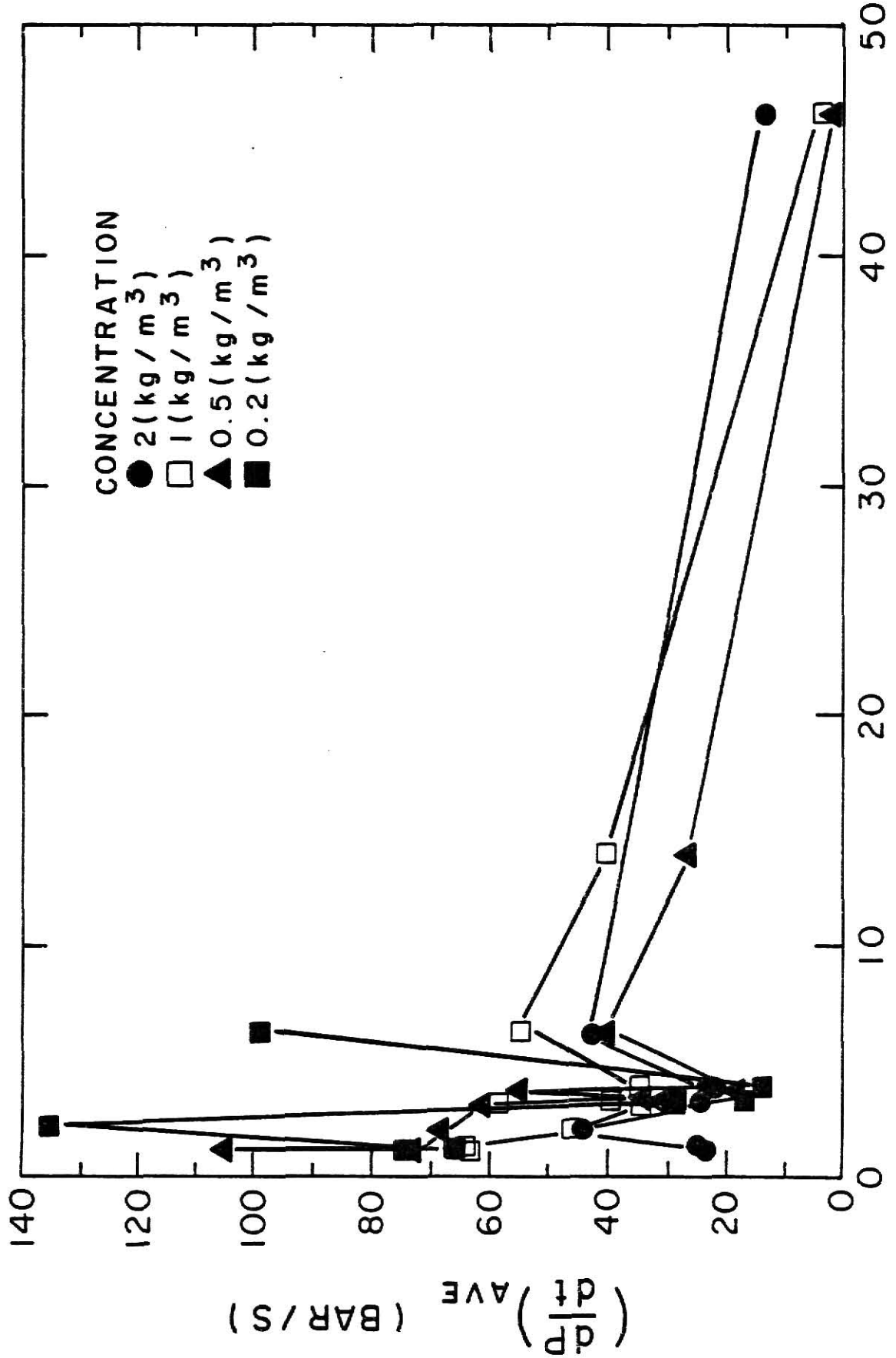

Fig. 5.67 The Relationship between the Average Rate of Pressure Rise and the Ash Content for Corn Dust

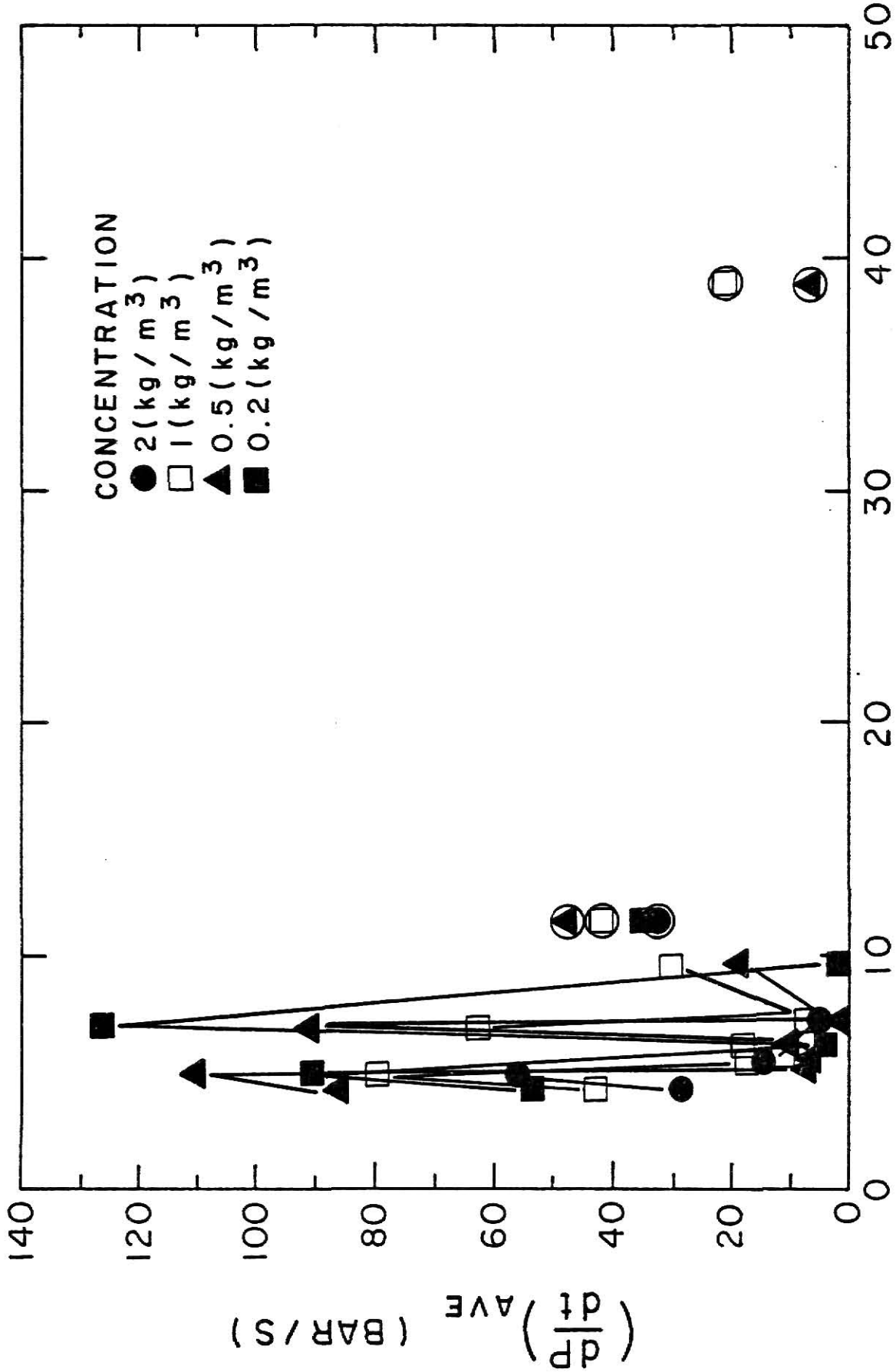

Fig. 5.68 The Relationship between the Average Rate of Pressure Rise and the Ash Content for Grain Sorghum Dust

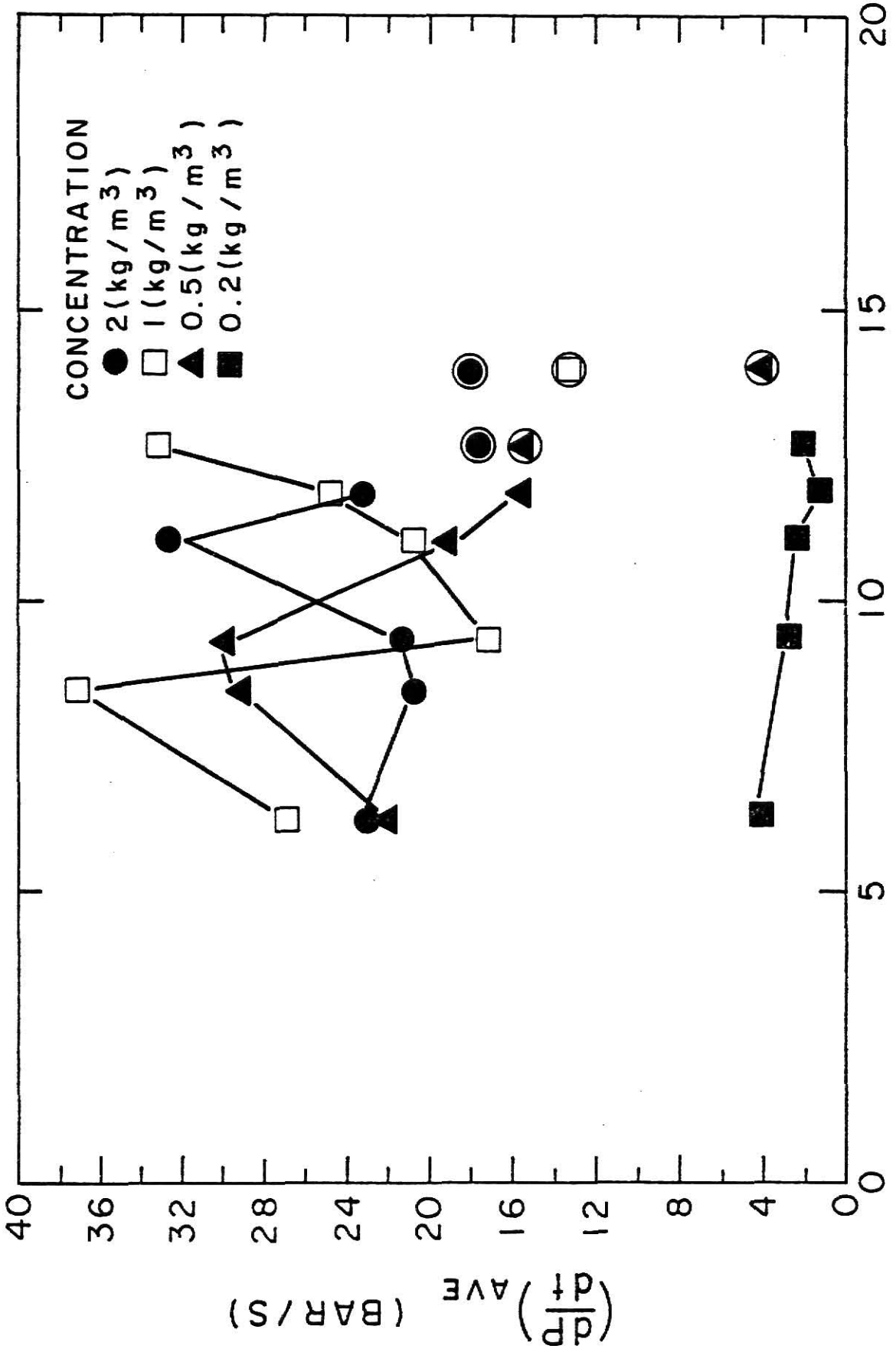

Fig. 5.69 The Relationship between the Average Rate of Pressure Rise and the Protein Content for Wheat Dust

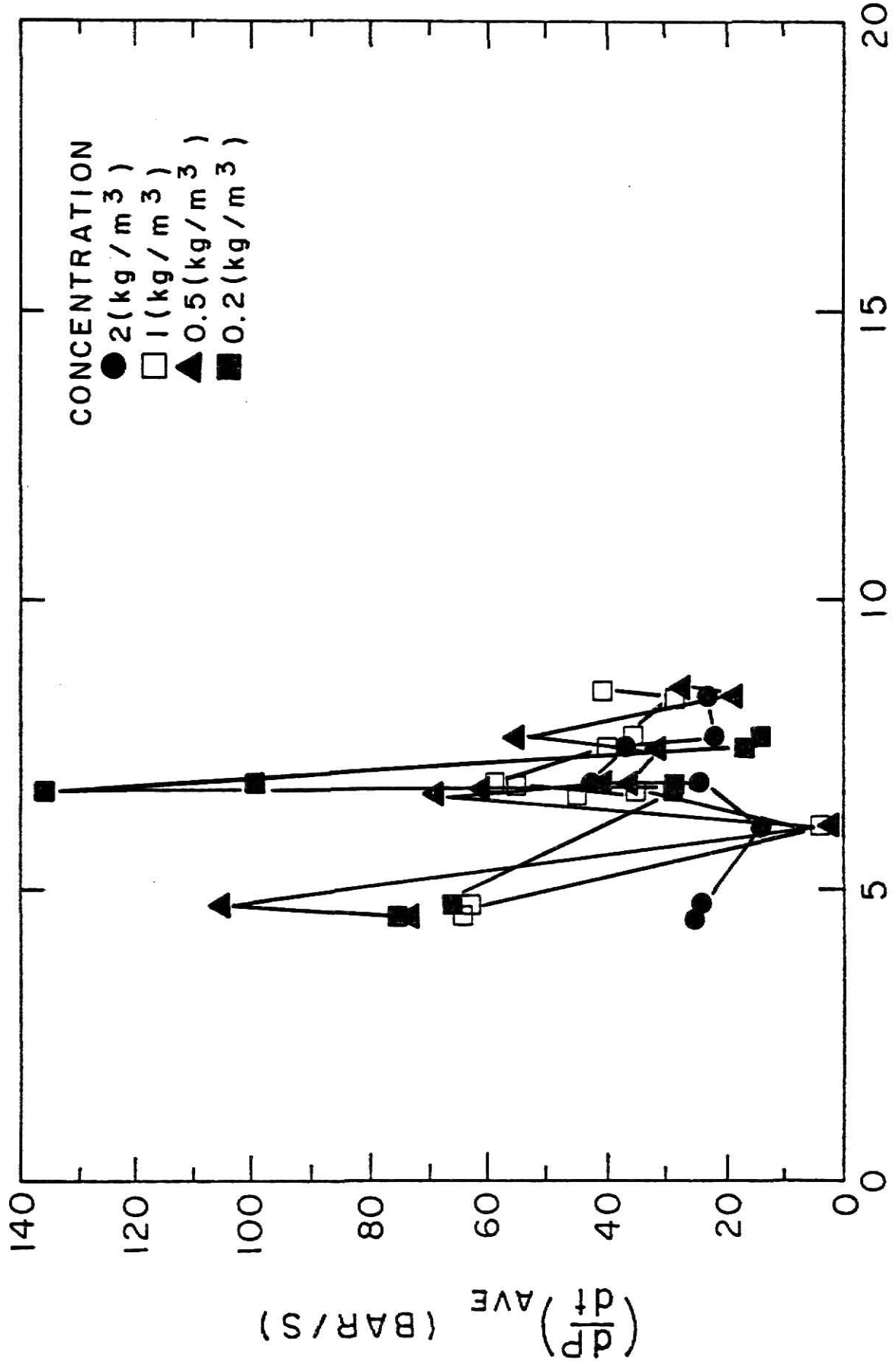

Fig. 5.70 The Relationship between the Average Rate of Pressure Rise and the Protein Content for Corn Dust

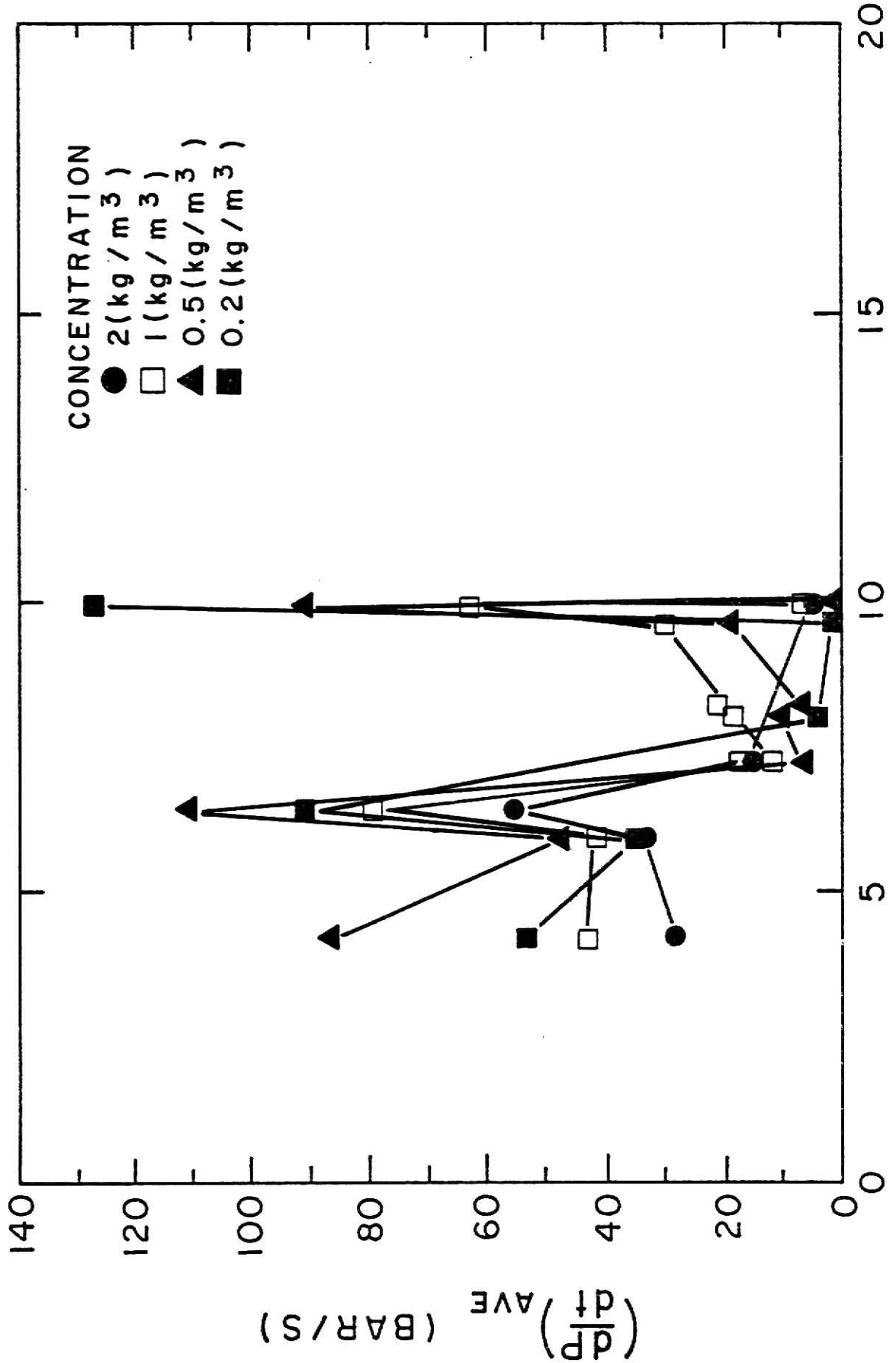

Fig. 5.71 The Relationship between the Average Rate of Pressure Rise and the Protein Content for Grain Sorghum Dust

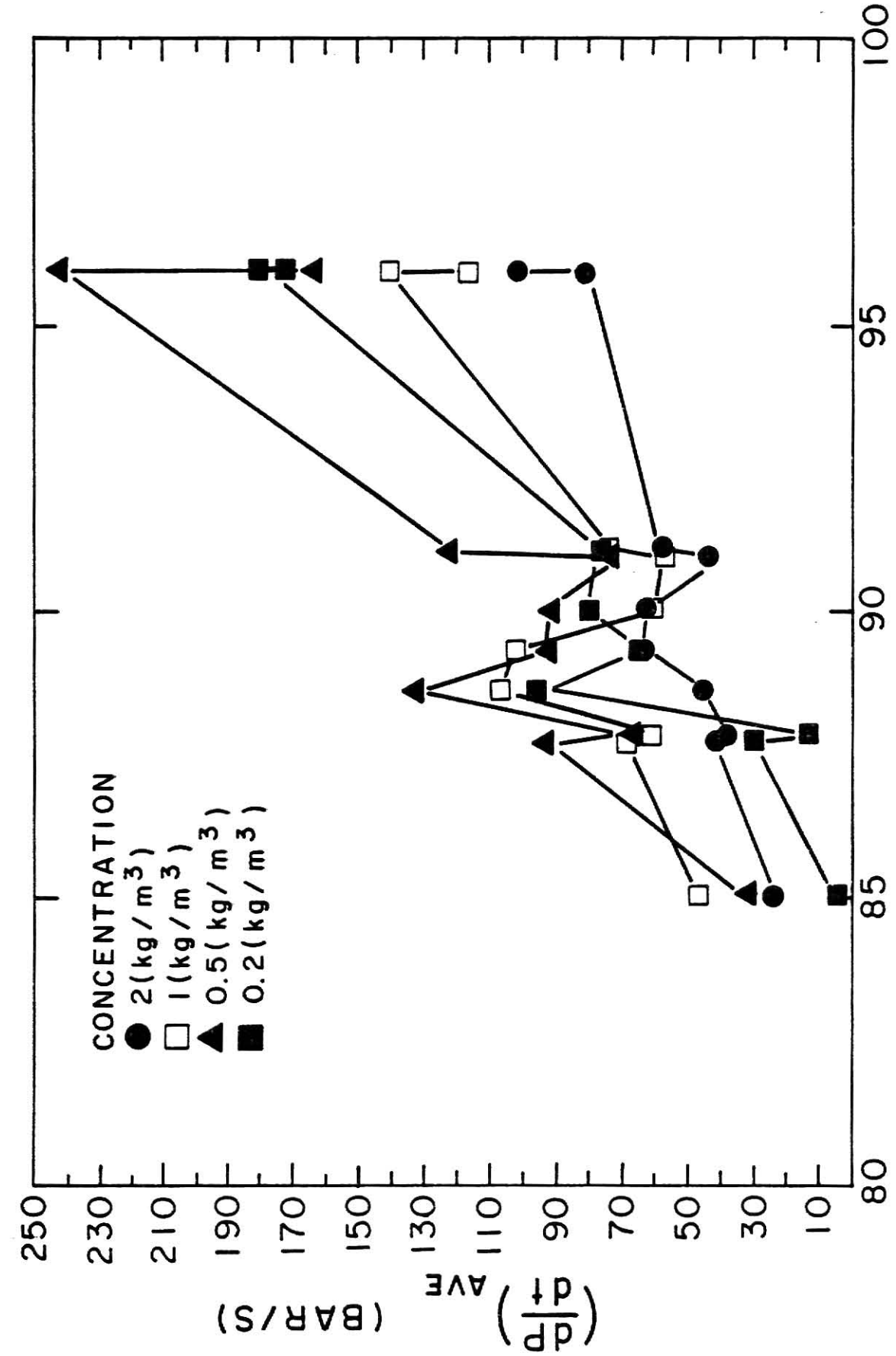

Fig. 5.72 The Relationship between the Average Rate of Pressure Rise and the Starch and Fiber Content for Cornstarch

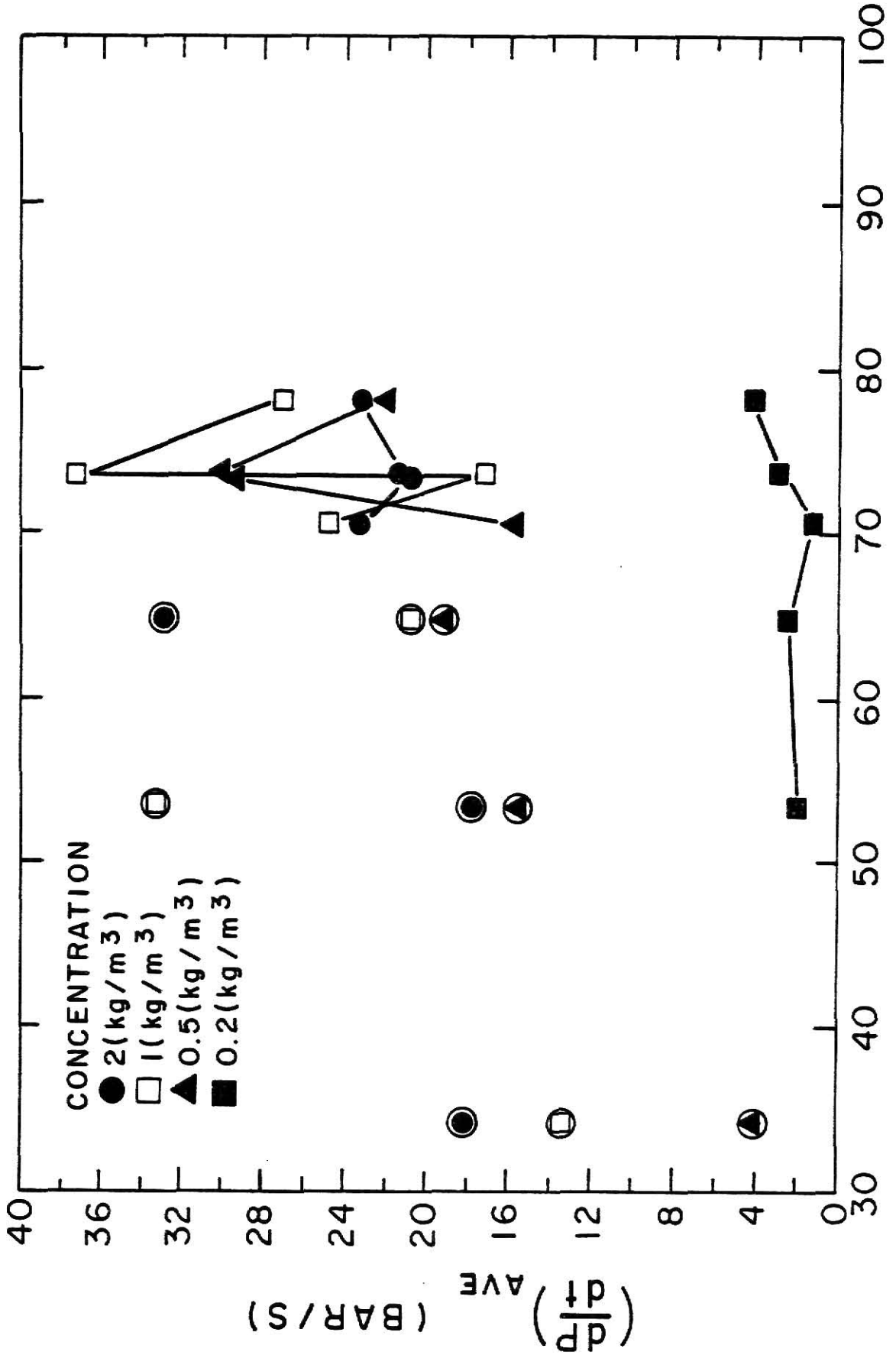

Fig. 5.73 The Relationship between the Average Rate of Pressure Rise and the Starch and Fiber Content for Wheat Dust

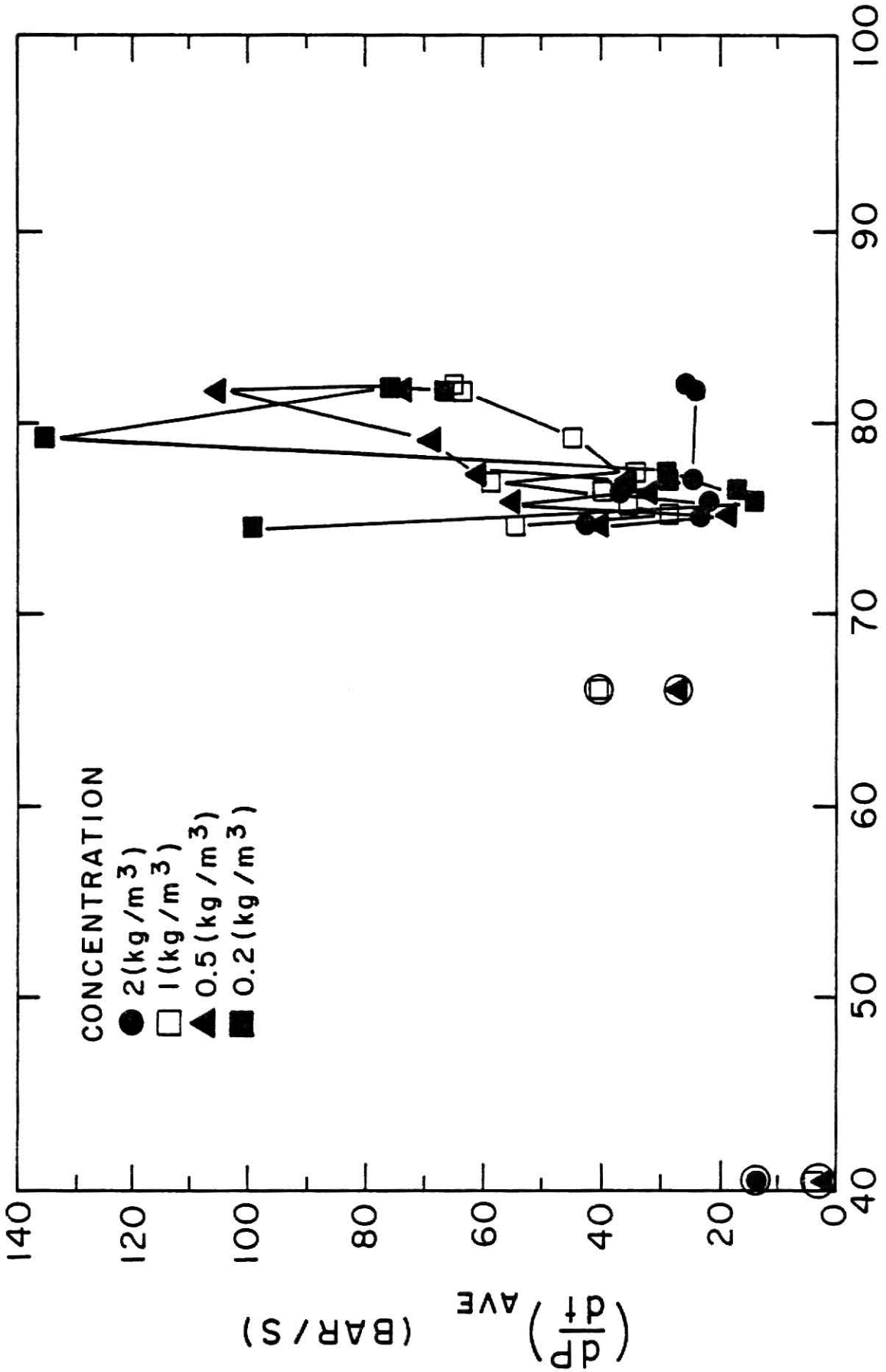

Fig. 5.74 The Relationship between the Average Rate of Pressure Rise and the Starch and Fiber Content for Corn Dust

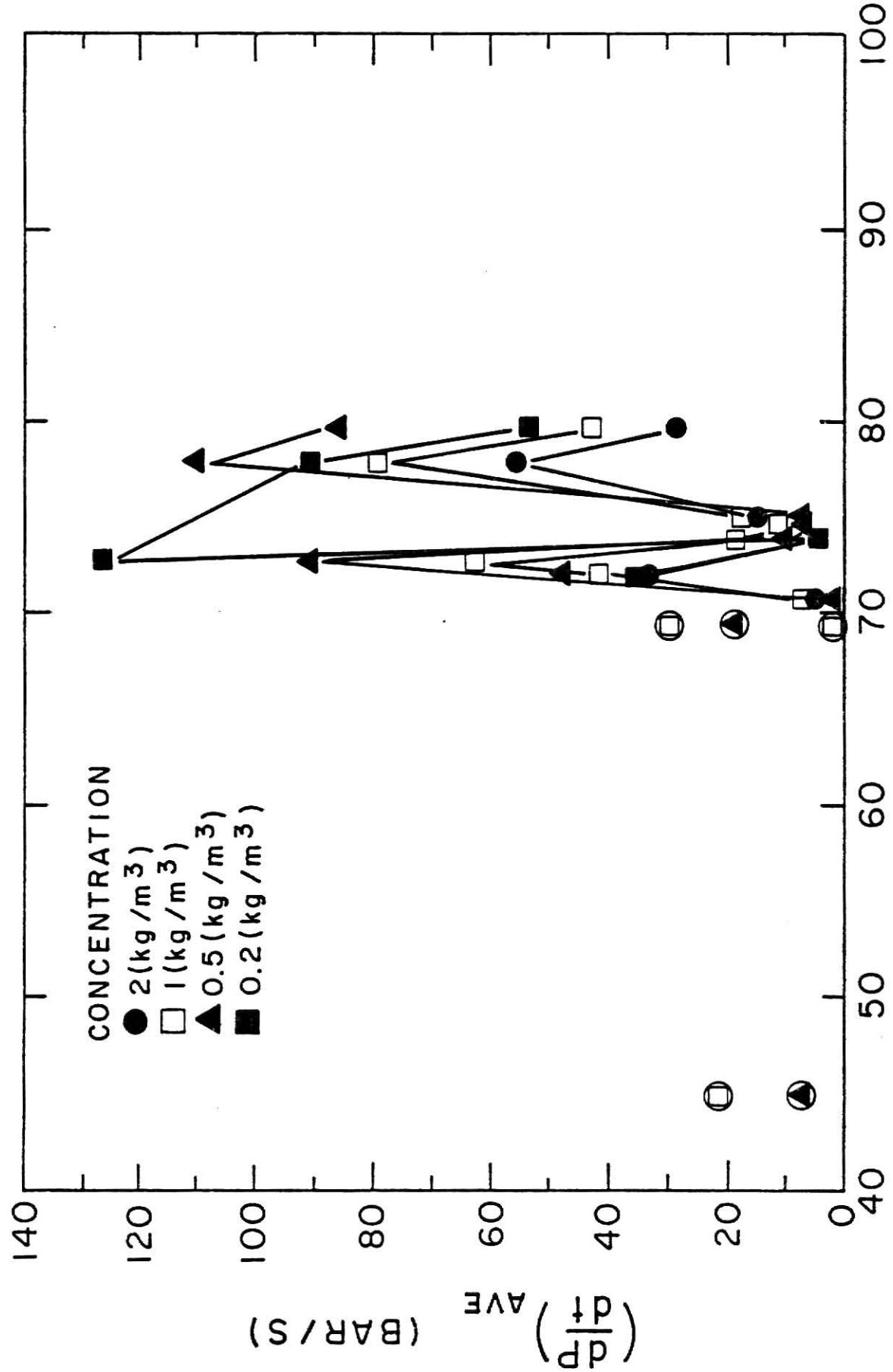

Fig. 5.75 The Relationship between the Average Rate of Pressure Rise and the Starch and Fiber Content for Grain Sorghum Dust

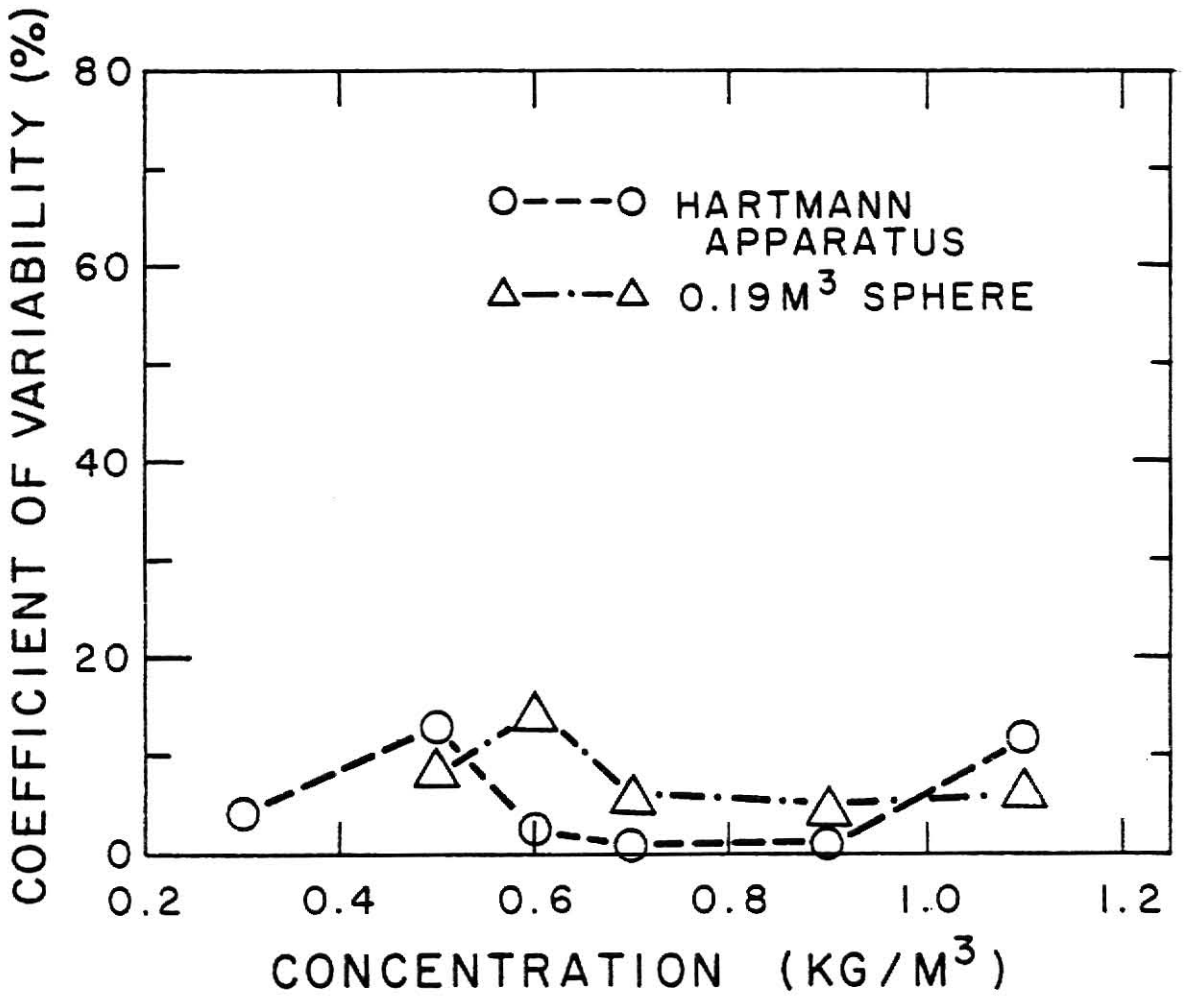

Fig. 5.76 The Coefficient of Variability between Repetitions of the Maximum Explosion Pressure as Affected by Concentration for Both Hartmann Apparatus and 0.19 m^3 Spherical Apparatus

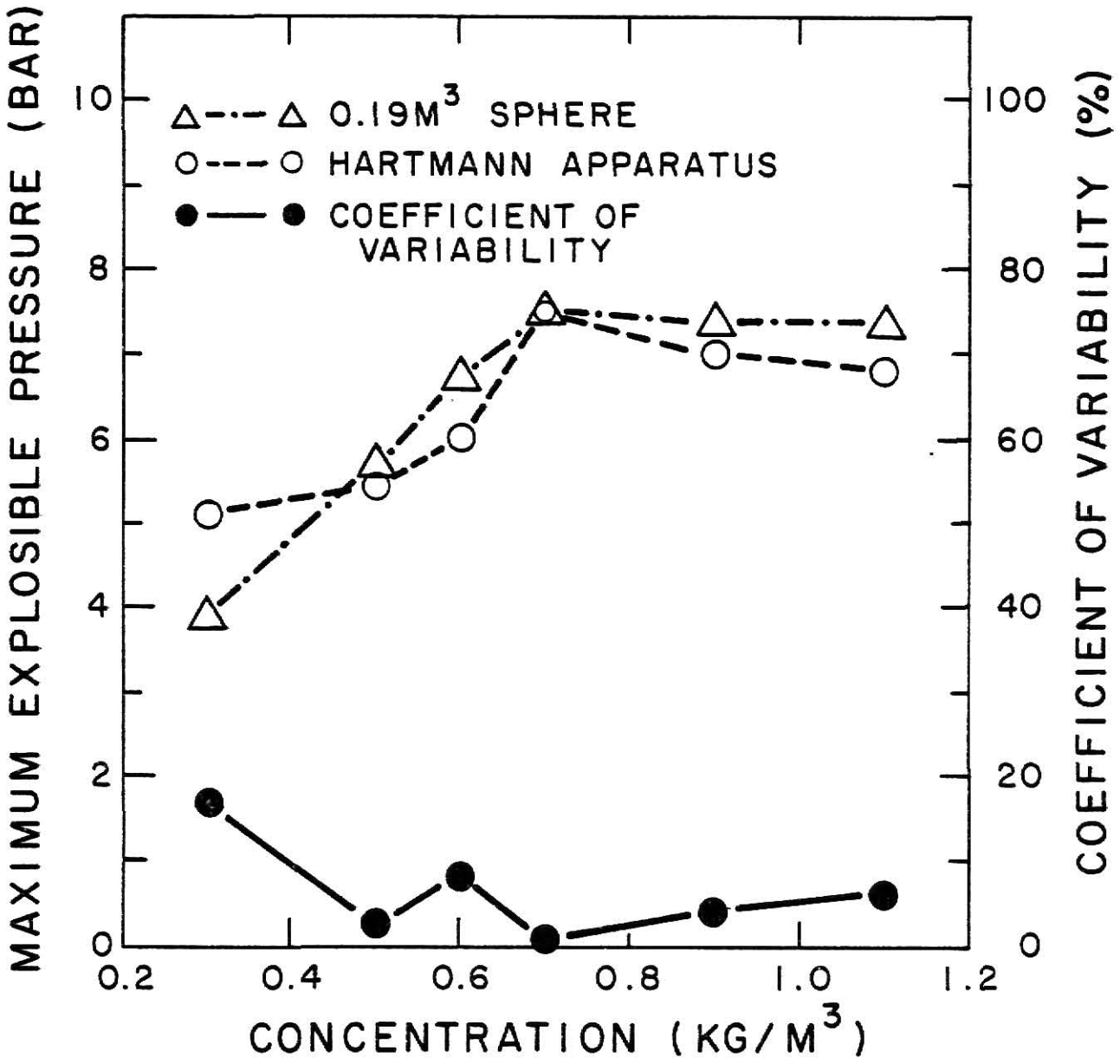

Fig. 5.77 Comparison of the Maximum Explosion Pressures Obtained from the Hartmann Apparatus with Those Obtained from the 0.19 m^3 Spherical Apparatus

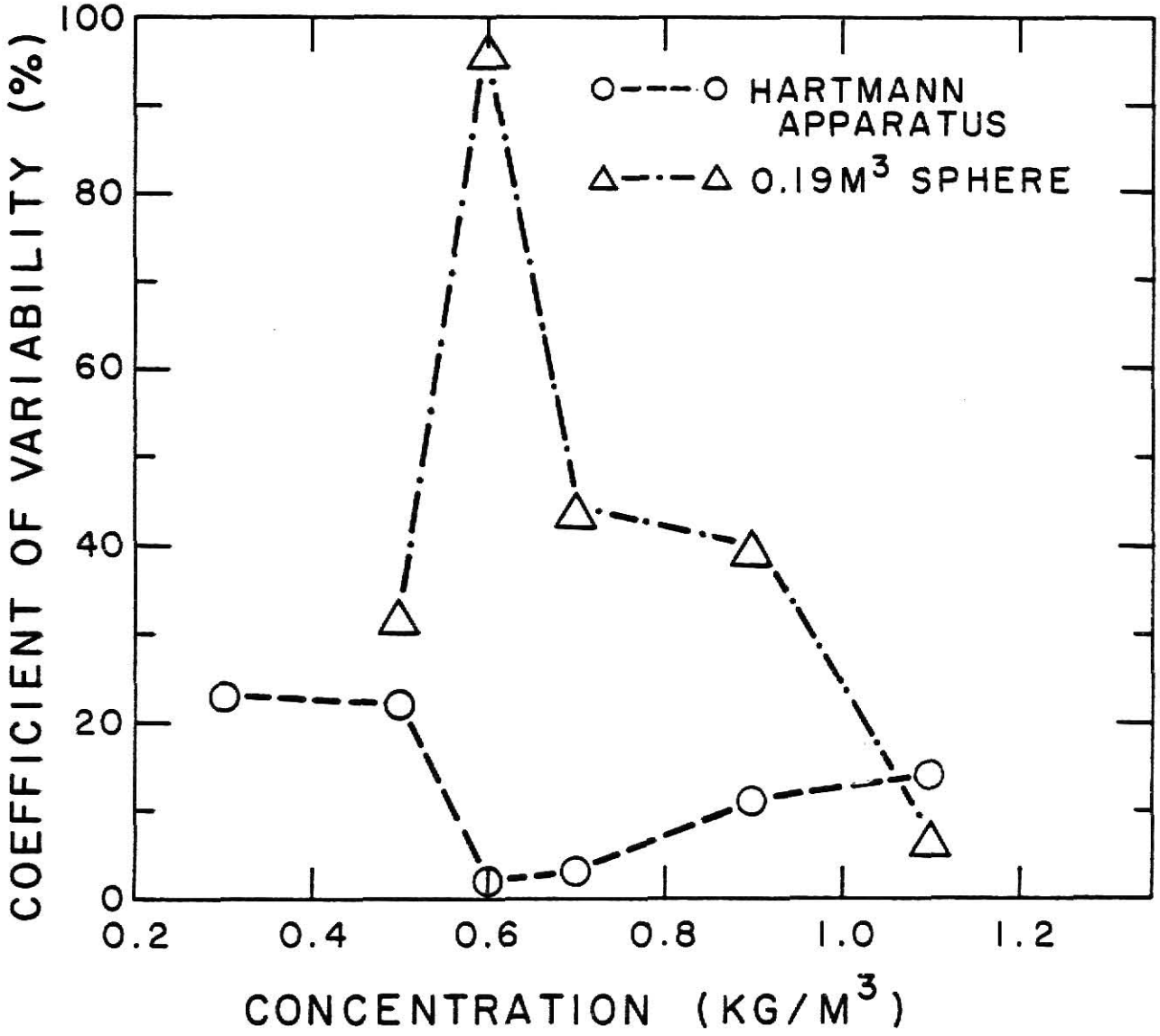

Fig. 5.78 The Coefficients of Variability between Repetitions of the K_{st} Values as Affected by Concentration for the Hartmann Apparatus and the 0.19 m^3 Spherical Apparatus

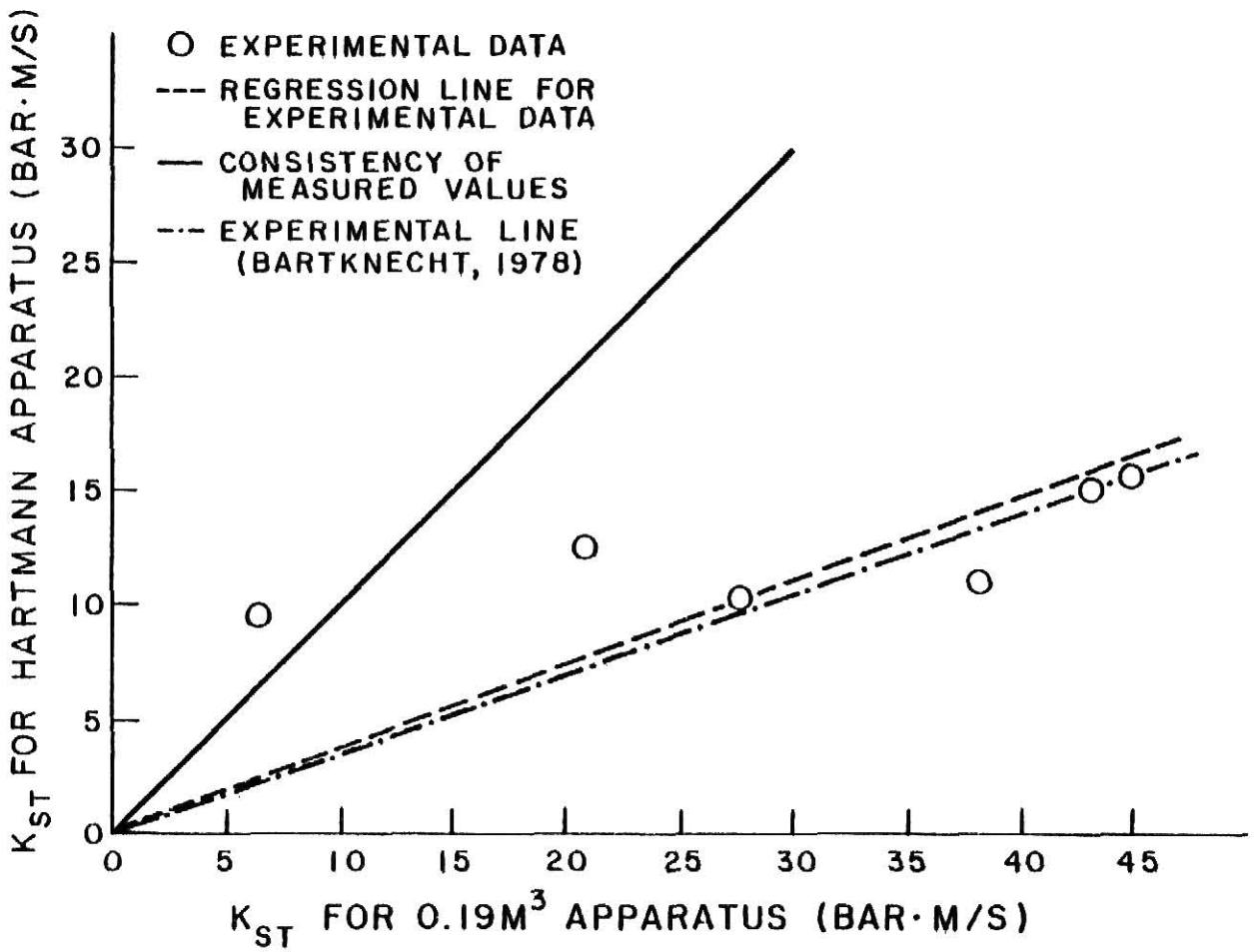

Fig. 5.79 Comparison of the Values of K_{st} Obtained from the Hartmann Apparatus with Those from 0.19 m^3 Spherical Apparatus

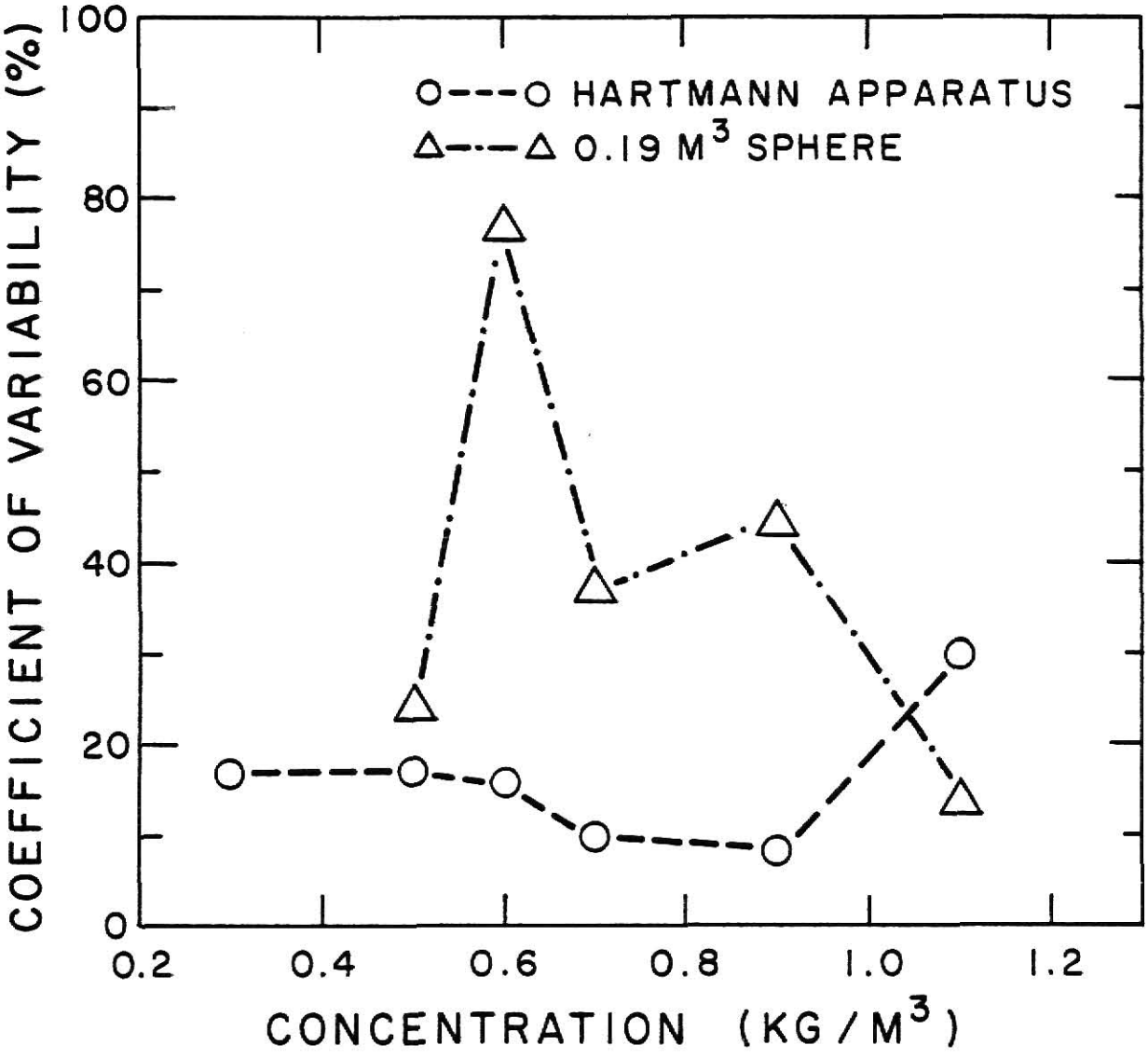

Fig. 5.80 The Coefficients of Variability between Repetitions of the $K_{st.ave}$ Values as Affected by Concentration for Hartmann and 0.19 m^3 Spherical Apparatus

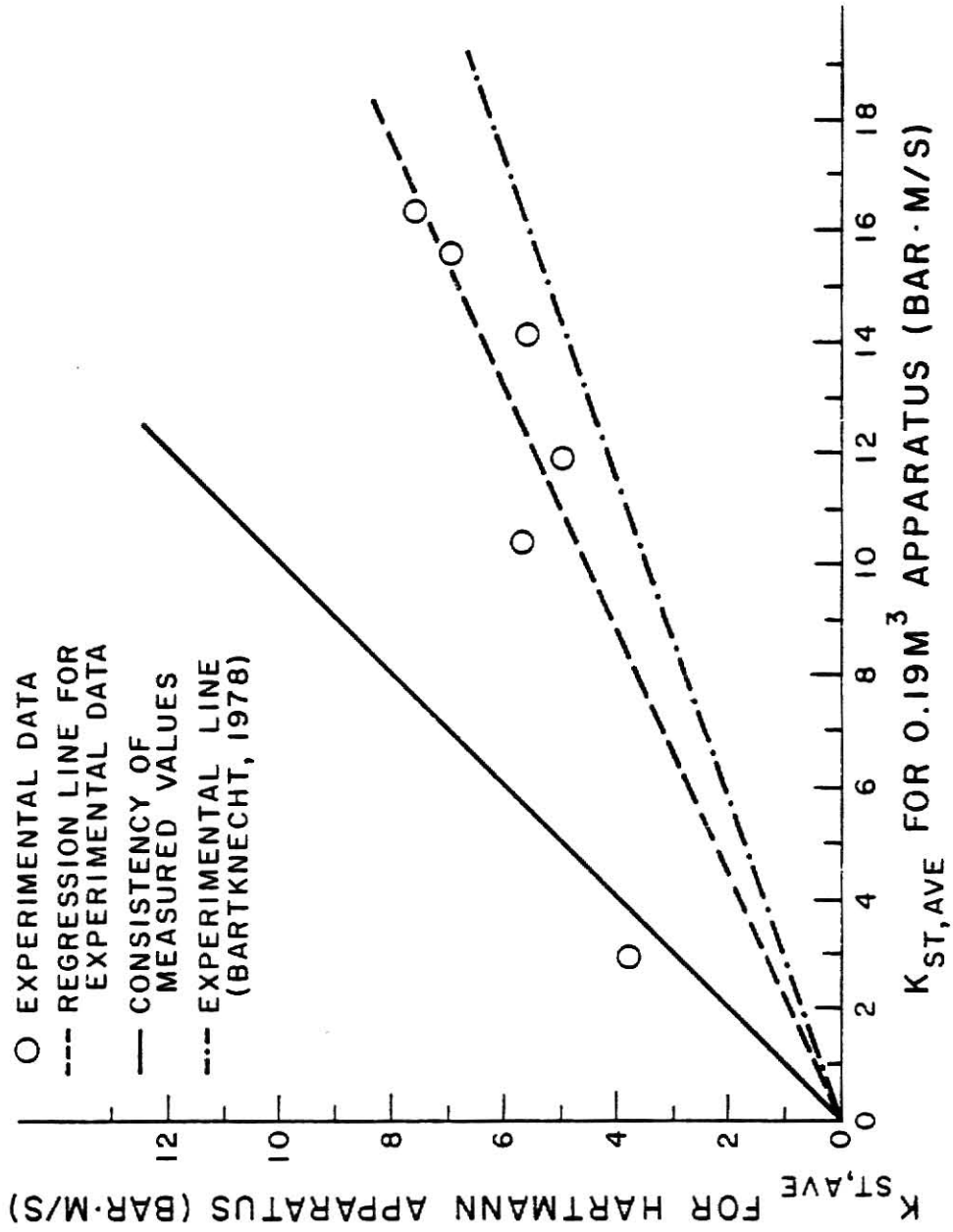

Fig. 5.81 Comparison of the Values of $K_{St,ave}$ Obtained from the Hartmann Apparatus with Those Obtained from the 0.19 m^3 Spherical Apparatus

CHAPTER 6

CONCLUSIONS AND RECOMMENDATIONS

Wheat dust, corn dust, and grain sorghum dust were very similar in composition and in ranges of particle diameters. Sieve classification, unless performed very carefully, can result in carry-over of large numbers of small diameter particles in these types of dust. A large portion of the ash content was contained in separate particles consisting almost entirely of ash. Thus the ash content of the dust particles appeared to be only approximately 2% and did not vary much between size fractions or types of dust. The starch & fiber content also did not appear to vary tremendously. No correlation was found between the mass mean diameter of a size fraction and its contents of moisture, ash, protein, or starch & fiber. The log normal approximation of a distribution can have the same coefficient of determination as that of another distribution; however, the deviation between the moments calculated from the actual distribution and that from each of the log normal approximations can be quite different. For a weight distribution, how well the distribution estimates the weight percent of the particles with diameters less than the mass mean diameter can be very critical when calculating moments of the distributions. The mass mean diameter, or and geometric mean diameter, is questionable as an average diameter because of its limitations in describing the distribution.

The minimum explosible concentration of all the dusts are similar. The order of explosibility is cornstarch, corn dust, grain sorghum dust, and wheat dust. Milo dust and corn dust yield very similar values of C_{min}. Particles with smaller diameters have lower values of C_{min}; however, the moisture content seems to be an important variable. Cornstarch yielded values of 40 kg/m^3

for 4% moisture and appear to become non-explosible at values approximately 15.8%. The remaining dust also become non-explosible at values ranging from 13% to 15% depending on the ash content. Ash content did not enter in except at high values of approximately 25%. The data for wheat dust indicated by extrapolation that approximately 73% ash is necessary to energize wheat dust. Reasonably good correlations were obtained between $1/C_{min}$ and S_{ext} or ash content or moisture content. There appears to be a long ignition delay, approximately 100-200 msec, for most dusts. For a transite experiment this could have serious implications.

The smallest size fraction of grain sorghum dust yielded the largest maximum explosion pressure, P_{max}, of 7.8 bar at a concentration of 1.0 kg/m^3. At the highest dust concentration of 2.0 kg/m^3, the highest value of P_{max} for the remaining three dusts ranged from approximately 6.0 to 6.5 bar.

For grain sorghum dust and corn dust, P_{max} remained essentially constant at 6.0 bar as the mass mean diameter decreased from approximately 50 to 15 μm for the concentrations of 1.0 and 2.0 kg/m^3. At a concentration of 0.5 kg/m^3, P_{max} increased with decreasing diameter until values of approximately 6.0 bar for grain sorghum dust and 4.7 for corn dust were attained at a diameter of 15 μm. Below a diameter of approximately 15 μm, P_{max} remained essentially constant or decreased for these three concentrations; except in the case of grain sorghum dust at a concentration of 1.0 kg/m^3. For a concentration of 0.2 kg/m^3, P_{max} increased for all diameters; it never attained a value of 6.0 bar.

A model has been developed, which correlates P_{max} with the specific external surface area, S_{ext}. The data for grain sorghum dust were fitted to the model and show a linear correlation between P_{max} and S_{ext} up to a certain point, depending on the concentration. Above this point, P_{max} rapidly

approached a constant value. The coefficients of determination, R^2, for grain sorghum dust were, 0.95, 0.78, and 0.88 for the concentrations of 0.5, 1.0, and 2.0 kg/m^3, respectively.

The maximum explosion pressure is linearly correlated with the ash content for values above approximately 10% for grain sorghum, wheat, and corn dusts. The maximum explosion pressure is quadratically correlated with the moisture content for cornstarch. Moisture contents ranging from approximately 16% to greater than 20% cause P_{max} to become zero. For both grain sorghum dust and corn dust, the correlations between P_{max} and the moisture content indicate that moisture content becomes the dominating variable that suppresses P_{max} for values above approximately 11%.

For all size fractions of grain sorghum dust and corn dust, the maximum rate of pressure rise, $(dP/dt)_{max}$, attained values so high as approximately 380 bar/s whereas those for wheat dust were approximately 1/2 of those for grain sorghum dust. For low moisture contents of approximately 4%, $(dP/dt)_{ave}$ for cornstarch attained values so high as 680 bar/s.

For the concentrations of 0.5, 1.0, and 2.0 kg/m^3 for grain sorghum dust and corn dust, $(dP/dt)_{max}$ increased as the mass mean diameter decreased down to approximately 15 μm. Below 15 μm, $(dP/dt)_{max}$ decreased sharply for those three concentrations. At a concentration of 0.2 kg/m^3, $(dP/dt)_{max}$ increased for the entire range of D_m.

For diameters below approximately 20 μm, the highest values of $(dP/dt)_{max}$ were obtained at the concentration of 0.5 kg/m^3. For D_m below approximately 15 μm, however, the highest values of $(dP/dt)_{max}$ were obtained at a concentration of 0.2 kg/m^3.

A model has been developed which correlates $(dP/dt)_{max}$ with the specific external surface area, S_{ext}. As in the case of P_{max}, data for grain sorghum

dust, and corn dust were fitted to the model and the results exhibited a linear correlation up to certain values of S_{ext}. For grain sorghum dust, the coefficients of determination obtained were 0.92, 0.92, 0.90 and 0.80 for concentrations of 0.2, 0.5, 1.0, and 2.0 kg/m^3, respectively. For the lowest concentration, the correlation was linear for the entire range of S_{ext}.

For all types of dust, the correlation between $(dP/dt)_{max}$ and the ash content were similar to those between P_{max} and the ash content. These correlations indicate that ash contents above approximately 50% are necessary to cause $(dP/dt)_{max}$ to become zero. The higher the dust concentration, the higher the ash content necessary to cause $(dP/dt)_{max}$ to become zero. The correlations between $(dP/dt)_{max}$ and the moisture content were also similar to those between P_{max} and the moisture content. For cornstarch, however, the correlations appear to be linear. The coefficients of determination were 0.94, 0.64, 0.56, and 0.78, for dust concentrations of 0.2, 0.5, 1.0, and 2.0 kg/m^3, respectively. From the extrapolation of these regression equations, the moisture contents that cause $(dP/dt)_{max}$ to approach zero are 14.6, 16.3, 17.9, and 18.6%, for concentrations of 0.2, 0.5, 1.0, and 2.0 kg/m^3, respectively.

The values of $(dP/dt)_{ave}$ for all types of dust were 1/2 to 1/3 of the values of $(dP/dt)_{max}$. The correlations for $(dP/dt)_{ave}$ were very similar to those for $(dP/dt)_{max}$. A model also has been developed which correlates $(dP/dt)_{ave}$ to S_{ext}. As in the case of $(dP/dt)_{max}$, the correlations were linear up to specific values of S_{ext} with coefficients of determination of 0.95, 0.88, 0.94, and 0.87 for concentrations of 0.2, 0.5, 1.0, and 2.0 kg/m^3.

Bartknecht (1979) experimentally demonstrated that $(dP/dt)_{max}$ data from an explosion apparatus with a volume less than approximately 20 l can not be easily scaled to larger volumes. Such an apparatus was not available for the

present investigation. A similar investigation with this type of apparatus would be recommended.

In this investigation, only five levels of the dust concentration were utilized. Concentration, however, appeared to be an important factor in the determination of the explosion characteristics P_{max}, $(dP/dt)_{max}$, and $(dP/dt)_{ave}$. A more detailed and complete analysis of the effect of the dust concentration on these explosion characteristics would be desirable, especially at levels approaching the minimum explosible concentration.

The specific external surface area, S_{ext}, utilized in this investigation is only an approximation of the external surface area of a particle. The total specific surface area of a porous dust particle could be much larger. The total specific surface area could be a closer approximation of the surface area available for a surface reaction. The correlation between each explosion characteristic and the total specific surface area could, therefore, be quite significant.

A large ignition delay between the arrival of the dust at the ignition electrode and the ignition of the dust cloud was noted for the minimum explosible concentration determinations. This appeared to be undesirable in the determination of the explosion characteristics. The use of a higher energy ignition source could alleviate the difficulty. In addition, a higher energy ignition source would yield the lowest C_{min} and the highest values of P_{max}, $(dP/dt)_{max}$, and $(dP/dt)_{ave}$.

A mathematical model was developed in this investigation. The solution of these models was beyond the scope of this investigation. With an expression for (D/D_0), however, these models could be solved numerically.

Radiation heat transfer was not included in the models developed in this work. At high temperatures, however, heat transfer by radiation could become

important. The addition of radiation heat transfer between the dust and the gas phases, between the dust phase and the vessel wall, and between the gas phase and the vessel wall could improve the predicted value of the explosion characteristics.

ACKNOWLEDGEMENTS

I first wish to extend my deep appreciation to both of my major advisors, Dr. L. T. Fan and Dr. F. S. Lai. Their suggestions, availability, and counsel have contributed immensely to this present work.

For their helpful suggestions and assistance, I wish to express my appreciation to David Aldis, Charles Martin, and Dr. R. S. Lee. I would also like to extend my appreciation to Tara Cupps and Jeanne Streeter for their encouragement and diligent assistance in the completion of this thesis.

The financial support has been provided by the United States Department of Agriculture Grain Marketing Research Laboratory.

Lastly, I extend my humble appreciation to the creator GOD of the universe who has said, "Cast all your anxiety upon Me because I care for you." His promises have sustained me physically, emotionally, and spiritually.

STUDY OF MECHANISMS OF GRAIN DUST EXPLOSION AS AFFECTED BY PARTICLE SIZE AND COMPOSITION

by

DAVID WAYNE GARRETT

B.S., Kansas State University, 1977

AN ABSTRACT OF A MASTER'S THESIS

submitted in partial fulfillment of the

requirements for the degree

MASTER OF SCIENCE

Department of Chemical Engineering

KANSAS STATE UNIVERSITY
Manhattan, Kansas

1981

ABSTRACT

Grain dust explosions have become a topic of much concern in the last few years. A dust explosion is essentially a very rapid combustion reaction of a solid reactant, e.g., grain dust. Thus, the composition and the particle size of the dust particles might be expected to be important parameters. In the literature, much has been postulated about the effect of particle size and composition and some studies have been performed on various types of dust. Little has been done, however, to study the explosibility of different size particles and the composition of a specific type of grain dust.

Each of three types of grain dust, namely, grain sorghum, corn, and wheat dust, or cornstarch was divided into 6 to 11 size fractions utilizing air and sieve classifications. The particle size distribution and the composition, in terms of the contents of moisture, ash, protein, and starch & fiber were determined for each size fraction. Large amounts of particles with diameters smaller than the sieve aperatures were retained on the sieve unless the sieving was carried out carefully. Particles consisting almost entirely of ash material were found to concentrate in particular air classified size fractions. The average diameter based on external surface area, the average diameter based on mass, and the coefficient of variability were calculated from each experimental particle size distribution utilizing a piecewise log normal approximation. These values were compared to those calculated from a least squares fitted log normal approximation of the actual distribution.

The minimum explosible concentration, C_{min}, of the dust in each size fraction was determined using the Hartmann apparatus. The minimum explosible concentration was correlated to the mass mean diameter, D_m, and to each of the composition components. Correlations between C_{min} and D_m for corn dust and

grain sorghum dust, and between C_{min} and moisture content for corn dust, grain sorghum dust, and cornstarch were found to be significant. According to models developed in this work, a linear correlation should exist between $1/C_{min}$ and the specific external surface area, S_{ext}, and also between $1/C_{min}$ and each composition component. In addition, the models were fitted to the experimental data. The coefficients of determination ranged from 0.80 to 0.94. The experimental results and the analysis indicated that the moisture content and the ash content were the major variables for these four types of dust. Extrapolation of the models to a moisture-free basis yielded values of C_{min} that were consistent with those reported in the literature. Extrapolation of the models to the moisture and ash contents which are necessary for a completely inert dust sample yielded values of the moisture and ash content consistent with those reported in the literature. The ignition delay between the dispersion and the ignition of the dust was also examined optically.

The maximum explosion pressure, the maximum rate of pressure rise, and the average rate of pressure rise were determined for the dust in all size fractions. Each of the characteristics were correlated with the mass mean diameter and with every composition component. According to models developed in this work, a linear correlation between each of the characteristics and S_{ext} should exist. For grain sorghum dust and corn dust, each characteristic exhibited a linear correlation below a particular value of S_{ext}. The contents of ash and moisture appeared to be determining factors for weight percents above approximately 12% and 15% - 25%, respectively. The effect of concentration on each correlation was also examined. For particles with diameters less than approximately 15 μm, the most hazardous condition occurred at the lowest concentration examined, 0.2 kg/m^3.